

Synthesis of covalent and non-covalent photoswitchable derivatives and their biological applications

Dissertation

Zur Erlangung des Doktorgrades der Naturwissenschaften

(Dr. rer. nat.)

an der Fakultät für Chemie und Pharmazie

der Universität Regensburg



vorgelegt von

Ranit Lahmy

aus Melbourne, Australia

2023

The experimental work was carried out at the Institute of Organic Chemistry at the University of Regensburg under the supervision of Prof. Dr. Burkhard König between March 2018 and June 2022.

Date of submission: 19.09.2023

Date of colloquium: 09.11.2023



Board of examiners:

Chair: Apl. Prof. Dr. Rainer Müller

1st Referee: Prof. Dr. Burkhard König

2nd Referee: Prof. Dr. Oliver Reiser

Examiner: Prof. Dr. Joachim Wegener

This thesis is dedicated to

My parents Anna & Coco, as well as my brother Doron

TABLE OF CONTENTS

1. Photoswitchable Fentanyl Derivatives for Controlled μ-Opioid Receptor Activation	1
1.1 Abstract	3
1.2 Introduction	5
1.2.1 Fentanyl – the Controversy	5
1.2.2 Fentanyl and the μ -Opioid GPCR.....	5
1.2.3 Photoswitchable Ligands as GPCR Probes	5
1.2.4 Photoswitchable Fentanyl Ligands	6
1.2.5 Expanding the Photofentanyl Toolbox	6
1.3 Results and Discussion.....	8
1.3.1 Design of Photofentanyl Ligands	8
1.3.2 Synthesis of Photofentanyl Ligands	10
1.3.3 Photophysical Investigations of Photofentanyl Ligands.....	15
1.3.4 Biochemical Evaluation of Photofentanyl Ligands.....	18
1.4 Conclusion and Outlook.....	26
1.5 Acknowledgements.....	27
1.6 References.....	28
1.7 Supplementary Information.....	31
1.7.1 Supplementary Molecular Modeling Information.....	31
1.7.2 Supplementary Chemical Information.....	32
1.7.3 Supplementary Photophysical Information	56
1.7.4 Supplementary Biochemical Information.....	66
1.7.5 NMR Spectra.....	70
1.7.6 References.....	71
2. Tethered Photoswitchable Derivatives of Fentanyl that Target the μ-Opioid Receptor	73
2.1 Abstract	75
2.2 Introduction	77

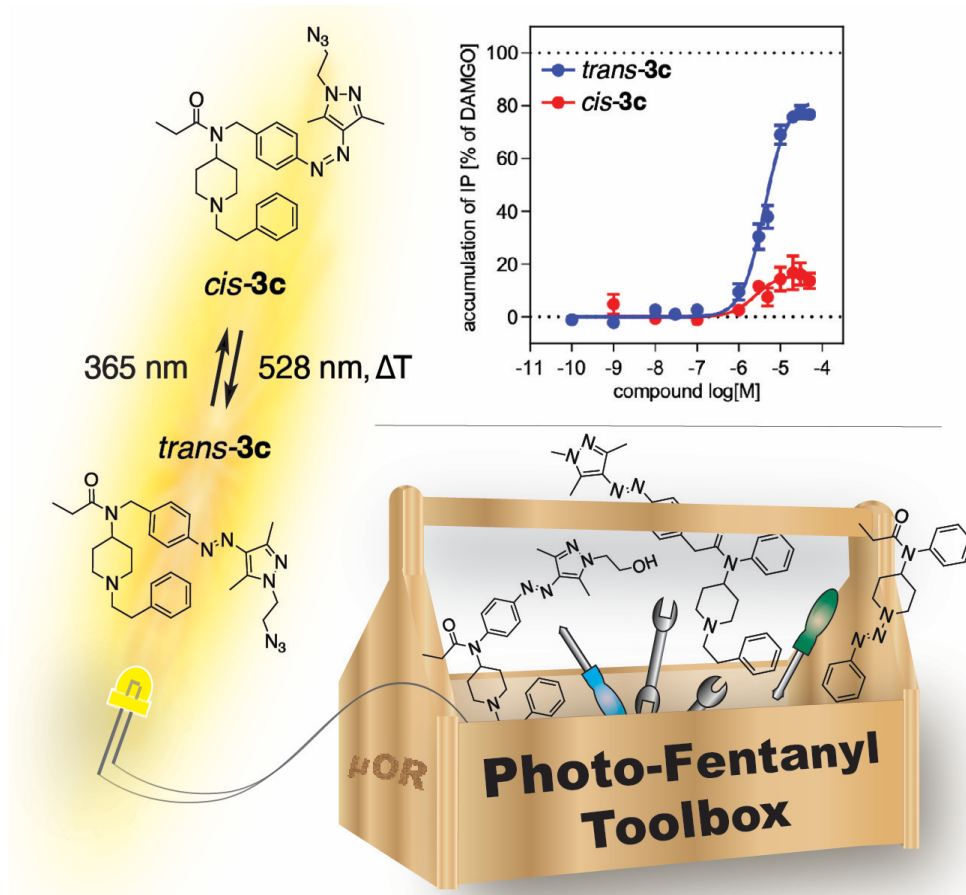
2.2.1	Photoswitchable Ligands as Novel Probes	77
2.2.2	The μ -Opioid Receptor – a GPCR	77
2.2.3	Targeting μ OR with Photoswitchable Fentanyl Ligands	77
2.2.4	Photoswitchable Tethered Fentanyl Ligands	78
2.3	Results and Discussion	80
2.3.1	Design of Fentanyl-based PTLs	80
2.3.2	Synthesis of Fentanyl-based PTLs	82
2.3.3	Photophysical Investigations of Fentanyl-based PTLs	87
2.3.4	Biochemical Evaluation of Fentanyl-based PTLs	90
2.4	Conclusion and Outlook.....	95
2.5	Acknowledgements	96
2.6	References.....	97
2.7	Supplementary Information	99
2.7.1	Supplementary Chemical Information.....	99
2.7.2	Supplementary Photophysical Information	123
2.7.3	Supplementary Biochemical Information.....	143
2.7.4	NMR Spectra	148
2.7.5	References	149
3.	Covalent and Photochromic Derivatives of the Potent Synthetic Opioid Isotonitazene and Other Nitazenes.....	151
3.1	Abstract.....	153
3.2	Introduction.....	155
3.2.1	Re-emergence of the Potent Opioid Isotonitazene	155
3.2.2	Isotonitazene Sparks Investigations into Nitazenes	155
3.2.3	Covalent and Photoswitchable Nitazenes	156
3.3	Results and Discussion	158
3.3.1	Design of Photoswitchable Nitazenes	158
3.3.2	Synthesis of Photoswitchable Nitazenes	160
3.3.3	Photophysical Investigations of Photoswitchable Nitazenes.....	163
3.3.4	Biochemical Evaluation of Photoswitchable Nitazenes	167

3.4	Conclusion and Outlook	178
3.5	Acknowledgements	179
3.6	References	180
3.7	Supplementary Information	183
3.7.1	Supplementary Chemical Information.....	183
3.7.2	Supplementary Photophysical Information	198
3.7.3	Supplementary Biochemical Information.....	221
3.7.4	Supplementary Information for 96-Well Plate LED Device.....	225
3.7.5	Supplementary Crystallographic Information.....	226
3.7.6	NMR Spectra.....	230
3.7.7	References.....	231
4.	Site Selective Insertion of Motions into ImGPS and its Influence on Enzymatic Activity	233
4.1	Abstract	235
4.2	Introduction	237
4.2.1	Dynamic Motions in Enzymes.....	237
4.2.2	Photoswitches as Tools to Create Motion	238
4.2.3	Azobenzene Phenylalanine in ImGPS.....	238
4.3	Results and Discussion	241
4.3.1	Photocontrol of ImGPS Activity with Continuous Irradiation.....	241
4.3.2	Photophysical Investigations with Pulsing Irradiation	244
4.3.3	Pulsing AzoF to Transfer Rapid Motions into ImGPS.....	247
4.3.4	Temperature Studies	253
4.3.5	Reversible Dynamic Control of ImGPS(hW123AzoF)	256
4.4	Conclusion and Outlook	258
4.5	Acknowledgements	258
4.6	References	259
4.7	Supplementary Information	261
4.7.1	Materials and Methods	261
4.7.2	Supplementary Figures and Tables.....	265

4.7.3	References	273
5.	Expanding the Repertoire of Photoswitchable Unnatural Amino Acids	275
5.1	Abstract & Introduction	277
5.2	Results and Discussion	279
5.2.1	Design of Photoswitchable Phenylalanine Derivatives	279
5.2.2	Synthesis of Photoswitchable Phenylalanine Derivatives	282
5.2.3	Photophysical Investigations	284
5.3	Conclusion and Outlook.....	287
5.4	Acknowledgements	287
5.5	References.....	288
5.6	Supplementary Information	289
5.6.1	Supplementary Chemical Information.....	289
5.6.2	Supplementary Photophysical Information	302
5.6.3	NMR Spectra	307
5.6.4	References	308
6.	Summary.....	311
7.	Appendix	315
7.1	Abbreviations.....	315
7.2	Appendix for Chapter 1.....	319
7.2.1	Analytical HPLC Chromatograms for Purity Determination	319
7.2.2	Analytical HPLC Chromatogram for PSS Determination.....	325
7.2.3	NMR Spectra	341
7.3	Appendix for Chapter 2	371
7.3.1	Analytical HPLC Chromatograms for Purity Determination	371
7.3.2	Analytical HPLC Chromatogram for PSS Determination.....	380
7.3.3	NMR Spectra	398
7.4	Appendix for Chapter 3	419
7.4.1	Analytical HPLC Chromatograms for Purity Determination	419

7.4.2	NMR Spectra.....	430
7.5	Appendix for Chapter 5.....	443
7.5.1	Analytical HPLC Chromatograms for Purity Determination	443
7.5.2	Analytical HPLC Chromatogram for PSS Determination.....	446
7.5.3	NMR Spectra.....	458
8.	Curriculum Vitae	469
9.	Acknowledgements	473

1. Photoswitchable Fentanyl Derivatives for Controlled μ -Opioid Receptor Activation



CHAPTER 1

1.1 Abstract

Photoswitchable ligands as biological tools provide an opportunity to explore the kinetics and dynamics of the clinically-relevant μ -opioid receptor. These ligands can potentially activate and deactivate the receptor when desired, using light. Spatial and temporal control of biological activity allows for application in a diverse range of biological investigations. Photoswitchable ligands have been developed in this work, modeled on the known agonist fentanyl, with the aim of expanding the current ‘toolbox’ of fentanyl photoswitchable ligands. In doing so, ligands have been developed that change geometry (isomerize) upon exposure to light, with varying photophysical and biochemical properties. This variation in properties may be valuable in further studying the functional significance of the μ -opioid receptor.

Major parts of this chapter have been published in:

R. Lahmy, H. Hübner, M. F. Schmidt, D. Lachmann, P. Gmeiner, B. König, *Chem. Eur. J.* **2022**, *28*, e202201515.

Reprinted (adapted) with permission from R. Lahmy, H. Hübner, M. F. Schmidt, D. Lachmann, P. Gmeiner, B. König, *Chem. Eur. J.* **2022**, *28*, e202201515. Copyright 2022 Wiley-VCH GmbH.

Author contributions:

RL was the first to synthesize compounds **1**, **3a**, **3c**, **6-9**, **18-20** and **24-27**, and performed the corresponding chemical and photophysical evaluations. DL was the first to synthesize compounds **2**, **3b**, **11-15**, **17** and **21-23**, and performed the corresponding chemical and photophysical evaluations. HH performed the biochemical measurements and evaluations. MS performed the molecular modeling studies and provided corresponding edits to Section 1.3.1. The manuscript was written by RL, with the biochemical section (Section 1.3.4) written by both HH and RL. BK and PG supervised the project and are the corresponding authors.

1.2 Introduction

1.2.1 Fentanyl – the Controversy

In recent years, the potent μ -opioid receptor (μ OR) agonist fentanyl has attracted significant media attention as a controversial medicine for the treatment of severe pain. Despite having advantageous analgesic properties, which is particularly useful in a clinical setting, this commercially available opioid also causes sedation and euphoria.^[1] The potency of fentanyl to induce these physiological effects has been linked to drug dependency and tolerance in clinical patients, which can ultimately lead to substance abuse with devastating consequences.^[1a, 2] As a result, there has been an increasing demand to better understand the mechanism of the μ OR and interacting opioid ligands. A better understanding of this complex system is important in the pursuit of physiologically-biased opioids that solely induce the desired analgesic response, and not the unwanted side effects.^[3]

1.2.2 Fentanyl and the μ -Opioid GPCR

The μ OR is a G-protein-coupled receptor (GPCR), containing the characteristic seven-transmembrane cellular domain with an extracellular N-terminus and a cytoplasmic C-terminus. Once agonists bind on the extracellular surface, the heterotrimeric $G_{i/o}$ protein, which is specific to this class of GPCR, dissociates into $G_{\alpha i}$ and $G_{\beta\gamma}$ subunits. This induces intracellular transduction pathways, including the inhibition of cyclic adenosine monophosphate (cAMP) production and the activation of G-protein-coupled inward-rectifying potassium (GIRK) channels, that ultimately result in various physiological responses.^[3b, 4] Current challenges in studying such GPCRs are their low expression levels in native cells, their flexibility and instability once purified from cell cultures, and their low affinity for their endogenous proteins.^[5] Advancements in technology have been pivotal for the development of numerous selective and potent ligands that can be used as probe molecules to overcome some of these issues.^[5-6] These compounds have been implemented in a diverse range of chemical, biological, microscopic and spectroscopic techniques in order to further elucidate GPCR receptor signaling pathways and their resulting cellular responses.^[6-7]

1.2.3 Photoswitchable Ligands as GPCR Probes

Over the past few decades, there has been an increasing interest in using photochemical tools for such purposes.^[8] Despite being investigated as early as 1969, photoswitchable

ligands have only recently received increasing attention and have been described as new-age powerful biological tools.^[9] Photoswitchable ligands are composed of two main components: a selective bioactive small molecule and a photoswitchable moiety that has either been incorporated into or linked to the structure of the molecule. Upon exposure to light, the photoswitchable functionality undergoes a reversible change in structure and/or properties.^[9b, 10] This change may result in a significant change in receptor affinity, thus resulting in compounds that have a biologically active and inactive state. The main advantage in developing such a photoswitchable ligand is that it could allow for spatial and temporal control of drug activity. Such examples have been documented, including those that are relevant to the GPCR field.^[11] A tool with this capability is useful to further understand receptor mechanism and signaling pathways through kinetic and dynamic studies.^[9b] For example, current limitations in the use of conventional probes are the inability to have a uniform start and stop time of receptor activation in biological and biochemical experiments.

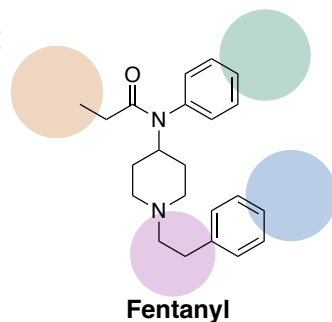
1.2.4 Photoswitchable Fentanyl Ligands

The most explored class of photoswitchable ligands that undergoes a change in geometry are the azobenzenes.^[9b] This change in geometry is a result of a *trans* to *cis* isomerization upon light exposure. Azobenzenes and their derivatives can then revert to the more stable *trans*-isomer either thermally or upon exposure with light of a different wavelength.^[12] A recent application of this was performed by Trauner *et al.*, who developed the first fentanyl azobenzene photoswitches.^[4b] Incorporating azobenzene on the terminus of the phenethyl moiety to form photofentanyl 1 (**PF1**), diminished receptor agonism, however, incorporation on the phenyl propanamide unit to obtain photofentanyl 2 (**PF2**) provided a successful candidate (Figure 1). By monitoring potassium influx through GIRK channels, it was revealed that switching **PF2** to the *trans*-isomer (irradiation with blue light) resulted in a potassium influx through the GIRK channels, while the *cis*-isomer (irradiation with 360 nm) retracted this μ OR activation.^[4b]

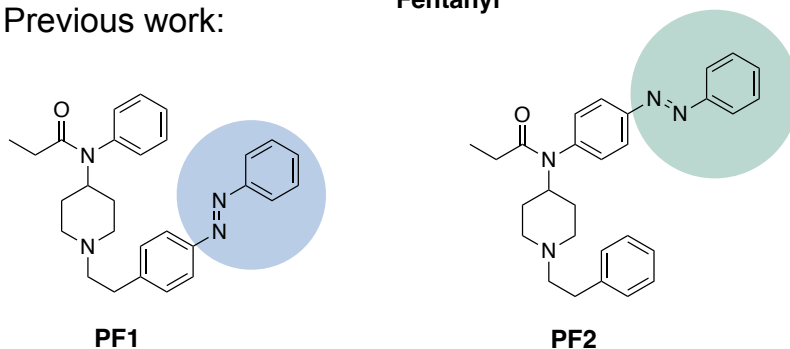
1.2.5 Expanding the Photofentanyl Toolbox

Due to the clinical significance of fentanyl, the work described herein aims to expand the repertoire of photochromic fentanyl ligands. Creating such a repertoire would provide access to a ‘toolbox’ of photochromic fentanyl ligands, with various photophysical properties and biological potencies that cater to a broader range of assays (Figure 1).

Model compound:



Previous work:



This work - expanding the toolbox:

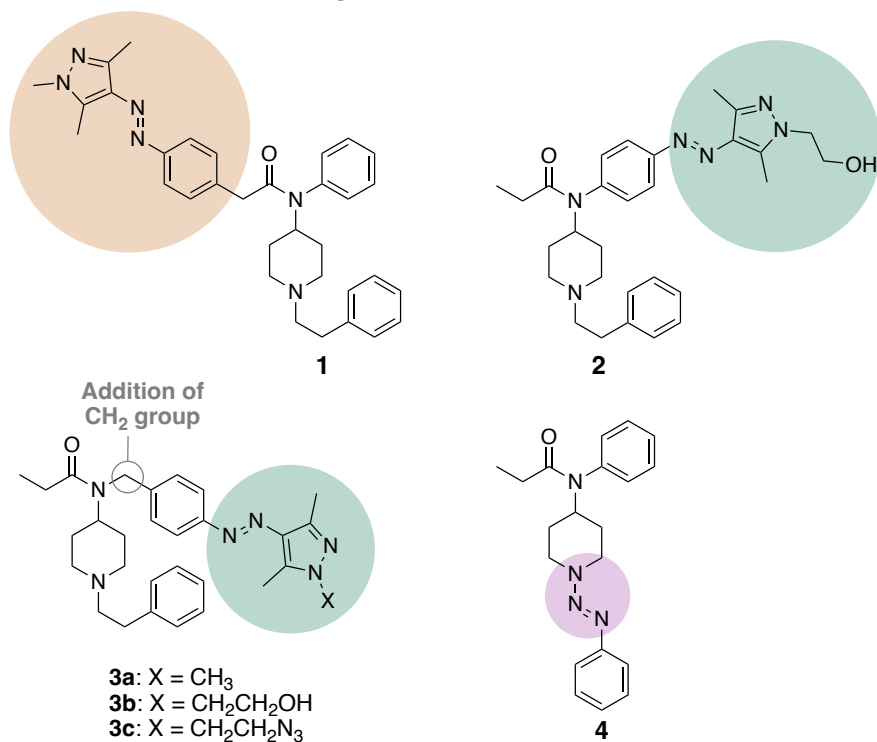


Figure 1. Structures of photoswitch-containing ligands that target the μ OR, modeled on the fentanyl pharmacophore (top). Previous work by Trauner et al.^[4b] attached the azobenzene photoswitch moiety to the pharmacophore in two positions (middle). The work herein expands the biological ‘toolbox’ of fentanyl photoswitchable ligands by attaching a reversibly switchable arylazopyrazole unit in various positions, or by incorporating triazene into the core structure of fentanyl (bottom).

1.3 Results and Discussion

1.3.1 Design of Photofentanyl Ligands

In order to obtain the next generation of photoswitchable fentanyl ligands, the azobenzene moiety was replaced with an arylazopyrazole, as the latter has been shown to provide superior photophysical properties (Figure 1).^[13] A shift of the $n\text{-}\pi^*$ transition when compared to azobenzenes, provides a red-shifted absorbance band for the *cis*-isomer of arylazopyrazole. This is ideal for biological studies as it circumvents the sole use of UV irradiation for isomerization.^[14] This shift and thus, separation between the absorbance bands of *trans*- and *cis*-isomers, also provides near quantitative switching. In addition, the substitution pattern of these arylazopyrazole-based photoswitches can be modified to tune the thermal stabilities of the *cis*-isomer to range from seconds to weeks.^[15]

Pyrazole systems exist in nature, therefore, adapting the benzene moiety from the literature reported **PF2** structure into a pyrazole that contains 2 nitrogen atoms may result in further binding interactions in the μ OR active site.^[16] For this work, the ‘4-pyrazoles’ system was chosen due to the reported long thermal half-life of the *cis*-isomer.^[15] The arylazopyrazole was attached to either the benzeneacetamide unit (compound **1**) or the phenylpropanamide unit (compound **2**) of fentanyl, as shown in (Figure 1). When the azopyrazole was directly attached to the phenylpropanamide unit, the resulting photophysical properties included a fast-thermal back-isomerization of the *cis*-isomer within seconds (described in more detail below). This may be due to the presence of a strong push-pull system, as previously described.^[13, 17] To obtain more thermally stable photochromic ligands, the compound **3** series were designed to contain an extra methylene group to insulate phenyl from the anilino nitrogen, as shown in (Figure 1). A fentanyl analogue that contains such a methylene insertion (referred to as fentanyl-CH₂) has been previously reported to maintain high binding affinity to the μ OR, as well as full agonist activity.^[18] Furthermore, in this work, molecular modeling studies were performed with fentanyl-CH₂ (Figure 2). The results indicated that a key interaction is maintained between a conserved aspartic acid residue (Asp147^{3,32}) on transmembrane helix 3 of μ OR and a charged amine on the N-piperidinyl unit of fentanyl-CH₂.^[19] This interaction has been reported to be crucial for receptor function.^[19] Interestingly, a novel μ OR-G α_{i1} cryoEM structure was reported very recently in complex with the fentanyl derivative lofentanil while this study was underway.^[20] Of particular note, the calculated binding poses of fentanyl-CH₂ are in accordance with the reported binding mode of lofentanil at the μ OR.

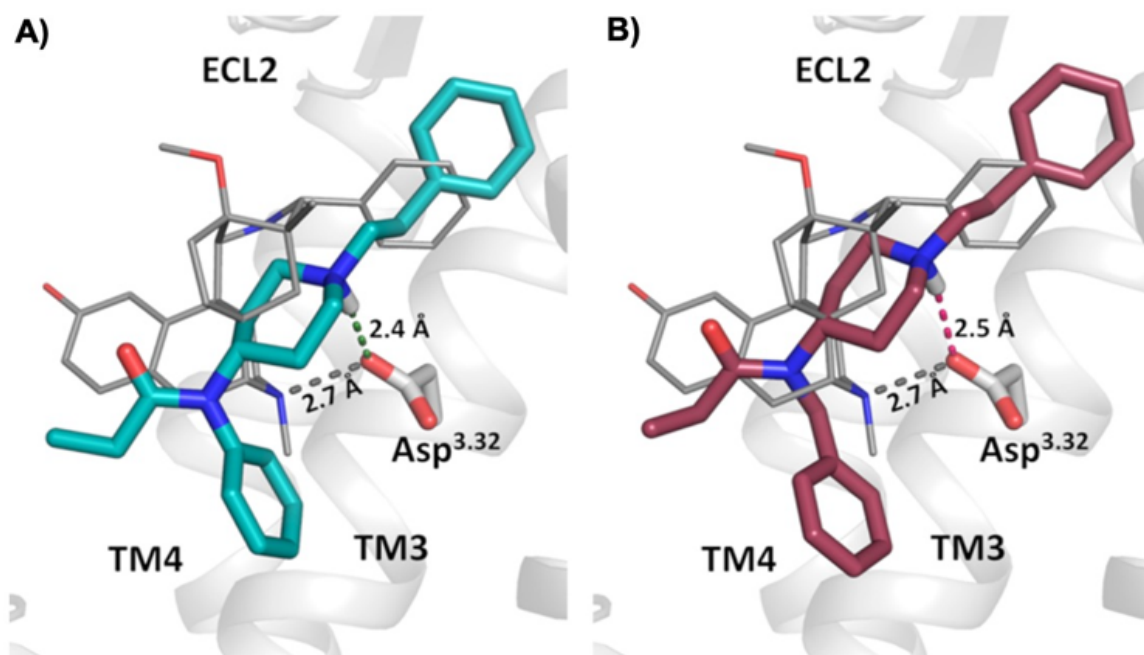
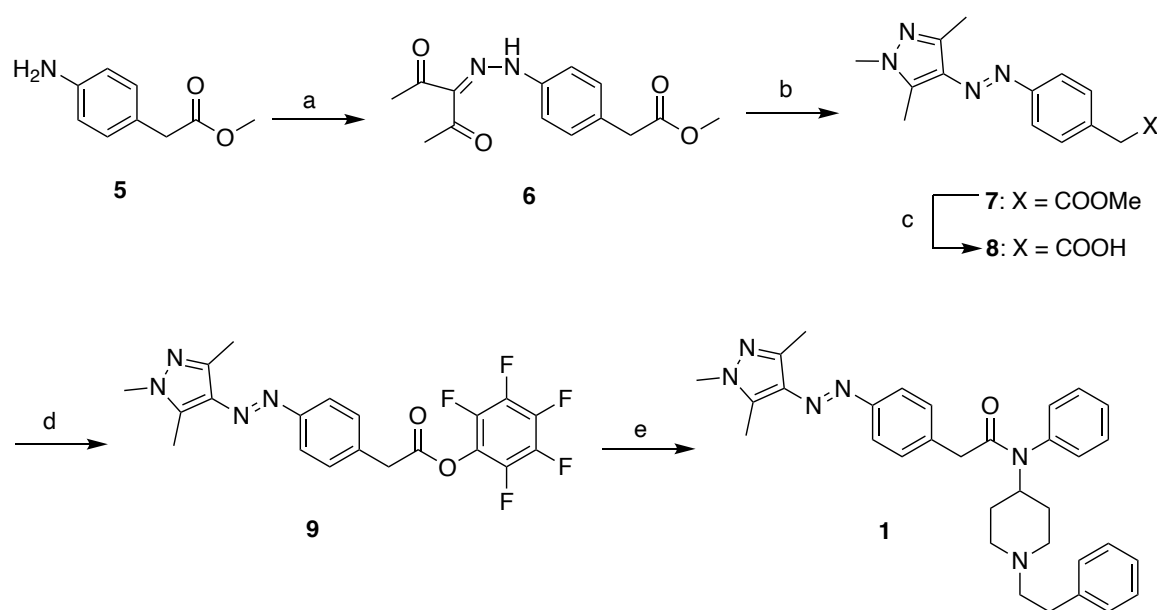


Figure 2. Modeled binding poses of fentanyl (A) and its higher homologue fentanyl-CH₂ (B) using the active-state BU72-bound μ OR-Nb39 X-ray structure (PDB-ID 5C1M).^[2] For each ligand, the best-scored poses are shown in comparison with the binding mode of BU72 in its μ OR co-crystal structure (grey sticks). As observed for BU72, both ligands form the canonical salt bridge of the protonated tertiary amine with Asp1473.32.

Compound **3a** that contains a methyl-capped pyrazole unit was selected due to reported long thermal stabilities of the *cis*-isomer.^[15] The addition of a hydroxyl group (**3b**) and an azide moiety (**3c**) was chosen to allow for differing binding interactions within the active site of μ OR. Compound **4** was designed to include a triazene unit within the structure of fentanyl. While π -conjugated triazenes have been reported to isomerize upon exposure to irradiation, linear triazenes have been found to undergo photofragmentation.^[21] Even though the latter class would be unable to reversibly isomerize, it was still of interest to incorporate such a structure into the pharmacophore due to synthetic accessibility. This class was designed to be incorporated within the core structure of fentanyl (compound **4**), and if photodegradation would indeed occur then that could involve the removal of the phenethyl moiety.^[21c-e] This phenethyl moiety has been reported to be important for binding to the μ OR, and therefore, removal of this moiety may result in diminished potency.^[19, 22] Such probes that are either irreversibly activated or deactivated using light have been explored in the field of photopharmacology.^[23]

1.3.2 Synthesis of Photofentanyl Ligands

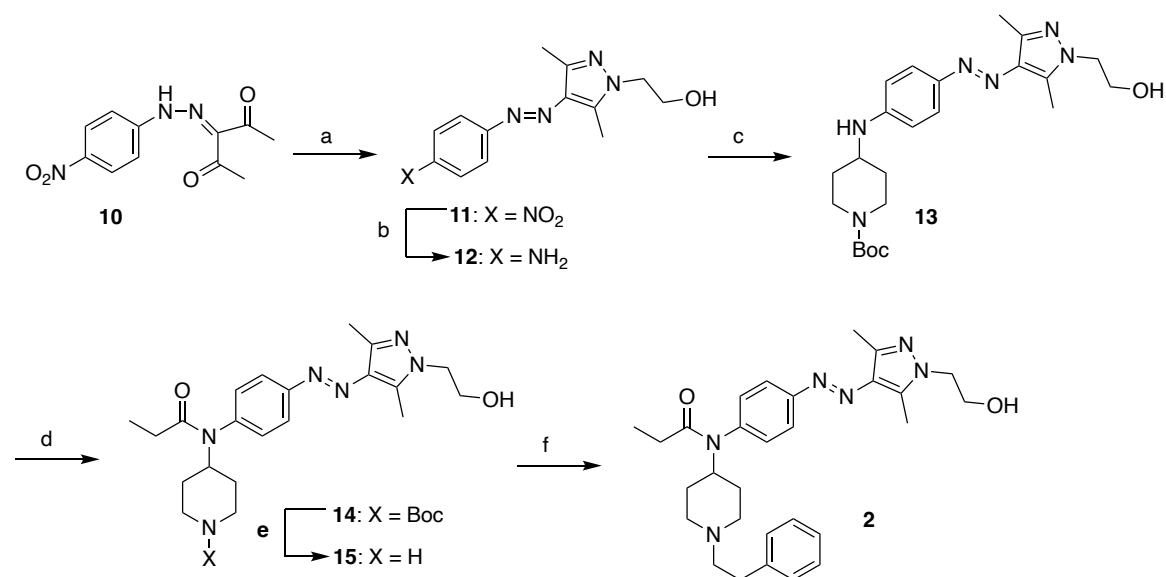
To obtain target compound **1**, commercially available starting material **5** was utilized in a diazotisation reaction to obtain diketone **6** (Scheme 1). This was followed by a condensation reaction that successfully resulted in azopyrazole **7** with 93% yield. Following treatment with lithium hydroxide to form **8**, the free acid was reacted with pentafluorophenol to form intermediate **9** in 34% yield. A coupling reaction with the previously synthesized *N*-[1-(2-phenylethyl)-4-piperidinyl]aniline resulted in target compound **1** in 8% yield.^[24]



Scheme 1. Synthesis of target compound **1**. (a) Methyl(4-aminophenyl)acetate, NaNO_2 , HCl , H_2O , AcOH , $0\text{ }^\circ\text{C}$, 45 min, then acetylacetone, NaOAc , EtOH , $0\text{ }^\circ\text{C} \rightarrow \text{rt}$, 1 h, 27%; (b) Methylhydrazine, EtOH , reflux, 3 h, 93%; (c) LiOH , $\text{THF}:\text{H}_2\text{O}$ (3:1), rt , 4 h, 85%; (d) Pentafluorophenol, EDCI , DMAP , THF , rt , 18 h, 34%; (e) *N*-[1-(2-phenylethyl)-4-piperidinyl]aniline, dry DMF , N_2 , rt , 16 h, 8%.

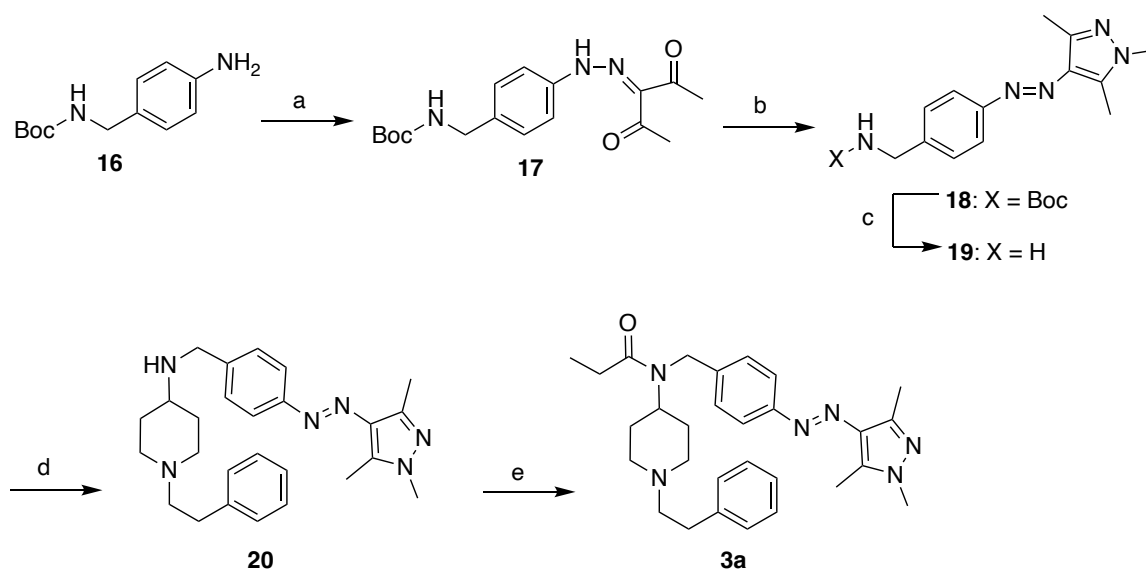
The synthesis of target compound **2** resembled a synthesis strategy used in the publication of *Trauner et al.* (Scheme 2).^[4b] A condensation reaction with previously reported diketone **10** allowed azopyrazole **11** to be obtained in 98% yield.^[25] The nitro group of intermediate **11** was then reduced to amine **12** in 67% yield. The pharmacophore moiety was then attached via reductive amination to obtain compound **13** in 77% yield. Acylation of secondary amine **13** yielded intermediate **14** in poor yield due to an unwanted diacylated product. Following Boc-deprotection under acidic conditions to obtain intermediate **15**,

reductive amination was performed with phenylacetaldehyde to obtain target compound **2** in 45% yield.



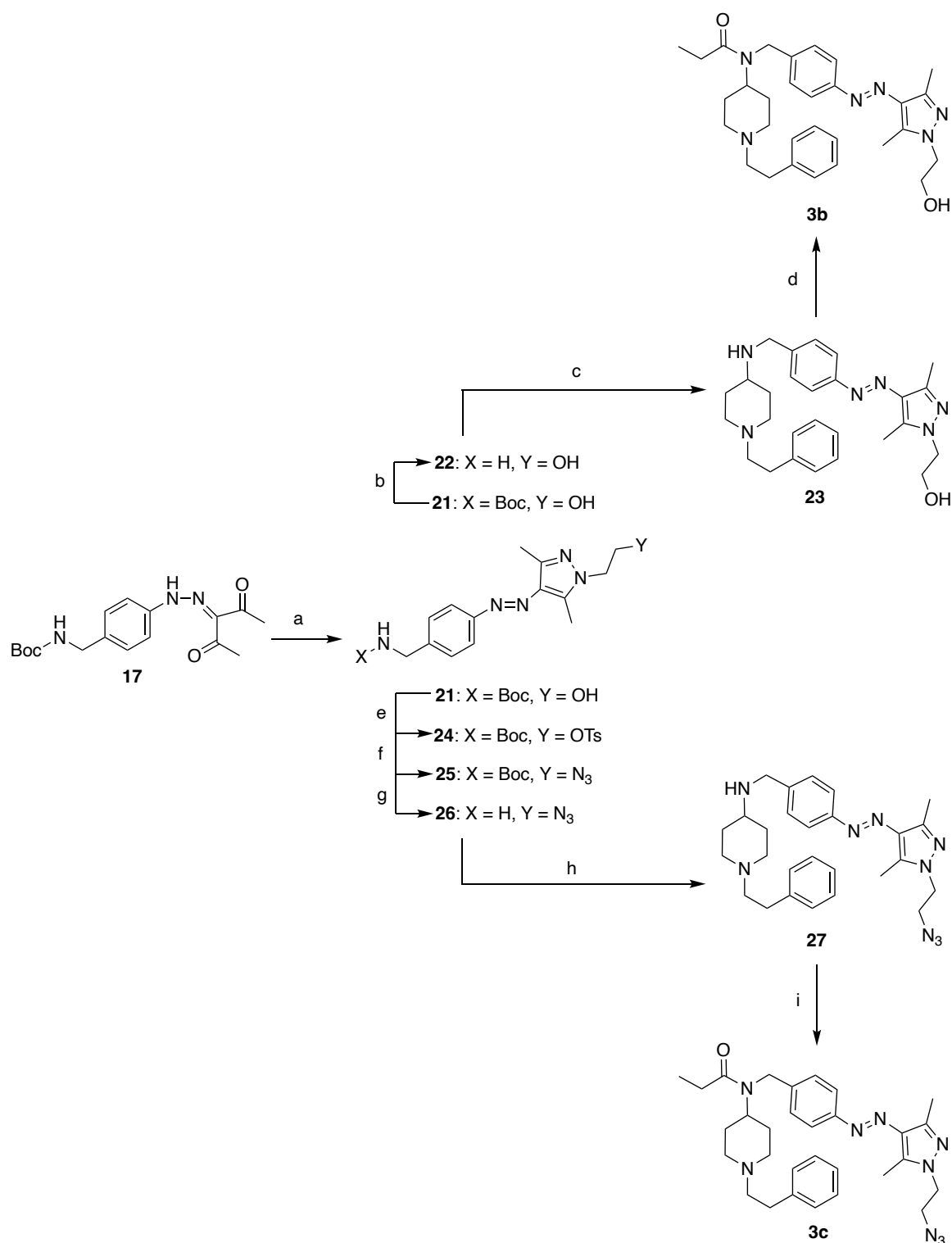
Scheme 2. Synthesis of target compound **2**. (a) 3-(2-(4-nitrophenyl)hydrazono)pentane-2,4-dione, 2-hydrazinoethanol, EtOH, reflux, 3 h, 98%; (b) Na₂S, THF/H₂O, 80 °C, 3 h, 67%; (c) 1-Boc-4-piperidone, NaBH(OAc)₃, AcOH, DCE, rt, 24 h, 77%; (d) Propionic anhydride, DMAP, dry toluene, N₂, rt, 24 h, 10%; (e) TFA, DCM, 0 °C → rt, 1 h, 77%; (f) Phenylacetaldehyde, NaBH(OAc)₃, AcOH, DCE, rt, 24 h, 45%.

The synthesis of target compound **3a** began with the commercially available 4-[(N-Boc)aminomethyl]aniline **16** that was employed in a diazotisation reaction to obtain intermediate **17** in 74% yield (Scheme 3). Intermediate **17** was utilized in a condensation reaction with commercially available methylhydrazine to obtain the azopyrazole-containing intermediate **18**. Boc-deprotection using trifluoroacetic acid then afforded amine **19** in quantitative yield. Reductive amination with 1-phenethyl-4-piperidone resulted in intermediate **20**, which was then acylated to obtain target compound **3a** in 12% yield.



Scheme 3. Synthesis of target compound **3a**. (a) 4-[(N-Boc)aminomethyl]aniline, NaNO_2 , HCl , H_2O , AcOH , $0\text{ }^\circ\text{C}$, 45 min, then acetylacetone, NaOAc , EtOH , $0\text{ }^\circ\text{C} \rightarrow \text{rt}$, 1 h, 74%; (b) Methylhydrazine, EtOH , reflux, 3 h, 97%; (c) TFA , DCM , $0\text{ }^\circ\text{C} \rightarrow \text{rt}$, 1 h, 99%; (d) 1-Phenethyl-4-piperidone, $\text{NaBH}(\text{OAc})_3$, AcOH , DCE , rt , 20 h, 34%; (e) Propionyl chloride, Et_3N , DCM , 1 h, rt , 12%.

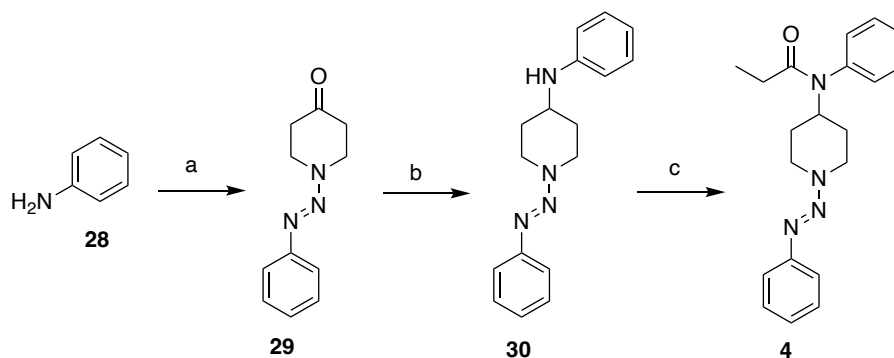
The synthesis of target compounds **3b** and **3c** involved a condensation reaction using intermediate **17** and 2-hydrazinoethanol that resulted in the azobenzene-containing compound **21** (Scheme 4). For **3b**, the Boc-containing intermediate **21** was deprotected under acidic conditions, obtaining **22** in quantitative yield. Reductive amination to form **23**, followed by N-acylation, yielded target compound **3b** in 7% yield. The synthesis of **3c** was inspired by a previously reported literature procedure^[26], where intermediate **21** was activated using p-toluenesulfonyl chloride to form **24** in 76% yield. Azide **25** was then obtained in 72% yield upon reaction with sodium azide. Boc-deprotection using trifluoroacetic acid then afforded amine **26** in quantitative yield. Reductive amination with commercially available 1-phenethyl-4-piperidone resulted in compound **27**, which was then acylated to obtain target compound **3c** in 71% yield.



Scheme 4. Synthesis of target compound **3b** and **3c**. (a) Intermediate **17**, 2-hydrazinoethanol, EtOH, reflux, 3 h, 99%; (b) TFA, DCM, 1 h, 0 °C \rightarrow rt, 95%; (c) 1-Phenethyl-4-piperidone, NaBH(OAc)₃, AcOH, DCE, 20 h, rt, 37%; (d) Propionyl chloride, Et₃N, DCM, 10 min, rt, 7%; (e) TsCl, Et₃N, DCM, 16 h, rt, 76%; (f) NaN₃, NaI, dry DMSO, N₂, 65 °C, 24 h, 72%; (g) TFA, DCM, 0 °C \rightarrow rt, 1 h, 99%; (h) 1-Phenethyl-4-piperidone, NaBH(OAc)₃, AcOH, DCE, 20 h, rt, 64%; (i) Propionyl chloride, Et₃N, DCM, rt, 1 h, 71%.

Photoswitchable Fentanyl Derivatives for Controlled μ -Opioid Receptor Activation

Synthesis of target compound **4** began with a diazotisation reaction of aniline **28** with commercially available 4-piperidone to obtain triazene **29** in 52% yield (Scheme 5). Triazene **29** has been previously obtained via an alternative synthetic route.^[27] Reductive amination with aniline resulted in precursor **30** in 31% yield. An acylation reaction allowed access to target compound **4** in 51% yield.



Scheme 5. Synthesis of target compound **4**. (a) Aniline, NaNO_2 , HCl , $\text{MeCN}/\text{H}_2\text{O}$ (2:1), 0°C , 45 min, then 4-piperidone, K_2CO_3 , rt, 1 h, 52%; (b) Aniline, $\text{NaBH}(\text{OAc})_3$, AcOH , DCE , rt, 20 h, 31%; (c) Propionyl chloride, Et_3N , DCM , rt, 1 h, 51%.

1.3.3 Photophysical Investigations of Photofentanyl Ligands

The photophysical properties of compounds **1**, **2**, **3a**, **3b**, **3c** and **4** were evaluated. This involved obtaining UV/Vis absorption spectra of thermal equilibrium, *trans*- and *cis*-isomers, as well as evaluating thermal stability of the *cis*-isomer, cycle performance and photostationary states (Table 1, Figure 3 and Supplementary Information).

Table 1. Summary of experimental photophysical properties.^[a]

Compound	Solvent	PSS	PSS	$t_{1/2}$ [days] <i>cis</i> -isomer ^[d]
		<i>cis</i> \rightarrow <i>trans</i> <i>trans:cis</i> ^[b]	<i>trans</i> \rightarrow <i>cis</i> <i>trans:cis</i> ^[b]	
1	DMSO	94:6	6:94	6.2
1	Buffer ^[c]	99:1	7:93	6.4
2	DMSO	99:1	20:80 ^[e]	26 ^[f]
3a	DMSO	95:5	7:93	5.3
3a	Buffer ^[c]	93:7	6:94	6.0
3b	DMSO	96:4	7:93	6.4
3b	Buffer ^[c]	97:3	7:93	10
3c	DMSO	94:6	4:96	8.7
3c	Buffer ^[c]	93:7	9:91	11

^[a]Isomerization was obtained by irradiation of 365 nm (*cis*-isomer) and 528 nm (*trans*-isomer) at 25 °C, except for compound **2** that required 400 nm to obtain the *cis*-isomer. ^[b]PSS was determined by HPLC measurements. ^[c]Buffer solution (TrisHCl Buffer, pH 7.5) + 0.2% or 0.5% DMSO, see Supplementary Information. ^[d]Experiment was performed at 27 °C. ^[e]Estimated PSS by UV/VIS absorption measurements with irradiation wavelength of 400 nm to obtain *cis*-isomer. ^[f]Value reported in seconds.

Compounds **1**, **3a**, **3b** and **3c** displayed similar and promising photophysical properties. When compared to the previously reported azobenzene analogue (**PF2**),^[4b] the respective *cis*-isomers of compounds **1** and series **3** displayed an increase of the $n \rightarrow \pi^*$ transition, allowing for a red-shifted wavelength of 528 nm to be utilized for isomerization back to the *trans*-isomer.

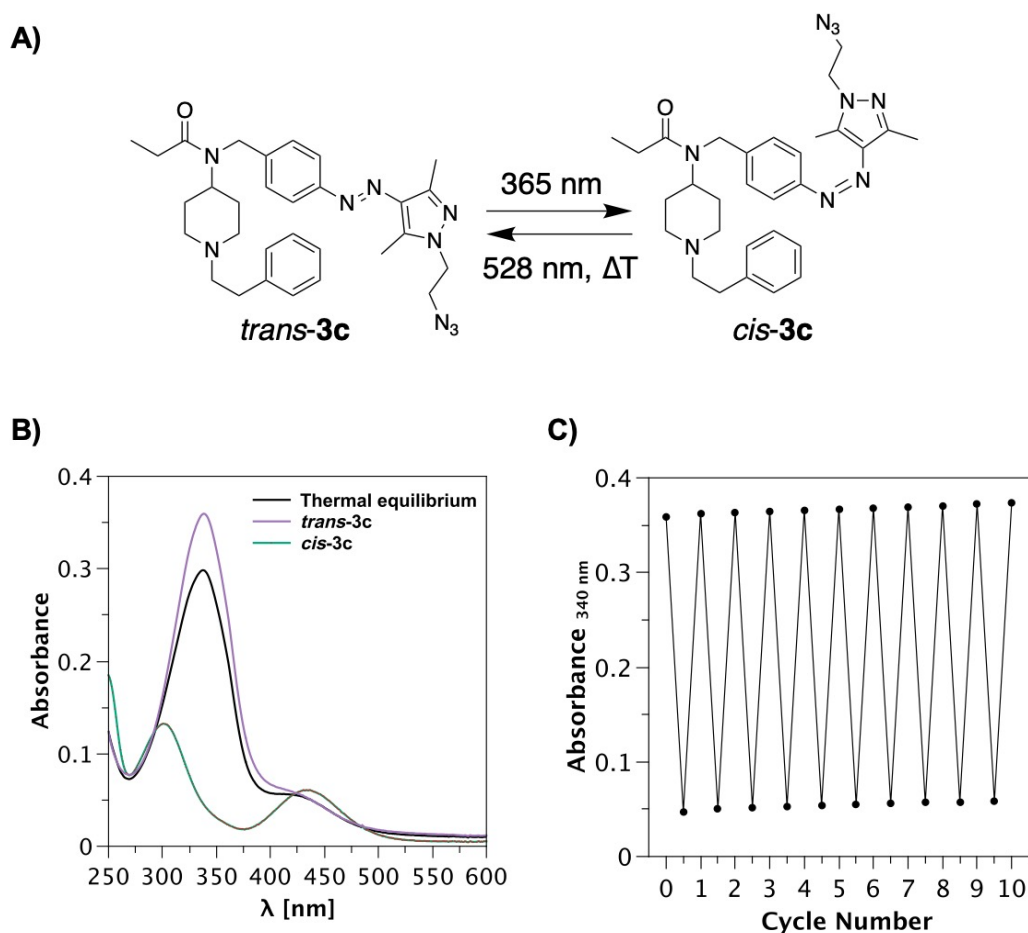


Figure 3. Light-induced isomerization and cycle performance of ligand **3c**. This ligand is shown here as a representative, as compounds **1**, **3a**, **3b** and **3c** displayed similar photophysical properties (See Supplementary Information). A) Depiction of the structural changes that ensue upon photo-induced isomerization of **3c**. B) UV/Vis absorption spectra of thermal equilibrium, *trans*-isomer and *cis*-isomer. The *cis*-isomer was accessed via irradiation with 365 nm, while the *trans*-isomer was obtained with 528 nm irradiation. C) Cycle performance of **3c** upon alternating irradiation of 365 nm and 528 nm. Data points were recorded at the absorbance maximum of the respective *trans*-isomer (340 nm). Results are shown of **3c** (20 μ M) in buffer solution (TrisHCl Buffer, pH 7.5) + 0.2% DMSO at 25 $^{\circ}$ C.

In addition, these compounds exhibited long thermal half-lives of their respective *cis*-isomer, ranging from 5 to 11 days in both DMSO and buffer solutions (Table 1). Compounds **1**, **3a**, **3b** and **3c** also exhibited resistance to cycle fatigue, as toggling between *trans*- and *cis*-isomers was achieved for at least 10 cycles (Figure 3 and Supplementary Information). Exciting the $\pi \rightarrow \pi^*$ transition of *trans*-**2** to obtain the *cis*-isomer, required a wavelength of 400 nm to be utilized. Such a red-shifted photoswitch is ideal for biological purposes and was the result of a slight bathochromic shift in absorbance. However, the resulting *cis*-isomer of compound **2** was found to be significantly less thermally stable ($t_{1/2} = 26$ seconds, Table 1). Even though a thermally non-stable ligand was outside the scope of the biological investigations described herein, such a ligand may be valuable when investigating receptor function, especially the role of dynamics. Interestingly, while compounds **1**, **2** and **3** possess an arylazopyrazole that undergoes isomerization upon exposure to light, compound **4** that possesses a triazene was found to decompose upon exposure to UV irradiation. This finding was consistent with literature and was confirmed by UV/Vis Spectroscopy and HPLC measurements (see Supplementary Information).^[21b-d]

1.3.4 Biochemical Evaluation of Photofentanyl Ligands

1.3.4.1 Radioligand Binding Studies

Lead photoswitchable compounds **1**, **3a**, **3b** and **3c**, as well as previously reported **PF2**, were subjected to radioligand binding studies to determine compound affinity for the μ OR. To obtain each of the respective isomers, each compound in solution was irradiated with their corresponding wavelength prior to biological analysis. Each isomer was then subjected to evaluation, with results shown in Table 2. Control compounds in these investigations included fentanyl and the previously reported fentanyl-CH₂.^[18b] In these studies, fentanyl displayed a binding affinity of 10 nM to the μ OR. This low nanomolar binding affinity was maintained after substitution in *para*-position of the aniline to obtain the **PF2** photoswitchable system, since *trans*-**PF2** and *cis*-**PF2** were found to have K_i values of 16 nM and 44 nM, respectively. Although the insertion of a methylene unit in fentanyl-CH₂ attenuated binding to a K_i value of 100 nM, this range of affinity was considered as a good starting point for the development of azopyrazole photoswitchable analogs. Here, it could be observed that the introduction of an azopyrazole photoswitch moiety in compounds **1**, **3a**, **3b** and **3c** led to binding affinities that range from 690 nM to 3 μ M. Compared to their respective *trans*-isomers, both methylpyrazoles *cis*-**1** and *cis*-**3a** showed approximately a two-fold higher binding affinity, with obtained values of 690 nM and 980 nM, respectively. When extending the substituent in position 1 of the pyrazole with a hydroxyethyl group, affinity slightly decreased to 3 μ M for both the isomers *trans*-**3b** and *cis*-**3b**. In contrast, replacing the methyl group of **1** by azidoethyl in **3c**, resulted in K_i values of 880 nM and 1.7 μ M for *trans*-**3c** and *cis*-**3c**, respectively. Here, *trans*-**3c** binds to μ OR with two-fold higher affinity than *cis*-**3c**.

Table 2. Radioligand binding studies.^[a]

Compound	μ OR _{wt}		
	K_i [nM \pm S.E.M.] ^[b]	K_i ratio ^[c]	(n) ^[d]
Fentanyl	10 \pm 0.15		
Fentanyl-CH ₂	100 \pm 28		5
<i>trans</i> -PF2 ^[e]	16 \pm 0.58	2.8 (<i>trans</i>)	3
<i>cis</i> -PF2	44 \pm 9.8		5
<i>trans</i> -1	1,400 \pm 260	2.0 (<i>cis</i>)	4
<i>cis</i> -1	690 \pm 93		5
<i>trans</i> -3a	1,400 \pm 260	1.4 (<i>cis</i>)	4
<i>cis</i> -3a	980 \pm 170		4
<i>trans</i> -3b	3,000 \pm 170	1.0	4
<i>cis</i> -3b	3,000 \pm 700		3
<i>trans</i> -3c	880 \pm 210	1.9 (<i>trans</i>)	4
<i>cis</i> -3c	1,700 \pm 500		5
4	960 \pm 88		6

^[a]Binding data to wild-type μ OR (μ OR_{wt}) determined by competition binding with [³H]diprenorphine; samples were pre-irradiated prior to the assay, with 365 nm for isomerization to obtain the *cis*-isomer and 528 nm for isomerization to obtain the *trans*-isomer. ^[b]Mean K_i value in [nM \pm S.E.M.]. ^[c]The isomer shown in brackets has a lower K_i value than its respective isomer. ^[d]Number of individual experiments each performed in triplicate. ^[e]Irradiation of 420 nm required for isomerization to the *trans*-isomer.

1.3.4.2 Ligand-mediated Activation Studies

As the binding profiles for compounds **1**, **3a**, **3b** and **3c** displayed moderate differences between *trans*- and *cis*-isomers, it became of interest to determine whether these photoswitches and their respective isomers show a larger difference in activating the μ OR. Therefore, ligand-mediated μ OR activation was evaluated in a G-protein activation assay (IP-One[®]), measuring the agonist-stimulated accumulation of IP in HEK293T cells that were transiently co-transfected with the receptor and the hybrid G-protein $G\alpha_{qi5HA}$.^[28] Each photoswitch-containing compound was irradiated prior to biological analysis with the appropriate wavelength to obtain either their respective *trans*- or *cis*-isomer, which were then used to determine dose-response curves in comparison to the full agonist reference DAMGO (Table 3, Figure 4 and Supplementary Information).

Fentanyl and the homologous fentanyl-CH₂ both behaved as full agonists with potencies of 2.6 nM and 77 nM, respectively. These results demonstrated that the insertion of the methylene group into fentanyl is well tolerated for receptor activation, though at reduced potency. Surprisingly, we could not determine any significant difference in activation properties between *trans*- and *cis*-**PF2** (*trans*-**PF2**: EC₅₀ = 96 nM, E_{max} = 93%; *cis*-**PF2**: EC₅₀ = 85 nM, E_{max} = 95%) (see Supplementary Information). These results are different to previously published data that describes agonist activity for *trans*-**PF2** and after irradiation, an inactive effect for *cis*-**PF2**.^[4b] This may be explained by the application of different biological assays. In contrast to monitoring the ionotropic response,^[4b] this work focused on examining the metabotropic response.

As observed for the binding affinity of the new photoswitch ligands, the addition of an azopyrazole to the aniline moiety of fentanyl-CH₂ resulted in an attenuation of activation potency for *trans/cis*-**3a,b,c** with EC₅₀ values that range from 1,600 nM (for *cis*-**3b**) to 7,900 nM (for *cis*-**3a**). These compounds displayed agonist properties with intrinsic activities, described by E_{max} values, that range from 18% (for *cis*-**3c**) to 100% (for *cis*-**3b**). Interestingly, the addition of the azopyrazole photoswitch unit to the acylamide of fentanyl-CH₂ in *trans/cis*-**1** resulted in a complete loss of intrinsic activity (Table 3 and Figure 4A). Within the series of azopyrazole-substituted anilines, the *N*-methyl derivative **3a** and the hydroxyethyl derivative **3b** displayed little to moderate differences in the activation profile between their respective *trans*- and *cis*-isomers.

Table 3. Ligand-mediated activation of the μ OR.^[a]

Compound	μ OR _{wt}				(n) ^[f]
	EC ₅₀ [nM \pm S.E.M.] ^[b]	EC ₅₀ ratio ^[c]	E _{max} [% \pm S.E.M.] ^[d]	Δ E _{max} [%] ^[e]	
DAMGO	5.0 \pm 0.62		100		7
Fentanyl	2.6 \pm 0.27		99 \pm 3		6
Fentanyl-CH ₂	77 \pm 19		102 \pm 2		6
<i>trans</i> -PF2	96 \pm 16		93 \pm 5		4
<i>cis</i> -PF2	85 \pm 43	1.1 (<i>cis</i>)	95 \pm 8	2 (<i>cis</i>)	3
<i>trans</i> -1	n/a		<5		4
<i>cis</i> -1	n/a		<5		4
<i>trans</i> -3a	2,400 \pm 350		93 \pm 2		10
<i>cis</i> -3a	7,900 \pm 690	3.3 (<i>trans</i>)	69 \pm 5	24 (<i>trans</i>)	8
<i>trans</i> -3b	2,000 \pm 440		88 \pm 5		8
<i>cis</i> -3b	1,600 \pm 510	1.3 (<i>cis</i>)	100 \pm 3	12 (<i>cis</i>)	9
<i>trans</i> -3c	4,700 \pm 510		90 \pm 2		11
<i>cis</i> -3c	2,300 \pm 550	2.0 (<i>cis</i>)	18 \pm 5	72 (<i>trans</i>)	7
4	2,400 \pm 400		106 \pm 2		8

^[a]IP-One accumulation assay (Cisbio) with HEK293T cells transiently co-transfected with the cDNAs of the human μ OR and the hybrid G-protein G α_{q15HA} . ^[b]Mean EC₅₀ values are given in [nM \pm S.E.M.]. ^[c]The isomer shown in brackets has a lower EC₅₀ value than its respective isomer. ^[d]Maximum receptor activation in [% \pm S.E.M.] relative to the full effect of DAMGO. ^[e] Δ E_{max} refers to the difference between E_{max} values. The isomer shown in brackets has a higher E_{max} value than its respective isomer. ^[f]Number of individual experiments each performed in duplicates. n/a: not applicable due to poor receptor activity.

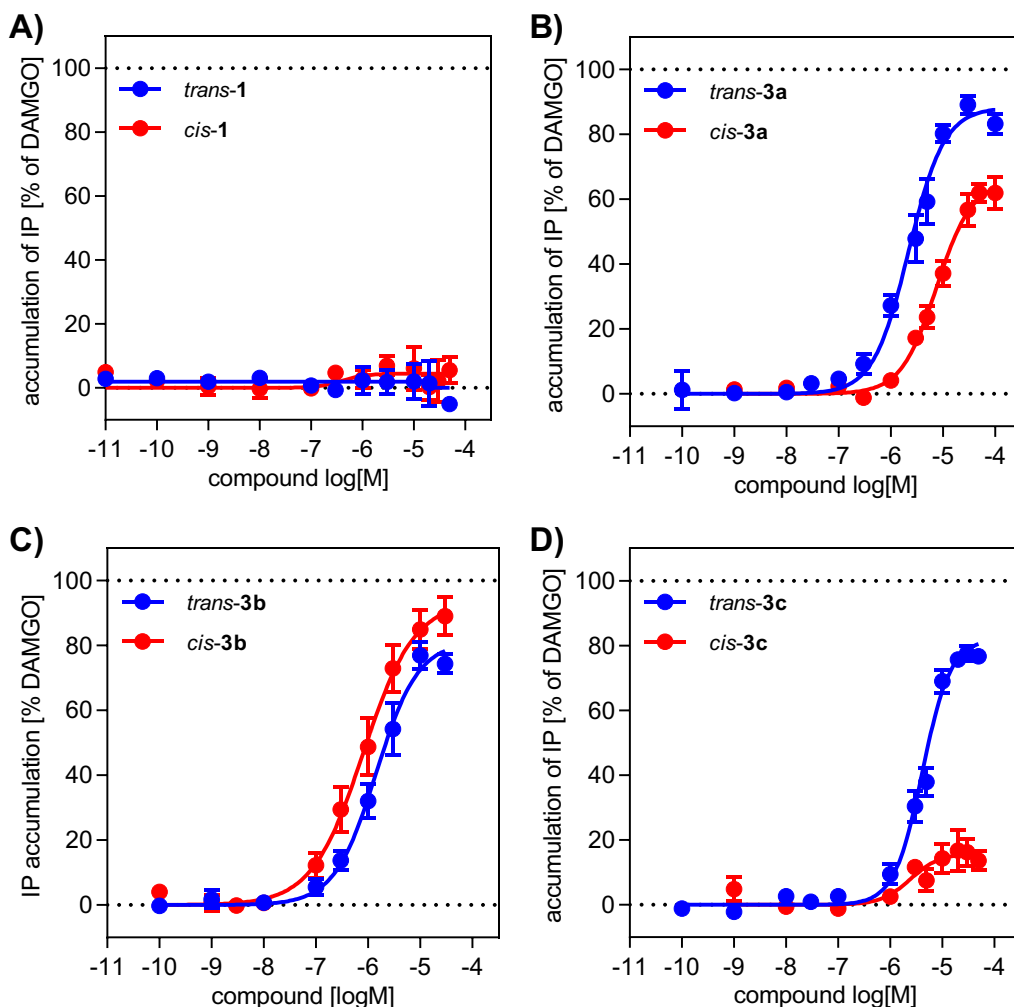


Figure 4. Activation of the μ OR by selected photoswitches. G-protein-mediated receptor activation by *trans-1*, *cis-1* (A), *trans-3a*, *cis-3a* (B), *trans-3b*, *cis-3b* (C), and *trans-3c*, *cis-3c* (D) was measured by applying the IP-One[®] accumulation assay in HEK293T cells transiently co-transfected with μ OR and the hybrid G-protein $G\alpha_{q5HA}$. While *trans-1* and *cis-1* behave as antagonists, *trans-3a,b,c* and *cis-3a,b* show strong partial agonist activity and *cis-3c* reveals only weak partial agonist activity. The great difference in activation between *trans-* and *cis-* isomers of **3c** indicates *trans/cis-3c* as a promising tool for photoswitch experiments. Graphs show mean curves (\pm S.E.M.) of 4-11 single experiments each performed in duplicate.

Compound *trans-3b* displayed a potency of 2,000 nM and an efficacy of 88%, while its respective isomer *cis-3b* activated μ OR with an EC_{50} of 1,600 nM and an E_{max} of 100%. A better difference in activity could be observed for *trans-3a* when compared to *cis-3a*, with a 3-fold higher activity found for the former isomer ($EC_{50} = 2,400$ nM, $E_{max} = 93\%$) than that found for the latter ($EC_{50} = 7,900$ nM, $E_{max} = 69\%$). Most interestingly, the azidoethyl derivative **3c** revealed substantial differences in the activation profile of both isomers. While

Photoswitchable Fentanyl Derivatives for Controlled μ -Opioid Receptor Activation

trans-**3c** acts as a strong partial agonist with an efficacy of 90% ($EC_{50} = 4,700$ nM), its isomer *cis*-**3c** only displayed weak partial agonist properties with an E_{max} value of 18% ($EC_{50} = 2,300$ nM). This clear difference in efficacy offers the opportunity to use *trans/cis*-**3c** as a photoswitch tool that allows targeted *on*- and *off*-switching of μ OR activity by irradiation.

Although compound **4** decomposes upon irradiation, we were interested in its biological properties at the μ OR. Binding affinity was determined with a K_i value of 960 nM and the potency to activate μ OR was measured showing an EC_{50} of 2,400 nM (Table 2 and Table 3). These values are about 100-fold and 1,000-fold worse than for fentanyl, which may be explained by an attenuated basicity induced by the inductive effect of the azo group.^[29]

1.3.4.3 *In Vitro* Photoisomerization

With the identification of *trans/cis-3c* as a photoswitch compound that displays different activation properties for its *trans*- and *cis*-isomers, it became of interest to determine whether this tool could also be switched during a cell incubation experiment and thereby, enable the activation and inactivation of μ OR *in situ*. To prove this, cells were incubated with 30 μ M of *trans/cis-3c* in a micro-plate format (Figure 5). Incubation of the cells was initiated by irradiation of the wells with a wavelength of 528 nm (for 180 sec) to obtain the *trans*-isomer and at 365 nm (for 20 sec) to obtain the *cis*-isomer. *In situ* photoisomerization was performed after 30 min and second messenger accumulation was continued for a total incubation time of 120 min. To be able to compare the amount of IP accumulation at the time of *in situ* switching to that after *in situ* switching, receptor activation was additionally determined after 30 min.

After 120 min, *trans-3c* and *cis-3c* activated μ OR with an efficacy of 76% and 26%, respectively (Figure 5A,B), which reflected the strong and weak partial agonist properties that were determined for both isomers in dose-response experiments (Table 3, Figure 4). A similar ratio of efficacy between these two isomers (25% for *trans-3c*, 10% for *cis-3c*) was found after 30 min. Switching *trans-3c* to *cis-3c* resulted in receptor activation of 38% (Figure 5C, red stripes). Given that *trans-3c* induces approximately 25% of second messenger (within 30 min), the additionally formed IP (13% during 90 min) indicated a complete transformation of the strong partial agonist *trans-3c* to the weakly activating *cis-3c*.

For the inverse approach, the shorter 30 min incubation with *cis-3c* and subsequent switching to *trans-3c* resulted in an efficacy of 71%. Here, the additionally accumulated IP (61% during 90 min) can clearly be explained by the fact that conversion of *cis-3c* to *trans-3c* was successfully achieved (Figure 5C, blue stripes). With compound *trans/cis-3c*, a photoswitch tool has been developed that displays very promising activation properties, which enable the control of activation states of the μ -opioid receptor *in vitro*. When switched to the *trans*-isomer, compound *trans-3c* elicits a near full agonist receptor response, and when switched to the *cis*-isomer, receptor activation is diminished. This is a significant finding since developing a 'switch on' and 'switch off' tool has been an obstacle in the field of photopharmacology so far, especially when applied to commercially accessible and cell-based assays.^[30] Switching receptor efficacy by non-invasive means, such as irradiation by light, reveals azopyrazole **3c** to be a useful tool for future mechanistic investigations of the μ OR.

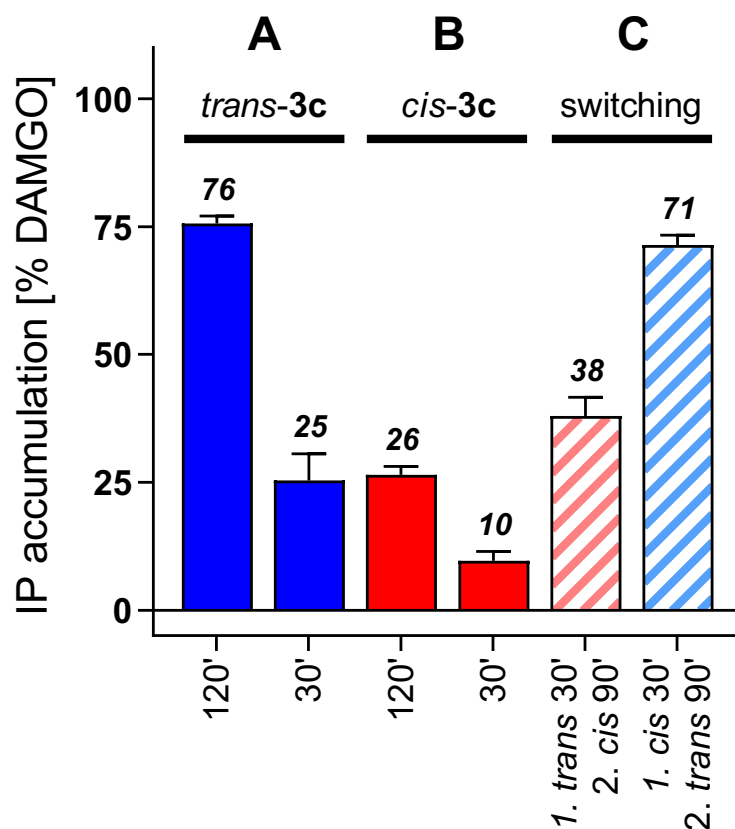


Figure 5. Photoisomerization of *trans/cis-3c* during incubation of μ OR expressing HEK293T cells determined in an IP accumulation assay. Receptor efficacy induced by 30 μ M of *trans-3c* (A) and *cis-3c* (B) after 30 or 120 min. In situ photo-induced switching of *trans-3c* to *cis-3c* (red stripes) or for *cis-3c* to *trans-3c* (blue stripes) after 30 min reveals full conversion of *trans/cis-* and *cis/trans-*isomers, resulting in differing μ OR activation (C). Incubation was initiated by irradiation with 528 nm for 180 sec for *trans-3c* (A,C) or with 365 nm for 20 sec to obtain *cis-3c* (B,C). For switching during incubation, a second irradiation step was performed after 30 min with 365 nm for 20 sec (red stripes) and 528 nm for 180 sec (blue stripes) (C). Bars represent efficacy relative to the effect of DAMGO (after 120 min) as mean values ($\% \pm$ S.E.M.) of 6-11 single experiments each done in quadruplicates.

1.4 Conclusion and Outlook

The work herein describes the generation of diverse photoresponsive fentanyl-based ligands, with differing photophysical and biochemical properties. In doing so, a ‘toolbox’ was developed that could be applied in a diverse range of biochemical investigations to better understand the μ OR. By attaching an azopyrazole photoswitch on the benzeneacetamide moiety (compound **1**), receptor activation was abolished. This may indicate that large modifications in this position of fentanyl are less tolerated.

While most of the compounds in the series displayed relatively long thermal stabilities of the *cis*-isomer, compound **2** isomerized back to the *trans*-isomer with a thermal half-life of 26 seconds. This may be beneficial for dynamic investigations that require a fast-switching ligand. However, continuous near-UV irradiation is required (400 nm), which may not be as compatible with cell-based assays.

Each of the compounds in series **3** exhibited excellent photophysical properties, with good PSS values and the ability to switch between isomers for at least 10 cycles. The lead ligand in this series was azide **3c** that displayed a significant difference between *trans*- and *cis*-isomer when comparing the maximum response of receptor activation. The *trans*-isomer of compound **3c** was able to activate the μ OR to a 90% response, while the *cis*-isomer significantly reduced the maximum activation response to 18%. This suggests compound **3c** to be a valuable tool that potently targets μ OR and displays ‘switch on’ and ‘switch off’ capabilities, which can be accessed non-invasively using light. Importantly, photo-induced switching, and the resulting biological effects of *trans/cis*-**3c** that ensue, was successfully achieved *in situ*. Furthermore, the azide moiety allows this ligand to be accessible to further bioorthogonal reactions, such as the known ‘click’ reaction, to covalently attach the ligand to the μ OR.^[31]

Compound **4** proved not to be able to reversibly switch between isomers but decomposed upon exposure to UV irradiation. This could have provided an opportunity to irreversibly deactivate ligand activity *in situ* using light, however, the incorporation of the triazene unit into the fentanyl structure diminished ligand potency towards μ OR. The combination of results described herein establishes the diverse range of photoswitchable fentanyl ligands that have been developed, which provides access to beneficial tool compounds that may aid in the pursuit of better understanding dynamic and/or kinetic mechanisms surrounding μ OR and interacting ligands.

1.5 Acknowledgements

This work was supported by the Deutsche Forschungsgemeinschaft, RTG 1910, and a Minerva PhD Fellowship to RL. We thank Prof. Kevin Burgess for ligand design inspiration.

1.6 References

- [1] a) M. J. Brownstein, *Proc. Natl. Acad. Sci. U. S. A.* **1993**, *90*, 5391-5393; b) P. W. Peng, A. N. Sandler, *Anesthesiology* **1999**, *90*, 576-599.
- [2] W. Huang, A. Manglik, A. J. Venkatakrisnan, T. Laeremans, E. N. Feinberg, A. L. Sanborn, H. E. Kato, K. E. Livingston, T. S. Thorsen, R. C. Kling, S. Granier, P. Gmeiner, S. M. Husbands, J. R. Traynor, W. I. Weis, J. Steyaert, R. O. Dror, B. K. Kobilka, *Nature* **2015**, *524*, 315-321.
- [3] a) A. Manglik, H. Lin, D. K. Aryal, J. D. McCorvy, D. Dengler, G. Corder, A. Levit, R. C. Kling, V. Bernat, H. Hübner, X. P. Huang, M. F. Sassano, P. M. Giguère, S. Löber, D. Da, G. Scherrer, B. K. Kobilka, P. Gmeiner, B. L. Roth, B. K. Shoichet, *Nature* **2016**, *537*, 185-190; b) E. A. Johnson, S. Oldfield, E. Braksator, A. Gonzalez-Cuello, D. Couch, K. J. Hall, S. J. Mundell, C. P. Bailey, E. Kelly, G. Henderson, *Mol. Pharmacol.* **2006**, *70*, 676-685.
- [4] a) K. P. Minneman, L. L. Iversen, *Nature* **1976**, *262*, 313-314; b) M. Schönberger, D. Trauner, *Angew. Chem. Int. Ed. Engl.* **2014**, *53*, 3264-3267.
- [5] a) D. M. Rosenbaum, S. G. Rasmussen, B. K. Kobilka, *Nature* **2009**, *459*, 356-363; b) D. Weichert, P. Gmeiner, *ACS Chem. Biol.* **2015**, *10*, 1376-1386.
- [6] D. Weichert, A. C. Kruse, A. Manglik, C. Hiller, C. Zhang, H. Hübner, B. K. Kobilka, P. Gmeiner, *Proc. Natl. Acad. Sci. U. S. A.* **2014**, *111*, 10744-10748.
- [7] a) A. S. Hauser, M. M. Attwood, M. Rask-Andersen, H. B. Schiöth, D. E. Gloriam, *Nat. Rev. Drug Discov.* **2017**, *16*, 829-842; b) G. W. Pasternak, Y. X. Pan, *Pharmacol. Rev.* **2013**, *65*, 1257-1317.
- [8] F. Ciruela, K. A. Jacobson, V. Fernández-Dueñas, *ACS Chem. Biol.* **2014**, *9*, 1918-1928.
- [9] a) J. Bieth, S. M. Vratsanos, N. Wassermann, B. F. Erlanger, *Proc. Natl. Acad. Sci. U. S. A.* **1969**, *64*, 1103-1106; b) W. Szymański, J. M. Beierle, H. A. Kistemaker, W. A. Velema, B. L. Feringa, *Chem. Rev.* **2013**, *113*, 6114-6178; c) W. A. Velema, W. Szymanski, B. L. Feringa, *J. Am. Chem. Soc.* **2014**, *136*, 2178-2191.
- [10] a) D. Lachmann, R. Lahmy, B. König, *Eur. J. Org. Chem.* **2019**, *2019*, 5018-5024; b) C. Petermayer, H. Dube, *Acc. Chem. Res.* **2018**, *51*, 1153-1163.
- [11] a) M. M. Lerch, M. J. Hansen, G. M. van Dam, W. Szymanski, B. L. Feringa, *Angew. Chem. Int. Ed. Engl.* **2016**, *55*, 10978-10999; b) P. Donthamsetti, N. Winter, A. Hoagland, C. Stanley, M. Visel, S. Lammel, D. Trauner, E. Isacoff, *Nat. Commun.* **2021**, *12*, 4775; c) D. Prischich, A. M. J. Gomila, S. Milla-Navarro, G. Sangüesa, R. Diez-Alarcia, B. Preda, C. Matera, M. Batlle, L. Ramírez, E. Giralt, J. Hernando, E. Guasch, J. J. Meana, P. de la Villa, P. Gorostiza, *Angew. Chem. Int. Ed. Engl.* **2021**, *60*, 3625-3631; d) J. Morstein, G. Romano, B. E. Hetzler, A. Plante, C. Haake, J. Levitz, D. Trauner, *Angew. Chem. int. Ed.* **2022**, *61*, e202117094.
- [12] J. Dokić, M. Gothe, J. Wirth, M. V. Peters, J. Schwarz, S. Hecht, P. Saalfrank, *J. Phys. Chem. A.* **2009**, *113*, 6763-6773.
- [13] C. E. Weston, R. D. Richardson, P. R. Haycock, A. J. White, M. J. Fuchter, *J. Am. Chem. Soc.* **2014**, *136*, 11878-11881.
- [14] a) L. Stricker, E.-C. Fritz, M. Peterlechner, N. L. Doltsinis, B. J. Ravoo, *J. Am. Chem. Soc.* **2016**, *138*, 4547-4554; b) A. A. Beharry, O. Sadovski, G. A. Woolley, *J. Am. Chem. Soc.* **2011**, *133*, 19684-19687.
- [15] J. Calbo, C. E. Weston, A. J. P. White, H. S. Rzepa, J. Contreras-García, M. J. Fuchter, *J. Am. Chem. Soc.* **2017**, *139*, 1261-1274.
- [16] N. E. Santos, A. R. F. Carreira, V. L. M. Silva, S. S. Braga, *Molecules* **2020**, *25*, 1364.
- [17] J. Garcia-Amorós, M. C. R. Castro, P. Coelho, M. M. M. Raposo, D. Velasco, *Chem. Commun.* **2013**, *49*, 11427-11429.

- [18] a) G. Weltrowska, N. N. Chung, C. Lemieux, J. Guo, Y. Lu, B. C. Wilkes, P. W. Schiller, *J. Med. Chem.* **2010**, *53*, 2875-2881; b) A. F. Casy, M. R. Huckstep, *J. Pharm. Pharmacol.* **1988**, *40*, 605-608.
- [19] Q. N. Vo, P. Mahinthichaichan, J. Shen, C. R. Ellis, *Nat. Commun.* **2021**, *12*, 984.
- [20] Q. Qu, W. Huang, D. Aydin, J. M. Paggi, A. B. Seven, H. Wang, S. Chakraborty, T. Che, J. F. DiBerto, M. J. Robertson, A. Inoue, B. L. Roth, S. Majumdar, R. O. Dror, B. K. Kobilka, G. Skiniotis, *bioRxiv* **2021**, 2021.2012.2007.471645.
- [21] a) S. Patil, A. Bugarin, *Eur. J. Org. Chem.* **2016**, *2016*, 860-870; b) M. Nagel, R. Hany, T. Lippert, M. Molberg, F. A. Nüesch, D. Rentsch, *Macromol. Chem. Phys.* **2007**, *208*, 277-286; c) P. Klán, T. Šolomek, C. G. Bochet, A. Blanc, R. Givens, M. Rubina, V. Popik, A. Kostikov, J. Wirz, *Chem. Rev.* **2013**, *113*, 119-191; d) D. Enders, C. Rijksen, E. Bremus-Köbberling, A. Gillner, J. Köbberling, *Tetrahedron Lett.* **2004**, *45*, 2839-2841; e) O. Nwajobi, A. K. Verma, M. Raj, *J. Am. Chem. Soc.* **2022**, *144*, 4633-4641.
- [22] P. F. J. Lipiński, P. Kosson, J. Matalińska, P. Roszkowski, Z. Czarnocki, M. Jarończyk, A. Misicka, J. C. Dobrowolski, J. Sadlej, *Molecules* **2019**, *24*, 740.
- [23] a) W. Lee, Z.-H. Li, S. Vakulenko, S. Mobashery, *J. Med. Chem.* **2000**, *43*, 128-132; b) A. V. Yadykov, A. M. Scherbakov, V. V. Trofimova, A. G. Lvov, A. I. Markosyan, I. V. Zavarzin, V. Z. Shirinian, *Org. Lett.* **2019**, *21*, 9608-9612; c) V. Arkhipova, H. Fu, M. W. H. Hoorens, G. Trinco, L. N. Lameijer, E. Marin, B. L. Feringa, G. J. Poelarends, W. Szymanski, D. J. Slotboom, A. Guskov, *J. Am. Chem. Soc.* **2021**, *143*, 1513-1520; d) A. Deiters, *ChemBioChem* **2010**, *11*, 47-53.
- [24] C. A. Valdez, R. N. Leif, B. P. Mayer, *PLoS One* **2014**, *9*, e108250.
- [25] L. Stricker, M. Böckmann, T. M. Kirse, N. L. Doltsinis, B. J. Ravoo, *Chem. Eur. J.* **2018**, *24*, 8639-8647.
- [26] D. Weichert, M. Stanek, H. Hübner, P. Gmeiner, *Bioorg. Med. Chem.* **2016**, *24*, 2641-2653.
- [27] R. Lazny, M. Sienkiewicz, S. Bräse, *Tetrahedron* **2001**, *57*, 5825-5832.
- [28] a) H. Liu, J. Hofmann, I. Fish, B. Schaake, K. Eitel, A. Bartuschat, J. Kaindl, H. Rapp, A. Banerjee, H. Hübner, M. J. Clark, S. G. Vincent, J. T. Fisher, M. R. Heinrich, K. Hirata, X. Liu, R. K. Sunahara, B. K. Shoichet, B. K. Kobilka, P. Gmeiner, *Proc. Natl. Acad. Sci. U. S. A.* **2018**, *115*, 12046-12050; b) C. Gentzsch, K. Seier, A. Drakopoulos, M.-L. Jobin, Y. Lanoiselée, Z. Koszegi, D. Maurel, R. Sounier, H. Hübner, P. Gmeiner, S. Granier, D. Calebiro, M. Decker, *Angew. Chem. Int. Ed. Engl.* **2020**, *59*, 5958-5964.
- [29] X. Creary, *J. Org. Chem.* **2022**, *87*, 2241-2254.
- [30] a) X. Gómez-Santacana, S. M. de Munnik, P. Vijayachandran, D. Da Costa Pereira, J. P. M. Bebelman, I. J. P. de Esch, H. F. Vischer, M. Wijtmans, R. Leurs, *Angew. Chem. Int. Ed. Engl.* **2018**, *57*, 11608-11612; b) M. V. Westphal, M. A. Schafroth, R. C. Sarott, M. A. Imhof, C. P. Bold, P. Leippe, A. Dhopeshwarkar, J. M. Grandner, V. Katritch, K. Mackie, D. Trauner, E. M. Carreira, J. A. Frank, *J. Am. Chem. Soc.* **2017**, *139*, 18206-18212; c) M. Wijtmans, I. Josimovic, H. F. Vischer, R. Leurs, *Curr. Opin. Pharmacol.* **2022**, *63*, 102192.
- [31] a) C. G. Parker, M. R. Pratt, *Cell* **2020**, *180*, 605-632; b) S. L. Scinto, D. A. Bilodeau, R. Hincapie, W. Lee, S. S. Nguyen, M. Xu, C. W. am Ende, M. G. Finn, K. Lang, Q. Lin, J. P. Pezacki, J. A. Prescher, M. S. Robillard, J. M. Fox, *Nat. Rev. Dis. Primers* **2021**, *1*, 30.

1.7 Supplementary Information

1.7.1 Supplementary Molecular Modeling Information

1.7.1.1 General Information

Molecular docking was conducted using GLIDE software (Schrödinger LLC). Geometries of fentanyl and fentanyl-CH₂ were prepared and energetically optimized using the LigPrep module (Schrödinger LLC). The tertiary amines were protonated, resulting in a formal charge of +1 for each ligand. The recently disclosed active-state μ OR-Nb39 X-ray structure bound to the agonist BU72 (PDB-ID 5C1M)^[1] was used as receptor and was prepared by means of the Protein Preparation Wizard module (Schrödinger LLC). Water molecules within the orthosteric binding site were kept. Amino acid side chains containing hydrogen-bond donors and acceptors were optimized for hydrogen bonding and were modelled in their dominant protonation state at pH 7. The residue Asp147^{3,32} was chosen as box center for the grid box. Molecular Docking was performed using the default settings of the obtained docking poses were inspected manually and according to the GLIDE docking score. Visualization was performed using the PyMOL Molecular Graphics System, Version 2.1.1 (Schrödinger, LLC).

1.7.2 Supplementary Chemical Information

1.7.2.1 Materials and Methods

Commercial reagents were obtained from Merck, Sigma-Aldrich, TCI Deutschland GmbH, ABCR GmbH or Fluorochem, and were used without further purification. Solvents were used in P.A. quality and if necessary, dried according to common procedures. Anhydrous reactions were performed using dried glassware under a nitrogen or argon atmosphere, unless otherwise specified. Technical grade solvents were used for column chromatography without further purification. Flash chromatography was performed using Biotage Isolera One System for normal phase chromatography, using Davisil Chromatographic Silica Media 60 Å (particle size 40-63 μ M, Merck). For reversed phase chromatography, Biotage SNAP Cartridges KP-C18-HS were used. Analytical thin layer chromatography (TLC) was performed on silica gel 60 F-254 with a 0.2 mm layer and aluminium-backed plates (Merck). Visualization was obtained by fluorescence quenching under UV light (short and long wave) and/or by staining the plate with potassium permanganate stain (60 mM KMnO_4 , 480 mM K_2CO_3 and 5% w/v NaOH) and vanillin- H_2SO_4 solution (0.5 g vanillin, 85 mL ethanol, 10 mL conc. acetic acid, 3 mL conc. H_2SO_4). Preparative high-performance liquid chromatography (HPLC) was performed using Agilent 1100 Series with a Phenomenex Luna 10 μ M C18 column (100 Å, 250 x 21.2 mm) and a solvent flow rate of 20 mL/min. Analytic HPLC measurements were performed using Agilent 1220 Infinity LC System (column: Phenomenex Luna, 3 μ M C18(2), 100 Å 150 x 2.00 mm). All biologically tested compounds possessed a purity of $\geq 95\%$, which was determined by analytical HPLC with wavelength detections of 220 nm and 254 nm. Infrared (IR) Spectroscopy was recorded using Agilent Cary 630 FTIR instrument. NMR spectra were recorded on a Bruker Avance III HD 600 (^1H 600.25 MHz, ^{13}C 150.95 MHz, T = 300K), with solvents specified. The chemical shifts were reported as δ values in parts per million (ppm), referenced to the appropriate and specified solvent peak. Resonance multiplicity is abbreviated as: 's' (singlet), 'd' (doublet), 't' (triplet), 'q' (quartet) and 'm' (multiplet). J-coupling constants (J) were recorded in Hz. Mass spectra were recorded using Finnigan MAT-SSQ 710 A, ThermoQuest Finnigan TSQ 7000, Agilent 6540 UHD Q-TOF, or a JeolAccuTOF GCX instrument.

1.7.2.2 Chemistry Synthesis Procedures

Compound **10**^[2], **PF2**^[3] and **fentanyl-CH₂**^[4] were synthesized according to literature procedures.

General Procedure 1: Diazotisation

A mixture of the respective aniline derivative (1.0 eq.), acetic acid (2 mL/mmol) and conc. HCl (0.25 mL/mmol) was allowed to stir at 0 °C. A solution of NaNO₂ (1.2 eq.) dissolved in a minimum amount of water was added dropwise to the reaction mixture. After stirring for 45 min at 0 °C, the resulting diazonium salt mixture was added to a suspension of acetylacetone (1.3 eq.) and NaOAc (3.0 eq.) in EtOH (2 mL/mmol). The reaction mixture was then stirred at room temperature for 1 h. The resulting bright yellow-orange precipitate was collected, filtered, washed with ice-cold water and hexane (1:1), and dried *in vacuo*. The desired product was obtained without further purification.

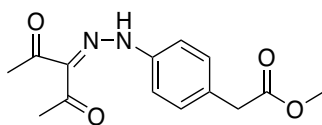
General Procedure 2: Pyrazole formation

To a stirred solution of the respective diketone (1.0 eq.) in EtOH (10 mL/mmol), 2-hydrazinoethanol (1.1 eq.) was added. The reaction mixture was allowed to reflux for 3 h. After cooling to room temperature, the solvent was removed *in vacuo*, yielding the desired product. If necessary, further purification was employed, as specified.

General Procedure 3: Deprotection of the Boc-protecting group

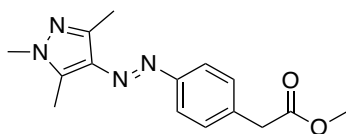
To a stirred solution of the Boc-protected amine (1.0 eq.) and DCM (10 mL/mmol), TFA (1 mL/mmol) was added dropwise at 0 °C. After 1 h of stirring at room temperature, the reaction was quenched with 2M NaOH (10 mL/mmol), followed by an extraction with DCM. The combined organic layer was dried with Na₂SO₄ and filtered. The solvent was then removed *in vacuo* to afford the desired product. If necessary, further purification was employed, as specified.

Methyl 2-(4-(2-(2,4-dioxopent-3-ylidene)hydrazineyl)phenyl)acetate (6)



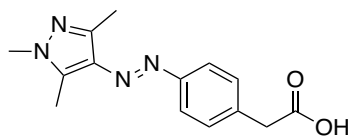
General Procedure 1 was followed, using commercially available methyl(4-aminophenyl)acetate (479 mg, 2.90 mmol) to obtain **6** as a yellow solid (198 mg, 0.717 mmol, 27%). ¹H-NMR (400 MHz, CDCl₃): δ (ppm) = 7.39-7.37 (m, 2H), 7.33-7.31 (m, 2H), 3.71 (s, 3H), 3.64 (s, 2H), 2.60 (s, 3H), 2.48 (s, 3H). ¹³C-NMR (101 MHz, CDCl₃): δ = 198.14, 197.24, 171.89, 140.81, 133.40, 131.82, 130.75, 116.60, 52.32, 40.73, 31.82, 26.78. ESI-MS (m/z): [M+H]⁺ found: 277.1188.

Methyl (*E*)-2-(4-((1,3,5-trimethyl-1*H*-pyrazol-4-yl)diazenyl) phenyl)acetate (7)



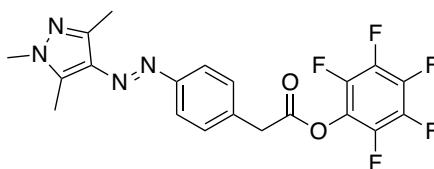
General Procedure 2 was followed, using intermediate **6** (178 mg, 0.644 mmol) and methylhydrazine (0.03 mL, 0.644 mmol, 1.0 eq.). The crude product was subjected to automated flash column chromatography, eluting at 100% DCM to 10% MeOH/DCM to obtain **7** as a yellow oil (172 mg, 0.601 mmol, 93%). ¹H-NMR (400 MHz, CDCl₃): δ (ppm) = 7.73 (d, J = 8.35 Hz, 2H), 7.36 (d, J = 8.35 Hz, 2H), 3.77 (s, 3H), 3.70 (s, 3H), 3.68 (s, 2H), 2.56 (s, 3H), 2.49 (s, 3H). ¹³C-NMR (101 MHz, CDCl₃): δ (ppm) = 171.90, 152.84, 142.55, 138.86, 135.25, 135.21, 129.96, 122.06, 52.24, 41.11, 36.09, 13.93, 10.07. ESI-MS (m/z): [M+H]⁺ found: 287.1505.

(*E*)-2-(4-((1,3,5-trimethyl-1*H*-pyrazol-4-yl)diazenyl)phenyl)acetic acid (**8**)



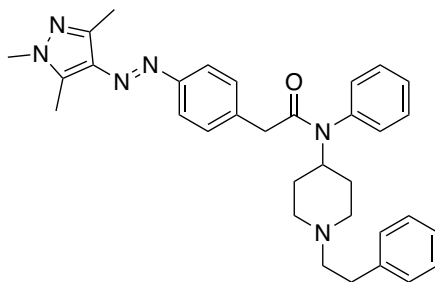
A mixture of **7** (157 mg, 0.548 mmol) and LiOH·H₂O (0.03 mL, 0.644 mmol, 1.0 eq.) in THF (7.0 mL) and water (2.3 mL) was allowed to stir at room temperature. After 18 h, 10% citric acid solution (5 mL) was added, and the resulting solution was extracted with ethyl acetate (2 x 10 mL). The combined organic layer was then washed with 10% NaHCO₃ (1 x 10 mL), followed by a wash with sat. NaCl solution (1 x 10 mL). This solution was then dried with Na₂SO₄ and concentrated *in vacuo* to obtain **8** as an orange solid (127 mg, 0.466 mmol, 85%). ¹H-NMR (400 MHz, MeOD): δ (ppm) = 7.72 (d, *J* = 8.40 Hz, 2H), 7.40 (d, *J* = 8.40 Hz, 2H), 3.78 (s, 3H), 3.67 (s, 2H), 2.59 (s, 3H), 2.45 (s, 3H). ¹³C-NMR (101 MHz, MeOD): δ = 175.22, 153.86, 143.05, 143.05, 140.99, 137.76, 135.89, 131.11, 122.78, 41.64, 36.05, 13.83, 9.75. ESI-MS (*m/z*): [*M*+H]⁺ found: 273.1349.

Perfluorophenyl-(*E*)-2-(4-((1,3,5-trimethyl-1*H*-pyrazol-4-yl)diazenyl)phenyl)acetate (**9**)



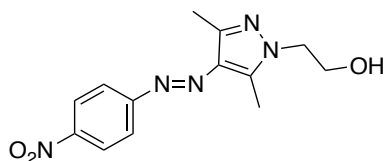
To a solution of intermediate **8** (116 mg, 0.43 mmol) in THF (5 mL), pentafluorophenol (78.4 mg, 0.43 mmol, 1 eq.), EDCI (66.1 mg, 0.84 mmol, 1.0 eq.) and DMAP (5.2 mg, 0.08 mmol, 0.1 eq.) was added. The reaction mixture was allowed to stir for 16 h at rt. The mixture was then filtered, and the resulting filtrate was then concentrated *in vacuo*. The crude product was subjected to automated flash column chromatography, eluting at 100% DCM to 10% MeOH/DCM to obtain **9** as an orange solid (63 mg, 0.144 mmol, 34%). ¹H-NMR (400 MHz, CDCl₃): δ (ppm) = 7.79 (d, *J* = 8.36 Hz, 2H), 7.45 (d, *J* = 8.35 Hz, 2H), 4.02 (s, 2H), 3.79 (s, 3H), 2.58 (s, 3H), 2.50 (s, 3H). ¹³C-NMR (101 MHz, CDCl₃): δ = 167.40, 153.24, 142.67, 139.13, 135.27, 133.10, 129.99, 122.38, 40.11, 36.09, 13.92, 10.11. ESI-MS (*m/z*): [*M*+H]⁺ found: 439.1195.

(*E*)-*N*-(1-phenethylpiperidin-4-yl)-*N*-phenyl-2-(4-((1,3,5-trimethyl-1*H*-pyrazol-4-yl)diazenyl) phenyl)acetamide (**1**)



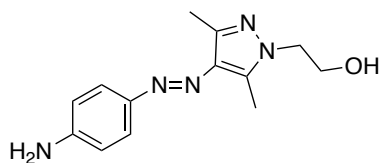
A solution of pentafluorophenyl ester **9** (50 mg, 0.11 mmol), *N*-[1-(2-phenylethyl)-4-piperidinyl]aniline^[5] (32 mg, 0.11 mmol, 1.0 eq.) and Et₃N (0.05 mL, 0.34 mmol, 3.0 eq.) in DMF (3 mL) was stirred at room temperature. After 16 h, the solvent was removed under reduced pressure and the crude product was subjected to automated flash column chromatography, eluting at 100% DCM to 10% MeOH/DCM. The product was further purified by preparative HPLC (solvent A: H₂O [0.05 Vol% TFA], solvent B: MeCN; gradient A/B: 0-20 min: 90/10 to 2/98, 20-25 min: 2/98), eluting at 40% MeCN, to obtain target compound **1** as an orange solid (4.6 mg, 0.009 mmol, 8%). ¹H-NMR (400 MHz, MeOD): δ (ppm) = 7.65 (d, *J* = 8.36 Hz, 2H), 7.52-7.51 (m, 3H), 7.34-7.20 (m, 7H), 7.11 (d, *J* = 8.35 Hz, 2H), 3.78 (s, 3H), 3.68-3.65 (m, 2H), 3.46 (s, 2H), 3.29-3.26 (m, 2H), 3.22-3.16 (m, 2H), 3.00-2.96 (m, 2H), 2.59 (s, 3H), 2.44 (s, 3H), 2.19-2.16 (m, 2H), 1.76-1.65 (m, 2H). ¹³C-NMR (101 MHz, MeOD): δ = 173.04, 153.78, 143.03, 141.01, 138.00, 135.89, 131.70, 130.96, 130.76, 130.51, 130.01, 129.72, 128.35, 122.73, 58.94, 53.32, 51.62, 42.58, 36.07, 31.41, 28.96, 13.82, 9.73. HR-ESI-MS (*m/z*): [*M*+H]⁺ calculated: 535.3117; found: 535.3190.

(E)-2-(3,5-dimethyl-4-((4-nitrophenyl)diazenyl)-1H-pyrazol-1-yl)-ethan-1-ol (**11**)



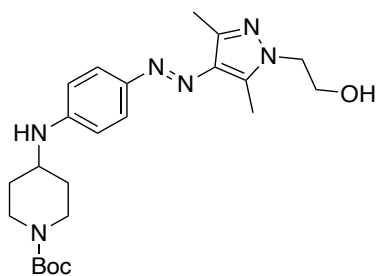
General Procedure 2 was followed, using compound previously synthesized compound **10**^[2] to obtain **11** as an orange solid (98%). ¹H-NMR (400 MHz, CDCl₃): δ = 8.32 (d, J = 9.1 Hz, 2H), 7.87 (d, J = 9.0 Hz, 2H), 4.18 (t, J = 4.8 Hz, 2H), 4.07 (t, J = 4.8 Hz, 2H), 2.64 (s, 3H), 2.51 (s, 3H). ¹³C-NMR (101 MHz, CDCl₃): δ = 157.17, 147.79, 143.38, 141.61, 135.80, 124.83, 122.47, 61.47, 50.56, 14.32, 10.08. ESI-MS (m/z): [M+H]⁺ found: 290.1257.

(E)-2-(4-((4-aminophenyl)diazenyl)-3,5-dimethyl-1H-pyrazol-1-yl)ethan-1-ol (**12**)



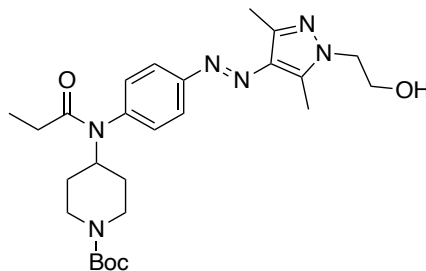
Intermediate **11** (1.0 g, 3.5 mmol, 1.0 eq.) was dissolved in a solvent mixture of THF/H₂O (3:1, 60 mL), and Na₂S (1.0 g, 12.8 mmol, 3.4 eq.) was then added. The resulting mixture was stirred at reflux for 4 h. Afterwards, the reaction mixture was cooled to room temperature and the organic solvent was removed *in vacuo*. Aqueous 1 M NaOH and EtOAc were then added and after separation of the aqueous layer, the organic layer was extracted with sat. NaHCO₃ solution (1 x 50 mL) and sat. NaCl solution (1 x 50 mL). The organic layer was dried with Na₂SO₄, filtered and the solvent removed *in vacuo*. The crude product was subjected to automated flash column chromatography, eluting at 100% DCM (0.1% Et₃N) to 20% MeOH/DCM (0.1% Et₃N) to obtain compound **12** (0.6 g, 2.31 mmol, 67%) as an orange solid. ¹H-NMR (400 MHz, DMSO-D₆): δ = 7.49 (d, J = 8.7 Hz, 2H), 6.62 (d, J = 8.8 Hz, 2H), 4.04 (t, J = 5.6 Hz, 2H), 3.71 (q, J = 5.5 Hz, 2H), 2.51 (s, 3H), 2.34 (s, 3H). ¹³C-NMR (101 MHz, DMSO-D₆): δ = 150.83, 143.80, 139.89, 138.01, 133.79, 123.22, 113.40, 60.06, 50.91, 13.92, 9.47. ESI-MS (m/z): [M+H]⁺ found: 260.1533.

tert-butyl (*E*)-4-((4-((1-(2-hydroxyethyl)-3,5-dimethyl-1*H*-pyrazol-4-yl)diazenyl)phenyl)amino) piperidine-1-carboxylate (**13**)



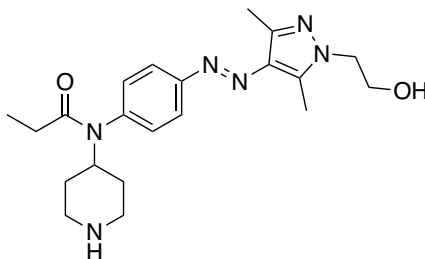
A solution of intermediate **12** (0.7 g, 2.7 mmol, 1.05 eq.), commercially available 1-boc-4-piperidone (0.5 g, 2.6 mmol, 1.0 eq.) and AcOH (169 μ L, 2.7 mmol, 1.0 eq.) in dichloroethane (50 mL) was stirred at room temperature. Afterwards, $\text{NaBH}(\text{OAc})_3$ (0.8 g, 3.5 mmol, 1.0 eq.) was slowly added over 15 mins, and the mixture was then stirred at room temperature for 24 h. The reaction mixture was diluted with EtOAc and the organic layer was extracted with 1 M NaOH (2 x 50 mL), sat. NaHCO_3 solution (1 x 50 mL) and sat. NaCl solution (1 x 50 mL). The organic layer was dried with Na_2SO_4 , filtered and the solvent removed *in vacuo*. The crude product was subjected to automated flash column chromatography, eluting at 100% DCM (0.1% Et_3N) to 10% MeOH/DCM (0.1% Et_3N) to obtain compound **13** as a yellow solid (0.8 g, 0.2 mmol, 77%). $^1\text{H-NMR}$ (400 MHz, DMSO-D_6): δ = 7.54 (d, J = 8.9 Hz, 2H), 6.67 (d, J = 8.9 Hz, 2H), 4.04 (t, J = 5.6 Hz, 2H), 3.90-3.87 (m, 2H), 3.71 (t, J = 5.6 Hz, 2H), 3.01-2.84 (m, 2H), 2.51 (s, 3H), 2.34 (s, 3H), 1.91-1.88 (m, 2H), 1.41 (s, 9H), 1.30-1.22 (m, 2H). $^{13}\text{C-NMR}$ (101 MHz, DMSO-D_6): δ = 153.95, 149.28, 143.75, 139.91, 138.05, 133.84, 123.28, 112.01, 78.62, 60.06, 50.92, 48.60, 28.10, 13.93, 9.49. ESI-MS (m/z): $[M+H]^+$ found: 443.2784.

tert-butyl (*E*)-4-(*N*-(4-((1-(2-hydroxyethyl)-3,5-dimethyl-1*H*-pyrazol-4-yl)diazenyl)phenyl)propionamido)piperidine-1-carboxylate (**14**)



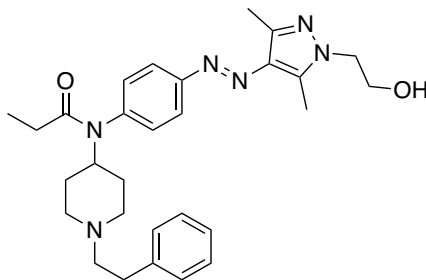
Compound **13** (1.1g, 2.5 mmol, 1.0 eq.) was dissolved in anhydrous toluene (35 mL) under argon atmosphere. DMAP (0.62 g, 5.1 mmol, 2.0 eq), propionic anhydride (0.65 mL, 5.1 mmol, 2 eq.) and Et₃N (1.8 mL, 12.7 mmol, 5.0 eq.) were added and the mixture was stirred at room temperature for 16 h. The solvent was removed *in vacuo*, and the crude product was subjected to automated flash column chromatography, eluting at 100% PE to 90% EtOAc /PE to obtain **14** as a slightly yellow-coloured oil (0.1 g, 0.31 mmol, 10%). ¹H-NMR (400 MHz, CDCl₃): δ = 7.66 (d, J = 7.9 Hz, 2H), 6.61 (d, J = 7.8 Hz, 2H), 4.41 (t, J = 5.3 Hz, 2H), 4.26 (t, J = 5.3 Hz, 2H), 3.95-4.09 (m, 2H), 3.51-3.46 (m, 1H), 2.93 (t, J = 11.9 Hz, 2H), 2.54 (s, 3H), 2.46 (s, 3H), 2.32-2.26 (m, 2H), 2.08-2.03 (m, 2H), 1.45 (s, 9H), 1.39-1.31 (m, 2H), 1.10-1.06 (m, 3H). ¹³C-NMR (101 MHz, CDCl₃): δ = 174.13, 154.85, 148.29, 145.68, 142.74, 137.92, 134.90, 123.81, 112.84, 79.80, 77.48, 77.16, 76.84, 62.88, 50.12, 47.49, 32.30, 28.50, 27.44, 13.87, 9.86, 9.02. ESI-MS (m/z): [M+H]⁺ found: 499.3028.

(*E*)-*N*-(4-((1-(2-hydroxyethyl)-3,5-dimethyl-1*H*-pyrazol-4-yl)diazenyl)phenyl)-*N*-(piperidin-4-yl) propionamide (**15**)



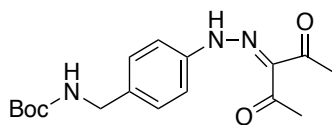
Intermediate **14** (196 mg, 0.39 mmol, 1 eq.) was dissolved in a solvent mixture of DCM/THF (1:1). Afterwards, 4N HCl in dioxane (5 mL) was added and the mixture was stirred at room temperature for 1.5 h. The solvent was removed *in vacuo* and the crude product was then purified by reverse phase column chromatography (solvent A: H₂O [0.05 Vol% TFA], solvent B: MeCN; gradient A/B: 0-20 min: 90/10 to 2/98, 20-25 min: 2/98). After lyophilization, compound **15** was obtained as a white solid (120 mg, 0.3 mmol, 77%). ¹H-NMR (400 MHz, DMSO-D₆): δ = 7.56 (d, *J* = 8.8 Hz, 2H), 6.71 (d, *J* = 8.8 Hz, 2H), 4.36-4.33 (m, 2H), 4.29-4.26 (m, 2H), 3.66-3.60 (m, 1H), 3.33-3.30 (m, 2H), 3.06-2.98 (m, 2H), 2.51 (s, 3H), 2.34 (s, 3H), 2.28 (q, *J* = 7.5 Hz, 2H), 2.08-2.05 (m, 2H), 1.64-1.56 (m, 2H), 0.98 (t, *J* = 7.5 Hz, 3H). ¹³C-NMR (101 MHz, DMSO-D₆): δ = 173.32, 149.10, 143.82, 140.33, 137.88, 133.93, 123.33, 111.99, 62.31, 47.14, 46.19, 42.07, 28.31, 26.67, 13.86, 9.26, 8.84. ESI-MS (*m/z*): [*M*+H]⁺ found: 399.2517.

(*E*)-*N*-(4-((1-(2-hydroxyethyl)-3,5-dimethyl-1*H*-pyrazol-4-yl)diazenyl)phenyl)-*N*-(1-phenethyl piperidin-4-yl)propionamide (**2**)



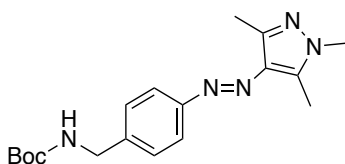
Compound **15** (1.6 g, 4.0 mmol, 1.0 eq.) was dissolved in dichloroethane (100 mL) and stirred at room temperature. Phenylacetaldehyde (0.72 g, 6.0 mmol, 1.5 eq.) and $\text{NaBH}(\text{OAc})_3$ (7.7 g, 36 mmol, 6.0 eq.) were added and the mixture was stirred under argon atmosphere for 16 h. The reaction mixture was diluted with EtOAc and the organic mixture was extracted with 1 M NaOH (1 x 100 mL), sat. NaHCO_3 (1 x 100 mL) and sat. NaCl solution (1 x 100 mL). The organic layer was dried with Na_2SO_4 , filtered and the solvent was removed *in vacuo*. The crude product was purified automated flash column chromatography, eluting at 100% DCM to 8% MeOH/DCM to afford target compound **2** as an orange solid (0.9 g, 1.8 mmol, 45%). $^1\text{H-NMR}$ (400 MHz, MeOD): δ = 7.62 (d, J = 8.8 Hz, 2H), 7.28-7.24 (m, 2H), 7.19-7.17 (m, 3H), 6.66 (d, J = 8.9 Hz, 2H), 4.39 (t, J = 5.2 Hz, 2H), 4.27 (t, J = 5.2 Hz, 2H), 3.38-3.33 (m, 1H), 3.00-2.97 (m, 2H), 2.81-2.77 (m, 2H), 2.61-2.57 (m, 2H), 2.54 (s, 3H), 2.42 (s, 3H), 2.28 (q, J = 7.6, 2H), 2.24-2.21 (m, 2H), 2.05-2.02 (m, 2H), 1.59-1.50 (m, 2H), 1.04 (t, J = 7.6, 3H). $^{13}\text{C-NMR}$ (101 MHz, MeOD): δ = 175.50, 151.19, 146.02, 143.22, 141.19, 139.47, 135.73, 129.66, 129.50, 127.19, 124.82, 113.42, 63.70, 61.59, 53.37, 50.45, 48.43, 34.18, 32.64, 28.07, 13.95, 9.86, 9.30. HR-ESI-MS (m/z): $[M+H]^+$ calculated: 503.3129; found: 503.3134.

***tert*-Butyl (4-(2-(2,4-dioxopentan-3-ylidene)hydrazineyl)benzyl)carbamate (17)**



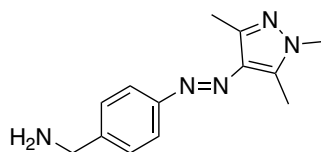
General Procedure 1 was followed, using commercially available 4-[(N-Boc)-aminomethyl]aniline **16** (1.00 g, 4.50 mmol) to obtain **17** as a yellow solid (1.11 g, 3.33 mmol, 74%). $^1\text{H-NMR}$ (400 MHz, CDCl_3): δ = 7.38-7.30 (m, 4H), 4.30 (br s, 2H), 2.59 (s, 3H), 2.48 (s, 3H), 1.46 (s, 9H). $^{13}\text{C-NMR}$ (101 MHz, CDCl_3): δ = 198.09, 197.21, 156.01, 140.89, 137.01, 133.36, 128.90, 116.56, 79.83, 44.28, 31.79, 28.53, 26.76. ESI-MS (m/z): $[M+H]^+$ found: 334.18.

***tert*-butyl (*E*)-(4-((1,3,5-trimethyl-1*H*-pyrazol-4-yl)diazenyl)benzyl)carbamate (18)**



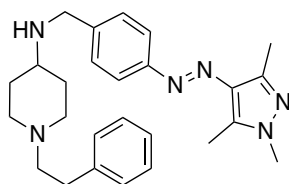
General Procedure 2 was followed, using intermediate **17** (520 mg, 1.56 mmol) and methylhydrazine (82 μL , 1.56 mmol, 1.0 eq.) to obtain **18** as a yellow solid (520 mg, 1.51 mmol, 97%). $^1\text{H-NMR}$ (400 MHz, CDCl_3): δ (ppm) = 7.74 (d, J = 8.30 Hz, 2H), 7.36 (d, J = 8.21 Hz, 2H), 4.36 (br s, 2H), 3.78 (s, 3H), 2.57 (s, 3H), 2.49 (s, 3H), 1.47 (s, 9H). $^{13}\text{C-NMR}$ (101 MHz, CDCl_3): δ = 155.91, 152.95, 142.45, 140.13, 138.73, 135.12, 127.99, 121.99, 120.62, 77.23, 44.44, 28.42, 13.81, 9.98. ESI-MS (m/z): $[M+H]^+$ found: 344.2087.

(E)-4-((1,3,5-trimethyl-1H-pyrazol-4-yl)diazenyl)phenylmethanamine (19)



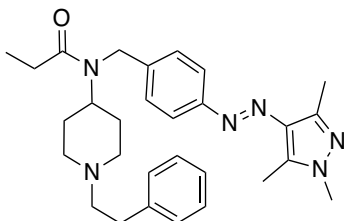
General Procedure 3 was followed, using intermediate **18** (510 mg, 1.49 mmol) to obtain **19** as an orange oil (358 mg, 1.47 mmol, 99%). $^1\text{H-NMR}$ (400 MHz, MeOD): δ (ppm) = 7.82 (d, J = 8.42 Hz, 2H), 7.57 (d, J = 8.42 Hz, 2H), 4.18 (s, 2H), 3.78 (s, 3H), 2.60 (s, 3H), 2.45 (s, 3H). $^{13}\text{C-NMR}$ (101 MHz, MeOD): δ = 155.21, 143.16, 141.56, 136.01, 135.56, 130.85, 123.30, 119.68, 116.76, 43.96, 36.12, 13.89, 9.76. ESI-MS (m/z): $[M+H]^+$ found: 244.1557.

(E)-1-phenethyl-N-(4-((1,3,5-trimethyl-1H-pyrazol-4-yl)diazenyl)benzyl)piperidin-4-amine (20)



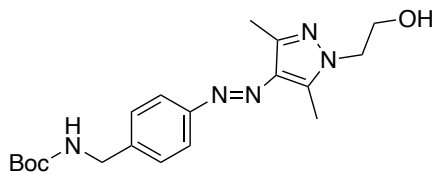
To a solution of 1-phenethyl-4-piperidone (298 mg, 1.47 mmol, 1.05 eq.) in DCE (30 mL), was added sequentially to intermediate **19** (340 mg, 1.40 mmol), $\text{NaBH}(\text{OAc})_3$ (415 mg, 2.88 mmol, 1.4 eq.) and AcOH (0.08 mL, 1.40 mmol, 1.0 eq.). The bright orange reaction mixture was allowed to stir overnight at room temperature. After 15 h, the reaction mixture was diluted with EtOAc (2 x 10 mL), washed with 1M NaOH (1x 5 mL), sat. NaHCO_3 (1 x 5 mL), sat. aqueous NaCl (1 x 10 mL). The combined organic layers were dried (Na_2SO_4), filtered and concentrated *in vacuo*. The crude product was subjected to automated flash column chromatography, eluting at 100% DCM (0.01% Et_3N) to 20% DCM/MeOH (0.01% Et_3N) to obtain **20** as an orange oil (205 mg, 0.48 mmol, 34%). $^1\text{H-NMR}$ (400 MHz, CDCl_3): δ (ppm) = 7.76-7.73 (m, 3H), 7.44-7.39 (m, 3H), 7.31-7.27 (m, 1H), 7.23-7.16 (m, 2H), 3.93 (s, 2H), 3.88 (s, 1H), 3.77- 3.74 (m, 5H), 3.17-3.14 (m, 1H), 2.87-2.81 (m, 4H), 2.57 (s, 3H), 2.55 (s, 1H), 2.49-2.48 (m, 5H), 2.08-2.05 (m, 1H), 1.72-1.69 (m, 2H). $^{13}\text{C-NMR}$ (101 MHz, MeOD): 155.20, 143.16, 141.55, 135.46, 131.78, 130.84, 129.92, 129.79, 128.76, 123.35, 123.32, 122.84, 73.49, 51.87, 44.50, 43.99, 36.13, 36.06, 31.81, 13.89, 13.84, 9.77. ESI-MS (m/z): $[M+H]^+$ found: 431.2918.

(*E*)-*N*-(1-phenethylpiperidin-4-yl)-*N*-(4-((1,3,5-trimethyl-1*H*-pyrazol-4-yl)diazenyl)benzyl) propionamide (**3a**)



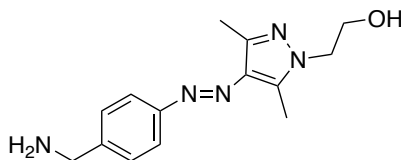
To a solution of intermediate **20** (180 mg, 0.42 mmol) in dry DCM (6 mL), triethylamine (0.11 mL, 0.84 mmol, 2.0 eq.) was added, followed by propionyl chloride (0.73 mL, 0.84 mmol, 2.0 eq.). The reaction mixture was allowed to stir for 24 h under N_2 atmosphere. Water (5 mL) was then added, and the organic phase was extracted with DCM (2 x 5 mL). The pooled organic phase was washed with sat. $NaHCO_3$ (1 x 5 mL) and sat. aqueous $NaCl$ (1 x 5 mL). The organic phase was then dried over Na_2SO_4 and concentrated. The crude residue was subjected to automated flash column chromatography, eluting at 100% DCM to 10% MeOH/DCM. The product was further purified by preparative HPLC (solvent A: H_2O [0.05 Vol% TFA], solvent B: MeCN; gradient A/B: 0-20 min: 90/10 to 2/98, 20-25 min: 2/98), eluting at 65% MeCN, to obtain **3a** as an orange oil (21 mg, 0.04 mmol, 12%). 1H -NMR (400 MHz, MeOD): δ (ppm) = 7.80-7.69 (m, 2H), 7.41-7.23 (m, 7H), 4.69 (s, 2H), 4.54-4.27 (m, 1H), 3.77 (s, 3H), 3.68-3.65 (m, 2H), 3.29-3.27 (m, 2H), 3.15-3.00 (m, 4H), 2.70-2.64 (m, 1H), 2.58 (s, 3H), 2.46-2.41 (m, 4H), 2.22-2.09 (m, 2H), 1.98-1.94 (m, 2H), 1.25-1.11 (m, 3H). ^{13}C -NMR (101 MHz, MeOD): δ = 177.34, 154.39, 143.05, 141.19, 140.62, 137.46, 135.94, 129.98, 129.75, 128.44, 128.31, 127.93, 123.27, 122.89, 59.00, 53.47, 53.19, 52.35, 36.08, 31.42, 29.24, 28.25, 27.91, 27.59, 13.85, 9.82, 9.75. HR-ESI-MS (m/z): $[M+H]^+$ calculated: 487.3117; found: 487.3190.

tert-butyl(*E*)-4-((1-(2-hydroxyethyl)-3,5-dimethyl-1*H*-pyrazol-4-yl)diazenyl)benzyl)carbamate (**21**)



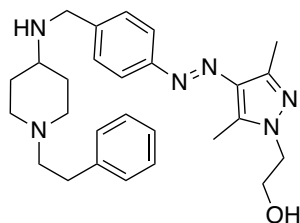
General procedure 2 was followed, using intermediate **17** (1.13 g, 3.39 mmol) to obtain intermediate **21** as a yellow solid (1.30 g, 3.48 mmol, 99%). ¹H-NMR (400 MHz, CDCl₃): δ = 7.72 (d, *J* = 8.6 Hz, 2H), 7.34 (d, *J* = 8.6 Hz, 2H), 4.35-4.33 (m, 2H), 4.15-4.10 (m, 2H), 4.05-4.00 (m, 2H), 2.58 (s, 3H), 2.47 (s, 3H), 1.46 (s, 9H). ¹³C-NMR (101 MHz, CDCl₃): 155.96, 152.80, 142.67, 140.37, 139.63, 134.89, 127.96, 122.04, 116.44, 79.65, 61.37, 50.27, 44.39, 28.42, 13.96, 9.85. δ = [M+H]⁺ found: 374.2240.

(*E*)-2-(4-((4-(aminomethyl)phenyl)diazenyl)-3,5-dimethyl-1*H*-pyrazol-1-yl)ethan-1-ol (**22**)



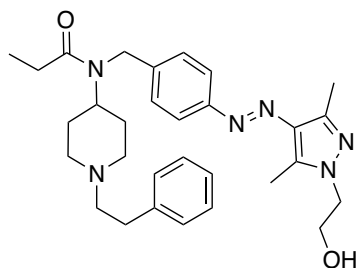
General Procedure 3 was followed, using intermediate **21** to obtain compound **22** as yellow crystals (95%). ¹H-NMR (400 MHz, CDCl₃): δ = 7.70 (d, *J* = 8.4 Hz, 2H), 7.32 (d, *J* = 8.6 Hz, 2H), 4.11 (t, *J* = 4.8 Hz, 2H), 3.99 (t, *J* = 4.9 Hz, 2H), 3.84 (s, 2H), 2.58 (s, 3H), 2.46 (s, 3H). ¹³C-NMR (101 MHz, CDCl₃): δ = 152.62, 144.39, 142.71, 139.77, 134.96, 127.62, 122.08, 61.24, 50.65, 46.16, 14.14, 9.96. ESI-MS (*m/z*): [M+H]⁺ found: 274.15.

(*E*)-2-(3,5-dimethyl-4-((4-(((1-phenethylpiperidin-4-yl)amino)methyl)phenyl)diazenyl)-1*H*-pyrazol-1-yl)ethan-1-ol (**23**)



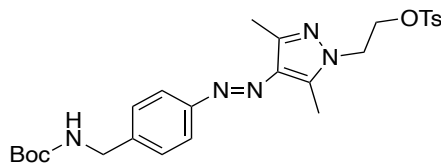
Intermediate **22** (600 mg, 1.61 mmol, 1.0 eq.), 1-phenethyl-4-piperidone (444 mg, 1.61 mmol, 1.0 eq.) and AcOH (0.13 mL, 1.61 mmol, 1.0 eq.) was dissolved in dichloroethane (80 mL). To this reaction mixture, NaBH(OAc)₃ (651 mg, 3.07 mmol, 1.9 eq.) was slowly added over 15 mins. The mixture was stirred at room temperature for 24 h. The reaction mixture was diluted with EtOAc (120 mL) and the organic layer was extracted with 1 M NaOH (100 mL), sat. aqueous NaHCO₃ solution (100 mL) and sat. aqueous NaCl solution (100 mL). The organic layer was dried with Na₂SO₄, filtered and the solvent was removed *in vacuo*. The crude product was subjected to automated flash column chromatography, eluting at 100% DCM (0.01% Et₃N) to 20% DCM/MeOH (0.01% Et₃N) to obtain intermediate **23** as a yellow solid (270 mg, 0.59 mmol, 37%). ¹H-NMR (400 MHz, CDCl₃): δ = 7.74 (d, J = 8.3 Hz, 2H), 7.40 (d, J = 8.3 Hz, 2H), 7.30-7.27 (m, 2H), 7.20-7.19 (m, 3H), 4.13 (t, J = 4.8 Hz, 2H), 4.02 (t, J = 4.9 Hz, 2H), 3.86 (s, 2H), 2.98-2.95 (m, 2H), 2.82-2.78 (m, 3H), 2.60 (s, 3H), 2.59-2.55 (m, 2H), 2.50 (s, 3H), 2.09-2.04 (m, 2H), 1.94-1.91 (m, 2H), 1.52-1.42 (m, 2H). ¹³C-NMR (101 MHz, CDCl₃): δ = 152.74, 142.81, 142.23, 140.53, 139.60, 135.03, 128.78, 128.64, 128.46, 126.09, 121.95, 61.34, 60.70, 54.11, 52.53, 50.49, 33.87, 32.74, 14.12, 9.97. ESI-MS (m/z): [M+H]⁺ found: 461.3032.

(*E*)-*N*-(4-((1-(2-hydroxyethyl)-3,5-dimethyl-1*H*-pyrazol-4-yl)diazenyl)benzyl)-*N*-(1-phenethyl piperidin-4-yl)propionamide (**3b**)



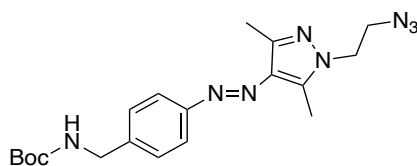
Intermediate **23** (270 mg, 0.587 mmol, 1.0 eq.), DMAP (86.0 mg, 0.704 mmol, 1.2 eq.), propionic anhydride (90 μ L, 0.704 mmol, 1.2 eq.) and DIPEA (0.5 mL, 2.93 mmol, 5 eq.) were dissolved in DCM (10 mL) and stirred at room temperature for 24 h. The solvent was removed *in vacuo* and the crude product was subjected to automated flash column chromatography, eluting at 100% DCM to 15% MeOH/DCM. The product was further purified by preparative HPLC (solvent A: H₂O [0.05 Vol% TFA], solvent B: MeCN; gradient A/B: 0-20 min: 10/98, 20-25 min: 2/98; t_R = 10 min). The resulting compound was dissolved in MeOH/H₂O (9:1, 10 mL) and then KOH (164 mg, 2.93 mmol, 5.0 eq.) was added. The mixture was stirred for 16 h and then acidified with 2M HCl and extracted with DCM (3 x 50 mL). The combined organic layers were dried with Na₂SO₄, filtered and the solvent was removed *in vacuo*. The product was purified by preparative HPLC (solvent A: H₂O [0.05 Vol% TFA], solvent B: MeCN; gradient A/B: 0-20 min: 90/10 to 2/98, 20-25 min: 2/98), eluting at 70% MeCN, to obtain target compound **3b** as a yellow residue (20 mg, 0.038 mmol, 7%). ¹H-NMR (400 MHz, CDCl₃): δ = 7.72 (d, J = 8.4 Hz, 2H), 7.30-7.27 (m, 2H), 7.25-7.19 (m, 5H), 4.89 (br s, 1H), 4.64 (s, 2H), 4.14 (t, J = 4.8 Hz, 2H), 4.03 (t, J = 4.8 Hz, 2H), 3.60-3.58 (m, 2H), 3.15 (br s, 4H), 2.78-2.75 (m, 2H), 2.58 (s, 3H), 2.51-2.42 (m, 5H), 2.35-2.28 (m, 2H), 2.80-1.77 (m, 2H), 1.14-1.09 (m, 3H). ¹³C-NMR (101 MHz, CDCl₃): δ = 175.37, 153.02, 142.90, 139.87, 136.07, 135.07, 129.11, 128.78, 127.44, 126.36, 122.39, 61.51, 58.65, 52.77, 50.47, 48.91, 46.36, 30.59, 27.37, 27.16, 26.42, 14.13, 9.99, 9.58. HR-ESI-MS (m/z): [$M+H$]⁺ calculated: 517.3286; found: 517.3292.

(*E*)-2-(4-((4-(((*tert*-butoxycarbonyl)amino)methyl)phenyl)diazenyl)-3,5-dimethyl-1*H*-pyrazol-1-yl)ethyl 4-methylbenzenesulfonate (**24**)



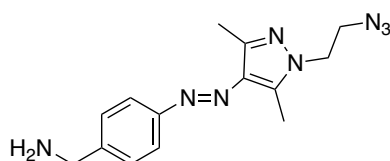
To a solution of intermediate **21** (1.30 g, 3.48 mmol) in DCM (80 mL), Et₃N (1.46 mL, 10.4 mmol, 3.0 eq.) was added, followed by the dropwise addition of *p*-toluenesulfonyl chloride (0.73 g, 3.83 mmol, 1.1 eq.) at room temperature. After 16 h of stirring, water was added (60 mL), and the mixture was extracted with DCM (2 x 40 mL). The combined organic layers were dried (Na₂SO₄), filtered and concentrated *in vacuo*. The crude residue was subjected to automated flash column chromatography, eluting at 100% DCM to 20% MeOH/DCM to obtain **24** as yellow crystals (1.40 mg, 2.65 mmol, 76%). ¹H-NMR (400 MHz, CDCl₃): δ = 7.75 (d, *J* = 8.29 Hz, 2H), 7.59 (d, *J* = 8.29 Hz, 2H), 7.39 (d, *J* = 8.13 Hz, 2H), 7.18 (d, *J* = 8.17 Hz, 2H), 4.43 (t, *J* = 4.94 Hz, 2H), 4.39-4.37 (m, 2H), 4.27 (t, *J* = 4.92 Hz, 2H), 2.54 (s, 3H), 2.35 (s, 3H), 2.34 (s, 3H), 1.48 (s, 9H). ¹³C-NMR (101 MHz, CDCl₃): δ = 156.04, 152.83, 145.18, 142.79, 140.68, 134.92, 132.22, 129.98, 128.16, 127.86, 122.45, 122.24, 77.36, 68.37, 47.70, 28.55, 21.78, 13.86, 9.89. ESI-MS (*m/z*): [*M*+H]⁺ found: 528.23.

***tert*-butyl (*E*)-(4-((1-(2-azidoethyl)-3,5-dimethyl-1*H*-pyrazol-4-yl)diazenyl)benzyl) carbamate (**25**)**



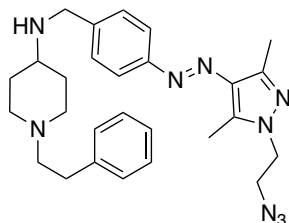
Compound **24** (1.30 g, 2.46 mmol) was dissolved in anhydrous DMSO (55 mL). Afterwards, NaN_3 (641 mg, 9.86 mmol, 4.0 eq.) and NaI (369 mg, 2.46 mmol, 1.0 eq.) were added and the reaction mixture was heated to 65 °C for 24 h under N_2 atmosphere. The reaction was allowed to cool to room temperature, water (50 mL) was added, and the mixture was extracted with DCM (2 x 30 mL). The combined organic layers were dried (Na_2SO_4), filtered and concentrated *in vacuo*. The crude residue was subjected to automated flash column chromatography, eluting at 100% DCM to 20% MeOH/DCM to obtain **25** as a yellow oil (714 mg, 1.79 mmol, 72%). $^1\text{H-NMR}$ (400 MHz, CDCl_3): δ = 7.74 (d, J = 8.33 Hz, 2H), 7.36 (d, J = 8.09 Hz, 2H), 4.36-4.35 (m, 2H), 4.17 (t, J = 5.68 Hz, 2H), 3.77 (t, J = 5.68 Hz, 2H), 2.62 (s, 3H), 2.50 (s, 3H), 1.46 (s, 9H). $^{13}\text{C-NMR}$ (101 MHz, CDCl_3): δ = 156.04, 152.94, 143.30, 140.09, 135.21, 128.09, 122.19, 116.55, 77.37, 50.79, 47.84, 44.53, 28.53, 14.13, 9.94. ESI-MS (m/z): $[M+H]^+$ found: 399.2260.

***E*-(4-((1-(2-azidoethyl)-3,5-dimethyl-1*H*-pyrazol-4-yl)diazenyl)phenyl)methanamine (**26**)**



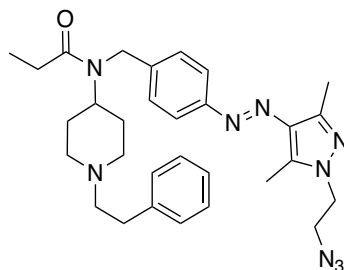
General Procedure 3 was followed, using intermediate **25** (704 mg, 1.79 mmol) to obtain compound **26** as an orange oil (675 mg, 2.26 mmol, 99%). $^1\text{H-NMR}$ (400 MHz, CDCl_3): δ = 7.76 (d, J = 8.32 Hz, 2H), 7.40 (d, J = 8.24 Hz, 2H), 4.16 (t, J = 5.67 Hz, 2H), 3.93 (s, 2H), 3.77 (t, J = 5.67 Hz, 2H), 2.62 (s, 3H), 2.51 (s, 3H), 1.81 (s, 2H). $^{13}\text{C-NMR}$ (101 MHz, CDCl_3): δ = 152.61, 144.40, 143.28, 139.76, 135.15, 127.66, 122.05, 50.70, 47.74, 46.16, 14.10, 9.82. ESI-MS (m/z): $[M+H]^+$ found: 299.17.

(*E*)-*N*-(4-((1-(2-azidoethyl)-3,5-dimethyl-1*H*-pyrazol-4-yl)diazenyl)benzyl)-1-phenethylpiperidin-4-amine (**27**)



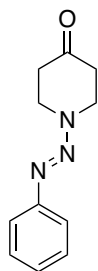
To a solution of 1-phenethylpiperidin-4-one (465 mg, 2.29 mmol, 1.05 eq.) in DCE (10 mL), was added sequentially to **26** (650 mg, 2.18 mmol), NaBH(OAc)₃ (646 mg, 3.05 mmol, 1.4 eq.) and AcOH (0.12 mL, 2.18 mmol, 1.0 eq.). The bright orange reaction mixture was allowed to stir overnight at room temperature. After 15 h, the reaction mixture was diluted with EtOAc (2 x 10 mL), washed with 1M NaOH (1x 5 mL), sat. NaHCO₃ (1 x 5 mL), sat. NaCl solution (1 x 10 mL). The combined organic layers were dried with Na₂SO₄, filtered and concentrated *in vacuo*. The crude residue was subjected to automated flash column chromatography, eluting at 100% DCM to 10% MeOH/DCM to obtain **27** as an orange oil (680 mg, 1.40 mmol, 64%). ¹H-NMR (400 MHz, CDCl₃): δ = 7.75 (d, *J* = 8.3 Hz, 2H), 7.43 (d, *J* = 8.3 Hz, 2H), 7.30-7.27 (m, 2H), 7.21-7.18 (m, 3H), 4.17 (t, *J* = 5.7 Hz, 2H), 3.89 (s, 2H), 3.77 (t, *J* = 5.7 Hz, 2H), 3.10-3.07 (m, 2H), 2.89-2.2.85 (m, 2H), 2.72-2.68 (m, 2H), 2.62 (s, 3H), 2.51 (s, 3H), 2.30-2.25 (m, 2H), 2.03 (s, 2H), 2.01 (br s, 1H), 1.67-1.61 (m, 2H), ¹³C-NMR (101 MHz, CDCl₃): δ = 152.94, 143.44, 139.97, 135.30, 128.90, 128.85, 128.64, 126.42, 122.10, 59.96, 51.65, 51.63, 50.83, 50.30, 47.88, 32.98, 31.34, 14.23, 9.96. ESI-MS (*m/z*): [*M*+H]⁺ found: 486.3088.

E-*N*-(4-((1-(2-azidoethyl)-3,5-dimethyl-1*H*-pyrazol-4-yl)diazenyl)benzyl)-*N*-(1-phenethylpiperidin-4-yl)propionamide (**3c**)



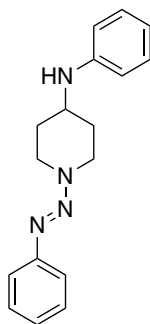
To a solution of **27** (660 mg, 1.36 mmol) in anhydrous DCM (15 mL), Et₃N (0.37 mL, 2.72 mmol, 2 eq.) was added, followed by propionyl chloride (0.24 mL, 2.72 mmol, 2.0 eq.). The reaction mixture was allowed to stir for 24 h under N₂ atmosphere at room temperature. Water was then added, and the organic phase was extracted with DCM (2 x 10 mL). The pooled organic phase was washed with sat. NaHCO₃ (1x 20 mL) and sat. NaCl solution (1 x 20 mL). The combined organic layers were dried (Na₂SO₄), filtered and concentrated *in vacuo*. The crude residue was subjected to automated flash column chromatography, eluting at 100% DCM to 10% MeOH/DCM. The product was further purified by preparative HPLC (solvent A: H₂O [0.05 Vol% TFA], solvent B: MeCN; gradient A/B: 0-20 min: 90/10 to 2/98, 20-25 min: 2/98), eluting at 70% MeCN, to obtain **3c** as an orange oil (525 mg, 0.97 mmol, 71%). ¹H-NMR (400 MHz, CDCl₃): δ = 7.77 (d, J = 8.3 Hz, 2H), 7.32-2.25 (m, 5H), 7.17 (d, J = 8.2 Hz, 2H), 4.93-4.87 (m, 1H), 4.61 (s, 2H), 4.19 (t, J = 5.6 Hz, 2H), 3.78 (t, J = 5.6 Hz, 2H), 3.67-3.64 (m, 2H), 3.18-3.14 (m, 2H), 3.06-3.02 (m, 2H), 2.79-2.74 (m, 2H), 2.63 (s, 3H), 2.51 (s, 3H), 2.37 (q, J = 7.3 Hz, 2H), 2.21-2.15 (m, 2H), 1.85-1.82 (m, 2H), 1.15 (t, J = 7.3 Hz, 3H). ¹³C-NMR (101 MHz, CDCl₃): δ = 175.46, 153.08, 143.46, 140.35, 139.13, 135.79, 135.22, 129.19, 128.72, 127.56, 126.30, 122.54, 58.52, 52.70, 50.81, 48.87, 47.83, 46.30, 30.60, 27.16, 26.50, 14.04, 9.94, 9.63. HR-ESI-MS (m/z): [M+H]⁺ calculated: 542.3284; found: 542.3357. IR: ν [cm⁻¹]: 2933, 2803, 2102, 1733, 1640, 1558, 1502, 1409, 1375, 1282, 1233, 1200, 1118, 1077, 1033, 999, 936, 824, 749.

(*E*)-1-(phenyldiazenyl)piperidin-4-one (**29**)



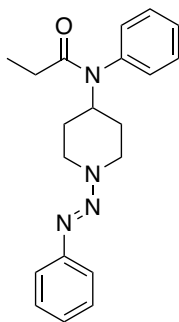
To a stirred solution of aniline **28** (1.0 g, 10.7 mmol, 1.0 eq.) dissolved in a mixture of acetonitrile and water (2:1, 15 mL), 12 M HCl (3.6 mL, 43.0 mmol, 4.0 eq.) was added dropwise at 0 °C. In dark conditions, the reaction mixture was further cooled to -5 °C and an aqueous solution of NaNO₂ (1.1 g, 34 mmol, 1.5 eq.) dissolved in a minimal amount of water was added dropwise and stirred for 0.5 h. At 0 °C, the reaction mixture was added slowly to a stirred solution of 4-piperidone (3.1 mL, 26.9 mmol, 2.5 eq.) and potassium carbonate (7.73 g, 55.9 mmol, 5.2 eq.) in a 2:1 mixture of acetonitrile and water (60 mL). The reaction mixture was allowed to warm to room temperature and stirred for 1 h. The mixture was then extracted with DCM (2 x 30 mL). The combined organic layer was washed with sat. NaHCO₃ (1 x 30 mL), dried with Na₂SO₄, and solvent removed *in vacuo*. The crude residue was subjected to automated flash column chromatography in dark conditions, eluting at 100% DCM to 10% MeOH/DCM to obtain **29** as a red oil (1.127 g, 5.55 mmol, 52%). ESI-MS (m/z): [M+H]⁺ found: 204.1136. Compound characterization matches that previously reported.^[6]

(*E*)-*N*-phenyl-1-(phenyldiazenyl)piperidin-4-amine (**30**)



To a solution of **29** (1.05 g, 5.19 mmol, 1.05 eq.) in DCE (30 mL), was added sequentially aniline (0.50 mL, 5.45 mmol, 1.05 eq.), NaBH(OAc)₃ (1.54 g, 7.27 mmol, 1.4 eq.) and AcOH (0.30 mL, 5.19 mmol, 1.0 eq.). The bright orange reaction mixture was allowed to stir overnight at room temperature. After 15 h, the reaction mixture was diluted with EtOAc (2 x 10 mL), washed with 1M NaOH (1x 5 mL), sat. NaHCO₃ (1 x 5 mL), brine (1 x 10 mL). The combined organic layers were dried (Na₂SO₄), filtered and concentrated *in vacuo*. The crude residue was subjected to automated flash column chromatography, eluting at 100% DCM (0.01% Et₃N) to 20% DCM/MeOH (0.01% Et₃N) to obtain **30** as a dark orange residue (453 mg, 1.62 mmol, 31%). ¹H-NMR (400 MHz, CDCl₃): δ (ppm) = 7.55-7.53 (m, 2H), 7.45-7.41 (m, 2H), 7.30-7.28 (m, 2H), 7.25-7.21 (m, 1H), 6.83-6.80 (m, 1H), 6.76-6.70 (m, 2H), 4.54-4.50 (m, 2H), 3.68-3.62 (m, 1H), 3.40-3.35 (m, 2H), 2.23-2.24 (m, 2H), 1.66-1.56 (m, 2H). ¹³C-NMR (101 MHz, CDCl₃): δ = 150.56, 146.72, 129.51, 129.36, 128.98, 126.15, 120.75, 117.77, 115.18, 113.48, 50.00, 31.63. ESI-MS (*m/z*): [*M*+H]⁺ found: 281.1759.

(*E*)-*N*-phenyl-*N*-(1-(phenyldiazenyl)piperidin-4-yl)propionamide (**4**)



To a solution of intermediate **30** (360 mg, 0.42 mmol) in dry DCM (6 mL), triethylamine (0.35 mL, 2.57 mmol, 2.0 eq.) was added, followed by propionyl chloride (0.22 mL, 2.57 mmol, 2.0 eq.). The reaction mixture was allowed to stir for 24 h under N_2 atmosphere. Water (5 mL) was then added, and the organic phase was extracted with DCM (2 x 5 mL). The pooled organic phase was washed with sat. $NaHCO_3$ (1 x 5 mL) and brine (1 x 5 mL). The organic phase was then dried over Na_2SO_4 and concentrated. The crude residue was subjected to automated flash column chromatography, eluting at 100% DCM to 10% MeOH/DCM to obtain target compound **4** as a red oil (220 mg, 0.654 mmol, 51%). 1H -NMR (400 MHz, $CDCl_3$): δ (ppm) = 7.28-7.24 (m, 5H), 7.19-7.16 (m, 2H), 7.03-6.99 (m, 1H), 6.96-6.94 (m, 2H), 4.85-4.78 (m, 1H), 4.47-4.44 (m, 2H), 3.03-2.97 (m, 2H), 1.85-1.80 (m, 4H), 1.35-1.24 (m, 2H), 0.91 (t, J = 7.44 Hz, 3H). ^{13}C -NMR (101 MHz, $CDCl_3$): δ = 173.67, 150.43, 138.65, 130.25, 129.55, 128.86, 128.62, 126.00, 120.62, 52.01, 43.66, 30.00, 28.53, 9.64. ESI-MS (m/z): $[M+H]^+$ found: 337.2020.

1.7.2.1 Purity Measurements

All purity measurements can be found in the appendix (Section 7.2.1) under ‘Analytical HPLC Chromatograms for Purity Determination’.

1.7.3 Supplementary Photophysical Information

1.7.3.1 Materials and Methods

For determination of thermal equilibrium and isomer spectra, as well as determination of cycle performance and thermal half-life, UV/Vis absorption spectroscopy was employed. UV/Vis absorption spectroscopy was performed using Agilent 8453 UV/Vis spectrophotometer or Agilent Varian Cary[®] 50 UV/Vis spectrophotometer, in 10 mm quartz cuvettes. To determine PSS values at the respective isosbestic points of compounds (50 μ M), analytical HPLC was performed using Agilent 1220 Infinity LC System (column: Phenomenex Luna, 3 μ M C18(2), 100 Å 150 x 2.0 mm; flow rate of 0.3 mL/min at 20 °C; solvent A: Milli-Q water with 0.05 wt% TFA; solvent B: MeCN). LED light sources for irradiation: λ =265 nm (Nikkiso, VPC131, 350 mA, 6.3 V), λ =285 nm (Nikkiso, VPS173, 500 mA, 6.0 V), λ =365 nm (Seoul Viosys, CUN66A1B, 700 mA, 3.6 V), λ =400 nm (Luxeon LHUV-0400-0450, SZ-01-S2, 1000 mA, 3.2 V), λ =420 nm (Mouser, L1F3-U410200012000, 700 mA, 3.4 V), λ =451 nm (LED-TECH, Oslon SSL 80, LDCQ7P-2U3U, 700 mA, 3.2 V), λ =528 nm (LED-TECH, Oslon SSL 80, LDCQ7P-2U3U, 700 mA, 3.5 V), λ =645 nm (LED-TECH, Oslon SSL 80, LHCP7P-2T3T, 700 mA, 2.6 V). The details of these light sources are based on the supplier specifications upon purchase.

1.7.3.2 UV/Vis Absorption Spectra, Cycle Performance and Thermal Stabilities

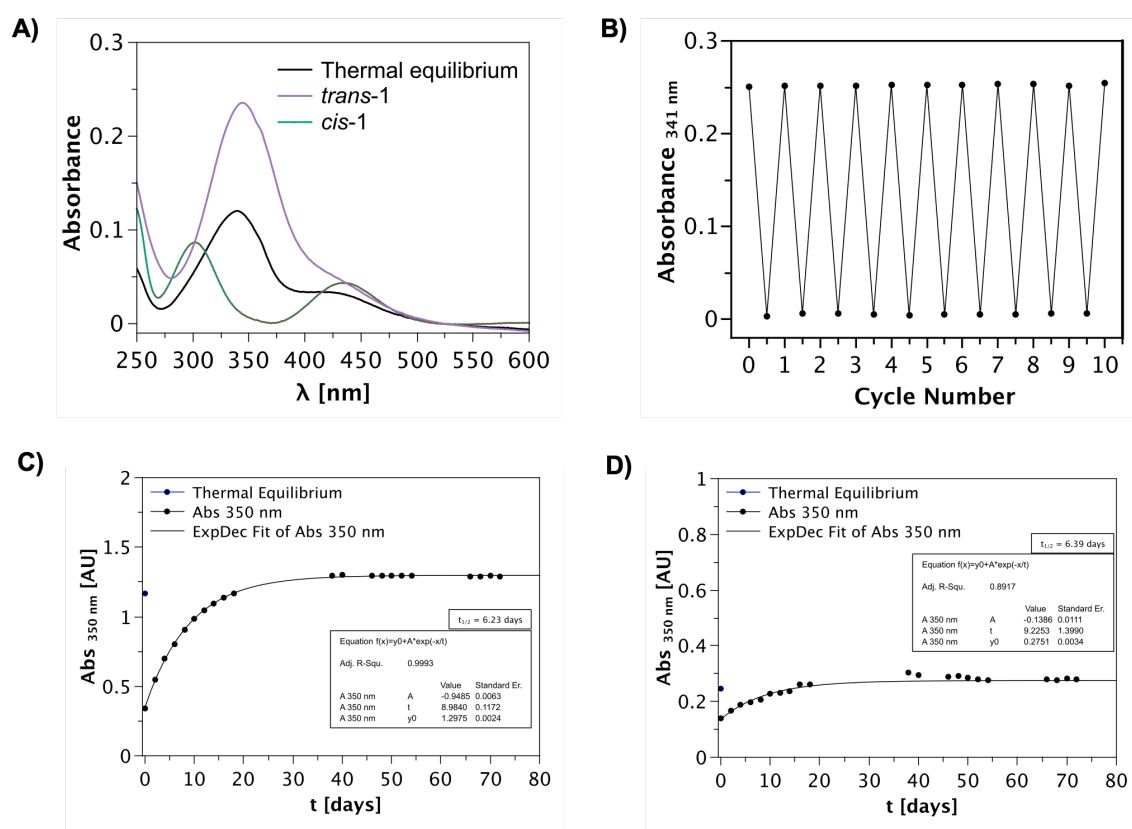


Figure 6. Photophysical properties of compound **1**. Compound ($20 \mu\text{M}$) was evaluated in buffer solution (TrisHCl Buffer, pH 7.5) + 0.2% DMSO at 25°C , unless otherwise specified. A) UV/Vis absorption spectra data of thermal equilibrium, *trans*-isomer and *cis*-isomer. The *cis*-isomer was accessed via irradiation with 365 nm, while the *trans*-isomer was obtained with 528 nm irradiation. B) Cycle performance upon alternating irradiation of 365 nm and 528 nm. Data points were recorded at the absorbance maximum of the *trans*-isomer (341 nm). C) Thermal half-life of compound **1** ($150 \mu\text{M}$) measured at 27°C in DMSO. D) Thermal half-life of compound **1** ($50 \mu\text{M}$) measured at 27°C in buffer solution (TrisHCl Buffer, pH 7.5) + 0.5% DMSO.

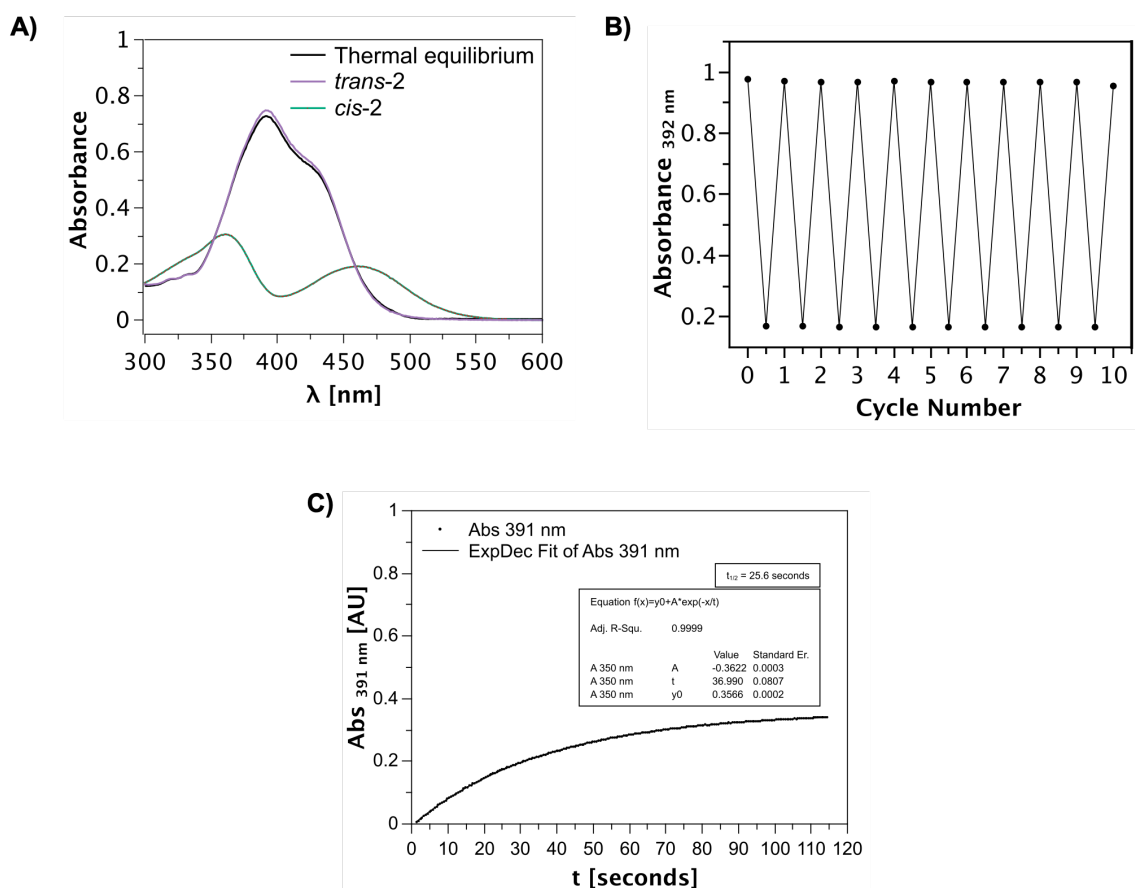


Figure 7. Photophysical properties of compound **2**. Compound (50 μ M) was evaluated in DMSO at 25 $^{\circ}$ C, unless otherwise specified. A) UV/Vis absorption spectra data of thermal equilibrium, *trans*-isomer and *cis*-isomer. The *cis*-isomer was accessed via continuous irradiation with 400 nm, while the *trans*-isomer was obtained via irradiation with 528 nm. B) Cycle performance upon alternating irradiation of 365 nm and darkness. Data points were recorded at the absorbance maximum of the *trans*-isomer (392 nm). C) Thermal half-life of compound **2** (50 μ M) measured at 27 $^{\circ}$ C in DMSO. UV/Vis trace obtained every 0.5 seconds.

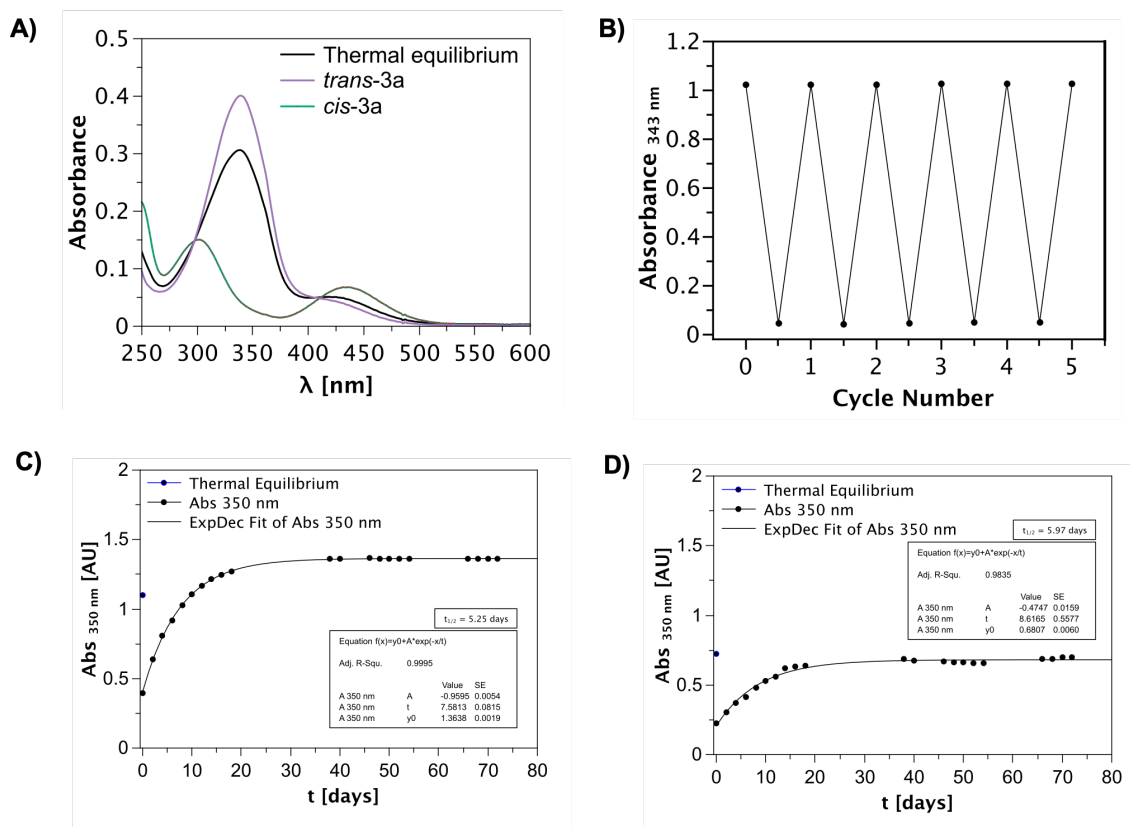


Figure 8. Photophysical properties of compound **3a**. Compound (20 μ M) was evaluated in buffer solution (TrisHCl Buffer, pH 7.5) + 0.2% DMSO at 25 °C, unless otherwise specified. A) UV/Vis absorption spectra data of thermal equilibrium, *trans*-isomer and *cis*-isomer. The *cis*-isomer was accessed via irradiation with 365 nm, while the *trans*-isomer was obtained with 528 nm irradiation. B) Cycle performance upon alternating irradiation of 365 nm and 528 nm. Data points were recorded at the absorbance maximum of the *trans*-isomer (343 nm). C) Thermal half-life of compound **3a** (150 μ M) measured at 27 °C in DMSO. D) Thermal half-life of compound **3a** (150 μ M) measured at 27 °C in buffer solution (TrisHCl Buffer, pH 7.5) + 1.5% DMSO.

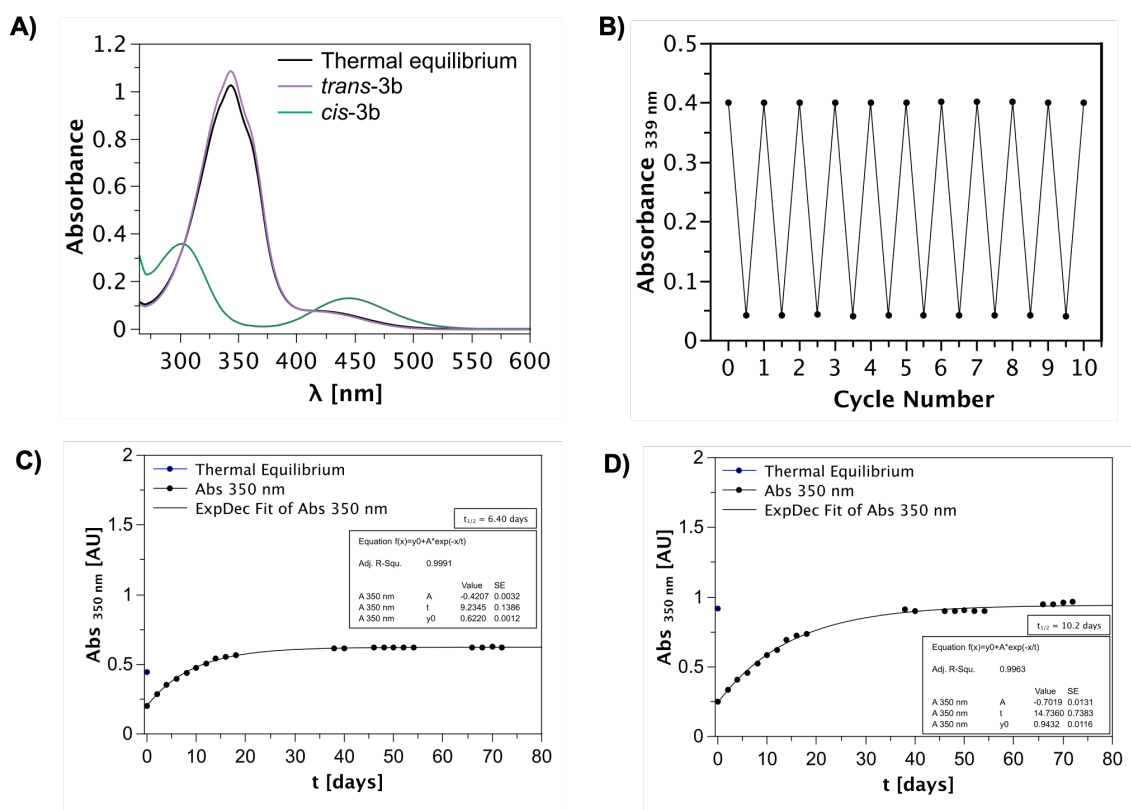


Figure 9. Photophysical properties of compound **3b**. Compound (50 μ M) was evaluated in buffer solution (TrisHCl Buffer, pH 7.5) + 0.5% DMSO at 25 $^{\circ}$ C, unless otherwise specified. A) UV/Vis absorption spectra data of thermal equilibrium, *trans*-isomer and *cis*-isomer. The *cis*-isomer was accessed via irradiation with 365 nm, while the *trans*-isomer was obtained with 528 nm irradiation. B) Cycle performance upon alternating irradiation of 365 nm and 528 nm. Data points were recorded at the absorbance maximum of the *trans*-isomer (339 nm). C) Thermal half-life of compound **3b** (50 μ M) measured at 27 $^{\circ}$ C in DMSO. D) Thermal half-life of compound **3b** (150 μ M) measured at 27 $^{\circ}$ C in buffer solution (TrisHCl Buffer, pH 7.5) + 1.5% DMSO.

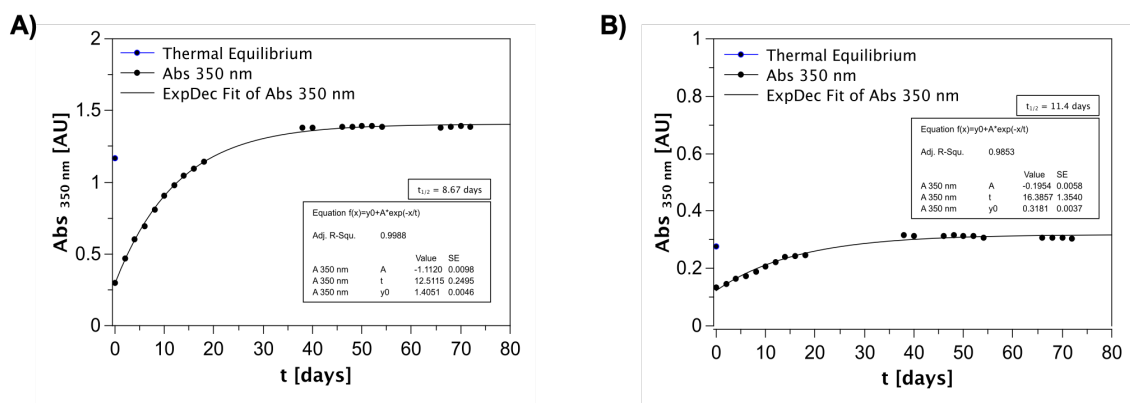


Figure 10. Photophysical properties of compound **3c**. A) Thermal half-life of compound **3c** (150 μ M) measured at 27 $^{\circ}$ C in DMSO. B) Thermal half-life of compound **3c** (50 μ M) measured at 27 $^{\circ}$ C in buffer solution (TrisHCl Buffer, pH 7.5) + 0.5% DMSO.

1.7.3.3 Supplementary Data that Suggest Compound 4 Degradation Upon Exposure to UV Irradiation

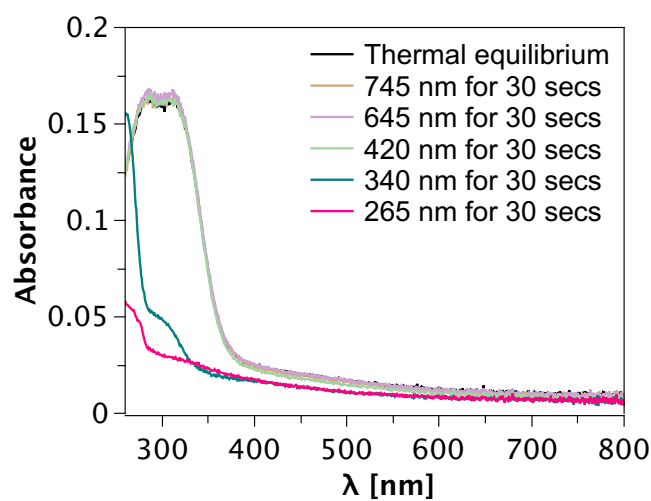


Figure 11. UV/Vis absorbance spectra of compound 4 upon light exposure with various wavelengths. Irradiation with wavelengths of 745, 645, 528 and 420 nm did not significantly change UV/Vis spectral absorbance, when compared to thermal equilibrium. However, irradiation of 340 and 265 nm significantly diminished absorbance. Compound 4 (50 μ M) was evaluated in buffer solution (TrisHCl Buffer, pH 7.5) + 0.5% DMSO at 25 $^{\circ}$ C.

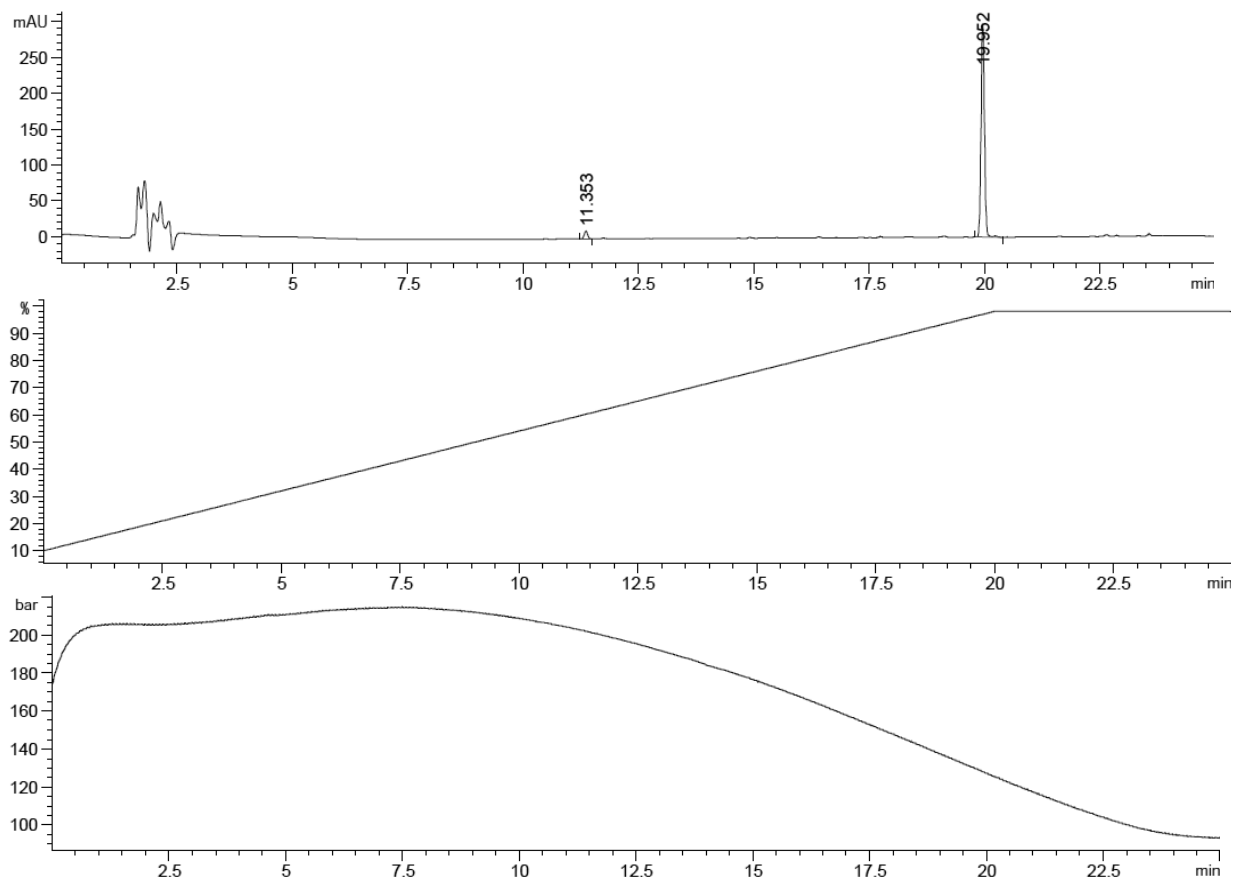
Photoswitchable Fentanyl Derivatives for Controlled μ -Opioid Receptor Activation

Analytical HPLC to Monitor Effects of Light Exposure:

Compound 4 (50 μ M solution in TrisHCl buffer, pH 7.4 + 0.2% DMSO) in dark conditions:

Detection at 280 nm: tR = 19.952 min.

Figures of analytical HPLC trace, solvent gradient (acetonitrile/H₂O + 0.01% TFA), pressure profile and data analysis:



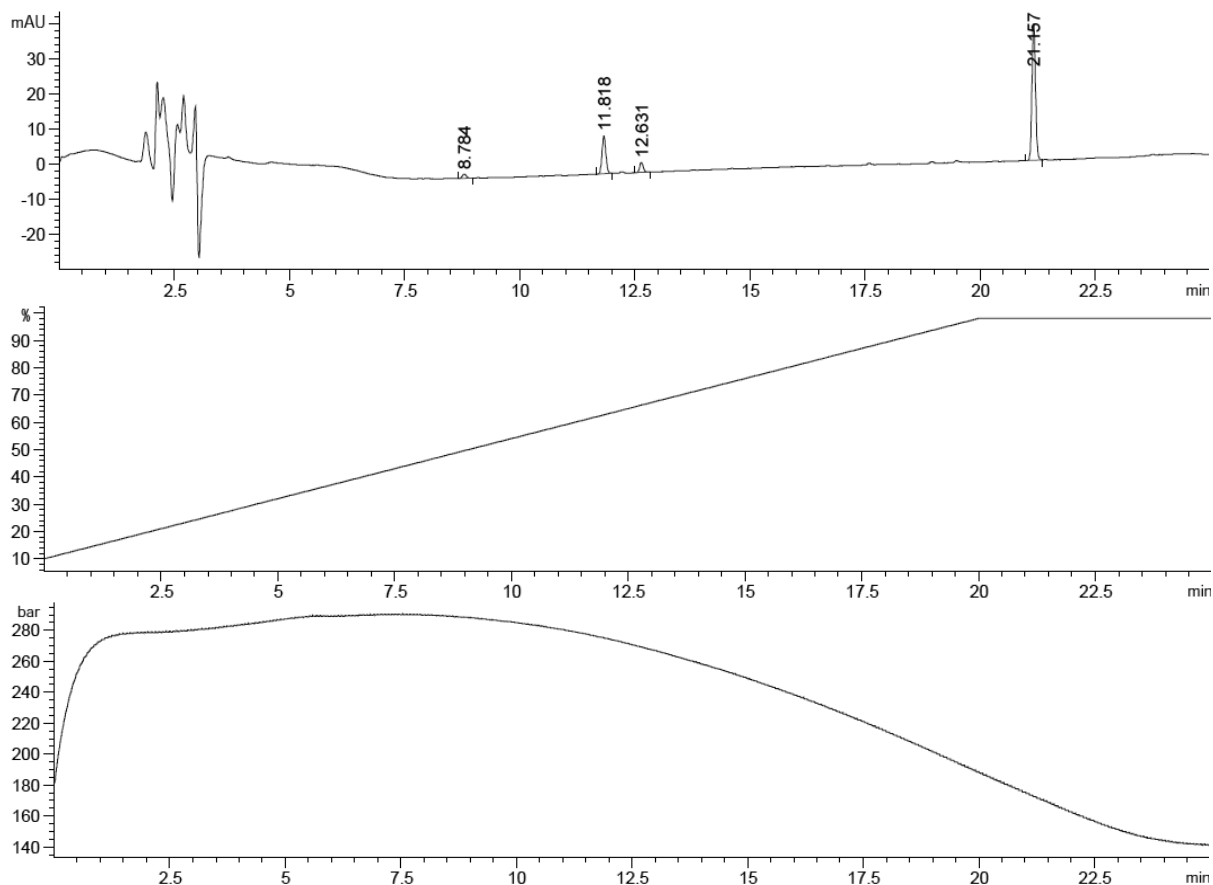
Signal 3: DAD1 C, Sig=280,4 Ref=off

Peak #	RetTime [min]	Type	Width [min]	Area [mAU*s]	Height [mAU]	Area %
1	11.353	BB	0.0803	57.70715	11.15608	3.6514
2	19.952	BV R	0.0795	1522.69250	297.17880	96.3486

Photoswitchable Fentanyl Derivatives for Controlled μ -Opioid Receptor Activation

The same sample of compound **4** after irradiation with $\lambda = 285$ nm for 20 seconds, with the same HPLC instrument, set-up and conditions.

Detection at 280 nm: tR = 21.157 min. A significant reduction in absorbance height (mAU) can be observed.



Signal 3: DAD1 C, Sig=280,4 Ref=off

Peak #	RetTime [min]	Type	Width [min]	Area [mAU*s]	Height [mAU]	Area %
1	8.784	BB	0.0960	7.59672	1.23146	2.5574
2	11.818	BB	0.0913	62.59029	10.85392	21.0706
3	12.631	BB	0.0855	16.27894	2.89927	5.4802
4	21.157	BB	0.0828	210.58388	39.12384	70.8918

1.7.3.1 PSS Evaluation

All PSS measurements can be found in the appendix (Section 7.2.2) under 'Analytical HPLC Chromatograms for PSS Determination'.

1.7.4 Supplementary Biochemical Information

1.7.4.1 Materials and Methods

Radioligand Binding

Binding affinities towards the human opioid receptor μ OR were determined as described previously.^[7] In brief, membranes were prepared from HEK293T cells transiently transfected with the cDNA for μ OR (gift from the Ernest Gallo Clinic and Research Center, UCSF, CA) and incubated with the radioligand [³H]diprenorphine (specific activity 31 Ci/mmol; PerkinElmer, Rodgau, Germany) at concentrations of 0.2 to 0.3 nM. Homogenates expressing μ OR with a Bmax of 2200 ± 360 fmol/mg protein and a KD of 0.089 ± 0.01 nM were incubated at an amount of protein of 3-10 μ g/well with radioligand and varying concentrations of test compound (in the range of 10 pM-100 μ M) for 60 min in binding buffer (50 mM TRIS, pH 7.4) and filtered on glass fiber mats presoaked with 0.3% PEI solution. Trapped radioactivity was measured with a microplate reader (Microbeta Trilux, Perkin Elmer) by scintillation counting. To measure the photoswitchable compounds 200-300 μ L of a working solution was irradiated with a single LED at 528 nm for 180 sec to switch to the *trans*-isomer and at 365 nm for 20 sec to obtain the *cis*-isomer. For switching *trans*-PF2 irradiation was done at 420 nm for 120 sec. Unspecific binding was determined in the presence of 10 μ M of naloxone. Protein concentration was determined employing the method of Lowry with bovine serum albumin as standard.^[8] The resulting competition curves of the receptor binding experiments were analyzed by nonlinear regression using the algorithms in PRISM 9.0 (GraphPad Software, San Diego, USA). The data were initially fit using a sigmoid model to provide IC₅₀ values which were subsequently transformed to K_i values according to the equation of Cheng and Prusoff.^[9]

IP Accumulation Assay for Receptor Activation

The determination of receptor mediated G-protein signaling by μ OR activation was performed applying an IP accumulation assay (IP-One HTRF[®], PerkinElmer-Cisbio, Rodgau, Germany) according to the manufacturer's protocol and in analogy to previously described protocols.^[10] In brief, HEK293T cells were co-transfected with the cDNA for μ OR and the hybrid G-protein G α qi5HA (G α q protein with the last five amino acids at the C-terminus replaced by the corresponding sequence of G α i (gift from The J. David

Photoswitchable Fentanyl Derivatives for Controlled μ -Opioid Receptor Activation

Gladstone Institutes, San Francisco, CA), respectively and transferred into 384 well micro plates. Cells were incubated with test compound for 120 min and accumulation of second messenger was stopped by adding detection reagents (IP1-d2 conjugate and Anti-IP1cryptate TB conjugate). After 60 min, TR-FRET was measured with a Clariostar plate reader. FRET emission was measured at 620 nm and 665 nm, the corresponding ratio (emission at 665 nm/emission at 620 nm) was calculated and normalized to vehicle (0%) and the maximum effect of the reference DAMGO (100%). Each single experiment, performed in duplicate, was analyzed applying the algorithms for four parameter non-linear regression implemented in Prism 9.0 to get dose-response curves representing EC_{50} and E_{max} values and was repeated to get 3 to 11 independent values.

Photoisomerization experiments were performed by measuring IP accumulation as described above. In detail, 10,000 cells transiently co-transfected with μ OR and $G\alpha_{qi5}HA$ were seeded in each well of a 96 well microplate (Greiner Bio-One, Frickenhausen, Germany). On the day of experiment, medium was removed by stimulation buffer supplemented with 30 μ M of *trans/cis*-**3c** or 1 μ M of DAMGO as a reference. Incubation was initiated by irradiation at 365 nm (for 20 sec) or 528 nm (for 180 sec) with LEDs directly placed upon the wells. As a reference, buffer and DAMGO were irradiated in parallel to the photoswitch ligand **3c** for each irradiation condition. The second irradiation step was performed similarly. Accumulation of IP was determined by TR-FRET measurement and normalized to the effect of buffer (0%) and DAMGO (100%), which resulted after an incubation of 120 min. Each experiment was performed in quadruplicate and was repeated to get 6 to 11 individual values.

1.7.4.1 Supplementary Figures and Tables

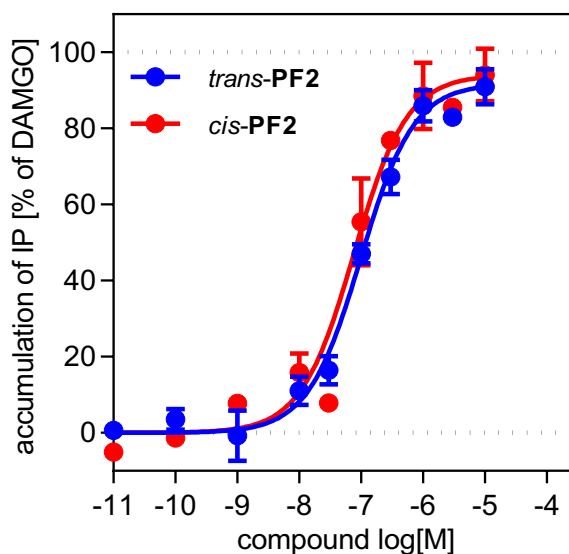


Figure 12. Activation of the μ OR by *trans*-PF2 and *cis*-PF2, measured by applying the IP-One[®] accumulation assay in HEK293T cells transiently co-transfected with μ OR and the hybrid G-protein G α qi5HA. Both *trans*-PF2 and *cis*-PF2 show full agonist properties with E_{max} values of 93% and 95%, respectively, and similar EC₅₀ potencies of 96 nM and 85 nM, respectively. Graphs show mean curves (\pm S.E.M.) of 3-4 single experiments, each performed in duplicate.

Photoswitchable Fentanyl Derivatives for Controlled μ -Opioid Receptor Activation

Table 4. Photoisomerization of *trans/cis*-**3c** during cell incubation, indicated by μ OR-stimulated IP accumulation.

	IP accumulation ^[a]	
	E_{\max} [% \pm S.E.M.] ^[b]	(n) ^[c]
A) <i>trans</i> - 3c		
120 min	76 \pm 1	11
30 min	25 \pm 5	6
B) <i>cis</i> - 3c		
120 min	26 \pm 2	11
30 min	10 \pm 2	6
C) switching		
<i>trans</i> 30 min / <i>cis</i> 90 min	38 \pm 4	6
<i>cis</i> 30 min / <i>trans</i> 90 min	71 \pm 2	6

^[a]IP accumulation was determined by applying the IP-One[®] assay (Cisbio/PerkinElmer) with HEK293T cells transiently co-transfected with the human μ OR and the hybrid G-protein $G\alpha_{q15HA}$. ^[b]Mean EC_{50} value [% \pm S.E.M.] normalized to the full effect of DAMGO after an incubation time of 120 min. ^[c]Number of individual experiments, each performed in duplicate.

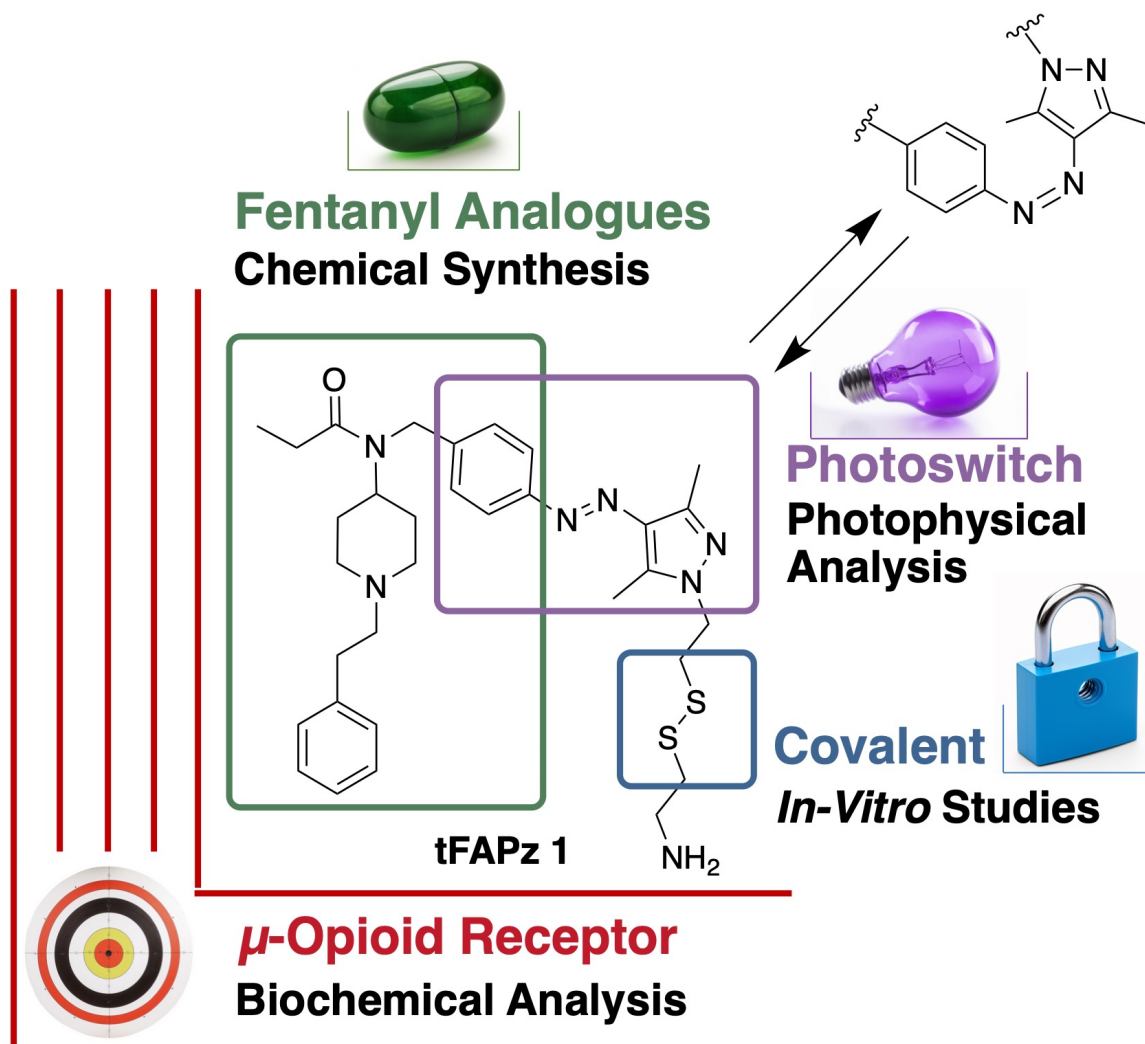
1.7.5 NMR Spectra

All NMR spectra can be found in the appendix (Section 7.2.3).

1.7.6 References

- [1] W. Huang, A. Manglik, A. J. Venkatakrishnan, T. Laeremans, E. N. Feinberg, A. L. Sanborn, H. E. Kato, K. E. Livingston, T. S. Thorsen, R. C. Kling, S. Granier, P. Gmeiner, S. M. Husbands, J. R. Traynor, W. I. Weis, J. Steyaert, R. O. Dror, B. K. Kobilka, *Nature* **2015**, *524*, 315-321.
- [2] L. Stricker, M. Böckmann, T. M. Kirse, N. L. Doltsinis, B. J. Ravoo, *Chem. Eur. J.* **2018**, *24*, 8639-8647.
- [3] M. Schönberger, D. Trauner, *Angew. Chem. Int. Ed. Engl.* **2014**, *53*, 3264-3267.
- [4] A. F. Casy, M. R. Huckstep, *J. Pharm. Pharmacol.* **1988**, *40*, 605-608.
- [5] C. A. Valdez, R. N. Leif, B. P. Mayer, *PLoS One* **2014**, *9*, e108250.
- [6] R. Lazny, M. Sienkiewicz, S. Bräse, *Tetrahedron* **2001**, *57*, 5825-5832.
- [7] a) H. Hübner, C. Haubmann, W. Utz, P. Gmeiner, *J. Med. Chem.* **2000**, *43*, 756-762; b) A. Drakopoulos, Z. Koszegi, Y. Lanoiselée, H. Hübner, P. Gmeiner, D. Calebiro, M. Decker, *J. Med. Chem.* **2020**, *63*, 3596-3609.
- [8] O. H. Lowry, N. J. Rosebrough, A. L. Farr, R. J. Randall, *J. Biol. Chem.* **1951**, *193*, 265-275.
- [9] Y. C. Cheng, W. H. Prusoff, *Biochem. Pharmacol.* **1973**, *22*, 3099-3108.
- [10] a) H. Liu, J. Hofmann, I. Fish, B. Schaake, K. Eitel, A. Bartuschat, J. Kaindl, H. Rampp, A. Banerjee, H. Hübner, M. J. Clark, S. G. Vincent, J. T. Fisher, M. R. Heinrich, K. Hirata, X. Liu, R. K. Sunahara, B. K. Shoichet, B. K. Kobilka, P. Gmeiner, *Proc. Natl. Acad. Sci. U. S. A.* **2018**, *115*, 12046-12050; b) C. Gentzsch, K. Seier, A. Drakopoulos, M.-L. Jobin, Y. Lanoiselée, Z. Koszegi, D. Maurel, R. Sounier, H. Hübner, P. Gmeiner, S. Granier, D. Calebiro, M. Decker, *Angew. Chem. Int. Ed. Engl.* **2020**, *59*, 5958-5964.

2. Tethered Photoswitchable Derivatives of Fentanyl that Target the μ -Opioid Receptor



CHAPTER 2

2.1 Abstract

Converting known ligands into photoswitchable derivatives offers the opportunity to modulate compound structure with light and hence, biological activity. In doing so, these probes provide unique control when evaluating G-protein-coupled receptor (GPCR) mechanism and function. Further conversion of such compounds into covalent probes, known as photoswitchable tethered ligands (PTLs), offers additional advantages. These include localization of the PTLs to the receptor binding pocket. Covalent localization increases local ligand concentration, improves site-selectivity and may improve the biological differences between the respective isomers. This work describes chemical, photophysical and biochemical characterizations of a variety of PTLs designed to target the μ -opioid receptor (μ OR). These PTLs were modeled on fentanyl, with the lead disulfide-containing agonist found to covalently interact with a cysteine-enriched mutant of this medically-relevant receptor.

Major parts of this chapter have been published in:

R. Lahmy, H. Hübner, D. Lachmann, P. Gmeiner, B. König, *ChemMedChem.* **2023**, e202300228.

Reprinted (adapted) with permission from R. Lahmy, H. Hübner, D. Lachmann, P. Gmeiner, B. König, *ChemMedChem.* **2023**. Copyright 2023 Wiley-VCH GmbH.

Author contributions:

RL was the first to synthesize compounds **2a**, **2b**, **2c**, **2d**, **2e**, **2f**, **2g**, **3** and **10-15**, and performed the corresponding chemical and photophysical evaluations. DL was the first to synthesize compounds **1**, **4-9**, and performed the corresponding chemical and photophysical evaluations. HH performed the biochemical measurements and evaluations. The manuscript was written by RL, with the biochemical section (Section 2.3.4) written by both HH and RL. BK and PG supervised the project and are the corresponding authors.

2.2 Introduction

2.2.1 Photoswitchable Ligands as Novel Probes

Throughout the past decade, extensive research has been conducted in expanding the repertoire of photoswitchable ligands that interact with a range of biological targets.^[1] The attractiveness of photoswitchable probes stems from the ability to use light to reversibly change their chemical structure and/or properties. Importantly, this change may also alter the inherent biological activity of these compounds, resulting in photocontrol of ligand activity.^[1] Such spatial, temporal and non-invasive control may be beneficial in enhancing kinetic and dynamic investigations.^[2] This includes overcoming limitations of non-uniform start times in kinetic studies, as well as exploring receptor-ligand interactions and associated conformational changes in dynamic studies.^[2] These investigations are particularly important for understanding the mechanisms and interactions of medically-relevant receptors, including G-protein-coupled receptors (GPCRs).^[3]

2.2.2 The μ -Opioid Receptor – a GPCR

Approximately 34% of clinically approved drugs exert their mechanism of action by modulating GPCR signaling.^[4] Despite the successful application into clinics of drugs that target this class of receptors, there is still a knowledge gap in the research surrounding GPCR mechanisms and interactions.^[5] This knowledge gap is particularly evident for the μ -opioid receptor (μ OR). The μ OR is notably targeted for pain relief, with drugs such as fentanyl and morphine available on the medical market. However, despite its importance, this GPCR plays a leading role in opioid addiction and the current opioid epidemic.^[6] In order to better understand the μ OR, a wide range of valuable research has been accomplished over decades.^[7]

2.2.3 Targeting μ OR with Photoswitchable Fentanyl Ligands

In the field of photopharmacology, fentanyl was developed by *Trauner et al.*^[8] and later by our group^[9] into photoswitchable ligands that enabled photocontrol of a μ OR ionotropic and metabotropic response, respectively (Figure 13). For ionotropic photocontrol, the *trans*-isomer (blue light irradiation) of photofentanyl 2 (**PF2**) was found to trigger μ OR-mediated potassium influx through G-protein-coupled inward-rectifying potassium (GIRK) channels, while its respective *cis*-isomer (360 nm irradiation) retracted this μ OR activation.^[8] For metabotropic photocontrol, a photoswitchable ligand that is named here as fentanyl

Tethered Photoswitchable Derivatives of Fentanyl that Target the μ -Opioid Receptor

azopyrazole 1 (**FAPz 1**), displayed significant receptor efficacy differences between its respective *trans*- (528 nm irradiation) and *cis*-isomers (365 nm irradiation) in a G-protein activation assay (IP-One[®]).^[9]

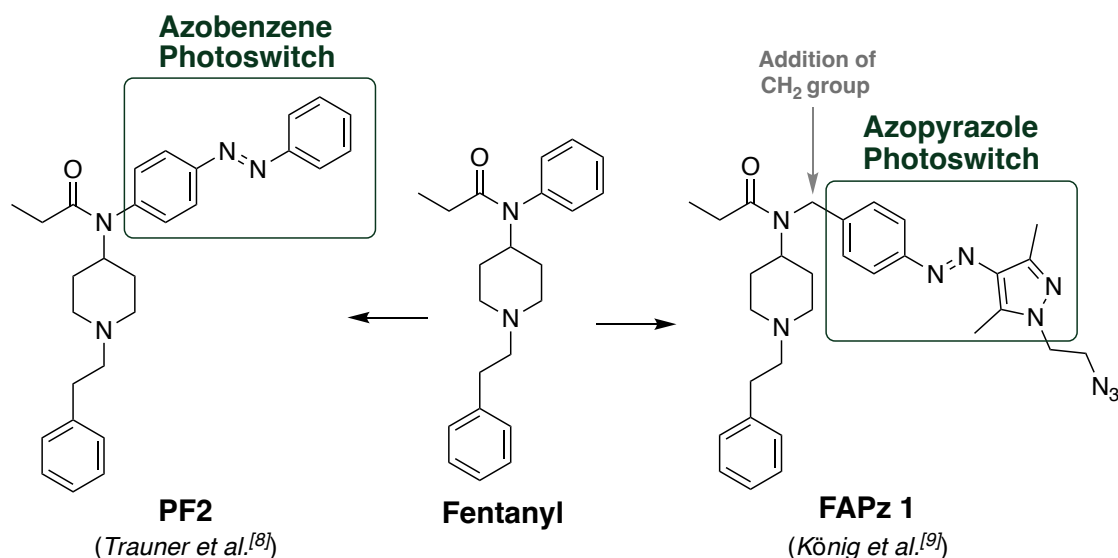


Figure 13. Structures of previously reported photoswitch-containing ligands that target the μ OR (left and right), modeled on the fentanyl pharmacophore (middle). Previous work by Trauner et al.^[8] attached an azobenzene photoswitch to the core structure of fentanyl, named photofentanyl 2 (**PF2**), while previous work by our group (König et al.^[9]) attached an azopyrazole photoswitch unit (**FAPz 1**). When compared to fentanyl, **FAPz 1** contains a methylene insertion (+CH₂), which was reported to improve the photophysical properties of **FAPz 1**.^[9]

2.2.4 Photoswitchable Tethered Fentanyl Ligands

In order to further exploit the possibilities of **FAPz 1** as a biochemical tool, this photoresponsive ligand was modified in this work into a range of tethered fentanyl azopyrazole (**tFAPz**) derivatives. These compounds were designed to contain a reactive group that could covalently interact with μ OR (Figure 14). More specifically, these fentanyl derivatives were designed in accordance with a class of covalent photoswitchable molecules, known as photoswitchable tethered ligands (PTLs), which offer several advantages that are discussed below. To date, there have been no PTLs that target μ OR, and as a result, the work herein describes findings in the pursuit of these ligands.

FAPz 1 Structural Core

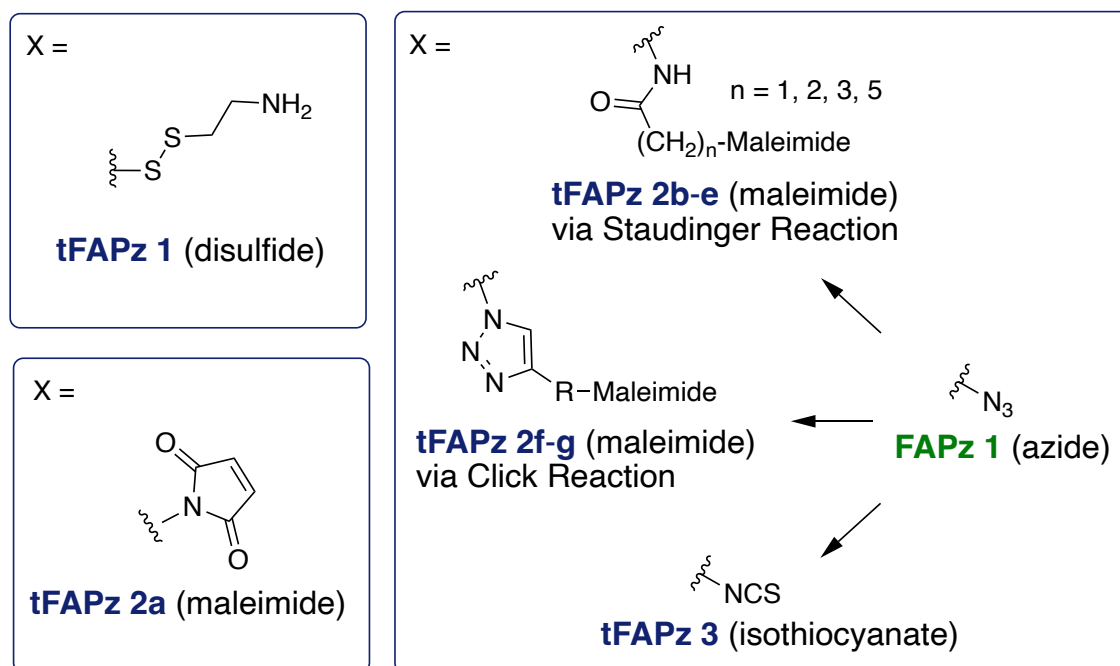
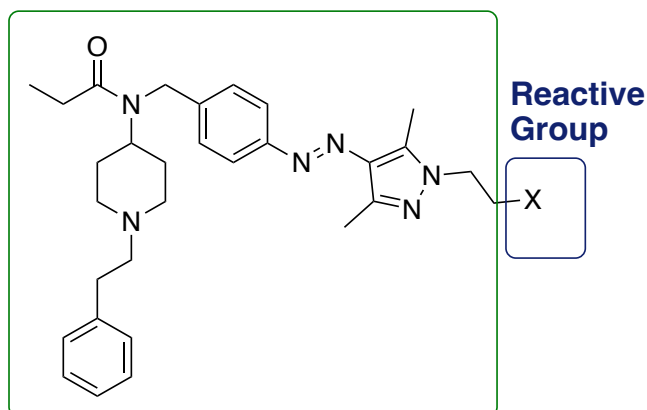


Figure 14. Structures of **tFAPz** that target the μ OR, modeled on **FAPz 1**. The **tFAPz** explored in this work contain disulfide, maleimide or isothiocyanate reactive groups. Furthermore, maleimides **tFAPz 2b-g** and isothiocyanate **tFAPz 3** were synthetically accessed directly from **FAPz 1**.

2.3 Results and Discussion

2.3.1 Design of Fentanyl-based PTLs

PTLs have been successfully applied in targeting GPCRs, ion channels and enzymes.^[10] These tool compounds are composed of a pharmacophore that is attached to a photoswitch unit, which in turn, is attached to a reactive unit.^[11] The two segments that link these 3 components may vary in length. Longer segments result in a greater separation between these components, which may be beneficial in maintaining pharmacophore affinity. A greater separation between these components may also allow for more dramatic displacement of the pharmacophore from the binding pocket upon photoisomerization; however, too much flexibility could oppose this effect. Once the PTL is drawn by affinity to its respective binding site, the reactive unit is able to form a covalent bond via a cross-linking reaction, localizing the ligand to its biological target.^[12] In doing so, PTLs overcome several limitations of freely diffusible photoswitchable ligands.^[12] Covalent localization to the target receptor may improve site-selectivity, minimize off-target interactions, and is resistant towards sample washing or dilution.

One of the most established extracellular bioconjugation techniques using PTLs has been the cysteine-maleimide system.^[13] In this system, a sulfhydryl group of a cysteine residue near the receptor binding pocket reacts with an electrophilic maleimide moiety installed on the PTL, forming a covalent bond. Since reduced and solvent-exposed cysteine residues have a low natural abundance in proteins, mutation of amino acids near the binding site to a cysteine residue has commonly been required to allow for bioconjugation.^[12] Despite the possibility for introduced cysteines to undergo oxidation reactions that may affect protein folding,^[14] the disadvantages can be considered minor when compared to other biorthogonal approaches that require fusion proteins or other larger modifications.^[10e] For example, the azide group of **FAPz 1** could be directly used in a bioorthogonal approach to covalently attach this fentanyl-based probe to the binding pocket of μ OR,^[15] however, this may require more complex genetic engineering of μ OR. Furthermore, due to the low natural abundance and good reactivity of 'free' sulfhydryl groups, cysteine residues are considered to be one of the most convenient targets for selective bioconjugation.^[16]

Overall, PTLs offer significant advantages as biochemical tools. As a result, it became of interest to expand **FAPz 1** that already possesses desirable biochemical and photophysical properties into PTLs.^[9] Since **FAPz 1** already contains the fentanyl pharmacophore and an

Tethered Photoswitchable Derivatives of Fentanyl that Target the μ -Opioid Receptor

azopyrazole photoswitch unit, a reactive group was attached to the photoswitch unit via various linker lengths, resulting in an array of **tFAPz** derivatives (Figure 14). Various lengths of this linking segment were explored in order to achieve covalent interaction in or near the μ OR binding pocket. The longest segment designed in this series was the PEG-4 linker in **tFAPz 2g**. This derivative was hypothesized to form covalent interactions more distal to the ligand-receptor binding pocket in accordance with the design approach of photoswitchable orthogonal remotely tethered ligands (PORTLs).^[11]

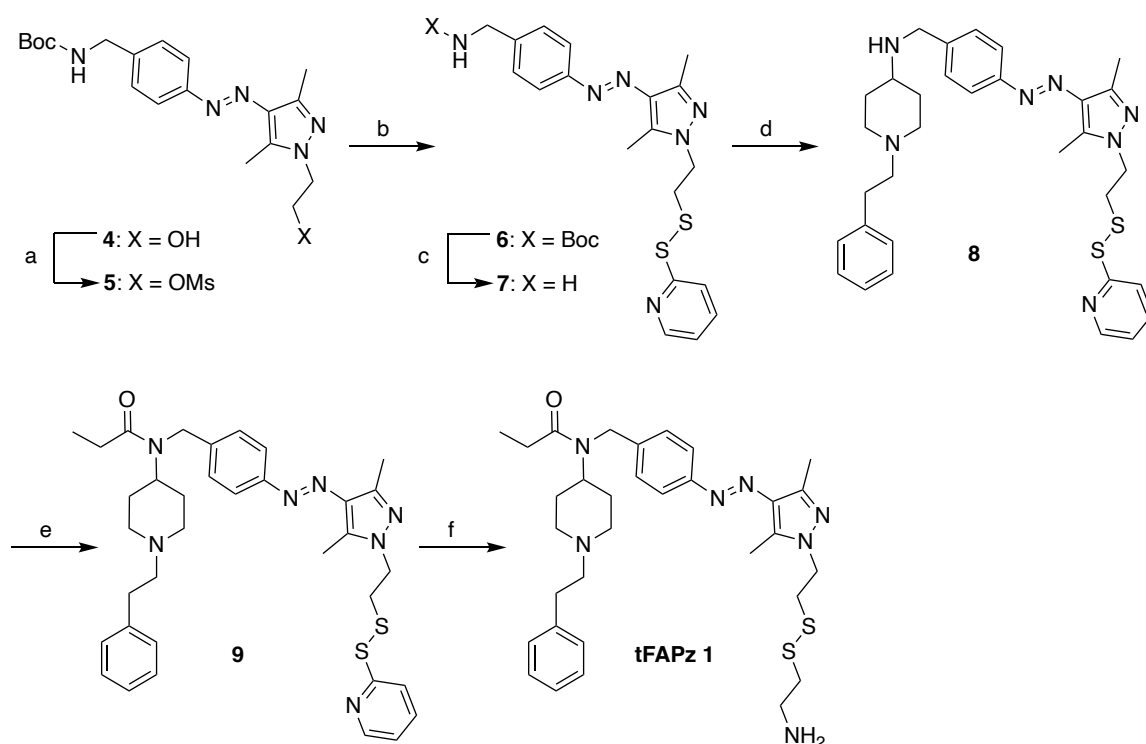
Following these strategies, a maleimide series was developed (**tFAPz 2a-g**) using different synthesis techniques for maleimide attachment to **FAPz 1**, including the well-known ‘click’ and ‘Staudinger’ reaction methods (Figure 14).^[17] Even though maleimides have been effectively used in bioconjugation, hydrolysis and other drawbacks provided incentive to synthesize additional PTLs with other reactive groups.^[16] The disulfide reactive group is highly selective for cysteine residues via disulfide exchange with free thiol groups. Despite susceptibility to reduction, disulfides have been proven valuable in bioconjugation for targeting GPCRs,^[18] as a result, a disulfide-containing PTL was designed (**tFAPz 1**). Similarly, isothiocyanate **tFAPz 3** was developed due to promising properties. Isothiocyanates have been shown to react with both sulfhydryl and amine nucleophiles, depending on pH, with a resistance towards water and alcohol-mediated hydrolysis.^[18] It should be mentioned that in previous literature, an isothiocyanate group was attached to the terminus of the phenethyl moiety of fentanyl to form a covalent ligand (FIT or further modifications to SUPERFIT).^[19] Despite possessing covalent properties, these ligands resulted in selectivity for δ OR instead of μ OR.

Further modifications were explored in other literature work in attempts to obtain a fentanyl-based ligand that covalently targets μ OR.^[20] This included the incorporation of a reactive acryloyl group to the benzeneacetamide unit of fentanyl, however, a covalent ligand did not result.^[20a] In 1990, an azido-containing photoaffinity derivative of carfentanil was developed that was successfully able to irreversibly label μ OR.^[20b] A drawback of this probe was the prolonged periods of 315 nm exposure that was required to activate the azide moiety, which may not be compatible with several biological assays.^[1a, 1b, 21] The desire to expand the repertoire of fentanyl-based covalent probes provided further incentive for the development of the proposed **tFAPz** ligands.

2.3.2 Synthesis of Fentanyl-based PTLs

The synthesis of **tFAPz** either required the development of individual synthetic routes (**tFAPz 1** and **tFAPz 2a**) or could be easily accessed from **FAPz 1** via a one-pot synthesis reaction (**tFAPz 2b-g** and **3**).

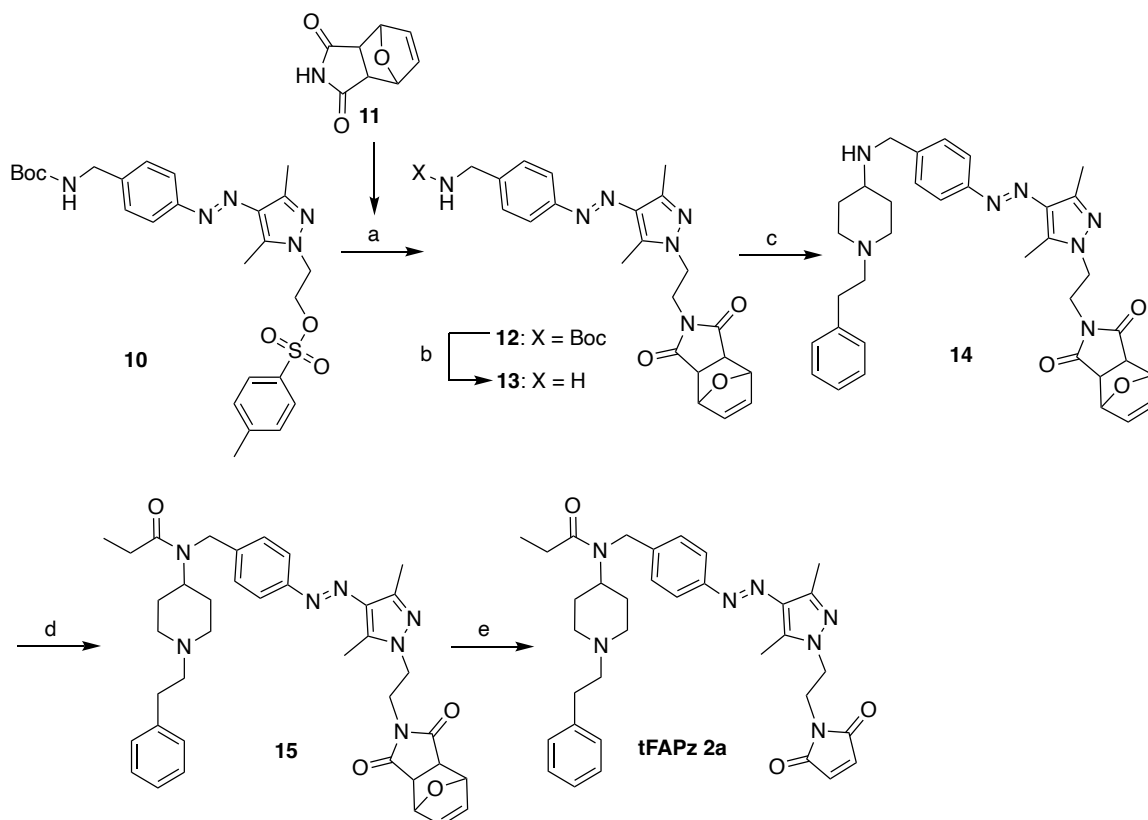
To obtain **tFAPz 1** (Scheme 6), arylazopyrazole **4** that was synthesized according to literature procedures^[9] was activated using methanesulfonyl chloride to form **5** in 97% yield. Nucleophilic substitution with potassium thioacetate resulted in a thioester, which was directly transformed to pyridyl disulfide **6** using AldrithiolTM-2 in an overall yield of 67%. Boc-deprotection with trifluoroacetic acid then afforded amine **7** in high yield. Subsequent reductive amination with 1-phenethyl-4-piperidone, afforded intermediate **8** in 88% yield, which was then acylated to obtain intermediate **9** in 95% yield. Treatment with cysteamine, following previous literature,^[22] afforded **tFAPz 1** in 95% yield.



Scheme 6. Synthesis of **tFAPz 1**. (a) MsCl, Et₃N, DCM, 0 °C → rt, 1 h, 97%; (b) KSAc, acetone, reflux, 3 h; and then, AldrithiolTM-2, NaOMe, MeOH, rt, 16 h, 67% (overall yield); (c) TFA, DCM, 0 °C → rt, 1 h, 95%; (d) 1-Phenethyl-4-piperidone, NaBH(OAc)₃, AcOH, DCE, argon., rt, 20 h, 88%; (e) Propionyl chloride, Et₃N, DCM, 10 min, rt, 95%; (f) Cysteamine hydrochloride, MeOH, argon, rt, 0.5 h, 95%.

Tethered Photoswitchable Derivatives of Fentanyl that Target the μ -Opioid Receptor

The synthesis of **tFAPz 2a** (Scheme 7) involved preparing precursors **10** and **11** via previously reported procedures.^[9, 23] Using these materials, nucleophilic substitution yielded intermediate **12** in 56% yield. Boc-deprotection with trifluoroacetic acid afforded amine **13** in quantitative yield. Reductive amination with 1-phenethyl-4-piperidone resulted in intermediate **14** in 61% yield. An acylation reaction then afforded intermediate **15** in 34% yield. The 2,5-dimethylfuran-protected maleimide was deprotected at 110 °C to afford **tFAPz 2a** in 51% yield.

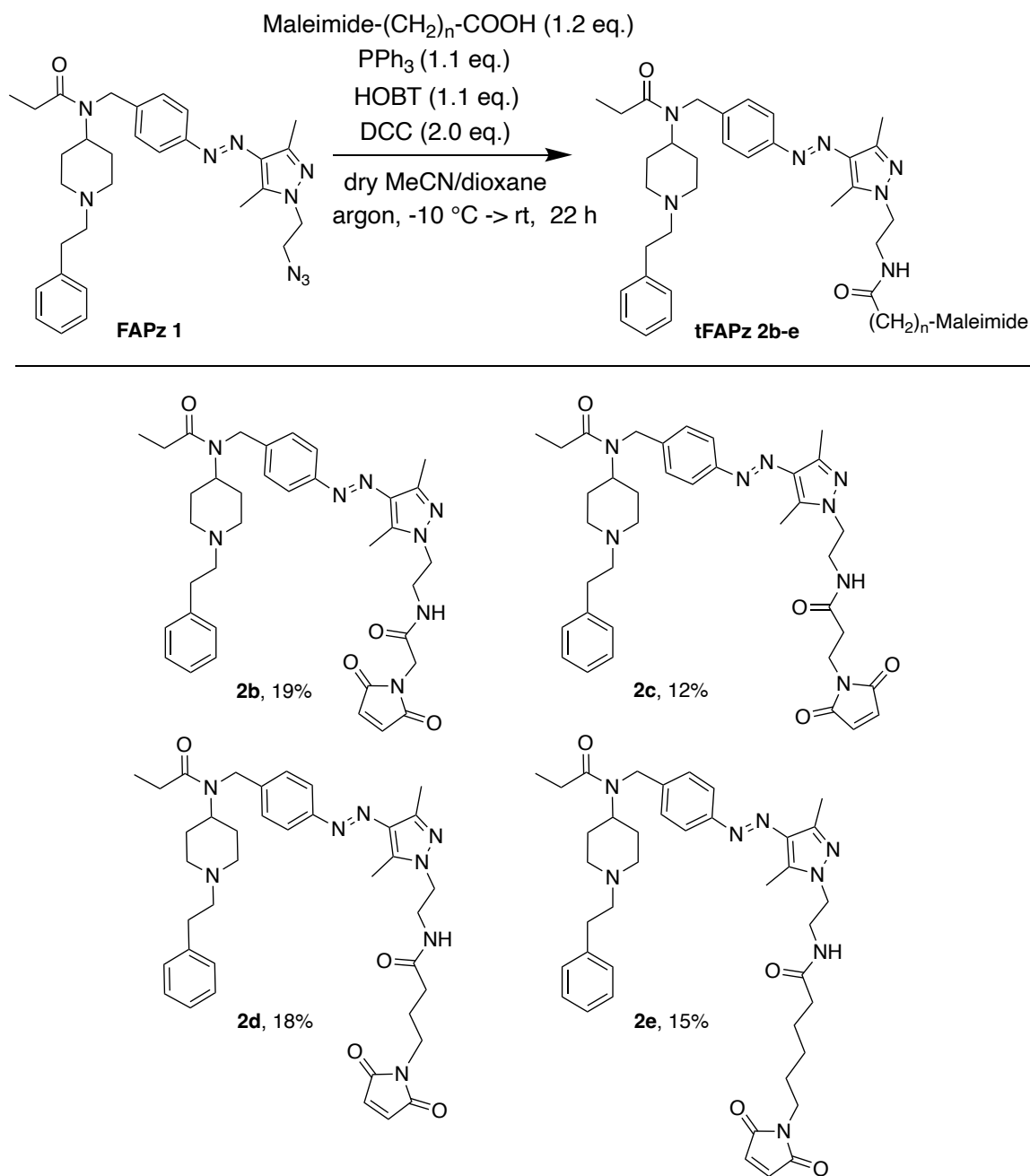


Scheme 7. Synthesis of **tFAPz 2a**. (a) K_2CO_3 , DMF, 50 °C, 3 h, 56%; (b) TFA, DCM, 0 °C \rightarrow rt, 1 h, 99%; (c) 1-Phenethyl-4-piperidone, $\text{NaBH}(\text{OAc})_3$, AcOH, DCE, rt, 16 h, 61%; (d) Propionyl chloride, Et_3N , DCM, N_2 , 24 h, rt, 34%; (e) DMSO (dried), 110 °C, 3 h, 51%.

For the synthesis of **tFAPz 2b-e**, an adapted Staudinger reaction was employed, using a previously reported procedure (Scheme 8).^[24] The classic Staudinger reaction involves the reaction of an azide with triphenylphosphine to form an iminophosphorane intermediate. This species has been shown in modified procedures to react with activated carboxylic acids or esters to form an amide bond, instead of hydrolyzing to an amine.^[17] In this adapted procedure, the carboxylic acid was first activated by HOBt. Activated esters were then reacted under dry conditions with the iminophosphorane intermediate of **FAPz 1**, using

Tethered Photoswitchable Derivatives of Fentanyl that Target the μ -Opioid Receptor

DCC as a coupling reagent, to form **tFAPz 2b**, **2c**, **2d** and **2e** in 19%, 12%, 18% and 15% yield, respectively.

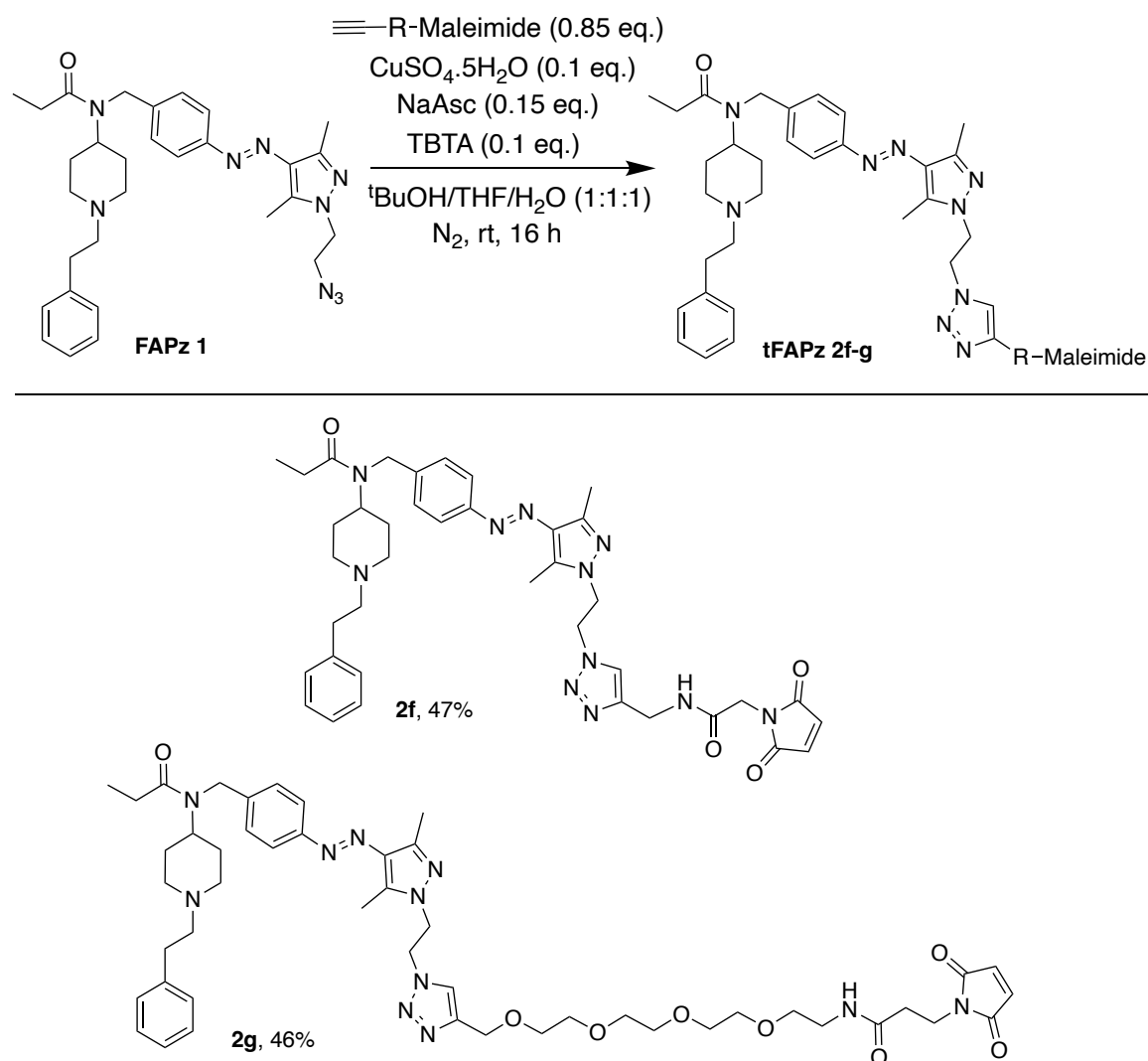


Scheme 8. Synthesis of **tFAPz 2b-2e** via an adapted Staudinger reaction. Yields of isolated products are shown. Please refer to Supplementary Information for detailed synthesis methods.

In order to improve synthesis yields, Cu(II)-assisted click chemistry was employed to generate additional maleimide-containing PTLs (Scheme 9). This was achieved using a similar method to that previously reported.^[25] Using this approach, the azide of **FAPz 1** was reacted

Tethered Photoswitchable Derivatives of Fentanyl that Target the μ -Opioid Receptor

with alkyne derivatives that contained a maleimide group to obtain **tFAPz 2f** and **2g**. The alkyne used to obtain **tFAPz 2f** was synthesized via the reaction of activated 2-maleimidoacetic acid with N-propargylamine (see Supplementary Information), while the alkyne used to obtain **tFAPz 2g** was commercially obtained. In this assisted cycloaddition reaction, sodium ascorbate was used as an initiating reagent and Cu(II) was chelated with TBTA, which yielded **tFAPz 2f** and **2g** in higher yields of 47% and 46%, respectively.

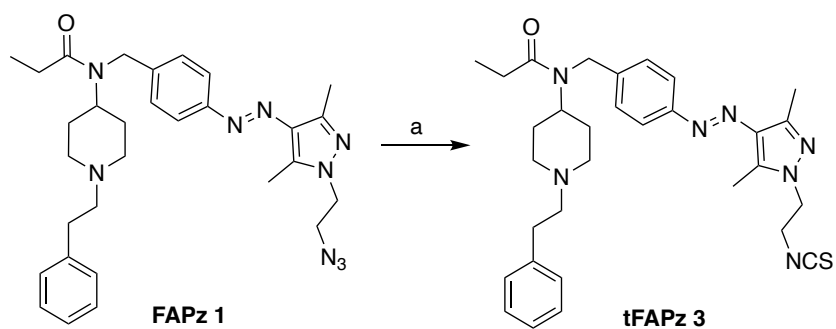


Scheme 9. Synthesis of **tFAPz 2f-2g** via Cu(II)-mediated click reaction. Yields of isolated products are shown. Please refer to Supplementary Information for detailed synthesis methods.

To obtain isothiocyanate **tFAPz 3** (Scheme 10), previously synthesized **FAPz 1** was directly subjected to a one-pot reaction that has been previously reported.^[26] This involved

Tethered Photoswitchable Derivatives of Fentanyl that Target the μ -Opioid Receptor

generating an iminophosphorane from the azide of **FAPz 1**, followed by a condensation reaction with carbon disulfide to afford **tFAPz 3** in 42% yield.



Scheme 10. Synthesis of **tFAPz 3**. (a) PPh₃, CS₂, dry THF, N₂, reflux, 16 h, 42%.

2.3.3 Photophysical Investigations of Fentanyl-based PTLs

Once these PTLs were synthesized, it was important to evaluate their photophysical properties. This involved obtaining UV/Vis absorption spectra of *trans*- and *cis*-isomers, as well as evaluating cycle performance and photostationary states (PSS) in DMSO and buffer solution (Table 5, Figure 15 and Supplementary Information). Further studies included thermal stability evaluations of the respective *cis*-isomers, with results shown in Table 5.

Table 5. Summary of experimental photophysical properties.^[a]

tFAPz	Solvent	PSS <i>cis</i> \rightarrow <i>trans</i> <i>trans:cis</i> ^[b]	PSS <i>trans</i> \rightarrow <i>cis</i> <i>trans:cis</i> ^[b]	t _{1/2} [days] ^[c] <i>cis</i> -isomer
1	DMSO	93:7	5:95	6.6
1	Buffer ^[d]	89:11	3:97	12.2
2a	DMSO	93:7	7:93	10.5
2a	Buffer ^[d]	87:13	22:78	15.2
2b	DMSO	95:5	15:85	7.1
2b	Buffer ^[d]	87:13	12:88	6.0
2c	DMSO	95:5	10:90	6.1
2c	Buffer ^[d]	89:11	10:90	4.3
2d	DMSO	96:4	31:69	4.8
2d	Buffer ^[d]	90:10	9:91	≥ 9.9
2e	DMSO	95:5	13:87	6.8
2e	Buffer ^[d]	89:11	9:91	≥ 6.9
2f	DMSO	94:6	4:96	9.1
2f	Buffer ^[d]	91:9	12:88	13.9
2g	DMSO	94:6	6:94	9.0
2g	Buffer ^[d]	92:8	10:90	20.9
3	DMSO	94:6	4:96	3.7
3	Buffer ^[d]	92:8	5:95	11.1

^[a]Isomerization was obtained by irradiation of 365 nm (*cis*-isomer) and 528 nm (*trans*-isomer) at 25 °C. ^[b]PSS was determined by HPLC measurements. ^[c]Thermal half-life measurements of respective *cis*-isomers, performed at 27 °C. ^[d]Buffer solution (TrisHCl Buffer, pH 7.5) + 0.2-1.5% DMSO, see Supplementary Information.

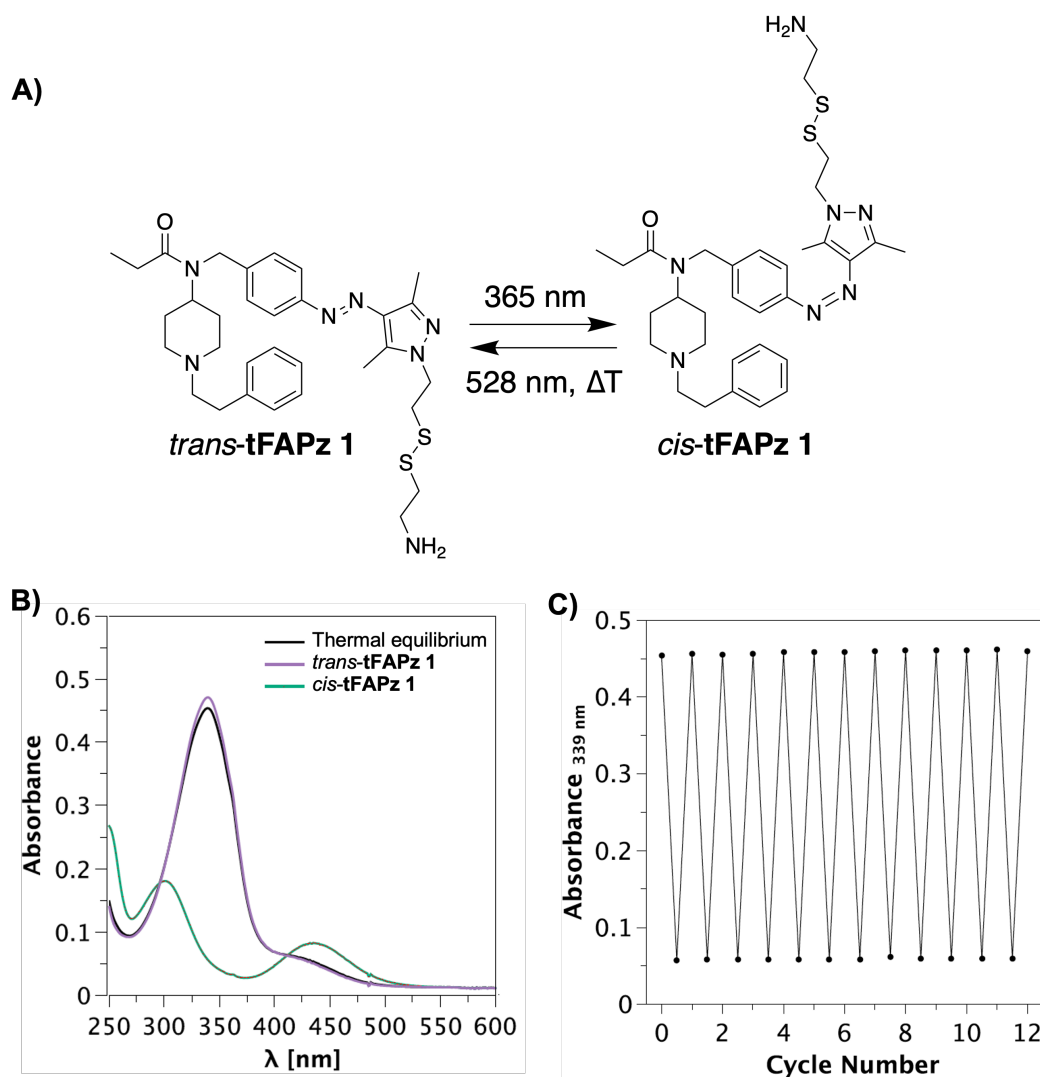


Figure 15. Photoinduced isomerization and cycle performance of **tFAPz 1**, shown as a representative compound. A) Depiction of geometrical changes that occur upon photoinduced isomerization of **tFAPz 1**. B) UV/Vis absorption spectra of thermal equilibrium, *trans*-isomer and *cis*-isomer. C) Cycle performance (12 cycles) of **tFAPz 1** upon alternating irradiation of 365 nm and 528 nm, recorded at the absorbance maximum of the *trans*-isomer (339 nm). Results are shown of **tFAPz 1** (20 μ M) in buffer solution (TrisHCl Buffer, pH 7.5) + 0.2% DMSO at 25 $^{\circ}$ C.

Overall, these ligands possessed desirable photophysical properties that were similar to that of the previously reported **FAPz 1**.^[9] Similar to **FAPz 1**, irradiation wavelengths of 365 nm could be used to obtain the *cis*-isomers of these **tFAPz** ligands, while a desirable red-shifted wavelength (528 nm) could be used to obtain the *trans*-isomers. In addition, **tFAPz** ligands displayed resistance towards cycle fatigue, as toggling between respective *cis*- and *trans*-isomers for each compound was achieved for at least 5 cycles in both DMSO and buffer solution (Figure 15 and Supplementary Information). As displayed in Table 5, the

Tethered Photoswitchable Derivatives of Fentanyl that Target the μ -Opioid Receptor

experimental PSS values suggested that upon irradiation with 365 nm, a greater abundance of *cis*-isomer could be obtained for each of the **tFAPz** derivatives, while a greater abundance of the respective *trans*-isomer could be obtained upon irradiation with 528 nm. In addition, these compounds exhibited *cis*-isomer thermal half-lives of at least 3 days in both DMSO and buffer solution (Table 5). Such long thermal half-lives allow for good photocontrol, as the abundance of either *cis*- or *trans*-isomer can be spatially and temporally modulated by irradiation with either 365 nm or 528 nm, respectively.

2.3.4 Biochemical Evaluation of Fentanyl-based PTLs

2.3.4.1 Ligand-mediated Activation and Binding Studies

Since the PTLs displayed desirable photophysical properties, it was next important to determine whether **tFAPz 1**, **2a-g** and **3** displayed a potency towards wild-type μ OR (μ OR_{wt}). These PTLs were subjected to a ligand-mediated μ OR activation screen at 10 μ M ligand concentration, using a G-protein activation assay (IP-One[®]).^[27] This assay measures agonist-stimulated accumulation of IP in HEK293T cells, which were transiently co-transfected with the receptor and the hybrid G-protein $G\alpha_{q5HA}$.^[27] Each PTL was irradiated prior to biological analysis with the appropriate wavelength in order to obtain either the respective *trans*- or *cis*-isomer, and were compared to the full agonist reference DAMGO. In this screen, **tFAPz 2a-g** and **3** displayed weak receptor activation (SI Table 7). After an IP accumulation period of 3h, both *cis*- and *trans*-isomers of **tFAPz 2b**, **2d** and **2f** displayed less than 31% μ OR_{wt} maximum receptor response, while both respective isomers of **tFAPz 2a**, **2c**, **2e**, **2g** and **3** displayed no significant μ OR activation. These poor activation profiles, especially when compared to fentanyl (100% response), may be due to suboptimal modifications to the pharmacophore or may be due to off-target interactions of the reactive tethering groups. In contrast to these derivatives, the disulfide-containing **tFAPz 1** displayed full agonist activity ($E_{max} = 100\%$) similar to the efficacy stimulated by fentanyl. As a result, **tFAPz 1** was identified as a lead compound in this work.

The use of disulfide-containing compounds to covalently bind to GPCRs have been proven successful in generating stable and functional GPCR-ligand complexes.^[18] Once such ligands diffuse via intrinsic affinity into the receptor binding pocket, a chemoselective disulfide exchange proceeds between the disulfide unit of the ligand and a nearby sulfhydryl group of a free cysteine residue.^[28] This highly selective reaction reduces the risk of off-target interactions with other nucleophilic amino acids and ultimately, would result in covalent binding to the target site. In order to ensure that **tFAPz 1** binds to an appropriate cysteine residue, a site-specific μ OR mutant (N127^{2.63}C, abbreviated as μ OR_{M1}) was established that contains a free cysteine residue in the μ OR binding pocket.^[7d,29]

Using this μ OR mutant, ligand-mediated activation and binding affinity of **tFAPz 1** to μ OR_{M1} were evaluated (Figure 16, Table 6). In order to determine ligand-mediated activation, full-dose response curves of both *trans*- and *cis*-isomers of **tFAPz 1** were generated using the IP-One[®] assay. In this study, both isomers of **tFAPz 1** behaved as full agonists with

Tethered Photoswitchable Derivatives of Fentanyl that Target the μ -Opioid Receptor

potencies of 480 nM (*trans*-isomer) and 810 nM (*cis*-isomer). Despite the reduction in potency when compared to fentanyl, both *trans*- and *cis*-isomers were still able to activate the receptor in a nM range, with approximately 2-fold higher activity found for *trans*-**tFAPz 1** than *cis*-**tFAPz 1**. Importantly, the previously published efficacy ligand **FAPz 1** possessed a lower potency than **tFAPz 1** in the same activation assay with wild-type μ OR (*trans*-**FAPz 1**: $EC_{50} = 4,700$ nM; *cis*-**FAPz 1**: $EC_{50} = 2,300$ nM; compare with fentanyl: $EC_{50} = 2.6$ nM).^[9] These results suggest that modification of **FAPz 1** to **tFAPz 1** by replacing the azide moiety with a disulfide unit may be better tolerated for receptor activation. Radioligand binding studies revealed competitive binding of **tFAPz 1** to μOR_{M1} , with K_i values of 42 nM and 80 nM obtained for its *trans*- and *cis*-isomers, respectively (Table 6). Similar to activation studies, *trans*-**tFAPz 1** displayed approximately 2-fold higher affinity for μOR_{M1} than *cis*-**tFAPz 1**. Furthermore, the former isomer displayed only a 3.8-fold attenuation in binding affinity when compared to fentanyl, which establishes the affinity of this ligand towards μOR_{M1} .

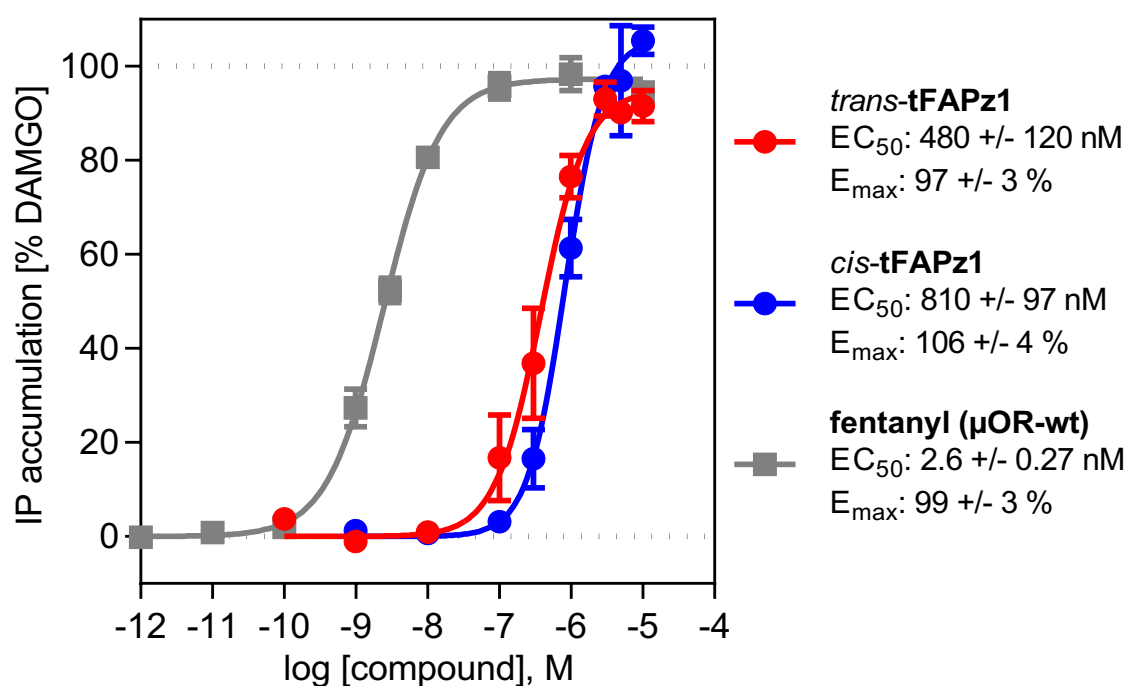


Figure 16. Activation of μ OR by **tFAPz 1** and fentanyl. G-protein-mediated receptor activation by *trans*-**tFAPz 1**, *cis*-**tFAPz 1** and fentanyl was measured by applying the IP-One[®] accumulation assay in HEK293T cells transiently co-transfected with μOR_{M1} or the wild-type μ OR (for fentanyl) and the hybrid G-protein $G\alpha_{qi5}HA$. Graphs show mean curves (\pm S.E.M.) of 4 (*cis*-**tFAPz 1**), 6 (*trans*-**tFAPz 1**) or 7 (fentanyl) individual experiments, each performed in duplicate.

Tethered Photoswitchable Derivatives of Fentanyl that Target the μ -Opioid Receptor

Table 6. Ligand-mediated activation and radioligand binding with μ ORM1.

Ligand-mediated activation^[a]				
Compound	EC ₅₀ [nM \pm S.E.M.]	EC ₅₀ ratio ^[b]	E _{max} [% \pm S.E.M.] ^[c]	(n) ^[d]
<i>trans</i> - tFAPz 1	480 \pm 120	1.7	97 \pm 3	6
<i>cis</i> - tFAPz 1	810 \pm 97	(<i>trans</i>)	106 \pm 4	4
Fentanyl ^[e]	2.6 \pm 0.27		99 \pm 3	7
Radioligand binding studies^[f]				
Compound	K _i [nM \pm S.E.M.]	K _i ratio ^[b]		(n) ^[g]
<i>trans</i> - tFAPz 1	42 \pm 10	1.9 (<i>trans</i>)		6
<i>cis</i> - tFAPz 1	80 \pm 28			6
Fentanyl ^[e]	11 \pm 1.8			7
<i>trans</i> - tFAPz 1 ^[e]	85 \pm 32	1.3 (<i>trans</i>)		4
<i>cis</i> - tFAPz 1 ^[e]	110 \pm 27			3

^[a]IP-One accumulation assay (Cisbio). ^[b]The isomer shown in brackets has a greater potency than its respective isomer. ^[c]Maximum receptor activation in % \pm S.E.M. relative to the full effect of DAMGO. ^[d]Number of individual experiments, each performed in duplicate. ^[e]Data is derived from experiments conducted with the μ OR wild-type receptor. ^[f]Binding data to μ OR_{M1} was determined by competition binding with [³H]diprenorphine. ^[g]Number of individual experiments, each performed in triplicate.

2.3.4.1 Biochemical Evaluation of Covalent Properties

Since **tFAPz 1** displayed significant affinity and activation profiles towards μ OR_{M1}, it was crucial to determine whether this lead PTL was able to covalently bind to μ OR_{M1}. Specific binding of [³H]diprenorphine was determined, according to previous procedures,^[28, 30] for membranes pre-treated with *trans*- or *cis*-**tFAPz 1**. Corresponding findings were compared to a control homogenate that was incubated with the reversible ligand naloxone or fentanyl. For membranes that were treated with **tFAPz 1**, the determined specific binding indicates the amount of blocked receptor binding sites by covalently bound ligand after washing and exposure to excess radioligand. In comparison to the control, both isomers of this newly synthesized PTL were able to covalently bind to μ OR_{M1} (Figure 17).

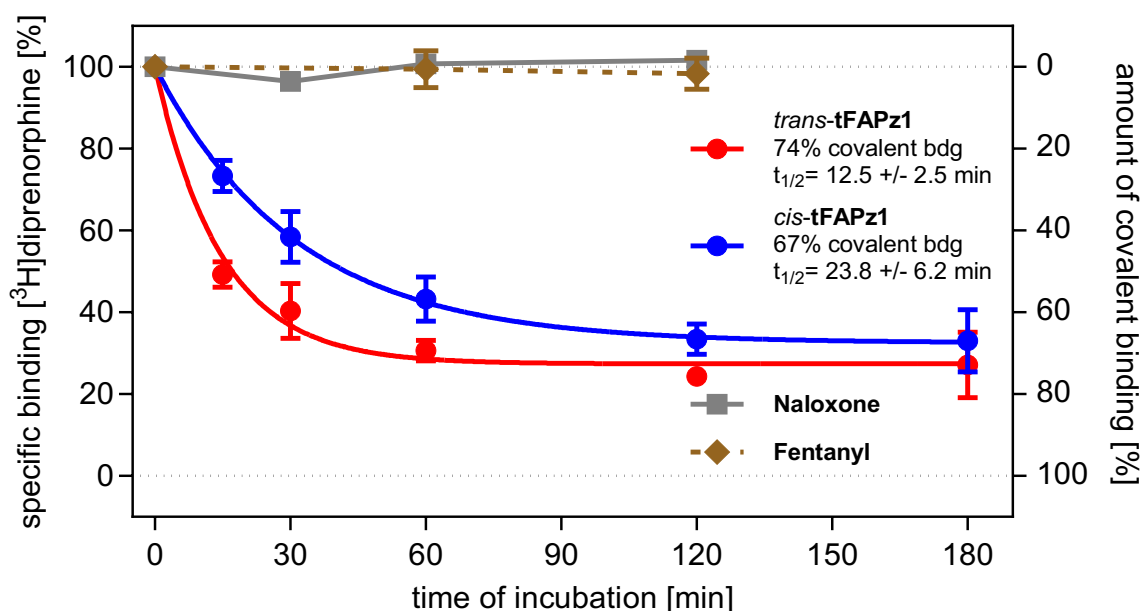


Figure 17. Covalent binding of **tFAPz 1**. Covalent binding was determined in a radioligand depletion assay, with membranes from μ OR_{M1}, expressing HEK293T cells and the radioligand [³H]diprenorphine. The PTL **tFAPz 1** displayed significant covalent binding, with a covalent binding maximum of $74 \pm 1\%$ by *trans*-**tFAPz 1** ($1 \mu\text{M}$) and $67 \pm 4\%$ by *cis*-**tFAPz 1** ($1 \mu\text{M}$), while the reversible control ligands naloxone ($0.1 \mu\text{M}$) and fentanyl ($0.1 \mu\text{M}$) displayed no covalent binding properties. Kinetic analysis of this covalent process revealed a 2-fold faster interaction of *trans*-**tFAPz 1** ($t_{1/2} = 12.5 \text{ min}$) with the orthosteric binding site, compared to *cis*-**tFAPz 1** ($t_{1/2} = 23.8 \text{ min}$). Graphs show mean curves (\pm S.E.M.) of 3 (for naloxone) or 6 (for **tFAPz 1** and for fentanyl) individual experiments, each performed in quadruplicate.

Tethered Photoswitchable Derivatives of Fentanyl that Target the μ -Opioid Receptor

After an incubation time of 45 min, *trans*-**tFAPz 1** was able to covalently bind to $74\pm 1\%$ of μOR_{M1} binding sites, as indicated by the curve shown in Figure 17. In contrast, *cis*-**tFAPz 1** was only able to covalently bind to $67\pm 4\%$ of μOR_{M1} binding sites after 120 min. The superiority of the *trans*-isomer over the *cis*-isomer was also reflected by the kinetics of covalent binding. While *cis*-**tFAPz 1** displayed covalent binding to the receptor with a half-life ($t_{1/2}$) of 23.8 min, a $t_{1/2}$ of 12.5 min was obtained for *trans*-**tFAPz 1**. This result indicates 2-fold faster kinetics for the latter isomer (Figure 17, SI Table 8). These findings were further validated by the observation that *trans*-**tFAPz 1** decreased specific binding by 51% after 15 min, while *cis*-**tFAPz 1** only decreased specific binding by 27% in the same amount of time. Since differences in covalent binding properties were observed between the isomers of **tFAPz 1**, it may be inferred that the differing geometry of each isomer was maintained upon diffusion into the receptor binding pocket and during the process of ligand-receptor complexing. These findings establish **tFAPz 1** as an attractive probe that can localize and covalently bind to μOR_{M1} .

2.4 Conclusion and Outlook

The work described herein focuses on the development of PTLs, modeled on the potent μ OR agonist fentanyl. Each newly synthesized ligand displayed ideal photophysical properties that were similar to that of the previously reported **FAPz 1**, including long thermal half-lives (in the hours range) and cycle performance resistance (for at least 5 cycles) in both buffer and DMSO systems.^[9] Furthermore, respective *cis*-isomers could be accessed with 365 nm irradiation and respective *trans*-isomers could be accessed using a desirable red-shifted wavelength of 528 nm. The lead disulfide-containing PTL **tFAPz 1** displayed full agonist properties in a metabotropic functional assay, with significant potencies towards μ OR_{M1} (*trans*-**tFAPz 1**: EC₅₀ = 480 nM; *cis*-**FAPz 1**: EC₅₀ = 810 nM). High binding affinities were further validated in a radioligand binding assay (*trans*-**tFAPz 1**: K_i = 42 nM; *cis*-**FAPz 1**: K_i = 80 nM). Notably, the *trans*-**tFAPz 1** displayed nearly 2-fold greater potency than its respective *cis*-isomer in both assays. Importantly, **tFAPz 1** was found to form covalent ligand-receptor complexes with μ OR_{M1}, with differences observed between isomers. Covalent binding of *trans*-**tFAPz 1** proceeded with a t_{1/2} of 12.5 min and a maximum of 74±1%. In contrast, covalent binding of *cis*-**tFAPz 1** proceeded at approximately half the rate (t_{1/2} = 23.8 min), with a maximum of 67±4%.

These findings not only establish **tFAPz 1** as a photoswitchable agonist that can form covalent ligand-receptor complexes in this system but demonstrate that the structural differences between isomers were maintained upon covalent interaction with μ OR_{M1}. Future work may consist of minor structural modifications to **tFAPz 1** in order to further enhance biological differences between isomers. For example, lower affinity PTLs may allow for more significant compound placement/displacement in/out of the receptor binding pocket upon photoisomerization.^[10e] Due to the high binding affinity of *trans*-**tFAPz 1** (K_i = 42 nM) and *cis*-**tFAPz 1** (K_i = 80 nM), structural modifications to slightly reduce affinity may be beneficial. Further work may also consist of exploring isomer activity differences of the ligand once in complex with the receptor, which could be best explored using different systems, including both metabotropic and ionotropic systems.^[8-9] As a result, the development and confirmation of **tFAPz 1** as a covalent and photoswitchable μ OR probe, provides a foundation to further expand and improve the repertoire of **tFAPz** ligands. Furthermore, this covalent probe may be beneficial in future biochemical investigations surrounding μ OR and fentanyl-based structure relations, with the added advantage of utilizing the photoswitchable properties of **tFAPz 1** when desired.

2.5 Acknowledgements

This work was supported by the Deutsche Forschungsgemeinschaft, RTG 1910, and a Minerva PhD Fellowship to RL.

2.6 References

- [1] a) W. A. Velema, W. Szymanski, B. L. Feringa, *J. Am. Chem. Soc.* **2014**, *136*, 2178-2191; b) M. M. Lerch, M. J. Hansen, G. M. van Dam, W. Szymanski, B. L. Feringa, *Angew. Chem. Int. Ed. Engl.* **2016**, *55*, 10978-10999; c) M. J. Fuchter, *J. Med. Chem.* **2020**, *63*, 11436-11447.
- [2] a) W. Szymański, J. M. Beierle, H. A. Kistemaker, W. A. Velema, B. L. Feringa, *Chem. Rev.* **2013**, *113*, 6114-6178; b) E. Sengupta, Y. Yan, X. Wang, K. Munechika, D. S. Ginger, *ACS Nano* **2014**, *8*, 2625-2631; c) N. Barbosa, L. Sagresti, G. Brancato, *Phys. Chem. Chem. Phys.* **2021**, *23*, 25170-25179.
- [3] a) M. Wijnmans, I. Josimovic, H. F. Vischer, R. Leurs, *Curr. Opin. Pharmacol.* **2022**, *63*, 102192; b) J. Morstein, G. Romano, B. E. Hetzler, A. Plante, C. Haake, J. Levitz, D. Trauner, *Angew. Chem. Int. Ed.* **2022**, *61*, e202117094; c) P. Donthamsetti, N. Winter, A. Hoagland, C. Stanley, M. Visel, S. Lammel, D. Trauner, E. Isacoff, *Nat. Commun.* **2021**, *12*, 4775; d) D. Prischich, A. M. J. Gomila, S. Milla-Navarro, G. Sangüesa, R. Diez-Alarcia, B. Preda, C. Matera, M. Battle, L. Ramírez, E. Giralto, J. Hernando, E. Guasch, J. J. Meana, P. de la Villa, P. Gorostiza, *Angew. Chem. Int. Ed. Engl.* **2021**, *60*, 3625-3631; e) D. Lachmann, R. Lahmy, B. König, *Eur. J. Org. Chem.* **2019**, *2019*, 5018-5024; f) X. Rovira, A. Traperero, S. Pittolo, C. Zussy, A. Faucherre, C. Jopling, J. Giraldo, J. P. Pin, P. Gorostiza, C. Goudet, A. Llebaria, *Cell Chem. Biol.* **2016**, *23*, 929-934.
- [4] A. S. Hauser, M. M. Attwood, M. Rask-Andersen, H. B. Schiöth, D. E. Gloriam, *Nat. Rev. Drug Discov.* **2017**, *16*, 829-842.
- [5] a) D. M. Rosenbaum, S. G. Rasmussen, B. K. Kobilka, *Nature* **2009**, *459*, 356-363; b) D. Hilger, M. Masureel, B. K. Kobilka, *Nat. Struct. Mol. Biol.* **2018**, *25*, 4-12.
- [6] a) A. D. Kaye, M. R. Jones, A. M. Kaye, J. G. Ripoll, V. Galan, B. D. Beakley, F. Calixto, J. L. Bolden, R. D. Urman, L. Manchikanti, *Pain Physician* **2017**, *20*, S93-s109; b) T. Y. Lim, E. J. Stringfellow, C. A. Stafford, C. DiGennaro, J. B. Homer, W. Wakeland, S. L. Eggers, R. Kazemi, L. Glos, E. G. Ewing, C. B. Bannister, K. Humphreys, D. C. Throckmorton, M. S. Jalali, *Proc. Natl. Acad. Sci. U. S. A.* **2022**, *119*, e2115714119.
- [7] a) Q. Qu, W. Huang, D. Aydin, J. M. Paggi, A. B. Seven, H. Wang, S. Chakraborty, T. Che, J. F. DiBerto, M. J. Robertson, A. Inoue, C.-M. Suomivuori, B. L. Roth, S. Majumdar, R. O. Dror, B. K. Kobilka, G. Skiniotis, *Nat. Chem. Biol.* **2023**, *19*, 423-430; b) P. Mahinthichaichan, Q. N. Vo, C. R. Ellis, J. Shen, *JACS Au* **2021**, *1*, 2208-2215; c) R. J. Valentino, N. D. Volkow, *Neuropsychopharmacology* **2018**, *43*, 2514-2520; d) A. Manglik, H. Lin, D. K. Aryal, J. D. McCorvy, D. Dengler, G. Corder, A. Levit, R. C. Kling, V. Bernat, H. Hübner, X. P. Huang, M. F. Sassano, P. M. Giguère, S. Löber, D. Da, G. Scherrer, B. K. Kobilka, P. Gmeiner, B. L. Roth, B. K. Shoichet, *Nature* **2016**, *537*, 185-190; e) W. Huang, A. Manglik, A. J. Venkatakrisnan, T. Laeremans, E. N. Feinberg, A. L. Sanborn, H. E. Kato, K. E. Livingston, T. S. Thorsen, R. C. Kling, S. Granier, P. Gmeiner, S. M. Husbands, J. R. Traynor, W. I. Weis, J. Steyaert, R. O. Dror, B. K. Kobilka, *Nature* **2015**, *524*, 315-321; f) G. W. Pasternak, Y. X. Pan, *Pharmacol. Rev.* **2013**, *65*, 1257-1317.
- [8] M. Schönberger, D. Trauner, *Angew. Chem. Int. Ed. Engl.* **2014**, *53*, 3264-3267.
- [9] R. Lahmy, H. Hübner, M. F. Schmidt, D. Lachmann, P. Gmeiner, B. König, *Chem. Eur. J.* **2022**, *28*, e202201515.
- [10] a) W.-C. Lin, M.-C. Tsai, R. Rajappa, R. H. Kramer, *J. Am. Chem. Soc.* **2018**, *140*, 7445-7448; b) A. Acosta-Ruiz, V. A. Gutzeit, M. J. Skelly, S. Meadows, J. Lee, P. Parekh, A. G. Orr, C. Liston, K. E. Pleil, J. Broichhagen, J. Levitz, *Neuron* **2020**, *105*, 446-463.e413; c) J. Levitz, J. Broichhagen, P. Leippe, D. Konrad, D. Trauner, E. Y. Isacoff, *Proc. Natl. Acad. Sci. U. S. A.* **2017**, *114*, E3546-E3554; d) P. C. Donthamsetti, N.

Tethered Photoswitchable Derivatives of Fentanyl that Target the μ -Opioid Receptor

- Winter, M. Schönberger, J. Levitz, C. Stanley, J. A. Javitch, E. Y. Isacoff, D. Trauner, *J. Am. Chem. Soc.* **2017**, *139*, 18522-18535; e) J. Broichhagen, D. Trauner, *Curr. Opin. Chem. Biol.* **2014**, *21*, 121-127; f) P. Gorostiza, M. Volgraf, R. Numano, S. Szobota, D. Trauner, E. Y. Isacoff, *Proc. Natl. Acad. Sci. U. S. A.* **2007**, *104*, 10865-10870.
- [11] M. A. Kienzler, E. Y. Isacoff, *Curr. Opin. Neurobiol.* **2017**, *45*, 202-209.
- [12] M. Izquierdo-Serra, A. Bautista-Barrufet, A. Trapero, A. Garrido-Charles, A. Díaz-Tahoces, N. Camarero, S. Pittolo, S. Valbuena, A. Pérez-Jiménez, M. Gay, A. García-Moll, C. Rodríguez-Esrich, J. Lerma, P. de la Villa, E. Fernández, M. Pericàs, A. Llebaria, P. Gorostiza, *Nat. Commun.* **2016**, *7*, 12221.
- [13] a) P. Leippe, J. Koehler Leman, D. Trauner, *Biochemistry* **2017**, *56*, 5214-5220; b) A. Acosta-Ruiz, J. Broichhagen, J. Levitz, *Methods Mol. Biol.* **2019**, *1947*, 103-136.
- [14] N. Stephanopoulos, M. B. Francis, *Nat. Chem. Biol.* **2011**, *7*, 876-884.
- [15] C. J. Pickens, S. N. Johnson, M. M. Pressnall, M. A. Leon, C. J. Berkland, *Bioconjug. Chem.* **2018**, *29*, 686-701.
- [16] C. Sornay, V. Vaur, A. Wagner, G. Chaubet, *R. Soc. Open Sci.* **2022**, *9*, 211563.
- [17] R. E. Bird, S. A. Lemmel, X. Yu, Q. A. Zhou, *Bioconjug. Chem.* **2021**, *32*, 2457-2479.
- [18] D. Weichert, P. Gmeiner, *ACS Chem. Biol.* **2015**, *10*, 1376-1386.
- [19] a) K. C. Rice, A. E. Jacobson, T. R. Burke, Jr., B. S. Bajwa, R. A. Streaty, W. A. Klee, *Science* **1983**, *220*, 314-316; b) T. R. Burke, Jr., A. E. Jacobson, K. C. Rice, J. V. Silverton, W. F. Simonds, R. A. Streaty, W. A. Klee, *J. Med. Chem.* **1986**, *29*, 1087-1093.
- [20] a) I. Ujváry, R. Jorge, R. Christie, T. Le Ruez, H. V. Danielsson, R. Kronstrand, S. Elliott, A. Gallegos, R. Sedefov, M. Evans-Brown, *Forensic Toxicol.* **2017**, *35*, 232-243; b) J. L. Galzi, A. Mejean, M. Goeldner, C. Hirth, B. Ilien, *Eur J Pharmacol* **1990**, *188*, 321-328; c) J. L. Galzi, A. Mejean, B. Ilien, C. Mollereau, J. C. Meunier, M. Goeldner, C. Hirth, *J. Med. Chem.* **1990**, *33*, 2456-2464.
- [21] D. Y. Wong, T. Ranganath, A. M. Kasko, *PLoS One* **2015**, *10*, e0139307.
- [22] D. M. Rosenbaum, C. Zhang, J. A. Lyons, R. Holl, D. Aragao, D. H. Arlow, S. G. Rasmussen, H. J. Choi, B. T. Devree, R. K. Sunahara, P. S. Chae, S. H. Gellman, R. O. Dror, D. E. Shaw, W. I. Weis, M. Caffrey, P. Gmeiner, B. K. Kobilka, *Nature* **2011**, *469*, 236-240.
- [23] J.-Y. Wu, C.-D. Kuo, C.-Y. Chu, M.-S. Chen, J.-H. Lin, Y.-J. Chen, H.-F. Liao, *Molecules* **2014**, *19*, 6911-6928.
- [24] I. Kosiova, A. Janicova, P. Kois, *Beilstein J. Org. Chem.* **2006**, *2*, 23.
- [25] A. Banerjee, S. Maschauer, H. Hübner, P. Gmeiner, O. Prante, *Bioorganic Med. Chem. Lett.* **2013**, *23*, 6079-6082.
- [26] S. Gosling, C. E. Amri, A. Tatibouët, *Synthesis* **2014**, *46*, 1079-1084.
- [27] a) H. Liu, J. Hofmann, I. Fish, B. Schaake, K. Eitel, A. Bartuschat, J. Kaindl, H. Rampp, A. Banerjee, H. Hübner, M. J. Clark, S. G. Vincent, J. T. Fisher, M. R. Heinrich, K. Hirata, X. Liu, R. K. Sunahara, B. K. Shoichet, B. K. Kobilka, P. Gmeiner, *Proc. Natl. Acad. Sci. U. S. A.* **2018**, *115*, 12046-12050; b) C. Gentzsch, K. Seier, A. Drakopoulos, M.-L. Jobin, Y. Lanoiselée, Z. Koszegi, D. Maurel, R. Sounier, H. Hübner, P. Gmeiner, S. Granier, D. Calebiro, M. Decker, *Angew. Chem. Int. Ed. Engl.* **2020**, *59*, 5958-5964.
- [28] D. Weichert, A. C. Kruse, A. Manglik, C. Hiller, C. Zhang, H. Hübner, B. K. Kobilka, P. Gmeiner, *Proc. Natl. Acad. Sci. U. S. A.* **2014**, *111*, 10744-10748.
- [29] a) J. Einsiedel, M. F. Schmidt, H. Hübner, P. Gmeiner, *Bioorg. Med. Chem.* **2022**, *61*, 116720; b) T. Schwalbe, H. Hübner, P. Gmeiner, *Bioorg. Med. Chem.* **2019**, *27*, 2959-2971; c) T. Schwalbe, J. Kaindl, H. Hübner, P. Gmeiner, *Bioorg. Med. Chem.* **2017**, *25*, 5084-5094.
- [30] R. C. Kling, M. Plomer, C. Lang, A. Banerjee, H. Hübner, P. Gmeiner, *ACS Chem. Biol.* **2016**, *11*, 869-875.

2.7 Supplementary Information

2.7.1 Supplementary Chemical Information

2.7.1.1 Materials and Methods

Commercial reagents were obtained from Merck, Sigma-Aldrich, TCI Deutschland GmbH, ABCR GmbH or Fluorochem, and were used without further purification. Solvents were used in P.A. quality and if necessary, dried according to common procedures. Anhydrous reactions were performed using dried glassware under a nitrogen or argon atmosphere, unless otherwise specified. Technical grade solvents were used for column chromatography without further purification. Flash chromatography was performed using Biotage Isolera One System for normal phase chromatography, using Davisil Chromatographic Silica Media 60 Å (particle size 40-63 μ M, Merck). For reversed phase chromatography, Biotage SNAP Cartridges KP-C18-HS were used. Analytical thin layer chromatography (TLC) was performed on silica gel 60 F-254 with a 0.2 mm layer and aluminium-backed plates (Merck). Visualization was obtained by fluorescence quenching under UV light (short and long wave) and/or by staining the plate with potassium permanganate stain (60 mM KMnO_4 , 480 mM K_2CO_3 and 5% w/v NaOH) and vanillin- H_2SO_4 solution (0.5 g vanillin, 85 mL ethanol, 10 mL conc. acetic acid, 3 mL conc. H_2SO_4). Preparative high-performance liquid chromatography (HPLC) was performed using Agilent 1100 Series with a Phenomenex Luna 10 μ M C18 column (100 Å, 250 x 21.2 mm) and a solvent flow rate of 20 mL/min, with solvents and gradients specified in the respective synthesis procedures. All biologically tested compounds possessed a purity of $\geq 90\%$, which was determined by analytical HPLC with wavelength detections of 220 nm and 254 nm. Analytic HPLC measurements were performed using Agilent 1220 Infinity LC System (column: Phenomenex Luna, 3 μ M C18(2), 100 Å 150 x 2.00 mm), with a flow rate of 0.3 mL/min at 20 °C. For these measurements (solvent A: Milli-Q water with 0.05 wt% TFA; solvent B: MeCN), a solvent gradient of 10-98% B (0-20 min) and then 98% B (20-40 min) was utilized. NMR spectra were recorded on a Bruker Avance III HD 600 (^1H 600.25 MHz, ^{13}C 150.95 MHz, T = 300K), with solvents specified. The chemical shifts were reported as δ values in parts per million (ppm), referenced to the appropriate and specified solvent peak. Resonance multiplicity is abbreviated as: 's' (singlet), 'd' (doublet), 't' (triplet), 'q' (quartet) and 'm' (multiplet). J-coupling constants (J) were recorded in Hz. Mass spectra were recorded

Tethered Photoswitchable Derivatives of Fentanyl that Target the μ -Opioid Receptor

using Finnigan MAT-SSQ 710 A, ThermoQuest Finnigan TSQ 7000, Agilent 6540 UHD Q-TOF, or a JeolAccuTOF GCX instrument.

2.7.1.2 Chemistry Synthesis Procedures

Compound **FAPz 1**^[1], **4**^[1], **10**^[1] and **11**^[2] were synthesized according to literature procedures.

General Procedure 1: Deprotection of the Boc-protecting group

Boc-protected amine (1.0 eq.) was dissolved in DCM (10 mL/mmol) and cooled to 0 °C. To the cooled reaction mixture, TFA (1 mL/mmol) was added dropwise. After 1 h of stirring at room temperature, the reaction was quenched with 2M NaOH (10 mL/mmol) and then extracted with DCM. The combined organic layers were dried with Na₂SO₄ and filtered. The solvent was then removed *in vacuo* to afford the desired product.

General Procedure 2: Adapted Staudinger Reaction^[3]

Step 1: Previously synthesized azide **FAPz 1** (1.0 eq.) was dissolved in dry MeCN (50 mL/mmol), and PPh₃ (1.1 eq.) was added. The reaction mixture was stirred at room temperature under Ar atmosphere for 6 h and then used immediately in Step 3.

Step 2: Separately, respective carboxylic acid (1.2 eq.) was dissolved in dry THF (50 mL/mmol). Afterwards, HOBt (1.1 eq.) and DCC (2.0 eq.) were then added. The reaction mixture was stirred at room temperature for 2 h. The mixture was then diluted with dry MeCN (50 mL/mmol) and cooled to -10 °C.

Step 3: The mixture from Step 1 was added dropwise to the cooled mixture from Step 2 under Ar atmosphere. The resulting mixture was then allowed to warm to room temperature. After 16 h of stirring, the crude material was directly purified by preparative HPLC (solvent A: H₂O [0.05 Vol% TFA]; solvent B: MeCN; gradient: 10-98% B from 0-20 min, and then 98% B from 20-25 min) to obtain the desired product.

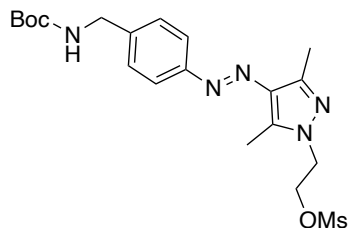
Tethered Photoswitchable Derivatives of Fentanyl that Target the μ -Opioid Receptor

General Procedure 3: Cu(II)-Mediated Click Reaction

To a solution of *t*BuOH/H₂O/THF (1:1:1; 100 mL/mmol), the respective alkyne (1.0 eq.) and previously synthesized azide **FAPz 1** (1.15 eq.) were added under N₂ atmosphere. After stirring for 5 minutes at room temperature, CuSO₄·5H₂O (0.1 eq.), TBTA (0.1 eq.), (+)-sodium-L-ascorbate (0.15 eq.) were then added. The reaction was allowed to stir for 16 h at room temperature, and afterwards, the solvent was removed *in vacuo*. The crude product was purified by preparative HPLC (solvent A: H₂O [0.05 Vol% TFA]; solvent B: MeCN; gradient: 10-98% B from 0-20 min, and then 98% B from 20-25 min) to obtain the desired product.

Tethered Photoswitchable Derivatives of Fentanyl that Target the μ -Opioid Receptor

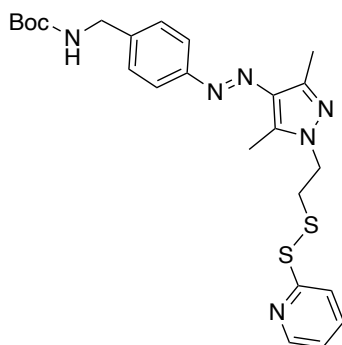
(E)-2-(4-((4-(((*tert*-butoxycarbonyl)amino)methyl)phenyl)diazenyl)-3,5-dimethyl-1H-pyrazol-1-yl)ethyl methanesulfonate (5)



A solution of previously synthesized **4** (4.0 g, 11.0 mmol, 1.0 eq.) in DCM (150 mL) was cooled to 0 °C and allowed to stir. Afterwards, Et₃N (2.2 mL, 16.5 mmol, 1.5 eq.) and methanesulfonyl chloride (2.20 mL, 11.1 mmol, 1.05 eq.) were added. While stirring, the mixture was then allowed to warm to room temperature over 1 h. Water (100 mL) was then added and the aqueous layer was extracted with DCM (2 x 100 mL). The combined organic layers were dried with Na₂SO₄, filtered and the solvent removed *in vacuo* to obtain compound **5** as a yellow oil (4.80 g, 10.6 mmol, 97%). ¹H-NMR (400 MHz, CDCl₃): δ (ppm) = 7.74 (d, J = 8.4 Hz, 2H), 7.37 (d, J = 8.3 Hz, 2H), 4.63 (t, J = 5.2 Hz, 2H), 4.37-4.34 (m, 4H), 2.87 (s, 3H), 2.62 (s, 3H), 2.49 (s, 3H), 1.47 (s, 9H). ¹³C-NMR (101 MHz, CDCl₃): δ = 162.7, 156.0, 152.9, 143.5, 140.4, 135.3, 128.1, 122.2, 79.8, 67.8, 47.8, 44.5, 37.4, 28.6, 14.2, 9.9. ESI-MS (m/z): [M+H]⁺ found: 452.20.

Tethered Photoswitchable Derivatives of Fentanyl that Target the μ -Opioid Receptor

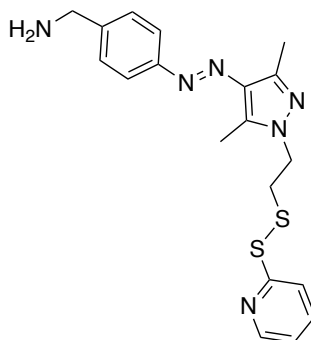
tert-butyl (*E*)-4-((3,5-dimethyl-1-(2-(pyridin-2-yl)disulfaneyl)ethyl)-1*H*-pyrazol-4-yl)diazenyl)benzyl)carbamate (**6**)



Potassium thioacetate (0.51 g, 3.79 mmol, 2.0 eq.) was added to a stirred mixture of compound **5** (1.0 g, 1.89 mmol, 1.0 eq) in acetone (80.0 mL). The mixture was refluxed for 3 h and subsequently cooled to room temperature. The solvent was removed under reduced pressure and the residue was dissolved in H₂O and extracted with EtOAc (3 x 80.0 mL). The combined organic layers were dried with Na₂SO₄, filtered and the solvent removed *in vacuo* to obtain the intermediate thioester as an orange solid. This intermediate was then dissolved in a 0.5 M NaOMe solution in MeOH under Ar atmosphere. To this, Aldrithiol™-2 (0.46 g, 2.08 mmol, 1.1 eq) was added and the mixture was stirred for 16 h at room temperature. The solvent was removed *in vacuo* and the crude product subjected to automated flash column chromatography, eluting at 5% EtOAc/PE to 80% EtOAc/PE to afford **6** as a yellow oil (0.63 g, 1.26 mmol, 67%). ¹H-NMR (400 MHz, CDCl₃): δ (ppm) = 8.50-8.48 (m, 1H), 7.73 (d, *J* = 8.4, 2H), 7.65 (d, *J* = 1.4, 2H), 7.36 (d, *J* = 8.3, 2H), 7.13-7.10 (m, 1H), 4.37 (m, 4H), 3.26 (t, *J* = 6.8, 2H), 2.58 (s, 3H), 2.48 (s, 3H), 1.66 (br s, 2H), 1.47 (s, 9H). ¹³C-NMR (101 MHz, CDCl₃): δ = 159.3, 153.1, 150.0, 143.2, 137.3, 135.2, 128.1, 122.2, 121.2, 120.3, 79.8, 47.3, 44.6, 37.7, 28.6, 14.2, 10.1. ESI-MS (*m/z*): [*M*+H]⁺ found: 499.19.

Tethered Photoswitchable Derivatives of Fentanyl that Target the μ -Opioid Receptor

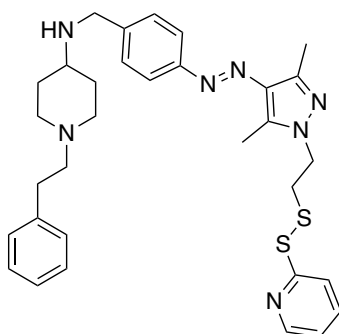
(*E*)-(4-((3,5-dimethyl-1-(2-(pyridin-2-yl)disulfaneyl)ethyl)-1*H*-pyrazol-4-yl)diazenyl)phenyl) methanamine (**7**)



General Procedure 1 was followed, using intermediate **6** (0.60 g, 1.20 mmol) to obtain **7** as yellow crystals (455 mg, 1.14 mmol, 95%). $^1\text{H-NMR}$ (400 MHz, CDCl_3): δ = 8.47 (d, J = 4.9, 1H), 7.68-7.66 (m, 4H), 7.37 (d, J = 8.4, 2H), 7.17-7.14 (m, 1H), 4.33 (t, J = 6.6, 2H), 3.93 (s, 2H), 3.21 (t, J = 6.6, 2H), 2.50 (s, 3H), 2.39 (s, 3H). $^{13}\text{C-NMR}$ (101 MHz, CDCl_3): δ = 158.8, 153.8, 149.1, 143.3, 140.4, 138.3, 135.0, 133.4, 129.9, 122.5, 121.7, 121.0, 77.4, 47.1, 43.5, 37.7, 13.9, 10.0. ESI-MS (m/z): $[M+H]^+$ found: 399.14.

Tethered Photoswitchable Derivatives of Fentanyl that Target the μ -Opioid Receptor

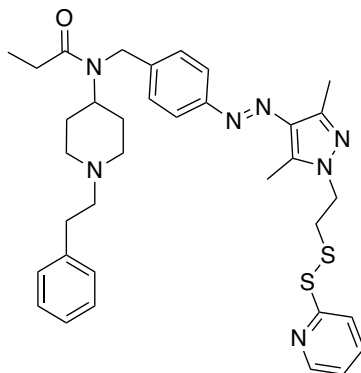
(*E*)-*N*-(4-((3,5-dimethyl-1-(2-(pyridin-2-yl)disulfaneyl)ethyl)-1*H*-pyrazol-4-yl)diazenyl)benzyl)-1-phenethylpiperidin-4-amine (**8**)



To a solution of commercially available 1-phenethyl-4-piperidone (162 mg, 1.0 mmol, 1.0 eq.) in dichloroethane (40 mL), was added sequentially compound **7** (400 mg, 1.0 mmol, 1.0 eq.), $\text{NaBH}(\text{OAc})_3$ (391 mg, 1.4 mmol, 1.4 eq.) and AcOH (0.08 mL, 1.4 mmol, 1.0 eq) under Ar atmosphere. The bright orange reaction mixture was stirred overnight at room temperature. After 20 h, the reaction mixture was diluted with EtOAc (100 mL), washed with 1M NaOH (50 mL), followed by aqueous sat. NaHCO_3 (50 mL) and then aqueous sat. NaCl solution (50 mL). The combined organic layers were dried with Na_2SO_4 , filtered and concentrated *in vacuo*. The crude product was subjected to automated flash column chromatography, eluting at 100% DCM to 10% MeOH/DCM to obtain **8** as an orange oil (342 mg, 0.58 mmol, 88%). $^1\text{H-NMR}$ (400 MHz, CDCl_3): δ (ppm) = 8.48 (dt, $J = 4.7, 1.4$, 1H), 7.73 (d, $J = 8.3$, 2H), 7.62-7.60 (m, 2H), 7.41 (d, $J = 8.3$, 2H), 7.27-7.24 (m, 2H), 7.18-7.17 (m, 3H), 7.10 (m, 1H), 4.34 (t, $J = 6.8$, 2H), 3.86 (s, 2H), 3.23 (t, $J = 6.8$, 2H), 2.99-2.96 (m, 2H), 2.82-2.78 (m, 2H), 2.61-2.58 (m, 3H), 2.56 (s, 3H), 2.47 (s, 3H), 2.13-2.07 (m, 2H), 1.97-1.94 (m, 2H), 1.57-1.47 (m, 2H). $^{13}\text{C-NMR}$ (101 MHz, CDCl_3): $\delta = 159.2, 152.8, 149.9, 143.0, 141.6, 140.2, 139.4, 137.2, 135.0, 128.7, 128.4, 126.1, 121.9, 121.1, 120.1, 77.36, 60.4, 53.8, 52.2, 50.3, 47.2, 37.6, 33.6, 32.2, 14.1, 9.9$. ESI-MS (m/z): $[M+H]^+$ found: 586.28.

Tethered Photoswitchable Derivatives of Fentanyl that Target the μ -Opioid Receptor

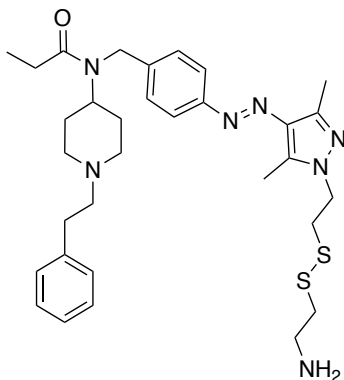
(*E*)-*N*-(4-((3,5-dimethyl-1-(2-(pyridin-2-yl)disulfaneyl)ethyl)-1*H*-pyrazol-4-yl)diazenyl)benzyl)-*N*-(1-phenethylpiperidin-4-yl)propionamide (**9**)



Compound **8** (200 mg, 0.34 mmol, 1.0 eq) was dissolved in DCM and propionylchloride (40 μ L, 0.41 mmol, 1.2 eq) and Et₃N (240 μ L, 1.71 mmol, 5.0 eq) were added at room temperature. The mixture was then allowed to stir for 10 min. The reaction was quenched by H₂O and extracted with DCM (3 x 50 mL). The combined organic layers were dried with Na₂SO₄, filtered and concentrated *in vacuo*. The crude product was purified by automated reverse phase column chromatography (H₂O + 0.05% TFA/MeCN, 10-98% MeCN) to obtain **9** as a yellow powder (208 mg, 0.32 mmol, 95%). ¹H-NMR (400 MHz, MeOD): δ (ppm) = 8.41 (d, *J* = 4.8 Hz, 1H), 7.81-7.78 (m, 3H), 7.73-7.69 (m, 1H), 7.40-7.31 (m, 5H), 7.27-7.24 (m, 3H), 4.70 (s, 2H), 4.50-4.45 (m, 1H), 4.41 (t, *J* = 6.4 Hz, 2H), 3.67 (d, *J* = 11.4 Hz, 2H), 3.19-2.99 (m, 6H), 2.68-2.62 (m, 5H), 2.45-2.43 (m, 5H), 2.19-2.13 (m, 2H), 1.99-1.96 (m, 2H), 1.15-1.12 (m, 3H). ¹³C-NMR (101 MHz, MeOD): δ = 177.2, 154.4, 150.4, 143.7, 141.6, 140.7, 139.4, 137.4, 136.0, 130.0, 129.8, 128.4, 128.0, 123.3, 122.7, 121.6, 59.0, 53.5, 39.1, 31.4, 28.0, 14.1, 9.9, 9.8. ESI-MS (*m/z*): [*M*+H]⁺ found: 642.31.

Tethered Photoswitchable Derivatives of Fentanyl that Target the μ -Opioid Receptor

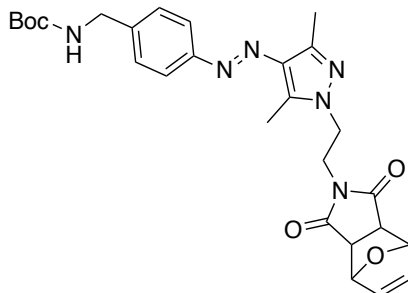
(*E*)-*N*-(4-((1-(2-((2-aminoethyl)disulfaneyl)ethyl)-3,5-dimethyl-1*H*-pyrazol-4-yl)diazenyl)benzyl)-*N*-(1-phenethylpiperidin-4-yl)propionamide (**tFAPz 1**)



Compound **9** (6.0 mg, 9.35 μ mol, 1.0 eq) was dissolved in MeOH (10 mL) at room temperature under Ar atmosphere. To this solution, cysteamine hydrochloride (1.2 mg, 10 μ mol, 1.1 eq) was added and the mixture was stirred at room temperature for 0.5 h. The solvent was removed carefully *in vacuo* and the crude product was purified by preparative HPLC (solvent A: H₂O [0.05 Vol% TFA]; solvent B: MeCN; gradient: 10-98% B from 0-20 min, and then 98% B from 20-25 min; t_R = 7.9 min). Lyophilization afforded target compound **tFAPz 1** as a pale-yellow solid (5.4 mg, 8.88 μ mol, 95%). ¹H-NMR (400 MHz, MeOD): δ (ppm) = 7.80 (d, J = 8.2 Hz, 2H), 7.39 (d, J = 8.1 Hz, 2H), 7.33-7.31 (m, 3H), 7.27 (s, 2H), 4.71 (s, 2H), 4.51-4.47 (m, 1H), 4.42 (t, J = 6.5 Hz, 2H), 3.67 (d, J = 11.8 Hz, 2H), 3.29-3.28 (m, 2H), 3.21 (t, J = 6.6 Hz, 2H), 3.13-3.09 (m, 2H), 3.03-2.98 (m, 4H), 2.69-2.97 (m, 2H), 2.65 (s, 3H), 2.47 (s, 3H), 2.45-2.42 (m, 2H), 2.22-2.15 (m, 2H), 1.99-1.97 (m, 2H), 1.13 (t, J = 7.2 Hz, 3H). ¹³C-NMR (101 MHz, MeOD): δ = 177.4, 154.4, 143.8, 141.9, 140.8, 137.4, 136.0, 130.0, 129.8, 128.4, 128.0, 123.3, 59.0, 53.5, 53.2, 52.5, 45.3, 39.1, 38.0, 35.2, 31.4, 29.3, 28.3, 27.9, 27.6, 14.1, 9.9, 9.8. HR-ESI-MS (m/z): [$M+H$]⁺ calculated: 608.3237; found: 608.3207.

Tethered Photoswitchable Derivatives of Fentanyl that Target the μ -Opioid Receptor

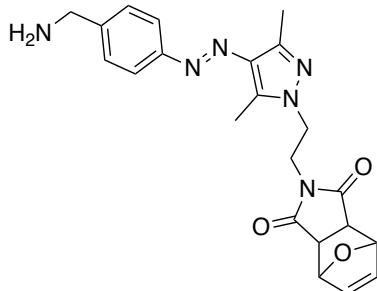
tert-butyl(*E*)-(4-((1-(2-(1,3-dioxo-1,3,3a,4,7,7a-hexahydro-2*H*-4,7-epoxyisindol-2-yl)ethyl)-3,5-dimethyl-1*H*-pyrazol-4-yl)diazenyl)benzyl)carbamate (**12**)



A mixture of previously synthesized **10** (280 mg, 0.53 mmol) and previously synthesized **11** (96.2 mg, 0.58 mmol, 1.1 eq.), K_2CO_3 (110 mg, 0.79 mmol, 1.5 eq.) and DMF (22 mL) was heated to 50 °C and stirred for 3 h. The reaction mixture was allowed to cool and then diluted with water (30 mL) and ethyl acetate (20 mL). The organic layer was further washed with water (2 x 10 mL), brine (1 x 10 mL), dried (Na_2SO_4), filtered and concentrated *in vacuo*. The crude residue was subjected to automated flash column chromatography, eluting at a gradient of 100% DCM to 20% MeOH/DCM to obtain compound **12** as a yellow solid (155 mg, 0.30 mmol, 56%). 1H -NMR (400 MHz, $CDCl_3$): δ (ppm) = 7.73 (d, J = 8.3 Hz, 2H), 7.35 (d, J = 8.3 Hz, 2H), 6.50 (s, 2H), 5.24 (s, 2H), 4.36 (d, J = 5.4 Hz, 2H), 4.23 (t, J = 6.3 Hz, 2H), 3.90 (t, J = 6.3 Hz, 2H), 2.84 (s, 2H), 2.58 (s, 3H), 2.46 (s, 3H), 1.47 (s, 9H). ^{13}C -NMR (101 MHz, $CDCl_3$): δ = 175.82, 156.03, 152.92, 142.76, 140.61, 139.55, 136.66, 135.27, 128.12, 122.25, 80.98, 77.48, 77.36, 77.16, 76.84, 47.69, 45.81, 44.58, 38.20, 34.60, 28.55, 13.84, 9.82. ESI-MS (m/z): $[M+H]^+$ found: 521.3.

Tethered Photoswitchable Derivatives of Fentanyl that Target the μ -Opioid Receptor

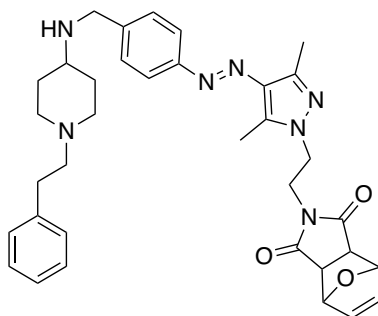
(E)-2-(2-(4-((4-(aminomethyl)phenyl)diazenyl)-3,5-dimethyl-1*H*-pyrazol-1-yl)ethyl)-3a,4,7,7a-tetrahydro-1*H*-4,7-epoxyisoindole-1,3(2*H*)-dione (**13**)



General Procedure 1 was followed, using intermediate **12** (110 mg, 1.79 mmol) to obtain **13** as an orange oil (108 mg, 0.21 mmol, 99%). $^1\text{H-NMR}$ (400 MHz, MeOD): δ (ppm) = 7.83 (d, $J = 8.3$ Hz, 2H), 7.57 (d, $J = 8.3$ Hz, 2H), 6.52 (s, 2H), 5.11 (s, 2H), 4.28 (t, $J = 6.0$ Hz, 2H), 4.18 (s, 2H), 3.89 (t, $J = 6.0$ Hz, 2H), 2.90 (s, 2H), 2.60 (s, 3H), 2.43 (s, 3H). $^{13}\text{C-NMR}$ (101 MHz, CDCl_3): $\delta = 178.00, 155.26, 143.72, 142.20, 137.62, 136.29, 135.50, 130.81, 123.39, 82.15, 49.28, 46.89, 44.00, 38.96, 14.03, 9.67$. ESI-MS (m/z): $[M+H]^+$ found: 421.2.

Tethered Photoswitchable Derivatives of Fentanyl that Target the μ -Opioid Receptor

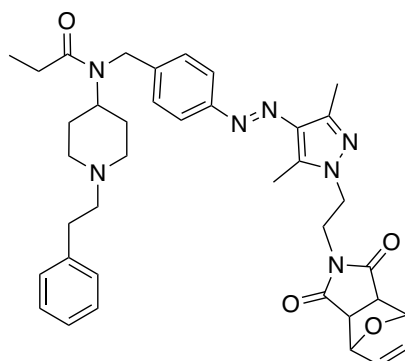
(E)-2-(2-(3,5-dimethyl-4-((4-(((1-phenethylpiperidin-4-yl)amino)methyl)phenyl) diazenyl)-1H-pyrazol-1-yl)ethyl)-3a,4,7,7a-tetrahydro-1H-4,7-epoxyisoindole-1,3(2H)-dione (14)



To a solution of commercially available 1-phenethyl-4-piperidone (64.5 mg, 0.32 mmol, 1.05 eq.) in DCE (10 mL) was added sequentially **13** (157 mg, 0.30 mmol), NaBH(OAc)₃ (89.7 mg, 0.42 mmol, 1.4 eq.) and AcOH (0.04 mL, 0.63 mmol, 2.0 eq.). The bright orange reaction mixture was allowed to stir overnight at room temperature. After 16 h, the reaction mixture was diluted with EtOAc (2 x 10 mL), washed with 1M NaOH (1x 5 mL), sat. NaHCO₃ (1x 5 mL), followed by brine (1 x 10 mL). The combined organic layers were dried (Na₂SO₄), filtered and concentrated *in vacuo*. The crude residue was subjected to automated flash column chromatography, eluting at 100% DCM to 10% MeOH/DCM to obtain **14** as an orange oil (112 mg, 0.18 mmol, 61%). ¹H-NMR (400 MHz, CDCl₃): δ (ppm) = 7.73 (d, J = 8.3 Hz, 1H), 7.43 (d, J = 8.3 Hz, 1H), 7.31-7.27 (m, 2H), 7.22-7.19 (m, 5H), 6.50 (s, 2H), 5.24 (s, 2H), 4.22 (t, J = 6.3 Hz, 2H), 3.89-3.88 (m, 2H), 3.08-3.04 (m, 2H), 2.95-2.89 (m, 5H), 2.83 (s, 2H), 2.74-2.69 (m, 4H), 2.57 (s, 3H), 2.45 (s, 3H), 2.09-2.03 (m, 4H), 1.72-1.66 (m, 2H). ¹³C-NMR (101 MHz, CDCl₃): δ = 175.78, 152.96, 143.01, 139.32, 136.67, 135.39, 128.92, 128.83, 128.67, 126.47, 122.08, 80.98, 77.36, 60.14, 47.62, 45.98, 45.69, 38.22, 33.61, 33.14, 14.11, 9.82. ESI-MS (m/z): [M+H]⁺ found: 608.3.

Tethered Photoswitchable Derivatives of Fentanyl that Target the μ -Opioid Receptor

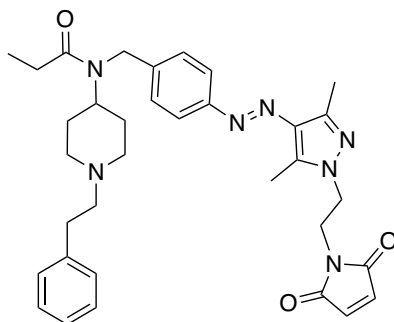
(*E*)-*N*-(4-((1-(2-(1,3-dioxo-1,3,3a,4,7,7a-hexahydro-2*H*-4,7-epoxyisindol-2-yl)ethyl)-3,5-dimethyl-1*H*-pyrazol-4-yl)diazenyl)benzyl)-*N*-(1-phenethylpiperidin-4-yl)propionamide (**15**)



To a solution of **14** (93 mg, 0.15 mmol) in anhydrous DCM (2.5 mL), Et₃N (0.06 mL, 0.46 mmol, 3.0 eq.) was added, followed by propionyl chloride (0.02 mL, 0.18 mmol, 1.2 eq.). The reaction mixture was allowed to stir for 24 h under N₂ atmosphere at room temperature. Water was then added, and the organic phase was extracted with DCM (2 x 10 mL). The pooled organic phase was washed with sat. NaHCO₃ (1x 20 mL) and brine (1 x 20 mL). The combined organic layers were dried (Na₂SO₄), filtered and concentrated *in vacuo*. The crude residue was subjected to automated flash column chromatography, eluting at 100% DCM to 10% MeOH/DCM to obtain **15** as an orange oil (35 mg, 0.05 mmol, 34%). ¹H-NMR (400 MHz, CDCl₃): δ (ppm) = 7.74 (d, *J* = 8.1 Hz, 2H), 7.32-7.24 (m, 5H), 7.17 (d, *J* = 7.1 Hz, 2H), 6.49 (s, 2H), 5.22 (s, 2H), 4.93-4.88 (m, 1H), 4.62 (s, 2H), 4.27 (t, *J* = 6.2 Hz, 2H), 3.89 (t, *J* = 6.1 Hz, 2H), 3.65-3.63 (m, 2H), 3.17-3.08 (m, 4H), 2.84 (s, 2H), 2.82-2.76 (m, 2H), 2.58 (s, 3H), 2.46 (s, 3H), 2.38-2.33 (m, 2H), 1.85-1.82 (m, 2H), 1.14 (t, *J* = 7.3 Hz, 3H). ¹³C-NMR (101 MHz, CDCl₃): δ = 175.79, 175.66, 161.26, 160.88, 153.02, 143.08, 139.75, 139.07, 136.65, 135.72, 135.24, 129.20, 128.73, 127.59, 126.30, 122.59, 117.26, 114.39, 80.97, 77.37, 58.58, 52.77, 48.97, 47.61, 46.39, 45.73, 38.13, 30.60, 27.18, 26.49, 13.68, 9.80, 9.63. ESI-MS (*m/z*): [*M*+H]⁺ found: 664.4.

Tethered Photoswitchable Derivatives of Fentanyl that Target the μ -Opioid Receptor

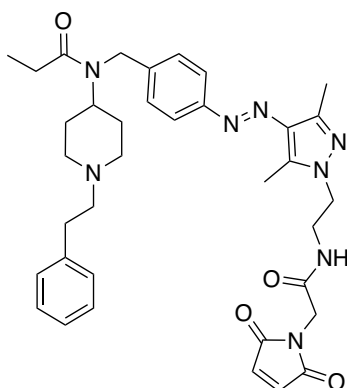
(E)-*N*-(4-((1-(2-(2,5-dioxo-2,5-dihydro-1*H*-pyrrol-1-yl)ethyl)-3,5-dimethyl-1*H*-pyrazol-4-yl)diazenyl)benzyl)-*N*-(1-phenethylpiperidin-4-yl)propionamide (**tFAPz 2a**)



To a solution of the protected maleimide **15** (15.0 mg, 22.6 μ mol), dry DMSO (1 mL) was added and the solution was heated to 110 $^{\circ}$ C. After 3 h, the mixture was cooled, and the resulting crude material was directly purified by preparative HPLC (solvent A: H₂O [0.05 Vol% TFA]; solvent B: MeCN; gradient: 10-98% B from 0-20 min, and then 98% B from 20-25 min). This yielded target compound **tFAPz 2a** as an orange oil (6.9 mg, 11.6 μ mol, 51%). ¹H-NMR (400 MHz, CDCl₃): δ (ppm) = 7.74 (d, *J* = 8.2 Hz, 2H), 7.32-7.29 (m, 3H), 7.25-7.24 (m, 2H), 7.17 (d, *J* = 7.2 Hz, 2H), 6.70 (s, 2H), 4.93-4.87 (m, 1H), 4.60 (s, 2H), 4.27 (t, *J* = 6.0 Hz, 2H), 3.94 (t, *J* = 6.0 Hz, 2H), 3.64 (d, *J* = 11.5 Hz, 2H), 3.18-3.14 (m, 2H), 3.06-3.02 (m, 2H), 2.79-2.73 (m, 2H), 2.55 (s, 3H), 2.44 (s, 3H), 2.39-2.34 (m, 4H), 2.25-2.17 (m, 2H), 1.83 (d, *J* = 12.9 Hz, 2H), 1.15 (t, *J* = 7.3 Hz, 3H). ¹³C-NMR (101 MHz, CDCl₃): δ = 175.40, 170.19, 153.12, 143.32, 139.28, 139.05, 135.84, 135.39, 134.43, 129.21, 128.76, 127.57, 126.30, 122.54, 77.36, 58.52, 52.67, 48.90, 46.46, 46.29, 37.26, 30.67, 27.18, 26.60, 13.92, 9.83, 9.66. HR-ESI-MS (*m/z*): [*M*+*H*]⁺ calculated: 596.3381; found: 596.3354.

Tethered Photoswitchable Derivatives of Fentanyl that Target the μ -Opioid Receptor

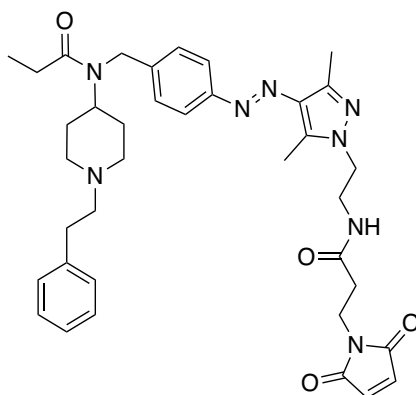
(E)-*N*-(4-((1-(2-(2-(2,5-dioxo-2,5-dihydro-1*H*-pyrrol-1-yl)acetamido)ethyl)-3,5-dimethyl-1*H*-pyrazol-4-yl)diazenyl)benzyl)-*N*-(1-phenethylpiperidin-4-yl)propionamide (**tFAPz 2b**)



General procedure 2 was followed using **FAPz 1** (45 mg, 83.1 μ mol) and commercially available 2-maleimido acetic acid (15.5 mg, 99.7 μ mol, 1.2 eq.) to yield target compound **tFAPz 2b** as a yellow solid (9.2 mg, 14.1 μ mol, 17%). $^1\text{H-NMR}$ (400 MHz, DMSO-D_6): δ (ppm) = 7.75-7.66 (m, 2H), 7.39-7.32 (m, 4H), 7.27-7.24 (m, 3H), 7.09 (s, 2H), 4.61-4.46 (m, 3H), 4.09 (t, $J = 5.9$ Hz, 2H), 3.99 (s, 2H), 3.58-3.56 (m, 2H), 3.45 (q, $J = 5.7$ Hz, 2H), 3.27-3.22 (m, 2H), 3.11-3.05 (m, 2H), 2.96-2.94 (m, 2H), 2.59-2.54 (m, 1H), 2.52 (s, 3H), 2.39 (s, 3H), 2.33-2.27 (m, 1H), 1.97-1.78 (m, 4H), 1.11-0.98 (m, 3H). $^{13}\text{C-NMR}$ (101 MHz, DMSO-D_6): $\delta = 170.62, 166.72, 138.18, 134.91, 129.01, 128.91, 128.68, 127.39, 127.02, 126.91, 121.74, 121.43, 56.48, 51.44, 51.37, 49.82, 47.48, 46.76, 43.62, 40.06, 38.76, 29.71, 27.67, 26.41, 26.37, 25.96, 14.07, 9.69, 9.21$. HR-ESI-MS (m/z): $[M+H]^+$ calculated: 653.3592; found: 653.3566.

Tethered Photoswitchable Derivatives of Fentanyl that Target the μ -Opioid Receptor

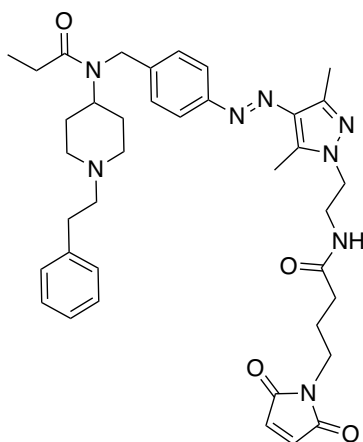
(E)-*N*-(2-(3,5-dimethyl-4-((4-((*N*-(1-phenethylpiperidin-4-yl)propionamido)methyl)phenyl)diazenyl)-1*H*-pyrazol-1-yl)ethyl)-3-(2,5-dioxo-2,5-dihydro-1*H*-pyrrol-1-yl)propanamide (**tFAPz 2c**)



General procedure 2 was followed using **FAPz 1** (85 mg, 156.9 μ mol) and commercially available 3-maleimidopropionic acid (31.9 mg, 188.3 μ mol, 1.2 eq.) to yield target compound **tFAPz 2c** as a yellow solid (12.0 mg, 18.0 μ mol, 12%). $^1\text{H-NMR}$ (400 MHz, CDCl_3): δ (ppm) = 7.76 (d, J = 8.3 Hz, 2H), 7.32-7.27 (m, 4H), 7.25-7.23 (m, 1H), 7.17 (d, J = 6.9 Hz, 2H), 6.64 (s, 2H), 4.94-4.88 (m, 1H), 4.61 (s, 2H), 4.17-4.14 (m, 2H), 3.82 (t, J = 7.0 Hz, 2H), 3.72-3.63 (m, 4H), 3.18-3.14 (m, 2H), 3.06-3.02 (m, 2H), 2.76 (t, J = 12.1 Hz, 2H), 2.56 (s, 3H), 2.53-2.50 (m, 2H), 2.49 (s, 3H), 2.36 (q, J = 7.3 Hz, 2H), 2.24-2.15 (m, 2H), 1.83 (d, J = 12.9 Hz, 2H), 1.15 (t, J = 7.3 Hz, 3H). $^{13}\text{C-NMR}$ (101 MHz, CDCl_3): δ = 175.39, 170.58, 170.37, 153.06, 143.08, 139.83, 139.22, 135.82, 135.17, 134.31, 129.21, 128.75, 127.58, 126.34, 122.56, 77.36, 58.51, 52.68, 48.87, 47.49, 46.27, 39.13, 34.87, 34.28, 30.66, 27.17, 26.60, 14.01, 9.87, 9.66. HR-ESI-MS (m/z): $[M+H]^+$ calculated: 667.3747; found: 667.3720.

Tethered Photoswitchable Derivatives of Fentanyl that Target the μ -Opioid Receptor

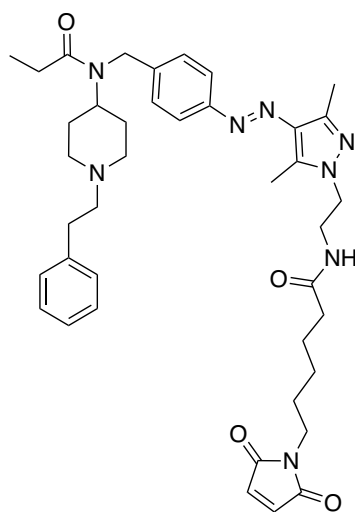
(*E*)-*N*-(2-(3,5-dimethyl-4-((4-((*N*-(1-phenethylpiperidin-4-yl)propionamido)methyl)phenyl)diazenyl)-1*H*-pyrazol-1-yl)ethyl)-4-(2,5-dioxo-2,5-dihydro-1*H*-pyrrol-1-yl)butanamide (**tFAPz 2d**)



General procedure 2 was followed using **FAPz 1** (85 mg, 156.9 μ mol) and commercially available 4-maleimidobutyric acid (34.5 mg, 188.3 μ mol, 1.2 eq.) to yield target compound **tFAPz 2d** as a yellow solid (19.1 mg, 28.1 μ mol, 18%). $^1\text{H-NMR}$ (400 MHz, CDCl_3): δ (ppm) = 7.75 (d, J = 8.2 Hz, 2H), 7.32-7.28 (m, 3H), 7.24-7.22 (m, 2H), 7.16 (d, J = 7.1 Hz, 2H), 6.66 (s, 2H), 4.93-4.87 (m, 1H), 4.60 (s, 2H), 4.22 (t, J = 5.7 Hz, 2H), 3.73-3.64 (m, 4H), 3.53 (t, J = 6.5 Hz, 2H), 3.19-3.15 (m, 2H), 3.05-3.01 (m, 2H), 2.78 (t, J = 11.9 Hz, 2H), 2.58 (s, 3H), 2.49 (s, 3H), 2.36 (q, J = 7.3 Hz, 2H), 2.20-2.14 (m, 4H), 1.93-1.82 (m, 4H), 1.14 (t, J = 7.4 Hz, 3H). $^{13}\text{C-NMR}$ (101 MHz, CDCl_3): δ = 175.47, 172.70, 170.98, 153.01, 142.99, 139.97, 139.21, 135.71, 135.09, 134.24, 129.20, 128.71, 127.59, 126.32, 122.59, 77.36, 58.51, 52.70, 48.90, 47.53, 46.30, 39.22, 37.13, 33.48, 30.64, 27.16, 26.59, 24.71, 13.77, 9.86, 9.63. HR-ESI-MS (m/z): $[M+H]^+$ calculated: 681.391; found: 681.388.

Tethered Photoswitchable Derivatives of Fentanyl that Target the μ -Opioid Receptor

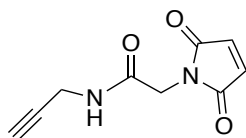
(*E*)-*N*-(2-(3,5-dimethyl-4-((4-(*N*-(1-phenethylpiperidin-4-yl)propionamido)methyl)phenyl)diazenyl)-1*H*-pyrazol-1-yl)ethyl)-6-(2,5-dioxo-2,5-dihydro-1*H*-pyrrol-1-yl)hexanamide (**tFAPz 2e**)



General procedure 2 was followed using **FAPz 1** (85 mg, 156.9 μ mol) and commercially available 6-maleimidohexanoic acid (39.8 mg, 188.3 μ mol, 1.2 eq.) to yield target compound **tFAPz 2e** as an orange oil (16.9 mg, 23.8 μ mol, 15%). $^1\text{H-NMR}$ (400 MHz, CDCl_3): δ (ppm) = 7.75 (d, J = 8.1 Hz, 2H), 7.32-7.28 (m, 3H), 7.24-7.22 (m, 2H), 7.17 (d, J = 7.3 Hz, 2H), 6.65 (s, 2H), 4.94-4.87 (m, 1H), 4.60 (s, 2H), 4.17 (t, J = 5.5 Hz, 2H), 3.71-3.62 (m, 4H), 3.46 (t, J = 7.2 Hz, 2H), 3.17-3.13 (m, 2H), 3.06-3.02 (m, 2H), 2.79-2.73 (m, 2H), 2.56 (s, 3H), 2.49 (s, 3H), 2.35 (q, J = 7.2 Hz, 2H), 2.22-2.13 (m, 4H), 1.84-1.81 (m, 2H), 1.64-1.53 (m, 4H), 1.32-1.24 (m, 2H), 1.14 (t, J = 7.2 Hz, 3H). $^{13}\text{C-NMR}$ (101 MHz, CDCl_3): δ = 173.38, 170.94, 135.87, 134.17, 133.50, 133.40, 130.01, 129.88, 129.17, 128.74, 127.53, 126.30, 122.49, 58.44, 52.60, 48.83, 47.61, 46.23, 39.24, 37.63, 36.38, 30.64, 28.32, 27.15, 26.57, 26.39, 25.00, 14.12, 9.86, 9.63. HR-ESI-MS (m/z): $[M+H]^+$ calculated: 709.4222; found: 709.4194.

Tethered Photoswitchable Derivatives of Fentanyl that Target the μ -Opioid Receptor

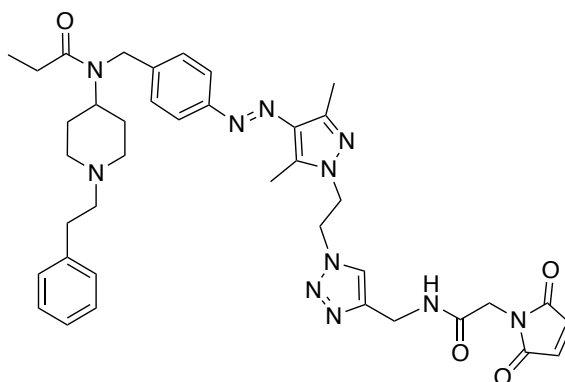
2-(2,5-dioxo-2,5-dihydro-1H-pyrrol-1-yl)-N-(prop-2-yn-1-yl)acetamide (**16**)



Commercially available 2-maleimidoacetic acid (100 mg, 0.65 mmol, 1.0 eq.) was dissolved in a solution of DCM/DMF (100:1, 5 mL). Oxalylchloride (123 mg, 0.97 mmol, 1.5 eq.) was then added dropwise to this reaction mixture and allowed to stir for 2 h at room temperature. The solvent was removed *in vacuo* and the residue was redissolved in THF (4.0 mL). These previous steps followed literature methods.^[4] This mixture was then added to a solution of N-propargylamine (50 μ L, 0.78 mmol, 1.2 eq.) and DIPEA (0.23 mL, 1.3 mmol, 2.0 eq.) in THF (4.0 mL) at 0 °C. The mixture was allowed to stir for 1 h at room temperature and afterwards, the solvent was removed *in vacuo* and the crude mixture was purified by automated flash column chromatography, eluting at 100% PE to 80% EtOAc/PE to yield alkyne **16** as a white powder (50 mg, 0.26 mmol, 40%). ¹H-NMR (400 MHz, CDCl₃): δ (ppm) = 6.80 (s, 2H), 4.19 (s, 2H), 4.08-4.06 (m, 2H), 2.26 (t, J = 2.6 Hz, 1H). ¹³C-NMR (101 MHz, CDCl₃): δ = 170.14, 165.67, 134.69, 77.36, 72.42, 40.50, 29.68. ESI-MS (m/z): [M+H]⁺ found: 193.06

Tethered Photoswitchable Derivatives of Fentanyl that Target the μ -Opioid Receptor

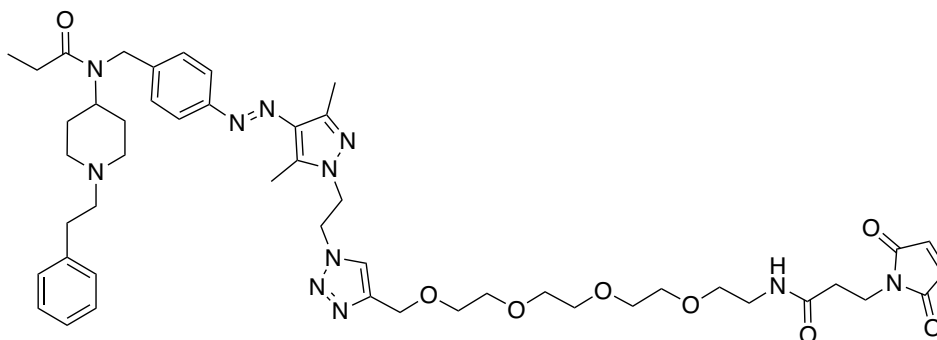
(E)-*N*-(4-((1-(2-(4-((2-(2,5-dioxo-2,5-dihydro-1*H*-pyrrol-1-yl)acetamido)methyl)-1*H*-1,2,3-triazol-1-yl)ethyl)-3,5-dimethyl-1*H*-pyrazol-4-yl)diazenyl)benzyl)-*N*-(1-phenethylpiperidin-4-yl) propionamide (**tFAPz 2f**)



General procedure 3 was followed using alkyne **16** (15.0 mg, 78.1 μ mol, 1.0 eq.) and **FAPz 1** (48.6 mg, 89.8 μ mol, 1.15 eq.) to yield target compound **tFAPz 2f** as an orange solid (27.0 mg, 36.8 μ mol, 47%). $^1\text{H-NMR}$ (400 MHz, CDCl_3): δ (ppm) = 7.74 (d, J = 8.3 Hz, 2H), 7.32-7.28 (m, 3H), 7.25-7.23 (m, 2H), 7.15 (d, J = 7.0 Hz, 2H), 6.73 (s, 2H), 4.91-4.88 (m, 1H), 4.86 (t, J = 5.5 Hz, 2H), 4.59 (s, 2H), 4.53 (t, J = 5.5 Hz, 2H), 4.41 (d, J = 5.8 Hz, 2H), 4.05 (s, 2H), 3.67 (d, J = 11.8 Hz, 2H), 3.20-3.16 (m, 2H), 3.04-3.00 (m, 2H), 2.82-2.77 (m, 2H), 2.52 (s, 3H), 2.39 (q, J = 7.4 Hz, 2H), 2.22-2.09 (m, 5H), 1.85-1.81 (m, 2H), 1.15 (t, J = 7.4 Hz, 3H). $^{13}\text{C-NMR}$ (101 MHz, CDCl_3): δ = 175.65, 170.16, 166.71, 152.92, 144.16, 140.64, 139.15, 135.59, 134.93, 134.59, 129.23, 128.70, 127.64, 126.47, 124.16, 122.66, 77.36, 58.57, 52.81, 49.91, 49.04, 48.09, 46.43, 40.26, 34.40, 30.62, 27.20, 26.65, 13.95, 9.67, 9.13. HR-ESI-MS (m/z): $[M+H]^+$ calculated: 734.3927; found: 734.3899.

Tethered Photoswitchable Derivatives of Fentanyl that Target the μ -Opioid Receptor

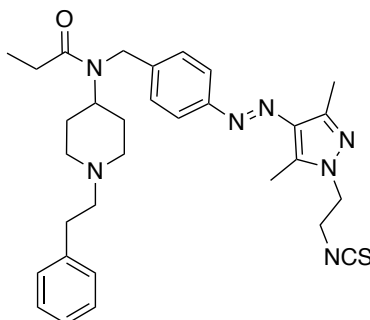
(*E*)-*N*-(1-(1-(2-(3,5-dimethyl-4-((4-((*N*-(1-phenethylpiperidin-4yl)propionamido)methyl)phenyl)diazenyl)-1*H*-pyrazol-1-yl)ethyl)-1*H*-1,2,3-triazol-4-yl)-2,5,8,11-tetraoxatridecan-13-yl)-3-(2,5-dioxo-2,5-dihydro-1*H*-pyrrol-1-yl)propanamide (tFAPz 2g)



General procedure 3 was followed using commercially available alkyne-PEG4-maleimide (10.0 mg, 26.2 μ mol, 1.0 eq.) and **FAPz 1** (16.3 mg, 30.1 μ mol, 1.15 eq.) to yield target compound **tFAPz 2g** as a yellow oil (7.9 mg, 8.55 μ mol, 46%). $^1\text{H-NMR}$ (400 MHz, CDCl_3): δ (ppm) = 7.72 (d, J = 8.3 Hz, 2H), 7.32-7.28 (m, 3H), 7.25-7.24 (m, 2H), 7.17 (d, J = 7.0 Hz, 2H), 6.65 (s, 2H), 4.90-4.88 (m, 2H), 4.62-4.60 (m, 3H), 4.54-4.51 (m, 2H), 3.77 (t, J = 7.0 Hz, 2H), 3.67-3.53 (m, 12H), 3.38-3.37 (m, 2H), 3.18-3.14 (m, 2H), 3.06-3.02 (m, 2H), 2.80-2.75 (m, 2H), 2.50 (s, 3H), 2.47-2.33 (m, 10H), 2.23-2.14 (m, 5H), 1.85-1.81 (m, 2H), 1.15 (t, J = 7.3 Hz, 3H). $^{13}\text{C-NMR}$ (101 MHz, CDCl_3): δ = 170.70, 170.66, 135.89, 134.30, 129.22, 128.76, 127.59, 126.38, 122.53, 77.37, 70.30, 70.15, 58.54, 52.70, 48.88, 48.35, 46.29, 43.87, 39.25, 34.55, 34.46, 30.65, 26.61, 14.22, 9.17. HR-ESI-MS (m/z): $[M+H]^+$ calculated: 924.5124; found: 924.5510.

Tethered Photoswitchable Derivatives of Fentanyl that Target the μ -Opioid Receptor

(*N*-4-((1-(2-isothiocyanatoethyl)-3,5-dimethyl-1*H*-pyrazol-4-yl)diazenyl)benzyl)-*N*-(1-phenethylpiperidin-4-yl)propionamide (**tFAPz 3**)



Previously synthesized **FAPz 1** (40 mg, 73.8 μ mol) was dissolved in dry THF (1.0 mL), and PPh_3 (39 mg, 148 μ mol, 2.0 eq.) was added under N_2 atmosphere. Carbon disulfide (0.05 mL, 738 μ mol, 10.0 eq.) was then added dropwise. The mixture was heated to reflux and stirred for 16 h. The solvent was removed *in vacuo* and the crude product was directly purified by preparative HPLC (solvent A: H_2O [0.05 Vol% TFA]; solvent B: MeCN; gradient: 10-98% B from 0-20 min, and then 98% B from 20-25 min) to yield target compound **tFAPz 3** as a yellow solid (17.4 mg, 31.2 μ mol, 42%). $^1\text{H-NMR}$ (400 MHz, CDCl_3): δ (ppm) = 7.77 (d, J = 8.3 Hz, 2H), 7.32-7.27 (m, 3H), 7.25-7.23 (m, 2H), 7.18-7.16 (m, 2H), 4.93-4.87 (m, 1H), 4.61 (s, 2H), 4.29 (t, J = 5.7 Hz, 2H), 4.02 (t, J = 5.6 Hz, 2H), 3.67-3.64 (m, 2H), 3.19-3.14 (m, 2H), 3.06-3.02 (m, 2H), 2.80-2.74 (m, 2H), 2.66 (s, 3H), 2.50 (s, 3H), 2.37 (q, J = 7.3 Hz, 2H), 2.24-2.16 (m, 2H), 1.85-1.82 (m, 2H), 1.15 (t, J = 7.3 Hz, 3H). $^{13}\text{C-NMR}$ (101 MHz, CDCl_3): δ = 175.47, 153.07, 143.86, 140.29, 139.14, 135.74, 135.33, 134.30, 129.20, 128.73, 127.58, 126.30, 122.60, 77.35, 58.53, 52.71, 48.92, 47.96, 46.31, 45.16, 30.65, 27.17, 26.58, 14.10, 9.97, 9.64. HR-ESI-MS (m/z): $[M+H]^+$ calculated: 558.304; found: 558.301.

2.7.1.3 Purity Measurements

All purity measurements can be found in the appendix (Section 7.3.1) under ‘Analytical HPLC Chromatograms for Purity Determination’.

2.7.2 Supplementary Photophysical Information

2.7.2.1 Materials and Methods

For determination of thermal equilibrium and isomer spectra, as well as determination of cycle performance and thermal half-life, UV/Vis absorption spectroscopy was employed. Compounds were irradiated with 365 nm for 5 sec to obtain the respective *cis*-isomers or with 528 nm for 2 min to obtain the respective *trans*-isomers. UV/Vis absorption spectroscopy was performed using Agilent 8453 UV/Vis spectrophotometer or Agilent Varian Cary[®] 50 UV/Vis spectrophotometer, in 10 mm quartz cuvettes. PSS values of both *cis*- (365 nm irradiation for 5 sec) and *trans*-isomers (528 nm irradiation for 2 min) were evaluated at the respective isosbestic points (as specified) of compounds (20 or 50 μ M, as specified), using analytical HPLC. Analytical HPLC was performed using Agilent 1220 Infinity LC System (column: Phenomenex Luna, 3 μ M C18(2), 100 Å 150 x 2.0 mm; flow rate of 0.3 mL/min at 20 °C; solvent A: Milli-Q water with 0.01 wt% TFA; solvent B: MeCN). The solvent gradient for **tFAPz 1** was 10-98% B from 0-20 min, and then 98% B from 20-30 min. The solvent gradient for **tFAPz 2a, 2b, 2c, 2d, 2e, 2g** and **3** was 10-98% B from 0-15 min, and then 98% B from 15-20 min. The solvent gradient for **tFAPz 2f** was 10-98% B from 0-25 min, and then 98% B from 25-40 min. For compounds **2a, 2c, 2d** and **2e** splitting of both *cis*- and *trans*-isomer peaks could be observed in buffer solution. While compound degradation post-irradiation cannot be entirely excluded as a potential cause, the observed splitting was believed to occur from compound interaction with the HPLC column during separation under the described experimental conditions. Accordingly, PSS values for the given compounds were assessed by grouping the *cis*-isomer peaks and separately, the *trans*-isomer peaks to determine respective isomer abundances. The *cis*-isomer peaks were distinguished from the *trans*-isomer peaks via the analysis of corresponding UV/Vis absorption spectra that were measured simultaneously with the HPLC run. Furthermore, the general influence of TFA on inducing back-isomerization to the thermally stable *trans*-isomer during PSS evaluation cannot be excluded, which may lead to an overall underrepresentation of *cis*-isomer abundances for the evaluated compounds. LED light sources for irradiation: λ =365 nm (Seoul Viosys, CUN66A1B, 700 mA, 3.6 V) and λ =528 nm (LED-TECH, Oslon SSL 80, LDCQ7P-2U3U, 700 mA, 3.5 V). The details of these light sources are based on the supplier specifications upon purchase.

2.7.2.2 UV/Vis Absorption Spectra, Cycle Performance and Thermal Stabilities

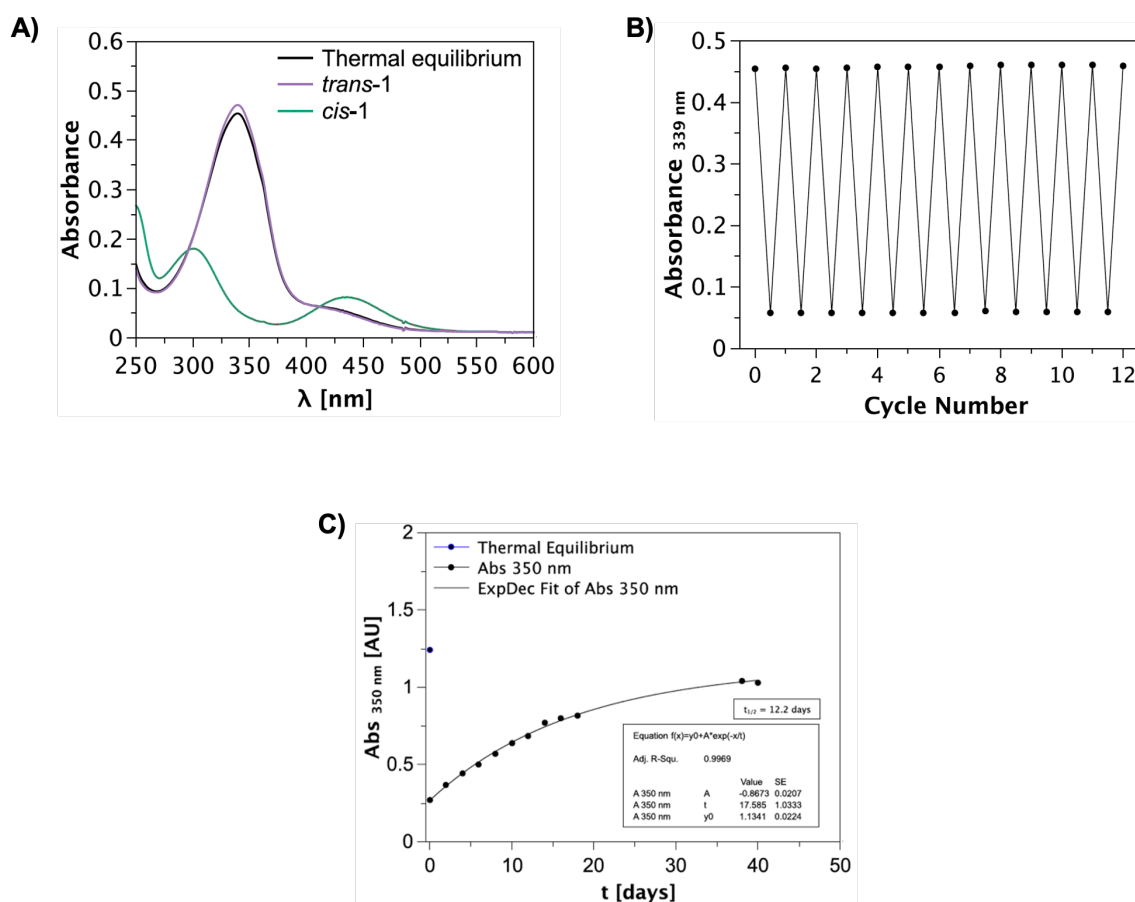


Figure 18. Photophysical properties of **tFAPz 1** (40 μ M) in buffer solution (TrisHCl Buffer, pH 7.5) + 0.4% DMSO at 25 $^{\circ}$ C. A) UV/Vis absorption spectra data of thermal equilibrium, *trans*-isomer and *cis*-isomer. The *cis*-isomer was accessed via irradiation with 365 nm, while the *trans*-isomer was obtained with 528 nm irradiation. B) Cycle performance upon alternating irradiation of 365 nm and 528 nm. Data points were recorded at the absorbance maximum of the *trans*-isomer (339 nm). C) Thermal half-life of compound **1** (150 μ M), measured at 27 $^{\circ}$ C in buffer solution (TrisHCl Buffer, pH 7.5) + 1.5% DMSO.

Tethered Photoswitchable Derivatives of Fentanyl that Target the μ -Opioid Receptor

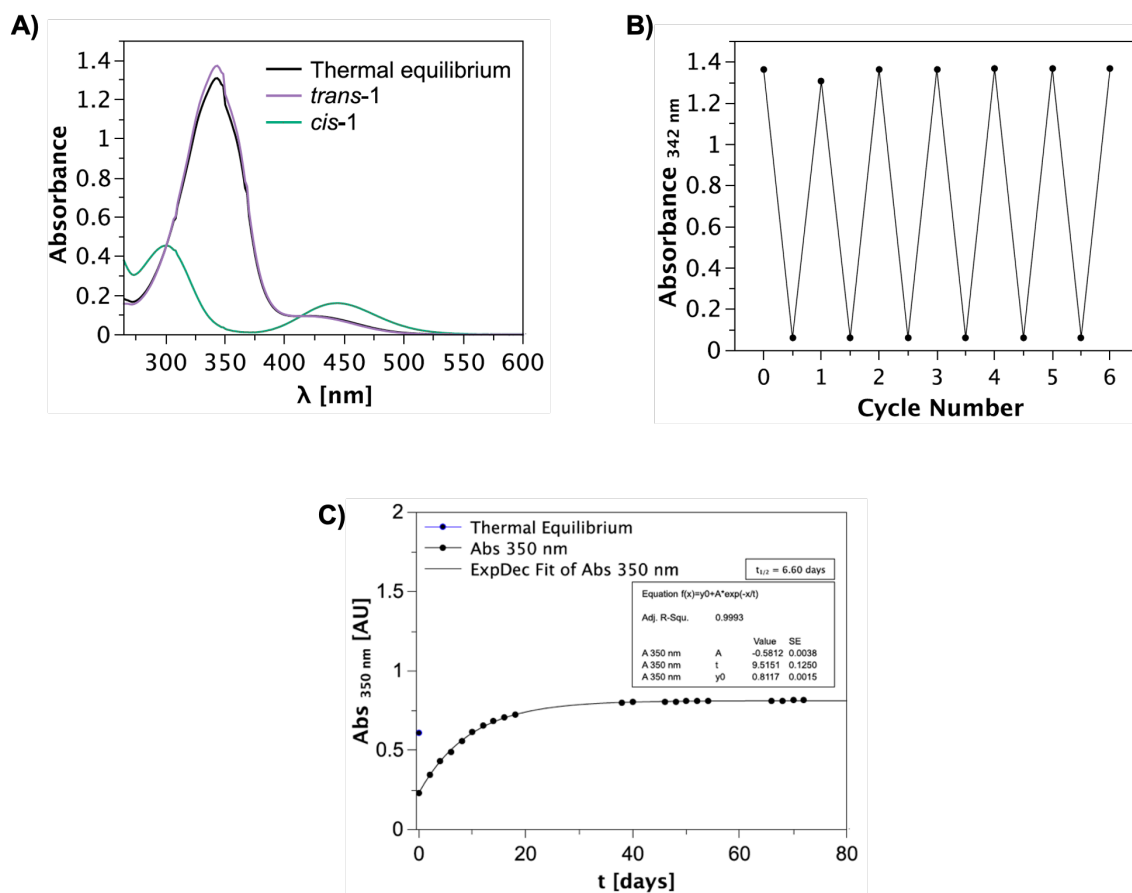


Figure 19. Photophysical properties of **tFAPz 1** (50 μ M) in DMSO at 25 $^{\circ}$ C. A) UV/Vis absorption spectra data of thermal equilibrium, *trans*-isomer and *cis*-isomer. The *cis*-isomer was accessed via irradiation with 365 nm, while the *trans*-isomer was obtained with 528 nm irradiation. B) Cycle performance upon alternating irradiation of 365 nm and 528 nm. Data points were recorded at the absorbance maximum of the *trans*-isomer (342 nm). C) Thermal half-life of compound **1** (50 μ M), measured at 27 $^{\circ}$ C.

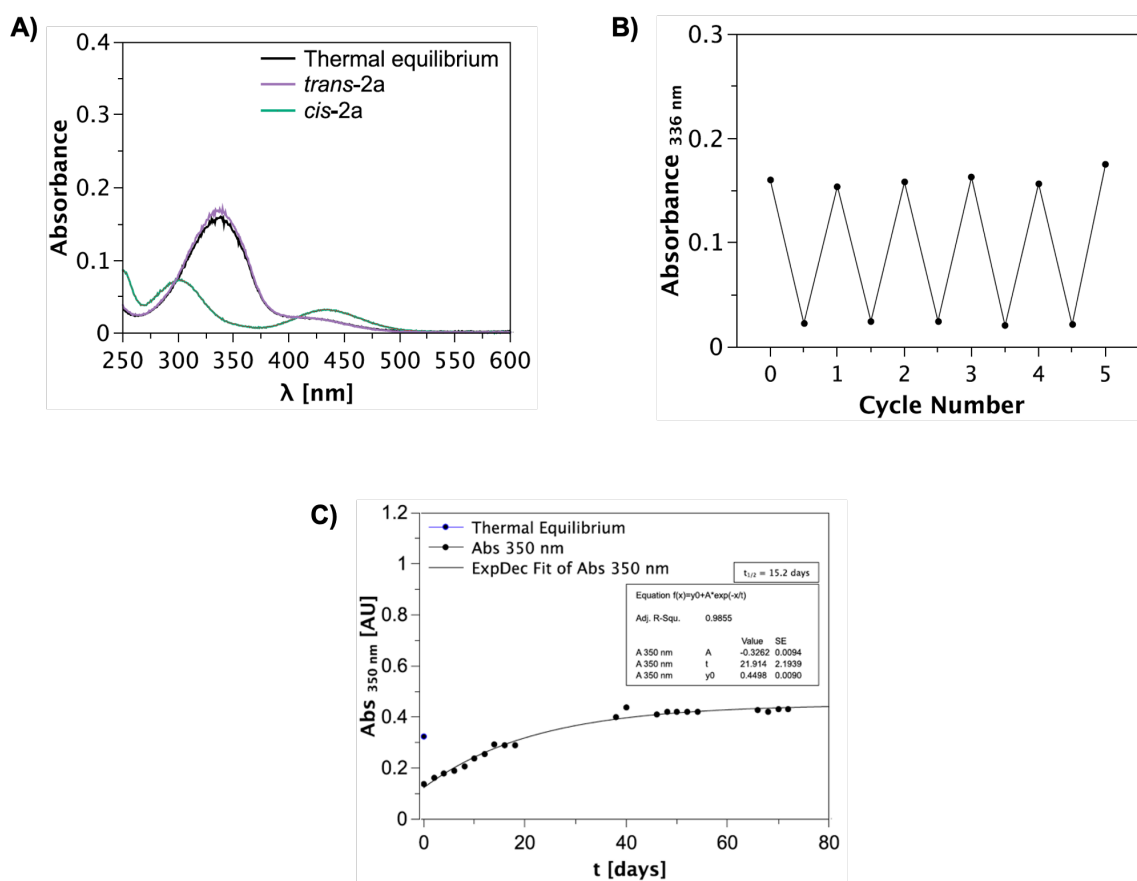


Figure 20. Photophysical properties of **tFAPz 2a** (20 μ M) in buffer solution (TrisHCl Buffer, pH 7.5) + 0.2% DMSO at 25 °C. A) UV/Vis absorption spectra data of thermal equilibrium, *trans*-isomer and *cis*-isomer. The *cis*-isomer was accessed via irradiation with 365 nm, while the *trans*-isomer was obtained with 528 nm irradiation. B) Cycle performance upon alternating irradiation of 365 nm and 528 nm. Data points were recorded at the absorbance maximum of the *trans*-isomer (336 nm). C) Thermal half-life of compound **2a** (50 μ M), measured at 27 °C in buffer solution (TrisHCl Buffer, pH 7.5) + 0.5% DMSO.

Tethered Photoswitchable Derivatives of Fentanyl that Target the μ -Opioid Receptor

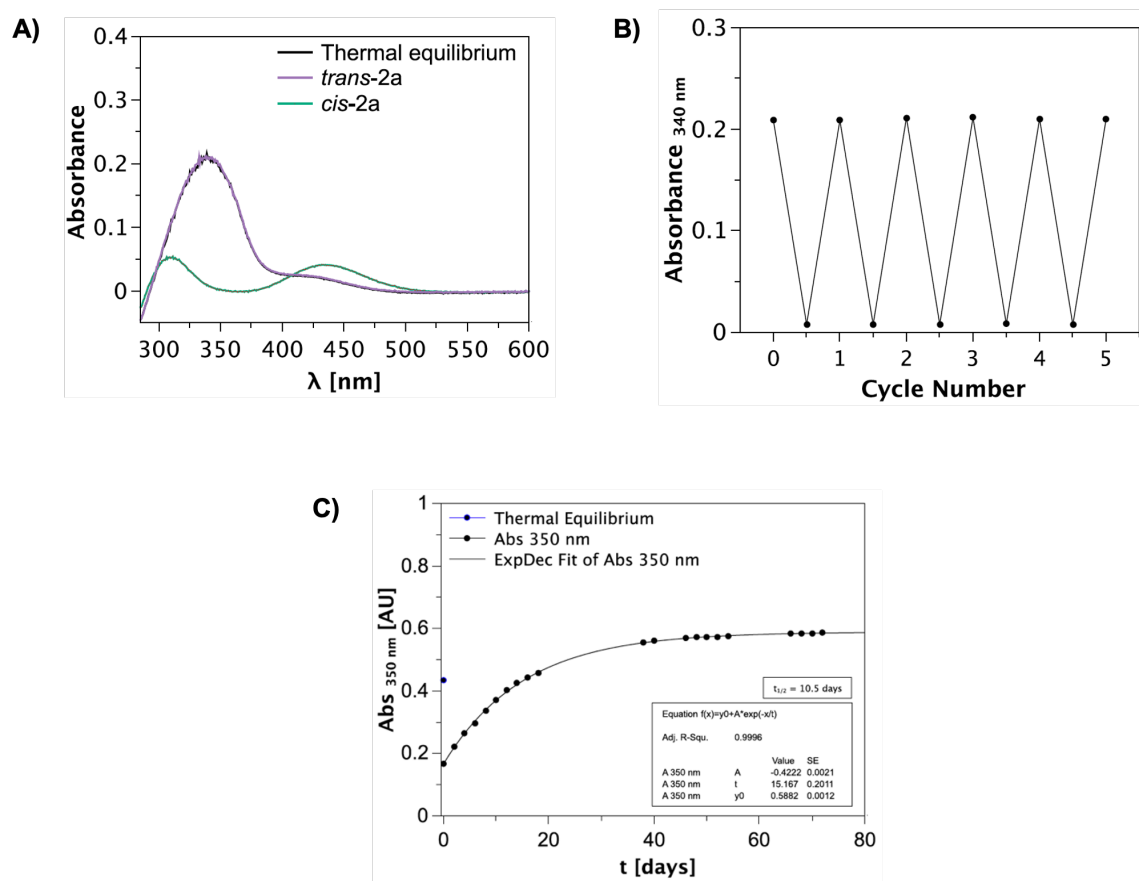


Figure 21. Photophysical properties of **tFAPz 2a** (20 μ M) in DMSO at 25 $^{\circ}$ C. A) UV/Vis absorption spectra data of thermal equilibrium, *trans*-isomer and *cis*-isomer. The *cis*-isomer was accessed via irradiation with 365 nm, while the *trans*-isomer was obtained with 528 nm irradiation. B) Cycle performance upon alternating irradiation of 365 nm and 528 nm. Data points were recorded at the absorbance maximum of the *trans*-isomer (340 nm). C) Thermal half-life of compound **2a** (50 μ M), measured at 27 $^{\circ}$ C.

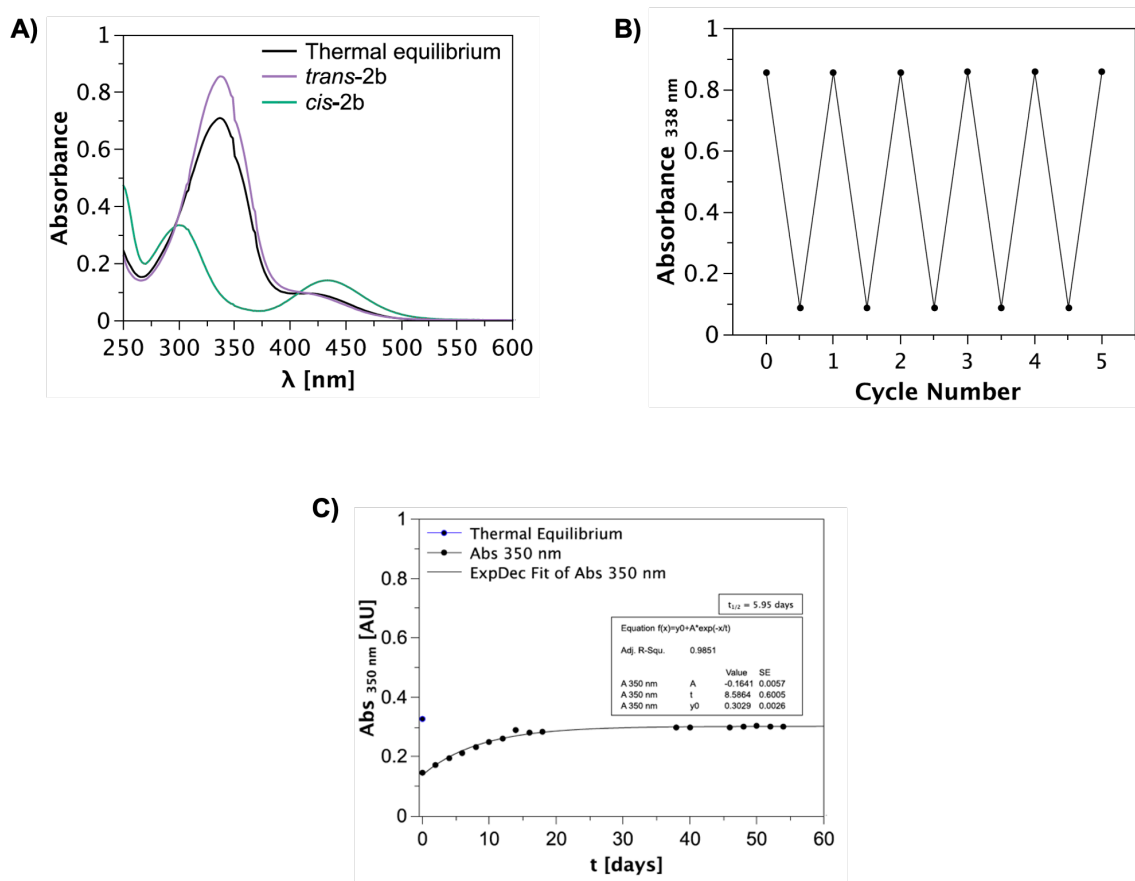


Figure 22. Photophysical properties of **tFAPz 2b** (50 μ M) in buffer solution (TrisHCl Buffer, pH 7.5) + 0.5% DMSO at 25 °C. A) UV/Vis absorption spectra data of thermal equilibrium, *trans*-isomer and *cis*-isomer. The *cis*-isomer was accessed via irradiation with 365 nm, while the *trans*-isomer was obtained with 528 nm irradiation. B) Cycle performance upon alternating irradiation of 365 nm and 528 nm. Data points were recorded at the absorbance maximum of the *trans*-isomer (338 nm). C) Thermal half-life of compound **2b** (50 μ M), measured at 27 °C in buffer solution (TrisHCl Buffer, pH 7.5) + 0.5% DMSO.

Tethered Photoswitchable Derivatives of Fentanyl that Target the μ -Opioid Receptor

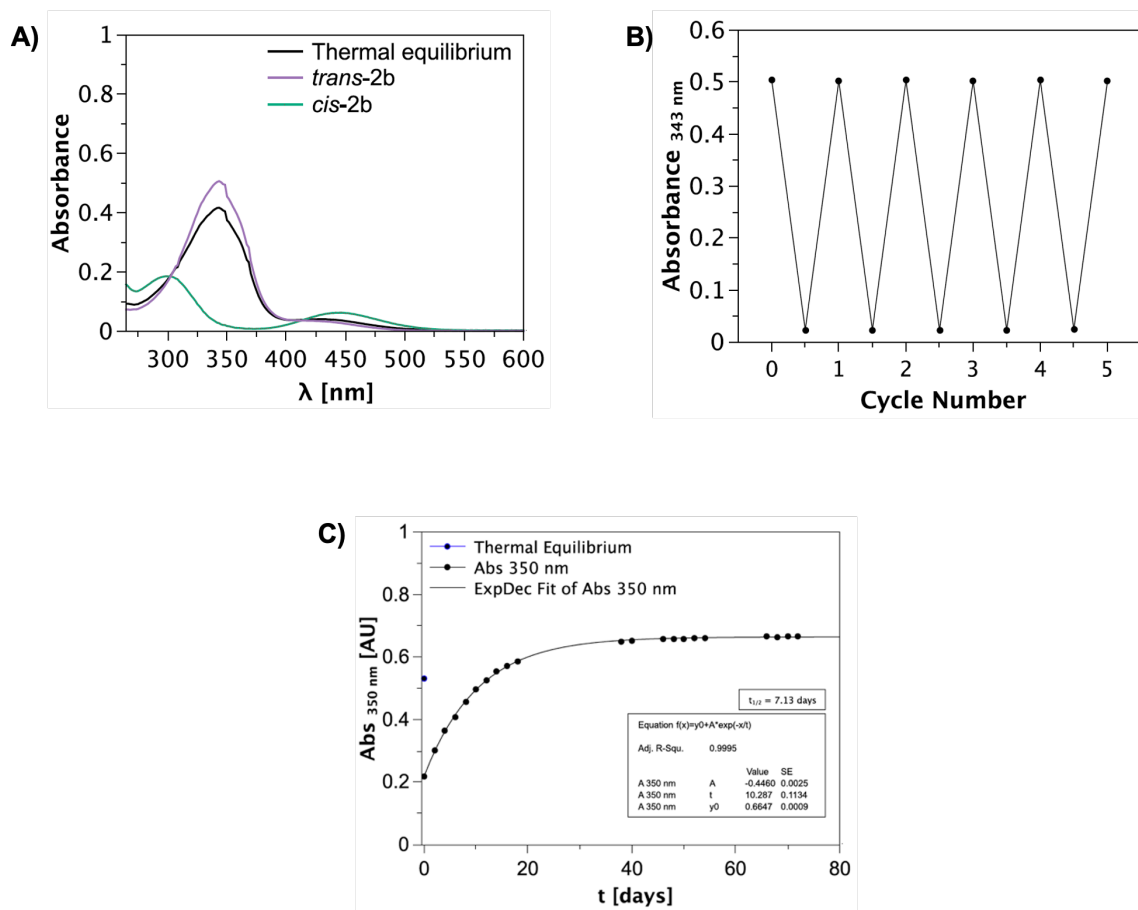


Figure 23. Photophysical properties of **tFAPz 2b** (20 μ M) in DMSO at 25 $^{\circ}$ C. A) UV/Vis absorption spectra data of thermal equilibrium, *trans*-isomer and *cis*-isomer. The *cis*-isomer was accessed via irradiation with 365 nm, while the *trans*-isomer was obtained with 528 nm irradiation. B) Cycle performance upon alternating irradiation of 365 nm and 528 nm. Data points were recorded at the absorbance maximum of the *trans*-isomer (343 nm). C) Thermal half-life of compound **2b** (50 μ M), measured at 27 $^{\circ}$ C.

Tethered Photoswitchable Derivatives of Fentanyl that Target the μ -Opioid Receptor

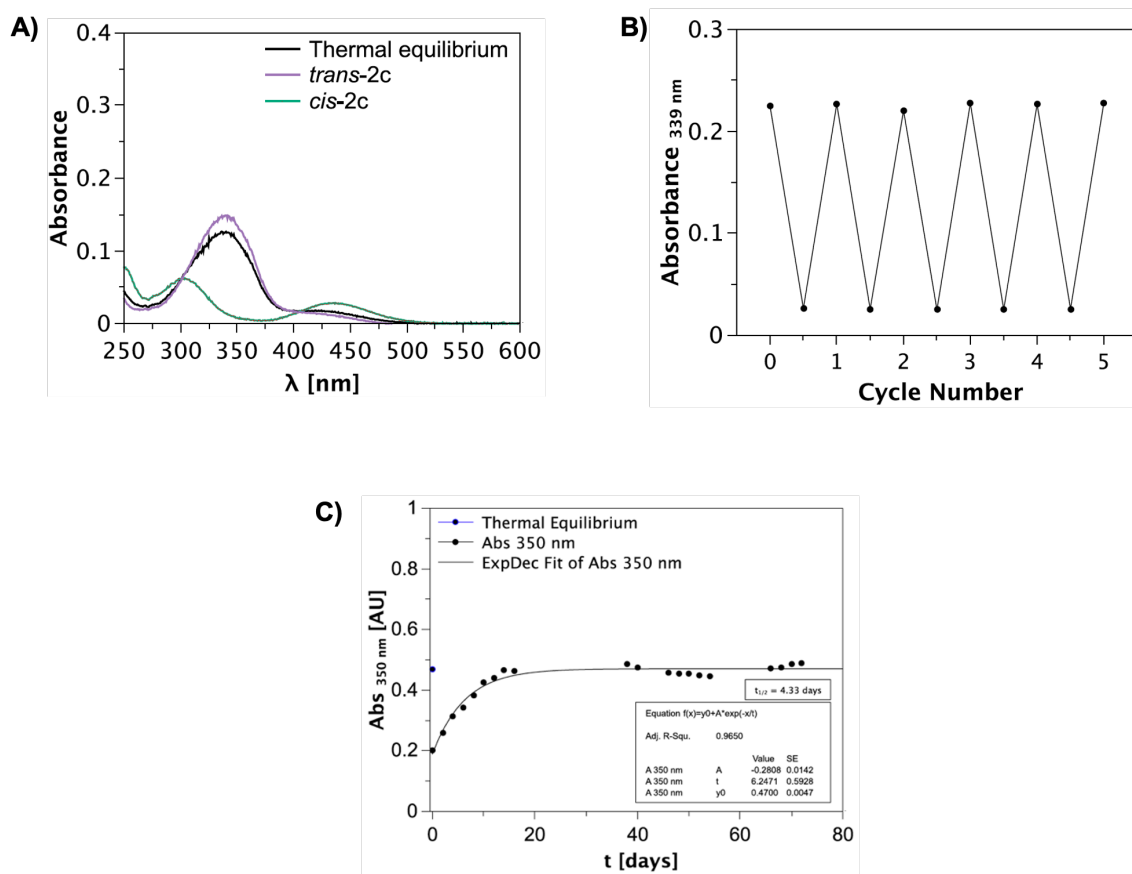


Figure 24. Photophysical properties of **tFAPz 2c** (20 μ M) in buffer solution (TrisHCl Buffer, pH 7.5) + 0.2% DMSO at 25 $^{\circ}$ C. A) UV/Vis absorption spectra data of thermal equilibrium, *trans*-isomer and *cis*-isomer. The *cis*-isomer was accessed via irradiation with 365 nm, while the *trans*-isomer was obtained with 528 nm irradiation. B) Cycle performance upon alternating irradiation of 365 nm and 528 nm. Data points were recorded at the absorbance maximum of the *trans*-isomer (339 nm). C) Thermal half-life of compound **2c** (50 μ M), measured at 27 $^{\circ}$ C in buffer solution (TrisHCl Buffer, pH 7.5) + 0.5% DMSO.

Tethered Photoswitchable Derivatives of Fentanyl that Target the μ -Opioid Receptor

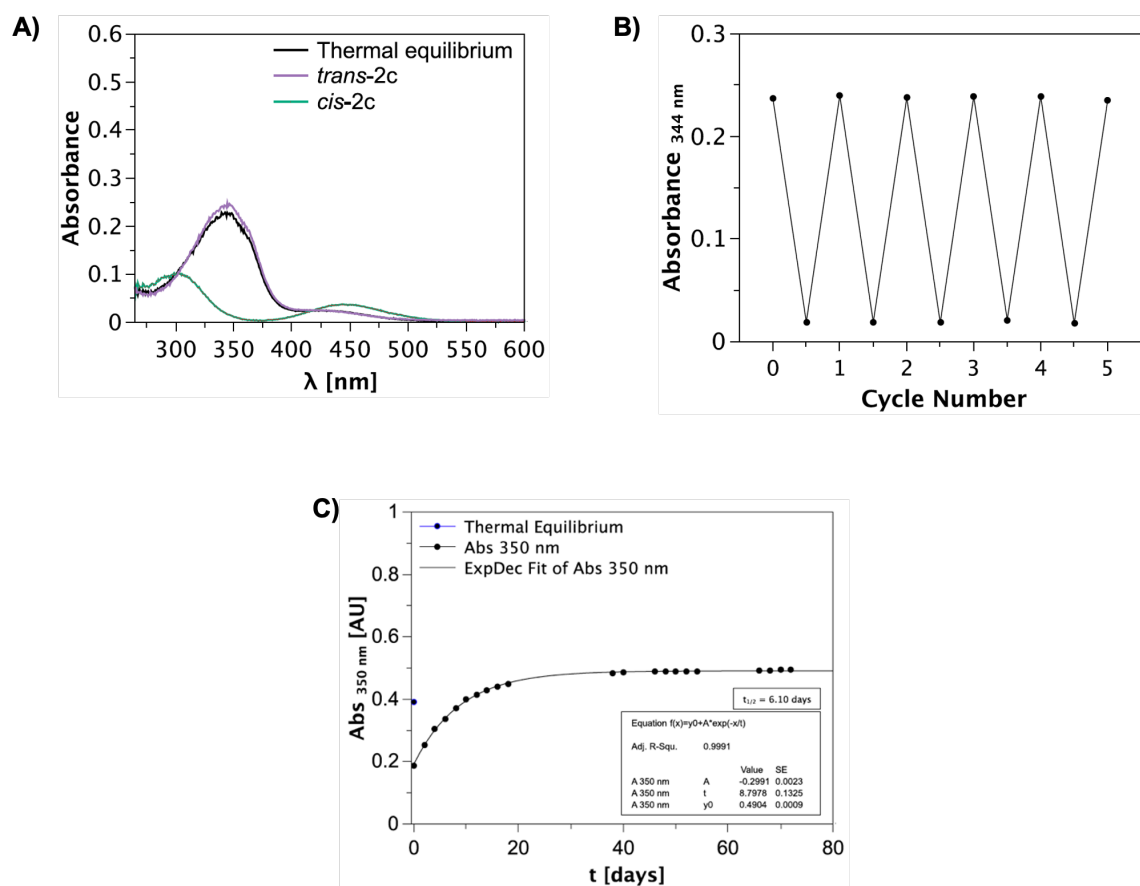


Figure 25. Photophysical properties of **tFAPz 2c** (20 μ M) in DMSO at 25 °C. A) UV/Vis absorption spectra data of thermal equilibrium, *trans*-isomer and *cis*-isomer. The *cis*-isomer was accessed via irradiation with 365 nm, while the *trans*-isomer was obtained with 528 nm irradiation. B) Cycle performance upon alternating irradiation of 365 nm and 528 nm. Data points were recorded at the absorbance maximum of the *trans*-isomer (344 nm). C) Thermal half-life of compound **2c** (50 μ M), measured at 27 °C.

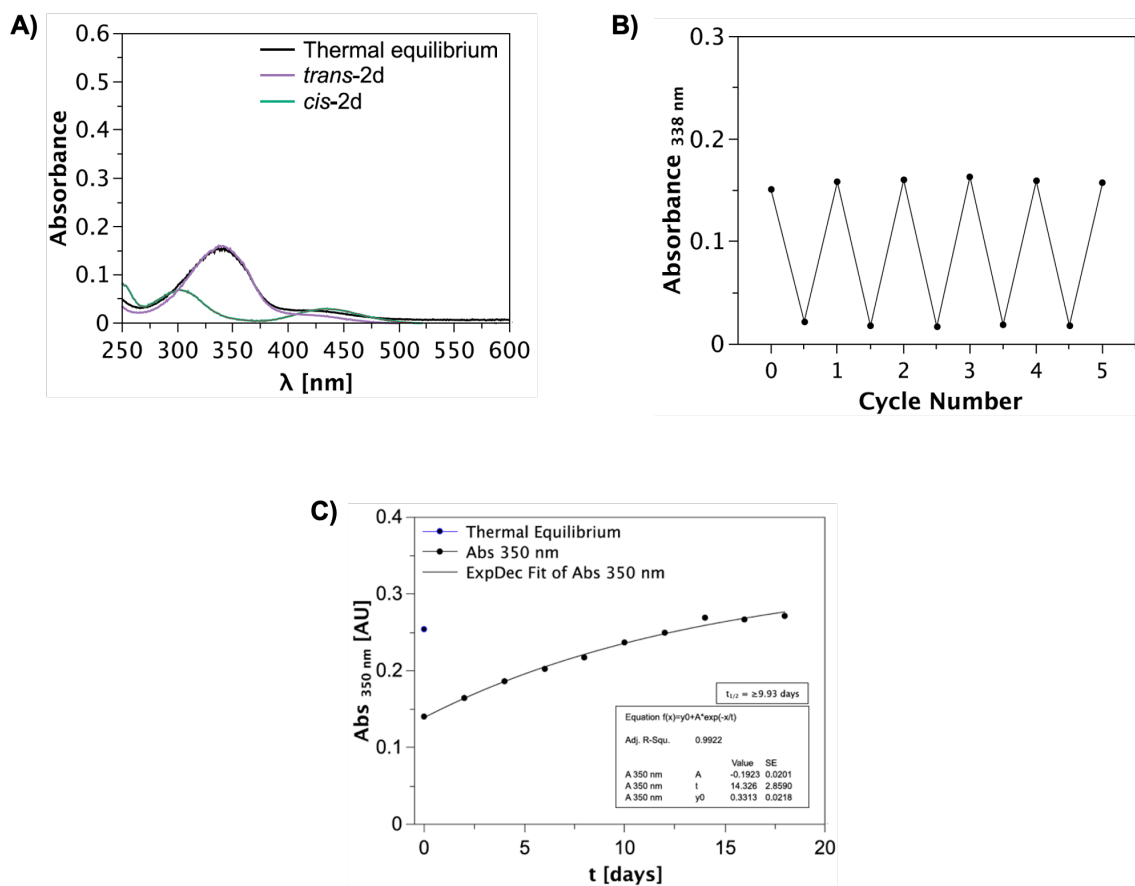


Figure 26. Photophysical properties of **tFAPz 2d** (20 μ M) in buffer solution (TrisHCl Buffer, pH 7.5) + 0.2% DMSO at 25 °C. A) UV/Vis absorption spectra data of thermal equilibrium, *trans*-isomer and *cis*-isomer. The *cis*-isomer was accessed via irradiation with 365 nm, while the *trans*-isomer was obtained with 528 nm irradiation. B) Cycle performance upon alternating irradiation of 365 nm and 528 nm. Data points were recorded at the absorbance maximum of the *trans*-isomer (338 nm). C) Thermal half-life of compound **2d** (50 μ M), measured at 27 °C in buffer solution (TrisHCl Buffer, pH 7.5) + 0.5% DMSO. The symbol ‘ \geq ’ indicates ‘at least’, since the curve did not plateau.

Tethered Photoswitchable Derivatives of Fentanyl that Target the μ -Opioid Receptor

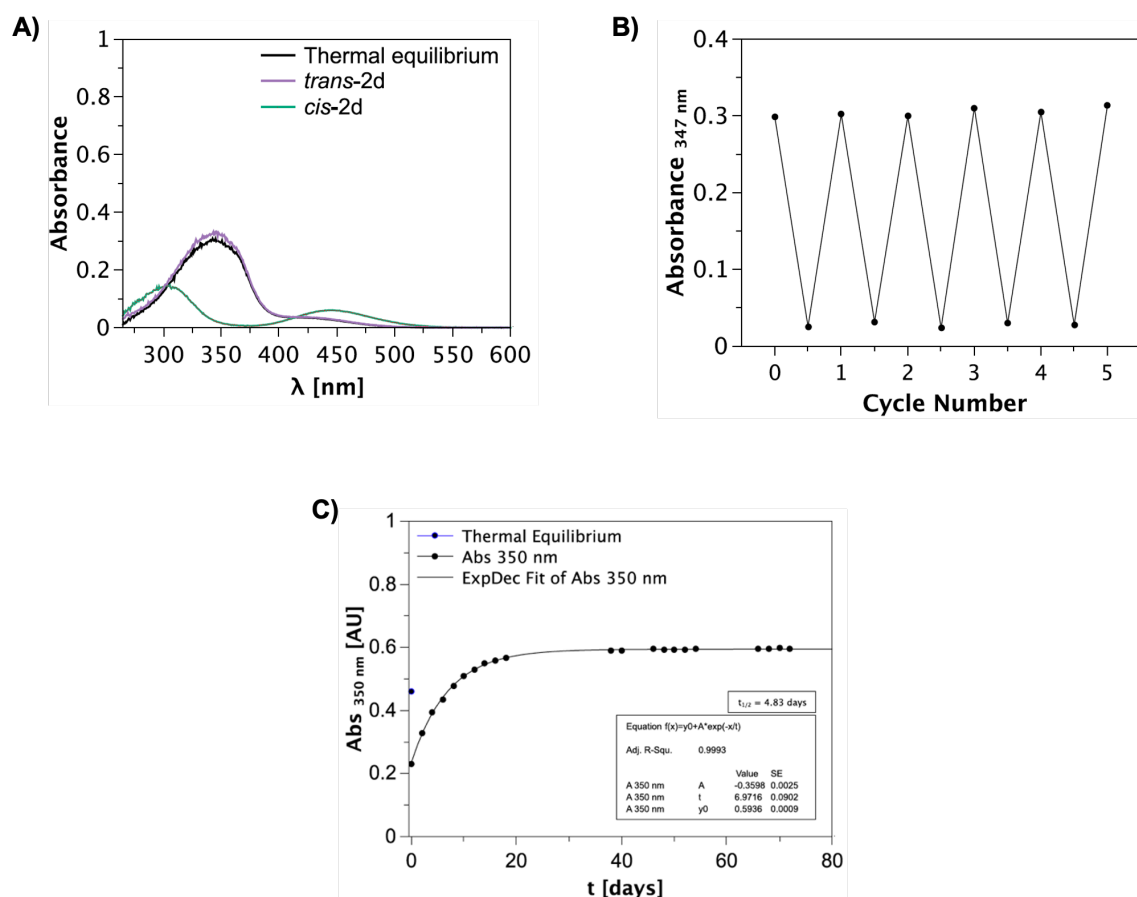


Figure 27. Photophysical properties of **tFAPz 2d** (20 μ M) in DMSO at 25 $^{\circ}$ C. A) UV/Vis absorption spectra data of thermal equilibrium, *trans*-isomer and *cis*-isomer. The *cis*-isomer was accessed via irradiation with 365 nm, while the *trans*-isomer was obtained with 528 nm irradiation. B) Cycle performance upon alternating irradiation of 365 nm and 528 nm. Data points were recorded at the absorbance maximum of the *trans*-isomer (347 nm). C) Thermal half-life of compound **2d** (50 μ M), measured at 27 $^{\circ}$ C.

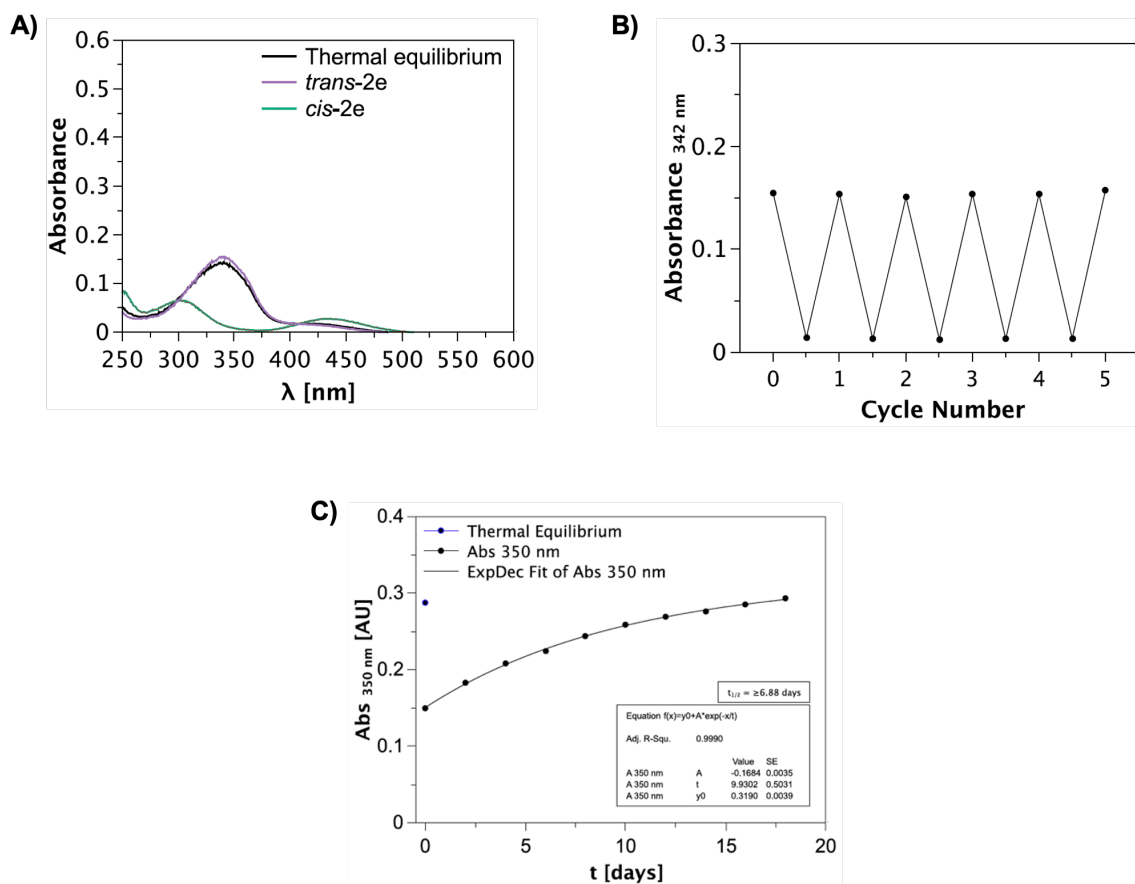


Figure 28. Photophysical properties of **tFAPz 2e** (20 μ M) in buffer solution (TrisHCl Buffer, pH 7.5) + 0.2% DMSO at 25 $^{\circ}$ C. A) UV/Vis absorption spectra data of thermal equilibrium, *trans*-isomer and *cis*-isomer. The *cis*-isomer was accessed via irradiation with 365 nm, while the *trans*-isomer was obtained with 528 nm irradiation. B) Cycle performance upon alternating irradiation of 365 nm and 528 nm. Data points were recorded at the absorbance maximum of the *trans*-isomer (342 nm). C) Thermal half-life of compound **2e** (50 μ M), measured at 27 $^{\circ}$ C in buffer solution (TrisHCl Buffer, pH 7.5) + 0.5% DMSO. The symbol ' \geq ' indicates 'at least', since the curve did not plateau.

Tethered Photoswitchable Derivatives of Fentanyl that Target the μ -Opioid Receptor

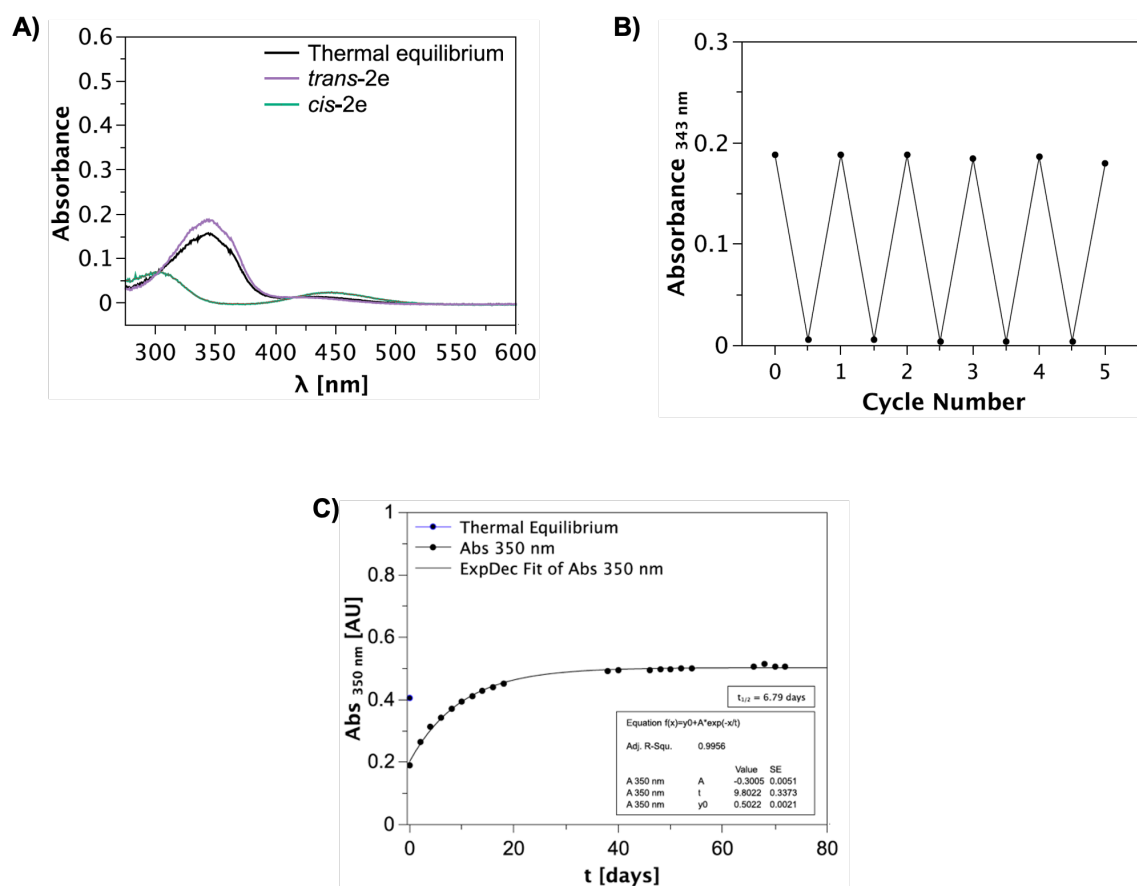


Figure 29. Photophysical properties of **tFAPz 2e** (20 μ M) in DMSO at 25 $^{\circ}$ C. A) UV/Vis absorption spectra data of thermal equilibrium, *trans*-isomer and *cis*-isomer. The *cis*-isomer was accessed via irradiation with 365 nm, while the *trans*-isomer was obtained with 528 nm irradiation. B) Cycle performance upon alternating irradiation of 365 nm and 528 nm. Data points were recorded at the absorbance maximum of the *trans*-isomer (343 nm). C) Thermal half-life of compound **2e** (50 μ M), measured at 27 $^{\circ}$ C.

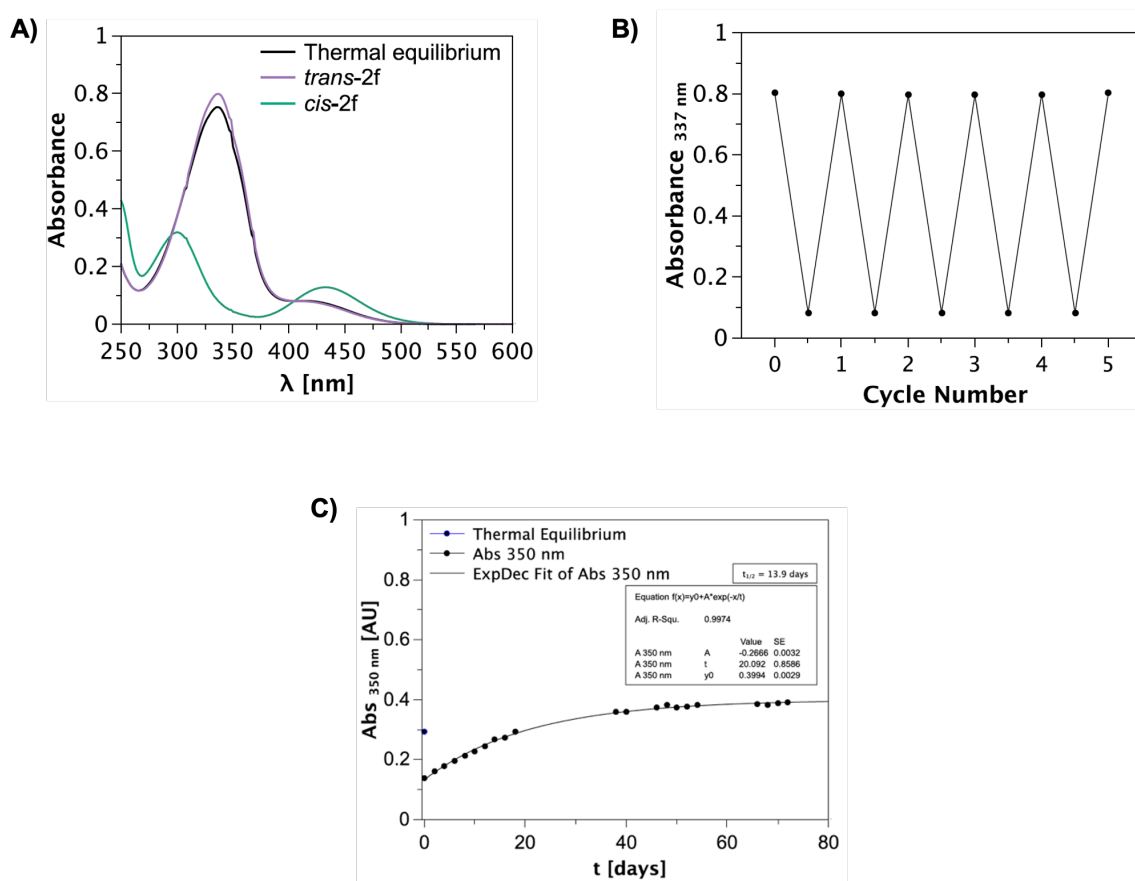


Figure 30. Photophysical properties of **tFAPz 2f** (50 μ M) in buffer solution (TrisHCl Buffer, pH 7.5) + 0.5% DMSO at 25 °C. A) UV/Vis absorption spectra data of thermal equilibrium, *trans*-isomer and *cis*-isomer. The *cis*-isomer was accessed via irradiation with 365 nm, while the *trans*-isomer was obtained with 528 nm irradiation. B) Cycle performance upon alternating irradiation of 365 nm and 528 nm. Data points were recorded at the absorbance maximum of the *trans*-isomer (337 nm). C) Thermal half-life of compound **2f**, measured at 27 °C in buffer solution (TrisHCl Buffer, pH 7.5) + 0.5% DMSO.

Tethered Photoswitchable Derivatives of Fentanyl that Target the μ -Opioid Receptor

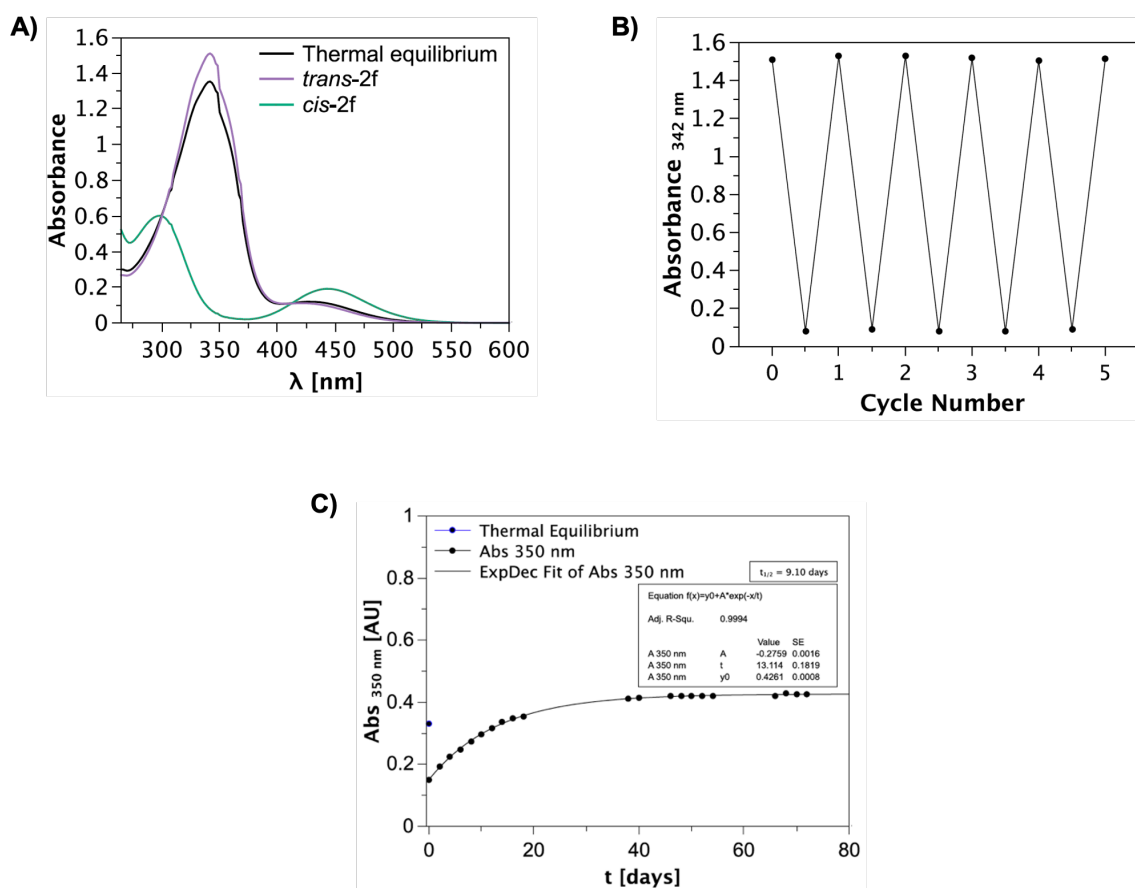


Figure 31. Photophysical properties of **tFAPz 2f** (50 μ M) in DMSO at 25 °C. A) UV/Vis absorption spectra data of thermal equilibrium, *trans*-isomer and *cis*-isomer. The *cis*-isomer was accessed via irradiation with 365 nm, while the *trans*-isomer was obtained with 528 nm irradiation. B) Cycle performance upon alternating irradiation of 365 nm and 528 nm. Data points were recorded at the absorbance maximum of the *trans*-isomer (342 nm). C) Thermal half-life of compound **2f**, measured at 27 °C.

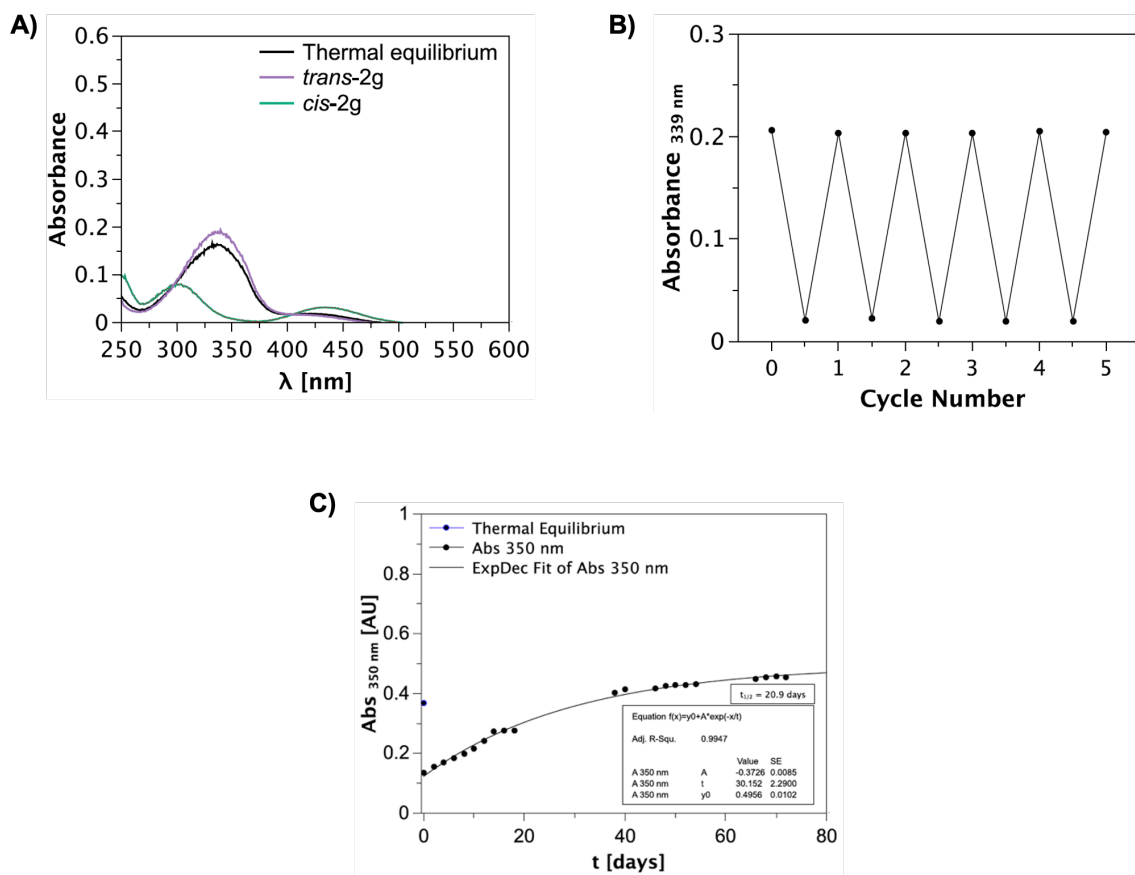


Figure 32. Photophysical properties of **tFAPz 2g** (20 μ M) in buffer solution (TrisHCl Buffer, pH 7.5) + 0.2% DMSO at 25 °C. A) UV/Vis absorption spectra data of thermal equilibrium, *trans*-isomer and *cis*-isomer. The *cis*-isomer was accessed via irradiation with 365 nm, while the *trans*-isomer was obtained with 528 nm irradiation. B) Cycle performance upon alternating irradiation of 365 nm and 528 nm. Data points were recorded at the absorbance maximum of the *trans*-isomer (339 nm). C) Thermal half-life of compound **2g** (50 μ M), measured at 27 °C in buffer solution (TrisHCl Buffer, pH 7.5) + 0.5% DMSO.

Tethered Photoswitchable Derivatives of Fentanyl that Target the μ -Opioid Receptor

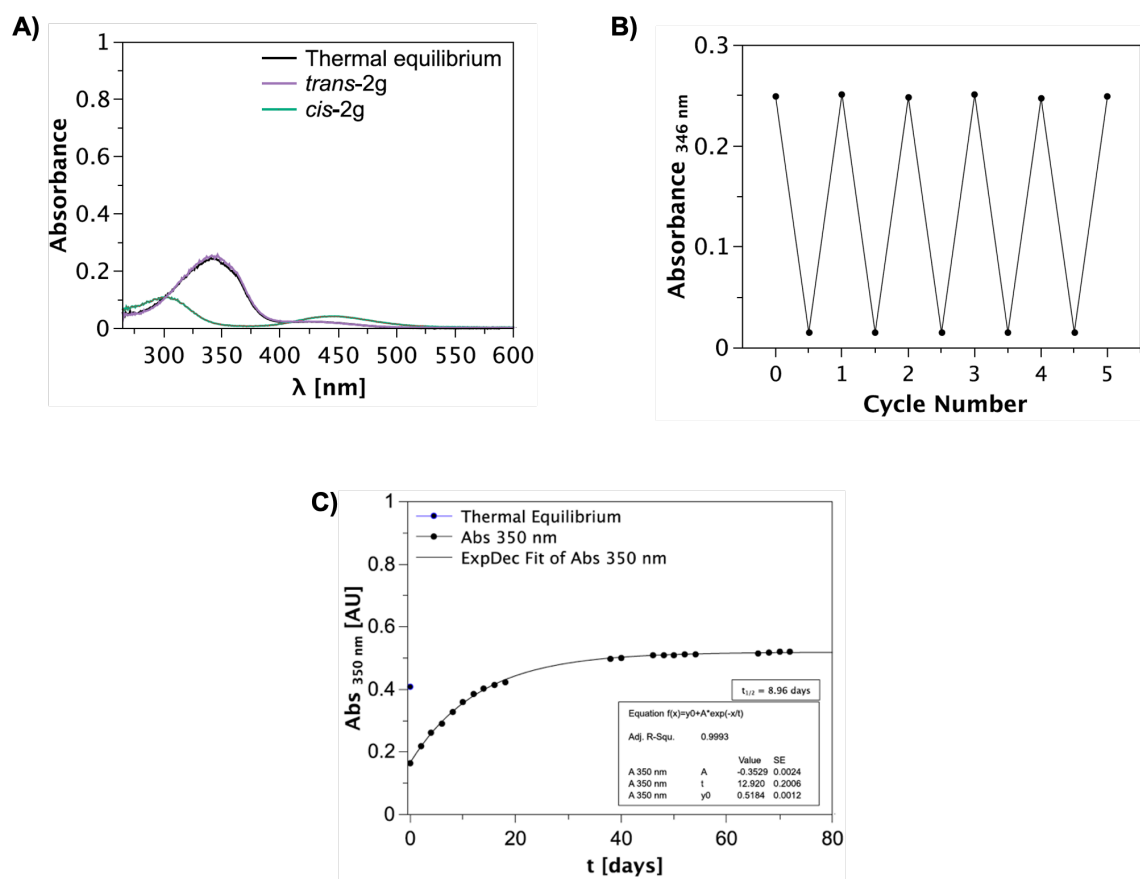


Figure 33. Photophysical properties of **tFAPz 2g** (20 μ M) in DMSO at 25 $^{\circ}$ C. A) UV/Vis absorption spectra data of thermal equilibrium, *trans*-isomer and *cis*-isomer. The *cis*-isomer was accessed via irradiation with 365 nm, while the *trans*-isomer was obtained with 528 nm irradiation. B) Cycle performance upon alternating irradiation of 365 nm and 528 nm. Data points were recorded at the absorbance maximum of the *trans*-isomer (346 nm). C) Thermal half-life of compound **2g** (50 μ M), measured at 27 $^{\circ}$ C.

Tethered Photoswitchable Derivatives of Fentanyl that Target the μ -Opioid Receptor

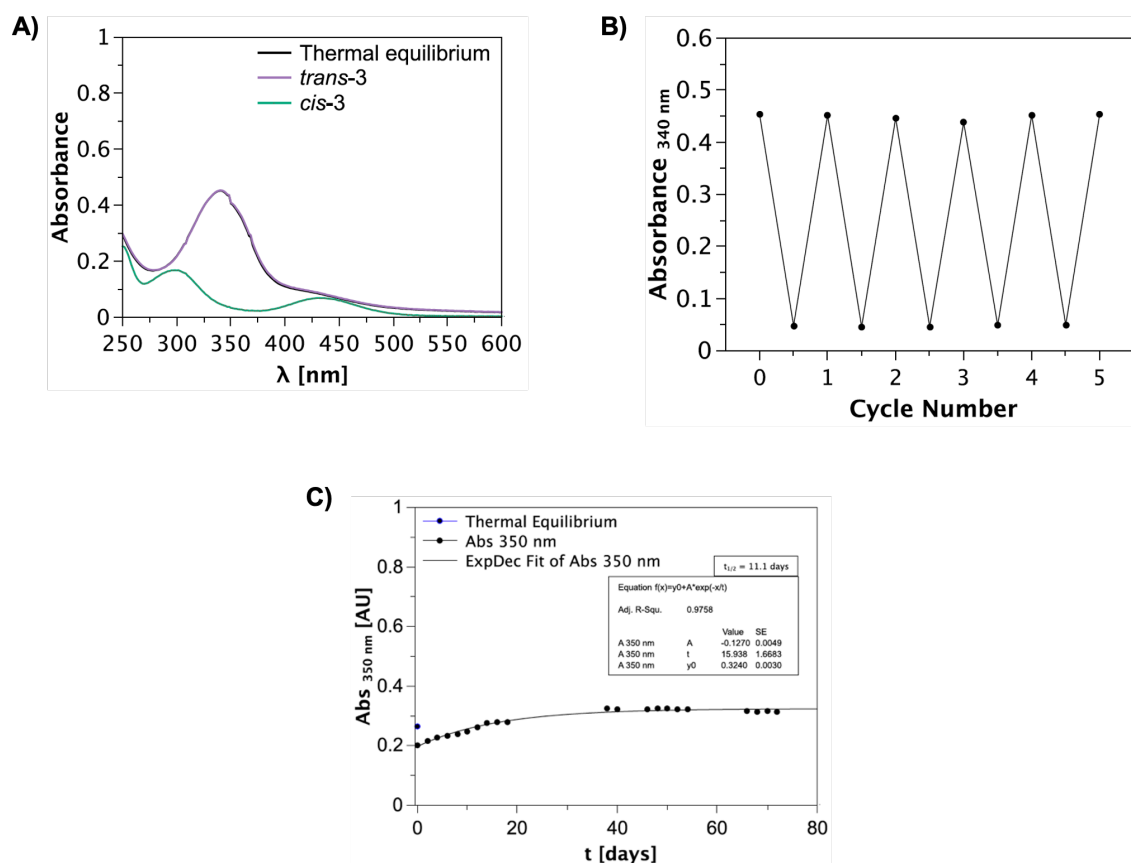


Figure 34. Photophysical properties of **tFAPz 3** (20 μ M) in buffer solution (TrisHCl Buffer, pH 7.5) + 0.2% DMSO at 25 $^{\circ}$ C. A) UV/Vis absorption spectra data of thermal equilibrium, *trans*-isomer and *cis*-isomer. The *cis*-isomer was accessed via irradiation with 365 nm, while the *trans*-isomer was obtained with 528 nm irradiation. B) Cycle performance upon alternating irradiation of 365 nm and 528 nm. Data points were recorded at the absorbance maximum of the *trans*-isomer (340 nm). C) Thermal half-life of compound **3** (50 μ M), measured at 27 $^{\circ}$ C in buffer solution (TrisHCl Buffer, pH 7.5) + 0.5% DMSO.

Tethered Photoswitchable Derivatives of Fentanyl that Target the μ -Opioid Receptor

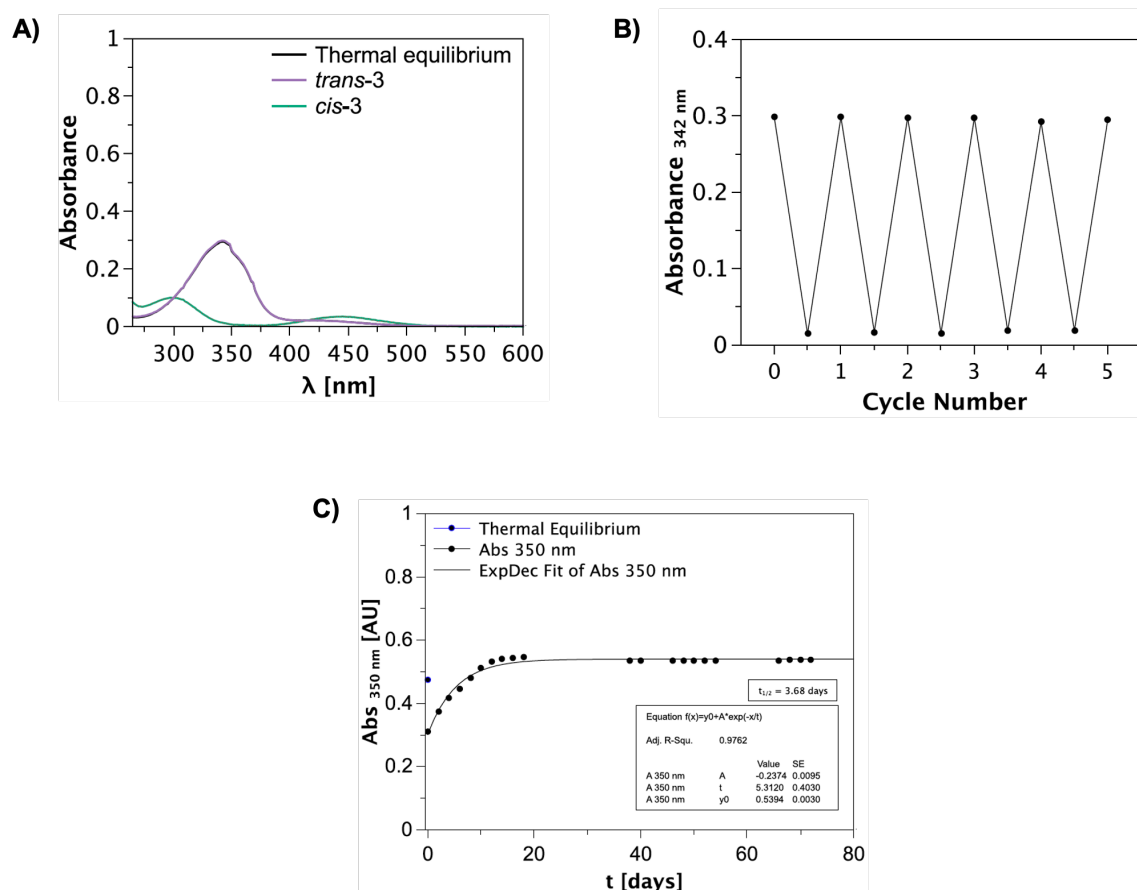


Figure 35. Photophysical properties of **tFAPz 3** (10 μ M) in DMSO at 25 °C. A) UV/Vis absorption spectra data of thermal equilibrium, *trans*-isomer and *cis*-isomer. The *cis*-isomer was accessed via irradiation with 365 nm, while the *trans*-isomer was obtained with 528 nm irradiation. B) Cycle performance upon alternating irradiation of 365 nm and 528 nm. Data points were recorded at the absorbance maximum of the *trans*-isomer (342 nm). C) Thermal half-life of compound **3** (50 μ M), measured at 27 °C.

2.7.2.3 PSS Evaluation

All PSS measurements can be found in the appendix (Section 7.3.2) under ‘Analytical HPLC Chromatograms for PSS Determination’.

2.7.3 Supplementary Biochemical Information

2.7.3.1 Materials and Methods

Radioligand Binding

Binding affinities towards the human opioid receptor μ OR and the mutant μ OR_{M1} were determined as described previously.^[1, 5] In brief, membranes were prepared from HEK293T cells transiently transfected with the cDNA for μ OR (gift from the Ernest Gallo Clinic and Research Center, UCSF, CA) or μ OR_{M1} (gift from B. Kobilka, Stanford University, CA) and incubated with the radioligand [³H]diprenorphine (specific activity 31 Ci/mmol; PerkinElmer, Rodgau, Germany) at concentrations of 0.2 to 0.3 nM for μ OR, and 0.15 to 0.2 nM for μ OR_{M1}, respectively. Homogenates expressing μ OR with a B_{\max} of 3000 ± 350 fmol/mg protein and a K_D of 0.11 ± 0.02 nM or membranes with from μ OR_{M1} expressing cells with a B_{\max} of 4500 ± 500 fmol/mg protein and a K_D of 0.12 ± 0.02 nM were incubated at an amount of protein of 4 μ g/well with radioligand and varying concentrations of test compound (in the range of 10 pM - 100 μ M) for 60 min in binding buffer (50 mM Tris, pH 7.4) and filtered on glass fiber mats presoaked with a 0.3% aqueous polyethyleneimine solution. Trapped radioactivity was determined with a microplate reader (Microbeta Trilux, Perkin Elmer) by scintillation counting. To measure the photoswitchable compounds, 200-300 μ L working solution was irradiated with a single LED at 528 nm for 180 sec to generate the *trans*-isomer or at 365 nm for 20 sec to obtain the *cis*-isomer.

Unspecific binding was determined in the presence of 10 μ M of naloxone. Protein concentration was determined employing the method of Lowry, with bovine serum albumin as standard.^[6] The resulting competition curves of the receptor binding experiments were analyzed by nonlinear regression, using the algorithms in PRISM 9.0 (GraphPad Software, San Diego, USA). The data were initially fit using a sigmoid model to provide IC_{50} values, which were subsequently transformed to K_i values according to the equation of Cheng and Prusoff.^[7] Mean K_i values were calculated from 3-7 individual experiments, each performed in triplicate.

Tethered Photoswitchable Derivatives of Fentanyl that Target the μ -Opioid Receptor

IP Accumulation Assay for Receptor Activation

The determination of receptor mediated G-protein signaling by μ OR and μ OR_{M1} activation was conducted applying an IP accumulation assay (IP-One HTRF[®], PerkinElmer, Rodgau, Germany), according to the manufacturer's protocol and in analogy to previously described protocols.^[1, 8] In brief, HEK293T cells were co-transfected with the cDNA for μ OR or μ OR_{M1} and the hybrid G-protein G α q5HA (G α q protein with the last five amino acids at the C-terminus replaced by the corresponding sequence of G α i (gift from The J. David Gladstone Institutes, San Francisco, CA), respectively and transferred into 384-well microplates. Cells were incubated with test compound for 180 min and accumulation of second messenger was stopped by adding detection reagents (IP1-d2 conjugate and Anti-IP1cryptate TB conjugate). After 60 min, TR-FRET was measured with a Clariostar plate reader. FRET emission was measured at 620 nm and 665 nm, the corresponding ratio (emission at 665 nm/emission at 620 nm) was calculated and normalized to vehicle (0%) and the maximum effect of the reference DAMGO (100%). Each single experiment, performed in duplicate, was analyzed applying the algorithms of four parameter non-linear regression, implemented in Prism 9.0 to get dose-response curves, EC₅₀ and E_{max} values, which was repeated to get 4-7 independent values.

Radioligand Depletion Assay for Determining Covalent Binding

Tests to determine covalent binding to the receptor were carried out as previously described.^[9] Briefly, membranes from HEK293T cells were transiently transfected with the human opioid receptor carrying the mutation N127^{2,63}C (μ OR_{M1}). Before the experiment, 200-300 μ L working solution of the PTLs were irradiated with a single LED at 528 nm for 180 sec to generate the *trans*-isomer or at 365 nm for 20 sec to obtain the *cis*-isomer. Membranes were preincubated with 1 μ M of *trans*-tFAPz **1** or *cis*-tFAPz **1** for 15, 30, 60, 120 and 180 min. Incubation was stopped by centrifugation and the amount of reversibly bound ligand was washed out three times (resuspension of the membranes in buffer for 30 min followed by centrifugation). Finally, the membranes were used for radioligand binding experiments with [³H]diprenorphine to determine the remaining specific binding according to the protocol described above. As controls, 100 nM of naloxone or fentanyl were evaluated under the same conditions. Data analysis was performed via normalization by defining unspecific binding equal to 0% and total binding equal to 100%. The amount of covalent

Tethered Photoswitchable Derivatives of Fentanyl that Target the μ -Opioid Receptor

binding was calculated by the equation [covalent binding [%] = 100 – specific binding [%]]. Kinetics of covalent binding was analyzed by nonlinear regression, using the equation for one phase exponential decay in PRISM 9.0 to get the rate constant and subsequently, the half-life for covalent binding and the maximum amount of covalent binding to receptor binding sites. Mean values were derived from 3-6 individual experiments each done in quadruplicate.

2.7.3.2 Supplementary Figures and Tables

Table 7. tFAPz-mediated activation screen at μ OR_{wt}.^{[a][b]}

Compound	μ OR _{wt}	
	E_{\max} [% \pm S.E.M.] ^[c]	(n) ^[d]
DAMGO	100	7
Fentanyl	100 \pm 2.4	7
<i>trans</i> -tFAPz 1	100 \pm 0.1	2
<i>cis</i> -tFAPz 1	101 \pm 0.8	2
<i>trans</i> -tFAPz 2a	<1	3
<i>cis</i> -tFAPz 2a	<1	2
<i>trans</i> -tFAPz 2b	<1	2
<i>cis</i> -tFAPz 2b	29 \pm 0.6	2
<i>trans</i> - tFAPz 2c	<1	2
<i>cis</i> -tFAPz 2c	<1	1
<i>trans</i> -tFAPz 2d	<1	2
<i>cis</i> -tFAPz 2d	31	1
<i>trans</i> -tFAPz 2e	<1	3
<i>cis</i> -tFAPz 2e	<1	2
<i>trans</i> -tFAPz 2f	18 \pm 1.7	2
<i>cis</i> -tFAPz 2f	16 \pm 5.5	2
<i>trans</i> -tFAPz 2g	<1	3
<i>cis</i> -tFAPz 2g	3 \pm 0.1	2
<i>trans</i> -tFAPz 3	<1	2
<i>cis</i> -tFAPz 3	<1	2

^[a]IP-One accumulation assay (Cisbio) with HEK293T cells transiently co-transfected with the cDNAs of the human μ OR and the hybrid G-protein $G_{\alpha_{q5HA}}$. ^[b]tFAPz ligands were evaluated with a concentration of 10 μ M, the references DAMGO and fentanyl were tested at 100 nM. ^[c]Maximum receptor activation in [% \pm S.E.M.] relative to the full effect of DAMGO. ^[d]Number of individual experiments each performed in duplicate.

Tethered Photoswitchable Derivatives of Fentanyl that Target the μ -Opioid Receptor

Table 8. Kinetics of **tFAPz**-mediated covalent binding at μ ORM1.^{[a][b]}

	Maximum specific binding [% \pm S.E.M.] ^[c]	Maximum covalent binding [% \pm S.E.M.] ^[d]	Rate constant of covalent binding <i>K</i> [min ⁻¹ \pm S.E.M.]	Half-life of covalent binding [min \pm S.E.M.]
<i>trans</i> - tFAPz 1	26 \pm 1	74 \pm 1	0.066 \pm 0.010	12.5 \pm 2.5
<i>cis</i> - tFAPz 1	33 \pm 4	67 \pm 4	0.036 \pm 0.005	23.8 \pm 6.2
Naloxone	~100	~ 0	---	---

^[a]Kinetic data were determined in a radioligand depletion assay with HEK293T cells transiently co-transfected with the cDNAs of the mutant μ OR N127^{2.63}C (μ OR_{M1}) and the hybrid G-protein G α_{q5} 5HA. ^[b]**tFAPz** ligands were evaluated with a concentration of 1 μ M in 6 independent experiments each performed in quadruplicate, naloxone was tested at 100 nM in 3 independent experiments. ^[c]Maximum specific binding after incubation with the PTL relative to specific binding measured with buffer in [% \pm S.E.M.]. ^[d]Maximum covalent binding derived from maximum specific binding by applying the equation [*covalent binding* = 100 – *specific binding*] in [% \pm S.E.M.].

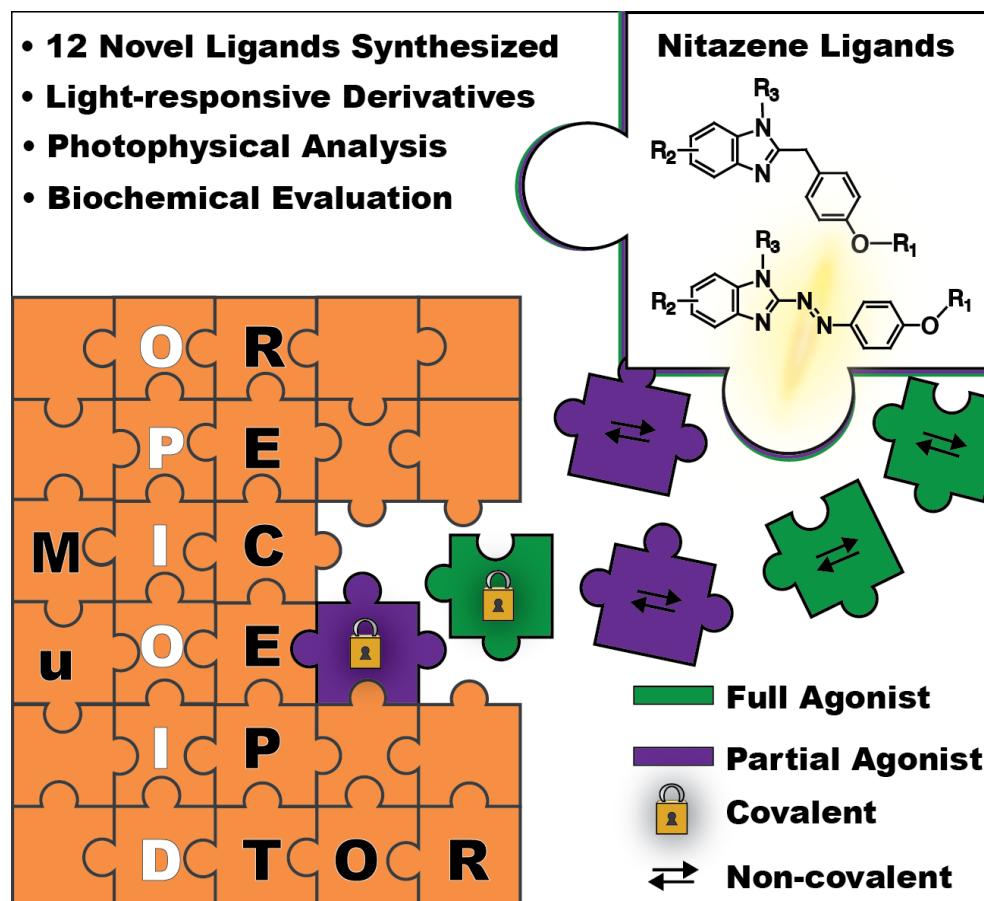
2.7.4 NMR Spectra

All NMR spectra can be found in the appendix (Section 7.3.3).

2.7.5 References

- [1] R. Lahmy, H. Hübner, M. F. Schmidt, D. Lachmann, P. Gmeiner, B. König, *Chem. Eur. J.* **2022**, *28*, e202201515.
- [2] J.-Y. Wu, C.-D. Kuo, C.-Y. Chu, M.-S. Chen, J.-H. Lin, Y.-J. Chen, H.-F. Liao, *Molecules* **2014**, *19*, 6911-6928.
- [3] I. Kosiova, A. Janicova, P. Kois, *Beilstein J. Org. Chem.* **2006**, *2*, 23.
- [4] P. C. Donthamsetti, N. Winter, M. Schönberger, J. Levitz, C. Stanley, J. A. Javitch, E. Y. Isacoff, D. Trauner, *J. Am. Chem. Soc.* **2017**, *139*, 18522-18535.
- [5] a) H. Hübner, C. Haubmann, W. Utz, P. Gmeiner, *J. Med. Chem.* **2000**, *43*, 756-762; b) A. Drakopoulos, Z. Koszegi, Y. Lanoiselée, H. Hübner, P. Gmeiner, D. Calebiro, M. Decker, *J. Med. Chem.* **2020**, *63*, 3596-3609.
- [6] O. H. Lowry, N. J. Rosebrough, A. L. Farr, R. J. Randall, *J. Biol. Chem.* **1951**, *193*, 265-275.
- [7] Y. C. Cheng, W. H. Prusoff, *Biochem. Pharmacol.* **1973**, *22*, 3099-3108.
- [8] a) H. Liu, J. Hofmann, I. Fish, B. Schaake, K. Eitel, A. Bartuschat, J. Kaindl, H. Rapp, A. Banerjee, H. Hübner, M. J. Clark, S. G. Vincent, J. T. Fisher, M. R. Heinrich, K. Hirata, X. Liu, R. K. Sunahara, B. K. Shoichet, B. K. Kobilka, P. Gmeiner, *Proc. Natl. Acad. Sci. U. S. A.* **2018**, *115*, 12046-12050; b) C. Gentzsch, K. Seier, A. Drakopoulos, M.-L. Jobin, Y. Lanoiselée, Z. Koszegi, D. Maurel, R. Sounier, H. Hübner, P. Gmeiner, S. Granier, D. Calebiro, M. Decker, *Angew. Chem. Int. Ed. Engl.* **2020**, *59*, 5958-5964.
- [9] a) D. Weichert, A. C. Kruse, A. Manglik, C. Hiller, C. Zhang, H. Hübner, B. K. Kobilka, P. Gmeiner, *Proc. Natl. Acad. Sci. U. S. A.* **2014**, *111*, 10744-10748; b) R. C. Kling, M. Plomer, C. Lang, A. Banerjee, H. Hübner, P. Gmeiner, *ACS Chem. Biol.* **2016**, *11*, 869-875.

3. Covalent and Photochromic Derivatives of the Potent Synthetic Opioid Isotonitazene and Other Nitazenes



CHAPTER 3

3.1 Abstract

Isotonitazene belongs to a potent class of μ -opioid receptor (μ OR) ligands, known as nitazenes. The lack of knowledge surrounding this agonist and others in its class has sparked thorough re-investigations. In order to aid in these investigations, a covalent and underexplored nitazene, BIT, was biochemically re-evaluated in this work. Furthermore, a derivative of BIT that was modeled on the structure of isotonitazene, Iso-BIT, was developed and exhibited slightly better covalent binding properties than BIT. Expanding the repertoire of nitazenes as probes was considered to be valuable in the pursuit of further understanding the mechanisms, functions and interactions of μ OR. As a result, photoswitchable probes were successfully developed in this work, modeled on the nitazene structure. Converting known ligands into azo-containing photoswitchable derivatives offers the opportunity to modulate ligand structure with light, allowing for photocontrol of compound activity. While photocontrol of μ OR activity could not be entirely achieved, photophysical evaluation of these arylazobenzimidazole derivatives revealed a novel photoswitch scaffold that responds to visible light. Furthermore, azo-containing **2e** and **3e** emerged as promising derivatives that were able to form an exceptionally high fraction of covalent-ligand receptor complexes with wild-type μ OR at physiological pH.

Major parts of this chapter are in the submission process:

R. Lahmy, H. Hübner, P. Gmeiner, B. König. **2023.**

Author contributions:

RL synthesized the compounds described in this chapter and performed the corresponding chemical and photophysical evaluations. HH performed the biochemical measurements and evaluations. The manuscript was written by RL, with the biochemical section (Section 3.3.4) written by both HH and RL. BK and PG supervised the project and are the corresponding authors.

3.2 Introduction

3.2.1 Re-emergence of the Potent Opioid Isotonitazene

Isotonitazene has been coined a ‘life-threatening’ substance that belongs to an emerging class of synthetic opioids, known as ‘nitazenes’.^[1] This potent agonist that targets the μ -opioid receptor (μ OR), a G-protein-coupled receptor (GPCR), has sparked great concern since its detection in 2019 on European, Canadian and USA illicit drug markets.^[1-2] Despite being first characterized in 1960 with a potency 500-fold greater than morphine,^[3] isotonitazene did not become a regulated drug in these regions until this recent detection and recent association with several fatal overdoses.^[1b, 4] Interestingly, isotonitazene was amongst several other potent 2-benzylbenzimidazole derivatives (nitazenes) that were investigated in the 50’s and 60’s as potential analgesics.^[3, 5] Even though these derivatives did not become clinically approved as medication, several analogues became officially regulated during this period.^[2b, 6] This includes a less potent structural analogue of isotonitazene, clonitazene, and the more potent structural analogue etonitazene, with the latter reported at that time to have 1000-fold greater potency than morphine.^[3-4] When compared to complex poppy alkaloids, synthetic nitazene opioids possess a simpler structure, rendering them more synthetically accessible. This access may also account for their increase in popularity and could become dangerous when considering the plethora of unregulated nitazene derivatives that could be produced in the future. As a result, the stark re-emergence of isotonitazene triggered concern for the lack of knowledge associated with this compound and its derivatives.^[4, 7]

3.2.2 Isotonitazene Sparks Investigations into Nitazenes

While numerous nitazenes, including isotonitazene, have very recently been re-investigated and reviewed,^[2, 4, 7-8] other derivatives require further attention. This includes the irreversible μ OR agonist BIT (reported as 2-(*p*-ethoxy-benzyl)-1-diethylaminoethyl-5-isothiocyanobenzimidazole isothiocyanate) that was first documented in 1983.^[9] The structure of BIT was modeled on the potent ligand etonitazene and contains a reactive isothiocyanate (SCN) in place of the 5-nitro group (Figure 36). Despite being used as a μ OR alkylating agent in the 80’s, 90’s and early 2000’s, BIT has seemingly ‘fallen off the radar’ in recent years, perhaps due to better non-nitazene alternatives.^[10] It should be noted that an azido etonitazene derivative was developed in 1990 as an effective photoactivatable μ OR alkylating agent, however, received even less attention.^[11] Nonetheless, an irreversible

Covalent and Photochromic Derivatives of the Potent Synthetic Opioid Isotonitazene and Other Nitazenes

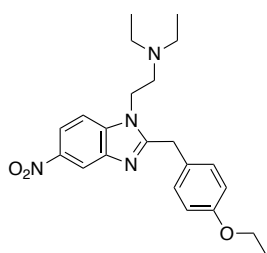
nitazene-based ligand that selectively targets the μ OR may be of interest in further understanding nitazene interactions with μ OR. Improved knowledge of this complex GPCR is important, especially for the desired development of physiologically-biased opioids that avoid harmful side effects and induce the medically-beneficial analgesic effect.^[12] Despite theoretical and computational research that elucidates the binding modes of isotonitazene and other nitazenes to μ OR,^[8e, 13] an irreversible ligand may allow access to further powerful technologies for clarifying these interactions, such as ligand-bound protein crystallography. Such developments may be necessary to better understand the impressive potencies of nitazenes.

3.2.3 Covalent and Photoswitchable Nitazenes

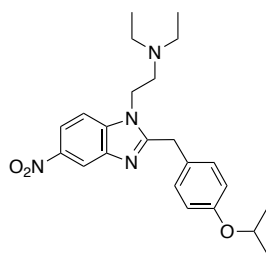
In this work, the potency and covalent properties of BIT towards μ OR were re-investigated, as well as the properties of a newly synthesized SCN-containing derivative that was modeled on the structure of isotonitazene, named here as Iso-BIT (**1**, Figure 36). In addition to covalent tools, other probe compounds may be beneficial in investigating μ OR and nitazene interactions with μ OR. Herein, photoswitchable probes modeled on both etonitazene and isotonitazene were developed, as well as reactive SCN derivatives, which all contain a photoswitchable azo group (Figure 36). The main advantage in developing photoswitchable ligands is that they can be used as tools to spatially and temporally control ligand activity using light, and are extensively explored in the field of photopharmacology.^[14] A tool with this capability may be useful in further understanding μ OR receptor mechanism and signaling pathways through kinetic and dynamic studies.^[14a, 15] Photophysical analysis of these photoswitchable nitazene derivatives also provides insight into the photophysical properties of arylazobenzimidazoles. This photoswitchable class is discussed in this work and belongs to the broader arylazoheterocycle class, which has received growing attention due to their wide range of desirable photophysical and biological properties.

Covalent and Photochromic Derivatives of the Potent Synthetic Opioid Isotonitazene and Other Nitazenes

Etonitazene and Isotonitazene

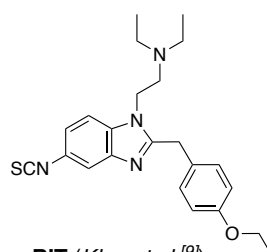


Etonitazene (Hoffmann *et al.*^[3])
'ethoxy-capped'

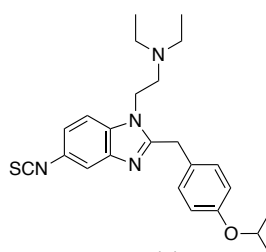


Isotonitazene (Hoffmann *et al.*^[3])
'isopropoxy-capped'

Covalent Nitazene Derivatives



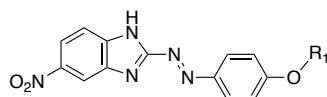
BIT (Klee *et al.*^[9])
'ethoxy-capped'



Iso-BIT (1)
'isopropoxy-capped'

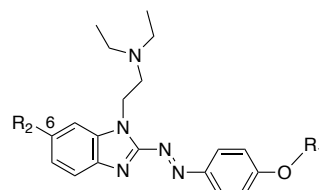
Novel Photochromic Nitazene Derivatives

Series 2: 'ethoxy-capped'
Series 3: 'isopropoxy-capped'



2a: R₁ = CH₂CH₃

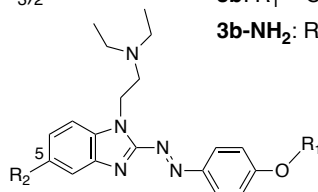
3a: R₁ = CH(CH₃)₂



2b: R₁ = CH₂CH₃; R₂ = NO₂

3b: R₁ = CH(CH₃)₂; R₂ = NO₂

3b-NH₂: R₁ = CH(CH₃)₂; R₂ = NH₂



2c: R₁ = CH₂CH₃; R₂ = NO₂

3c: R₁ = CH(CH₃)₂; R₂ = NO₂

2d: R₁ = CH₂CH₃; R₂ = NH₂

3d: R₁ = CH(CH₃)₂; R₂ = NH₂

2e: R₁ = CH₂CH₃; R₂ = NCS

3e: R₁ = CH(CH₃)₂; R₂ = NCS

Covalent Photochromic Nitazene Derivatives

Figure 36. Structures of nitazenes explored in this work that target μ OR. This includes etonitazene and isotonitazene, as well as their isothiocyanate-containing derivatives, BIT and Iso-BIT (1), respectively. The photoswitchable derivatives were modeled on etonitazene (series 2) and isotonitazene (series 3) and possess an arylazobenzimidazole core.

3.3 Results and Discussion

3.3.1 Design of Photoswitchable Nitazenes

In order to further expand the repertoire of nitazene probes, photoswitchable nitazenes were developed in this work. This involved incorporating a photoswitch unit into the core structures of etonitazene, isotonitazene, BIT and Iso-BIT, resulting in **2c**, **3c**, **2e** and **3e**, respectively (Figure 36). The most explored photoswitch unit are the azobenzenes, which can either be linked to or incorporated into the structure of a bioactive molecule.^[16] Upon exposure to light of a specific wavelength, azobenzenes undergo a reversible change in structure via isomerization. Once isomerization occurs, the *cis*-isomer typically can revert back to the more stable *trans*-isomer thermally or upon exposure with light of a different wavelength.^[16] The geometrical differences between *cis*- and *trans*-isomers may lead to differences in receptor binding, resulting in compounds that have a biologically active and inactive state. Such photoswitchable probes have been reported in the GPCR field.^[17]

In recent years, research in this field has expanded beyond azobenzenes and into a variety of arylazoheterocycles. The replacement of one or both benzene units by various heterocycles has been shown to diversify photophysical properties, which can be tuned with minor chemical modifications.^[18] In addition to these promising photophysical properties, such as red-shifted absorbances and quantitative photoisomerization, arylazoheterocycles are scaffolds present in various medically-relevant biomolecules that exhibit anti-cancer, anti-inflammatory and anti-microbial properties.^[19] As a result, arylazoheterocycles have received positive attention in the field of photopharmacology. Incorporation of the azo group into the structure of the described nitazenes, results in an arylazobenzimidazole core (Figure 37). Similar to other heterocycles, benzimidazoles have been reported as important scaffolds in a range of therapeutics.^[20] While valuable studies have been performed that describe the photophysical properties of arylazobenzimidazoles and similar structures,^[21] to our knowledge, little is known about these properties when the azo group is directly installed on position 2 of the benzimidazole unit, until very recently.^[22]

The development of these nitazene-based photoswitchable ligands resulted in arylazobenzimidazole precursors with various substitution patterns (Figure 36). This allowed access to evaluate the photophysical properties of various arylazobenzimidazoles. In regard to ligand design for biochemical analysis, the incorporation of the azo group into the core of these nitazenes were expected to alter the overall geometry of these molecules, which may

Covalent and Photochromic Derivatives of the Potent Synthetic Opioid Isotonitazene and Other Nitazenes

affect μ OR binding interactions (Figure 37). However, it was postulated that isomerization of this core may allow for biological differences between *trans*- and *cis*-isomers.

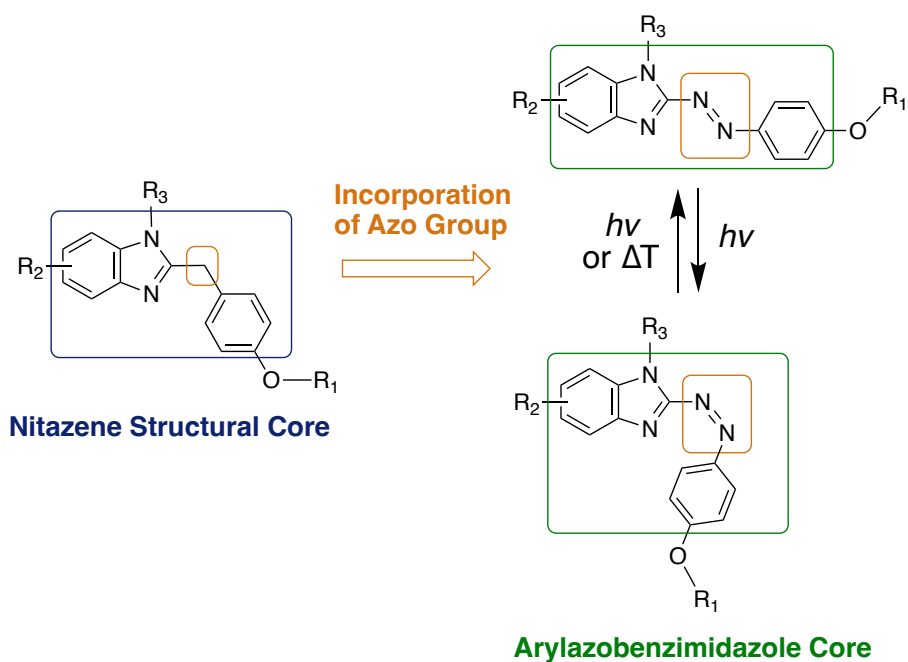
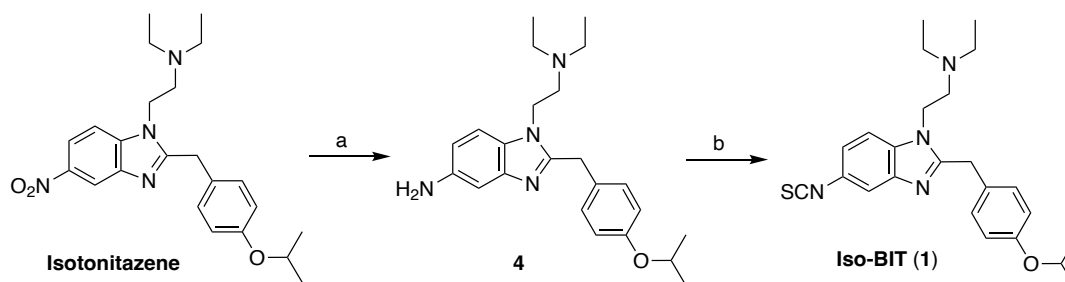


Figure 37. General design of nitazene-based photoswitchable ligands.

3.3.2 Synthesis of Photoswitchable Nitazenes

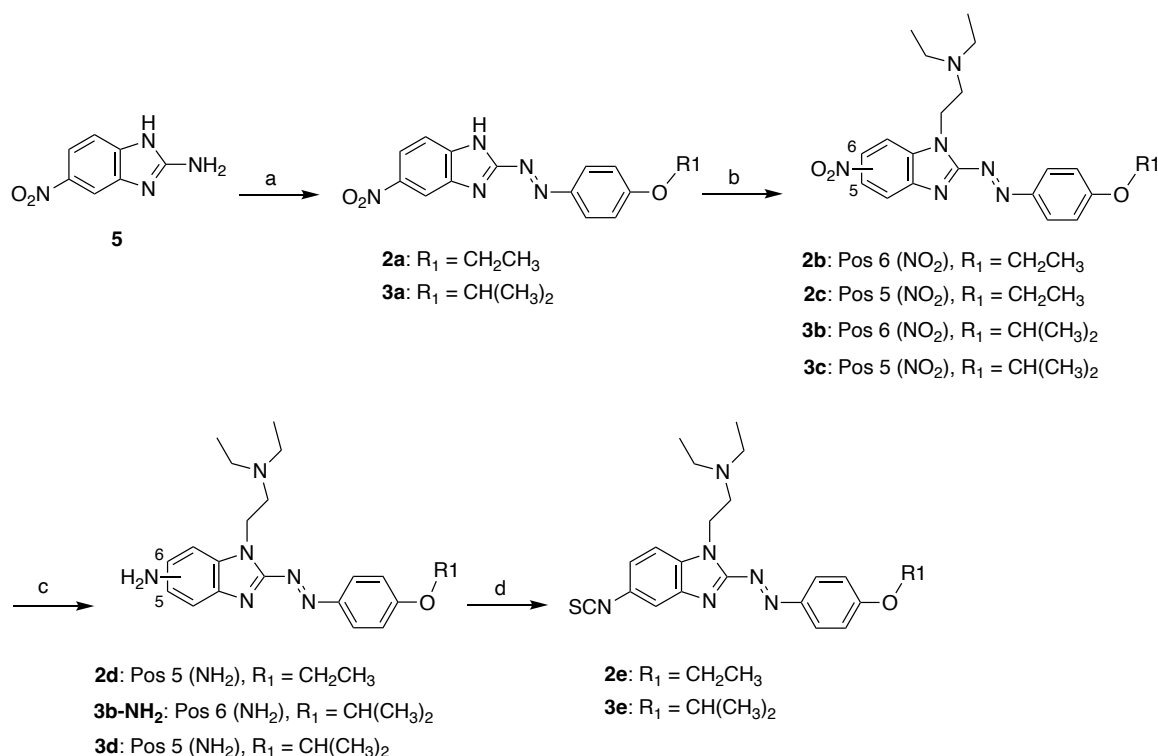
While BIT is commercially available, isotonitazene was synthesized as previously reported.^[4] To obtain the new Iso-BIT (**1**) derivative, the nitro group of isotonitazene was reduced to amine **4**, using H₂ and Pd/C (Scheme 11). Amine **4** was directly subjected to an SCN-forming reaction that has been previously reported,^[23] resulting in Iso-BIT with an overall yield of 29%.



Scheme 11. Synthesis of Iso-BIT (**1**). (a) Isotonitazene, H₂, Pd/C, methanol, rt, 3 h, to yield **4**, which was directly used in next step; (b) CS₂, Et₃N, THF, N₂, 0 °C → rt, 18 h, then TsCl, 0 °C → rt, 1 h, 29% overall yield.

The synthesis of the photochromic etonitazene series **2** began with commercially available 5-nitro-1*H*-benzimidazol-2-ylamine (**5**, Scheme 12). To form the azo-benzimidazole unit, an oxidative method was employed^[24] with *N*-chlorosuccinimide (NCS) as a mild oxidant, 1,8-diazabicyclo[5.4.0]undec-7-ene (DBU) in catalytic amounts and 4-ethoxyaniline to successfully obtain **2a** in 13% yield. This compound was then alkylated, using 2-chloro-*N,N*-diethylethylamine hydrochloride, where tautomerization resulted in isomers **2b** and **2c** with 22% and 16% yield, respectively. The former isomer is the 6-nitro regioisomer, while the latter is the 5-nitro isomer that is characteristic for etonitazene. The nitro group of **2c** was subsequently reduced to amine **2d** in 52% yield, using H₂ and Pd/C. A one-pot synthesis procedure allowed the conversion of amine **2d** to isothiocyanate **2e** in 49% yield.^[23]

Covalent and Photochromic Derivatives of the Potent Synthetic Opioid Isotonitazene and Other Nitazenes



Scheme 12. Synthesis of photochromic ethoxy (series **2**) and isopropoxy (series **3**) nitazene derivatives. (a) 5-nitro-1*H*-benzimidazol-2-ylamine (**5**), 4-ethoxyaniline, DBU, *N*-chlorosuccinimide, DCM, -78 °C, 0.5 h, 13% (**2a**) or 8% (**3a**); (b) 2-chloro-*N,N*-diethylethylamine hydrochloride, KOH, K₂CO₃, acetone, reflux, 3 h, 22% (**2b**), 16% (**2c**), 26% (**3b**) or 23% (**3c**); (c) H₂, Pd/C, methanol, rt, 3 h, 52% (**2d**), 8% (**3b-NH₂**) or 33% (**3d**); (d) CS₂, Et₃N, THF, N₂, 0 °C → rt, 18 h, then TsCl, 0 °C → rt, 1 h, 49% (**2e**) or 48% (**3e**).

For the photochromic isopropoxy series **3**, the same procedures were employed (Scheme 12). The azo unit was installed onto the commercially available precursor **5**, using NCS, DBU and 4-isopropoxyaniline to obtain **3a** in 8% yield. Subsequent alkylation with 2-chloro-*N,N*-diethylethylamine hydrochloride, afforded regioisomers **3b** and **3c** in 26% and 23% yield, respectively. X-ray crystal structures of these isomers were obtained, which validated their molecular structure and configuration (Figure 38). Reduction of the nitro group of both isomers (separately), resulted in amine **3b-NH₂** and **3d** in 8% and 33% yield, respectively. The lower yield of **3b-NH₂** was found to result from cleavage of the azo group during synthesis. A one-pot synthesis allowed the conversion of amine **3d** to the isothiocyanate **3e** in 48% yield.

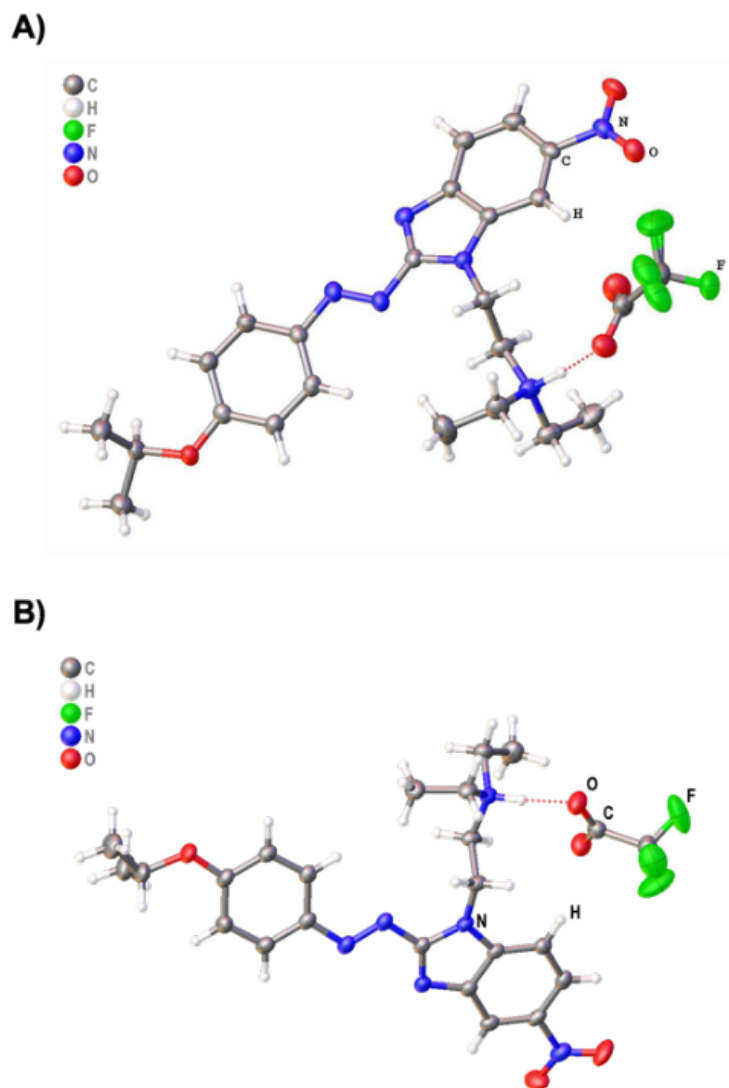


Figure 38. Crystal structure of A) isopropoxy **3b** (CCDC 2236462) and B) Isopropoxy **3c** (CCDC 2236450), both as TFA salts, shown as a 3D ball-and-stick representation. See Supplementary Information for further details.

3.3.3 Photophysical Investigations of Photoswitchable Nitazenes

The photophysical properties of compounds in both series **2** and **3** were evaluated. This involved evaluating UV/Vis absorption spectra of thermal equilibrium, *trans*- and *cis*-isomers, cycle performance and photostationary states, as well as determining thermal stabilities of *cis*-isomers (Figure 39, Table 9 and Supplementary Information). Compounds in both series **2** and **3** were able to reversibly isomerize between *trans*- and *cis*-isomers, except for compounds **2d**, **3d** and **3b-NH₂**. These latter derivatives contain an amine group on the 5- or 6-position of the benzimidazole unit. In UV/Vis absorption measurements, these compounds each displayed an absorbance band that ranged from approximately 300-600 nm in both DMSO and buffer solution (see Supplementary Information). In order to obtain and maintain their respective *cis*-isomers, compounds **2d**, **3d** and **3b-NH₂** were examined separately in time-resolved UV/Vis absorption experiments under continuous irradiation. Isomerization to the *cis*-isomer was attempted by separately irradiating these compounds with various wavelengths, ranging from 265 to 745 nm, however, no significant changes to absorbance were observed. These results suggested that the switching properties of these compounds could not be monitored or observably controlled under the described parameters.

Even though each of the lead photoswitchable compounds possessed different substitution patterns, their UV/Vis absorption spectra were relatively similar, with a slight bathochromic shift observed for compounds that contained an N-substitution on the benzimidazole core (**2b**, **2c**, **2e**, **3b**, **3c** and **3e**, compared to **2a** and **3a**, see Supplementary Information). This similarity may be due to all compounds possessing the strong electron donating ethoxy (series **2**) or isopropoxy groups (series **3**) linked to the benzene unit, with only minor chemical alterations to the electron withdrawing properties of the benzimidazole unit. The presence of these electron donating and electron withdrawing groups on opposite sides of the azo unit, may have induced a ‘push-pull’ effect. This effect has been shown to influence *cis*-isomer thermal stability and affect $\pi \rightarrow \pi^*$ and/or $n \rightarrow \pi^*$ transitions.^[25]

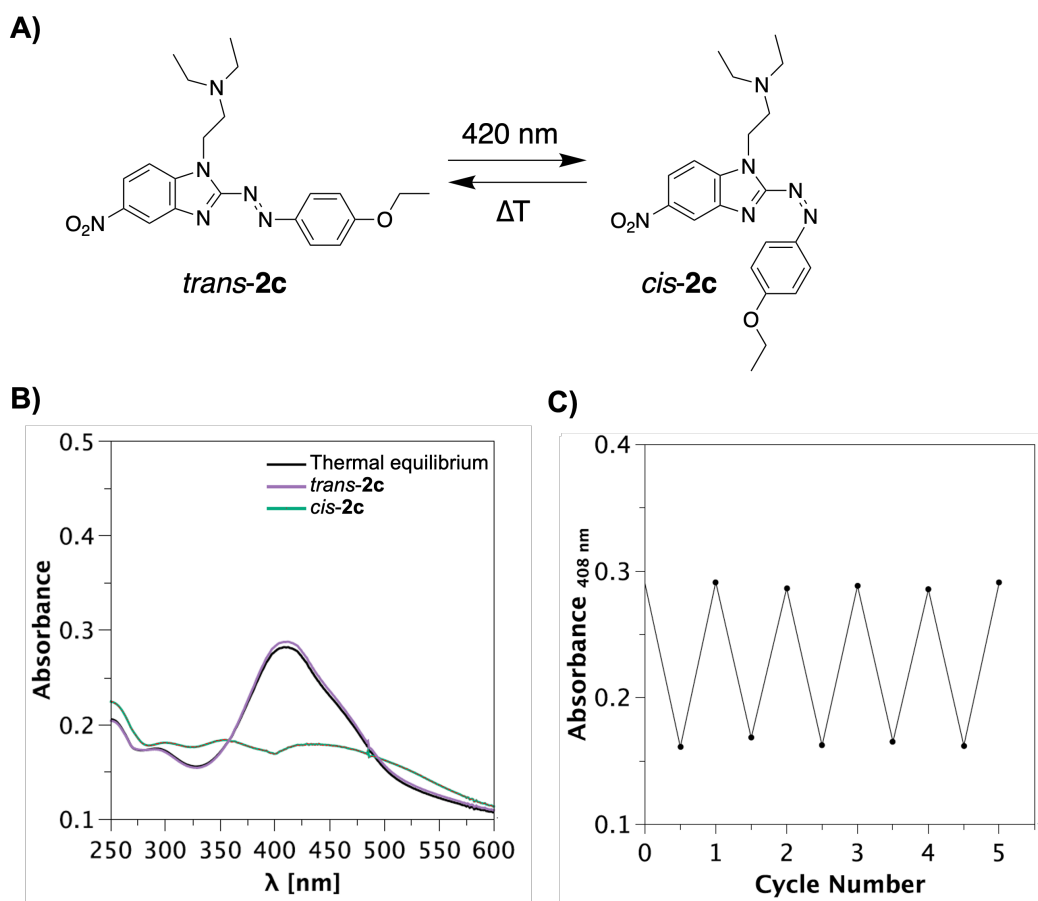


Figure 39. Light-induced isomerization and cycle performance of compound **2c**. This compound is shown here as a representative, as most compounds in both series **2** and **3** displayed similar photophysical properties (see Supplementary Information). A) Depiction of the structural changes that ensue upon photo-induced isomerization of **2c**. B) Online UV/Vis absorption spectra of thermal equilibrium, *trans*-isomer and *cis*-isomer. The *cis*-isomer was accessed via continuous irradiation with 420 nm, while the *trans*-isomer was obtained thermally under dark conditions. C) Cycle performance of **2c** upon alternating irradiation and dark conditions. Data points were recorded at the absorbance maximum of the respective *trans*-isomer (408 nm). Results are shown of **2c** (20 μ M) in buffer solution (TrisHCl Buffer, pH 7.5) + 0.2% DMSO at 25 $^{\circ}$ C.

When compared to common azobenzenes, the substitution patterns of the lead benzimidazole-based photoswitchable compounds in series **2** and **3** resulted in a red-shift of the $\pi \rightarrow \pi^*$ transition. As a result, this transition was able to be excited with 420 nm irradiation for each of the lead compounds, resulting in their respective *cis*-isomers. While the majority of azobenzenes require UV irradiation for isomerization to the *cis*-isomer, the use of red-shifted wavelengths is desirable for biological studies.^[14c, 25c] Since UV irradiation can be toxic to most biological material,^[14b] the ability to use blue light (420 nm) instead of UV irradiation can be considered less harmful and promising for the use of these compounds as

Covalent and Photochromic Derivatives of the Potent Synthetic Opioid Isotonitazene and Other Nitazenes

biochemical probes. Since an overlap of the π - π^* and n - π^* transitions were observed for the arylazobenzimidazoles described herein, quantitative switching was not obtained (Figure 39 and Table 9). PSS estimations indicated that the *cis*-isomers of compounds **2a**, **2b**, **2c**, **2e**, **3a**, **3b**, **3c** and **3e** constituted 45-80% *cis*-isomer (Table 9). Despite these findings, previous studies have reported non-quantitative photoswitchable ligands that displayed biological differences between isomers, therefore, biological activity of these compounds still remained of interest.^[26] While no direct correlation could be observed between the different substitution patterns of these compounds and their respective PSS values, thermal stability measurements proved insightful (Table 9 and Supplementary Information).

Table 9. Summary of photophysical properties in buffer solution.^{[a][b]}

Compound				PSS	PSS	$t_{1/2}$ [s]
	R_1	R_2	R_3	<i>TE</i>	<i>TE</i> \rightarrow <i>cis</i>	
				<i>trans:cis</i> ^[c]	<i>trans:cis</i> ^[c]	
2a	CH ₂ CH ₃	NO ₂	H	76:24	36:64	46.2
2b	CH ₂ CH ₃	6-NO ₂	X	80:20	37:63	6.9
2c	CH ₂ CH ₃	5-NO ₂	X	97:3	34:66	10.8
2e	CH ₂ CH ₃	5-NCS	X	83:17	52:48	15.1
3a	CH(CH ₃) ₂	NO ₂	H	76:24	55:45	65.4
3b	CH(CH ₃) ₂	6-NO ₂	X	72:28	37:63	5.2
3c	CH(CH ₃) ₂	5-NO ₂	X	93:7	20:80	15.5
3e	CH(CH ₃) ₂	5-NCS	X	92:8	55:45	15.1

^[a]Isomerization was achieved by 5-10 sec irradiation with 420 nm (for *cis*-isomer) or thermally under dark conditions (for *trans*-isomer) at 25 °C. ^[b]Buffer solution (TrisHCl Buffer, pH 7.5) + 0.2-1% DMSO. ^[c]PSS was estimated by UV/Vis spectroscopy measurements. The term ‘TE’ refers to thermal equilibrium.

Covalent and Photochromic Derivatives of the Potent Synthetic Opioid Isotonitazene and Other Nitazenes

In thermal stability measurements, the evaluated compounds exhibited fast thermal relaxation of their respective *cis*-isomer, ranging from 5-65 sec in buffer solution (Table 9). Here, differences could be observed between the N-substituted benzimidazole compounds (**2b**, **2c**, **2e**, **3b**, **3c** and **3e**) and the compounds that do not possess the N-diethylaminoethyl unit (**2a** and **3a**). The *cis*-isomers of the latter compounds displayed thermal half-lives of 46.2 and 65.4 sec, respectively, while that of the remaining compounds ranged from 5.2-15.5 sec. The greater thermal stability of *cis*-**2a** and *cis*-**3a** may be due to the lack of N-substitution, revealing a secondary amine on the benzimidazole. This may reduce electron withdrawing effects, and thus, slightly reduce the push-pull effects. These results are more pronounced in DMSO studies (SI Table 12). In DMSO studies, the *cis*-isomers of ethoxy **2a** and isopropoxy **3a** displayed thermal half-lives of 3.2 and 2.1 h, respectively, while that of the remaining compounds in series **2** ranged from 0.9-1.5 h and that of series **3** ranged from 18.1-32.6 min. These results suggested that the arylazobenzimidazole unit, like other arylazoheterocycles, may be susceptible to photophysical variations with only slight chemical modifications. The impacts of different solvents, including DMSO and water, on the thermal stability of *cis*-isomers have been previously investigated for phenylazoindole photoswitches.^[27] For the purposes of this project, the photophysical properties in buffer solution were of major interest, as these nitazene-based photoswitches were subjected to cell-based assays to evaluate compound affinity and activity towards μ OR.

While fast-relaxing systems may be valuable for a variety of material and biochemical applications,^[28] continuous irradiation was required to evaluate the biochemical properties of the *cis*-isomers in this series. For this, a new 96-well plate LED device was developed that allows for continuous irradiation of individual wells during cell-based assays. The advantage of this arylazobenzimidazole series is that continuous UV irradiation that typically harms cells can be mostly circumvented with the use of 420 nm irradiation for isomerization to the *cis*-isomer. Due to the fast-switching nature of these *cis*-isomers in buffer solution, the *trans*-isomer of these photoswitchable nitazenes can be obtained thermally. As a result, for biochemical investigations, dark conditions were employed to predominantly obtain the respective *trans*-isomers, while continuous 420 nm irradiation was employed to obtain the respective *cis*-enriched isomer states.

3.3.4 Biochemical Evaluation of Photoswitchable Nitazenes

3.3.4.1 Radioligand Binding Studies

Lead photoswitchable compounds **2a**, **2b**, **2c**, **2e**, **3a**, **3b**, **3c** and **3e** were subjected to radioligand binding studies to determine compound affinity towards μ OR (Table 10). These ligands were evaluated in their thermal equilibrium state, as their *trans*-enriched form, in order to screen for biochemically-relevant compounds. Reference compounds in these investigations included fentanyl, isotonitazene, BIT and newly synthesized Iso-BIT. In this system, isotonitazene ($K_i = 0.95$ nM) displayed a binding affinity that was 9-fold greater than fentanyl ($K_i = 8.3$ nM). These results were consistent to previously reported functional studies that describe a 9-fold greater potency of isotonitazene than fentanyl.^[4, 8c] In this work, both SCN-containing BIT ($K_i = 40$ nM) and Iso-BIT ($K_i = 27$ nM) displayed attenuated binding affinities when compared to isotonitazene and fentanyl, however, still in the nM range.

For the nitro-containing photoswitchable ligands (**2a-c** and **3a-c**), the methylene group as present in BIT and iso-BIT was substituted with an azo-group, which caused a substantial reduction in affinity (K_i from 720 to 10,000 nM). These photoswitchable compounds contained different substitution patterns, however, a particular trend in receptor binding could not be observed. Furthermore, substitution of the 5-NO₂ group in *trans*-**2c** and *trans*-**3c** with an isothiocyanate did not markedly influence the binding affinity for *trans*-**2e** ($K_i = 580$ nM) and *trans*-**3e** ($K_i = 620$ nM), however, K_i values in the submicromolar range were obtained. As a result, a more detailed biological investigation appeared promising and all test compounds were further evaluated in a functional assay to determine ligand-mediated receptor activation of μ OR.

Covalent and Photochromic Derivatives of the Potent Synthetic Opioid Isotonitazene and Other Nitazenes

Table 10. Binding affinities of *trans*-enriched photoswitchable ligands and reference compounds to the human opioid receptor μ OR derived from radioligand binding studies.^[a]

Photoswitchable Compounds:					
Compound	μ OR _{wt}				
	K_i [nM \pm S.E.M.] ^[b]				(n) ^[c]
Reference Compounds					
Fentanyl	8.3 \pm 1.5				11
Isotonitazene	0.95 \pm 0.31				6
BIT	40 \pm 6.6				5
Iso-BIT	27 \pm 8.7				4
New Photoswitchable Compounds					
	R ₁	R ₂	R ₃		
<i>trans</i> - 2a	CH ₂ CH ₃	NO ₂	H	10,000 \pm 4,200 ^[d]	2
<i>trans</i> - 2b	CH ₂ CH ₃	6-NO ₂	X	1,700 \pm 220	4
<i>trans</i> - 2c	CH ₂ CH ₃	5-NO ₂	X	1,100 \pm 220	5
<i>trans</i> - 3a	CH(CH ₃) ₂	NO ₂	H	720 \pm 130 ^[d]	2
<i>trans</i> - 3b	CH(CH ₃) ₂	6-NO ₂	X	970 \pm 190 ^[d]	2
<i>trans</i> - 3c	CH(CH ₃) ₂	5-NO ₂	X	800 \pm 420 ^[d]	2
New Covalent and/or Photoswitchable Compounds					
<i>trans</i> - 2e	CH ₂ CH ₃	5-SCN	X	580 \pm 130	4
<i>trans</i> - 3e	CH(CH ₃) ₂	5-SCN	X	620 \pm 28 ^[d]	2

^[a]Binding data to μ OR were determined using membrane preparations from HEK293T cells transiently transfected with μ OR and the radioligand [³H]diprenorphine. In the case of irreversible activity, K_i refers to pseudo- K_i . ^[b]Mean K_i values in [nM \pm S.E.M.] were derived from 3-11 individual experiments, each performed in triplicate. ^[c]Number of individual experiments. ^[d]Mean K_i \pm SD from two individual experiments.

3.3.4.2 Ligand-mediated Activation Studies

Ligand-mediated receptor activation was assessed via a biosensor-based BRET assay in HEK293T cells that were transiently transfected with human μ OR.^[29] Each photoswitchable ligand was irradiated with 420 nm for the full duration of incubation or was subjected to dark conditions to obtain either the respective *cis*- or *trans*-enriched isomer state (Figure 40 and Table 11). The reference agonist fentanyl and the nitazenes isotonitazene, BIT and Iso-BIT were measured for comparison. To examine whether continuous irradiation would interfere with the cellular assay, fentanyl and isotonitazene were additionally subjected to 420 nm irradiation. In this activation assay, isotonitazene behaved as a full agonist ($E_{\max} = 105\%$), with an EC_{50} value of 11 nM that was similar to fentanyl ($EC_{50} = 6.0$ nM). This finding differs to the obtained K_i values that showed a 9-fold better binding for isotonitazene than fentanyl, and differs to previously reported functional studies that describe a 9-fold greater potency for isotonitazene in a β -arrestin 2 assay ($EC_{50} = 1.6$ nM) and a mini- G_i recruitment assay ($EC_{50} = 3.7$ nM) in comparison to fentanyl ($EC_{50} = 14$ and 35 nM, respectively).^[4] Nonetheless, these results validated the strong potency of isotonitazene. Replacing the 5- NO_2 group in isotonitazene with 5-SCN caused a 16-fold reduction in potency for Iso-BIT, resulting in an EC_{50} value of 180 nM. In comparison to Iso-BIT, its ethoxy analogue BIT displayed a better potency of 63 nM. The overall reduction in potency of these isothiocyanate-containing derivatives is comparable to literature that describes a poorer potency for BIT than its nitro-containing analogue etonitazene.^[4, 10a] Despite the reduction in potency, both isothiocyanates behaved as full agonists ($E_{\max} = 98\%$ for Iso-BIT, 93% for BIT).

The functional data for fentanyl and isotonitazene when exposed to 420 nm irradiation, shown in Figure 40 and Table 11, revealed similar results to experiments performed in the dark (fentanyl: $EC_{50} = 6.0$ nM vs fentanyl [420 nm]: $EC_{50} = 6.3$ nM; isotonitazene: $EC_{50} = 11$ nM vs isotonitazene [420 nm]: $EC_{50} = 15$ nM). This finding suggests that the irradiation conditions required for evaluating the photoswitchable compounds were compatible with the employed functional study. Interestingly, when evaluating the photoswitchable ligands **2a-c** and **3a-c**, a strong structure-dependent activation profile could be observed (Figure 40 and Table 11). For *trans*-**2a** and *trans*-**3a**, which lack the N-diethylaminoethyl group, no explicit stimulation of the receptor could be measured up to a concentration of 10 μ M. This result is in good agreement with literature data that suggest the N-diethylaminoethyl substituent on the benzimidazole core to be important for nitazene- μ OR interactions.^[8c]

Covalent and Photochromic Derivatives of the Potent Synthetic Opioid Isotonitazene and Other Nitazenes

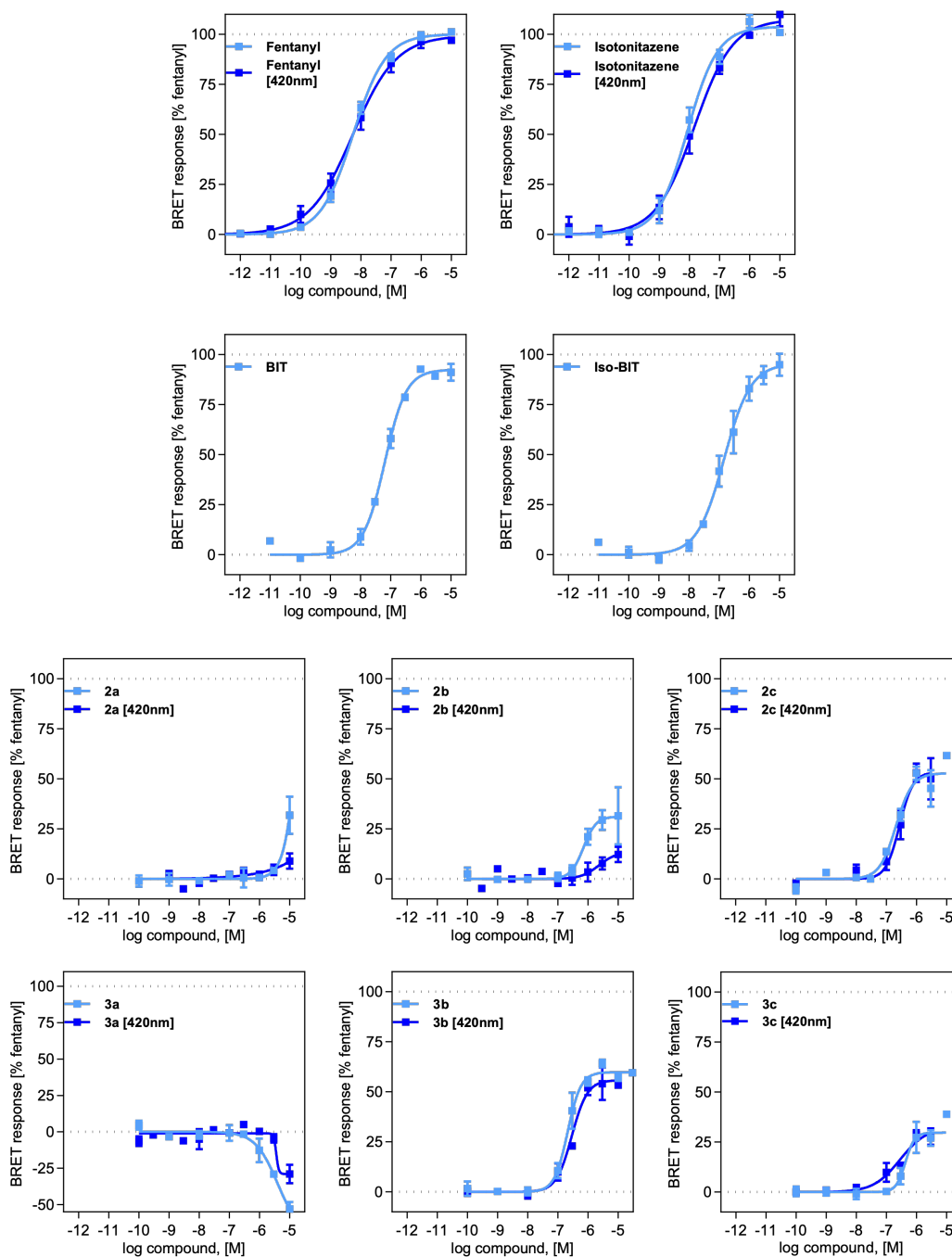


Figure 40. Activation of μ OR by synthetic opioids, measured via a biosensor-based BRET assay. Receptor activation was investigated for isotonitazene, BIT and Iso-BIT, as well as for the non-covalent (**2a-c** and **3a-c**) and covalent photoswitchable compounds (**2e** and **3e**) in HEK293T cells transiently co-transfected with μ OR and the hybrid G-protein $G\alpha_{q15HA}$ (light blue curves). To measure the activating effect of the *cis*-isomers, cells were irradiated with 420 nm for the full duration of the experiment (dark blue curves). As a control to evaluate any influence of irradiation on signaling, fentanyl and isotonitazene were subjected to the same irradiation conditions as that to obtain the respective *cis*-isomers (fentanyl [420 nm], isotonitazene [420 nm]; dark blue curves). Graphs show mean curves (\pm S.E.M.) of 3-7 individual experiments, each performed in duplicate.

Covalent and Photochromic Derivatives of the Potent Synthetic Opioid Isotonitazene and Other Nitazenes

For compounds that contained this basic entity, receptor activation substantially increased, with the best profiles obtained for *trans*-**2c** ($EC_{50} = 280$ nM and $E_{max} = 62\%$) and *trans*-**3b** ($EC_{50} = 250$ nM and $E_{max} = 60\%$). In regards to the positioning of the nitro group, it has previously been reported that the nitro group at position 5 in etonitazene offers improved μ OR-mediated analgesic effects than when placed at position 6.^[3, 8b, 8c] While this trend could be observed for the ethoxy derivative *trans*-**2c** that bears a 5-NO₂ substituent, the isopropoxy derivative *trans*-**3b** that bears a 6-NO₂ substituent emerged as the superior isopropoxy analogue. Comparing the activation data of the respective *trans*- and *cis*-isomers of the photoswitchable ligands revealed that both isomer-enriched states behaved similarly in activating μ OR (Figure 40; light blue and dark blue curves, respectively). The most expressed difference between both isomers could be observed for **2b**. While *cis*-**2b** displayed a weak efficacy ($E_{max} = 12\%$) and an EC_{50} value of 1400 nM, partial agonist activity could be observed for *trans*-**2b** ($E_{max} = 39\%$), with a 2-fold greater potency as exhibited by an EC_{50} value of 630 nM.

Unfortunately, the isothiocyanates **2e** and **3e** could not be measured in this assay as the detection signal was strongly diminished to an extent greater than 100% below basal activity (at concentrations greater than 3 μ M). This observation may be explained by an interference of these isothiocyanate derivatives with the BRET detection system. In order to validate the functional data obtained from the BRET assay, which measures receptor activation at equilibrium by monitoring G-protein dissociation, a FRET-based second messenger accumulation assay (IP-One[®] assay) was applied as an alternative test system. Furthermore, it was of interest to corroborate the receptor activation data of lead photoswitchable ligands **2c** and **3b** under alternative experimental conditions. The IP accumulation assay was performed with HEK293T cells that were transiently co-transfected with human μ OR and the hybrid G-protein $G\alpha_{qi5HA}$ (Figure 41 and Table 11).^[30] The *trans*-isomers of **2a-c**, **2e**, **3a-c** and **3e** were evaluated in the dark, while their respective *cis*-isomers were evaluated under continuous irradiation with 420 nm. For comparison, receptor activation of the reference fentanyl and isotonitazene (both in the dark and at 420 nm), as well as BIT and Iso-BIT, was determined. Except for isotonitazene, these compounds displayed comparable potencies, within less than a 2-fold range, to the data derived from the BRET system. Isotonitazene activated the μ OR with a 4-fold better potency in the accumulation assay, indicated by an EC_{50} value 2.8 nM.

Covalent and Photochromic Derivatives of the Potent Synthetic Opioid Isotonitazene and Other Nitzenes

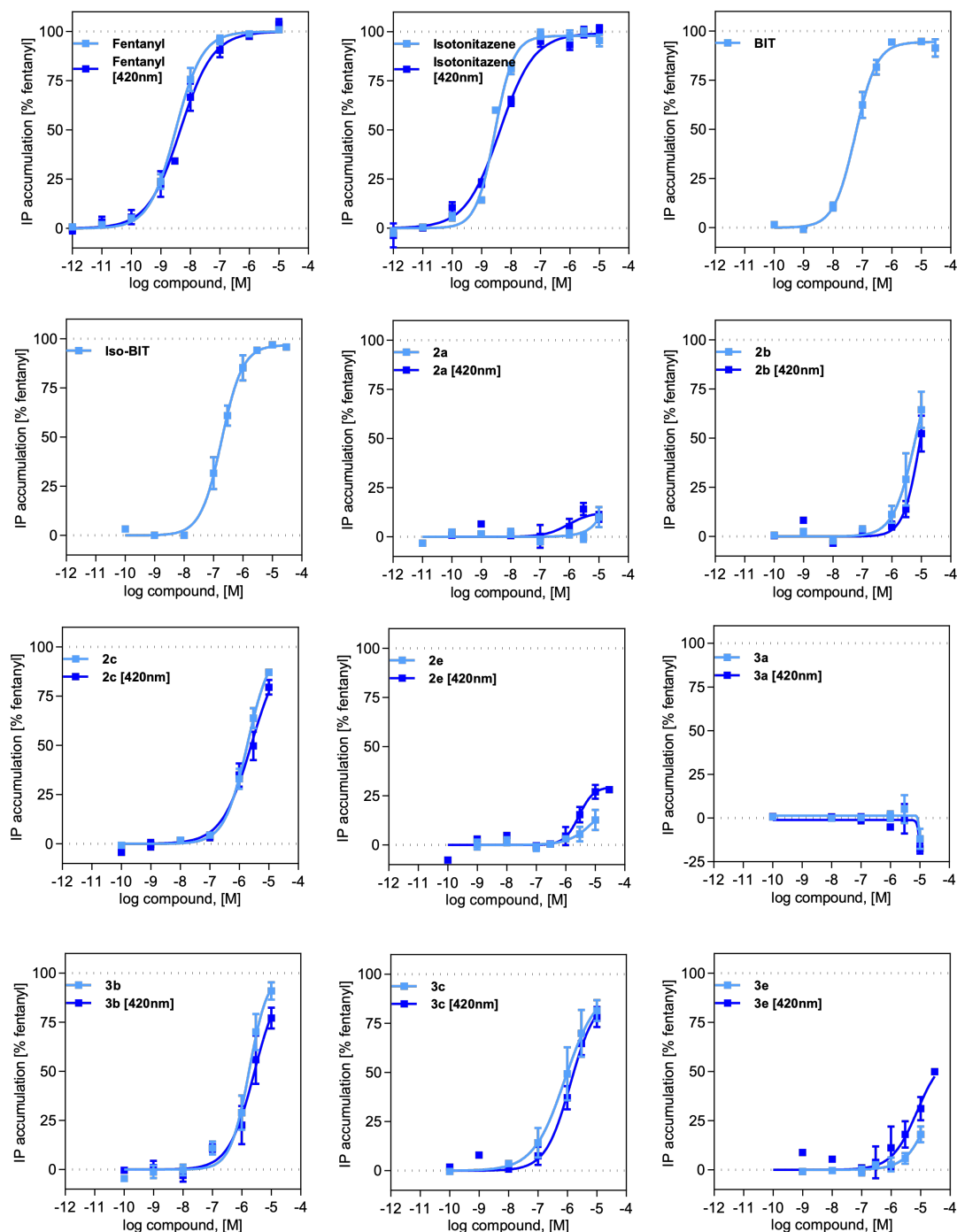
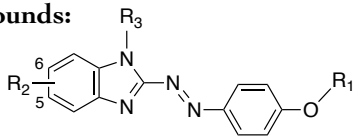
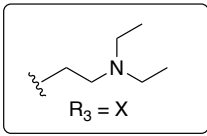


Figure 41. Activation of μ OR by synthetic opioids, measured via the IP-One[®] accumulation assay. G-protein-mediated μ OR activation was investigated for isotonitazene, BIT and Iso-BIT, as well as for the non-covalent (**2a-c** and **3a-c**) and covalent photoswitchable compounds (**2e** and **3e**) in HEK293T cells transiently co-transfected with μ OR and the hybrid G-protein $G\alpha_{q5HA}$ (light blue curves). The activating effect of the *cis*-isomers were determined under continuous irradiation at 420 nm (dark blue curves). As a control, fentanyl and isotonitazene were subjected to irradiation at 420 nm (fentanyl [420 nm], isotonitazene [420 nm]; dark blue curves). Graphs show mean curves (\pm S.E.M.) of 3-8 individual experiments, each performed in triplicate.

Covalent and Photochromic Derivatives of the Potent Synthetic Opioid Isotonitazene and Other Nitazenes

Table 11. Receptor activation of synthetic opioids at the μ -opioid receptor (μ OR).^[a]

Photoswitchable Compounds:									
									
Compound	Biosensor-based BRET assay (μ OR _{wt})			IP-One assay (μ OR _{wt})					
	EC ₅₀ [nM] ± S.E.M.] ^[b]	E _{max} [%] ± S.E.M.] ^[c]	(n) ^[d]	EC ₅₀ [nM] ± S.E.M.] ^[b]	E _{max} [%] ± S.E.M.] ^[c]	(n) ^[d]			
Reference Compounds (Non-Photoswitchable)									
Fentanyl	6.0 ± 1.0	100	7	3.7 ± 1.2	100	4			
Fentanyl [420 nm]	6.3 ± 1.9	100 ± 2	3	6.8 ± 2.1	101 ± 2	7			
Isotonitazene	11 ± 4.1	105 ± 3	5	2.8 ± 0.84	97 ± 2	4			
Isotonitazene [420 nm]	15 ± 5.5	104 ± 2	3	3.7 ± 0.66	97 ± 4	4			
BIT	63 ± 13	93 ± 2	3	64 ± 19	95 ± 2	4			
Iso-BIT	180 ± 75	98 ± 6	3	190 ± 48	93 ± 1	3			
New Photoswitchable Compounds									
	R ₁	R ₂	R ₃						
<i>trans</i> - 2a	CH ₂ CH ₃	NO ₂	H	n/q	32 ± 9 ^[f]	3	n/q	10 ± 5 ^[f]	3
<i>cis</i> - 2a	CH ₂ CH ₃	NO ₂	H	n/q	9 ± 4 ^[f]	3	720 ± 680	11 ± 3	3
<i>trans</i> - 2b	CH ₂ CH ₃	6-NO ₂	X	630 ± 150	39 ± 9	4	7100 ± 2200	68 ± 7	3
<i>cis</i> - 2b	CH ₂ CH ₃	6-NO ₂	X	1400 ± 830	12 ± 4	4	8300 ± 1400	52 ± 9	3
<i>trans</i> - 2c	CH ₂ CH ₃	5-NO ₂	X	280 ± 31	62 ± 5	4	2000 ± 430	99 ± 1	4
<i>cis</i> - 2c	CH ₂ CH ₃	5-NO ₂	X	410 ± 64	67 ± 4	3	2700 ± 630	96 ± 3	7
<i>trans</i> - 3a	CH(CH ₃) ₂	NO ₂	H	n/q	<0	3	n/q	-12 ± 6 ^[f]	3
<i>cis</i> - 3a	CH(CH ₃) ₂	NO ₂	H	n/q	<0	3	n/q	-18 ± 3 ^[f]	3
<i>trans</i> - 3b	CH(CH ₃) ₂	6-NO ₂	X	250 ± 46	60 ± 1	4	2300 ± 790	105 ± 4	5
<i>cis</i> - 3b	CH(CH ₃) ₂	6-NO ₂	X	340 ± 130	57 ± 5	3	3600 ± 1200	100 ± 3	5
<i>trans</i> - 3c	CH(CH ₃) ₂	5-NO ₂	X	540 ± 140	40 ± 4	4	2100 ± 1700	103 ± 7	3
<i>cis</i> - 3c	CH(CH ₃) ₂	5-NO ₂	X	470 ± 280	35 ± 5	4	1500 ± 260	83 ± 6	8

Covalent and Photochromic Derivatives of the Potent Synthetic Opioid Isotonitazene and Other Nitazenes

Table continued from previous page

New Covalent Photoswitchable Compounds

<i>trans-2e</i>	CH ₂ CH ₃	5-SCN	X	n/a	n/a	3	n/q	13 ± 5 ^[a]	3
<i>cis-2e</i>	CH ₂ CH ₃	5-SCN	X	n/a	n/a	2	3800 ± 1400	32 ± 2	4
<i>trans-3e</i>	CH(CH ₃) ₂	5-SCN	X	n/a	n/a	3	n/q	18 ± 4 ^[a]	3
<i>cis-3e</i>	CH(CH ₃) ₂	5-SCN	X	n/a	n/a	2	10000 ± 3800	60 ± 6	4

^[a]μOR activation was determined by either a biosensor-based BRET assay or the IP-One accumulation assay (Cisbio). ^[b]Potency for μOR activation shown as mean EC₅₀ in [nM ± S.E.M.]. ^[c]Mean value for maximum efficacy is reported as E_{max} in [% ± S.E.M.] relative to the full effect of fentanyl. ^[d]Number of individual experiments conducted in duplicate. ^[e]Number of individual experiments conducted in triplicate. ^[f]Efficacy at 10 μM. The abbreviation n/q refers to ‘not quantifiable’ and is applied when no complete sigmoidal curve could be analysed, while n/a refers to ‘not applicable’ when compounds were not compatible with the evaluation system.

Overall, the photoswitchable ligands exhibited similar structure-dependent activation profiles to that determined in the BRET system, however, with a 3- to 11-fold reduction in potency. Accordingly, the 5-nitro ethoxy derivative *trans-2c* exhibited the best activation profile in the ethoxy series, with an EC₅₀ value of 2,000 nM. However, in the isopropoxy series, both *trans-3b* (6-nitro) and *trans-3c* (5-nitro) emerged as lead compounds, with similar EC₅₀ values of 2,300 nM and 2,100 nM, respectively. In this assay, the *trans*-enriched form of **2c**, **3b** and **3c** all acted as full agonists as indicated by E_{max} values of 99%, 105% and 103%, respectively. In contrast, the isothiocyanates **2e** and **3e** revealed only partial agonist activity, with E_{max} values of 32% for *cis-2e* (EC₅₀ = 3,800 nM) and 60% for *cis-3e* (EC₅₀ = 10,000 nM). Accordingly, activity differences between the respective *cis*- and *trans*-isomers of **2e** and **3e** could be observed (Figure 41 and Table 11), whereby, the *cis*-isomers exhibited slightly superior activation profiles.

3.3.4.3 Biochemical Evaluation of Covalent Properties

Besides evaluating the receptor activation properties of these SCN-containing ligands, their ability to covalently interact with μ OR was of particular interest. As a result, a radioligand depletion assay was applied,^[31] using membranes of HEK293T cells that transiently express μ OR. Covalent interaction at the μ OR orthosteric binding site was monitored time-dependently by incubation with the isothiocyanates **2e** and **3e** in their thermal equilibrium state for 5, 15, 30 and 60 min (Figure 42, SI Table 13). At the end of the treatment, the reversibly bound ligands were carefully washed from the receptor and subsequently, the membranes were incubated with the radioligand [³H]diprenorphine. The amount of specific binding of radioligand indicates the number of accessible binding sites and consequently, the amount of covalent binding. As a negative control, the reversibly acting ligand isotonitazene was additionally evaluated. Remarkably, both photoswitches **2e** and **3e** displayed a strong and fast interaction with μ OR, indicated by a covalent binding maximum of 96% and 94%, respectively.

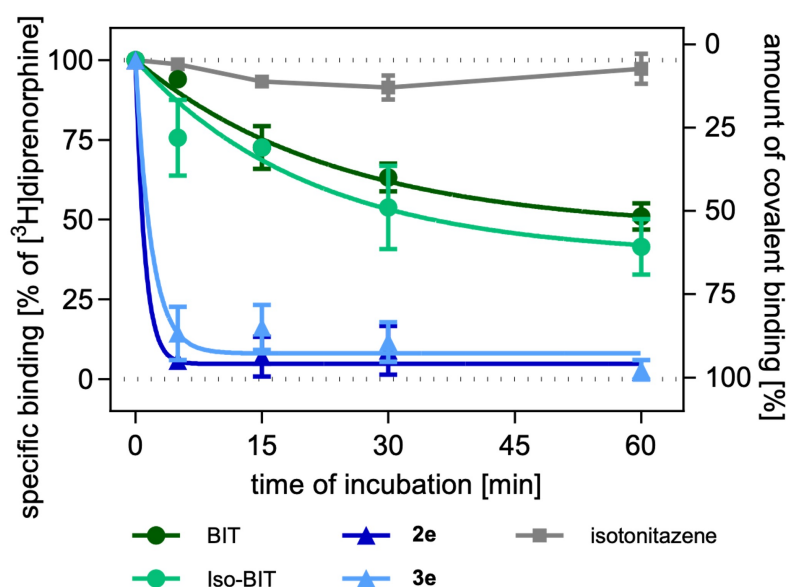


Figure 42. Covalent binding of SCN-containing nitazene compounds. Covalent binding of full efficacy agonists BIT and Iso-BIT, as well as azo-containing ligands **2e** and **3e** in their thermal equilibrium state was determined in a radioligand depletion assay with homogenates from HEK293T cell that express the human μ OR and the radioligand [³H]diprenorphine. Experiments were performed in comparison to the reversible control ligand isotonitazene. BIT and Iso-BIT displayed weak covalent binding of 53% and 58%, respectively, while near-complete blocking (greater than 90%) was obtained for **2e** and **3e** after only a 5-min incubation period. All test compounds were incubated at a concentration of 30- to 50-fold K_i (BIT (2 μ M), Iso-BIT (1 μ M), **2e** (20 μ M), **3e** (20 μ M) and isotonitazene (50 nM)). Graphs show mean curves (\pm S.E.M.) of 3 individual experiments, each performed in quadruplicate.

Covalent and Photochromic Derivatives of the Potent Synthetic Opioid Isotonitazene and Other Nitazenes

In a comparative study, the methylene-bearing reference BIT and its analogue Iso-BIT were tested under the same conditions (Figure 42, SI Table 13). Interestingly, both BIT and Iso-BIT were able to only partly block the μ OR, displaying a covalent binding maximum of 53% (BIT) and 58% (Iso-BIT) after 60 min. These results are somewhat comparable to studies that were performed in 1983 with rat brain membranes, which suggested BIT to covalently bind to 45% of μ OR after a 30-min incubation period.^[9] Overall, these findings indicate that BIT and iso-BIT exhibit substantially poorer covalent binding properties than the azo-containing derivatives **2e** and **3e**. The superior properties of these latter compounds become more pronounced when evaluating the kinetics of this reaction (SI Table 13). For **2e** and **3e**, the covalent binding half-life ($t_{1/2}$) was determined to be 3 min and 4 min, respectively, resulting in a receptor blocking of 96% (**2e**) and 94% (**3e**) after only a 5-min incubation period. In contrast, BIT and Iso-BIT both displayed a $t_{1/2}$ of 17 min. These findings establish **2e** and **3e** as attractive μ OR ligands that can localize and effectively covalently bind to μ OR at physiological pH.

3.4 Conclusion and Outlook

Nitazenes represent an underexplored class of potent μ OR ligands that have increasingly received attention. In this work, biochemical evaluations of the previously documented ligand BIT were undertaken, which included re-evaluating its covalent binding properties towards μ OR. In addition, an isopropoxy derivative of BIT, coined here as Iso-BIT, was synthesized. In biochemical evaluations, both BIT and Iso-BIT displayed binding affinities in the nM range ($K_i = 40$ and 27 nM, respectively). Furthermore, these full efficacy agonists exhibited nanomolar potencies, ranging from 63 to 190 nM, in two different G-protein signaling assays. In covalent binding studies, BIT was able to covalently block 53% of available μ OR binding sites after 60 min. Furthermore, the newly synthesized Iso-BIT displayed similar covalent properties but was able to covalently bind to 58% of available receptor sites.

In order to advance nitazene-based probes for future μ OR investigations and to search for new μ OR active ligands that possess chemical scaffolds different to the classic morphine structure, photoswitchable nitazene-based derivatives were developed. The successful synthesis of such ligands provided further insights into the photophysical properties of arylazobenzimidazoles. Substitution of the methylene group as present in BIT and Iso-BIT with the photoswitchable azo-group maintained agonist properties, but significantly reduced the potency for **2a-c** and **3a-c**. Furthermore, no clear functional activity differences between the *trans*- and the *cis*-isomers of these compounds could be observed. Importantly, the SCN-containing ligands **2e** and **3e** emerged as promising covalent ligands of μ OR. Despite possessing relatively attenuated activation profiles, these ligands both displayed excellent covalent binding properties. Remarkably, both **2e** and **3e** were able to form an exceptionally high fraction of covalent ligand-receptor complexes with wild-type μ OR after only a 5 -min incubation period. These covalent ligands may be beneficial in future biochemical evaluations of μ OR, including crystallographic investigations, as well as evaluations of other relevant receptors as μ OR alkylating agents. This successful finding further validates the potential of nitazenes, which may be beneficial in the pursuit of understanding the mechanisms, functions and interactions of the medically-significant μ OR.

3.5 Acknowledgements

This work was supported by the Deutsche Forschungsgemeinschaft, RTG 1910, and a Minerva PhD Fellowship to RL. We thank Julia Zach for assistance in developing the 96-well plate LED device, as well as the Electronics Workshop of the Department of Chemistry/Pharmacy (University of Regensburg) for manufacturing the device. We thank the X-Ray structure analysis department (University of Regensburg) for crystal structure determination and analysis.

3.6 References

- [1] a) EMCDDA, *Report on the risk assessment of N,N-diethyl-2-[[4-(1-methylethoxy)phenyl]methyl]-5-nitro-1H-benzimidazole-1-ethanamine (isotonitazene) in accordance with Article 5c of Regulation (EC) No 1920/2006 (as amended)*, https://www.emcdda.europa.eu/publications/risk-assessments/isotonitazene_en, **2020**. Accessed 01 Feb 2023; b) European Commission, *Commission Delegated Directive (EU) 2020/1687 of 2 September 2020 amending the Annex to Council Framework Decision 2004/757/JHA as regards the inclusion of the new psychoactive substance N,N-diethyl-2-[[4-(1-methylethoxy)phenyl]methyl]-5-nitro-1H-benzimidazole-1-ethanamine (isotonitazene) in the definition of 'drug'*, http://data.europa.eu/eli/dir_del/2020/1687/oj, **2020**. Accessed 01 Feb 2023.
- [2] a) A. J. Krotulski, D. M. Papsun, S. L. Kacinko, B. K. Logan, *J. Anal. Toxicol.* **2020**, *44*, 521-530; b) WHO, *Critical Review Report: ISOTONITAZENE*, <https://www.who.int/docs/default-source/controlled-substances/43rd-ecdd/isonitazene-43rd-final-complete-a.pdf>, **2020**. Accessed 01 Feb 2023.
- [3] A. Hunger, J. Kebrle, A. Rossi, K. Hoffmann, *Helv. Chim. Acta* **1960**, *43*, 1032-1046.
- [4] M. M. Vandeputte, K. Van Uytvanghe, N. K. Layle, D. M. St. Germaine, D. M. Iula, C. P. Stove, *ACS Chem. Neurosci.* **2021**, *12*, 1241-1251.
- [5] A. Hunger, J. Kebrle, A. Rossi, K. Hoffmann, *Experientia* **1957**, *13*, 400-401.
- [6] United Nations, *17. Protocol amending the Single Convention on Narcotic Drugs, 1961. Geneva, 25 March 1972*, https://treaties.un.org/Pages/ViewDetails.aspx?src=IND&mtdsg_no=VI-17&chapter=6&clang=en, **1975**. Accessed 01 Feb 2023.
- [7] F. Mueller, C. Bogdal, B. Pfeiffer, L. Andrello, A. Ceschi, A. Thomas, E. Grata, *Forensic Sci. Int.* **2021**, *320*, 110686.
- [8] a) M. M. Vandeputte, A. Cannart, C. P. Stove, *Arch. Toxicol.* **2020**, *94*, 3819-3830; b) P. Blanckaert, A. Cannart, K. Van Uytvanghe, F. Hulpia, E. Deconinck, S. Van Calenbergh, C. Stove, *Drug Test. Anal.* **2020**, *12*, 422-430; c) I. Ujváry, R. Christie, M. Evans-Brown, A. Gallegos, R. Jorge, J. de Moraes, R. Sedefov, *ACS Chem. Neurosci.* **2021**, *12*, 1072-1092; d) M. M. Vandeputte, A. J. Krotulski, D. M. Papsun, B. K. Logan, C. P. Stove, *J. Anal. Toxicol.* **2021**; e) M. A. De Luca, G. Tocco, R. Mostallino, A. Laus, F. Caria, A. Musa, N. Pintori, M. Ucha, C. Poza, E. Ambrosio, G. Di Chiara, M. P. Castelli, *Neuropharmacology* **2022**, *221*, 109263; f) P. Skolnick, *Pharmacol. Ther.* **2022**, *233*, 108019; g) K. Hasegawa, K. Minakata, M. Suzuki, O. Suzuki, *Forensic Toxicol.* **2022**, *40*, 234-243; h) A. L. A. Mohr, B. K. Logan, M. F. Fogarty, A. J. Krotulski, D. M. Papsun, S. L. Kacinko, M. A. Huestis, J. D. Roper-Miller, *J. Anal. Toxicol.* **2022**, *46*, e116-e185; i) M. M. Vandeputte, M. M. Tsai, L. Chen, G. C. Glatfelter, D. Walther, C. P. Stove, L. Shi, M. H. Baumann, *Drug Alcohol Depend.* **2023**, *249*, 109939; j) T. Kanamori, Y. Okada, H. Segawa, T. Yamamuro, K. Kuwayama, K. Tsujikawa, Y. T. Iwata, *Drug Test Anal.* **2023**, *15*, 449-457.
- [9] K. C. Rice, A. E. Jacobson, T. R. Burke, Jr., B. S. Bajwa, R. A. Streaty, W. A. Klee, *Science* **1983**, *220*, 314-316.
- [10] a) T. R. Burke, Jr., B. S. Bajwa, A. E. Jacobson, K. C. Rice, R. A. Streaty, W. A. Klee, *J. Med. Chem.* **1984**, *27*, 1570-1574; b) T. R. Burke Jr., K. C. Rice, A. E. Jacobson, W. F. Simonds, W. A. Klee, *J. Label. Compd. Radiopharm.* **1984**, *21*, 693-702; c) S. McLean, R. B. Rothman, A. E. Jacobson, K. C. Rice, M. Herkenham, *J. Comp. Neurol.* **1987**, *255*, 497-510; d) R. B. Rothman, V. Bykov, B. R. de Costa, A. E. Jacobson, K. C. Rice, L. S. Brady, *Peptides* **1990**, *11*, 311-331; e) B. Tocque, A. E. Jacobson, K. C. Rice, E. A. Frey, *Eur. J. Pharmacol.* **1987**, *143*, 127-130; f) J. A. Danks, F. C. Tortella, J. B. Long, V. Bykov, A. E. Jacobson, K. C. Rice, J. W. Holaday, R. B. Rothman, *Neuropharmacology*

- 1988, 27, 965-974; g) Q. Ni, H. Xu, J. S. Partilla, K. C. Rice, D. Matecka, S. N. Calderon, F. Porreca, J. Lai, H. Schmidhammer, R. Krassnig, R. B. Rothman, *Peptides* **1998**, 19, 1079-1090; h) G. R. Rios, T. R. Tephly, *Drug Metab. Dispos.* **2002**, 30, 1364-1367; i) R. B. Rothman, V. Bykov, J. A. Danks, A. E. Jacobson, T. R. Burke, K. C. Rice, M. Herkenham, *Neuropeptides* **1985**, 6, 503-516; j) R. B. Rothman, W. D. Bowen, V. Bykov, U. K. Schumacher, C. B. Pert, A. E. Jacobson, T. R. Burke, K. C. Rice, *Neuropeptides* **1984**, 4, 201-215; k) R. B. Rothman, J. B. Long, V. Bykov, A. E. Jacobson, K. C. Rice, J. W. Holaday, *Neuropharmacology* **1990**, 29, 805-810; l) D. J. J. Carr, B. R. DeCosta, C.-H. Kim, A. E. Jacobson, K. L. Bost, K. C. Rice, E. Blalock, *Neuroendocrinology* **2008**, 51, 552-560; m) J. K. Staley, R. B. Rothman, K. C. Rice, J. Partilla, D. C. Mash, *J. Neurosci.* **1997**, 17, 8225-8233; n) R. B. Rothman, J. A. Danks, A. E. Jacobson, T. R. Burke, K. C. Rice, C. B. Pert, *Neuropeptides* **1984**, 4, 311-317; o) H. Xu, J. S. Partilla, B. R. de Costa, K. C. Rice, R. B. Rothman, *Peptides* **1993**, 14, 893-907; p) R. A. Lessor, B. S. Bajwa, K. C. Rice, A. E. Jacobson, R. A. Streaty, W. A. Klee, C. B. Smith, M. D. Aceto, E. L. May, L. S. Harris, *J. Med. Chem.* **1986**, 29, 2136-2141; q) S. McLean, R. B. Rothman, D. M. Chuang, K. C. Rice, J. W. Spain, C. J. Coscia, B. L. Roth, *Brain Res. Dev. Brain Res.* **1989**, 45, 283-289.
- [11] J. L. Galzi, A. Mejean, B. Ilien, C. Mollereau, J. C. Meunier, M. Goeldner, C. Hirth, *J. Med. Chem.* **1990**, 33, 2456-2464.
- [12] A. E. Conibear, E. Kelly, *Mol. Pharmacol.* **2019**, 96, 542-549.
- [13] a) J. Shim, A. Coop, A. D. MacKerell, Jr., *J. Phys. Chem. B* **2011**, 115, 7487-7496; b) A. P. Feinberg, I. Creese, S. H. Snyder, *Proc. Natl. Acad. Sci. U. S. A.* **1976**, 73, 4215-4219.
- [14] a) W. Szymański, J. M. Beierle, H. A. Kistemaker, W. A. Velema, B. L. Feringa, *Chem. Rev.* **2013**, 113, 6114-6178; b) W. A. Velema, W. Szymanski, B. L. Feringa, *J. Am. Chem. Soc.* **2014**, 136, 2178-2191; c) M. M. Lerch, M. J. Hansen, G. M. van Dam, W. Szymanski, B. L. Feringa, *Angew. Chem. Int. Ed. Engl.* **2016**, 55, 10978-10999.
- [15] a) E. Sengupta, Y. Yan, X. Wang, K. Munechika, D. S. Ginger, *ACS Nano* **2014**, 8, 2625-2631; b) N. Barbosa, L. Sagresti, G. Brancato, *Phys. Chem. Chem. Phys.* **2021**, 23, 25170-25179.
- [16] M. J. Fuchter, *J. Med. Chem.* **2020**, 63, 11436-11447.
- [17] a) P. Donthamsetti, N. Winter, A. Hoagland, C. Stanley, M. Visel, S. Lammel, D. Trauner, E. Isacoff, *Nat. Commun.* **2021**, 12, 4775; b) X. Rovira, A. Trapero, S. Pittolo, C. Zussy, A. Faucherre, C. Jopling, J. Giraldo, J. P. Pin, P. Gorostiza, C. Goudet, A. Llebaria, *Cell Chem. Biol.* **2016**, 23, 929-934; c) M. Schönberger, D. Trauner, *Angew. Chem. Int. Ed. Engl.* **2014**, 53, 3264-3267; d) R. Lahmy, H. Hübner, M. F. Schmidt, D. Lachmann, P. Gmeiner, B. König, *Chem. Eur. J.* **2022**, 28, e202201515; e) D. Prischich, A. M. J. Gomila, S. Milla-Navarro, G. Sangüesa, R. Diez-Alarcia, B. Preda, C. Matera, M. Batlle, L. Ramírez, E. Giralt, J. Hernando, E. Guasch, J. J. Meana, P. de la Villa, P. Gorostiza, *Angew. Chem. Int. Ed. Engl.* **2021**, 60, 3625-3631; f) D. Lachmann, R. Lahmy, B. König, *Eur. J. Org. Chem.* **2019**, 2019, 5018-5024; g) J. Morstein, G. Romano, B. E. Hetzler, A. Plante, C. Haake, J. Levitz, D. Trauner, *Angew. Chem. int. Ed.* **2022**, 61, e202117094.
- [18] a) J. Calbo, C. E. Weston, A. J. P. White, H. S. Rzepa, J. Contreras-García, M. J. Fuchter, *J. Am. Chem. Soc.* **2017**, 139, 1261-1274; b) J. García-Amorós, M. C. R. Castro, P. Coelho, M. M. M. Raposo, D. Velasco, *Chem. Commun.* **2013**, 49, 11427-11429; c) R. Travieso-Puente, S. Budzak, J. Chen, P. Stacko, J. T. Jastrzebski, D. Jacquemin, E. Otten, *J. Am. Chem. Soc.* **2017**, 139, 3328-3331; d) C. E. Weston, R. D. Richardson, P. R. Haycock, A. J. White, M. J. Fuchter, *J. Am. Chem. Soc.* **2014**, 136, 11878-11881; e) L. Stricker, M. Böckmann, T. M. Kirse, N. L. Doltsinis, B. J. Ravoo, *Chem. Eur. J.* **2018**, 24, 8639-8647; f) A. D. W. Kennedy, I. Sandler, J. Andréasson, J. Ho, J. E. Beves, *Chem. Eur. J.* **2020**, 26, 1103-1110.

- [19] K. Mezgebe, E. Mulugeta, *RSC Adv.* **2022**, *12*, 25932-25946.
- [20] S. R. Brishty, M. J. Hossain, M. U. Khandaker, M. R. I. Faruque, H. Osman, S. M. A. Rahman, *Front. Pharmacol.* **2021**, *12*, 762807.
- [21] a) D. Dolles, A. Strasser, H.-J. Wittmann, O. Marinelli, M. Nabissi, R. G. Pertwee, M. Decker, *Adv. Ther.* **2018**, *1*, 1700032; b) S. Crespi, N. A. Simeth, A. Bellisario, M. Fagnoni, B. König, *J. Phys. Chem. A.* **2019**, *123*, 1814-1823; c) Y. Hasegawa, S. Kume, H. Nishihara, *Dalton Trans.* **2009**, 280-284; d) O. Shinzi, I. Syoji, M. Hiroshi, M. Mizuo, *Chem. Lett.* **2010**, *39*, 956-957.
- [22] S. A. M. Steinmüller, J. Fender, M. H. Deventer, A. Tutov, K. Lorenz, C. P. Stove, J. N. Hislop, M. Decker, *Angew. Chem. Int. Ed. Engl.* **2023**, e202306176.
- [23] R. Wong, S. J. Dolman, *J. Org. Chem.* **2007**, *72*, 3969-3971.
- [24] A. A. John, Q. Lin, *J. Org. Chem.* **2017**, *82*, 9873-9876.
- [25] a) F. Bureš, *RSC Advances* **2014**, *4*, 58826-58851; b) C. Knie, M. Utecht, F. Zhao, H. Kulla, S. Kovalenko, A. M. Brouwer, P. Saalfrank, S. Hecht, D. Bléger, *Chem. Eur. J.* **2014**, *20*, 16492-16501; c) M. Dong, A. Babalhavaeji, S. Samanta, A. A. Beharry, G. A. Woolley, *Acc. Chem. Res.* **2015**, *48*, 2662-2670; d) J. Garcia-Amoros, D. Velasco, *Beilstein J. Org. Chem.* **2012**, *8*, 1003-1017.
- [26] F. Riefolo, C. Matera, A. Garrido-Charles, A. M. J. Gomila, R. Sortino, L. Agnetta, E. Claro, R. Masgrau, U. Holzgrabe, M. Batlle, M. Decker, E. Guasch, P. Gorostiza, *J. Am. Chem. Soc.* **2019**, *141*, 7628-7636.
- [27] N. A. Simeth, S. Crespi, M. Fagnoni, B. König, *J. Am. Chem. Soc.* **2018**, *140*, 2940-2946.
- [28] a) L. Stricker, E.-C. Fritz, M. Peterlechner, N. L. Doltsinis, B. J. Ravoo, *J. Am. Chem. Soc.* **2016**, *138*, 4547-4554; b) M. A. Kienzler, A. Reiner, E. Trautman, S. Yoo, D. Trauner, E. Y. Isacoff, *J. Am. Chem. Soc.* **2013**, *135*, 17683-17686; c) A. A. Beharry, G. A. Woolley, *Chem. Soc. Rev.* **2011**, *40*, 4422-4437; d) C. Fedele, T.-P. Ruoko, K. Kuntze, M. Virkki, A. Priimagi, *Photochem. Photobiol. Sci.* **2022**, *21*, 1719-1734.
- [29] a) E. A. Fink, J. Xu, H. Hübner, J. M. Braz, P. Seemann, C. Avet, V. Craik, D. Weikert, M. F. Schmidt, C. M. Webb, N. A. Tolmachova, Y. S. Moroz, X. P. Huang, C. Kalyanaraman, S. Gahbauer, G. Chen, Z. Liu, M. P. Jacobson, J. J. Irwin, M. Bouvier, Y. Du, B. K. Shoichet, A. I. Basbaum, P. Gmeiner, *Science* **2022**, *377*, eabn7065; b) J. Quoyer, J. M. Janz, J. Luo, Y. Ren, S. Armando, V. Lukashova, J. L. Benovic, K. E. Carlson, S. W. Hunt, M. Bouvier, *Proc. Natl. Acad. Sci. U. S. A.* **2013**, *110*, E5088-E5097; c) C. Galés, J. J. Van Durm, S. Schaak, S. Pontier, Y. Percherancier, M. Audet, H. Paris, M. Bouvier, *Nat. Struct. Mol. Biol.* **2006**, *13*, 778-786.
- [30] a) H. Liu, J. Hofmann, I. Fish, B. Schaake, K. Eitel, A. Bartuschat, J. Kaindl, H. Rampf, A. Banerjee, H. Hübner, M. J. Clark, S. G. Vincent, J. T. Fisher, M. R. Heinrich, K. Hirata, X. Liu, R. K. Sunahara, B. K. Shoichet, B. K. Kobilka, P. Gmeiner, *Proc. Natl. Acad. Sci. U. S. A.* **2018**, *115*, 12046-12050; b) C. Gentzsch, K. Seier, A. Drakopoulos, M.-L. Jobin, Y. Lanoiselée, Z. Koszegi, D. Maurel, R. Sounier, H. Hübner, P. Gmeiner, S. Granier, D. Calebiro, M. Decker, *Angew. Chem. Int. Ed. Engl.* **2020**, *59*, 5958-5964.
- [31] a) D. Weichert, A. C. Kruse, A. Manglik, C. Hiller, C. Zhang, H. Hübner, B. K. Kobilka, P. Gmeiner, *Proc. Natl. Acad. Sci. U. S. A.* **2014**, *111*, 10744-10748; b) R. C. Kling, M. Plomer, C. Lang, A. Banerjee, H. Hübner, P. Gmeiner, *ACS Chem. Biol.* **2016**, *11*, 869-875.

3.7 Supplementary Information

3.7.1 Supplementary Chemical Information

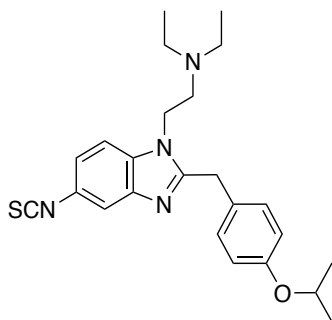
3.7.1.1 Materials and Methods

Commercial reagents were obtained from Merck, Sigma-Aldrich, TCI Deutschland GmbH, ABCR GmbH or Fluorochem, and were used without further purification. P.A. grade solvent were used and if necessary, dried according to common procedures. Anhydrous reactions were performed using dried glassware under a nitrogen or argon atmosphere, unless otherwise specified. Technical grade solvents were used for column chromatography without further purification. Flash chromatography was performed using Biotage Isolera One System for normal phase chromatography, using Davisil Chromatographic Silica Media 60 Å (particle size 40-63 µM, Merck). For reversed phase chromatography, Biotage SNAP Cartridges KP-C18-HS were used. Analytical thin layer chromatography (TLC) was performed on silica gel 60 F-254 with a 0.2 mm layer and aluminium-backed plates (Merck). Visualization was obtained by fluorescence quenching under UV light (short and long wave) and/or by staining the plate with potassium permanganate stain (60 mM KMnO₄, 480 mM K₂CO₃ and 5% w/v NaOH) and vanillin-H₂SO₄ solution (0.5 g vanillin, 85 mL ethanol, 10 mL conc. acetic acid, 3 mL conc. H₂SO₄). Preparative high-performance liquid chromatography (HPLC) was performed using Agilent 1100 Series with a Phenomenex Luna 10 µM C18 column (100 Å, 250 x 21.2 mm) and a solvent flow rate of 20 mL/min. Analytical HPLC measurements were performed using Agilent 1220 Infinity LC System (column: Phenomenex Luna, 3 µM C18(2), 100 Å 150 x 2.00 mm). Biologically tested compounds were further purified by preparative HPLC prior to biological testing and possessed a purity of ≥ 92%, which was determined by analytical HPLC with wavelength detections of 220 nm and 254 nm. NMR spectra were recorded on a Bruker Avance III HD 600 (¹H 600.25 MHz, ¹³C 150.95 MHz, T = 300K), with solvents specified. The chemical shifts were reported as δ values in parts per million (ppm), referenced to the appropriate and specified solvent peak. Resonance multiplicity is abbreviated as: 's' (singlet), 'd' (doublet), 't' (triplet), 'q' (quartet) and 'm' (multiplet). J-coupling constants (J) were recorded in Hz. Mass spectra were recorded using Finnigan MAT-SSQ 710 A, ThermoQuest Finnigan TSQ 7000, Agilent 6540 UHD Q-TOF, or a JeolAccuTOF GCX instrument.

3.7.1.2 Chemistry Synthesis Procedures

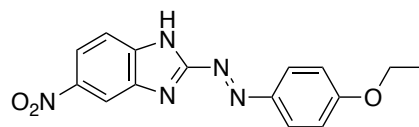
Isotonitazene was synthesized according to literature procedures.^[1]

N,N-diethyl-2-(2-(4-isopropoxybenzyl)-5-isothiocyanato-1*H*-benzo[*d*]imidazol-1-yl)ethan-1-amine (Iso-BIT, **1**)



Isotonitazene (60.0 mg, 0.15 mmol) was dissolved in anhydrous methanol (3 mL). Palladium, 10 wt% on activated carbon (17.3 mg, 0.015 mmol, 0.1 eq.) was added and the atmosphere from the flask was purged with hydrogen from a balloon. The mixture was then stirred under a hydrogen atmosphere at room temperature. After 3 hours, thin layer chromatography (DCM/MeOH 0.01% Et₃N, 20:1) followed by staining with ninhydrin showed complete consumption of starting material and formation of an amine. The mixture was filtered through a pad of celite, washed with anhydrous ethanol (5 mL), and then concentrated *in vacuo*. To this crude transparent yellow residue (55 mg, 0.14 mmol), Et₃N (0.081 mL, 0.58 mmol, 4.0 eq.) and THF (1 mL) were added, and then cooled with an ice bath under N₂ atmosphere. CS₂ (0.035 mL, 0.58 mmol, 4.0 eq.) was added over 0.5 h. After 2 h, additional CS₂ (0.035 mL, 0.58 mmol, 4.0 eq.) and Et₃N (0.081 mL, 0.58 mmol, 4.0 eq.) were added. After 18 h, the mixture was cooled with an ice bath and TsCl (30.3 mg, 0.16 mmol, 1.1 eq.) was added. After stirring at room temperature for 1 h, 1 M HCl (5 mL) and methyl tert-butyl ether (5 mL) were added to the mixture. The combined layers were washed with methyl tert-butyl ether (2 x 5 mL), dried over Na₂SO₄, filtered and concentrated *in vacuo*. The crude residue was subjected to automated flash column chromatography, eluting at 100% DCM to 20% MeOH/DCM to obtain isothiocyanate **1** as a light green residue (18.0 mg, 0.04 mmol, 29%). ¹H-NMR (400 MHz, CDCl₃): δ (ppm) = 7.60 (d, *J* = 1.8 Hz, 1H), 7.25-7.22 (m, 1H), 7.15-7.10 (m, 3H), 6.81 (d, *J* = 8.6 Hz, 2H), 4.48 (h, *J* = 6.1 Hz, 1H), 4.28 (s, 2H), 4.04 (t, *J* = 6.9 Hz, 2H), 2.51-2.42 (m, 6H), 1.30 (d, *J* = 6.1 Hz, 6H), 0.89 (t, *J* = 7.1 Hz, 6H). ¹³C-NMR (101 MHz, CDCl₃): δ = 157.18, 156.03, 142.91, 134.61, 133.63, 129.63, 127.80, 125.26, 120.78, 116.80, 116.41, 110.29, 77.36, 70.07, 52.06, 47.66, 33.87, 22.14, 11.75. HR-ESI-MS (*m/z*): [*M*+H]⁺ calculated: 423.2244; found: 423.2216.

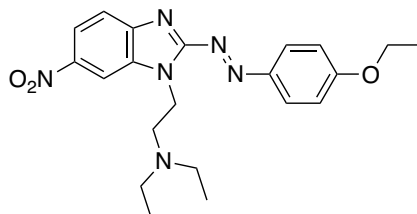
2-((4-ethoxyphenyl)diazenyl)-5-nitro-1*H*-benzo[*d*]imidazole (**2a**)



To a solution of commercially available 5-nitro-1*H*-benzimidazol-2-ylamine (2.0 g, 11.2 mmol) and 4-ethoxyaniline (1.45 mL, 11.2 mmol, 1.0 eq.) dissolved in DCM (50 mL), was added DBU (3.35 mL, 22.5 mmol, 2.0 eq.). The solution was stirred at room temperature for 5 min before being cooled down to -78 °C. N-chlorosuccinimide (3.0 g, 22.5 mmol, 2.0 eq.) was added to the reaction mixture. The solution was stirred for 0.5 h before being quenched by the addition of saturated NaHCO₃ solution. The organic layer was separated, washed with water (1 x 30 mL), dried (Na₂SO₄), filtered and concentrated *in vacuo*. The crude residue was subjected to automated flash column chromatography, eluting at 100% DCM to 20% MeOH/DCM. The product was further purified by automated reverse phase column chromatography (solvent A: H₂O [0.05 Vol% TFA], solvent B: MeCN; gradient A/B: 0-20 min: 10/98, 20-25 min: 2/98), yielded **2a** as a red solid (460 mg, 1.48 mmol, 13%). ¹H-NMR (400 MHz, MeOD): δ (ppm) = 8.60 (d, *J* = 2.1 Hz, 1H), 8.27 (dd, *J* = 6.8, 2.2 Hz, 1H), 8.11-8.08 (m, 2H), 7.78 (d, *J* = 9.0 Hz, 1H), 7.16-7.12 (m, 2H), 4.20 (q, *J* = 7.0 Hz, 2H), 1.46 (t, *J* = 7.0 Hz, 3H). ¹³C-NMR (101 MHz, MeOD): δ = 165.80, 161.66, 147.95, 145.52, 127.50, 120.66, 116.35, 114.38, 65.46, 14.95. HR-ESI-MS (*m/z*): [*M*+H]⁺ calculated: 312.1123; found: 312.1095.

Covalent and Photochromic Derivatives of the Potent Synthetic Opioid Isotonitazene and Other Nitazenes

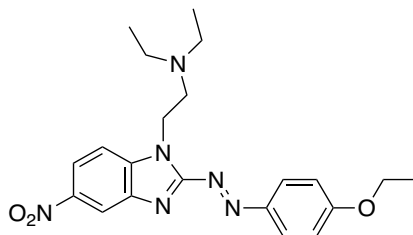
(*E*)-2-(2-((4-ethoxyphenyl)diazenyl)-6-nitro-1*H*-benzo[*d*]imidazol-1-yl)-*N,N*-diethylethan-1-amine (**2b**)



A mixture of compound **2a** (430 mg, 1.38 mmol), commercially available 2-chloro-*N,N*-diethylethylamine hydrochloride (238 mg, 1.38 mmol, 1.0 eq.), powdered KOH (188 mg, 3.36 mmol, 2.4 eq.), anhydrous K₂CO₃ (368 mg, 2.67 mmol, 1.9 eq.) and acetone (50 mL) was heated to reflux for 3 h, while stirring. The solvent was removed *in vacuo* and the residue was diluted with water (10 mL) and DCM (20 mL). The organic layer was further washed with DCM (1 x 10 mL), brine (1 x 10 mL), dried (Na₂SO₄), filtered and concentrated *in vacuo*. The crude residue was subjected to automated flash column chromatography, eluting at 10% ethyl acetate/petrolether to 100% ethyl acetate/petrolether to obtain compound **2b** as an orange solid (123 mg, 0.30 mmol, 22%). ¹H-NMR (400 MHz, CDCl₃): δ (ppm) = 8.57 (d, *J* = 1.8 Hz, 1H), 8.24 (dd, *J* = 9.0, 2.0 Hz, 1H), 8.14 (d, *J* = 9.0 Hz, 2H), 7.94 (d, *J* = 9.0 Hz, 1H), 7.05 (d, *J* = 9.0 Hz, 2H), 5.26-5.22 (m, 2H), 4.18 (q, *J* = 7.0 Hz, 2H), 3.55-3.51 (m, 2H), 3.34-3.28 (m, 4H), 1.49 (t, *J* = 7.0 Hz, 3H), 1.37 (t, *J* = 7.3 Hz, 6H). ¹³C-NMR (101 MHz, CDCl₃): δ = 165.27, 157.91, 147.89, 146.42, 144.67, 133.94, 127.51, 122.11, 120.04, 115.63, 106.72, 64.57, 50.42, 47.09, 38.81, 14.76, 8.44. HR-ESI-MS (*m/z*): [*M*+H]⁺ calculated: 411.2169; found: 411.2141.

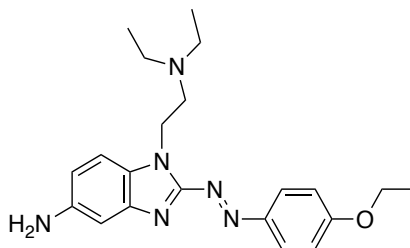
Covalent and Photochromic Derivatives of the Potent Synthetic Opioid Isotonitazene and Other Nitazenes

(*E*)-2-(2-((4-ethoxyphenyl)diazenyl)-5-nitro-1*H*-benzo[*d*]imidazol-1-yl)-*N,N*-diethylethan-1-amine (2c)



Following the synthesis procedure of compound **2b**, compound **2c** was obtained after automated flash column chromatography, eluting at 100% DCM to 20% MeOH/DCM as an orange solid (92.0 mg, 0.22 mmol, 16%). ¹H-NMR (400 MHz, CDCl₃): δ (ppm) = 8.74 (s, 1H), 8.33 (d, *J* = 9.0 Hz, 1H), 8.10 (d, *J* = 8.7 Hz, 2H), 7.83 (d, *J* = 9.0 Hz, 1H), 7.05 (d, *J* = 8.7 Hz, 2H), 5.23-5.19 (m, 2H), 4.19 (q, *J* = 6.9 Hz, 2H), 3.50-3.47 (m, 2H), 3.28 (br s, 4H), 1.49 (t, *J* = 6.9 Hz, 3H), 1.38 (t, *J* = 7.2 Hz, 6H). ¹³C-NMR (101 MHz, CDCl₃): δ = 165.03, 157.07, 147.74, 145.19, 141.47, 138.70, 127.15, 120.66, 118.33, 115.61, 110.43, 64.58, 50.51, 46.97, 38.90, 14.78, 8.38. HR-ESI-MS (*m/z*): [*M*+*H*]⁺ calculated: 411.2175; found: 411.2148.

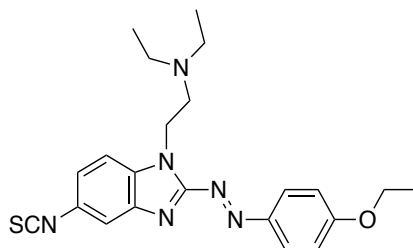
(*E*)-1-(2-(diethylamino)ethyl)-2-((4-ethoxyphenyl)diazenyl)-1*H*-benzo[*d*]imidazol-5-amine (2d)



Compound **2c** (90.0 mg, 0.22 mmol) was dissolved in anhydrous methanol (7 mL). Palladium, 10 wt% on activated carbon (2.60 mg, 0.02 mmol, 0.1 eq.) was added and the atmosphere from the flask was purged with hydrogen from a balloon. The atmosphere was evacuated from the flask and replaced with hydrogen twice. The mixture was then stirred under a hydrogen atmosphere at room temperature. After 3 hours, thin layer chromatography (DCM/MeOH 0.1% Et₃N, 20:1) followed by staining with ninhydrin showed complete consumption of starting material and formation of an amine. The mixture was filtered through a pad of celite, washed with anhydrous ethanol (5 mL), and then concentrated *in vacuo*. The crude residue was subjected to automated column chromatography, eluting at 100% DCM to 20% DCM/MeOH 0.1% Et₃N to obtain **2d** as a dark red oil (43.0 mg, 0.11 mmol, 52%). ¹H-NMR (400 MHz, CDCl₃): δ (ppm) = 8.04 (d, *J* = 9.0 Hz, 2H), 7.24 (s, 1H), 7.09-7.08 (m, 1H), 6.97 (d, *J* = 9.0 Hz, 2H), 6.76 (dd, *J* = 6.5, 2.1 Hz, 1H), 4.59 (t, *J* = 7.3 Hz, 2H), 4.11 (q, *J* = 7.0 Hz, 2H), 2.85 (t, *J* = 7.3 Hz, 2H), 2.55 (q, *J* = 7.1 Hz, 4H), 1.43 (t, *J* = 7.0 Hz, 3H), 0.93 (t, *J* = 7.1 Hz, 6H). ¹³C-NMR (101 MHz, CDCl₃): δ = 162.84, 155.52, 147.88, 143.82, 143.50, 129.89, 125.95, 115.14, 114.97, 110.66, 105.36, 77.48, 77.16, 76.84, 64.10, 53.11, 52.81, 47.71, 42.22, 29.81, 14.85, 12.21. HR-ESI-MS (*m/z*): [*M*+H]⁺ calculated: 381.2427; found: 381.2401.

Covalent and Photochromic Derivatives of the Potent Synthetic Opioid Isotonitazene and Other Nitazenes

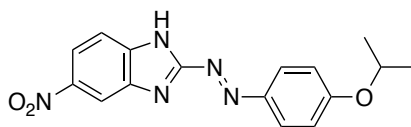
(*E*)-2-(2-((4-ethoxyphenyl)diazenyl)-5-isothiocyanato-1*H*-benzo[*d*]imidazol-1-yl)-*N,N*-diethylethan-1-amine (**2e**)



A mixture of **2d** (33.0 mg, 0.09 mmol) and Et₃N (0.12 mL, 0.87 mmol, 10.0 eq.) in THF (1.5 mL) was cooled with an ice bath under N₂ atmosphere. To the cooled solution, CS₂ (0.05 mL, 0.87 mmol, 10.0 eq.) was added drop-wise over 0.5 hours. A further addition of CS₂ (0.02 mL, 0.35 mmol, 4.0 eq.) and Et₃N (0.05 mL, 0.35 mmol, 4.0 eq.) was added after 4 hours, while stirring. After 16 hours of stirring at room temperature, the mixture was cooled with an ice bath and TsCl (18.2 mg, 0.10 mmol, 1.1 eq.) was added. After stirring at room temperature for 1 h, DCM (5 mL) and water (5 mL) were added to the mixture. The combined layers were washed with DCM (2 x 5 mL), dried over Na₂SO₄, filtered and concentrated *in vacuo*. The crude residue was subjected to automated flash column chromatography, eluting at 100% DCM to 20% MeOH/DCM. The product was further purified by preparative HPLC (solvent A: H₂O [0.05 Vol% TFA], solvent B: MeCN; gradient A/B: 0-20 min: 2/98) to obtain isothiocyanate **2e** as an orange oil (18.0 mg, 0.04 mmol, 49%). ¹H-NMR (400 MHz, CDCl₃): δ (ppm) = 8.10-8.08 (m, 2H), 7.71-7.70 (m, 1H), 7.45 (d, *J* = 8.6 Hz, 1H), 7.23 (dd, *J* = 6.7, 1.9 Hz, 1H), 7.03-7.01 (m, 2H), 4.65 (t, *J* = 6.9 Hz, 2H), 4.16 (q, *J* = 7.0 Hz, 2H), 2.87 (t, *J* = 6.9 Hz, 2H), 2.53 (q, *J* = 7.1 Hz, 4H), 1.47 (t, *J* = 7.0 Hz, 3H), 0.88 (t, *J* = 7.1 Hz, 6H). ¹³C-NMR (101 MHz, CDCl₃): δ = 163.57, 156.85, 147.68, 142.27, 134.50, 134.03, 126.50, 126.37, 122.28, 118.35, 115.04, 111.13, 64.13, 52.70, 47.52, 42.61, 14.71, 12.04. HR-ESI-MS (*m/z*): [*M*+H]⁺ calculated: 423.1995; found: 423.1967.

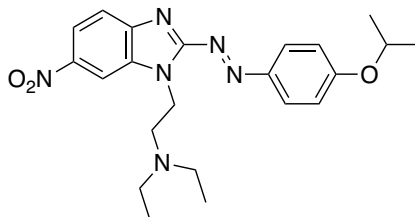
Covalent and Photochromic Derivatives of the Potent Synthetic Opioid Isotonitazene and Other Nitazenes

2-((4-isopropoxyphenyl)diazenyl)-5-nitro-1H-benzo[d]imidazole (**3a**)



To a solution of commercially available 5-nitro-1H-benzimidazol-2-ylamine (1.5 g, 8.42 mmol) and 4-isopropoxyaniline (1.29 mL, 8.42 mmol, 1.0 eq.) dissolved in DCM (50 mL), was added DBU (2.51 mL, 16.8 mmol, 2.0 eq.). The solution was stirred at room temperature for 5 min before being cooled down to -78 °C. Commercially available N-chlorosuccinimide (2.25 g, 16.8 mmol, 2.0 eq.) was added to the reaction mixture. The solution was stirred for 0.5 h before being quenched by the addition of saturated NaHCO₃ solution. The organic layer was separated, washed with water (30 mL), dried (Na₂SO₄), filtered and concentrated *in vacuo*. The crude residue was subjected to automated flash column chromatography, eluting at 100% DCM to 20% MeOH/DCM. Further purification was performed by automated reverse phase column chromatography (solvent A: H₂O [0.05 Vol% TFA], solvent B: MeCN; gradient A/B: 0-20 min: 10/98, 20-25 min: 2/98), yielded **3a** as an orange solid (215 mg, 0.66 mmol, 8%). ¹H-NMR (400 MHz, MeOD): δ (ppm) = 8.60 (br s, 1H), 8.26 (d, *J* = 8.7 Hz, 1H), 8.09-8.05 (m, 2H), 7.76 (br s, 1H), 7.14-7.10 (m, 2H), 4.84-4.76 (m, 1H), 1.40 (d, *J* = 6.0 Hz, 6H). ¹³C-NMR (101 MHz, MeOD): δ = 164.95, 147.93, 127.60, 117.27, 71.93, 22.19. HR-ESI-MS (*m/z*): [*M*+H]⁺ calculated: 326.1282; found: 326.1255.

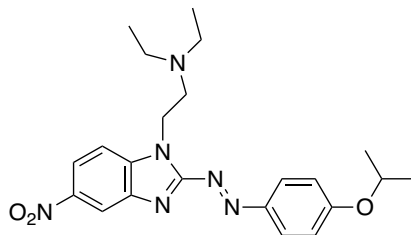
(*E*)-2-(2-((4-isopropoxyphenyl)diazenyl)-6-nitro-1*H*-benzo[*d*]imidazol-1-yl)-*N,N*-diethylethan-1-amine (**3b**)



A mixture of compound **3a** (195 mg, 0.60 mmol), commercially available 2-chloro-*N,N*-diethylethylamine hydrochloride (103 mg, 0.60 mmol, 1.0 eq.), powdered KOH (81.7 mg, 1.46 mmol, 2.4 eq.), anhydrous K₂CO₃ (160 mg, 1.16 mmol, 1.9 eq.) and acetone (40 mL) was heated to reflux for 3 h, while stirring. The solvent was removed *in vacuo* and the residue was diluted with water (10 mL) and DCM (20 mL). The organic layer was further washed with DCM (1 x 10 mL), brine (1 x 10 mL), dried (Na₂SO₄), filtered and concentrated *in vacuo*. The crude residue was subjected to automated flash column chromatography, eluting at 10% ethyl acetate/petrolether to 80% ethyl acetate/petrolether to obtain compound **3b** as an orange solid (65 mg, 0.153 mmol, 26%). ¹H-NMR (400 MHz, MeOD): δ (ppm) = 8.76 (d, *J* = 2.0 Hz, 1H), 8.27 (dd, *J* = 3.7 Hz, 1H), 8.10 (d, *J* = 9.1 Hz, 2H), 7.89 (d, *J* = 9.0 Hz, 1H), 7.13 (d, *J* = 9.1 Hz, 2H), 5.20 (t, *J* = 7.2 Hz, 2H), 4.83-4.79 (m, 1H), 3.79 (t, *J* = 7.2 Hz, 2H), 3.46-3.41 (m, 4H), 1.41 (d, *J* = 6.0 Hz, 6H), 1.34 (t, *J* = 7.3 Hz, 6H). ¹³C-NMR (101 MHz, CDCl₃): δ = 165.83, 159.50, 148.69, 146.95, 145.92, 135.45, 128.34, 121.93, 120.81, 117.44, 108.73, 72.24, 51.43, 39.62, 22.16, 9.06. HR-ESI-MS (*m/z*): [*M*+H]⁺ calculated: 425.2326; found: 425.2299. Crystal structure analysis: CCDC 2236462, X-ray grade crystals were obtained by vapor diffusion with diethyl ether and methanol at room temperature.

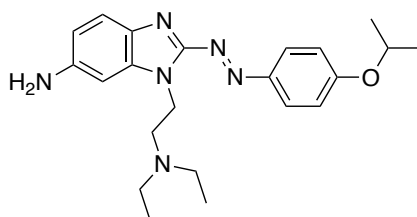
Covalent and Photochromic Derivatives of the Potent Synthetic Opioid Isotonitazene and Other Nitazenes

(*E*)-2-(2-((4-isopropoxyphenyl)diazenyl)-5-nitro-1*H*-benzo[*d*]imidazol-1-yl)-*N,N*-diethylethan-1-amine (**3c**)



Following the synthesis procedure of compound **3b**, compound **3c** was obtained after automated flash column chromatography, eluting at 80% ethyl acetate/petrolether to 100% ethyl acetate/petrolether as an orange solid (58 mg, 0.137 mmol, 23%). ¹H-NMR (400 MHz, MeOD): δ (ppm) = 8.56 (d, J = 2.1 Hz, 1H), 8.27 (dd, J = 3.7 Hz, 1H), 8.07-8.03 (m, 2H), 7.92 (d, J = 9.0 Hz, 1H), 7.11-7.08 (m, 2H), 5.17 (t, J = 7.4 Hz, 2H), 4.83-4.79 (m, 1H), 3.78 (t, J = 7.4 Hz, 2H), 3.45 (q, J = 7.2 Hz, 4H), 1.41 (d, J = 6.0 Hz, 6H), 1.36 (t, J = 7.3 Hz, 6H). ¹³C-NMR (101 MHz, MeOD): δ = 165.68, 158.76, 148.61, 146.19, 141.96, 140.01, 128.19, 120.92, 117.71, 117.38, 112.19, 72.21, 51.16, 39.61, 22.18, 9.04. HR-ESI-MS (m/z): $[M+H]^+$ calculated: 425.2326; found: 425.2299. Crystal structure analysis: CCDC 2236450, X-ray grade crystals were obtained by vapor diffusion with diethyl ether and dichloromethane at 5 °C.

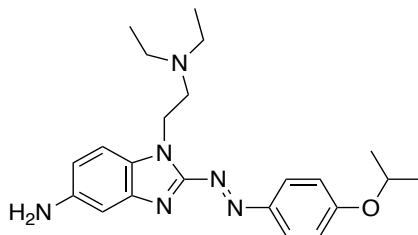
(*E*)-1-(2-(diethylamino)ethyl)-2-((4-isopropoxyphenyl)diazenyl)-1*H*-benzo[*d*]imidazol-6-amine (**3b-NH₂**)



Nitro-containing intermediate **3b** (205 mg, 0.48 mmol) was dissolved in anhydrous methanol (4 mL). Palladium, 10 wt% on activated carbon (5.72 mg, 0.05 mmol, 0.1 eq.) was added and the atmosphere from the flask was purged with hydrogen from a balloon. The atmosphere was evacuated from the flask and replaced with hydrogen twice. The mixture was then stirred under a hydrogen atmosphere at room temperature. After 3 hours, thin layer chromatography (DCM/MeOH 0.1% Et₃N, 20:1) followed by staining with ninhydrin showed complete consumption of starting material and formation of an amine. The mixture was filtered through a pad of celite, washed with anhydrous ethanol (5 mL), and then concentrated *in vacuo*. The crude residue was subjected to automated flash column chromatography, eluting at 100%DCM to 20% DCM/MeOH 0.1% Et₃N to obtain amine **3b-NH₂** as a dark red oil (15 mg, 0.038 mmol, 8%). ¹H-NMR (400 MHz, MeOD): δ (ppm) = 8.12 (d, *J* = 9.1 Hz, 2H), 7.63 (d, *J* = 8.8 Hz, 1H), 7.26 (d, *J* = 1.8 Hz, 1H), 7.17-7.11 (m, 3H), 5.14 (t, *J* = 7.2 Hz, 2H), 4.86-4.82 (m, 1H), 3.76 (t, *J* = 7.2 Hz, 2H), 3.43 (q, *J* = 7.3 Hz, 4H), 1.41 (d, *J* = 6.0 Hz, 6H), 1.35 (t, *J* = 7.3 Hz, 6H), ¹³C-NMR (101 MHz, MeOD): δ = 166.05, 153.39, 148.75, 136.13, 131.60, 128.47, 119.88, 119.45, 117.63, 97.57, 72.36, 50.67, 39.50, 22.15, 8.92. HR-ESI-MS (*m/z*): [*M*+*H*]⁺ calculated: 395.2591; found: 395.2562.

Covalent and Photochromic Derivatives of the Potent Synthetic Opioid Isotonitazene and Other Nitazenes

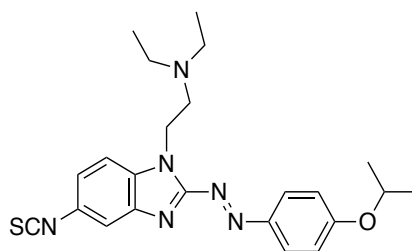
(*E*)-1-(2-(diethylamino)ethyl)-2-((4-isopropoxyphenyl)diazenyl)-1*H*-benzo[*d*]imidazol-5-amine (**3d**)



The synthesis procedure as for compound **3b-NH₂** was followed using nitro-containing intermediate **3c** (132 mg, 0.31 mmol) to obtain amine **3d** as a red solid (41.0 mg, 0.10 mmol, 33%). ¹H-NMR (400 MHz, MeOD): δ (ppm) = 8.18-8.14 (m, 2H), 7.85 (d, *J* = 8.8 Hz, 1H), 7.27-7.23 (m, 2H), 7.20-7.16 (m, 2H), 5.22 (t, *J* = 7.2 Hz, 2H), 4.86-4.83 (m, 1H), 3.79 (t, *J* = 7.2 Hz, 2H), 3.42 (q, *J* = 7.3 Hz, 4H), 1.41 (d, *J* = 6.0 Hz, 6H), 1.34 (t, *J* = 7.3 Hz, 6H). ¹³C-NMR (101 MHz, MeOD): δ = 166.42, 153.82, 148.77, 130.01, 128.77, 119.39, 117.70, 113.85, 104.67, 72.46, 50.99, 39.75, 22.15, 8.91. HR-ESI-MS (*m/z*): [*M*+H]⁺ calculated: 395.2583; found: 395.2554.

Covalent and Photochromic Derivatives of the Potent Synthetic Opioid Isotonitazene and Other Nitazenes

(*E*)-2-(2-((4-isopropoxyphenyl)diazenyl)-5-isothiocyanato-1*H*-benzo[*d*]imidazol-1-yl)-*N,N*-diethylethan-1-amine (**3e**)



A mixture of **3d** (47.0 mg, 0.12 mmol) and Et₃N (0.17 mL, 1.19 mmol, 10.0 eq.) in THF (2 mL) was cooled with an ice bath under N₂ atmosphere. To this cooled solution, CS₂ (0.07 mL, 1.19 mmol, 10.0 eq.) was added drop-wise over 0.5 hours. After 18 hours of stirring at room temperature, the mixture was cooled with an ice bath and TsCl (25.0 mg, 0.13 mmol, 1.1 eq.) was added. After stirring at room temperature for 1 h, DCM (5 mL) and water (5 mL) were added to the mixture. The combined layers were washed with DCM (2 x 5 mL), dried over Na₂SO₄, filtered and concentrated *in vacuo*. The crude residue was subjected to automated flash column chromatography, eluting at 100% DCM to 20% MeOH/DCM. The product was further purified by preparative HPLC (solvent A: H₂O [0.05 Vol% TFA], solvent B: MeCN; gradient A/B: 0-20 min: 2/98) to obtain isothiocyanate **3e** as an orange oil (25 mg, 0.057 mmol, 48%). ¹H-NMR (400 MHz, MeOD): δ (ppm) = 8.04 (d, *J* = 9.0 Hz, 2H), 7.81 (d, *J* = 8.7 Hz, 1H), 7.58 (d, *J* = 1.8 Hz, 1H), 7.31 (dd, *J* = 3.5 Hz, 1H), 7.10 (d, *J* = 9.1 Hz, 2H), 5.11 (t, *J* = 7.2 Hz, 2H), 4.82-4.78 (m, 1H), 3.71 (t, *J* = 7.2 Hz, 2H), 3.41 (q, *J* = 7.2 Hz, 4H), 1.40 (d, *J* = 6.0 Hz, 6H), 1.34 (t, *J* = 7.3 Hz, 6H). ¹³C-NMR (101 MHz, MeOD): δ = 165.23, 157.44, 148.61, 142.82, 137.07, 135.02, 129.00, 127.90, 124.02, 118.16, 117.35, 113.02, 72.06, 51.24, 39.42, 22.20, 9.00. HR-ESI-MS (*m/z*): [*M*+H]⁺ calculated: 437.2147; found: 437.2119.

3.7.1.3 Purity Measurements

All purity measurements can be found in the appendix (Section 7.4.1) under ‘Analytical HPLC Chromatograms for Purity Determination’.

3.7.1.1 Analysis of Isothiocyanate-containing Ligand Degradation

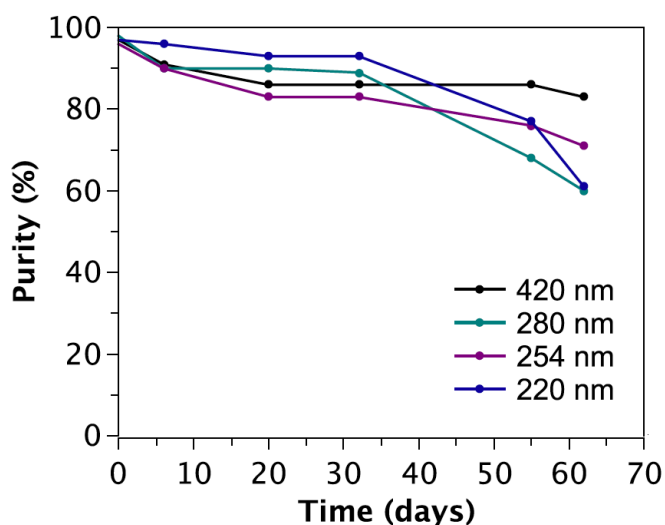


Figure 43. Evaluation of isothiocyanate-containing ligand degradation. Analytical HPLC analysis to determine the stability of compounds containing the isothiocyanate moiety, stored as DMSO stock solutions. This experiment was performed at 25 °C using isothiocyanate-containing compound **3e**, stored as a 10 mM stock solution in DMSO. Wavelengths 420, 280, 254 and 220 nm were used to determine the purity of the compound and for monitoring the appearance of impurities over 62 days. In between experiments, this compound was stored at -18 °C. At $t=0$ days and when the compound was first dissolved in DMSO, these wavelengths indicated compound purities of 97%, 98%, 96% and 97%, respectively. At $t=6$ days, purities were reduced to 91%, 90%, 90% and 96%, respectively. At $t=20$ days, purities were further reduced to 86%, maintained at 90%, reduced to 83% and 93%, respectively. At $t=32$ days, purities were maintained at 86%, reduced to 89%, maintained at 83% and 93%, respectively. At $t=55$ days, purities were maintained at 86%, and reduced to 68%, 76% and 77%, respectively. At $t=62$ days, purities were further reduced to 83%, 60%, maintained at 71% and 61%, respectively.

3.7.2 Supplementary Photophysical Information

3.7.2.1 Materials and Methods

For determination of thermal equilibrium and isomer spectra, as well as determination of cycle performance and thermal half-life, UV/Vis absorption spectroscopy was employed. UV/Vis absorption spectroscopy was performed using Agilent 8453 UV/Vis spectrophotometer for online measurements or Agilent Varian Cary® 50 UV/Vis spectrophotometer, in 10 mm quartz cuvettes. To determine PSS values, an estimation approach was implemented as reported in literature.^[2] Analytical HPLC was performed using Agilent 1220 Infinity LC System (column: Phenomenex Luna, 3 μ M C18(2), 100 Å 150 x 2.0 mm; flow rate of 0.3 mL/min at 20 °C; solvent A: Milli-Q water with 0.05 wt% TFA; solvent B: MeCN). LED light sources for irradiation: λ =265 nm (Nikkiso, VPC131, 350 mA, 6.3 V), λ =285 nm (Nikkiso, VPS173, 500 mA, 6.0 V), λ =340 nm (Seoul Viosys, CUC4AF1B, 500 mA, 4.3 V), λ =365 nm (Seoul Viosys, CUN66A1B, 700 mA, 3.6 V), λ =400 nm (Luxeon LHUV-0400-0450, SZ-01-S2, 1000 mA, 3.2 V), λ =420 nm (Mouser, L1F3-U410200012000, 700 mA, 3.4 V) or λ =420 nm LEDs (PUR-LED TECHNIK, 40301, 1000 Hz, 10% PW, 100 mA, 3.3 V), λ =451 nm (LED-TECH, Oslon SSL 80, LDCQ7P-2U3U, 700 mA, 3.2 V), λ =505 nm (LED-TECH, Oslon SSL 80, LVCK7P-JYKZ, 700 mA, 3.5 V), λ =528 nm (LED-TECH, Oslon SSL 80, LDCQ7P-2U3U, 700 mA, 3.5 V), λ =625 nm (LED-TECH, Oslon SSL 80, LRCP7P-JRJT, 700 mA, 2.8 V), λ =645 nm (LED-TECH, Oslon SSL 80, LHCP7P-2T3T, 700 mA, 2.6 V). The details of these light sources are based on the supplier specifications upon purchase. For lead photoswitchable compounds, respective *cis*-isomers in both DMSO and buffer solution was obtained via 5-10 sec irradiation with 420 nm. To obtain respective *trans*-isomers in DMSO, 1-3 min irradiation with 625 irradiation was required. Respective *trans*-isomers in buffer solutions were obtained thermally under dark conditions.

3.7.2.2 UV/Vis Absorption Spectra, Cycle Performance and Thermal Stabilities

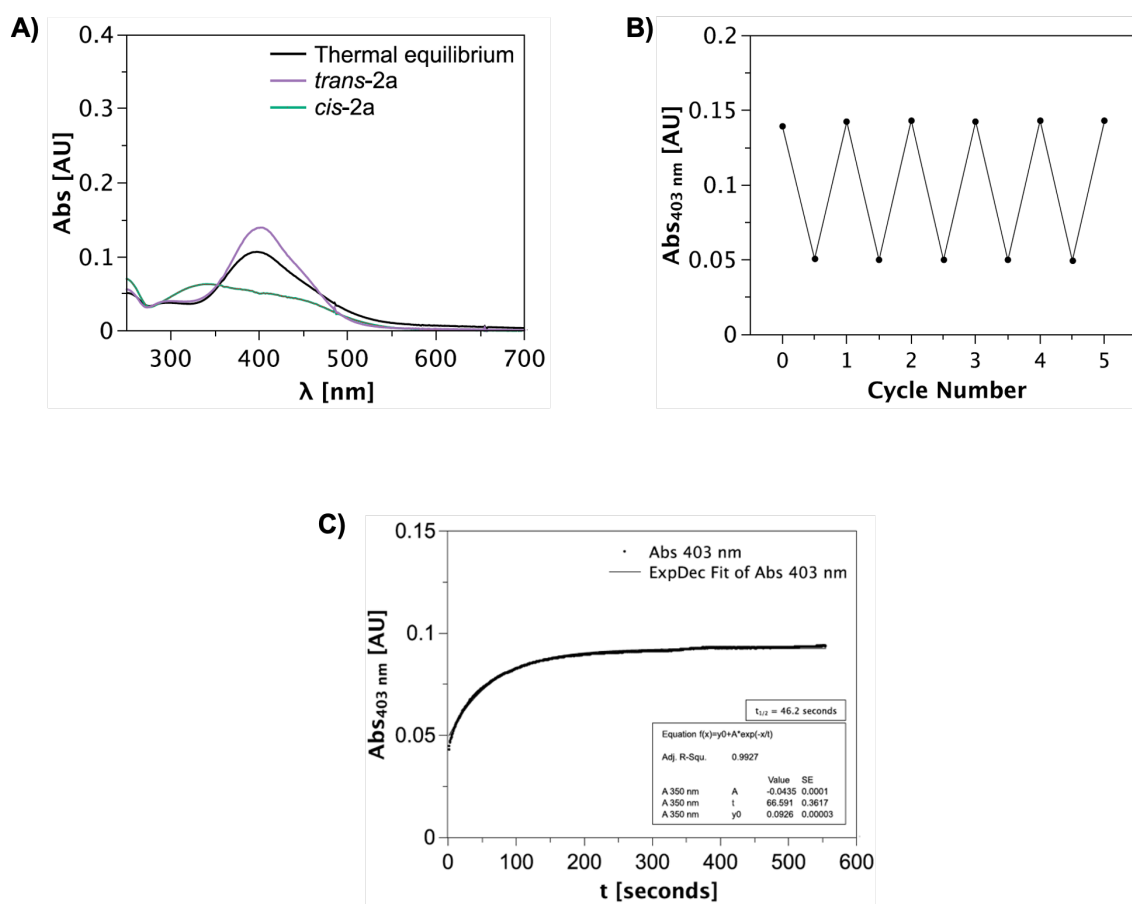


Figure 44. Photophysical properties of compound **2a** (20 μ M) in buffer solution (TrisHCl Buffer, pH 7.5) + 1% DMSO at 25 $^{\circ}$ C. A) Online UV/Vis absorption spectra of thermal equilibrium, *trans*-isomer and *cis*-isomer. The *cis*-isomer was accessed via continuous irradiation with 420 nm, while the *trans*-isomer was obtained thermally under dark conditions. B) Cycle performance when alternating between irradiation with 420 nm and dark conditions. Data points were recorded at the absorbance maximum of the *trans*-isomer (403 nm). C) Thermal half-life of compound **2a**, with each spectrum measured every 0.5 seconds.

Covalent and Photochromic Derivatives of the Potent Synthetic Opioid Isotonitazene and Other Nitazenes

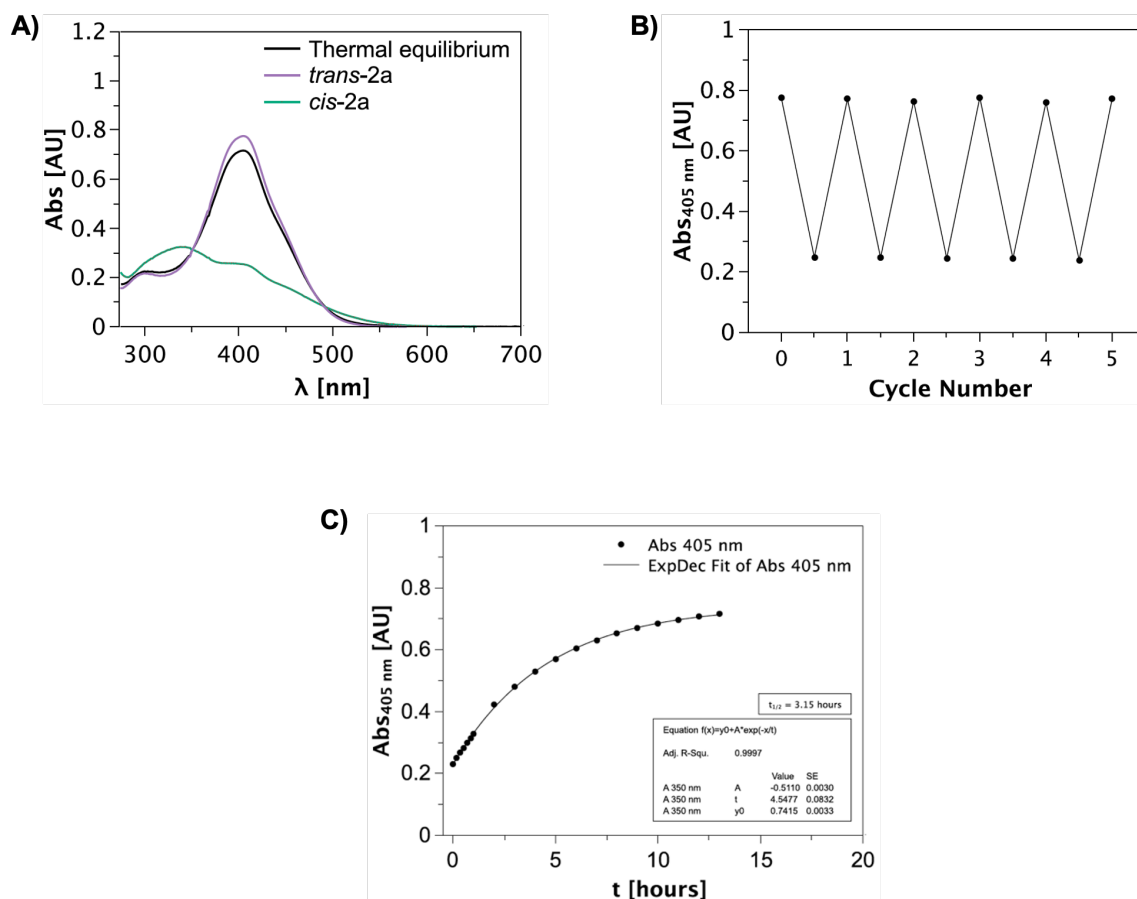


Figure 45. Photophysical properties of compound **2a** (50 μ M) in DMSO at 25 $^{\circ}$ C. A) UV/Vis absorption spectra of thermal equilibrium, *trans*-isomer and *cis*-isomer. The *cis*-isomer was accessed via irradiation with 420 nm, while the *trans*-isomer was obtained with 625 nm irradiation. B) Cycle performance upon alternating irradiation of 420 nm and 625 nm. Data points were recorded at the absorbance maximum of the *trans*-isomer (405 nm). C) Thermal half-life of compound **2a**.

Covalent and Photochromic Derivatives of the Potent Synthetic Opioid Isotonitazene and Other Nitazenes

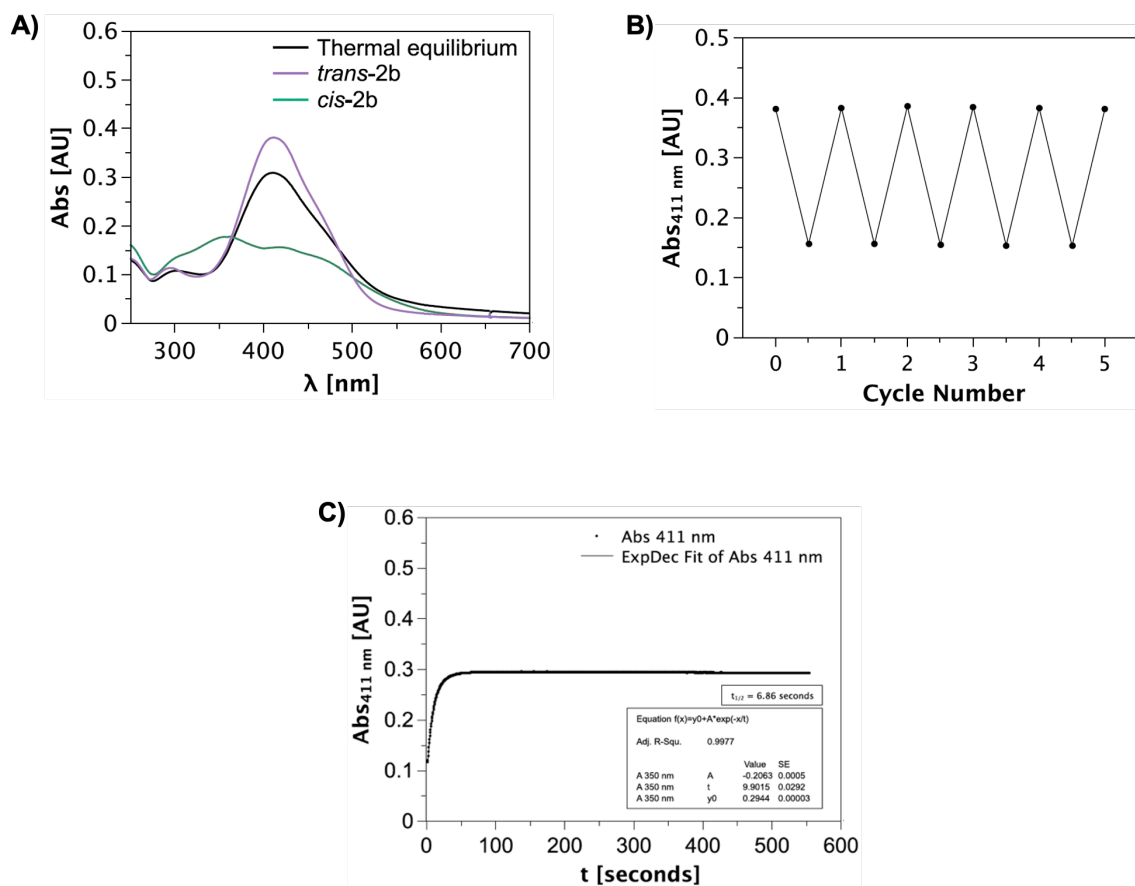


Figure 46. Photophysical properties of compound **2b** (20 μ M) in buffer solution (TrisHCl Buffer, pH 7.5) + 0.2% DMSO at 25 $^{\circ}$ C. A) Online UV/Vis absorption spectra of thermal equilibrium, *trans*-isomer and *cis*-isomer. The *cis*-isomer was accessed via continuous irradiation with 420 nm, while the *trans*-isomer was obtained thermally under dark conditions. B) Cycle performance when alternating between irradiation with 420 nm and dark conditions. Data points were recorded at the absorbance maximum of the *trans*-isomer (411 nm). C) Thermal half-life of compound **2b**, with each spectrum measured every 0.5 seconds.

Covalent and Photochromic Derivatives of the Potent Synthetic Opioid Isotonitazene and Other Nitazenes

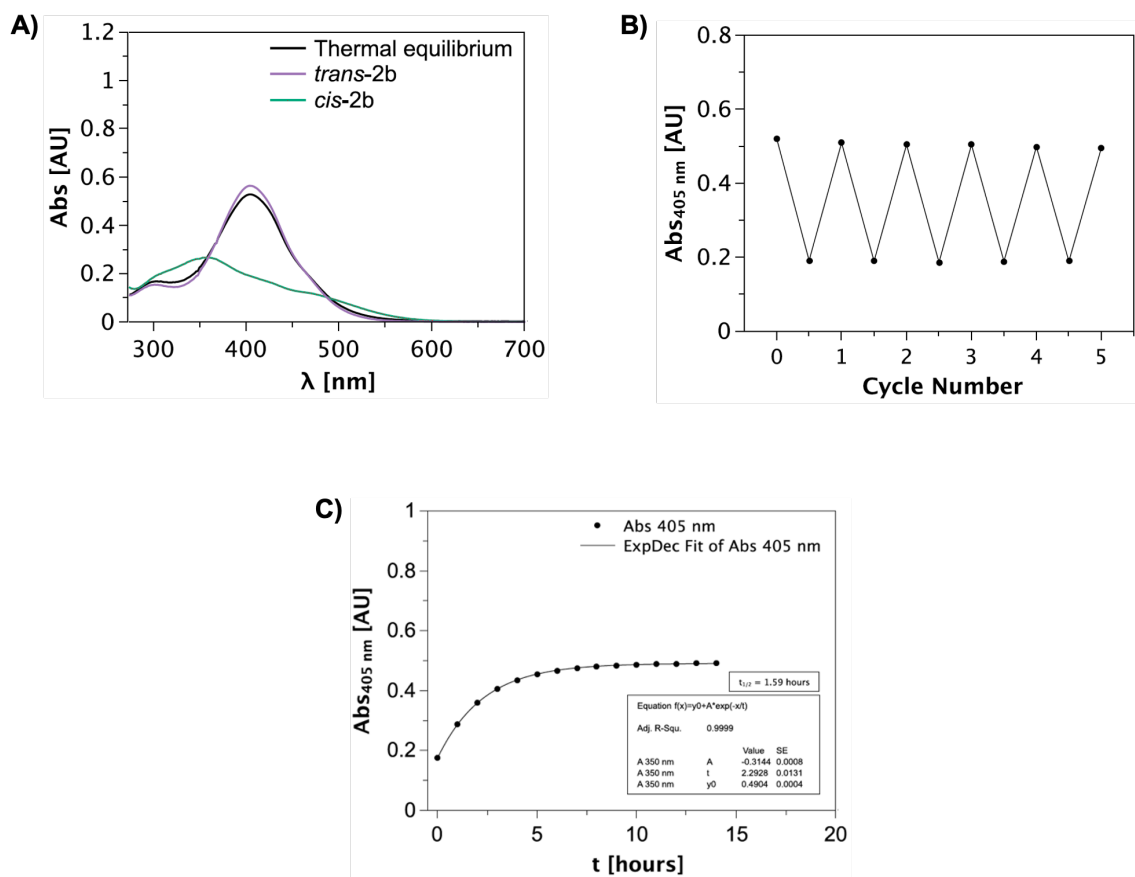


Figure 47. Photophysical properties of compound **2b** (20 μ M) in DMSO at 25 $^{\circ}$ C. A) UV/Vis absorption spectra of thermal equilibrium, *trans*-isomer and *cis*-isomer. The *cis*-isomer was accessed via irradiation with 420 nm, while the *trans*-isomer was obtained with 625 nm irradiation. B) Cycle performance upon alternating irradiation of 420 nm and 625 nm. Data points were recorded at the absorbance maximum of the *trans*-isomer (405 nm). C) Thermal half-life of compound **2b**.

Covalent and Photochromic Derivatives of the Potent Synthetic Opioid Isotonitazene and Other Nitazenes

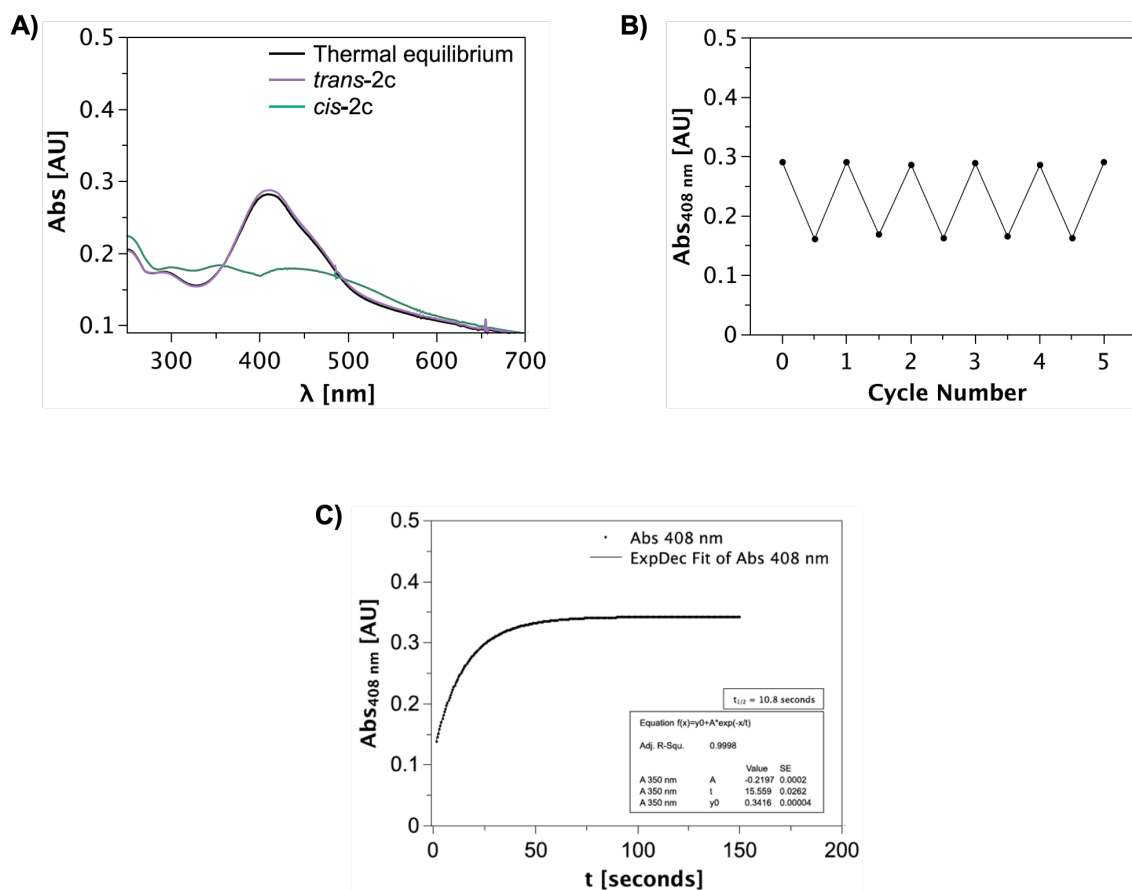


Figure 48. Photophysical properties of compound **2c** (20 μ M) in buffer solution (TrisHCl Buffer, pH 7.5) + 0.2% DMSO at 25 $^{\circ}$ C. A) Online UV/Vis absorption spectra of thermal equilibrium, *trans*-isomer and *cis*-isomer. The *cis*-isomer was accessed via continuous irradiation with 420 nm, while the *trans*-isomer was obtained thermally under dark conditions. B) Cycle performance when alternating between irradiation with 420 nm and dark conditions. Data points were recorded at the absorbance maximum of the *trans*-isomer (408 nm). C) Thermal half-life of compound **2c**, with each spectrum measured every 0.5 seconds.

Covalent and Photochromic Derivatives of the Potent Synthetic Opioid Isotonitazene and Other Nitazenes

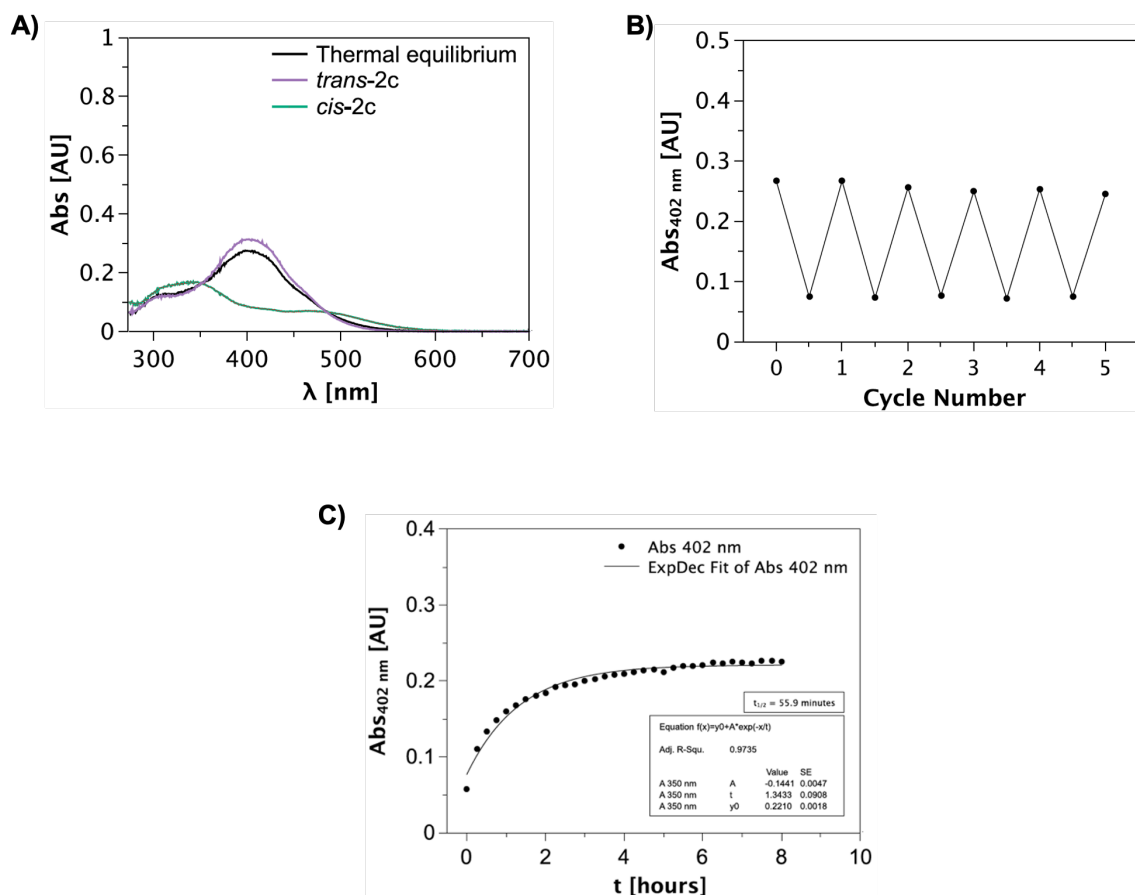


Figure 49. Photophysical properties of compound **2c** (10 μ M) in DMSO at 25 $^{\circ}$ C. A) UV/Vis absorption spectra of thermal equilibrium, *trans*-isomer and *cis*-isomer. The *cis*-isomer was accessed via irradiation with 420 nm, while the *trans*-isomer was obtained with 625 nm irradiation. B) Cycle performance upon alternating irradiation of 420 nm and 625 nm. Data points were recorded at the absorbance maximum of the *trans*-isomer (402 nm). C) Thermal half-life of compound **2c**.

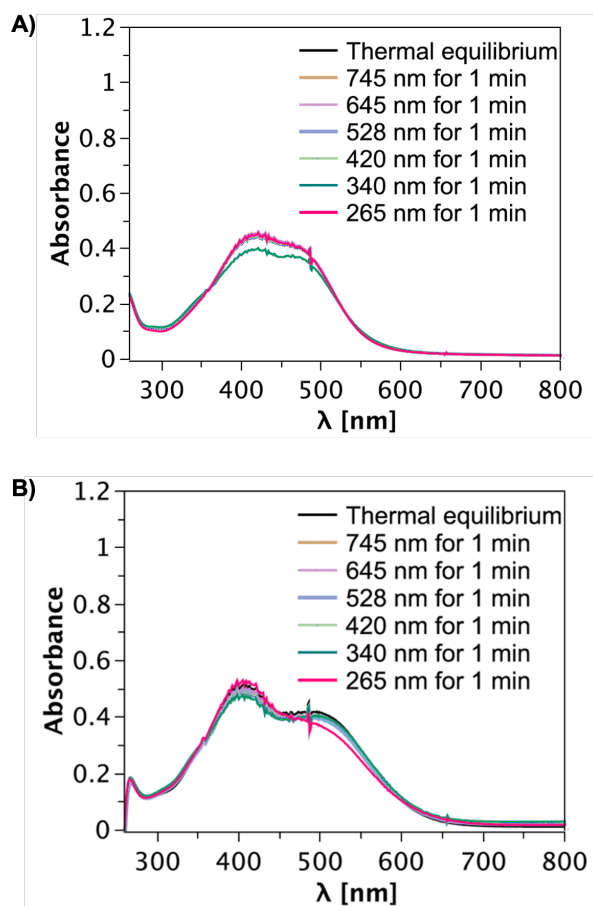


Figure 50. Online UV/Vis absorption spectra of compound **2d** (20 μM) upon light exposure with various wavelengths in A) TrisHCl Buffer (pH 7.5) + 0.2% DMSO, and B) in DMSO. Irradiation with wavelengths of 745, 645, 528, 420, 340 and 265 nm did not significantly change absorbance, when compared to thermal equilibrium. These results suggest that compound **2d** does not possess photoswitchable properties that are comparable to the other photoswitchable compounds in this series.

Covalent and Photochromic Derivatives of the Potent Synthetic Opioid Isotonitazene and Other Nitazenes

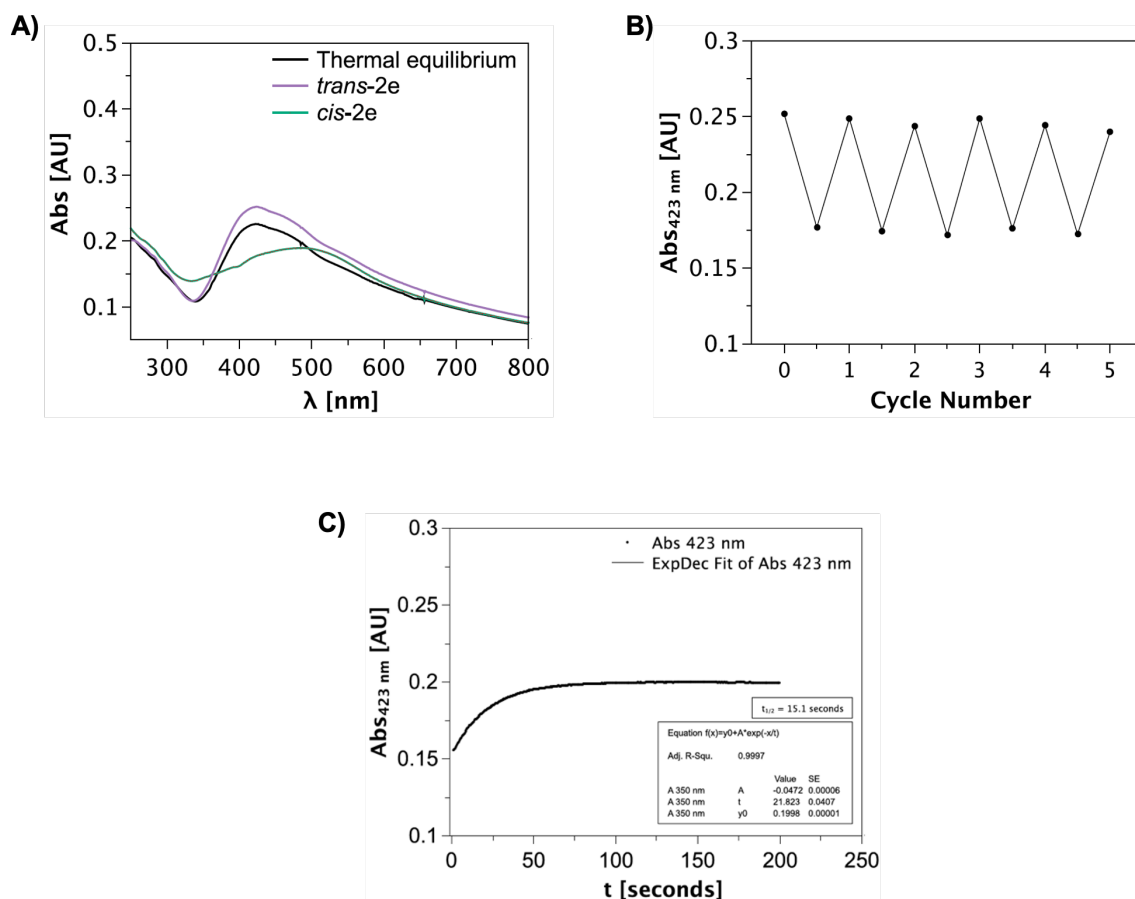


Figure 51. Photophysical properties of compound **2e** (20 μ M) in buffer solution (TrisHCl Buffer, pH 7.5) + 0.2% DMSO at 25 $^{\circ}$ C. A) Online UV/Vis absorption spectra of thermal equilibrium, *trans*-isomer and *cis*-isomer. The *cis*-isomer was accessed via continuous irradiation with 420 nm, while the *trans*-isomer was obtained thermally under dark conditions. B) Cycle performance when alternating between irradiation with 420 nm and dark conditions. Data points were recorded at the absorbance maximum of the *trans*-isomer (423 nm). C) Thermal half-life of compound **2e**, with each spectrum measured every 0.5 seconds.

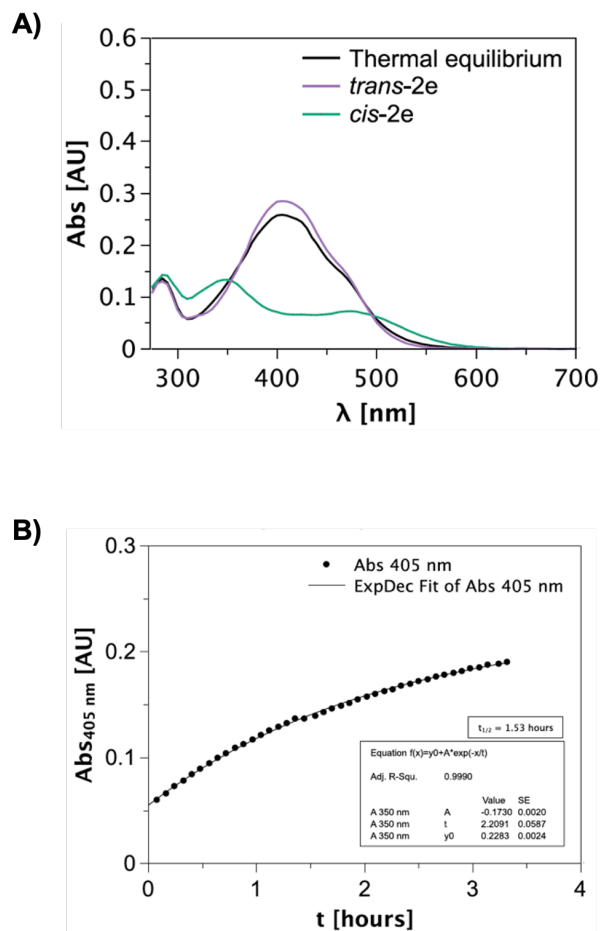


Figure 52. Photophysical properties of compound **2e** (20 μM) in DMSO at 25 °C. A) UV/Vis absorption spectra of thermal equilibrium, *trans*-isomer and *cis*-isomer. The *cis*-isomer was accessed via irradiation with 420 nm, while the *trans*-isomer was obtained with 625 nm irradiation. B) Thermal half-life of compound **2e**.

Covalent and Photochromic Derivatives of the Potent Synthetic Opioid Isotonitazene and Other Nitazenes

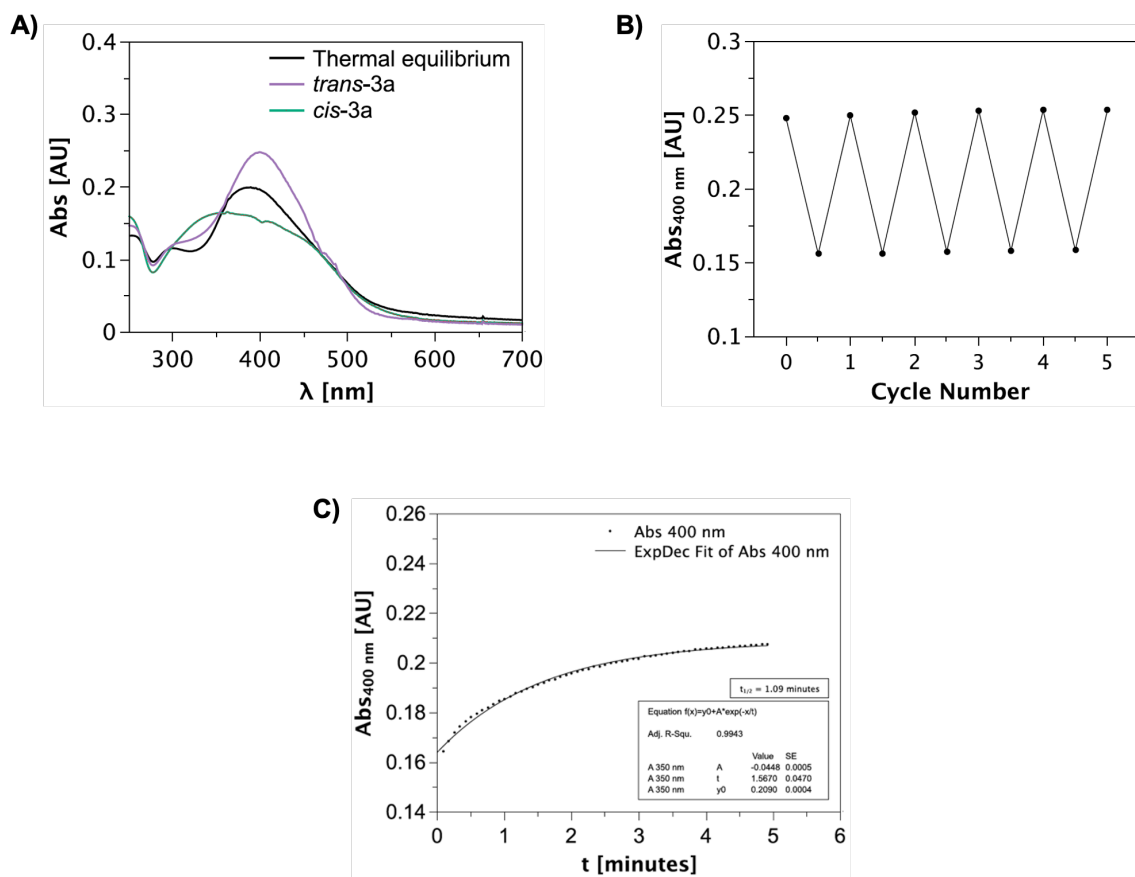


Figure 53. Photophysical properties of compound **3a** (20 μ M) in buffer solution (TrisHCl Buffer, pH 7.5) + 1% DMSO at 25 $^{\circ}$ C. A) Online UV/Vis absorption spectra of thermal equilibrium, *trans*-isomer and *cis*-isomer. The *cis*-isomer was accessed via continuous irradiation with 420 nm, while the *trans*-isomer was obtained thermally under dark conditions. B) Cycle performance when alternating between irradiation with 420 nm and dark conditions. Data points were recorded at the absorbance maximum of the *trans*-isomer (400 nm). C) Thermal half-life of compound **3a**, with each spectrum measured every 5 seconds.

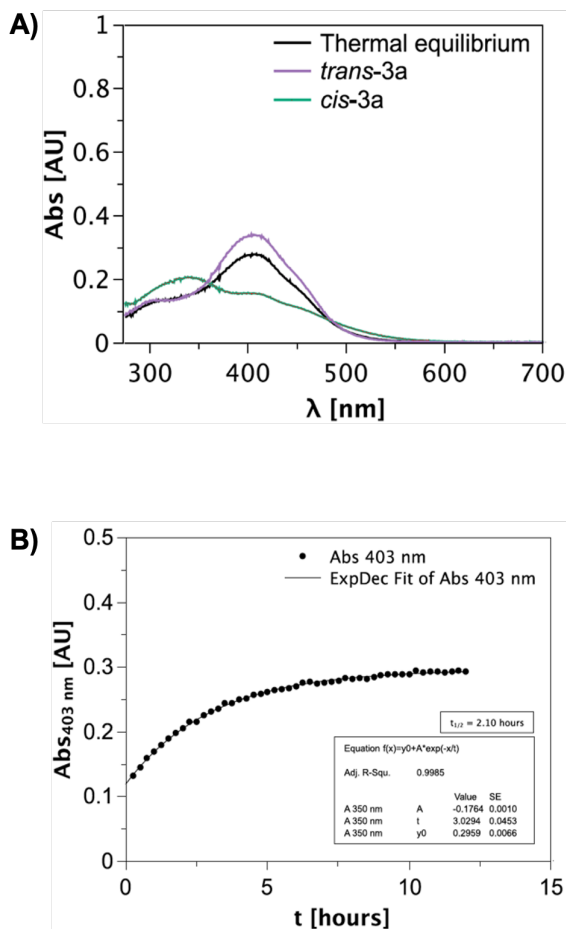


Figure 54. Photophysical properties of compound **3a** (20 μ M) in DMSO at 25 °C. A) UV/Vis absorption spectra of thermal equilibrium, *trans*-isomer and *cis*-isomer. The *cis*-isomer was accessed via irradiation with 420 nm, while the *trans*-isomer was obtained with 625 nm irradiation. B) Thermal half-life of compound **3a**, measured every 25 minutes.

Covalent and Photochromic Derivatives of the Potent Synthetic Opioid Isotonitazene and Other Nitazenes

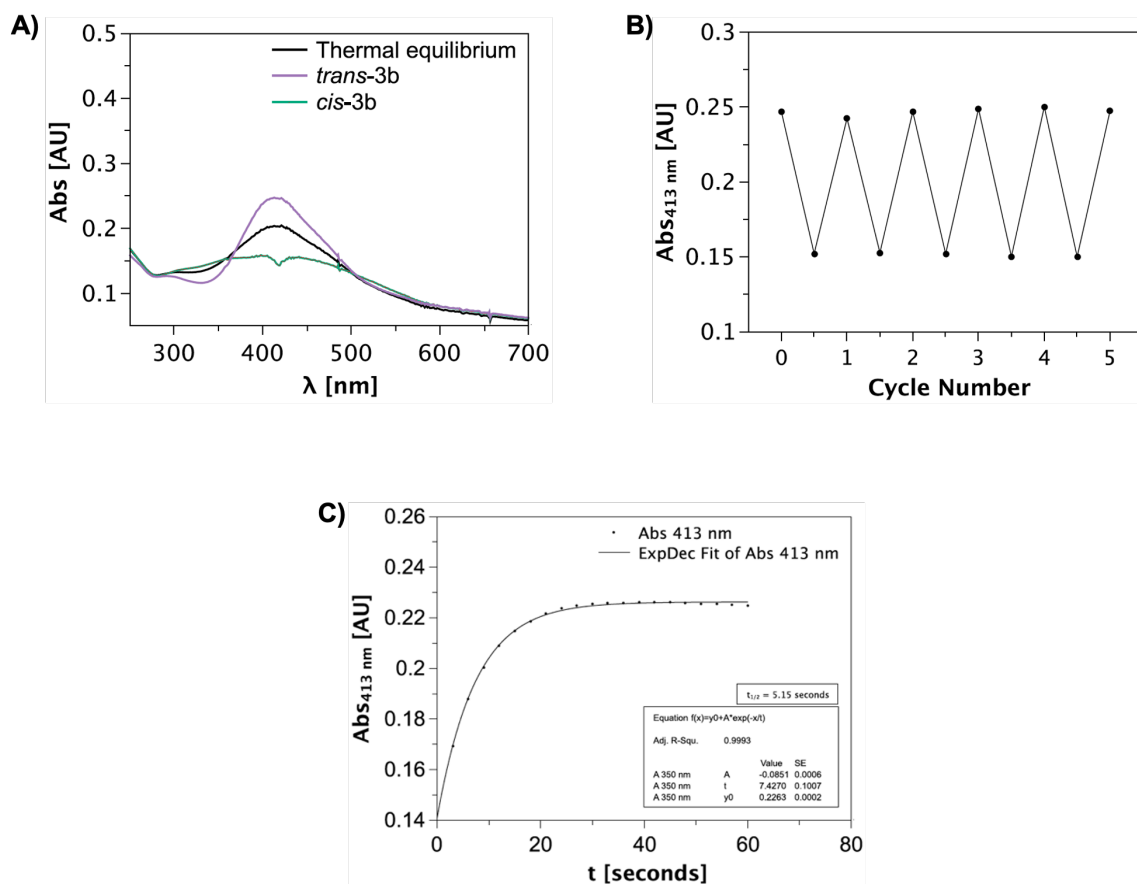


Figure 55. Photophysical properties of compound **3b** (20 μ M) in buffer solution (TrisHCl Buffer, pH 7.5) + 0.2% DMSO at 25 $^{\circ}$ C. A) Online UV/Vis absorption spectra of thermal equilibrium, *trans*-isomer and *cis*-isomer. The *cis*-isomer was accessed via continuous irradiation with 420 nm, while the *trans*-isomer was obtained thermally under dark conditions. B) Cycle performance when alternating between irradiation with 420 nm and dark conditions. Data points were recorded at the absorbance maximum of the *trans*-isomer (413 nm). C) Thermal half-life of compound **3b**, with each spectrum measured every 3 seconds.

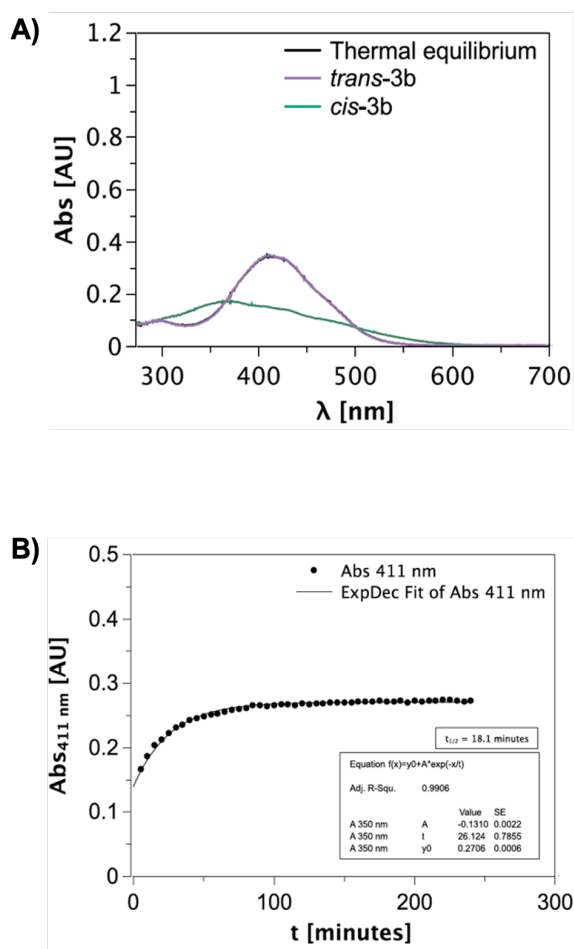


Figure 56. Photophysical properties of compound **3b** (20 μ M) in DMSO at 25 $^{\circ}$ C. A) UV/Vis absorption spectra of thermal equilibrium, *trans*-isomer and *cis*-isomer. The *cis*-isomer was accessed via irradiation with 420 nm, while the *trans*-isomer was obtained with 625 nm irradiation. B) Thermal half-life of compound **3b**, measured every 5 minutes.

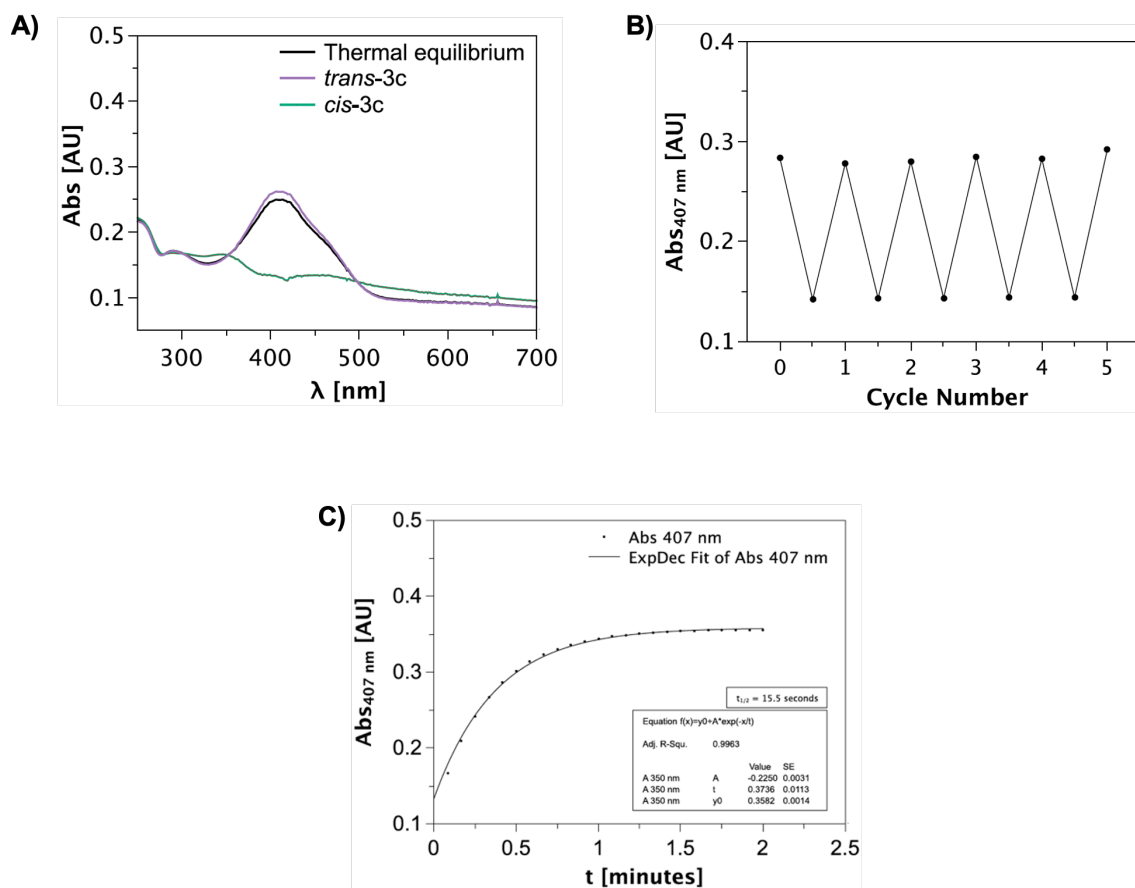


Figure 57. Photophysical properties of compound **3c** (20 μ M) in buffer solution (TrisHCl Buffer, pH 7.5) + 0.2% DMSO at 25 $^{\circ}$ C. A) Online UV/Vis absorption spectra of thermal equilibrium, *trans*-isomer and *cis*-isomer. The *cis*-isomer was accessed via continuous irradiation with 420 nm, while the *trans*-isomer was obtained thermally under dark conditions. B) Cycle performance when alternating between irradiation with 420 nm and dark conditions. Data points were recorded at the absorbance maximum of the *trans*-isomer (407 nm). C) Thermal half-life of compound **3c**, with each spectrum measured every 5 seconds.

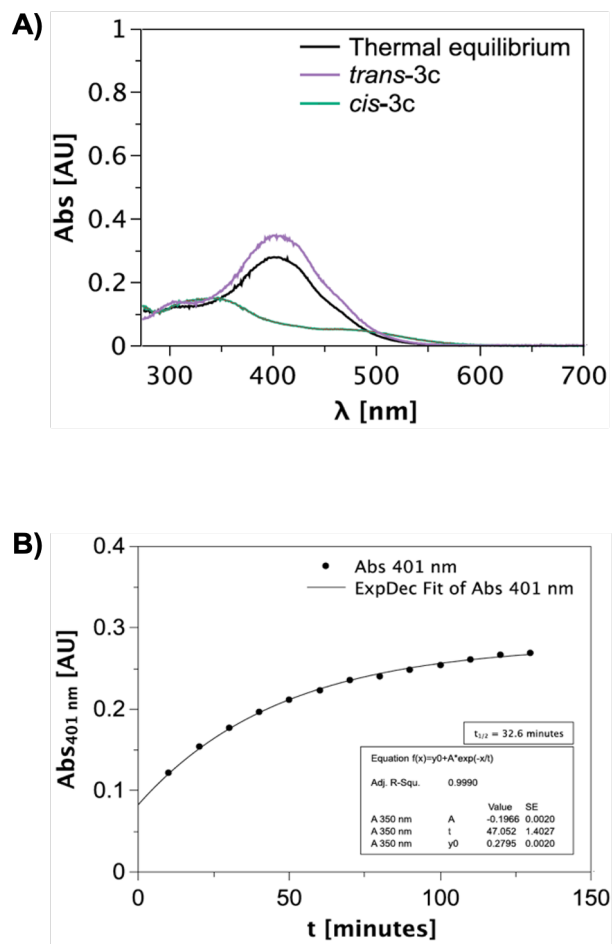


Figure 58. Photophysical properties of compound **3c** (20 μ M) in DMSO at 25 °C. A) UV/Vis absorption spectra of thermal equilibrium, *trans*-isomer and *cis*-isomer. The *cis*-isomer was accessed via irradiation with 420 nm, while the *trans*-isomer was obtained with 625 nm irradiation. B) Thermal half-life of compound **3c**, measured every 10 minutes.

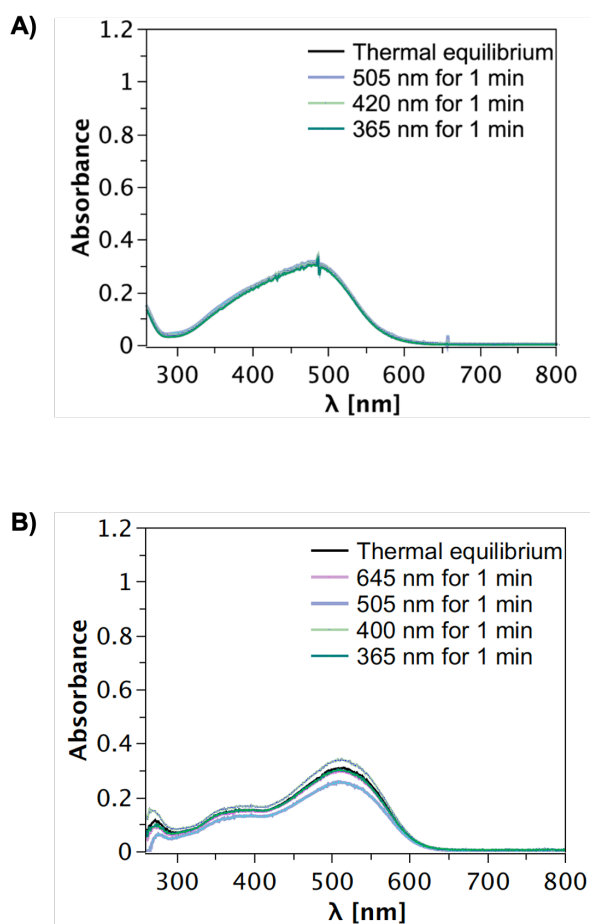


Figure 59. Online UV/Vis absorption spectra of compound **3b-NH₂** (20 μM) upon continuous light exposure with various wavelengths in A) TrisHCl Buffer (pH 7.5) + 0.2% DMSO, and B) in DMSO. Irradiation with various wavelengths did not significantly change absorbance, when compared to thermal equilibrium. These results suggest that compound **3b-NH₂** does not possess photoswitchable properties that are comparable to the other photoswitchable compounds in this series.

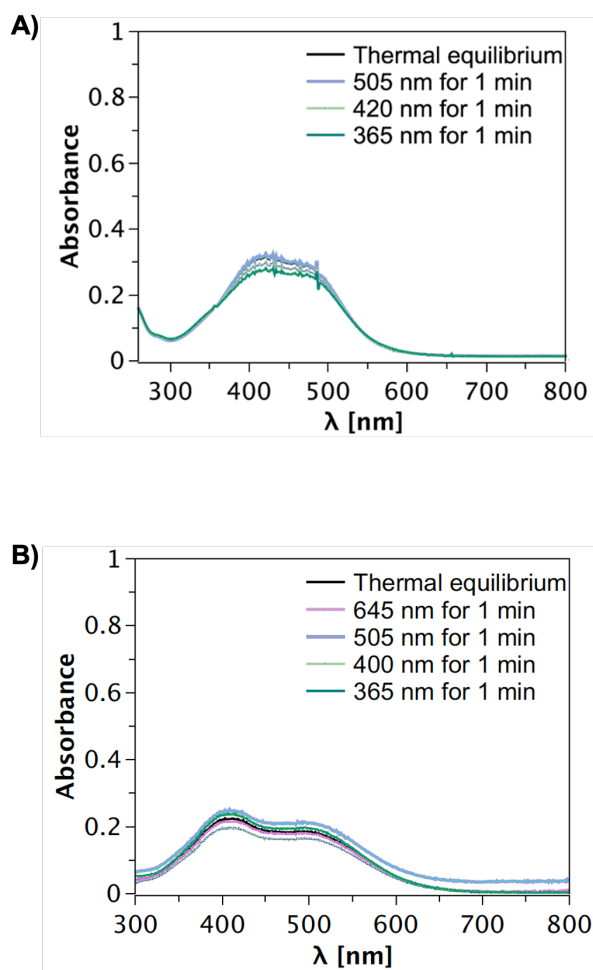


Figure 60. Online UV/Vis absorption spectra of compound **3d** (20 μM) upon continuous light exposure with various wavelengths in A) TrisHCl Buffer (pH 7.5) + 0.2% DMSO, and B) in DMSO. Irradiation with various wavelengths did not significantly change absorbance, when compared to thermal equilibrium. These results suggest that compound **3d** does not possess photoswitchable properties that are comparable to the other photoswitchable compounds in this series.

Covalent and Photochromic Derivatives of the Potent Synthetic Opioid Isotonitazene and Other Nitazenes

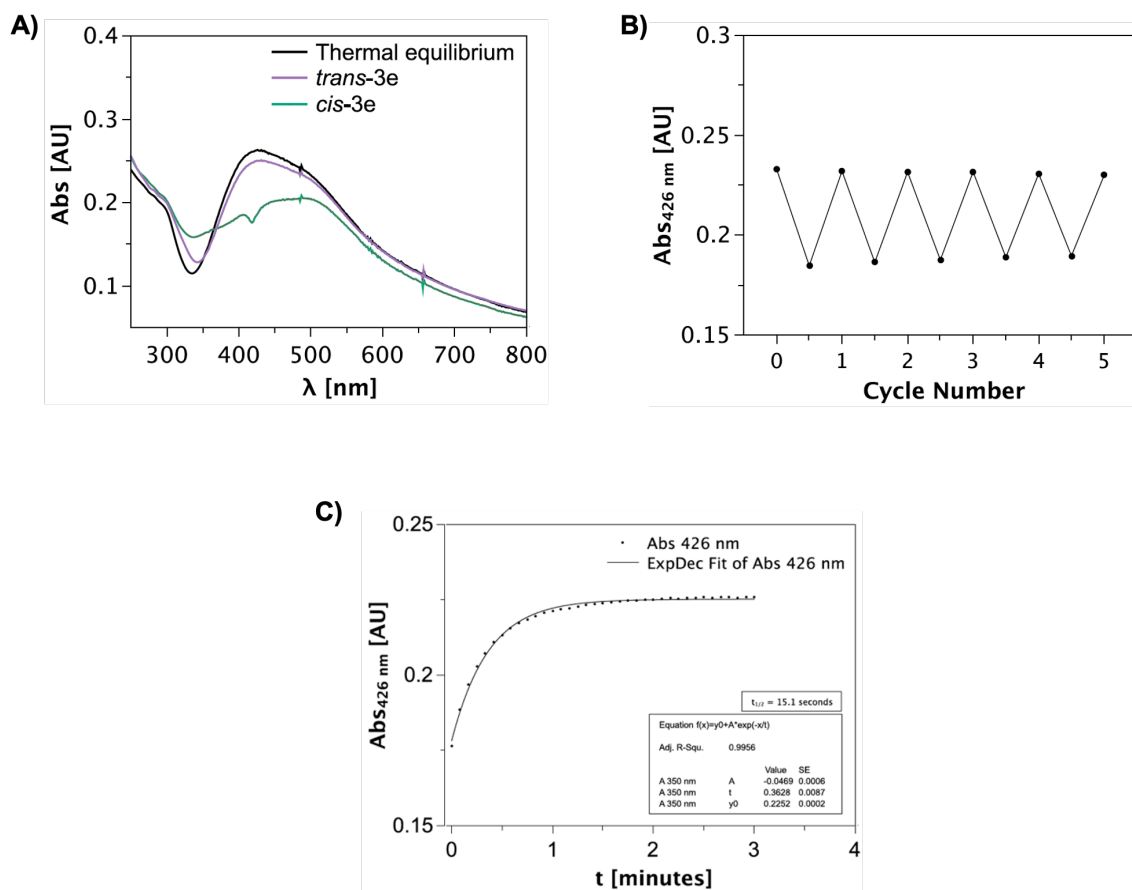


Figure 61. Photophysical properties of compound **3e** (20 μ M) in buffer solution (TrisHCl Buffer, pH 7.5) + 0.2% DMSO at 25 $^{\circ}$ C. A) Online UV/Vis absorption spectra of thermal equilibrium, *trans*-isomer and *cis*-isomer. The *cis*-isomer was accessed via continuous irradiation with 420 nm, while the *trans*-isomer was obtained thermally under dark conditions. B) Cycle performance when alternating between irradiation with 420 nm and dark conditions. Data points were recorded at the absorbance maximum of the *trans*-isomer (426 nm). C) Thermal half-life of compound **3e**, with each spectrum measured every 5 seconds.

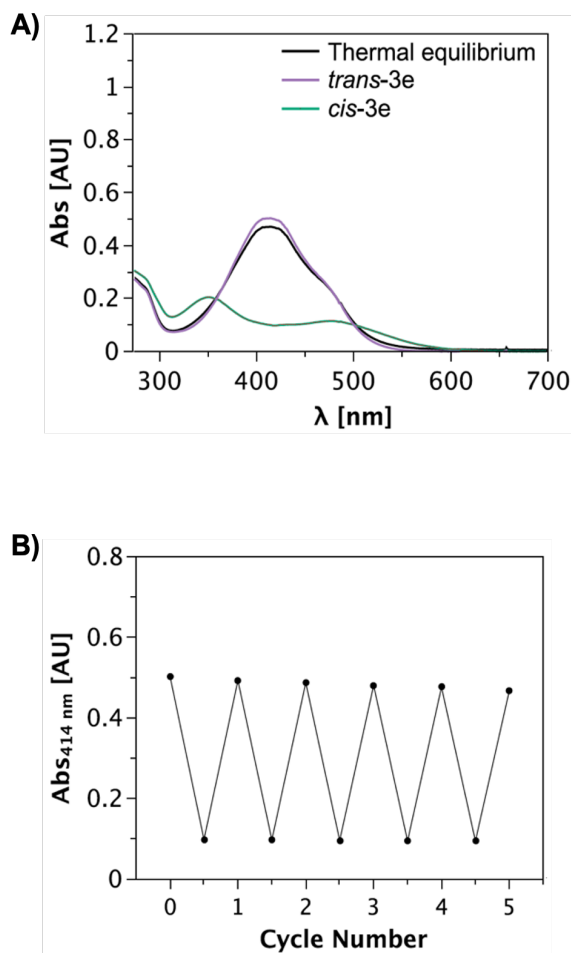


Figure 62. Photophysical properties of compound **3e** (20 μM) in DMSO at 25 °C. A) UV/Vis absorption spectra of thermal equilibrium, *trans*-isomer and *cis*-isomer. The *cis*-isomer was accessed via irradiation with 420 nm, while the *trans*-isomer was obtained with 625 nm irradiation. B) Cycle performance upon alternating irradiation of 420 nm and 625 nm. Data points were recorded at the absorbance maximum of the *trans*-isomer (414 nm).

Covalent and Photochromic Derivatives of the Potent Synthetic Opioid Isotonitazene and Other Nitazenes

3.7.2.3 Supplementary Figures and Tables

Table 12. Summary of experimental photophysical properties in DMSO.^[a]

Compound (DMSO)	PSS ^[b]	PSS ^[b]	t _{1/2}
	Thermal equilibrium <i>trans:cis</i>	<i>trans</i> → <i>cis</i> <i>trans:cis</i>	<i>cis</i> -isomer
2a	92:8	32:68	3.2 h
2b	94:6	32:68	1.6 h
2c	87:13	25:75	55.9 min
2e	91:9	23:77	1.5 h
3a	81:19	45:55	2.1 h
3b	98:2	42:58	18.1 min
3c	80:20	19:81	32.6 min
3e	94:6	19:81	-

^[a]Isomerization was obtained by irradiation of 420 nm (for *cis*-isomer) or 625 nm (for *trans*-isomer) at 25 °C. ^[b]PSS was estimated from UV/Vis spectroscopy measurements.

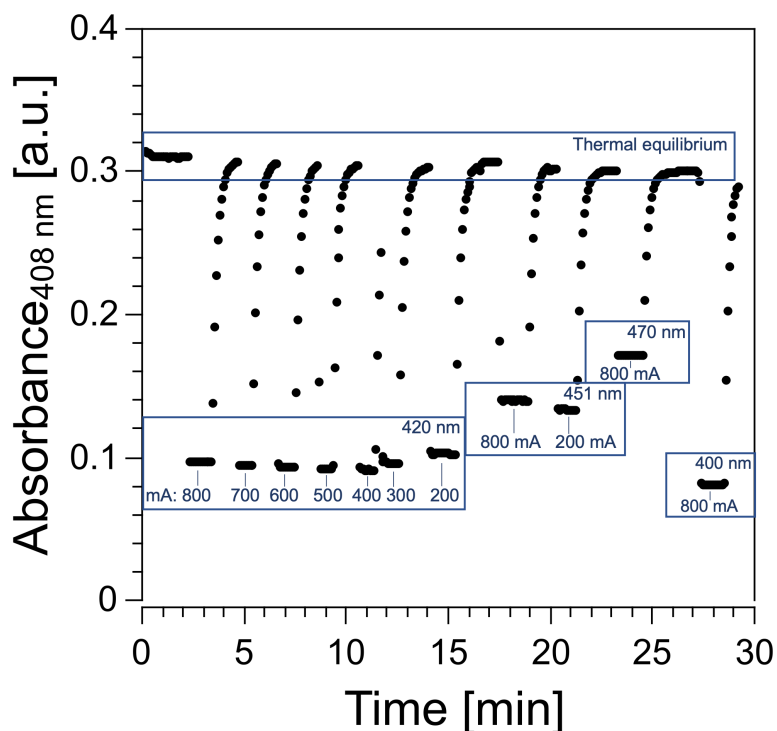


Figure 63. Time-resolved UV/Vis absorption spectroscopy measurements to determine optimal isomerization wavelengths and electric currents. It can be observed that the *cis*-isomer could be best obtained using the 420 nm LED with currents 300-800 mA, as well as the 400 nm LED with a current of 800 mA (bottom blue boxes). Isomerization to the *cis*-isomer was slightly reduced when using the 420 nm LED with a current of 200 mA. The use of the longer wavelengths 451 nm and 470 nm further reduced *cis*-isomerization. Data points were monitored at the absorbance maximum of the *trans*-isomer (408 nm), with each individual spectrum measured every 5 seconds. Compound **2c** (20 μ M) is shown here as a representative for compounds with similar substitution patterns.

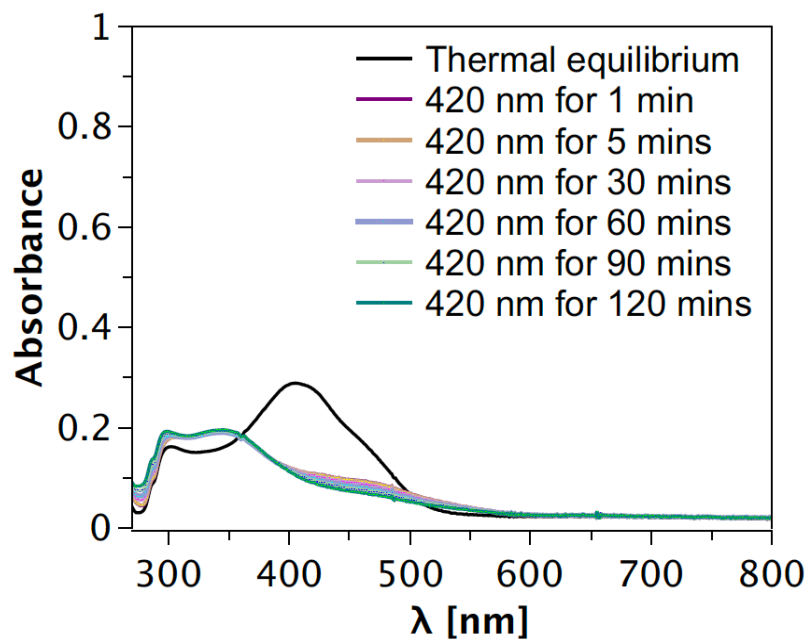


Figure 64. Online UV/Vis absorption spectroscopy to determine the effects of continuous irradiation on compound composition. Compound **3c** (20 μM) was continuously irradiated for a duration of 120 minutes. It can be observed that the *cis*-isomer was maintained for the entire irradiation duration of 120 minutes.

3.7.3 Supplementary Biochemical Information

3.7.3.1 Materials and Methods

Radioligand Binding

Receptor binding affinities of the test compounds to the human opioid receptor μ OR were determined as described previously.^[3] In brief, membranes were prepared from HEK293T cells transiently transfected with the cDNA for μ OR (gift from the Ernest Gallo Clinic and Research Center, UCSF, CA) and incubated with the radioligand [³H]diprenorphine (specific activity 31 Ci/mmol; PerkinElmer, Rodgau, Germany) at 0.2 nM. Membranes expressing μ OR with a receptor density of $B_{\max} = 2000 \pm 420$ fmol/mg protein and a $K_D = 0.11 \pm 0.02$ nM were incubated at an amount of protein of 3 to 8 μ g/well with radioligand and varying concentrations of test compound (in the range of 10 pM - 100 μ M) for 60 min in binding buffer (50 mM Tris, pH 7.4) and filtered on glass fiber mats soaked with a 0.3% aqueous polyethyleneimine solution. Trapped radioactivity was determined with a microplate reader (Microbeta Trilux, Perkin Elmer) by scintillation counting. Unspecific binding was determined in the presence of 10 μ M of naloxone. Protein concentration was measured employing the method of Lowry, with bovine serum albumin as the standard.^[4] The resulting competition curves were analyzed by nonlinear regression, using the algorithms in PRISM 9.0 (GraphPad Software, San Diego, USA). Data were initially fit using a sigmoid model to provide IC_{50} values, which were subsequently transformed to K_i values according to the equation of Cheng and Prusoff.^[5] Mean K_i values were calculated from 2-11 individual experiments, each performed in triplicate.

Radioligand Depletion Assay for Determining Covalent Binding

Tests to investigate the covalent binding of the isothiocyanate compounds to the wild-type μ OR receptor were carried out as previously described.^[6] Briefly, membranes from HEK293T cells that were transiently transfected with the human μ OR receptor were preincubated with 1 μ M (for Iso-BIT), 2 μ M (BIT), or 20 μ M (**2e** and **3e**) for 5, 15, 30, and 60 min, whereby, each concentration represented about 35- to 50-fold K_i . Incubation was stopped by centrifugation. Reversibly bound ligand was washed out three times by the procedure of resuspending the membranes in buffer for 30 min and subsequent centrifugation. Finally, the membranes were used in radioligand binding experiments with [³H]diprenorphine to determine the remaining specific binding, according to the protocol

Covalent and Photochromic Derivatives of the Potent Synthetic Opioid Isotonitazene and Other Nitazenes

described above. As a control, 0.05 μM of the reversibly acting analogue isotonitazene (50-fold K_i) was evaluated under the same conditions. Data analysis was performed by normalization of the raw data into specific binding (unspecific binding = 0%; binding in presence of buffer = 100%). The amount of covalent binding was calculated by the equation [covalent binding [%] = 100 – specific binding [%]]. Kinetics of covalent binding was analyzed by nonlinear regression, using the equation for one phase exponential decay in PRISM 9.0 and is expressed by the rate constant K and the half-life for covalent binding $t_{1/2}$. Mean values were derived from 3 individual experiments, each performed in quadruplicate.

Bioluminescence resonance energy transfer

G protein activation by the human μOR was monitored with $G\alpha_{i1}$ -RLucII together with $G\beta_1$ and $G\gamma_2$ -GFP₁₀.^[7] In brief, HEK293T cells were transfected with 200 ng receptor plasmid for G protein activation (receptor: $G\alpha$: $G\beta$: $G\gamma$ ratio 2:0.5:1:4) using linear polyethyleneimine (PEI, Polysciences, 3:1 PEI:DNA ratio). The DNA was complemented to a total amount of 1 μg DNA per $3 \cdot 10^5$ cells with ssDNA (Sigma Aldrich) and 10,000 cells per well were transferred into 96-well half-area plates (Greiner, Frickenhausen, Germany). After a 48 h transfection, the cell medium was exchanged with PBS (phosphate buffered saline) and cells were stimulated with ligands at 37°C for 15 min. For measuring the *cis*-isomers of the photoswitchable ligands, cells were permanently irradiated at 420 nm during the incubation. Coelenterazine 400a (abcr GmbH, Karlsruhe, Germany) at a final concentration of 2.5 μM was added 5 min before measurement. BRET was monitored on a CLARIOstar plate reader (BMG, Ortenberg, Germany) with the appropriate filter sets (donor 410/80 nm, acceptor 515/30 nm) and was calculated as the ratio of acceptor emission to donor emission. BRET ratio was normalized to the effect of buffer (0%) and the maximum effect of fentanyl (100%). For each compound 3 to 7 individual experiments were performed, with each performed in triplicate.

IP Accumulation Assay for Receptor Activation

To validate the functional data of receptor mediated G-protein signaling and to overcome experimental conditions that may disturb BRET signaling, an IP accumulation assay was performed (IP-One HTRF[®], PerkinElmer, Rodgau, Germany) as previously described.^[3c, 8] In brief, HEK293T cells were co-transfected with the cDNA for μOR and the

Covalent and Photochromic Derivatives of the Potent Synthetic Opioid Isotonitazene and Other Nitazenes

hybrid G-protein $G\alpha_{q5HA}$, which is a $G\alpha_q$ -protein with the last five amino acids at the C-terminus replaced by the corresponding sequence of $G\alpha_i$ (gift from The J. David Gladstone Institutes, San Francisco, CA), and transferred into 384-well microplates. Cells were incubated with test compound for 90 min and accumulation of second messenger was stopped by adding detection reagents (IP1-d2 conjugate and Anti-IP1cryptate TB conjugate). TR-FRET was monitored with a Clariostar plate reader. FRET emission was measured at 620 nm and 665 nm, and the corresponding ratio (emission at 665 nm/emission at 620 nm) was calculated and normalized to the vehicle (0%) and the maximum effect of the reference fentanyl (100%). For measuring the *cis*-isomers of the photoswitchable ligands, cells were incubated for 90 min under continuous irradiation with 420 nm. Data were analyzed by applying the algorithms of four parameter non-linear regression, implemented in Prism 9.0 to get dose-response curves, EC_{50} and E_{max} values. Individual experiments were performed 3-5 times, each in triplicate, to derive mean EC_{50} and E_{max} values.

Covalent and Photochromic Derivatives of the Potent Synthetic Opioid Isotonitazene and Other Nitazenes

3.7.3.2 Supplementary Figures and Tables

Table 13. Kinetics of the covalent blocking of the wild-type opioid receptor μ OR by the isothiocyanate derivatives BIT, Iso-BIT, and their photoswitchable analogues **2e** and **3e** in comparison to the reversible acting reference isotonitazene.^{[a][b]}

Compound	Maximum specific binding [% \pm S.E.M.] ^[c]	Maximum covalent binding [% \pm S.E.M.] ^[d]	Rate constant of covalent binding <i>K</i> [min ⁻¹ \pm S.E.M.]	Half-life of covalent binding [min \pm S.E.M.]
BIT (2 μ M)	46 \pm 5	53 \pm 8	0.046 \pm 0.010	17.0 \pm 5.0
Iso-BIT (1 μ M)	42 \pm 4	58 \pm 4	0.041 \pm 0.001	17.0 \pm 0.6
2e (20 μ M)	4 \pm 1	96 \pm 1	0.496 \pm 0.223	3.0 \pm 1.5
3e (20 μ M)	6 \pm 1	94 \pm 1	0.384 \pm 0.221	4.0 \pm 2.1
Isotonitazene (0.05 μ M)	~100	~ 0	---	---

^[a]Kinetic data were determined in a radioligand depletion assay with HEK293T cells transiently co-transfected with the cDNA of the wild-type μ OR. ^[b]Compounds were evaluated at concentrations that correspond to 30- to 50-fold K_i in three independent experiments, each performed in quadruplicate. ^[c]Maximum specific binding after incubation with the ligand relative to specific binding measured with buffer in [% \pm S.E.M.]. ^[d]Maximum covalent binding derived from maximum specific binding by applying the equation [*covalent binding* = 100 – *specific binding*] in [% \pm S.E.M.].

3.7.4 Supplementary Information for 96-Well Plate LED Device

A new 96-well plate LED set-up was designed to allow for continuous irradiation of compounds during cell-based assays. In this set-up, LEDs are fixed onto a specially designed lid that can be placed directly onto a non-transparent 96-well plate. This lid consists of 3 slots (Figure 65), which are separated by a barrier to prevent radiation leakage, which is especially important when LED boards that contain different irradiation wavelengths are employed. In these slots, boards of 3x8 LEDs (total of 24 LEDs) of a specific wavelength can be placed. The LEDs on these boards are positioned with precise measurements and dimensions so that each respective LED covers one individual well. The LED boards are connected to the respective output stages, power amplifiers, controller (with LC display) and power supply with a ribbon cable. The use of a ribbon cable allows the LED-containing lid to be extended into biochemical incubators, with the remaining equipment placed outside of the incubator. As a result, the LED-containing lid can be directly placed on top of the 96-well plate during incubation at 37 °C, with considerations of LED moisture resistance and LED temperature control. Due to the different electrical parameter requirements of LEDs with different wavelengths, each LED board is connected to individual and exchangeable output stages/amplifiers. This allows for modulation of electrical parameters, which can be useful in optimizing irradiation parameters in photophysical and biochemical experiments. The ability to interchange LED boards of various wavelengths and to modulate electrical parameters was found to be useful in investigating device compatibility with respective photophysical and biochemical experiments.



Figure 65. A photo of the 96-well plate LED lid, featuring exchangeable LED boards of a specific wavelength that allow for irradiation of 72 individual wells in a 96-well plate.

3.7.5 Supplementary Crystallographic Information

Compound **3b**

Crystallographic Experimental:

Single orange needle-shaped crystals of **3b** were used as supplied. A suitable crystal with dimensions $0.17 \times 0.02 \times 0.01 \text{ mm}^3$ was selected and mounted on a MITIGEN holder with inert oil on a XtaLAB Synergy R, DW system, HyPix-Arc 150 diffractometer. The crystal was kept at a steady $T = 123.00(10) \text{ K}$ during data collection. The structure was solved with the **ShelXT** 2018/2^[9] solution program using dual methods and by using **Olex2** 1.3-alpha^[10] as the graphical interface. The model was refined with **ShelXL** 2018/3^[11] using full matrix least squares minimisation on F^2 .

Crystal Data:

$\text{C}_{24}\text{H}_{29}\text{F}_3\text{N}_6\text{O}_5$, $M_r = 538.53$, orthorhombic, $Pna2_1$ (No. 33), $a = 20.4731(4) \text{ \AA}$, $b = 18.4549(4) \text{ \AA}$, $c = 6.78950(10) \text{ \AA}$, $\alpha = \beta = \gamma = 90^\circ$, $V = 2565.27(8) \text{ \AA}^3$, $T = 123.00(10) \text{ K}$, $Z = 4$, $Z' = 1$, $\mu(\text{Cu K}\alpha) = 0.971$, 20892 reflections measured, 4712 unique ($R_{\text{int}} = 0.0399$) which were used in all calculations. The final wR_2 was 0.1174 (all data) and R_1 was 0.0405 ($I \geq 2 \sigma(I)$).

CCDC: 2236462

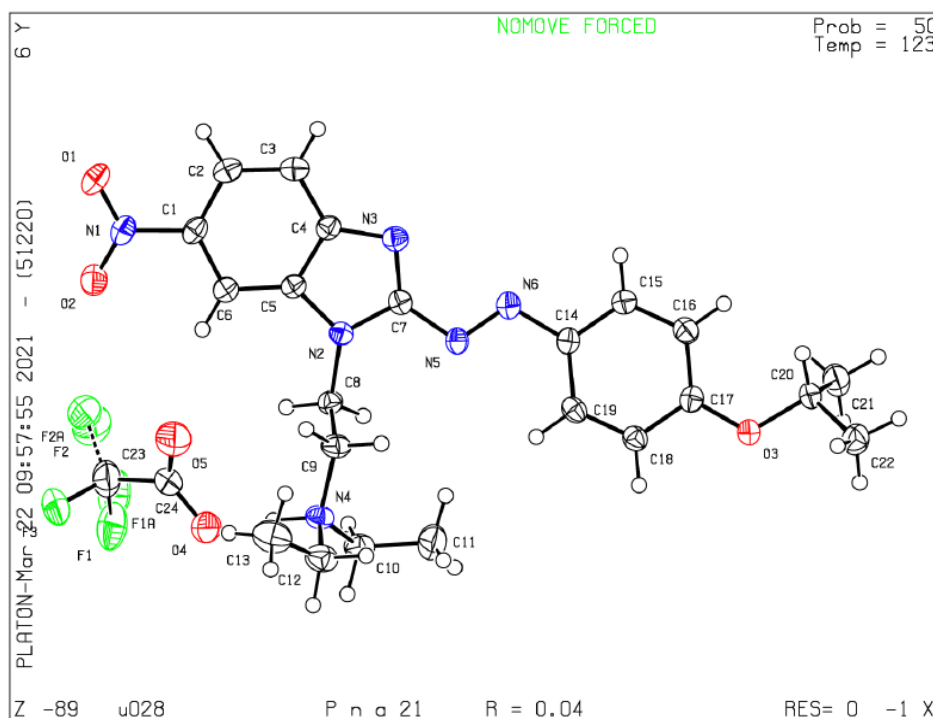


Figure 66. Crystal structure of **3b** as TFA salt, with ellipsoids shown at 50% probability level.

Covalent and Photochromic Derivatives of the Potent Synthetic Opioid Isotonitazene
and Other Nitazenes

Further Data for CCDC 2236462:

Compound	2236462
Formula	C ₂₄ H ₂₉ F ₃ N ₆ O ₅
<i>D</i> _{calc.} / g cm ⁻³	1.394
<i>μ</i> /mm ⁻¹	0.971
Formula Weight	538.53
Colour	orange
Shape	needle-shaped
Size/mm ³	0.17×0.02×0.01
<i>T</i> /K	123.00(10)
Crystal System	orthorhombic
Flack Parameter	0.6(2)
Hooft Parameter	0.59(8)
Space Group	<i>Pna</i> 2 ₁
<i>a</i> /Å	20.4731(4)
<i>b</i> /Å	18.4549(4)
<i>c</i> /Å	6.78950(10)
<i>α</i> /°	90
<i>β</i> /°	90
<i>γ</i> /°	90
<i>V</i> /Å ³	2565.27(8)
<i>Z</i>	4
<i>Z</i> '	1
Wavelength/Å	1.54184
Radiation type	Cu K _α
<i>θ</i> _{min} /°	3.224
<i>θ</i> _{max} /°	73.467
Measured Refl's.	20892
Indep't Refl's	4712
Refl's I ≥ 2 <i>σ</i> (I)	4139
<i>R</i> _{int}	0.0399
Parameters	371
Restraints	19
Largest Peak	0.218
Deepest Hole	-0.234
Goof	1.062
<i>wR</i> ₂ (all data)	0.1174
<i>wR</i> ₂	0.1118
<i>R</i> ₁ (all data)	0.0473
<i>R</i> ₁	0.0405

Compound **3c**

Crystallographic Experimental:

Single clear orange plate crystals of **3c** were used as supplied. A suitable crystal with dimensions $0.24 \times 0.06 \times 0.02 \text{ mm}^3$ was selected and mounted on a MITIGEN holder oil on a XtaLAB Synergy R, DW system, HyPix-Arc 150 diffractometer. The crystal was kept at a steady $T = 123.00(10) \text{ K}$ during data collection. The structure was solved with the **ShelXT** 2018/2^[9] solution program using dual methods and by using **Olex2** 1.3-alpha^[10] as the graphical interface. The model was refined with **ShelXL** 2018/3^[11] using full matrix least squares minimisation on F^2 .

Crystal Data:

$\text{C}_{24}\text{H}_{29}\text{F}_3\text{N}_6\text{O}_5$, $M_r = 538.53$, monoclinic, $P2_1/n$ (No. 14), $a = 18.8156(3) \text{ \AA}$, $b = 6.69980(10) \text{ \AA}$, $c = 21.3105(3) \text{ \AA}$, $\beta = 106.3210(10)^\circ$, $\alpha = \gamma = 90^\circ$, $V = 2578.16(7) \text{ \AA}^3$, $T = 123.00(10) \text{ K}$, $Z = 4$, $Z' = 1$, $\mu(\text{Cu K}\alpha) = 0.966$, 27341 reflections measured, 5002 unique ($R_{\text{int}} = 0.0298$) which were used in all calculations. The final wR_2 was 0.1255 (all data) and R_1 was 0.0450 ($I \geq 2 \sigma(I)$).

CCDC: 2236450

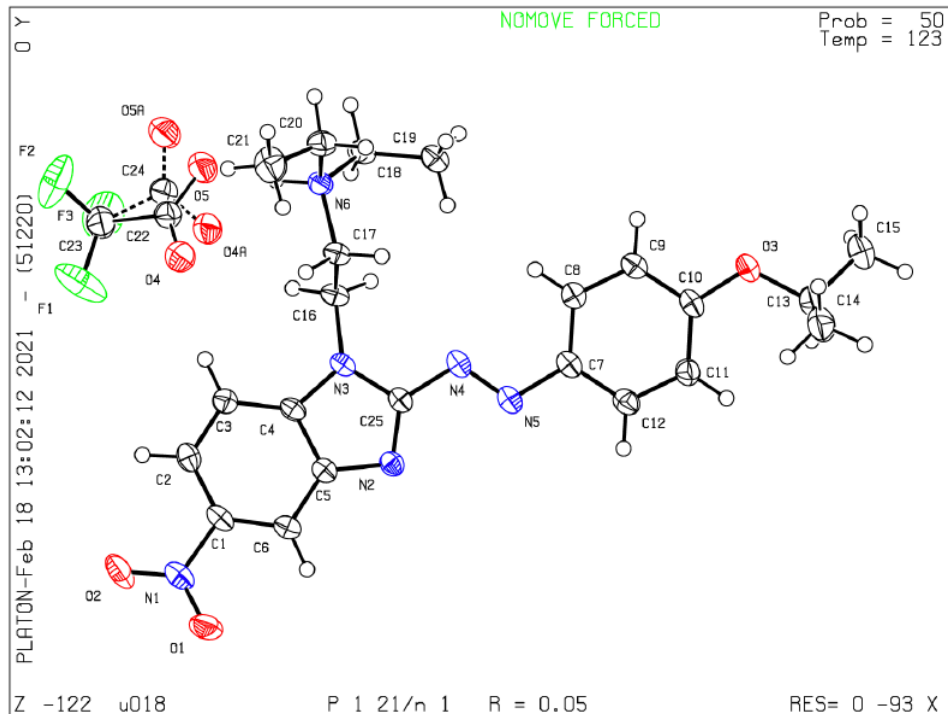


Figure 67. Crystal structure of **3c** as TFA salt, with ellipsoids shown at 50% probability level.

Covalent and Photochromic Derivatives of the Potent Synthetic Opioid Isotonitazene and Other Nitazenes

Further Data for CCDC 2236450:

Compound	2236450
Formula	C ₂₄ H ₂₉ F ₃ N ₆ O ₅
<i>D</i> _{calc.} / g cm ⁻³	1.387
μ /mm ⁻¹	0.966
Formula Weight	538.53
Colour	clear orange
Shape	plate
Size/mm ³	0.24×0.06×0.02
<i>T</i> /K	123.00(10)
Crystal System	monoclinic
Space Group	<i>P</i> 2 ₁ / <i>n</i>
<i>a</i> /Å	18.8156(3)
<i>b</i> /Å	6.69980(10)
<i>c</i> /Å	21.3105(3)
α /°	90
β /°	106.3210(10)
γ /°	90
<i>V</i> /Å ³	2578.16(7)
<i>Z</i>	4
<i>Z</i> '	1
Wavelength/Å	1.54184
Radiation type	Cu K α
θ _{min} /°	2.772
θ _{max} /°	73.196
Measured Refl's.	27341
Indep't Refl's	5002
Refl's I \geq 2 σ (I)	4203
<i>R</i> _{int}	0.0298
Parameters	379
Restraints	24
Largest Peak	0.350
Deepest Hole	-0.349
GooF	1.042
<i>wR</i> ₂ (all data)	0.1255
<i>wR</i> ₂	0.1198
<i>R</i> ₁ (all data)	0.0532
<i>R</i> ₁	0.0450

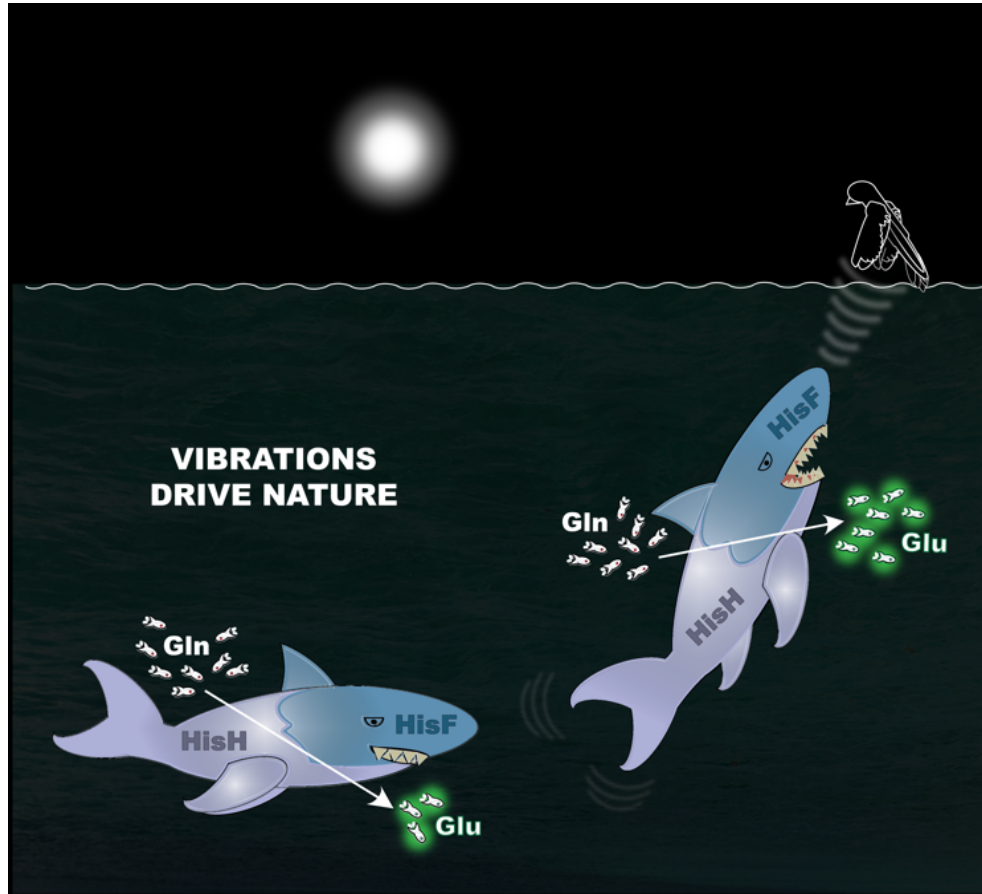
3.7.6 NMR Spectra

All NMR spectra can be found in the appendix (Section 7.4.2).

3.7.7 References

- [1] M. M. Vandeputte, K. Van Uytfanghe, N. K. Layle, D. M. St. Germaine, D. M. Iula, C. P. Stove, *ACS Chem. Neurosci.* **2021**, *12*, 1241-1251.
- [2] a) J. Calbo, C. E. Weston, A. J. P. White, H. S. Rzepa, J. Contreras-García, M. J. Fuchter, *J. Am. Chem. Soc.* **2017**, *139*, 1261-1274; b) A. C. Kneuttinger, C. Rajendran, N. A. Simeth, A. Bruckmann, B. König, R. Sterner, *Biochem.* **2020**, *59*, 2729-2742.
- [3] a) H. Hübner, C. Haubmann, W. Utz, P. Gmeiner, *J. Med. Chem.* **2000**, *43*, 756-762; b) A. Drakopoulos, Z. Koszegi, Y. Lanoiselée, H. Hübner, P. Gmeiner, D. Calebiro, M. Decker, *J. Med. Chem.* **2020**, *63*, 3596-3609; c) R. Lahmy, H. Hübner, M. F. Schmidt, D. Lachmann, P. Gmeiner, B. König, *Chem. Eur. J.* **2022**, *28*, e202201515.
- [4] O. H. Lowry, N. J. Rosebrough, A. L. Farr, R. J. Randall, *J. Biol. Chem.* **1951**, *193*, 265-275.
- [5] Y. C. Cheng, W. H. Prusoff, *Biochem. Pharmacol.* **1973**, *22*, 3099-3108.
- [6] a) D. Weichert, A. C. Kruse, A. Manglik, C. Hiller, C. Zhang, H. Hübner, B. K. Kobilka, P. Gmeiner, *Proc. Natl. Acad. Sci. U. S. A.* **2014**, *111*, 10744-10748; b) R. C. Kling, M. Plomer, C. Lang, A. Banerjee, H. Hübner, P. Gmeiner, *ACS Chem. Biol.* **2016**, *11*, 869-875.
- [7] a) E. A. Fink, J. Xu, H. Hübner, J. M. Braz, P. Seemann, C. Avet, V. Craik, D. Weikert, M. F. Schmidt, C. M. Webb, N. A. Tolmachova, Y. S. Moroz, X. P. Huang, C. Kalyanaraman, S. Gahbauer, G. Chen, Z. Liu, M. P. Jacobson, J. J. Irwin, M. Bouvier, Y. Du, B. K. Shoichet, A. I. Basbaum, P. Gmeiner, *Science* **2022**, *377*, eabn7065; b) J. Quoyer, J. M. Janz, J. Luo, Y. Ren, S. Armando, V. Lukashova, J. L. Benovic, K. E. Carlson, S. W. Hunt, M. Bouvier, *Proc. Natl. Acad. Sci. U. S. A.* **2013**, *110*, E5088-E5097; c) C. Galés, J. J. Van Durm, S. Schaak, S. Pontier, Y. Percherancier, M. Audet, H. Paris, M. Bouvier, *Nat. Struct. Mol. Biol.* **2006**, *13*, 778-786.
- [8] a) H. Liu, J. Hofmann, I. Fish, B. Schaake, K. Eitel, A. Bartuschat, J. Kaindl, H. Rapp, A. Banerjee, H. Hübner, M. J. Clark, S. G. Vincent, J. T. Fisher, M. R. Heinrich, K. Hirata, X. Liu, R. K. Sunahara, B. K. Shoichet, B. K. Kobilka, P. Gmeiner, *Proc. Natl. Acad. Sci. U. S. A.* **2018**, *115*, 12046-12050; b) C. Gentzsch, K. Seier, A. Drakopoulos, M.-L. Jobin, Y. Lanoiselée, Z. Koszegi, D. Maurel, R. Sounier, H. Hübner, P. Gmeiner, S. Granier, D. Calebiro, M. Decker, *Angew. Chem. Int. Ed. Engl.* **2020**, *59*, 5958-5964.
- [9] G. M. Sheldrick, *Acta Crystallogr. A Found. Adv.* **2015**, *71*, 3-8.
- [10] O. V. Dolomanov, L. J. Bourhis, R. J. Gildea, J. A. K. Howard, H. Puschmann, *J. Appl. Crystallogr.* **2009**, *42*, 339-341.
- [11] G. M. Sheldrick, *Acta Crystallogr. C Struct. Chem.* **2015**, *71*, 3-8.

4. Site Selective Insertion of Motions into ImGPS and its Influence on Enzymatic Activity



CHAPTER 4

4.1 Abstract

The importance of dynamic motions in proteins has been previously investigated in order to better understand protein mechanism and function. However, challenges remain that are predominantly due to the difficulty in identifying, characterizing and controlling such movement at an atomic level. Azobenzenes were utilized in this work to aid in these investigations, as their *E/Z* isomerization can be spatiotemporally controlled with light. More specifically, photoisomerizable azobenzenes were investigated as potential energy funnels for transferring motion into the allosteric enzyme imidazole glycerol phosphate synthase (ImGPS) at selected positions. This involved the use of azobenzene phenylalanine (AzoF) that was co-translationally incorporated into the protein sequence of ImGPS at the allosterically-relevant sites hW123 and fS55. Pulsing irradiation with alternating 365/420 nm was used to induce rapid isomerization of AzoF, presumably resulting in rapid motions at these sites. The protein complexes ImGPS(fS55AzoF) and ImGPS(hW123AzoF) were pulsed with alternating 365 nm and 420 nm irradiation at selected frequencies. The triggered motion of AzoF could then be directed towards the ImGPS complex, resulting in a substantial increase in the activity of ImGPS(hW123AzoF), while the catalytic activity of ImGPS(fS55AzoF) remained unaltered. This was a pivotal finding and validated the notion that dynamic processes can be induced site-selectively to alter enzymatic activity. Overall, the results obtained provide insights into the complex regulation of allosteric proteins and how these proteins can be modulated via the insertion of motions with spatiotemporal and remote control.

Major parts of this chapter are in the submission process:

The research in this chapter was performed in collaboration with the group of Prof. Dr. Reinhard Sterner (University of Regensburg) and the group of Dr. Andrea Kneuttinger (University of Regensburg).

R. Lahmy, C. Hiefinger, F. Zeqiri, A. Kneuttinger, R. Sterner, B. König.

Author contributions:

RL was responsible for experiment design, data processing, data analysis and wrote the draft shown here. CH edited the draft, including edits to figures and tables. FZ executed the experiments. RL synthesized AzoF. Proteins were obtained from the group of RS. AK, RS and BK supervised the project and are the corresponding authors.

4.2 Introduction

4.2.1 Dynamic Motions in Enzymes

Enzymes have been well characterized by steady-state kinetics in order to provide insight into their catalytic behavior. In doing so, the mechanism of catalytic activity has been commonly deciphered into single step reactions.^[1] Over the past few decades, a greater understanding into the macromolecular processes that occur prior, during and after these characterized steps has been pursued.^[1] This requires a more comprehensive understanding of the conformational and dynamic changes that occur within enzymes. Allosteric enzymes exemplify the presence of such dynamic processes.^[2] In addition to an active site, these enzymes have binding sites at distant locations. Upon interaction with an allosteric modulator, a conformational and/or dynamic change in the protein has been proposed, which is subsequently propagated throughout the protein scaffold.^[2b] This ultimately results in a particular effect in the enzyme, such as the enhancement of catalytic activity. Global changes in proteins that influence enzyme activity have been investigated and is still currently debated.^[3]

As early as 1967, studies were conducted to induce conformational changes in proteins in order to obtain dynamic control of enzymes.^[1] Such control would provide an alternative means of regulating enzymatic activity. Over the years, the link between dynamic motions and its influence on enzymatic activity has been investigated biochemically and computationally, as well as through quantum mechanical tunneling and various spectroscopic techniques.^[3-4] Importantly, the association between motions on the millisecond-picosecond timescale and their ability to influence rates of enzymatic activity has been explored, with a particular success in characterizing the presence of such dynamic processes on the millisecond timescale in biological systems.^[3-4] Furthermore, the effects of pressure on biological systems have been studied in order to monitor the effects of dynamic motions by promoting vibrations.^[5] Overall, rapid motions seem to play an important role in enzymatic activity, however, the ability to characterize and modulate these dynamic properties non-invasively requires further investigation.^[3-4] As a result, we hypothesized that an approach commonly used in photopharmacology may provide further insight into dynamic regulation of enzymatic activity, and that is, the use of photoswitches.^[6]

4.2.2 Photoswitches as Tools to Create Motion

The value of incorporating photoswitches into the scaffolds of biologically active molecules has been greatly explored in the field of photopharmacology.^[6-7] Azobenzenes represent one of the most explored class of photoswitches.^[8] Upon exposure to light of a certain wavelength, these light-sensitive molecules undergo a reversible change in structure (i.e., isomerization) that may induce significant differences in biological activity.^[9] As a result, spatial and temporal photocontrol of biological activity has been established in several cases.^[10] While azobenzenes and similar derivatives are commonly used to modulate biological systems by quantitatively switching these molecules into either their respective *E* or *Z* isomer states, the work described herein aims to use alternating pulsing irradiation to rapidly toggle between these isomers non-quantitatively. In doing so, the azobenzene molecules would presumably produce rapid motions that could be shuttled site-selectively into a candidate protein. Albeit for different purposes, the concept of using alternating pulsing irradiation to stimulate an azobenzene-containing molecule was recently investigated.^[11] Such irradiation was found to influence out-of-equilibrium enzymatic reactions, using α -chymotrypsin as a model enzyme and a reversible azobenzene-based α -chymotrypsin inhibitor.^[11]

4.2.3 Azobenzene Phenylalanine in ImGPS

In photopharmacology photoswitches are primarily employed as ligands that interact with the target protein post-translation, however, the method of genetic code expansion (GCE) involves the incorporation of photo-responsive elements co-translationally at a distinct site within the protein sequence.^[12] In previous work, azobenzene phenylalanine (AzoF) was co-translationally incorporated into the allosteric bienzyme complex imidazole glycerol phosphate synthase (ImGPS) at the conserved residue positions fS55 and hW123.^[13] While both positions are relevant in crucial conformation changes that regulate enzymatic activity, the former position is localized close to the allosteric sites of loop 1 and the latter is localized to a hinge position at the HisF:HisH (cyclase:glutaminase) subunit interface.^[13] Photocontrol of ImGPS activity at both these sites was achieved via *E/Z* isomerization (420 nm and 365 nm, respectively) of AzoF, represented in Figure 68.^[13] Furthermore, incorporation of AzoF at the hinge position W123 in HisH (hW123AzoF) of ImGPS was found to reinforce a catalytically-relevant conformational change in the enzyme, involving a closing of the cyclase:glutaminase subunit interface.^[13b]

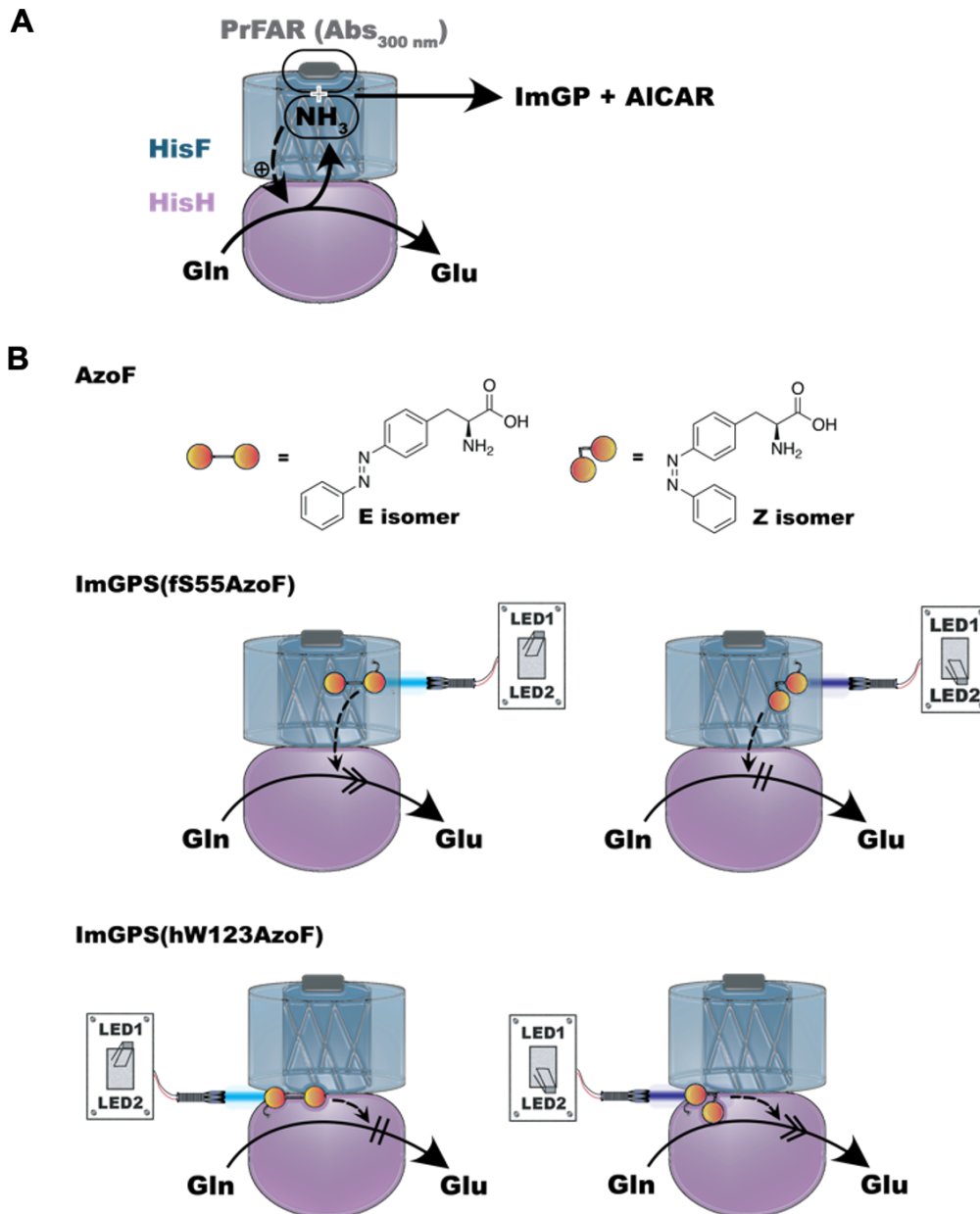


Figure 68. Activity, allostery and reversible photoregulation of ImGPS. A) ImGPS is activated by the binding of PrFAR to the HisF subunit (blue). This, in turn, stimulates the HisH subunit (purple) and leads to the turnover of glutamine to glutamate. Ammonia is produced from this reaction, which is subsequently shuttled back through HisF, where PrFAR is cleaved into 5-aminoimidazol-4-carboxamidribotide (AICAR) and Imidazole glycerol phosphate (ImGP).^[13-14] Deactivation of this complex occurs when these latter products dissociate from HisF. B) The photoisomerizable AzoF was previously incorporated into ImGPS at two distinct sites, resulting in ImGPS(fS55AzoF) and ImGPS(hW123AzoF).^[13] The *E* isomer of both ImGPS mutants was obtained via continuous irradiation with 420 nm (LED 1), while 365 nm was used to obtain the respective *Z* isomers (LED 2). Both ImGPS variants displayed an opposing effect on substrate turnover when present as either their *E* or *Z* isomer states.^[13]

The necessity of conformational changes for ImGPS activity was further validated by nuclear magnetic resonance spectroscopy and molecular dynamics simulations, with the signal transduction from the HisF to the HisH active site found to involve conformational fluctuations.^[13b, 14a] These findings becomes particularly relevant when considering the possibility to control such intrinsic fluctuations using site-selective rapid motions to ultimately control enzymatic activity. As a result, ImGPS was used as a model enzyme for the dynamic investigations explored in this work.

4.3 Results and Discussion

4.3.1 Photocontrol of ImGPS Activity with Continuous Irradiation

In previous work, reversible allosteric activation of ImGPS(fS55AzoF) and ImGPS(hW123AzoF) could be achieved by switching between the isomers of AzoF using light.^[13] When performing direct photocontrol measurements of HisH activity, both variants displayed significant differences in activity when present in their respective *Z* or *E* isomer states. Since W123 in HisH (hW123) and S55 in HisF (fS55) are known to be allosterically-relevant positions, it is not unlikely that dynamic motions induced by rapid toggling between the isomers of AzoF could propagate throughout the protein, influencing other residues along a putative allosteric pathway. Hence, monitoring the ImGPS activity instead of just the HisH activity may reflect potential alterations in allosteric communication between HisH and HisF more accurately. For this reason, direct photocontrol experiments were performed following the depletion of PrFAR at 300 nm in the ImGPS assay. For the sake of comparison with previously reported data from steady state kinetic measurements,^[13] light dependent ImGPS activity of both variants was determined using continuous irradiation (Figure 69).

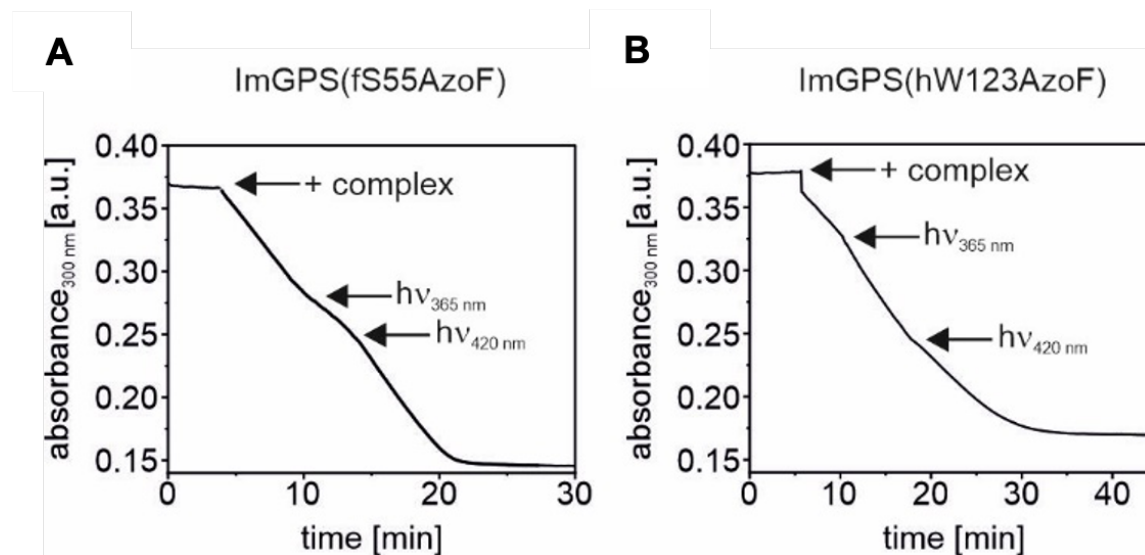


Figure 69. Direct photocontrol of ImGPS activity using continuous irradiation. Light-dependent activity of (A) ImGPS(fS55AzoF) and (B) ImGPS(hW123AzoF) was monitored at 300 nm. The reaction course shows the non-irradiated ‘as isolated’ complex that was subsequently continuously irradiated with 365 nm for 30 s for *E* to *Z* isomerization, while continuous irradiation with 420 nm for 1 min induced isomerization back to the *E* isomer. Samples were irradiated at the specified time points (black arrow) and irradiation was maintained until the end of the assay.

Catalytic activities were deduced from the reaction slopes and are depicted in Table 14. Changes in activity before and after irradiation at the specified wavelengths are described as light regulation factor (LRF). In establishing suitability of the irradiation conditions with the employed assay, previous work reported that the LRF of ImGPS(wt) was not significantly affected by continuous light exposure,^[13] with similar findings observed in this work (SI Figure 74, Table 14). Upon addition of ImGPS(fS55AzoF), the reaction was initiated as evident from the decrease in absorbance (Figure 69A). Conversion of ImGPS(fS55AzoF) to its *Z* isomer-enriched state [ImGPS(fS55AzoF^Z)] by continuous exposure to 365 nm irradiation for 30 s, resulted in a 32% decrease in substrate turnover as evident in the flattening of the slope, which remains constant post irradiation. Upon conversion back to the *E* isomer-enriched state [ImGPS(fS55AzoF^E)] by exposure to 420 nm irradiation for 1 min, substrate turnover increased by 60% and similarly remained constant post irradiation. In contrast, when ImGPS(hW123AzoF) was exposed to the same irradiation conditions, a 48% increase in substrate turnover was observed for ImGPS(hW123AzoF^Z) as apparent from a steeper slope upon illumination with 365 nm, while back isomerization to ImGPS(hW123^E) led to an observable 46% decrease in activity (Figure 69B, Table 14).

Table 14. Light-dependent catalytic activities of ImGPS(fS55AzoF) and ImGPS(hW123AzoF).^[a]

Protein	k_{cat}^{ai} [min ⁻¹] ^[b]	k_{cat}^Z [min ⁻¹] ^[b]	k_{cat}^E [min ⁻¹] ^[b]	LRF1 ^[c]	LRF2 ^[d]
ImGPS(wt)	19.9	18.9	17.3	0.95	0.92
ImGPS(fS55AzoF)	12.3 ± 0.1	8.4 ± 0.3	13.4 ± 0.9	0.68	1.60
ImGPS(hW123AzoF)	12.5 ± 1.0	18.5 ± 0.6	9.9 ± 0.4	1.48	0.54

^[a] k_{cat} apparent values were determined by linear equation fitting and normalization with enzyme concentration, based on previous literature.²⁸ Except for ImGPS(wt), which was a single measurement, data shown are the mean ± SEM of three independent experiments, with at least two biological replicates. ^[b]Apparent k_{cat} values of the non-irradiated samples ‘as isolated’ (*ai*), as well as the respective *E* and *Z* isomer-enriched samples. ^[c]LRF1 = $k_{\text{cat}}^Z/k_{\text{cat}}^{ai}$. ^[d]LRF2 = $k_{\text{cat}}^E/k_{\text{cat}}^Z$.

In addition, absorption spectra of the respective isomers of fS55AzoF and hW123AzoF could be reproduced as previously reported (SI Figure 75).^[13] The differences observed in

intrinsic catalytic activities before and after irradiation between the ImGPS mutants are discussed in more detail in previous work.^[13] However, it can be noted that the dissimilarity between the two mutants exemplifies the sensitivity of ImGPS towards configurational changes at particular sites within its scaffold, and are in accordance with the activity variations previously observed in a HisH assay.^[13] Furthermore, the k_{cat} values determined from the direct photocontrol of ImGPS activity coincide well with previously reported k_{cat} values.^[13]

4.3.2 Photophysical Investigations with Pulsing Irradiation

The photophysical properties of both AzoF-containing variants, including photostationary states (PSS), have been previously characterized.^[13] However, since rapid illumination with alternating 365/420 nm would be required to induce the desired rapid toggling between the isomers of AzoF, further photophysical evaluations were performed. Rapid illumination was achieved with pulsing irradiation, where the frequency of the light pulse could be precisely adjusted. On this account, UV/Vis spectroscopy was used to investigate whether pulsing irradiation could, in general, be used to switch between the isomers of AzoF (Figure 70). Both fS55AzoF and hW123AzoF were separately exposed to pulsing irradiation at 1000 Hz, with either 365 nm to obtain the *Z* isomer or 420 nm to obtain the *E* isomer. The spectra were similar to those obtained using continuous irradiation at the respective wavelength (SI Figure 75), suggesting that pulsing irradiation induces the same isomer states as continuous irradiation. Interestingly, the time to reach the maximum amount of *Z* or *E* isomer was 3 seconds at 365 nm or 5 seconds at 420 nm when pulsing and thus, was significantly reduced compared to continuous light exposure using the same LEDs (30 s at 365 nm, 1 min at 420 nm, SI Figure 75).

Once it was confirmed that pulsing irradiation was suitable for switching between the isomers of AzoF, it was next important to evaluate how many switching cycles both fS55AzoF and hW123AzoF can undergo. This is particularly important since the incorporated AzoF would be required to rapidly isomerize numerous times to obtain rapid motions. In principle, azobenzenes are known to be somewhat resistant towards photobleaching and have been proposed to withstand thousands of switching cycles.^[15] However, the impact of such a multitude of switching cycles on AzoF, and more importantly, on AzoF that is incorporated into a protein, has not to our knowledge been tested to this extent. It should be considered that besides photobleaching of AzoF, which may be dependent on its biochemical environment within the protein, the protein may sustain damage due to numerous switching cycles. Remarkably, when subjected to one hundred switching cycles, both fS55AzoF and hW123AzoF were quite robust as no significant signs of fatigue were observed (Figure 70B). Although the absorption of both isomers of hW123AzoF was constantly increasing, the amplitude remains constant, implying that this effect was rather attributed to the baseline shifting than to photobleaching. These results suggest that the incorporated azobenzene withstands multiple switching cycles, which constitutes an important requirement for pulsing experiments.

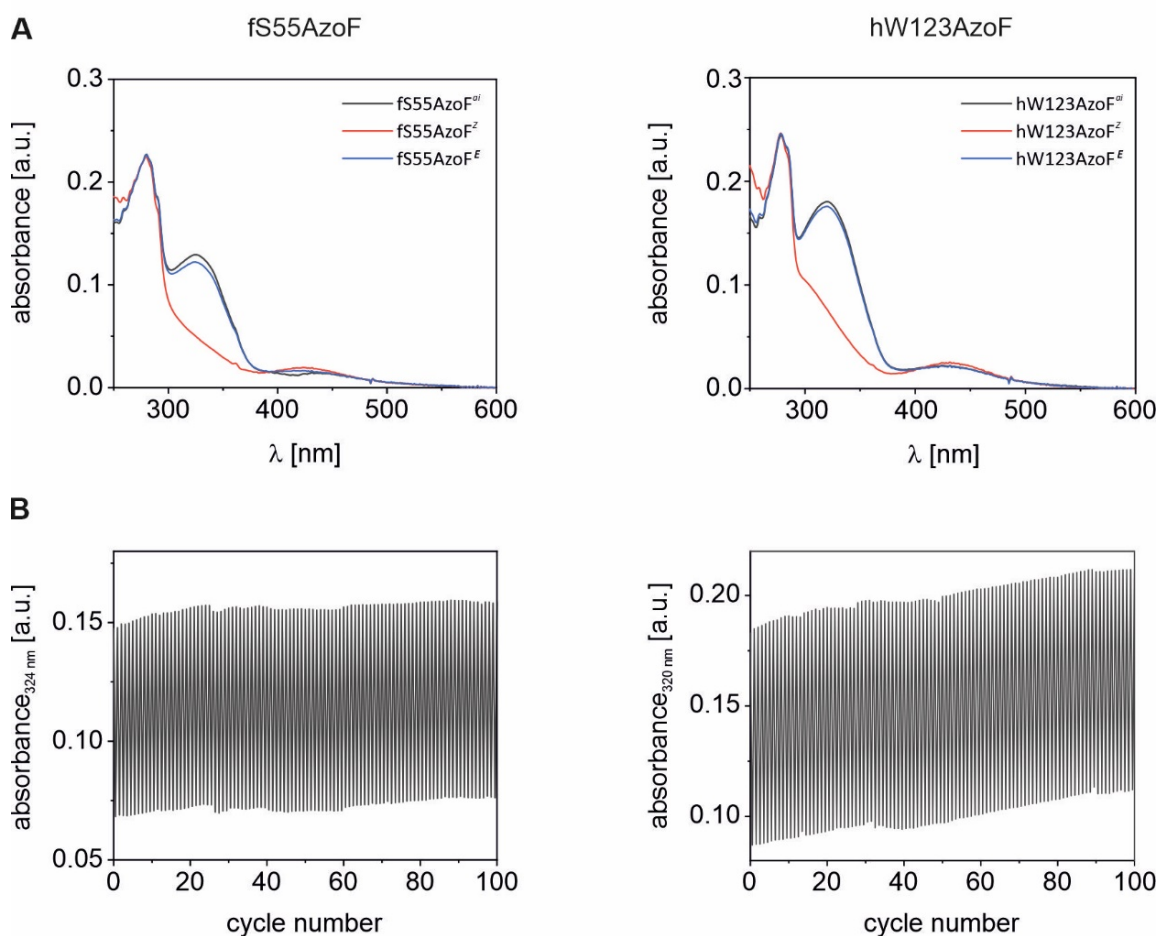


Figure 70. Impact of pulsing and repetitive switching on *E/Z* isomerization. (A) UV/Vis absorption spectra of fS55AzoF and hW123AzoF without any irradiation (black), as well as in their *Z* isomer (red) and *E* isomer (blue) states. Pulsing irradiation was performed at 1000 Hz with light of either 365 nm or 420 nm. (B) Cycle performance of S55AzoF and hW123AzoF. Repeated cycles of photoisomerization are displayed by monitoring the absorbance maximum of the respective *E* isomer. Pulsing irradiation with 365 nm (for 10 s) or 420 nm (for 10 s) was employed at 1000 Hz to obtain either *Z* or *E* isomers, respectively.

Despite these successful findings, it should be noted that pulsing with a frequency of 1000 Hz may require AzoF to be resistant to an even larger number of switching cycles. Due to the resolution of the UV/Vis spectrophotometer (0.5 scans/s), it is difficult to monitor isomerization at such high frequencies. On this account, recovery of the absorption spectra of the respective isomers after a certain period of pulsing was used as a measure for the resistance towards photodegradation. Both fS55AzoF and hW123AzoF were exposed to pulsing irradiation (1000 Hz) that alternated between 365 and 420 nm LEDs for 20 minutes (SI Figure 76). It was found that the AzoF present in both mutants could tolerate these

pulsing conditions, as *Z* and *E* isomer spectra for each mutant could be reproduced post pulsing.

4.3.3 Pulsing AzoF to Transfer Rapid Motions into ImGPS

The proven ability of AzoF to withstand a multitude of switching cycles between *E* and *Z* isomers constitutes an important prerequisite for its repurposing into an energy funnel. When pulsed with alternating 365/420 nm irradiation, the induced rapid isomerization (i.e., rapid motions) of AzoF may in turn, transfer dynamic motions site-selectively into the ImGPS system. The effects of such motions on substrate turnover of ImGPS(fS55AzoF), ImGPS(hW123AzoF), as well as ImGPS(wt) were evaluated by monitoring substrate turnover before pulsing and during pulsing. Representative turnover curves, where pulsing irradiation of alternating 365/420 nm was conducted at 1000 Hz, are shown in Figure 71. It can be observed that for ImGPS(wt), which does not contain AzoF, substrate turnover was unaffected by pulsing irradiation at 1000 Hz (Figure 71A). This indicated that the pulsing conditions were compatible with the chosen biological system and activity assay. Interestingly, when ImGPS(fS55AzoF) was exposed to these conditions, there was also no significant change in substrate turnover before pulsing and during pulsing (Figure 71B). In contrast, a key finding was observed when ImGPS(hW123AzoF) was subjected to the same pulsing conditions. When pulsed with 1000 Hz, a significant increase in ImGPS(hW123AzoF) activity was evident (Figure 71C) compared to the non-irradiated sample (Figure 71D). This was considered to be a consequence of the rapid motions induced, with subsequent experiments aimed to further address this.

In addition to 1000 Hz, the impact of other frequencies on the activity of these ImGPS variants was investigated. Corresponding pulsing regulation factors (PRFs) were deduced from the respective k_{cat} values when subjected to pulsing irradiation at four different frequencies (Table 15). The PRF is defined here as the ratio of k_{cat} values during pulsing irradiation to that before pulsing ($k_{\text{cat}}^{\text{pulsing irradiation}}/k_{\text{cat}}^{\text{#}}$). As the frequencies increase by intervals of 10, the PRF value of ImGPS(wt) remained close to 1, which indicated that there was no significant difference in substrate turnover before pulsing and during pulsing. These results confirmed that the various irradiation frequencies and assay conditions do not interfere with the intrinsic catalytic activity of ImGPS(wt). Despite containing the photoswitchable unit, similar values were obtained for ImGPS(fS55AzoF) independent of the pulsing frequency. This suggested that pulsing irradiation at the employed frequencies had no prominent effect on the catalytic behaviour of ImGPS(fS55AzoF).

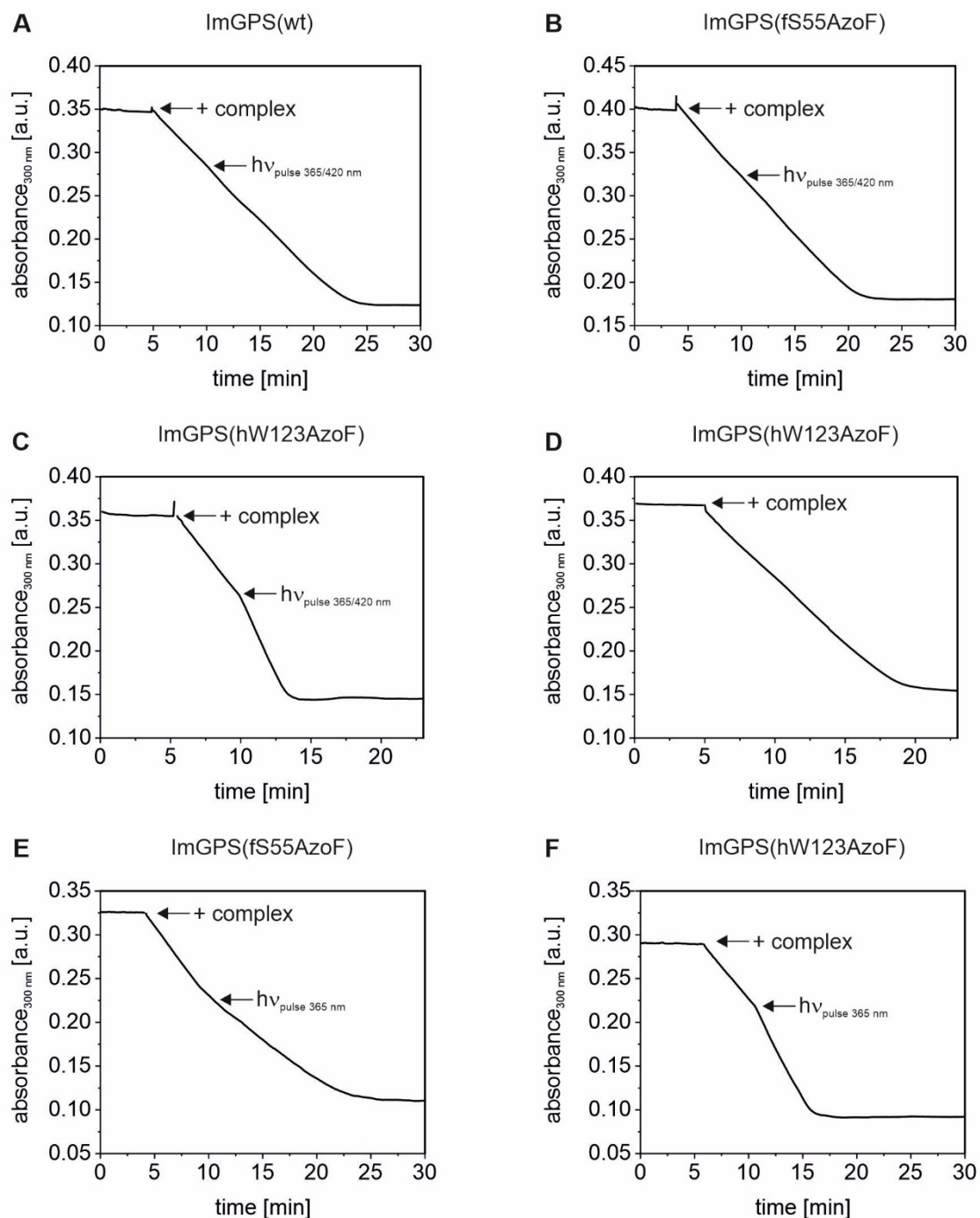


Figure 71. Effects of pulsing irradiation on ImGPS activity. Representative graphs of (A) ImGPS(wt), (B) ImGPS(fS55AzoF), and (C) ImGPS(hW123AzoF) when exposed to 1000 Hz pulsing with 365/420 nm. (D) The negative control of ImGPS(hW123AzoF) displays the reaction course without light. (E) Control experiment of ImGPS(fS55AzoF) with 365 nm pulsing (1000 Hz) only. (F) Control experiment of ImGPS(hW123AzoF) with 365 nm pulsing (1000 Hz) only. Samples were irradiated at a specified time point (black arrows) until the end of the assay.

In contrast, when exposed to pulsing irradiation at 1000 Hz, ImGPS(hW123AzoF) displayed a 72% increase in activity, characterized by a PRF of 1.72 (Figure 71C and Table 15). While the effect on the catalytic activity seemed to be independent of the pulsing frequency, it should be noted that all tested frequencies were within the millisecond timescale. Nonetheless, the different impact of pulsing irradiation on ImGPS(fS55AzoF) and ImGPS(hW123AzoF) was a pivotal aspect when considering the ability to induce dynamic motions. It remains unclear whether the activity of ImGPS(fS55AzoF) was unaltered because the motions triggered by rapid isomerization at position S55 in HisF did not influence the catalytic behaviour, or simply because there were no putative rapid motions induced at this specific position. However, the unambiguous effect of pulsing irradiation at 365/420 nm on ImGPS(hW123AzoF) may indicate the insertion of such motions. Moreover, it was possible to confirm that AzoF toggling can indeed be induced by 1 Hz pulsing irradiation, resolvable by online absorption spectroscopy, albeit not quantitatively (SI Figure 77). Isomerization at higher frequencies could not be monitored due to constraints in measurement velocity of the spectrophotometer device. However, since key dynamic movements of ImGPS(hW123AzoF), as well as ImGPS(wt), was previously found to occur on a millisecond timescale, it becomes conceivable that inducing rapid motions with frequencies on this scale (i.e., 1-1000 Hz) could affect catalytic activity.^[4c, 4d, 13b, 14c]

Table 15. PRF values of ImGPS activity when pulsing at various frequencies.^[a]

Protein	PRF				
	No pulsing ^[b]	Pulsing frequencies [Hz]			
		1	10	100	1000
ImGPS(wt)	0.98 ± 0.03	1.03 ± 0.04	1.03 ± 0.04	1.06 ± 0.04	1.01 ± 0.03
ImGPS(fS55AzoF)	1.02 ± 0.02	1.01 ± 0.05	0.96 ± 0.05	1.01 ± 0.04	1.01 ± 0.06
ImGPS(hW123AzoF)	0.96 ± 0.01	1.75 ± 0.05	1.64 ± 0.05	1.56 ± 0.15	1.72 ± 0.06

^[a]PRF = $k_{\text{cat}}^{\text{pulsing irradiation}}/k_{\text{cat}}^{\text{ai}}$. PRF < 1: decrease in ImGPS activity; PRF > 1: increase in ImGPS activity; PRF = 1: no change in ImGPS activity. Data shown are the mean ± SEM of at least three independent experiments, with 2-3 biological replicates. ^[b]Negative control (no irradiation): PRF values were determined using data at similar time points as that used in PRF calculations for pulsing measurements.

When providing experimental evidence that describes the influence of dynamic motions on catalytic activity and/or the ability to alter such motions, further considerations should be discussed. For example, it can be noted that similar PRF values were obtained when ImGPS(hW123AzoF) was pulsed with alternating 365 nm and 420 nm (Table 15) and when it was subjected to continuous irradiation with only 365 nm to obtain the *Z*-enriched isomer state (Table 14). These findings alone may suggest that pulsing between 365 nm and 420 nm may over time result in an abundance of the *Z* isomer, which may account for the similar PRF values obtained in both experiments. To evaluate this, further activity assays were performed where both variants were individually pulsed with either 365 nm or 420 nm to obtain either *Z* or *E* isomers, respectively, with results shown in Table 16. For these measurements, as well as subsequent experiments, 1000 Hz was employed as a representative frequency.

Table 16. PRF values of ImGPS activity when pulsing with only 365 nm or 420 nm.^[a]

Protein	PRF (Pulsing at 1000 Hz)	
	365 nm	420 nm
ImGPS(wt)	0.97 ± 0.04	0.99 ± 0.04
ImGPS(fS55AzoF)	0.58 ± 0.03	1.06 ± 0.05
ImGPS(hW123AzoF)	1.85 ± 0.01	0.97 ± 0.05

^[a]PRF = $k_{\text{cat}}^{\text{pulsing irradiation}}/k_{\text{cat}}^{\text{ir}}.$ PRF < 1: decrease in ImGPS activity; PRF > 1: increase in ImGPS activity; PRF = 1: no change in ImGPS activity. Data shown are the mean ± SEM of three independent experiments.

As expected, similar activity profiles were obtained when each respective variant was pulsed with only 365 nm (Figure 71E,F) compared to when continuously irradiated with the same wavelength (Figure 69), which is also reflected in the corresponding PRF values (Table 15, Table 16). Interestingly, comparable PRFs were also obtained for ImGPS(hW123AzoF) when this variant was pulsed with alternating 365 nm and 420 nm wavelengths (Table 15). If the reason for this similarity was indeed due to the predominance of the *Z* isomer when pulsing over time, then the same effect should be observed for ImGPS(fS55AzoF). While a 42% decrease in activity can be observed when ImGPS(fS55AzoF) was pulsed with only

365 nm to obtain the *Z* isomer (Figure 71E, Table 16), there was no significant change in activity when pulsed with alternating 365 nm and 420 nm wavelengths (Figure 71B, Table 15). The circumstance that ImGPS(fS55AzoF) does not reveal any effect upon pulsing with 365/420 nm, albeit the detectable effect upon isomerization to the *Z* isomer when pulsing with 365 nm, constitutes an important control in these experiments and demonstrates that the observed findings are not due to the predominance of the *Z* isomer. Pulsing both variants with only 420 nm did not result in any changes in activity, as the distribution of isomers in the induced *E*-enriched state is similar to that in the ‘*as isolated*’ state (Figure 70A).

To ultimately validate that the 72% increase in activity (1000 Hz, Table 15) was indeed due to alternating pulsing, resulting in putative toggling, and not due to the predominance of the *Z* isomer, further experiments were performed. This involved recording time-resolved UV/Vis absorbance spectra of hW123AzoF while being pulsed with alternating 365/420 nm irradiation over a period of 10 minutes at a scan rate of 2 sec⁻¹ (Figure 72). Although this scan rate is not sensitive enough to ascertain the motion of AzoF while switching at the high frequencies employed, this data provided further insight into the isomer abundance of hW123AzoF during pulsing. Starting from hW123AzoF^{ai}, the spectra recorded in the first minutes of pulsing seemed to approach the *Z* isomer spectrum as the characteristic absorbance of the *E* isomer decreased. However, the *Z* isomer spectrum was not reached. Instead, the absorbance at 320 nm increased again to reach a plateau by the end of the ten-minute pulsing period. As a result, even though similar PRF values were obtained for ImGPS(hW123AzoF) when pulsed with alternating 365 nm and 420 nm wavelengths (Table 15), compared to when pulsed with just 365 nm (Table 16), the mechanistic processes underlying the observed effects seem to be different.

Interestingly, the spectra during pulsing behaved similarly for fS55AzoF (SI Figure 78) although there was no observable effect on activity upon pulsing with 365/420 nm (Table 15). Considering the decrease in activity when fS55AzoF was pulsed with just 365 nm, these results substantiate the assumption that different activation processes are induced by pulsing with solely one wavelength and pulsing with 365/420 nm.

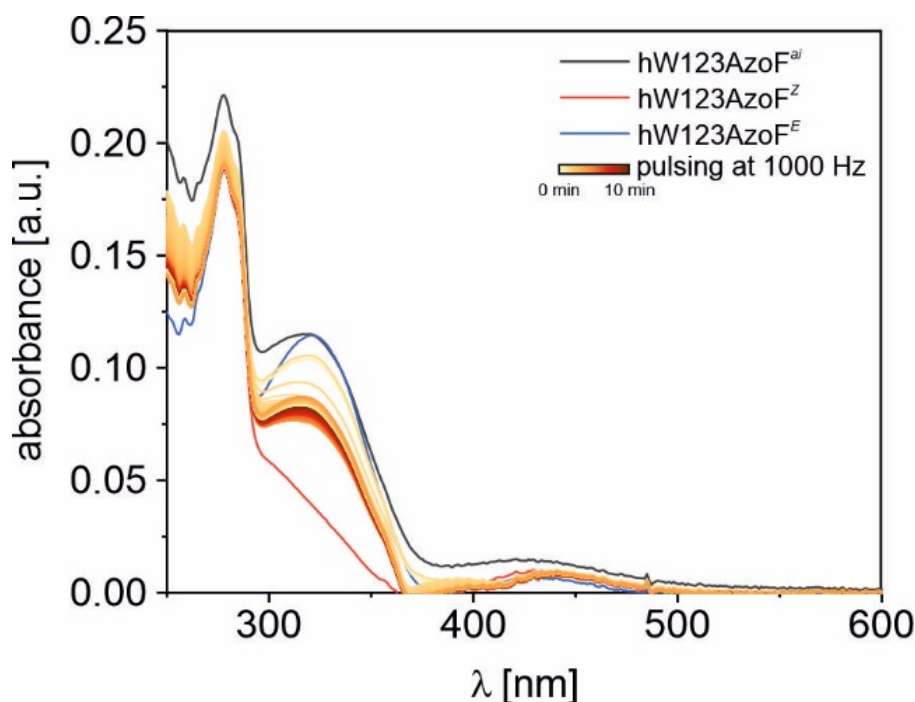


Figure 72. Time-resolved UV/Vis absorption spectroscopy to evaluate the effects of pulsing. Pulsing of hW123AzoF (10 μ M) with alternating 365/420 nm (1000 Hz) for 10 min. An absorbance spectrum was generated once every 2 seconds. Additional spectra are shown of the respective ‘as isolated’ state (black) prior to pulsing, as well as that of the *E* (blue) and *Z* isomers (red) post pulsing.

Furthermore, it was important to investigate whether the proposed dynamic findings result from simply exposing AzoF to both 365 nm and 420 nm at similar times. As a result, activity assays were performed where ImGPS(wt), ImGPS(fs55AzoF) and ImGPS(hW123AzoF) were subjected to continuous irradiation of both wavelengths at the same time (i.e., no pulsing). Assays were performed at room temperature, as well as at fixed temperatures of 20 °C (SI Table 18). Continuous irradiation with both LEDs was found to affect substrate turnover in all ImGPS(wt), ImGPS(fs55AzoF) and ImGPS(hW123AzoF). As a result, it can be concluded that continuous irradiation with both LEDs was not compatible with the employed biological system, and as a result, has a different effect than that produced by pulsing irradiation.

4.3.4 Temperature Studies

In previous experiments, ImGPS activity assays were conducted at room temperature, without temperature regulation. Since LEDs emit energy also in the form of heat, temperatures of the sample solutions could increase upon LED exposure. To investigate this, temperature changes in the sample solution were monitored during pulsing measurements. This involved exposing sample solution to pulsing irradiation with alternating 365 nm and 420 nm at 1000 Hz for 30 minutes, with temperature recorded at 5-minute intervals (SI Table 19). Results indicated a 1.8 °C increase in temperature after 5 minutes of pulsing irradiation and an increase of 6.8 °C increase after 30 minutes, with the former being closer to the standard conditions employed in this work. It is important to note that ImGPS(wt), ImGPS(fS55AzoF) and ImGPS(hW123AzoF) were all subjected to the same conditions. As a result, if the increase in heat from the LEDs was to indeed impact ImGPS activity, then this would be reflected in the PRF values for ImGPS(wt) assays, which is not the case (Table 15). In addition, when pulsed for 10 minutes with only 365 nm LEDs (Figure 71E), a PRF value of 0.58 ± 0.03 was obtained for ImGPS(fS55AzoF) despite any temperature increase. Nonetheless, further activity assays were performed at fixed temperatures.

When AzoF rapidly toggles between *E* and *Z* isomers in pulsing assays, as validated by UV/Vis measurements (SI Figure 77), the resulting rapid motion seems to result in an increase in ImGPS(hW123AzoF) activity (Table 15). The effects of fast-switching AzoF on ImGPS(hW123AzoF) may be rationalized in two ways, where both involve the ability of AzoF to act as an energy shuttle. One hypothesis is that the energy may be shuttled in the form of dynamic rapid motions (i.e., vibrations). In this case, the vibrations of AzoF could be transferred to ImGPS at the localized site of hW123, which ultimately, leads to an increase in catalytic activity. Another mechanistic rational that could be considered is the shuttling of energy from AzoF to ImGPS in the form of heat, and consequently, this site-selective heat transfer may result in an increase in catalytic activity.

Activity assays of ImGPS(hW123AzoF) were conducted separately at fixed temperatures of 4, 20, 30, and 40 °C, with corresponding k_{cat} and PRF values summarized in Table 17. Fixing the assay temperature to 4 °C, diminished the activity of the enzyme (SI Figure 79). Importantly, when assay temperatures were fixed at 20, 30 and 40 °C, an increase in substrate turnover was still obtained from pulsing, with PRF values of 1.70 ± 0.05 , 1.55 ± 0.08 and 1.69 ± 0.07 , respectively. This indicates that the effect of fast-switching AzoF on ImGPS activity was not simply due to an overall increase in temperature and further validates the

rapid motions hypothesis described in this work. Unfortunately, no significant trend in PRF values could be observed as the temperature increased. Even though a trend may be expected when dynamics is involved in the mechanism, the temperature dependencies of dynamic motions in biological systems have been previously described as complex.^[3e] In addition, when the temperature increases, the intrinsic catalytic activity of ImGPS also increases and reaction times significantly change (Table 17, SI Figure 79). As a result, it becomes difficult to directly compare PRF values between the different temperature experiments.

Table 17. Temperature-controlled measurements of ImGPS(hW123AzoF) activity.^[a]

Temperature [°C]	$k_{\text{cat}}^{\text{ai}}$ [min^{-1}] ^[b]	$k_{\text{cat}}^{\text{pulsing}}$ [min^{-1}] ^[b]	PRF ^[c]
No temp control	18.1 ± 1.5	30.2 ± 2.4	1.66 ± 0.02
4	N/A	N/A	N/A
20	11.3 ± 0.4	19.2 ± 1.0	1.70 ± 0.05
30	27.0 ± 0.7	41.6 ± 1.0	1.55 ± 0.08
40	52.9 ± 4.2	89.2 ± 5.2	1.69 ± 0.07

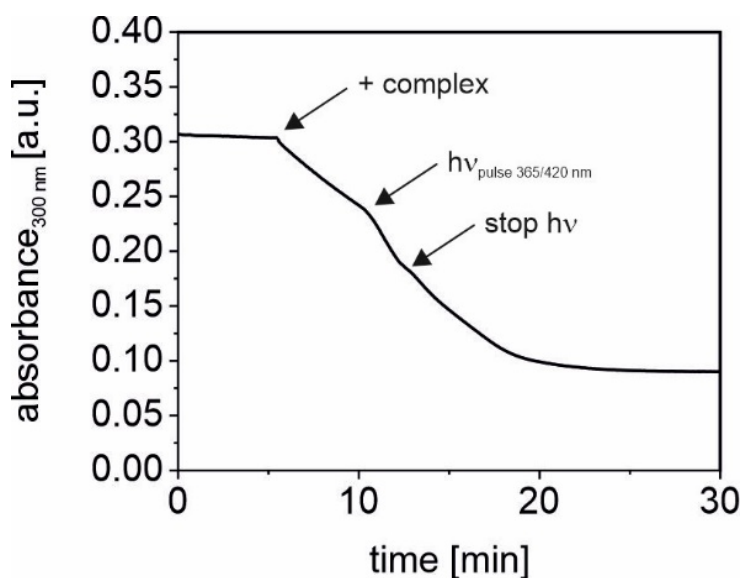
^[a]Experiments were conducted using 1000 Hz pulsing with 365/420 nm. *ai* = non-irradiated sample. Data shown are the mean ± SEM of three independent experiments. ^[b]Apparent k_{cat} values. ^[c]PRF = $k_{\text{cat}}^{\text{pulsing irradiation}}/k_{\text{cat}}^{\text{ai}}$. PRF < 1: decrease in ImGPS activity; PRF > 1: increase in ImGPS activity; PRF = 1: no change in ImGPS activity.

Furthermore, when discussing whether AzoF acts to induce vibrations into ImGPS(hW123AzoF) or whether this azobenzene acts to insert site-selective heat into the enzyme, these results become important. Even though it is difficult to directly monitor temperature changes at the specific site of hW123, it can be considered that by fixing the reaction temperature at higher temperatures (i.e., 40 °C, Table 17, SI Figure 79), the amount of heat that a fast-switching AzoF could shuttle into ImGPS at the location of hW123 may become less significant. Since high PRF values are still obtained at higher temperatures, this data suggests that the rapid motions of AzoF is most likely transferred to ImGPS at the site of hW123AzoF in the form of vibrations. This further establishes azobenzene as a tool to

induce site-selective motion and demonstrates the sensitivity of certain sites in ImGPS towards dynamic stimulation. As a result, these findings provide further insight into the importance of dynamic motion within selected regions of the enzyme and its influence on enzyme function.

4.3.5 Reversible Dynamic Control of ImGPS(hW123AzoF)

An important question that remained was whether the dynamic effect on ImGPS(hW123AzoF) was reversible or caused irreversible changes to the enzyme. Therefore, ImGPS(hW123AzoF) was pulsed for only 3 minutes and subsequently, the recovery of ImGPS activity was monitored post pulsing (Figure 73). Prior to pulsing, a k_{cat} value of 21.2 ± 0.8 was recorded, while a value of 43.7 ± 3.9 was obtained during pulsing at 1000 Hz. Interestingly, catalytic activity was restored to 22.1 ± 1.1 post pulsing.



$k_{\text{cat}}^{\text{at}}$ [min^{-1}]	$k_{\text{cat}}^{\text{pulsing}}$ [min^{-1}]	$k_{\text{cat}}^{\text{post pulsing}}$ [min^{-1}]
21.2 ± 0.8	43.7 ± 3.9	22.1 ± 1.1

Figure 73. Recovery of ImGPS(hW123AzoF) activity post pulsing. Reaction curve of ImGPS(hW123AzoF). The sample was pulsed with 365/420 nm irradiation at 1000 Hz. Pulsing was performed for 3 minutes and once stopped, the measurement was continued (graph above), with corresponding k_{cat} values reported in the table below. The k_{cat} values are shown as the mean \pm SEM of three independent experiments and one biological replicate.

These results indicated that the intrinsic catalytic activity of ImGPS(hW123AzoF) was not irreversibly hindered by the rapid motions induced by rapidly switching AzoF. Therefore, the ability to insert rapid motions into ImGPS to ultimately regulate catalytic activity was well tolerated by this enzyme. However, it should be noted that this particular biological replicate

exhibited higher intrinsic catalytic activity than previous replicates, and upon pulsing irradiation with alternating 365/420 nm, a 106% increase in activity could be observed. Nonetheless, these findings further validate that photobleaching does not occur from the pulsing conditions employed and these conditions do not appear to disturb the overall enzyme conformation required for catalytic activity. Importantly, these results validate fast-switching AzoF as a potential tool that can reversibly insert site-selective motion into an enzyme.

4.4 Conclusion and Outlook

The notion that rapid motions, in the form of vibrations, are present and are functionally-relevant in enzymes was further explored in this work. This involved the use of pulsing irradiation to rapidly toggle between the isomers of AzoF that was co-translationally incorporated into ImGPS at the allosterically-relevant sites hW123 and fS55. By rapidly switching between the isomers of AzoF, this unit could seemingly be repurposed into an energy funnel to transfer motions site-selectively into the ImGPS system. Even though both variants displayed a sensitivity towards AzoF isomerization when exposed to continuous irradiation with either 365 nm or 420 nm, pulsing irradiation with alternating 365/420 nm provided pivotal results. The presumable induced motions resulted in a substantial increase in the catalytic activity of ImGPS(hW123AzoF), while the activity of ImGPS(fS55AzoF) remained unaltered. The observable difference between these variants was a crucial aspect when considering the ability to induce such dynamic processes. In combination with further experiments, including time-resolved measurements, this finding substantiates the assumption that different activation processes were induced by pulsing irradiation in comparison to continuous irradiation. Overall, the results described in this work provide insights into the complex regulation of allosteric proteins and describe the possibility of modulating these proteins via the insertion of dynamic motions, using pulsing light.

4.5 Acknowledgements

This work was supported by the Deutsche Forschungsgemeinschaft, RTG 1910, and a Minerva PhD Fellowship to RL. We thank Karin Rustler and the Electronics Workshop of the Department of Chemistry/Pharmacy (University of Regensburg) for the development of the pulse generator, as well as Julia Zach for LED support.

4.6 References

- [1] R. Lovrien, T. Linn, *Biochem.* **1967**, *6*, 2281-2293.
- [2] a) R. A. Laskowski, F. Gerick, J. M. Thornton, *FEBS Lett.* **2009**, *583*, 1692-1698; b) J. Liu, R. Nussinov, *PLoS Comput. Biol.* **2016**, *12*, e1004966.
- [3] a) C. Narayanan, D. N. Bernard, N. Doucet, *Catalysts* **2016**, *6*; b) D. Petrovic, V. A. Risso, S. C. L. Kamerlin, J. M. Sanchez-Ruiz, *J. R. Soc. Interface* **2018**, *15*; c) B. M. Britt, *Biophys. Chem.* **1997**, *69*, 63-70; d) S. Hay, N. S. Scrutton, *Nat. Chem.* **2012**, *4*, 161-168; e) D. R. Glowacki, J. N. Harvey, A. J. Mulholland, *Nat. Chem.* **2012**, *4*, 169-176; f) P. A. Srere, *Trends Biochem. Sci.* **1984**, *9*, 387-390; g) A. J. Adamczyk, J. Cao, S. C. Kamerlin, A. Warshel, *Proc. Natl. Acad. Sci. U.S.A.* **2011**, *108*, 14115-14120; h) D. S. Goodsell, A. J. Olson, *Trends Biochem. Sci.* **1993**, *18*, 65-68.
- [4] a) D. D. Boehr, D. McElheny, H. J. Dyson, P. E. Wright, *Proc. Natl. Acad. Sci. U.S.A.* **2010**, *107*, 1373-1378; b) G. Bhabha, J. Lee, D. C. Ekiert, J. Gam, I. A. Wilson, H. J. Dyson, S. J. Benkovic, P. E. Wright, *Science* **2011**, *332*, 234-238; c) G. P. Lisi, K. W. East, V. S. Batista, J. P. Loria, *Proc. Natl. Acad. Sci.* **2017**, *114*, E3414-E3423; d) J. M. Lipchock, J. P. Loria, *Structure* **2010**, *18*, 1596-1607; e) L. Astl, A. Tse, G. M. Verkhivker, *Adv. Exp. Med. Biol.* **2019**, *1163*, 187-223.
- [5] a) S. Hay, M. J. Sutcliffe, N. S. Scrutton, *Proc. Natl. Acad. Sci. U.S.A.* **2007**, *104*, 507-512; b) S. M. Kandathil, M. D. Driscoll, R. V. Dunn, N. S. Scrutton, S. Hay, *Phys. Chem. Chem. Phys.* **2014**, *16*, 2256-2259.
- [6] a) W. A. Velema, W. Szymanski, B. L. Feringa, *J. Am. Chem. Soc.* **2014**, *136*, 2178-2191; b) M. M. Lerch, M. J. Hansen, G. M. van Dam, W. Szymanski, B. L. Feringa, *Angew. Chem. Int. Ed. Engl.* **2016**, *55*, 10978-10999.
- [7] a) D. Lachmann, R. Lahmy, B. König, *Eur. J. Org. Chem.* **2019**, *2019*, 5018-5024; b) R. Lahmy, H. Hübner, M. F. Schmidt, D. Lachmann, P. Gmeiner, B. König, *Chem. Eur. J.* **2022**, *28*, e202201515.
- [8] W. Szymański, J. M. Beierle, H. A. Kistemaker, W. A. Velema, B. L. Feringa, *Chem. Rev.* **2013**, *113*, 6114-6178.
- [9] H. Fliegl, A. Köhn, C. Hättig, R. Ahlrichs, *J. Am. Chem. Soc.* **2003**, *125*, 9821-9827.
- [10] a) I. Tochitsky, M. A. Kienzler, E. Isacoff, R. H. Kramer, *Chem. Rev.* **2018**, *118*, 10748-10773; b) K. Hull, J. Morstein, D. Trauner, *Chem. Rev.* **2018**, *118*, 10710-10747; c) A. A. Beharry, G. A. Woolley, *Chem. Soc. Rev.* **2011**, *40*, 4422-4437.
- [11] M. Teders, A. A. Pogodaev, G. Bojanov, W. T. S. Huck, *J. Am. Chem. Soc.* **2021**, *143*, 5709-5716.
- [12] a) M. Bose, D. Groff, J. Xie, E. Brustad, P. G. Schultz, *J. Am. Chem. Soc.* **2006**, *128*, 388-389; b) A. C. Kneuttinger, *Biol. Chem.* **2022**, *403*, 573-613; c) J. Luo, S. Samanta, M. Convertino, N. V. Dokholyan, A. Deiters, *ChemBioChem* **2018**, *19*, 2178-2185; d) N. Muranaka, T. Hohsaka, M. Sisido, *FEBS Lett.* **2002**, *510*, 10-12.
- [13] a) A. C. Kneuttinger, K. Straub, P. Bittner, N. A. Simeth, A. Bruckmann, F. Busch, C. Rajendran, E. Hupfeld, V. H. Wysocki, D. Horinek, B. König, R. Merkl, R. Sterner, *Cell Chem. Biol.* **2019**, *26*, 1501-1514 e1509; b) A. C. Kneuttinger, C. Rajendran, N. A. Simeth, A. Bruckmann, B. König, R. Sterner, *Biochem.* **2020**, *59*, 2729-2742.
- [14] a) G. P. Lisi, G. A. Manley, H. Hendrickson, I. Rivalta, V. S. Batista, J. P. Loria, *Structure* **2016**, *24*, 1155-1166; b) I. Rivalta, M. M. Sultan, N. S. Lee, G. A. Manley, J. P. Loria, V. S. Batista, *Proc. Natl. Acad. Sci. U.S.A.* **2012**, *109*, E1428-1436; c) C. Calvó-Tusell, M. A. Maria-Solano, S. Osuna, F. Feixas, *J. Am. Chem. Soc.* **2022**, *144*, 7146-7159.
- [15] a) M. Zhu, H. Zhou, *Org. Biomol. Chem.* **2018**, *16*, 8434-8445; b) J. D. Harris, M. J. Moran, I. Aprahamian, *Proc. Natl. Acad. Sci. U.S.A.* **2018**, *115*, 9414-9422.

4.7 Supplementary Information

4.7.1 Materials and Methods

Synthesis of AzoF

AzoF was synthesized according to literature procedures,^[1] with reagents obtained from Sigma-Aldrich. The synthesis has been modified to allow for easier access to higher purity and a more soluble product for biological purposes. Following literature procedures, the crude mixture was obtained, and solvent was removed *in vacuo*. Toluene (1 mL/mmol) was then added to facilitate the removal of 1,4-dioxane, and the solvent was once again removed *in vacuo*. Afterwards, the product was triturated with diethyl ether (3 x 1 mL/mmol), yielding AzoF in a purer and more water-soluble form, without further purification.

Expression Strains, Plasmids, Auxiliary Enzymes, and Chemicals

The bacterial strain *E. coli* BL21 Gold (DE3) that was used for production of proteins in this work was purchased from Agilent Technologies. The expression vectors pET21a_HisA,⁴⁴ pET28a_HisF,³⁷ pET28a_HisH,³⁷ pET28a_HisF_S55AzoF,³⁷ and pET28a_HisH_W123AzoF³⁸ were taken from previous work. Plasmid pEVOL_AzoF that was necessary for the incorporation of AzoF into proteins was provided by P. Schultz (Scripps Research Institute, La Jolla, CA).^[1a] The auxiliary enzyme HisA was expressed and purified according to a previously published protocol.^[1b, 2] Synthesis of AzoF (further optimized in this work) and ProFAR was performed as previously reported.^[1] Glutamate oxidase (GOX) and horseradish peroxidase type I (HRP) were purchased from Sigma-Aldrich. All other chemicals were purchased from commercial sources in analytical grade or higher.

Expression and Purification of ImGPS, hW123AzoF, and fS55AzoF

Wild type HisH and HisF from *Thermotoga maritima* were recombinantly expressed in *E. coli* BL21 Gold (DE3) and purified following a standard protocol as described previously.^[1b, 3] Briefly, the respective plasmids were co-transformed grown in 4 L of lysogeny broth (LB) medium at 37 °C. As soon as an OD₆₀₀ of 0.6 was reached, 0.5 mM isopropyl β-D-thiogalactopyranoside (IPTG) was added and protein expression proceeded at 30 °C overnight. Cells were harvested by centrifugation, resuspended in either 50 mM Tris-HCl pH 7.5, 100 mM NaCl, and 10 mM imidazole (HisF) or 50 mM potassium phosphate (KP) pH 7.5, 100 mM NaCl, and 10 mM imidazole (HisH) and lysed by sonification. *E. coli* proteins were precipitated by a heat step (65 °C, 15 min) and the proteins of interest were obtained from the supernatant after centrifugation. The proteins were subjected to nickel-affinity chromatography (HisTrap_FF Cruie column, 5 mL GE Healthcare) and elution was conducted with a linear gradient of imidazole (10-750 mM). Fractions containing the desired proteins were identified by sodium dodecyl sulfate-polyacrylamide gel electrophoresis (SDS-PAGE), pooled and further purified via size-exclusion chromatography (Superdex 75 HiLoad 26/600, GE Healthcare) using 50 mM HEPES pH 7.5, 100 mM NaCl as running buffer. Fractions containing protein with a purity of >90% were identified by means of SDS-PAGE, pooled, concentrated, and dripped into liquid nitrogen for storage at -80 °C.

For the expression of fS55AzoF and hW123AzoF, the respective plasmids were co-transformed with pEVOL_AzoF^[1a] into *E. coli* BL21 Gold (DE3). This plasmid harbours the orthogonal aminoacyl-tRNA synthetase adapted for AzoF binding as well as the respective orthogonal tRNA required for AzoF incorporation. Cells were grown at 37 °C in 6 L LB medium to reach an OD₆₀₀ of 0.6, harvested by centrifugation, and subsequently transferred to 600 mL terrific broth (TB) medium. Bacterial growth proceeded at 37 °C either until the OD₆₀₀ reached approximately 10 or for at least 6 hours. Protein expression was induced by addition of 0.5 mM IPTG, 0.02% L-arabinose, and 0.8 mM AzoF and the cultures were further incubated at 30 °C overnight. Protein purification was conducted as described above.

Pulse Generator to Produce Alternating Pulsing Irradiation

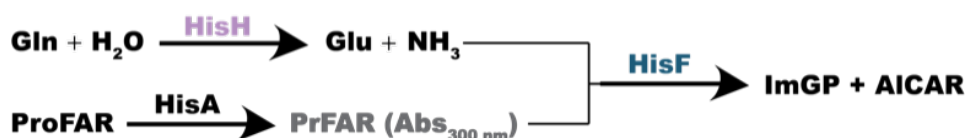
The LED pulse generator (rectangular pulses) was developed in-house, with two output channels that allow for simultaneous connection to a 365 nm LED (SSC VIOSYS CUN66A1B UV Z5 series) and a 420 nm LED (ILS ILH-XC01-S410-SC211-WIR200). Adjustable parameters include: current (100-800 mA), frequency (1-1000 Hz), and set duty cycles (10-100%). LEDs were installed perpendicular to the UV/Vis spectrophotometer measurement beam to allow for continuous irradiation or pulsing of the sample while measuring simultaneously. Continuous irradiation was conducted at 365 nm (400 mA) or 420 nm (400 mA). Pulsing experiments were performed by pulsing (1-1000 Hz) either at one wavelength (365 nm at 400 mA or 420 nm at 400 mA) or alternating between 365 nm (400 mA) and 420 nm (400 mA) at a set duty cycle ratio of 1:1.

UV/Vis Spectroscopy

UV/Vis spectra were recorded with an Agilent 8453 UV/Vis spectrophotometer in the range of 190–1100 nm. Spectra measurement was performed with 10–20 μM protein in 50 mM HEPES (pH 7.5) and 100 mM NaCl in a 10 mm cuvette (quartz) at room temperature, unless otherwise specified. Spectra were recorded of the non-irradiated protein sample (*as isolated*), as well as the respective *E* and *Z* isomer-enriched states. To obtain the respective *Z* or *E* isomer spectra, the sample was either continuously irradiated with 365 nm for 30 s or with 420 nm for 1 min, respectively, or was pulsed separately with 365 nm for 3 s or with 420 nm for 5 s prior to absorbance measurement. All spectra were baseline corrected. Cycle performance experiments were conducted by monitoring the absorbance maximum of the respective *E* isomer (320 nm for hW123AzoF and 324 nm for fS55AzoF) while pulsing with either 365 nm (10 s) and 420 nm (10 s) at 1000 Hz for 100 cycles. Alternatively, the frequency was set to 1 Hz while pulsing with alternating 365/420 nm, with spectra recorded every 2 s. To evaluate the photophysical effects of pulsing on hW123AzoF and fS55AzoF, 15 μM samples were pulsed with alternating 365/420 nm (1000 Hz) for a duration of 10 minutes, with absorbance spectra generated once every 2 seconds, unless otherwise specified.

Light-Dependent Measurement of ImGPS Activity

ImGPS activity of ImGPS(wt), ImGPS(hW123AzoF), and ImGPS(fS55AzoF) was measured using a continuous assay by following the turnover of PrFAR to AICAR and ImGP at 300 nm ($\Delta\epsilon_{300} = 5637 \text{ M}^{-1}\text{cm}^{-1}$),^[4] recorded with an Agilent 8453 UV/Vis spectrophotometer (Scheme 13).



Scheme 13. ImGPS activity assay. ImGPS activity was measured spectrophotometrically by continuously monitoring the turnover of PrFAR to AICAR and ImGP at 300 nm.

Reactions were conducted in 50 mM Tris–HCl pH 7.5, 0.6 μM HisA (to convert ProFAR to PrFAR), 40 μM (saturated) ProFAR, and 10 mM (saturated) glutamine at 25 $^\circ\text{C}$, unless stated otherwise. Prior to activity measurements, the ImGPS complex was formed by mixing the respective HisH and HisF monomers in equimolar concentrations in 50 mM HEPES pH 7.5, 100 mM NaCl. The reaction was started by adding 0.025 μM ImGPS(wt), 0.1 μM ImGPS(hW123AzoF), or 0.2 μM ImGPS(fS55AzoF) and monitored for up to 30 min. Irradiation of the sample was performed continuously or by pulsing at one wavelength or by alternating 365/420 nm with different frequencies (1, 10, 100 and 1000 Hz), concurrent with measuring. Measurements were performed in the number of specified repeats and catalytic activities were deduced from the slopes of the turnover curves and the enzyme concentration.

4.7.2 Supplementary Figures and Tables

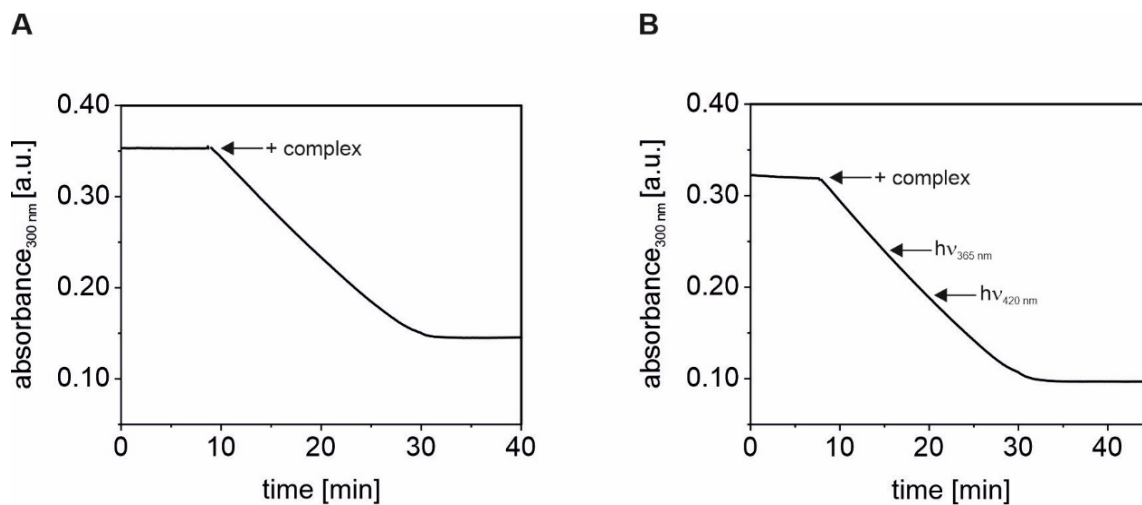


Figure 74. Direct photocontrol of ImGPS(wt) activity using continuous irradiation. (A) ImGPS(wt) control that was not exposed to any irradiation. (B) ImGPS(wt) exposed to continuous irradiation with 365 nm (at 15 min for 30 s) and 420 nm (at 20 min for 1 min). Both samples display the same reaction course, suggesting that irradiation has no significant influence on ImGPS(wt) activity and on the assay used.

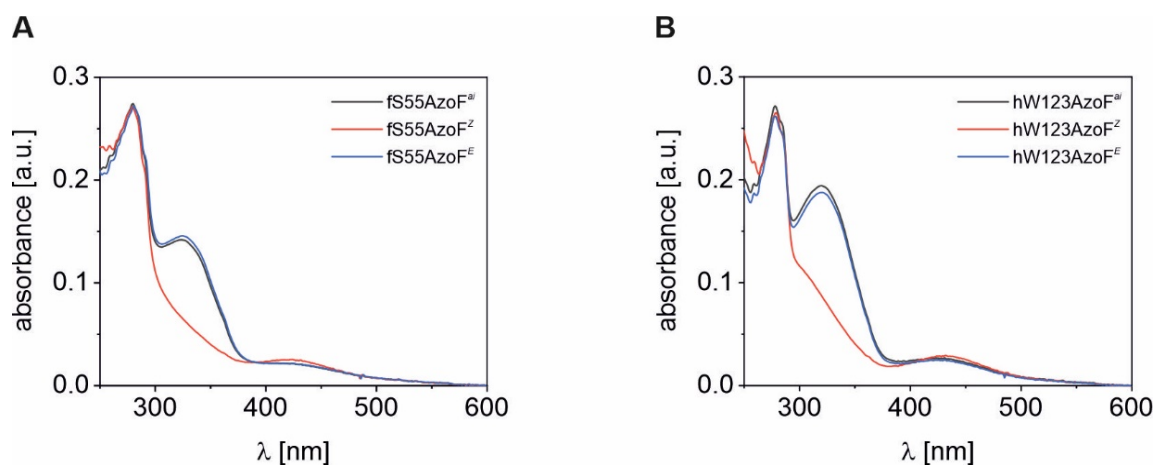


Figure 75. UV/Vis absorption spectra of ImGPS(fS55AzoF) and ImGPS(hW123AzoF), obtained with continuous irradiation. (A) Absorption spectra of 15 μ M non-irradiated fS55AzoF (ai, black), as well as of its *Z* isomer- (red) and *E* isomer-enriched (blue) state. (B) Absorption spectra of 15 μ M non-irradiated hW123AzoF (ai, black), as well as of its *Z* isomer- (red) and *E* isomer-enriched (blue) state. To obtain the *Z* isomer-enriched state, the samples were continuously irradiated with 365 nm for 30 s. To obtain the *E* isomer-enriched state, the samples were continuously irradiated with 420 nm for 1 min.

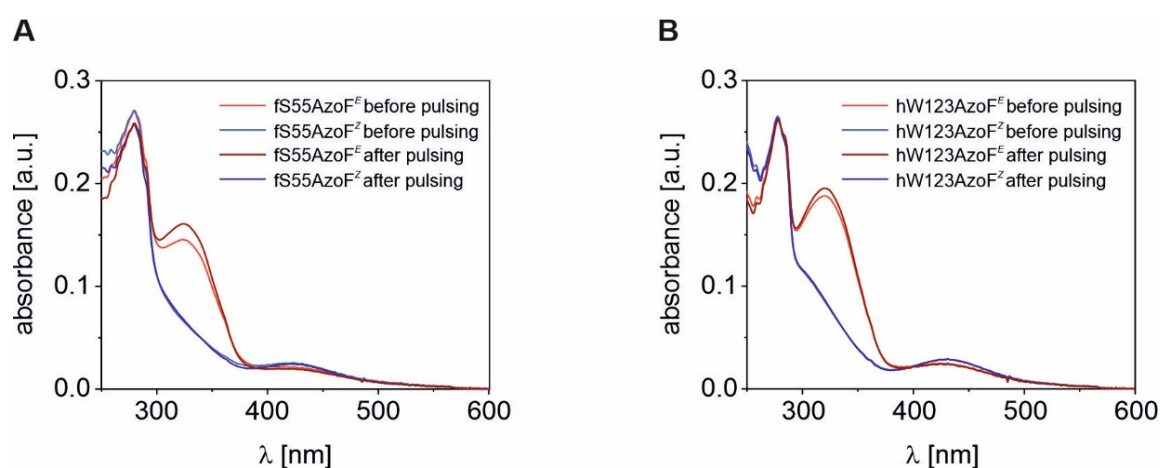


Figure 76. Regeneration of isomer spectra post 1000 Hz pulsing. (A) Absorption spectra of the *E* and *Z* isomer-enriched states of fS55AzoF (15 μ M) before and after pulsing. (B) Absorption spectra of the *E* and *Z* isomer-enriched states of hW123AzoF (15 μ M) before and after pulsing. Alternated pulsing with 365 nm and 420 nm was conducted at 1000 Hz for 20 min. After pulsing, the ability to isomerize between the *Z* and *E* isomers for both fS55AzoF and hW123AzoF was maintained.

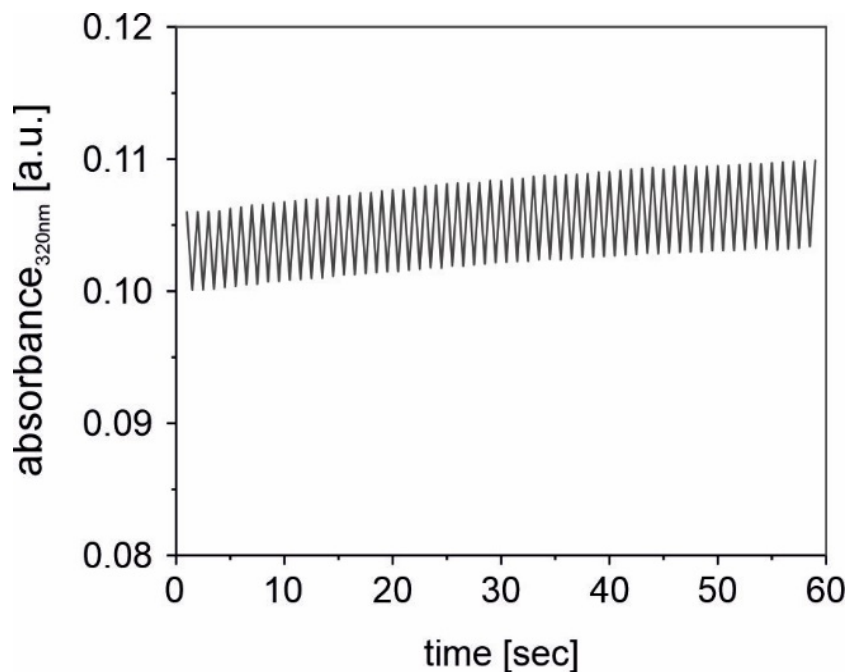


Figure 77. Isomerization of hW123AzoF when exposed to pulsing irradiation. A sample of 10 μM hW123AzoF was pulsed at 1 Hz for 1 min with alternating wavelengths of 365 nm and 420 nm to obtain respective *Z* and *E* isomers. The absorbance was recorded at the absorbance maximum of the *E* isomer (320 nm). Non-quantitative isomerization may be due to the frequency of alternating light or due to the resolution of the online UV/Vis spectrophotometer (0.5 scans/s).

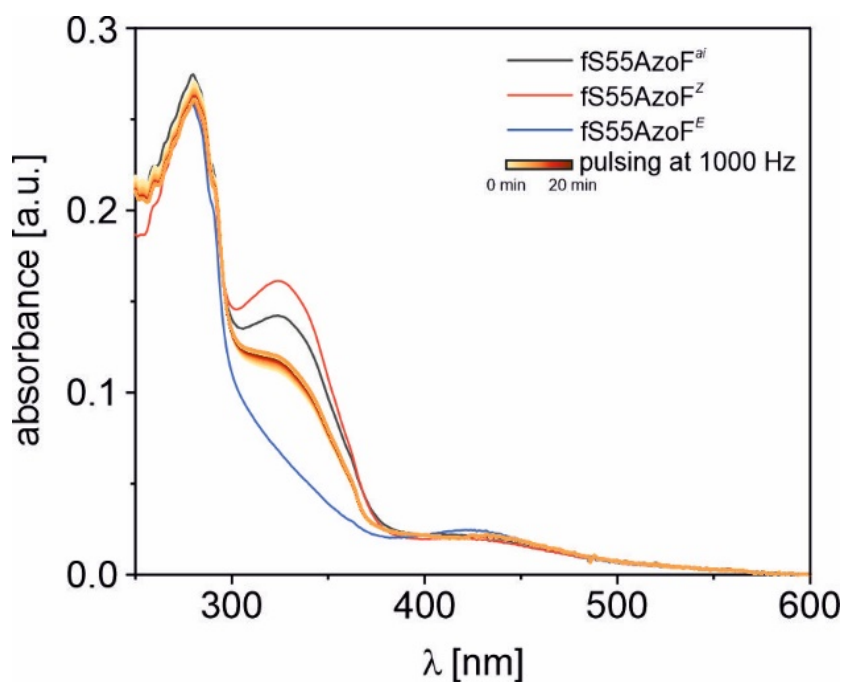


Figure 78. UV/Vis absorbance spectroscopy to evaluate the photophysical effect of pulsing. Pulsing of 15 μ M fS55AzoF with alternating 365/420 nm (1000 Hz) for 20 min. An absorbance spectrum was generated once every 2 seconds. Additional spectra were recorded of the 'as isolated' state (black) prior to pulsing, as well as of the *E* (blue) and *Z* isomers (red) post pulsing.

Table 18. Effects of continuous irradiation with both LEDs on ImGPS(wt) and ImGPS(AzoF).^[a]

Protein	LRF (Continuous irradiation with both LEDs) at rt	LRF (Continuous irradiation with both LEDs) at 20 °C
ImGPS(wt)	1.36	0.64
		0.85
	1.09	1.05
	1.18	0.73
		1.08
ImGPS(fS55AzoF)		0.78
	1.74	0.67
	1.19	1.02
		0.78
		1.06
ImGPS(hW123AzoF)	1.99	0.87
	1.97	0.71
	1.96	1.76
	1.70	2.06
	1.14	1.85

^[a]Data shown are individual repeats of at least two independent experiments, shown to demonstrate the fluctuation in results that occur upon continuous irradiation with both LEDs.

Table 19. Temperature changes to sample solution when exposed to pulsing irradiation (1000 Hz).^[a]

Time [min]	Room temperature [°C]	Temperature when fixed at 40 °C [°C]
0	23.2	39.0
5	25.0	39.0
10	26.4	39.0
15	29.0	39.0
20	29.0	39.0
25	30.0	39.0
30	30.0	39.0

^[a]Temperature changes in a cuvette filled with 700 μL (reaction volume) of 50 mM Tris-HCl (pH 7.5) buffer over a 30 min irradiation period, with temperature obtained every 5 min.

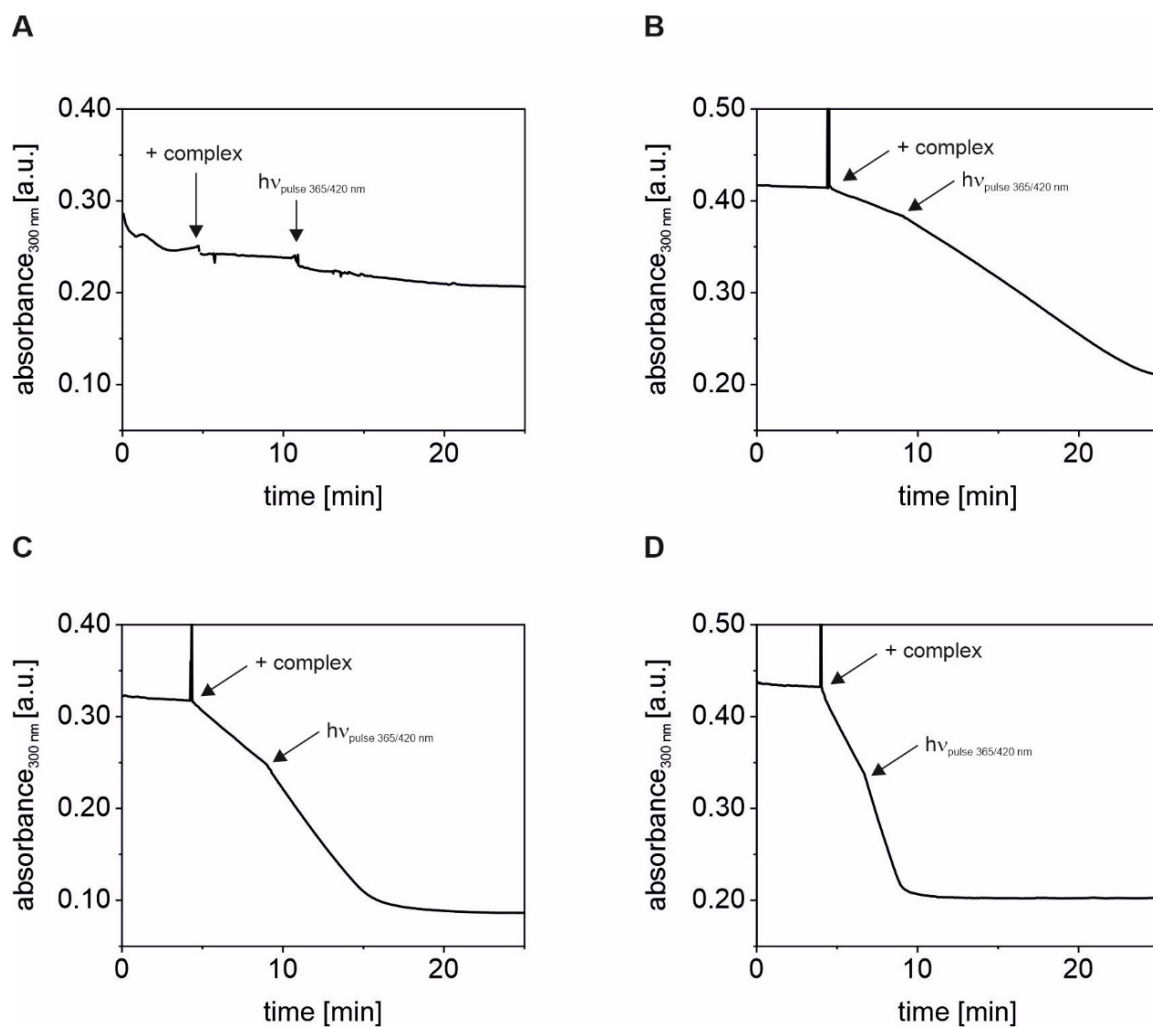
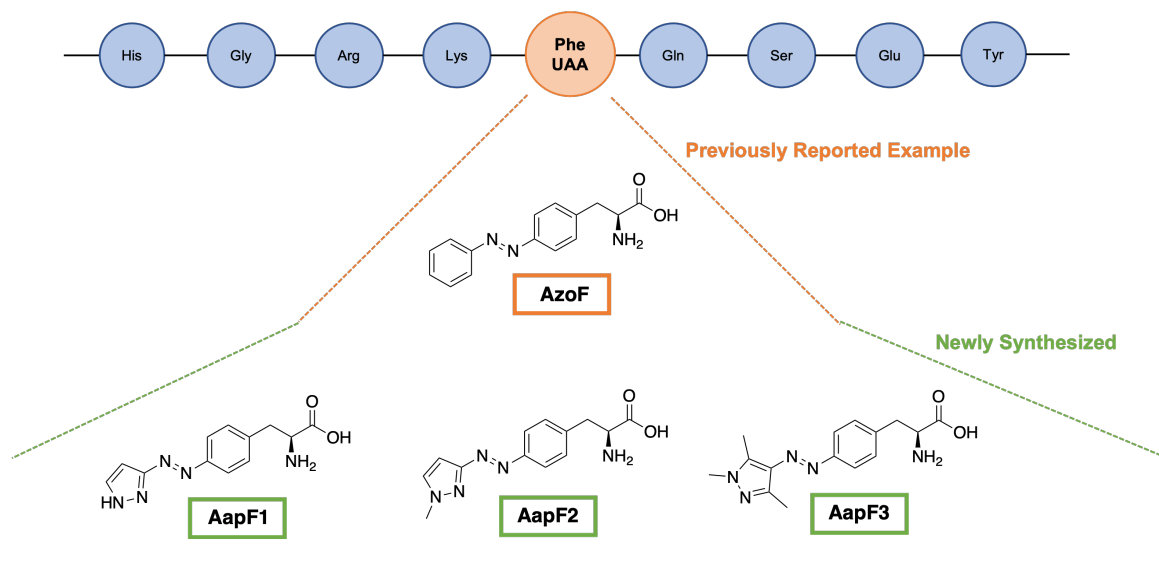


Figure 79. Temperature-controlled ImGPS activity experiments. Reaction curves of ImGPS(hW123AzoF) when pulsed (1000 Hz with 365/420 nm) at a fixed temperature of (A) 4, (B) 20, (C) 30, or (D) 40 °C.

4.7.3 References

- [1] a) M. Bose, D. Groff, J. Xie, E. Brustad, P. G. Schultz, *J. Am. Chem. Soc.* **2006**, *128*, 388-389; b) A. C. Kneutinger, K. Straub, P. Bittner, N. A. Simeth, A. Bruckmann, F. Busch, C. Rajendran, E. Hupfeld, V. H. Wysocki, D. Horinek, B. König, R. Merkl, R. Sterner, *Cell Chem. Biol.* **2019**, *26*, 1501-1514 e1509.
- [2] F. List, M. C. Vega, A. Razeto, Michaela C. Häger, R. Sterner, M. Wilmanns, *Chem. Biol.* **2012**, *19*, 1589-1599.
- [3] A. C. Kneutinger, C. Rajendran, N. A. Simeth, A. Bruckmann, B. König, R. Sterner, *Biochem.* **2020**, *59*, 2729-2742.
- [4] S. Beismann-Driemeyer, R. Sterner, *J. Biol. Chem.* **2001**, *276*, 20387-20396.

5. Expanding the Repertoire of Photoswitchable Unnatural Amino Acids



CHAPTER 5

5.1 Abstract & Introduction

The activity of imidazole glycerol phosphate synthase (ImGPS) was successfully modulated with light via an incorporated azobenzene phenylalanine (AzoF), as discussed in Chapter 4 of this thesis.^[1] Furthermore, the incorporation of AzoF at different positions in the ImGPS complex provided valuable insight into the allosteric activation mechanisms of ImGPS.^[1] Depending on the position of AzoF within ImGPS, isomerization of this unnatural amino acid (UAA) either interfered with existing allostery or induced an allosteric effect that influenced enzyme activity. To date, the current repertoire of reversible photoswitchable UAAs only consists of AzoF and similar derivatives.^[2] Expanding this repertoire to include phenylalanine UAAs with alternative photoswitchable moieties that contain different chemical structures and photophysical properties may provide further insight into the allosteric mechanisms of ImGPS. In addition, expanding this repertoire may be beneficial in obtaining even better photocontrol of ImGPS activity.

This chapter is unpublished work:

The research in this chapter was performed in collaboration with the group of Prof. Dr. Reinhard Sterner (University of Regensburg) and the group of Dr. Andrea Kneuttinger (University of Regensburg).

R. Lahmy, C. Hiefinger, A. Kneuttinger, R. Sterner, B. König.

Author contributions:

RL was responsible for compound design and synthesis procedures. RL and CH synthesized the compounds described in this chapter. CH performed the photophysical evaluations of **AapF1** and **AapF2** (as shown in this chapter), while RL performed thermal half-life measurements and the photophysical evaluations of **AapF3**. AK, RS and BK supervised the project and are the corresponding authors.

5.2 Results and Discussion

5.2.1 Design of Photoswitchable Phenylalanine Derivatives

As thoroughly discussed in Chapter 1 of this thesis, arylazopyrazoles are an alternative photoswitch group to azobenzenes that typically possess superior photophysical properties for biological purposes.^[3] These improved properties characteristically include higher PSS values, red-shifted absorbance bands and longer thermal half-lives of the *cis*-isomers.^[3] As a result, it became of interest to expand on AzoF by developing novel arylazopyrazole phenylalanine (AapF) derivatives (Figure 80).

Furthermore, pyrazole systems differ to 6-membered aromatic benzenes in that they are a five-membered aromatic ring that contain 2 nitrogen atoms.^[4] The presence of these nitrogen atoms may result in further interactions once incorporated into ImGPS, especially for the free amine-containing 3(5)-substituted azo-1*H*-pyrazole system^[5] that may participate in hydrogen bond interactions. As a result, an AapF that contains such a pyrazole system was developed, resulting in **AapF1**. In order to explore AapFs that do not contain an exposed secondary amine, **AapF2** was developed that contained a methyl substitution at position 1 of the pyrazole unit, resulting in a 1-methyl-3-arylazopyrazole system.^[3] The bulkiest AapF developed in this work was **AapF3** that contains a 1,3,5-trimethyl-4-arylazopyrazole system, with 3 methyl substituents on the pyrazole ring.^[3, 6] This AapF was developed due to this system being thoroughly investigated in previous literature and reported to have desirable photophysical properties, including long thermal half-lives of the *cis*-isomers and high photostationary states (PSS).^[3, 6-7]

Hemithioindigo phenylalanine 1 (**HtiF1**) and fulgimide phenylalanine 1 (**FulgF1**) were designed as compounds of interest that differ in chemical structure and/or properties to the arylazopyrazole class of photoswitchable ligands (Figure 80). **HtiF1** is comprised of a phenylalanine amino acid that is attached to a hemithioindigo (Hti) unit. Hti derivatives belong to another class of photoswitchable ligands that has been explored for biological purposes.^[8] These unsymmetrical molecules possess a thioindigo component that is connected to a stilbene component via a double bond. Isomerization of this double bond can be achieved with light, resulting in either the respective *cis*- or *trans*-isomer, depending on the wavelength of light employed.^[9] Importantly, both of these isomers can be accessed with visible light (>400 nm), making them valuable for biological use, as longer wavelengths tend to be less harmful to biological material.^[9-10] Despite having lower quantum yields when

compared to azobenzenes, Hti derivatives offer desirable photophysical properties, including good thermal stabilities and fatigue resistant photoisomerization.^[8-9]

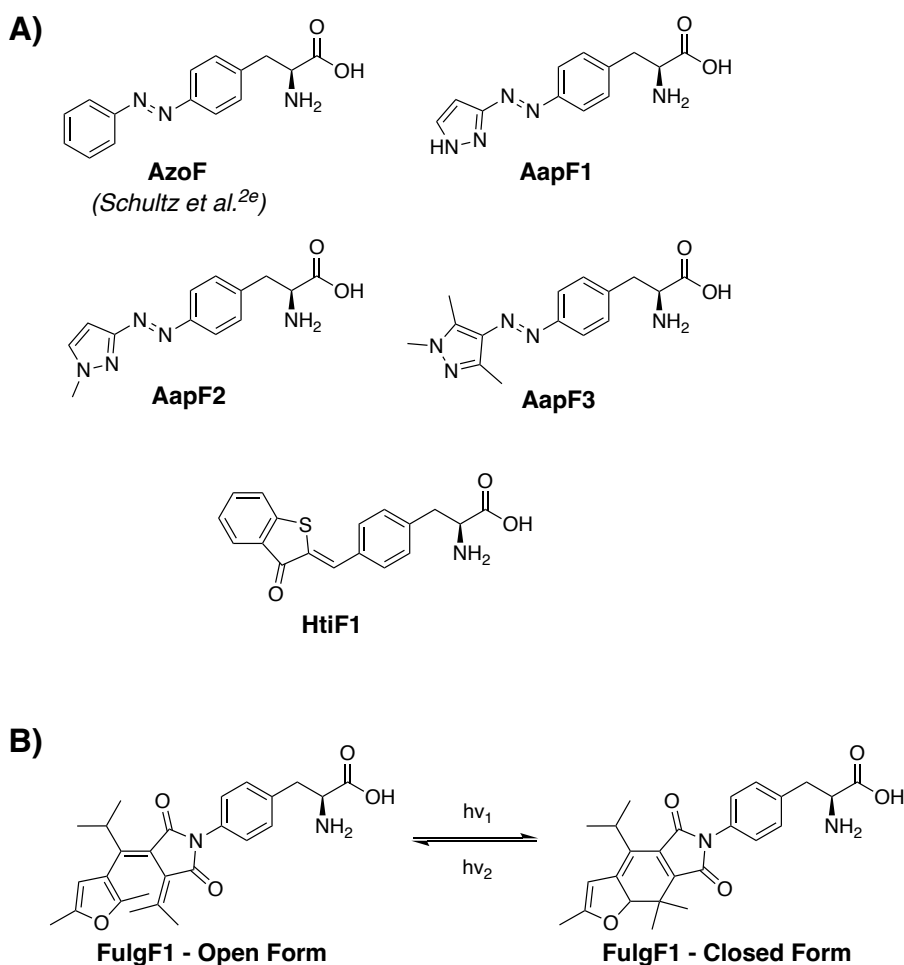


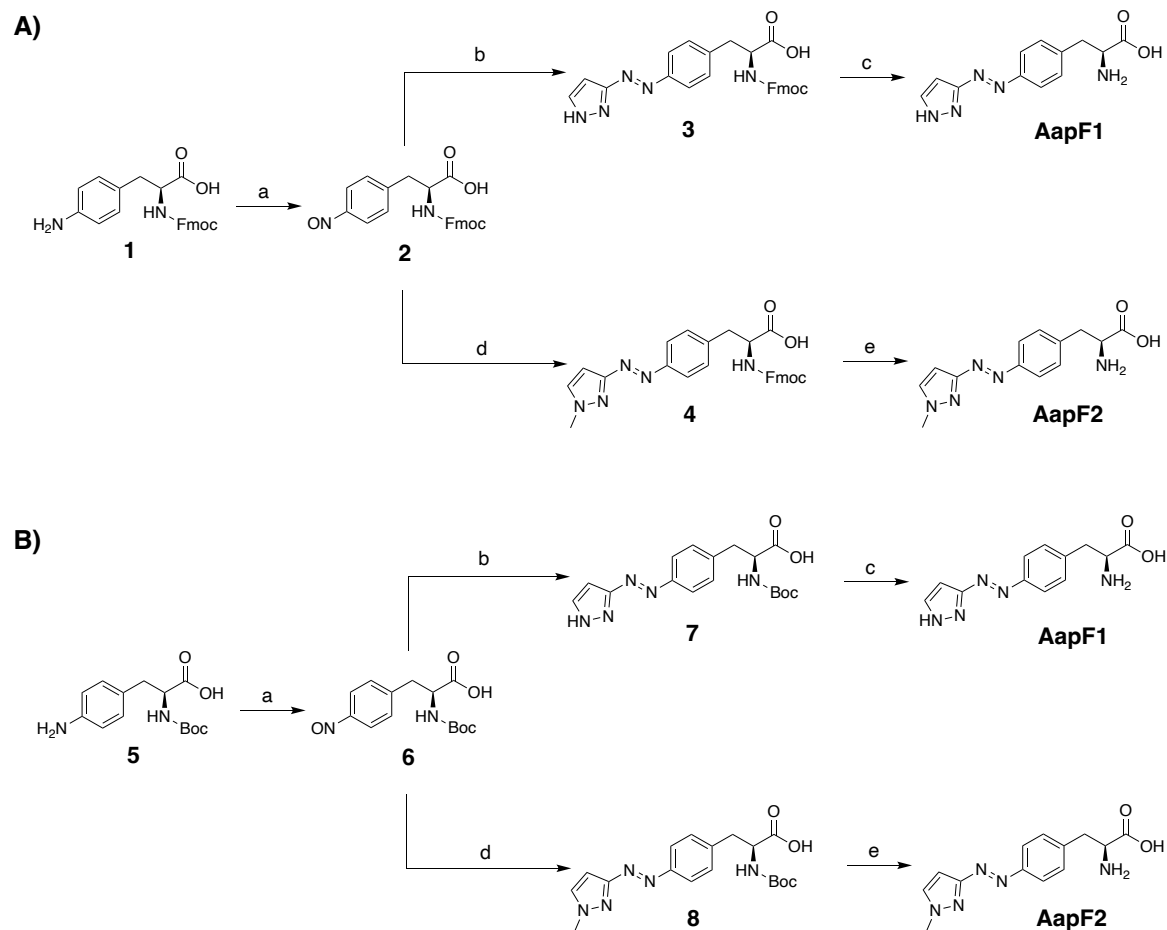
Figure 80. Chemical structures of previously reported AzoF^[2e] and newly designed photoswitchable UAAs. A) Chemical structures of photoisomerizable AzoF^[2e], novel phenylalanine-based arylazopyrazoles **AapF1-3** and hemithioindigo **HtiF1**. B) In addition to isomerization upon exposure to light, fulgimide **FulgF1** undergoes a change in electronic properties.

While hemithioindigos undergo *cis/trans*-isomerization similar to arylazopyrazoles and azobenzenes, fulgimides undergo a change in both structure and electronic properties. Upon exposure to light, fulgimides undergo a conrotatory electrocyclic reaction between an open and closed form that differs in both structure and electronic properties (Figure 80).^[11] Therefore, attaching a fulgimide photoswitch to the benzene moiety of phenylalanine may be beneficial in expanding the repertoire of UAA's. Despite being less explored in photopharmacology, recent papers display the benefits of this photoswitch for biological

applications.^[12] Furthermore, fulgimides offer advantageous photophysical properties, including good thermal stabilities and near-quantitative conversion between open and closed forms. This is discussed in more detail in our recent review.^[11] An isopropoxy substituent on the 1,3,5-hexatriene system was incorporated into the design of **FulgF1**, as this bulky substituent has been previously reported to prevent *cis*-isomerization, allowing exclusive access to the open (*trans*-isomer) and closed form of **FulgF1** upon light exposure.^[13] While both **HtiF1** and **FulgF1** were designed and identified as compounds of interest, completion of the synthesis was outside the scope of this thesis.

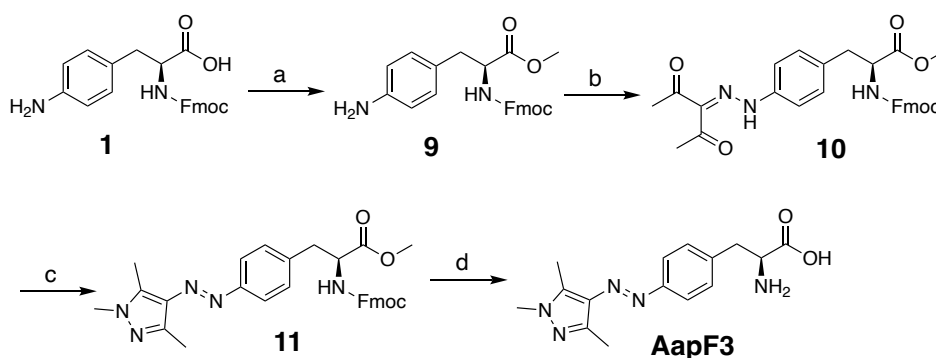
5.2.2 Synthesis of Photoswitchable Phenylalanine Derivatives

The synthesis of **AapF1** and **AapF2** was successfully achieved via the classic Mills reaction.^[14] Two synthesis routes were developed using either an Fmoc-4-amino-L-phenylalanine derivative (Scheme 14A) or a Boc-4-amino-L-phenylalanine derivative (Scheme 14B), which were both commercially available.



Scheme 14. Synthesis of novel phenylalanine-based arylazopyrazoles **AapF1** and **AapF2**. A) Synthesis via an Fmoc-protected phenylalanine starting material. (a) 4-Amino-N-Fmoc-L-phenylalanine, Oxone[®], DCM:H₂O (1:1), 0 °C → rt, 2 h, directly used in next step; (b) 3-Aminopyrazole, AcOH:DCM (1:1), rt, 48 h, overall yield 12%; (c) Piperidine, THF, rt, 16 h, 63%; (d) 3-Amino-1-methyl-1H-pyrazole, AcOH:DCM (1:1), rt, 48 h, overall yield 27%; (e) Piperidine, THF, rt, 16 h, 68%. B) Synthesis via a Boc-protected phenylalanine starting material. (a) 4-Amino-N-Boc-L-phenylalanine, Oxone[®], DCM:H₂O (1:1), 0 °C → rt, 2 h, directly used in next step; (b) 3-Aminopyrazole, AcOH:DCM (1:1), rt, 48 h, overall yield 13%; (c) 4N HCl, dioxane, 0 °C → rt, 16 h, 90%; (d) 3-Amino-1-methyl-1H-pyrazole, AcOH:DCM (1:1), rt, 48 h, overall yield 16%; (e) 4N HCl, dioxane, 0 °C → rt, 16 h, 89%.

Using the former derivative **1**, the secondary amine was oxidized to a nitroso group, using Oxone[®] (Scheme 14A). The nitroso intermediate **2** was directly used in a Mills reaction with 3-aminopyrazole to form the azo-containing intermediate **3** in an overall yield of 12%. The Fmoc group was removed under basic conditions, yielding **AapF1** in 63% yield. To obtain **AapF2**, nitroso **2** was reacted with commercially available 3-amino-1-methyl-1H-pyrazole to obtain intermediate **4** in an overall yield of 27%. Fmoc deprotection then resulted in **AapF2** in 68% yield. A similar procedure was employed for route 2, starting with a Boc-protected phenylalanine derivative **5** (Scheme 14B). The secondary amine of **5** was oxidized to a nitroso group, using Oxone[®]. The nitroso intermediate **6** was directly used in a Mills reaction with 3-aminopyrazole to form the azo-containing intermediate **7** in an overall yield of 13%. The Boc group was then removed under acidic conditions, yielding **AapF1** in 90% yield. To obtain **AapF2**, nitroso **2** was reacted with commercially available 3-amino-1-methyl-1H-pyrazole to obtain intermediate **8** in an overall yield of 16%. Boc deprotection then resulted in **AapF2** in 89% yield.



Scheme 15. Synthesis of novel phenylalanine-based arylazopyrazole **AapF3**. (a) 4-Amino-N-Fmoc-L-phenylalanine, thionyl chloride, MeOH, 0 °C → rt, 18 h, 99%; (b) NaNO₂, H₂O, HCl, AcOH, 0 °C, 45 min, then acetylacetone, NaOAc, EtOH, rt, 1 h, 38%; (c) Methylhydrazine, EtOH, reflux, 3 h, 43%; (d) LiOH·H₂O, THF:H₂O (3:1), rt, 19 h, 41%.

To obtain target compound **AapF3**, the carboxylic acid moiety of the commercially available starting material **1** was protected by esterification. This resulted in methyl ester **9** in quantitative yield (Scheme 15). Intermediate **9** was then utilized in a diazotisation reaction to obtain diketone **10** in 38% yield. This was followed by a condensation reaction that successfully resulted in azopyrazole **11** in 43% yield. Subsequent treatment with lithium hydroxide, resulted in both Fmoc deprotection and ester hydrolysis, obtaining **AapF3** in 41% yield.

5.2.3 Photophysical Investigations

Once synthesized, the photophysical properties of **AapF1**, **AapF2** and **AapF3** were evaluated. This involved obtaining UV/Vis absorption spectra of thermal equilibrium, *trans*- and *cis*-isomers, as well as evaluating thermal stability of the *cis*-isomer, PSS and cycle performance (Table 20, Figure 81 and Supplementary Information).

Table 20. Summary of experimental photophysical properties.^[a]

Compound	Solvent	PSS	PSS	PSS	t _{1/2} [days] <i>cis</i> -isomer ^[c]
		Therm. eq. <i>trans</i> : <i>cis</i> ^[b]	<i>cis</i> → <i>trans</i> <i>trans</i> : <i>cis</i> ^[b]	<i>trans</i> → <i>cis</i> <i>trans</i> : <i>cis</i> ^[b]	
AapF1	DMSO	95:5	69:31	8:92	6.0
AapF1	Buffer ^[d]	94:6	66:34	6:94	12.2
AapF2	DMSO	74:26	65:35	7:93	21.3
AapF2	Buffer ^[d]	75:25	61:39	10:90	17.4
AapF3	DMSO	93:7	92:8	4:96	4.4
AapF3	Buffer ^[d]	98:2	92:8	3:97	7.5

^[a]Isomerization was obtained by irradiation with 365 nm (*cis*-isomer) and 420 nm (*trans*-isomer **AapF1** and **AapF2**) or 528 nm (*trans*-isomer **AapF3**) at 25 °C. ^[b]PSS was determined by HPLC measurements. ^[c] Experiment was performed at 27 °C. ^[d] Buffer solution (TrisHCl Buffer, pH 7.5) + 0.2% or 0.5% DMSO, see Supplementary Information.

AapF1, **AapF2** and **AapF3** displayed slightly differing photophysical properties. Isomerization to the respective *cis*-isomers of **AapF1** and **AapF2** was achieved with 365 nm irradiation, while their respective *trans*-isomers were accessed with 420 nm. Even though the *cis*-isomer of **AapF3** was similarly accessed with 365 nm irradiation, a shift of the n-π* transition allowed for photoisomerization from *cis*- to *trans*-isomer with the desirable red-shifted wavelength of 528 nm (Figure 81). Further differences between these arylazopyrazoles could be observed when examining PSS values. Even though all compounds displayed high PSS values (>90%) upon photoisomerization to their respective *cis*-isomers, only **AapF3** displayed a high PSS value of more than 90% upon photoisomerization to the *trans*-isomer (Table 20).

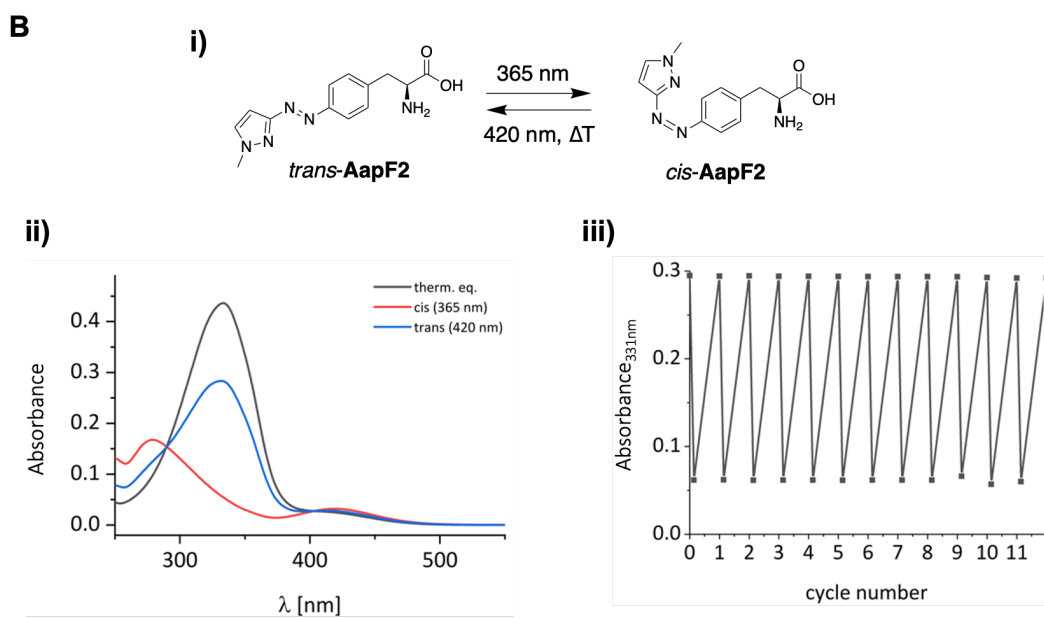
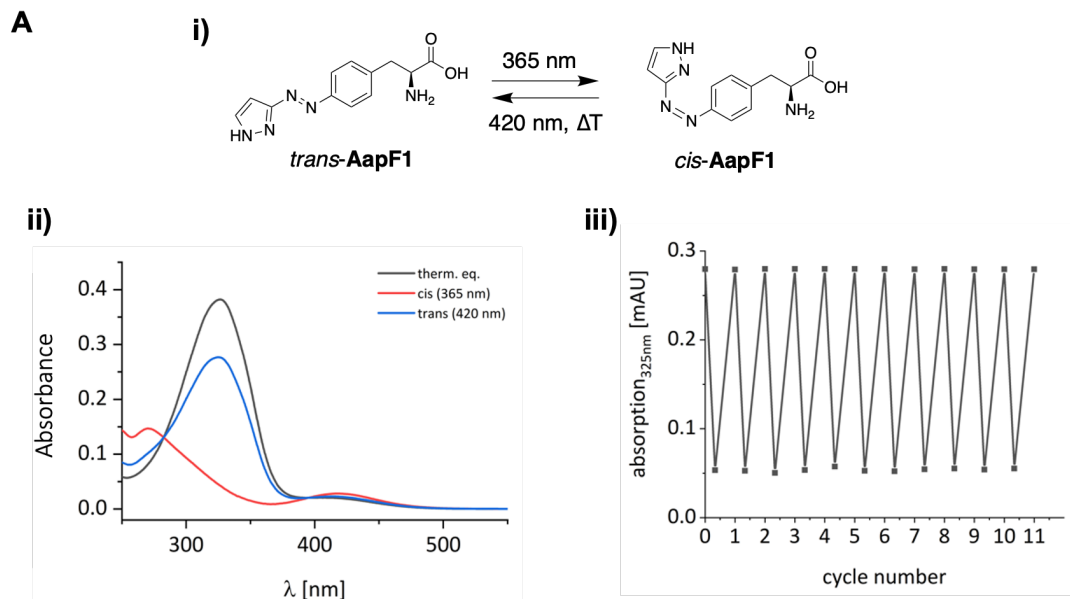


Figure continues on next page

Figure continued from previous page

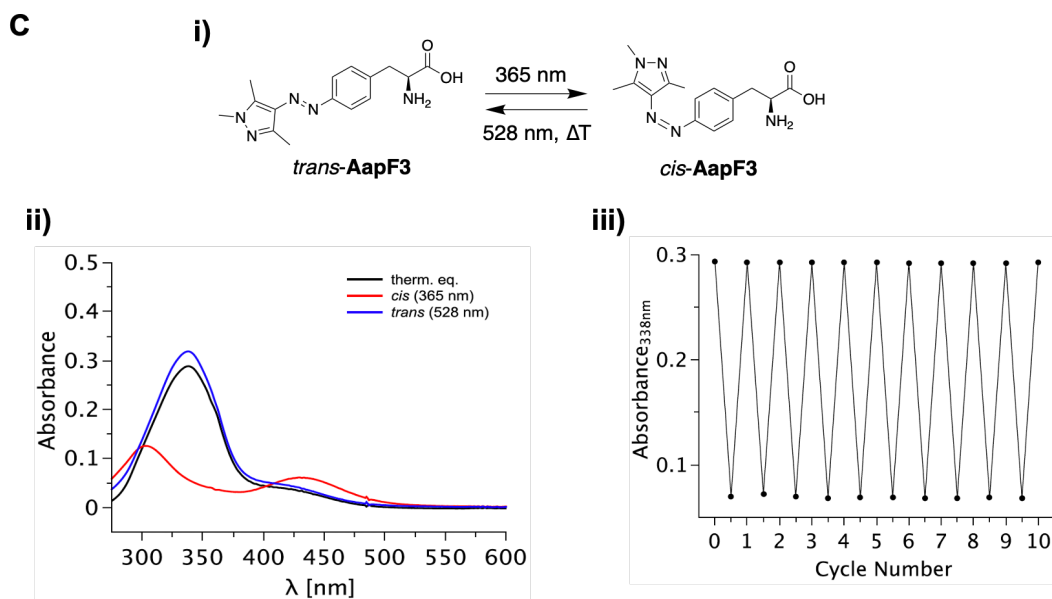


Figure 81. Photophysical analysis of **AapF1** (A), **AapF2** (B) and **AapF3** (C) in buffer solution. i) Depiction of geometrical changes that occur upon photoinduced isomerization. ii) UV/Vis absorption spectra of thermal equilibrium, *trans*-isomer and *cis*-isomer. iii) Cycle performance (at least 10 cycles) upon alternating irradiation of 365 nm (*cis*-isomer) and 420 nm (*trans*-isomer **AapF1** and **AapF2**) or 528 nm (*trans*-isomer **AapF3**), recorded at the absorbance maximum of the respective *trans*-isomer. Results are shown of AapF (20 μ M) in buffer solution (TrisHCl Buffer, pH 7.5) + 0.2% DMSO at 25 $^{\circ}$ C.

The poorer PSS values for *trans*-isomerization of **AapF1** and **AapF2** can be attributed to a greater overlap of the π - π^* and n - π^* transitions, and as a result, quantitative switching could not be obtained. Due to this, these compounds exhibited a higher abundance of their respective *trans*-isomers in thermal equilibrium (Table 20). Each AapF in this series exhibited long thermal half-lives of their respective *cis*-isomers, ranging from 4 to 21 days in both DMSO and buffer solution (Table 20). In particular, **AapF2** exhibited the longest thermal half-life of 21.3 days and 17.4 days in DMSO and buffer solution, respectively. In addition, **AapF1**, **AapF2** and **AapF3** all exhibited excellent resistance to cycle fatigue, as toggling between *trans*- and *cis*-isomers was achieved for at least 10 cycles (Figure 81 and Supplementary Information).

5.3 Conclusion and Outlook

In this work, novel phenylalanine-based photoswitchable compounds were designed and synthesized that differed in chemical structure and/or photophysical properties. Arylazopyrazole-containing **AapF1**, **AapF2** and **AapF3** were successfully synthesized via two methods, both only requiring a 3-step synthesis. Photophysical evaluations suggested that **AapF1**, **AapF2** and **AapF3** all displayed desirable photophysical properties for incorporation into and investigation of ImGPS. These desirable properties included long thermal half-lives of the respective *cis*-isomers and fatigue resistant photoisomerization. **AapF3** displayed slightly superior photophysical properties when compared to **AapF2** and **AapF3**. This included a desirable red-shifted absorbance band of the **AapF3** *cis*-isomer, allowing for 528 nm irradiation to be utilized for *trans*-isomerization instead of 420 nm that is required for the other arylazopyrazoles in this series. This absorbance band shift also allowed for higher PSS values to be obtained for *trans*-**AapF3**. Due to the differences in chemical properties, each of the AapFs represent novel UAAs that may provide differing interactions once incorporated into the target protein. In order to further investigate the allosteric mechanisms of ImGPS and to achieve further photocontrol of ImGPS, experiments are currently being performed by CH in the lab of RS and AK (Faculty of Biology and Preclinical Medicine, University of Regensburg). These experiments involve incorporating **AapF1**, **AapF2** and **AapF3** into ImGPS, and performing follow up experiments to achieve photocontrol of this enzyme, similar to that previously described in literature work.^[1]

5.4 Acknowledgements

This work was supported by the Deutsche Forschungsgemeinschaft, RTG 1910, and a Minerva PhD Fellowship to RL.

5.5 References

- [1] a) A. C. Kneuttinger, C. Rajendran, N. A. Simeth, A. Bruckmann, B. König, R. Sterner, *Biochem.* **2020**, *59*, 2729-2742; b) A. C. Kneuttinger, K. Straub, P. Bittner, N. A. Simeth, A. Bruckmann, F. Busch, C. Rajendran, E. Hupfeld, V. H. Wysocki, D. Horinek, B. König, R. Merkl, R. Sterner, *Cell Chem. Biol.* **2019**, *26*, 1501-1514.e1509.
- [2] a) N. Muranaka, T. Hohsaka, M. Sisido, *FEBS Lett.* **2002**, *510*, 10-12; b) J. Luo, S. Samanta, M. Convertino, N. V. Dokholyan, A. Deiters, *Chembiochem* **2018**, *19*, 2178-2185; c) A. A. John, C. P. Ramil, Y. Tian, G. Cheng, Q. Lin, *Org. Lett.* **2015**, *17*, 6258-6261; d) C. Hoppmann, L. Wang, *Meth. Enzymol.* **2019**, *624*, 249-264; e) M. Bose, D. Groff, J. Xie, E. Brustad, P. G. Schultz, *J. Am. Chem. Soc.* **2006**, *128*, 388-389; f) A. C. Kneuttinger, *Biol. Chem.* **2022**, *403*, 573-613.
- [3] J. Calbo, C. E. Weston, A. J. P. White, H. S. Rzepa, J. Contreras-García, M. J. Fuchter, *J. Am. Chem. Soc.* **2017**, *139*, 1261-1274.
- [4] N. E. Santos, A. R. F. Carreira, V. L. M. Silva, S. S. Braga, *Molecules* **2020**, *25*, 1364.
- [5] K. Rustler, P. Nitschke, S. Zahnbrecher, J. Zach, S. Crespi, B. König, *J. Org. Chem.* **2020**, *85*, 4079-4088.
- [6] C. E. Weston, R. D. Richardson, P. R. Haycock, A. J. White, M. J. Fuchter, *J. Am. Chem. Soc.* **2014**, *136*, 11878-11881.
- [7] L. Stricker, M. Böckmann, T. M. Kirse, N. L. Doltsinis, B. J. Ravoo, *Chem. Eur. J.* **2018**, *24*, 8639-8647.
- [8] a) A. Sailer, F. Ermer, Y. Kraus, F. H. Lutter, C. Donau, M. Bremerich, J. Ahlfeld, O. Thorn-Seshold, *Chembiochem* **2019**, *20*, 1305-1314; b) C. Petermayer, H. Dube, *Acc. Chem. Res.* **2018**, *51*, 1153-1163.
- [9] S. Wiedbrauk, H. Dube, *Tetrahedron Lett.* **2015**, *56*, 4266-4274.
- [10] W. A. Velema, W. Szymanski, B. L. Feringa, *J. Am. Chem. Soc.* **2014**, *136*, 2178-2191.
- [11] D. Lachmann, R. Lahmy, B. König, *Eur. J. Org. Chem.* **2019**, *2019*, 5018-5024.
- [12] a) D. Wutz, D. Gluhacevic, A. Chakrabarti, K. Schmidtkunz, D. Robaa, F. Erdmann, C. Romier, W. Sippl, M. Jung, B. König, *Org. Biomol. Chem.* **2017**, *15*, 4882-4896; b) D. Lachmann, C. Studte, B. Männel, H. Hübner, P. Gmeiner, B. König, *Chemistry* **2017**, *23*, 13423-13434; c) N. A. Simeth, L.-M. Altmann, N. Wössner, E. Bauer, M. Jung, B. König, *J. Org. Chem.* **2018**, *83*, 7919-7927; d) K. Rustler, G. Maleeva, A. M. J. Gomila, P. Gorostiza, P. Bregestovski, B. König, *Chemistry* **2020**, *26*, 12722-12727.
- [13] F. Strübe, R. Siewertsen, F. D. Sönnichsen, F. Renth, F. Temps, J. Mattay, *Eur. J. Org. Chem.* **2011**, *2011*, 1947-1955.
- [14] a) M. Schönberger, D. Trauner, *Angew. Chem. Int. Ed. Engl.* **2014**, *53*, 3264-3267; b) H. U. R. Shah, K. Ahmad, H. A. Naseem, S. Parveen, M. Ashfaq, T. Aziz, S. Shaheen, A. Babras, A. Shahzad, *J. Mol. Struct.* **2021**, *1244*, 131181.

5.6 Supplementary Information

5.6.1 Supplementary Chemical Information

5.6.1.1 Materials and Methods

Commercial reagents were obtained from Merck, Sigma-Aldrich, TCI Deutschland GmbH, ABCR GmbH or Fluorochem, and were used without further purification. Solvents were used in P.A. quality and if necessary, dried according to common procedures. Anhydrous reactions were performed using dried glassware under a nitrogen or argon atmosphere, unless otherwise specified. The development of **AapF1**^[1], **AapF2**^[2], and **AapF3**^[2-3] were based on previous literature. Technical grade solvents were used for column chromatography without further purification. Flash chromatography was performed using Biotage Isolera One System for normal phase chromatography, using Davisil Chromatographic Silica Media 60 Å (particle size 40-63 µM, Merck). For reversed phase chromatography, Biotage SNAP Cartridges KP-C18-HS were used. Analytical thin layer chromatography (TLC) was performed on silica gel 60 F-254 with a 0.2 mm layer and aluminium-backed plates (Merck). Visualization was obtained by fluorescence quenching under UV light (short and long wave) and/or by staining the plate with potassium permanganate stain (60 mM KMnO₄, 480 mM K₂CO₃ and 5% w/v NaOH) and vanillin-H₂SO₄ solution (0.5 g vanillin, 85 mL ethanol, 10 mL conc. acetic acid, 3 mL conc. H₂SO₄). Preparative high-performance liquid chromatography (HPLC) was performed using Agilent 1100 Series with a Phenomenex Luna 10 µM C18 column (100 Å, 250 x 21.2 mm) and a solvent flow rate of 20 mL/min. Analytic HPLC measurements were performed using Agilent 1220 Infinity LC System (column: Phenomenex Luna, 3 µM C18(2), 100 Å 150 x 2.00 mm). All biologically tested compounds possessed a purity of ≥ 95%, which was determined by analytical HPLC with wavelength detections of 220 nm and 254 nm. Infrared (IR) Spectroscopy was recorded using Agilent Cary 630 FTIR instrument. NMR spectra were recorded on a Bruker Avance III HD 600 (¹H 600.25 MHz, ¹³C 150.95 MHz, T = 300 K), with solvents specified. The chemical shifts were reported as δ values in parts per million (ppm), referenced to the appropriate and specified solvent peak. Resonance multiplicity is abbreviated as: 's' (singlet), 'd' (doublet), 't' (triplet), 'q' (quartet) and 'm' (multiplet). J-coupling constants (J) were recorded in Hz. Mass spectra were recorded using Finnigan MAT-SSQ 710 A, ThermoQuest Finnigan TSQ 7000, Agilent 6540 UHD Q-TOF, or a JeolAccuTOF GCX instrument.

5.6.1.2 Chemistry Synthesis Procedures

General Procedure 1: Nitroso formation^[4]

To a solution of amino acid (1.00 eq.) in DCM (15.0 mL/mmol) at 0 °C, oxone (potassium peroxymonosulfate) (1.00 eq.) in water (15.0 mL/mmol) was added. The orange, biphasic suspension was allowed to stir at 0 °C for 1 h, then for another 1 h at room temperature. Afterwards, the aqueous phase was decanted, and the organic phase was washed with water (2 x 30.0 mL), followed by decantation. The resulting organic mixture was used directly in the next step, unless otherwise specified.

General Procedure 2: Mills coupling^[4]

Following nitroso formation, glacial AcOH (15.0 mL/mmol) and respective pyrazole (1.50 eq.) were added to the previously formed nitroso intermediate, and the orange solution was allowed to stir for 48 h in dark conditions and under argon atmosphere. The solvent was then removed *in vacuo*. The crude product was subjected to automated flash column chromatography, eluting at 100% DCM (0.1% AcOH) to 10% MeOH/DCM (0.1% AcOH). The product was then further purified by reverse phase column chromatography (solvent A: H₂O [0.05 Vol% TFA], solvent B: MeCN; gradient A/B: 0/100 to 100/0).

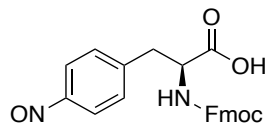
General Procedure 3: Deprotection of the Fmoc-protecting group

To a stirred solution of amino acid (1.00 eq.) in THF (30.0 mL/mmol), piperidine (50.0 eq.) was added and the mixture was allowed to stir for 7 h at room temperature. The reaction mixture was then concentrated *in vacuo* and purified by reverse phase column chromatography (solvent A: H₂O [0.05 Vol% TFA], solvent B: MeCN; gradient A/B: 0/100 to 100/0).

General Procedure 4: Deprotection of the Boc-protecting group

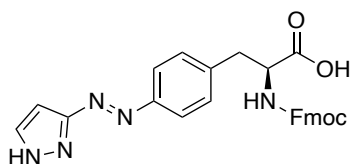
To a stirred solution of the Boc-protected amine (1.00 eq.) in dioxane (4.00 mL/mmol), 4N HCl (1.33 mL/mmol) was added dropwise at 0 °C. The reaction mixture was allowed to stir at room temperature for 16 h. Toluene (2.00 mL/mmol) was then added, and the solvents were removed *in vacuo*. The crude product was triturated with diethyl ether (3 x 2.00 mL/mmol) and subsequently purified by reverse phase column chromatography (solvent A: H₂O [0.05 Vol% TFA], solvent B: MeCN; gradient A/B: 0/100 to 100/0).

(*S*)-2-(((9*H*-fluoren-9-yl)methoxy)carbonyl)amino)-3-(4-nitrophenyl)propanoic acid (2**)**

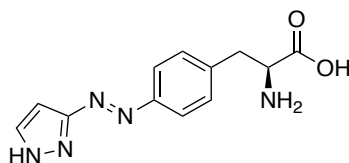


General Procedure 1 was followed, using commercially available Fmoc-4-amino-L-phenylalanine (1.00 g, 2.48 mmol). The crude product **2** was directly used in the next step without further purification.

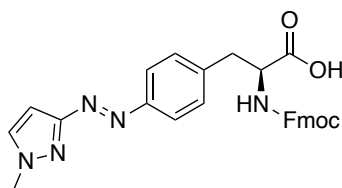
(*S,E*)-3-(4-((1*H*-pyrazol-3-yl)diazanyl)phenyl)-2-(((9*H*-fluoren-9-yl)methoxy)carbonyl)amino)propanoic acid (3**)**



General Procedure 2 was followed, using the previous nitroso intermediate **2** (1.03 g, 2.47 mmol) and 3-aminopyrazole (0.235 mL, 3.71 mmol, 1.50 eq.), without normal phase column chromatography purification, to obtain **3** as a yellow solid (139 mg, 0.289 mmol, 12%). ¹H-NMR (400 MHz, DMSO-*D*₆): δ (ppm) = 7.87-7.85 (m, 3H), 7.81-7.76 (m, 2H), 7.63 (t, *J* = 7.09 Hz, 2H), 7.51-7.46 (m, 2H), 7.41-7.36 (m, 2H), 7.32-7.25 (m, 2H), 6.55 (d, *J* = 2.32 Hz, 1H), 4.27-4.15 (m, 4H), 3.21-3.16 (m, 1H), 3.00-2.94 (m, 1H). ¹³C-NMR (101 MHz, DMSO-*D*₆): δ = 173.13, 155.95, 150.86, 143.75, 143.70, 141.66, 140.67, 130.18, 127.59, 127.04, 125.23, 125.17, 122.16, 120.09, 65.59, 55.19, 46.55, 36.26. ESI-MS (*m/z*): [*M*+*H*]⁺ found: 482.1828

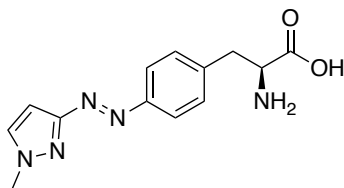
(*S,E*)-3-(4-((1*H*-pyrazol-3-yl)diazenyl)phenyl)-2-aminopropanoic acid (AapF1)

General Procedure 3 was followed, using intermediate **3** (100 mg, 0.208 mmol) to obtain target compound **AapF1** as a yellow solid (34.0 mg, 0.131 mmol, 63%). ¹H-NMR (400 MHz, MeOD): δ (ppm) = 7.91 (d, J = 8.36 Hz, 2H), 7.73 (d, J = 2.52 Hz, 1H), 7.49 (d, J = 8.36 Hz, 2H), 6.67 (d, J = 2.52 Hz, 1H), 4.32-4.28 (m, 1H), 3.43-3.38 (m, 1H), 3.28-3.22 (m, 1H). ¹³C-NMR (101 MHz, MeOD): δ = 171.27, 164.71, 153.57, 139.38, 132.47, 131.48, 124.31, 95.41, 55.06, 37.20. HR-ESI-MS (m/z): [M+H]⁺ calculated: 260.1142; found: 260.1143.

(*S,E*)-2-((((9*H*-fluoren-9-yl)methoxy)carbonyl)amino)-3-(4-((1-methyl-1*H*-pyrazol-3-yl)diazenyl)phenyl)propanoic acid (4**)**

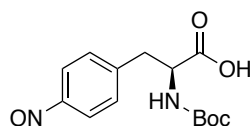
General Procedure 2 was followed, using the previous nitroso intermediate **2** (1.03 g, 2.47 mmol) and 3-amino-1-methyl-1*H*-pyrazole (0.322 mL, 3.71 mmol, 1.50 eq.) to obtain **4** as a yellow solid (335 mg, 0.676 mmol, 27%). ¹H-NMR (400 MHz, MeOD): δ (ppm) = 7.82-7.75 (m, 4H), 7.65 (d, J = 2.36 Hz, 1H), 7.57 (d, J = 7.44 Hz, 2H), 7.41-7.32 (m, 4H), 7.28-7.23 (m, 2H), 6.60 (d, J = 2.40 Hz, 1H), 4.51-4.47 (m, 1H), 4.35-4.22 (m, 2H), 4.15 (t, J = 6.83 Hz, 1H), 4.01 (s, 3H), 3.33-3.28 (m, 1H), 3.06-3.00 (m, 1H). ¹³C-NMR (101 MHz, MeOD): δ = 174.82, 164.92, 158.39, 152.91, 145.24, 145.15, 142.70, 142.55, 134.09, 131.28, 128.74, 128.15, 126.24, 126.16, 123.79, 120.86, 96.09, 67.89, 56.50, 49.64, 49.29, 39.63, 38.35. ESI-MS (m/z): [M+H]⁺ found: 496.1989.

(*S,E*)-2-amino-3-(4-((1-methyl-1*H*-pyrazol-3-yl)diazenyl)phenyl)propanoic acid (AapF2)



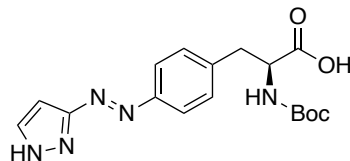
General Procedure 3 was followed, using intermediate **4** (300 mg, 0.605 mmol) to obtain target compound **AapF2** as a yellow solid (112 mg, 0.410 mmol, 68%). ¹H-NMR (400 MHz, MeOD): δ (ppm) = 7.89 (d, J = 8.40 Hz, 2H), 7.67 (d, J = 2.48 Hz, 1H), 7.48 (d, J = 8.40 Hz, 2H), 6.61 (d, J = 2.48 Hz, 1H), 4.31-4.28 (m, 1H), 4.01 (s, 3H), 3.43-3.38 (m, 1H), 3.27-3.21 (m, 1H). ¹³C-NMR (101 MHz, MeOD): δ = 171.32, 164.85, 153.56, 139.40, 134.19, 131.48, 124.28, 96.14, 55.11, 39.69, 37.22. HR-ESI-MS (m/z): [M+H]⁺ calculated: 274.1299; found: 274.1302.

(*S*)-2-((*tert*-butoxycarbonyl)amino)-3-(4-nitrosophenyl)propanoic acid (6**)**



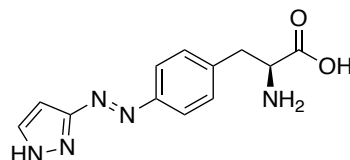
General Procedure 1 was followed, using commercially available Boc-4-amino-L-phenylalanine (2.00 g, 7.13 mmol). The crude product **6** was used directly in the next step without further purification.

(*S,E*)-3-(4-((1*H*-pyrazol-3-yl)diazenyl)phenyl)-2-((*tert*-butoxycarbonyl)amino)propanoic acid (7**)**

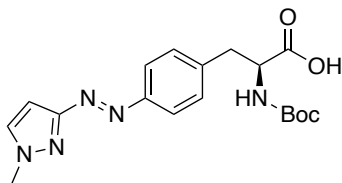


General Procedure 2 was followed, using the previous nitroso intermediate **6** (2.10 g, 7.14 mmol) and 3-aminopyrazole (0.679 mL, 10.7 mmol, 1.5 eq.), without normal phase column chromatography purification, to obtain **7** as a yellow solid (324 mg, 0.901 mmol, 13%). ¹H-NMR (400 MHz, MeOD): δ (ppm) = 7.84 (d, J = 8.25 Hz, 2H), 7.72 (d, J = 2.52 Hz, 1H), 7.42 (d, J = 8.29 Hz, 2H), 6.66 (d, J = 2.52 Hz, 1H), 4.44-4.40 (m, 1H), 3.29-3.24 (m, 1H), 3.03-2.98 (m, 1H), 1.38 (s, 9H). ¹³C-NMR (101 MHz, MeOD): δ = 175.09, 152.94, 142.77, 132.55, 131.31, 123.74, 95.43, 80.57, 56.08, 38.60, 28.66. ESI-MS (m/z): [M+H]⁺ found: 360.1672.

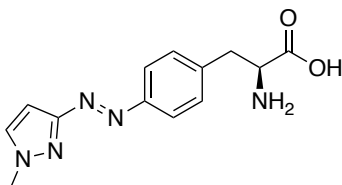
(*S,E*)-3-(4-((1*H*-pyrazol-3-yl)diazenyl)phenyl)-2-aminopropanoic acid (AapF1**)**



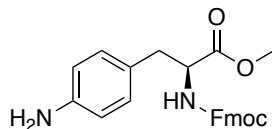
General Procedure 4 was followed, using intermediate **7** (300 mg, 0.835 mmol) to obtain target compound **AapF1** as a yellow solid (195 mg, 0.752 mmol, 90%). ¹H-NMR (400 MHz, MeOD): δ (ppm) = 7.91 (d, J = 8.36 Hz, 2H), 7.73 (d, J = 2.52 Hz, 1H), 7.49 (d, J = 8.36 Hz, 2H), 6.67 (d, J = 2.52 Hz, 1H), 4.32-4.28 (m, 1H), 3.43-3.38 (m, 1H), 3.28-3.22 (m, 1H). ¹³C-NMR (101 MHz, MeOD): δ = 171.27, 164.71, 153.57, 139.38, 132.47, 131.48, 124.31, 95.41, 55.06, 37.20. HR-ESI-MS (m/z): [M+H]⁺ calculated: 260.1142; found: 260.1143.

(*S,E*)-2-((*tert*-butoxycarbonyl)amino)-3-(4-((1-methyl-1*H*-pyrazol-3-yl)diazenyl)phenyl)propanoic acid (8**)**

General Procedure 2 was followed, using the previous nitroso intermediate **6** (2.10 g, 7.14 mmol) and 3-amino-1-methyl-1*H*-pyrazole (0.928 mL, 10.7 mmol, 1.50 eq.) to obtain **8** as a yellow solid (420 mg, 1.12 mmol, 16%). ¹H-NMR (400 MHz, DMSO-*D*₆): δ (ppm) = 7.82 (d, *J* = 2.40 Hz, 1H), 7.75 (d, *J* = 8.33 Hz, 2H), 7.44 (d, *J* = 8.33 Hz, 2H), 6.52 (d, *J* = 2.44 Hz, 1H), 4.20-4.14 (m, 1H), 3.97 (s, 3H), 3.14-3.09 (m, 1H), 2.95-2.89 (m, 1H), 1.31 (s, 9H). ¹³C-NMR (101 MHz, DMSO-*D*₆): δ = 173.40, 163.01, 155.45, 150.84, 141.79, 133.09, 130.18, 122.08, 94.48, 78.11, 54.86, 36.31, 28.13. ESI-MS (*m/z*): [*M*+*H*]⁺ found: 374.1829.

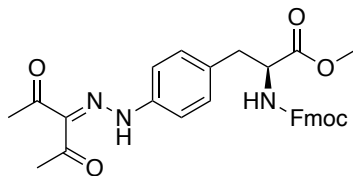
(*S,E*)-2-amino-3-(4-((1-methyl-1*H*-pyrazol-3-yl)diazenyl)phenyl)propanoic acid (AapF2**)**

General Procedure 4 was followed, using intermediate **8** (400 mg, 1.07 mmol) to obtain target compound **AapF2** as a yellow solid (262 mg, 0.959 mmol, 89%). ¹H-NMR (400 MHz, MeOD): δ (ppm) = 7.89 (d, *J* = 8.40 Hz, 2H), 7.67 (d, *J* = 2.48 Hz, 1H), 7.48 (d, *J* = 8.40 Hz, 2H), 6.61 (d, *J* = 2.48 Hz, 1H), 4.31-4.28 (m, 1H), 4.01 (s, 3H), 3.43-3.38 (m, 1H), 3.27-3.21 (m, 1H). ¹³C-NMR (101 MHz, MeOD): δ = 171.32, 164.85, 153.56, 139.40, 134.19, 131.48, 124.28, 96.14, 55.11, 39.69, 37.22. HR-ESI-MS (*m/z*): [*M*+*H*]⁺ calculated: 274.1299; found: 274.1302.

Methyl(*S*)-2-(((9*H*-fluoren-9-yl)methoxy)carbonyl)amino)-3-(4-aminophenyl)propanoate (9**)**

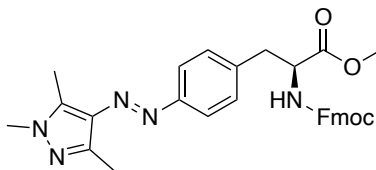
Thionylchloride (0.721 mL, 9.94 mmol, 2.00 eq.) was added dropwise to methanol (20.0 mL) at 0°C under nitrogen conditions. Commercially available Fmoc-4-amino-L-phenylalanine (2.00 g, 4.97 mmol) was then added, and the mixture was allowed to stir for 24 h at room temperature. The solution was then concentrated *in vacuo* without further purification to yield the methyl ester **9** as a pale-yellow oil (2.67 mg, 6.41 mmol, 99%). ¹H-NMR (400 MHz, MeOD): δ (ppm) = 7.79 (d, J = 7.45 Hz, 2H), 7.61 (t, J = 8.23 Hz, 2H), 7.41-7.37 (m, 4H), 7.31-7.30 (m, 4H), 4.47-4.44 (m, 1H), 4.28-4.26 (m, 2H), 4.16-4.12 (m, 1H), 3.71 (s, 3H), 3.25-3.21 (m, 1H), 3.30-2.94 (m, 1H). ¹³C-NMR (101 MHz, MeOD): δ = 173.42, 158.30, 145.13, 142.56, 140.19, 132.17, 130.44, 128.82, 128.14, 126.19, 124.09, 120.94, 67.93, 56.67, 52.90, 48.30, 37.93. ESI-MS (m/z): [M+H]⁺ found: 417.1741.

Methyl(*S*)-2-(((9*H*-fluoren-9-yl)methoxy)carbonyl)amino)-3-(4-(2-(2,4-dioxopentan-3-ylidene) hydrazineyl)phenyl)propanoate (10**)**

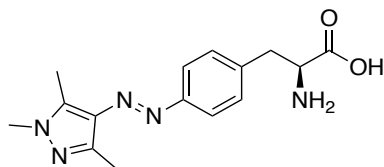


To a solution of intermediate of **9** (0.202 g, 4.85 mmol) in AcOH (14.0 mL) and 12 M HCl (12.0 M, 2.00 mL), NaNO₂ (0.402 g, 5.82 mmol, 1.20 eq.) dissolved in a minimum amount of water was added dropwise at 0 °C. Acetonitrile was then added (1.00 mL) and the mixture was stirred for 45 minutes at 0 °C. The resulting diazonium salt was then transferred to a suspension of pentane-2,4-dione (0.644 mL, 6.31 mmol, 1.30 eq.) and NaOAc (1.98 mg, 14.6 mmol, 3.00 eq.) in EtOH (24.0 mL). The mixture was stirred for 1.5 h at room temperature, and then cooled to 0 °C. The resulting yellow precipitate was collected via vacuum filtration, washed with ice-cold water/EtOH (1:1) and dried *in vacuo* to yield intermediate **10** as a bright yellow solid (0.959 mg, 1.82 mmol, 38%). ¹H-NMR (400 MHz, CDCl₃): δ (ppm) = 7.77 (d, J = 7.53 Hz, 2H), 7.58-7.55 (m, 2H), 7.40 (t, J = 7.45 Hz, 2H), 7.33-7.29 (m, 4H), 7.11 (d, J = 8.05 Hz, 2H), 4.70-4.65 (m, 1H), 4.50-4.34 (m, 2H), 4.19 (t, J = 6.71 Hz, 1H), 3.75 (s, 3H), 3.19-3.05 (m, 2H), 2.61 (s, 3H), 2.47 (s, 3H). ¹³C-NMR (101 MHz, CDCl₃): δ = 198.10, 197.18, 171.85, 155.61, 143.90, 143.82, 141.48, 140.77, 133.67, 133.35, 130.74, 127.89, 127.18, 125.18, 125.10, 120.16, 120.13, 116.54, 67.01, 54.86, 52.62, 47.33, 37.96, 31.80, 26.74. ESI-MS (m/z): [M+H]⁺: 528.2027.

Methyl(*S,E*)-2-(((9*H*-fluoren-9-yl)methoxy)carbonyl)amino)-3-(4-((1,3,5-trimethyl-1*H*-pyrazol-4-yl) diazenyl)phenyl) propanoate (11**)**



Methylhydrazine (0.600 mL, 11.4 mmol, 20.0 eq.) was added to a solution of intermediate **10** (0.300 g, 0.569 mmol) dissolved in ethanol (360 mL) and refluxed for 24 hours. The mixture was then concentrated *in vacuo* and the crude residue was subjected to automated flash column chromatography, with a gradient of 100% PE to 100% EtOAc. Further purification was performed with gradient 100% DCM to 10% MeOH/DCM to obtain the product **11** as a yellow oil (0.131 g, 0.243 mmol, 43%). ¹H-NMR (400 MHz, CDCl₃): δ (ppm) = 7.77-7.71 (m, 4H), 7.58-7.55 (m, 2H), 7.42-7.38 (m, 2H), 7.33-7.28 (m, 2H), 7.22-7.20 (m, 2H), 4.74-4.69 (m, 1H), 4.48-4.33 (m, 2H), 4.20 (t, J = 6.88 Hz, 1H), 3.94 (s, 3H), 3.76 (s, 3H), 3.26-3.12 (m, 2H), 2.62 (s, 3H), 2.60 (s, 3H). ¹³C-NMR (101 MHz, CDCl₃): δ = 171.86, 155.66, 152.31, 143.91, 143.82, 141.56, 141.45, 139.71, 134.58, 130.18, 127.87, 127.20, 125.22, 125.15, 122.45, 120.14, 67.13, 54.83, 52.63, 47.29, 38.27, 35.58, 12.61, 10.00. ESI-MS (m/z): [M+H]⁺ found: 538.2462.

(*S,E*)-2-amino-3-(4-((1,3,5-trimethyl-1*H*-pyrazol-4-yl)diazenyl)phenyl)propanoic acid (AapF3)

A mixture of intermediate **11** (0.131 g, 0.244 mmol) and LiOH·H₂O (0.046 g, 1.10 mmol, 4.50 eq.) in THF (3.50 ml) and water (1.00 mL) was allowed to stir at room temperature. After 18 h, the solvent was removed *in vacuo* and the crude product was directly subjected to preparative HPLC purification (solvent A: H₂O [0.05 Vol% TFA], solvent B: MeCN; gradient A/B: 0/100 to 100/0), eluting at 60% MeCN. Target compound **AapF3** was obtained as a bright yellow solid (0.03 g, 0.100 mmol, 41%). ¹H-NMR (400 MHz, MeOD): δ (ppm) = 7.77 (d, J = 8.38 Hz, 2H), 7.42 (d, J = 8.38 Hz, 2H), 4.28-4.25 (m, 1H), 3.78 (s, 3H), 3.40-3.35 (m, 1H), 3.23-3.18 (m, 1H), 2.59 (s, 3H), 2.44 (s, 3H). ¹³C-NMR (101 MHz, MeOD): δ = 171.40, 154.48, 143.09, 141.21, 137.28, 135.96, 131.22, 123.35, 55.23, 37.22, 36.10, 13.86, 9.75. HR-ESI-MS (m/z): [M+H]⁺ calculated: 302.1612; found: 302.1612.

5.6.1.3 Purity Measurements

All purity measurements can be found in the appendix (Section 7.5.1) under ‘Analytical HPLC Chromatograms for Purity Determination’.

5.6.2 Supplementary Photophysical Information

5.6.2.1 Materials and Methods

For determination of thermal equilibrium and isomer spectra, as well as determination of cycle performance and thermal half-life, UV/Vis absorption spectroscopy was employed. UV/Vis absorption spectroscopy was performed using Agilent 8453 UV/Vis spectrophotometer or Agilent Varian Cary[®] 50 UV/Vis spectrophotometer, in 10 mm quartz cuvettes. To determine PSS values at the respective isosbestic points of compounds (50 μM), analytical HPLC was performed using Agilent 1220 Infinity LC System (column: Phenomenex Luna, 3 μM C18(2), 100 Å 150 x 2.0 mm; flow rate of 0.3 mL/min at 20 °C; solvent A: Milli-Q water with 0.01 wt% TFA for **AapF1**, **AapF2** or without TFA for **AapF3**; solvent B: MeCN; gradient: 2/98 MeCN/H₂O to 100/0 MeCN/H₂O). LED light sources for irradiation: $\lambda=365$ nm (Seoul Viosys, CUN66A1B, 700 mA, 3.6 V), $\lambda=420$ nm (Mouser, L1F3-U410200012000, 700 mA, 3.4 V) and $\lambda=528$ nm (LED-TECH, Oslon SSL 80, LDCQ7P-2U3U, 700 mA, 3.5 V). The details of these light sources are based on the supplier specifications upon purchase.

5.6.2.2 UV/Vis Absorption Spectra, Cycle Performance and Thermal Stabilities

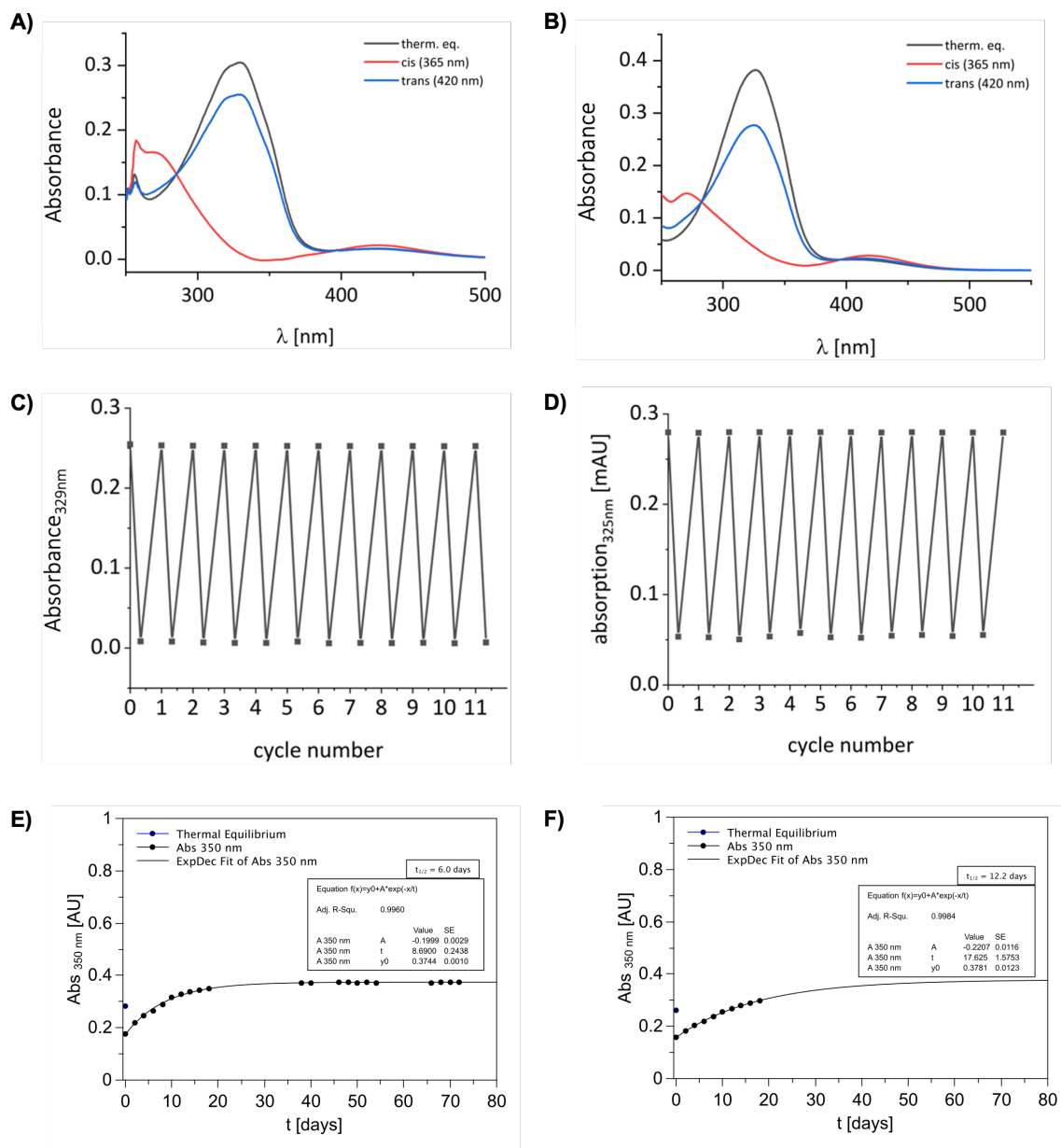


Figure 82. Photochemical evaluation of compound **AapF1**. The *cis*-isomer was accessed via irradiation with 365 nm, while the *trans*-isomer was obtained with 420 nm irradiation. A) UV/Vis absorption spectra (20 μM) of thermal equilibrium, *cis*-isomer and *trans*-isomer in DMSO. B) UV/Vis absorption spectra (20 μM) of thermal equilibrium, *cis*-isomer and *trans*-isomer in buffer solution. C) Cycle performance (20 μM) in DMSO. D) Cycle performance (20 μM) in buffer solution. E) Thermal half-life (50 μM) in DMSO, measured at 27 $^{\circ}\text{C}$. F) Thermal half-life (50 μM) in buffer solution (0.5% DMSO), measured at 27 $^{\circ}\text{C}$. After 18 days, compound began to crash out of the solution, and an extrapolation was performed over an 80-day period. Experiments were performed at room temperature and buffer solution consists of 50 mM TrisHCl, pH 7.5 + 0.2% DMSO, unless otherwise specified.

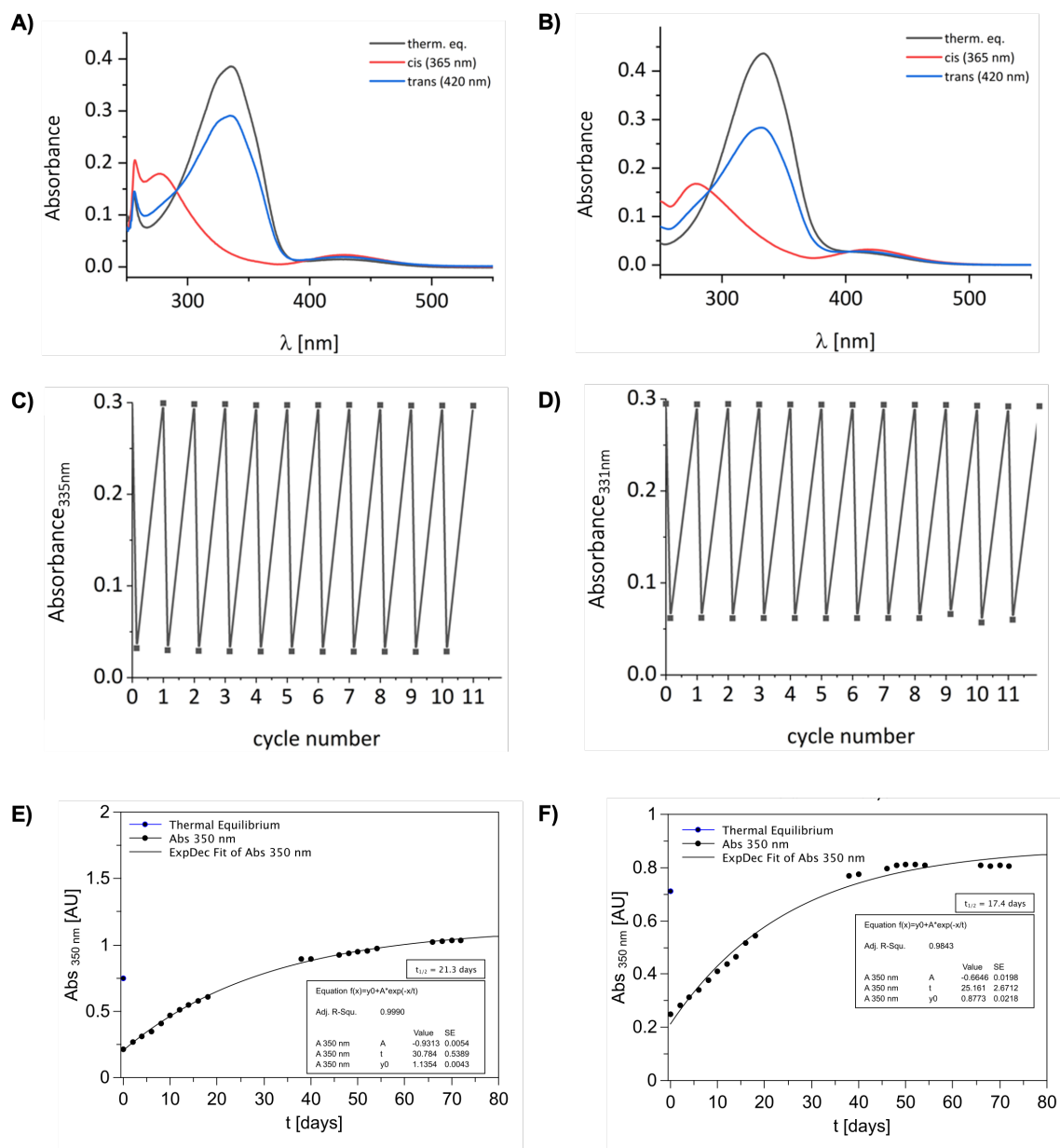


Figure 83. Photochemical evaluation of compound **AapF2**. The *cis*-isomer was accessed via irradiation with 365 nm, while the *trans*-isomer was obtained with 420 nm irradiation. A) UV/Vis absorption spectra (20 μM) of thermal equilibrium, *cis*-isomer and *trans*-isomer in DMSO. B) UV/Vis absorption spectra (20 μM) of thermal equilibrium, *cis*-isomer and *trans*-isomer in buffer solution. C) Cycle performance (20 μM) in DMSO. D) Cycle performance (20 μM) in buffer solution. E) Thermal half-life (150 μM) in DMSO, measured at 27 $^{\circ}\text{C}$. F) Thermal half-life (150 μM) in buffer solution (1.5% DMSO), measured at 27 $^{\circ}\text{C}$. Experiments were performed at room temperature, unless otherwise specified. Buffer solution consists of 50 mM TrisHCl, pH 7.5 + 0.2% DMSO, unless otherwise specified.

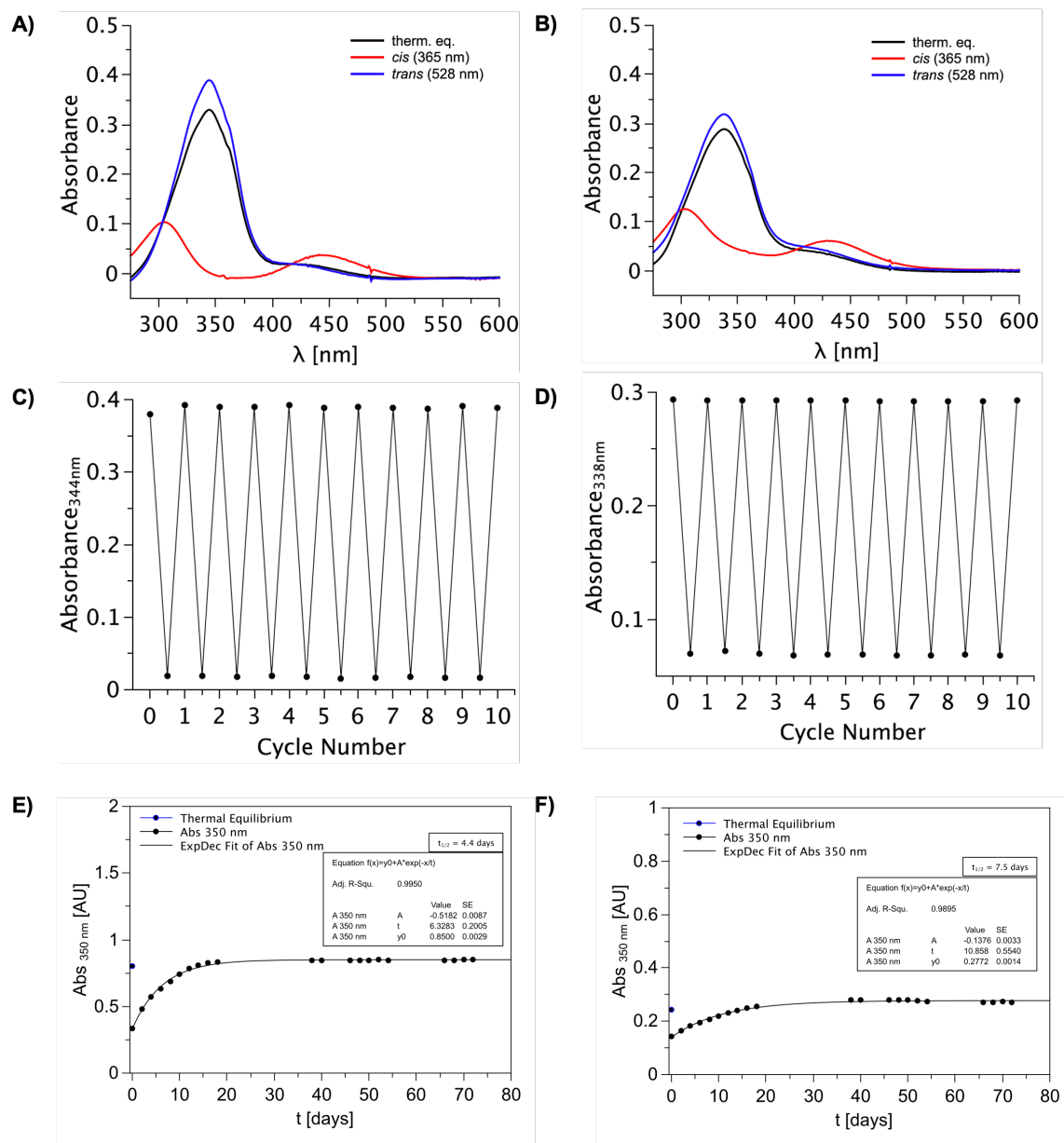


Figure 84. Photochemical evaluation of compound **AapF3**. The *cis*-isomer was accessed via irradiation with 365 nm, while the *trans*-isomer was obtained with 528 nm irradiation. A) UV/Vis absorption spectra (20 μM) of thermal equilibrium, *cis*-isomer and *trans*-isomer in DMSO. B) UV/Vis absorption spectra (20 μM) of thermal equilibrium, *cis*-isomer and *trans*-isomer in buffer solution. C) Cycle performance (20 μM) in DMSO. D) Cycle performance (20 μM) in buffer solution. E) Thermal half-life (50 μM) in DMSO, measured at 27 $^{\circ}\text{C}$. F) Thermal half-life (50 μM) in buffer solution (0.5% DMSO), measured at 27 $^{\circ}\text{C}$. Experiments were performed at room temperature, unless otherwise specified. Buffer solution consists of 50 mM TrisHCl, pH 7.5 + 0.2% DMSO, unless otherwise specified.

5.6.2.3 PSS Evaluation

All PSS measurements can be found in the appendix (Section 7.5.2) under ‘Analytical HPLC Chromatograms for PSS Determination’.

5.6.3 NMR Spectra

All NMR spectra can be found in the appendix (Section 7.5.3).

5.6.4 References

- [1] K. Rustler, P. Nitschke, S. Zahnbrecher, J. Zach, S. Crespi, B. König, *J. Org. Chem.* **2020**, *85*, 4079-4088.
- [2] J. Calbo, C. E. Weston, A. J. P. White, H. S. Rzepa, J. Contreras-García, M. J. Fuchter, *J. Am. Chem. Soc.* **2017**, *139*, 1261-1274.
- [3] C. E. Weston, R. D. Richardson, P. R. Haycock, A. J. White, M. J. Fuchter, *J. Am. Chem. Soc.* **2014**, *136*, 11878-11881.
- [4] M. Schönberger, D. Trauner, *Angew. Chem. Int. Ed. Engl.* **2014**, *53*, 3264-3267.

6. Summary

This thesis presents the design, synthesis and evaluation of covalent and non-covalent photoswitchable ligands for various biological purposes. One such purpose was to obtain photocontrol of μ -opioid receptor (μ OR) activity. This was achieved to varying degrees either by attaching a photoswitch unit to fentanyl (**Chapter 1 & 2**) or by incorporating a photoswitch unit into the nitazene structure (**Chapter 3**), with both ligands known to display a strong potency towards μ OR. Furthermore, covalent derivatives of both fentanyl and nitazene were successfully developed that offer differing functions than freely diffusible ligands, as discussed in **Chapter 2 & 3**. Alternatively, photoswitchable amino acids were covalently incorporated by means of co-translation into a protein of interest for a rather different biological purpose. This purpose was to evaluate whether photoswitches can be used as energy funnels to insert dynamic motions site-selectively into a protein via rapid photoisomerization, and to discern whether such processes could allow for dynamic control of protein activity (**Chapter 4**). In order to expand the repertoire of photoswitchable amino acids that could be co-translationally incorporated into proteins, arylazopyrazole derivatives of the amino acid phenylalanine were further developed and described in this thesis (**Chapter 5**).

In **Chapter 1**, a range of photoresponsive fentanyl-based ligands were synthesized, with differing photophysical and biochemical properties that may be applicable in future biochemical investigations of μ OR. This photofentanyl ‘toolbox’ was successfully obtained by chemically attaching an azopyrazole photoswitch to several positions on the fentanyl pharmacophore. The lead ligand **3c** displayed a significant difference in μ OR_{wt} efficacy between its respective *trans*- and *cis*-isomers, with the former isomer inducing a maximum receptor response of 90% (528 nm irradiation), while the latter isomer merely induced an 18% response (365 nm irradiation). Importantly, these findings could be reproduced upon *in situ* irradiation and suggest azide **3c** to be a valuable tool that can be used to ‘switch on/off’ μ OR activity with light.

While the former chapter focuses on the development of freely diffusible ligands, **Chapter 2** describes the development of covalent photoswitchable fentanyl derivatives for targeting μ OR. This involved the synthesis fentanyl derivatives that contained either maleimide, isothiocyanate or disulfide reactive groups for covalent interaction with nucleophilic amino acids present in or near the binding pocket of μ OR. The lead disulfide-containing ligand **tFAPz 1** displayed full agonist properties in a metabotropic functional

assay, with a 2-fold difference in potency between its respective light-accessible isomers. Importantly, **tFAPz 1** was found to covalently bind to a cysteine-containing μ OR mutant, with *trans*-**tFAPz 1** displaying a covalent binding maximum of 74% after a 45-min incubation period.

Chapter 3 encompasses the development of both covalent and non-covalent derivatives of nitazene-based ligands for targeting the μ OR. Nitazenes represent an underexplored class of potent μ OR ligands that have increasingly received attention. In order to achieve photocontrol of this ligand, an azo group was incorporated into the nitazene scaffold, which resulted in the formation of an arylazobenzimidazole. This photoswitch class with the corresponding substitution pattern, has not yet been thoroughly investigated and therefore, the synthesis of photoswitchable nitazene ligands with various substitution patterns provided access to investigating the photophysical properties of such arylazobenzimidazoles. While photocontrol of μ OR activity could not be entirely achieved with these ligands, azo-containing **2e** and **3e** emerged as particularly noteworthy as they were able to form an exceptionally high fraction of covalent-ligand receptor complexes with wild-type μ OR at physiological pH, after only a 5-min incubation period.

Chapter 4 presents a thorough investigation into the notion that dynamic motions can be site-selectively inserted into a protein via the use of photoswitches as energy funnels. In order to evaluate this, azobenzene phenylalanine (AzoF) was co-translationally incorporated into the protein sequence of imidazole glycerol phosphate synthase (ImGPS) at the allosterically-relevant sites hW123 and fS55. Subsequently, pulsing irradiation with alternating 365/420 nm was employed to rapidly toggle between the isomers of AzoF, which resulted in a pivotal finding. The presumable induced motions resulted in a substantial increase in the catalytic activity of ImGPS(hW123AzoF), while the activity of ImGPS(fS55AzoF) remained unaltered. Overall, the results described in this chapter provide insight into the complex regulation of allosteric proteins and describe the possibility of modulating these proteins via the insertion of dynamic motions.

While several unnatural amino acids have been previously developed to contain an azobenzene unit, such as in AzoF, **Chapter 5** describes the synthesis, chemical characterization and photophysical evaluation of arylazopyrazole-based phenylalanine derivatives. Arylazopyrazoles have been shown to possess superior photophysical properties, including high photostationary states and red-shifted absorbance bands. As a result, these

Summary

compounds were developed in order to provide alternative photoswitchable amino acids for co-translational incorporation into a selected protein.

7. Appendix

7.1 Abbreviations

°C	degree Celsius
A	ampere
Å	Ångström (10^{-10} m)
a.u.	arbitrary unit
AapF	arylazopyrazole phenylalanine
AcOH	acetic acid
<i>ai</i>	as isolated
AICAR	5-aminoimidazole-4-carboxamide ribonucleotide
Ar	aryl
Asp	aspartic acid
AzoF	azobenzene phenylalanine
BIT	2-(<i>p</i> -ethoxy-benzyl)-1-diethylaminoethyl-5-isothiocyanobenzimidazole isothiocyanate
Boc	<i>tert</i> -butyloxycarbonyl
br	broad
BRET	bioluminescence resonance energy transfer
Bu	butyl
calc.	calculated
cAMP	cyclic adenosine monophosphate
CDCl ₃	deuterated chloroform
cDNA	complimentary DNA
cm	centimeter
d	day
DAMGO	[D-Ala ² , NMe-Phe ⁴ , Gly-ol ⁵]-enkephalin
DBU	1,8-diazabicyclo[5.4.0]undec-7-ene
DCC	<i>N,N'</i> -dicyclohexylcarbodiimide
DCE	1,2-dichloroethane
DCM	dichloromethane
deg.	degassed
DIPEA	diisopropylethylamine
DMAP	4-dimethylaminopyridine
DMF	dimethylformamide
DMSO	dimethylsulfoxide
DMSO- <i>d</i> ₆	deuterated dimethylsulfoxide
EC ₅₀	half-maximal effective concentration
EDCI	1-ethyl-3-(3-dimethylaminopropyl)carbodiimide
E _{max}	maximal effect
eq.	equivalent
ESI	electrospray ionization

Appendix

Et	ethyl
EtOAc	ethylacetate
EtOH	ethanol
FAPz	fentanyl azopyrazole
FIT	fentanyl isothiocyanate (N-phenyl-N-[1-(2-(<i>p</i> -isothiocyano)phenyl-ethyl)-4-piperidinyl]propanamide)
Fmoc	fluorenylmethoxycarbonyl
FRET	fluorescence resonance energy transfer
FTIR	fourier transform infrared spectroscopy
Fulg	fulgimide
g	gram
GC	gas chromatography
GCE	genetic code expansion
GIRK	G-protein-coupled inward-rectifying potassium (ion channel)
Gln	glutamine
Glu	glutamate
GPCR	G-protein-coupled receptor
h	hour
HCl	hydrochloric acid
HEK	human embryonic kidney (cell line)
HEPES	4-(2-hydroxyethyl)-1-piperazineethanesulfonic acid
HOBT	1-hydroxybenzotriazole
HPLC	high-performance liquid chromatography
HRMS	high-resolution mass spectrometry
Hti	hemithioindigo
HTRF	homogeneous time-resolved fluorescence
Hz	Herz
h ν	photon energy
I	intensity
IC ₅₀	half-maximal inhibitory concentration
ImGP	imidazole glycerol phosphate
ImGPS	imidazole glycerol phosphate synthase
IP	inositol monophosphate
IR	infrared radiation
Iso	isopropyl
J	J-coupling constant
K _i	inhibitory constant
KOAc	potassium acetate
KSAc	potassium thioacetate
l	length
L	liter
LC	liquid chromatography
LED	light emitting diode

Appendix

M	molarity = mol/L
m	mass
M ⁺	molecular ion
mA	milliampere
Me	methyl
MeCN	acetonitrile
MeOH	methanol
mg	milligram
MgSO ₄	magnesium sulfate
MHz	megahertz
min	minute
mL	milliliter
mM	millimolar
mm	millimeter
mmol	millimole
mol%	mole percent
MS	mass spectrometry
n	number of experiments
n/a	not applicable
n/q	not quantifiable
Na ₂ SO ₄	sodium sulfate
NaAsc	sodium ascorbate
NaOAc	sodium acetate
NCS	N-chlorosuccinimide
nm	nanometer
nM	nanomolar
NMR	nuclear magnetic resonance
NP	normal phase
OTf	triflates
OTs	tosylate
PE	petroleum ether
PEG	polyethylene glycol
PF	photofentanyl
Ph	phenyl
PORTLs	photoswitchable orthogonal remotely tethered ligands
ppm	parts per million
PrFAR	N'-[(5'-phosphoribulosyl)formimino]-5-aminoimidazole-4-carboxamide ribonucleotide
ProFAR	N'-[(5'-phosphoribosyl)formimino]-5-aminoimidazole-4-carboxamide ribonucleotide
PSS	photostationary state
PTL	photoswitchable tethered ligands
Py	pyridine

Appendix

rt	room temperature
s	second
S.E.M.	standard error of mean
SCN	isothiocyanate
SD	standard deviation
sec	second
T	temperature
$t_{1/2}$	thermal half-life
TBTA	tris[(1-benzyl-1 <i>H</i> -1,2,3-triazol-4-yl)methyl]amine
tBu	tert-butyl
TFA	trifluoroacetic acid
tFAPz	tethered fentanyl azopyrazole
Therm. eq.	thermal equilibrium
THF	tetrahydrofuran
TLC	thin layer chromatography
t_R	retention time
Ts	toluenesulfonyl
UAA	Unnatural amino acid
UV	ultraviolet
V	volt
Vis	visible
W	watt
wt	wild-type
wt%	percentage by weight
z	Formal charge
ΔG	Gibbs free energy
ΔH	enthalpy
ϵ	molar extinction coefficient
λ	wavelength
μM	micromolar
μOR	μ -opioid receptor
μOR_{M1}	μ -opioid receptor mutant 1

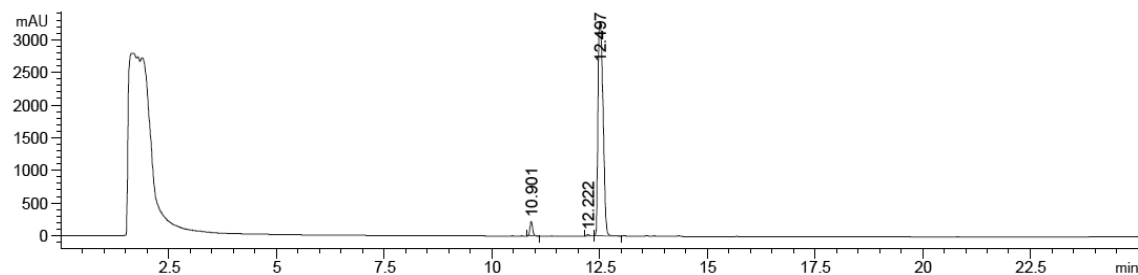
7.2 Appendix for Chapter 1

7.2.1 Analytical HPLC Chromatograms for Purity Determination

Experiments in this section were evaluated in DMSO.

Compound 1:

Detection at 220 nm: >99% purity

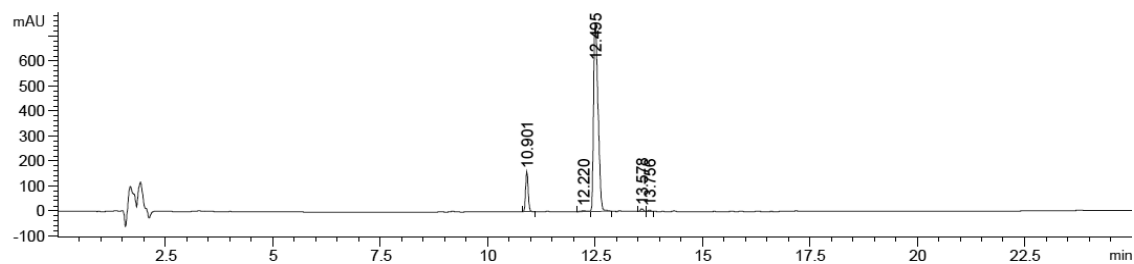


Signal 2: DAD1 B, Sig=220,4 Ref=off

Peak #	RetTime [min]	Type	Width [min]	Area [mAU*s]	Height [mAU]	Area %
1	10.901	BB	0.0655	944.72748	222.49606	3.3854
2	12.222	BB	0.0663	81.93166	19.00448	0.2936
3	12.497	BV R	0.1340	2.68792e4	3262.71216	96.3210

*Peak 1 and Peak 3 are *cis*- and *trans*-isomers of compound 1, respectively.

Detection at 254 nm: 99% purity



Signal 1: DAD1 A, Sig=254,4 Ref=off

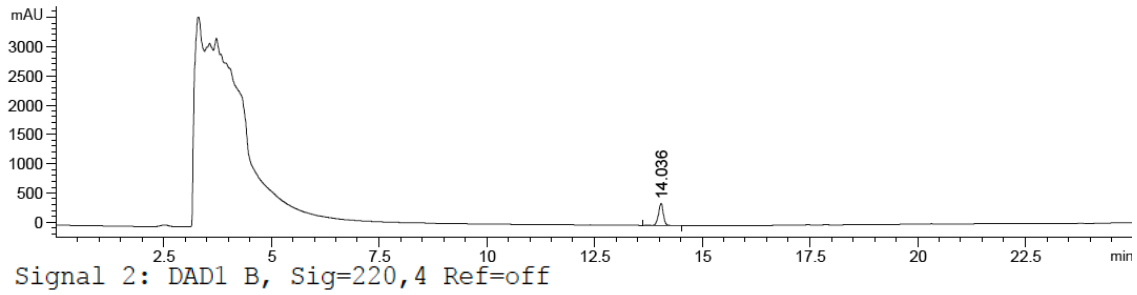
Peak #	RetTime [min]	Type	Width [min]	Area [mAU*s]	Height [mAU]	Area %
1	10.901	VB	0.0655	673.46973	158.75671	10.7275
2	12.220	BV E	0.0788	21.58519	4.00680	0.3438
3	12.495	VV R	0.1131	5518.78857	754.05664	87.9069
4	13.578	BV	0.0706	44.29095	9.82660	0.7055
5	13.756	VB	0.0675	19.86117	4.68273	0.3164

*Peak 1 and Peak 3 are *cis*- and *trans*-isomers of compound 1, respectively.

Appendix

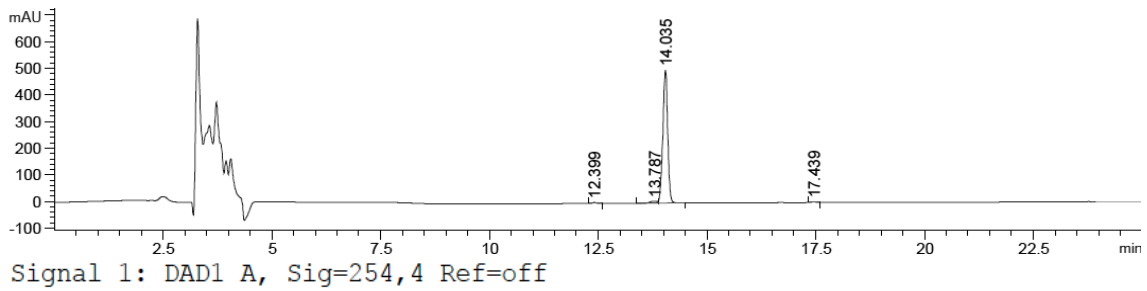
Compound 2:

Detection at 220 nm: >99% purity



Peak #	RetTime [min]	Type	Width [min]	Area [mAU*s]	Height [mAU]	Area %
1	14.036	VB R	0.1192	2952.95972	376.73669	100.0000

Detection at 254 nm: 97% purity

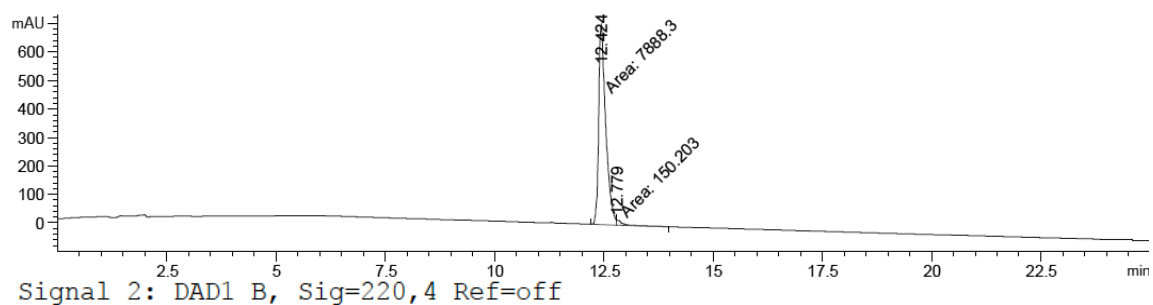


Peak #	RetTime [min]	Type	Width [min]	Area [mAU*s]	Height [mAU]	Area %
1	12.399	BB	0.0947	24.90855	4.11141	0.6172
2	13.787	BV E	0.1745	76.92455	7.21064	1.9061
3	14.035	VB R	0.1194	3913.41895	499.68018	96.9718
4	17.439	BB	0.0987	20.37437	3.26880	0.5049

Appendix

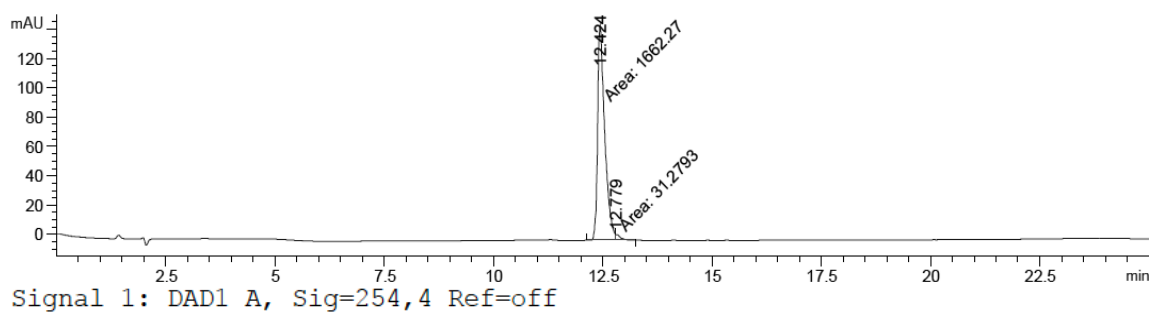
Compound **3a**:

Detection at 220 nm: 98% purity



Peak #	RetTime [min]	Type	Width [min]	Area [mAU*s]	Height [mAU]	Area %
1	12.424	MF	0.1877	7888.30420	700.51556	98.1315
2	12.779	FM	0.1446	150.20280	17.31518	1.8685

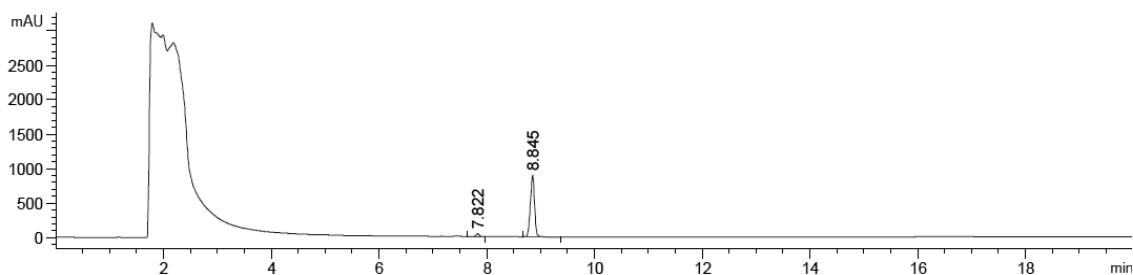
Detection at 254 nm: 98% purity



Peak #	RetTime [min]	Type	Width [min]	Area [mAU*s]	Height [mAU]	Area %
1	12.424	MF	0.1892	1662.26672	146.42648	98.1530
2	12.779	FM	0.1320	31.27930	3.95037	1.8470

Compound **3b**:

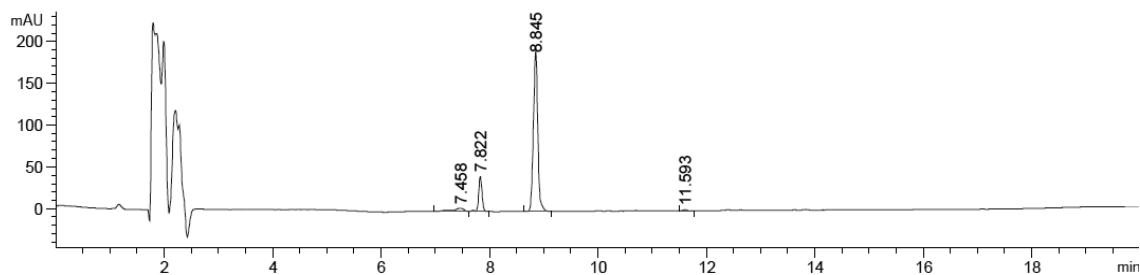
Detection at 220 nm: >99% purity



Peak #	RetTime [min]	Type	Width [min]	Area [mAU*s]	Height [mAU]	Area %
1	7.822	VB R	0.0660	180.70978	42.14679	3.5952
2	8.845	BV R	0.0832	4845.67578	894.04822	96.4048

*Peak 1 and Peak 2 are *cis*- and *trans*-isomers of compound **3b**, respectively.

Detection at 254 nm: 96% purity



Signal 1: DAD1 A, Sig=254,4 Ref=off

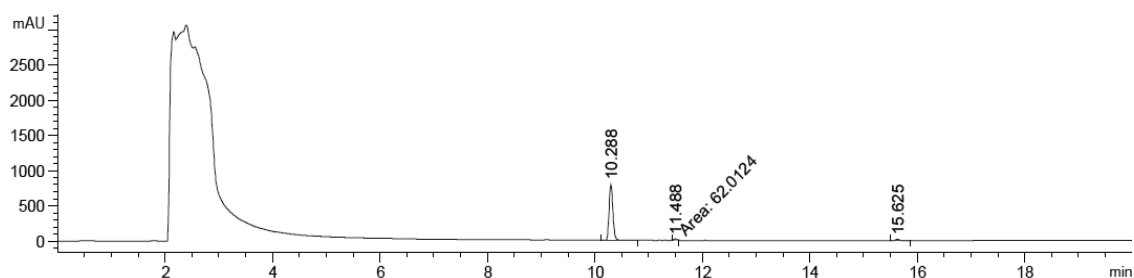
Peak #	RetTime [min]	Type	Width [min]	Area [mAU*s]	Height [mAU]	Area %
1	7.458	BV E	0.2028	55.41312	4.02104	4.1769
2	7.822	VB R	0.0651	182.76895	42.03464	13.7766
3	8.845	BB	0.0855	1082.79150	192.77330	81.6179
4	11.593	BB	0.0737	5.68597	1.19136	0.4286

*Peak 2 and Peak 3 are *cis*- and *trans*-isomers of compound **3b**, respectively.

Appendix

Compound 3c:

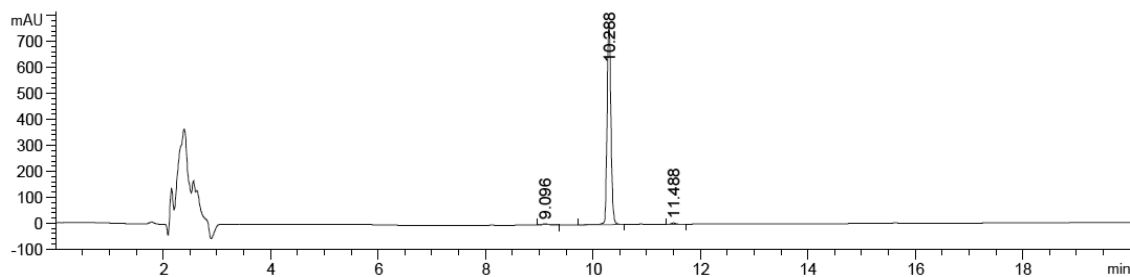
Detection at 220 nm: 96% purity



Signal 2: DAD1 B, Sig=220,4 Ref=off

Peak #	RetTime [min]	Type	Width [min]	Area [mAU*s]	Height [mAU]	Area %
1	10.288	BV R	0.0746	3870.74390	797.74713	95.5414
2	11.488	MM	0.0604	62.01241	17.10340	1.5306
3	15.625	BB	0.0811	118.62248	22.65009	2.9280

Detection at 254 nm: 98% purity

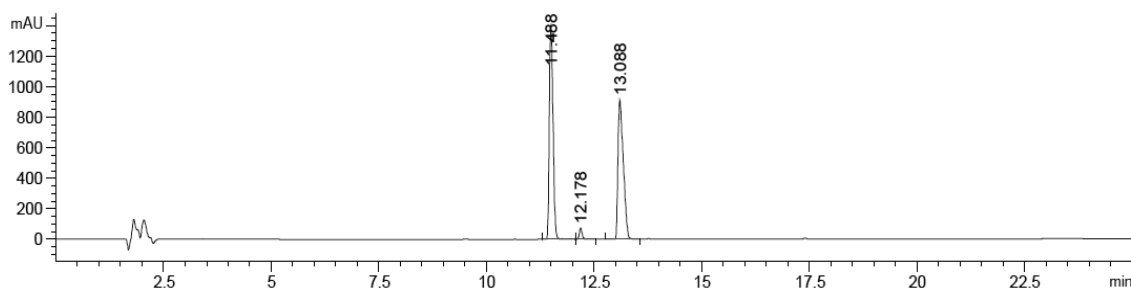


Signal 1: DAD1 A, Sig=254,4 Ref=off

Peak #	RetTime [min]	Type	Width [min]	Area [mAU*s]	Height [mAU]	Area %
1	9.096	BB	0.1030	35.88100	5.17085	0.9274
2	10.288	VB R	0.0747	3807.14722	779.84143	98.4018
3	11.488	BB	0.0789	25.95119	4.96788	0.6708

PF2:

Detection at 220 nm: 99% purity

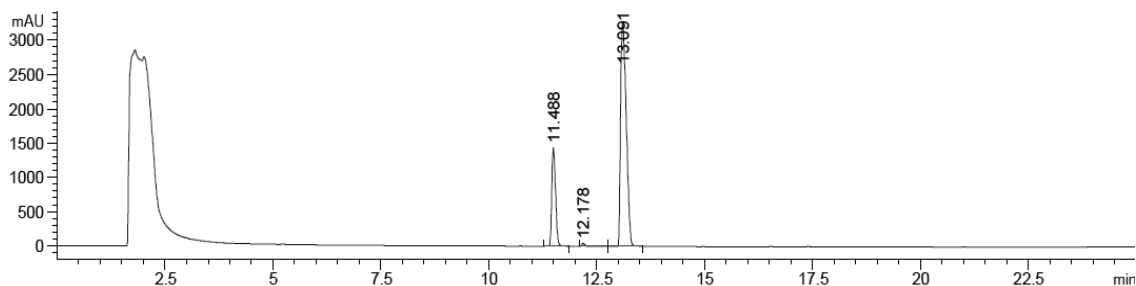


Signal 2: DAD1 B, Sig=220,4 Ref=off

Peak #	RetTime [min]	Type	Width [min]	Area [mAU*s]	Height [mAU]	Area %
1	11.488	VV R	0.0939	8630.08594	1435.03577	22.2835
2	12.178	BV R	0.0697	185.58174	40.29873	0.4792
3	13.091	VV R	0.1446	2.99129e4	3267.29736	77.2373

*Peak 1 and Peak 3 are *cis*- and *trans*-isomers of compound **PF2**, respectively.

Detection at 254 nm: 98% purity



Signal 1: DAD1 A, Sig=254,4 Ref=off

Peak #	RetTime [min]	Type	Width [min]	Area [mAU*s]	Height [mAU]	Area %
1	11.488	VV R	0.0937	8408.31250	1404.99841	50.4837
2	12.178	BV R	0.0699	340.14166	74.24352	2.0422
3	13.088	VV R	0.1267	7907.04053	913.79034	47.4741

*Peak 1 and Peak 3 are *cis*- and *trans*-isomers of compound **PF2**, respectively.

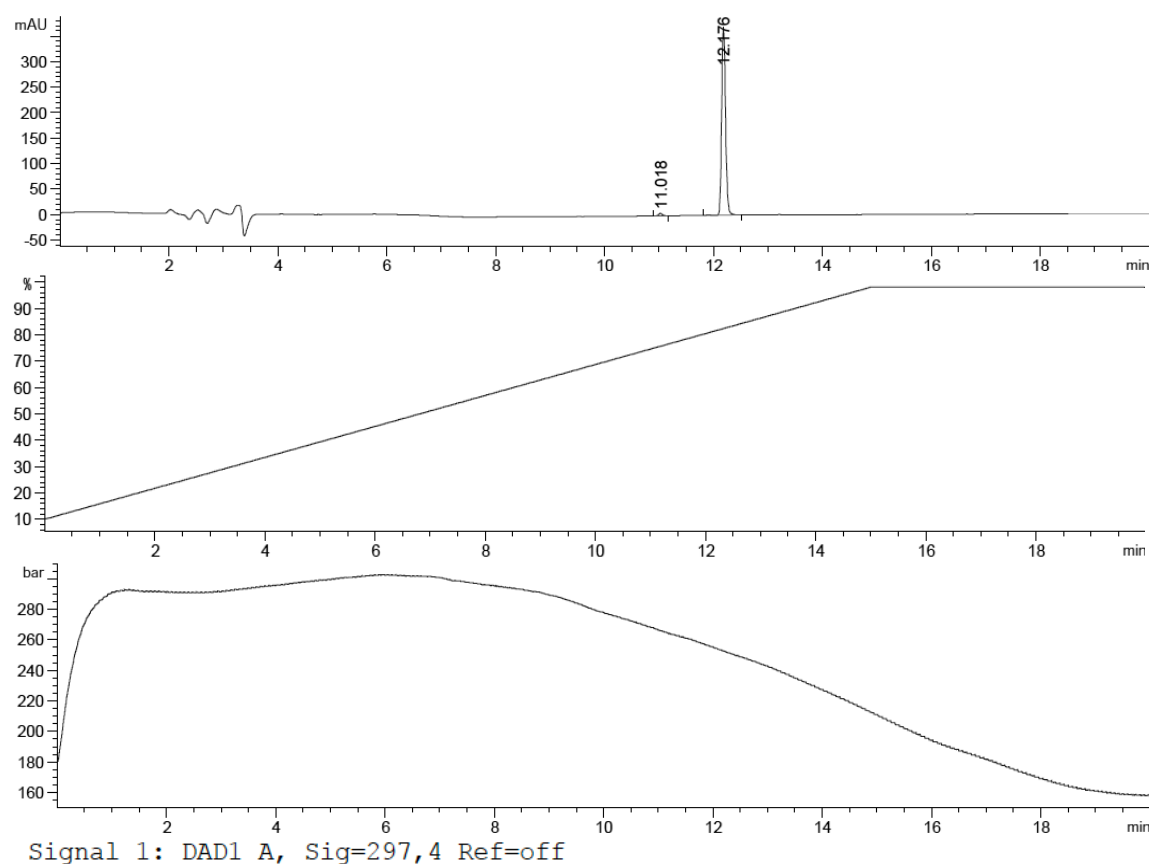
7.2.2 Analytical HPLC Chromatogram for PSS Determination

Compound 1 (50 μ M solution in TrisHCl Buffer + 0.5% DMSO, pH 7.5, injection volume 10 μ L):

Irradiation with $\lambda = 528$ nm for conversion from *cis*-isomer to *trans*-isomer.

Detection at 297 nm: t_R *cis*-isomer = 11.018 min (1%), t_R *trans*-isomer = 12.176 min (99%).

Figures of analytical HPLC trace, solvent gradient (acetonitrile/H₂O + 0.01% TFA), pressure profile and data analysis:



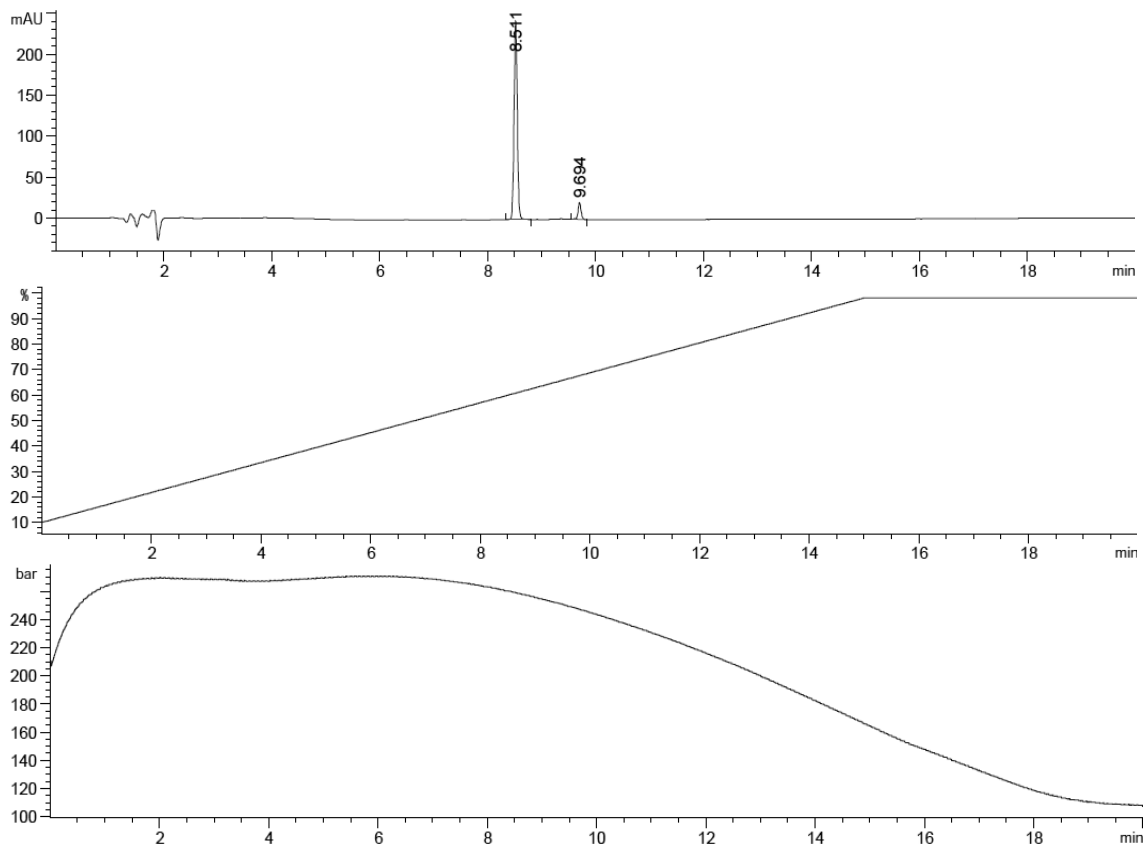
Peak #	RetTime [min]	Type	Width [min]	Area [mAU*s]	Height [mAU]	Area %
1	11.018	BB	0.0767	21.72623	4.46688	1.1498
2	12.176	VB R	0.0787	1867.78650	370.98001	98.8502

Appendix

Irradiation with $\lambda = 365$ nm for conversion from *trans*-isomer to *cis*-isomer.

Detection at 297 nm: t_R *cis*-isomer = 8.511 min (93%), t_R *trans*-isomer = 9.694 min (7%).

Figures of analytical HPLC trace, solvent gradient (acetonitrile/H₂O + 0.01% TFA), pressure profile and data analysis:



Signal 1: DAD1 A, Sig=297,4 Ref=off

Peak #	RetTime [min]	Type	Width [min]	Area [mAU*s]	Height [mAU]	Area %
1	8.511	BB	0.0652	1025.34265	243.28827	92.9756
2	9.694	BB	0.0592	77.46544	19.98244	7.0244

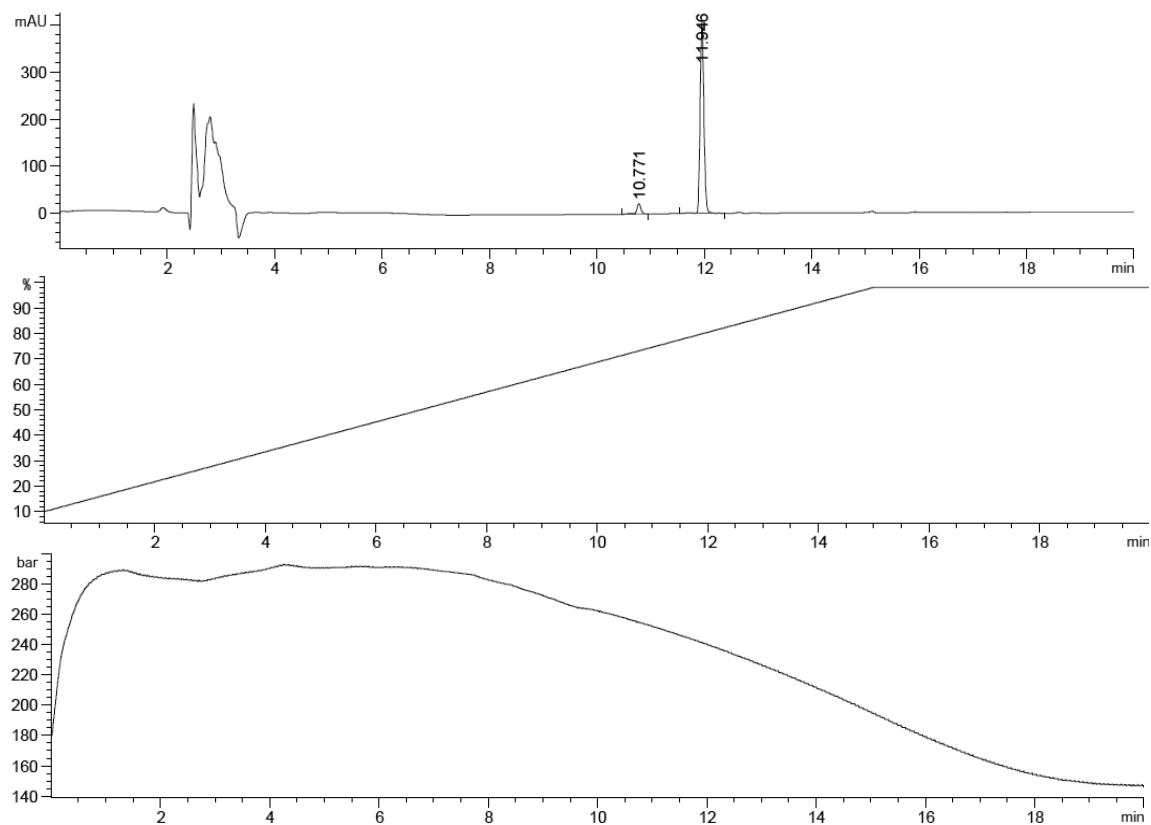
Appendix

Compound 1 (50 μ M solution in DMSO, injection volume 10 μ L):

Irradiation with $\lambda = 528$ nm for conversion from *cis*-isomer to *trans*-isomer.

Detection at 297 nm: t_R *cis*-isomer = 10.771 min (6%), t_R *trans*-isomer = 11.946 min (94%).

Figures of analytical HPLC trace, solvent gradient (acetonitrile/H₂O + 0.01% TFA), pressure profile and data analysis:



Signal 1: DAD1 A, Sig=297,4 Ref=off

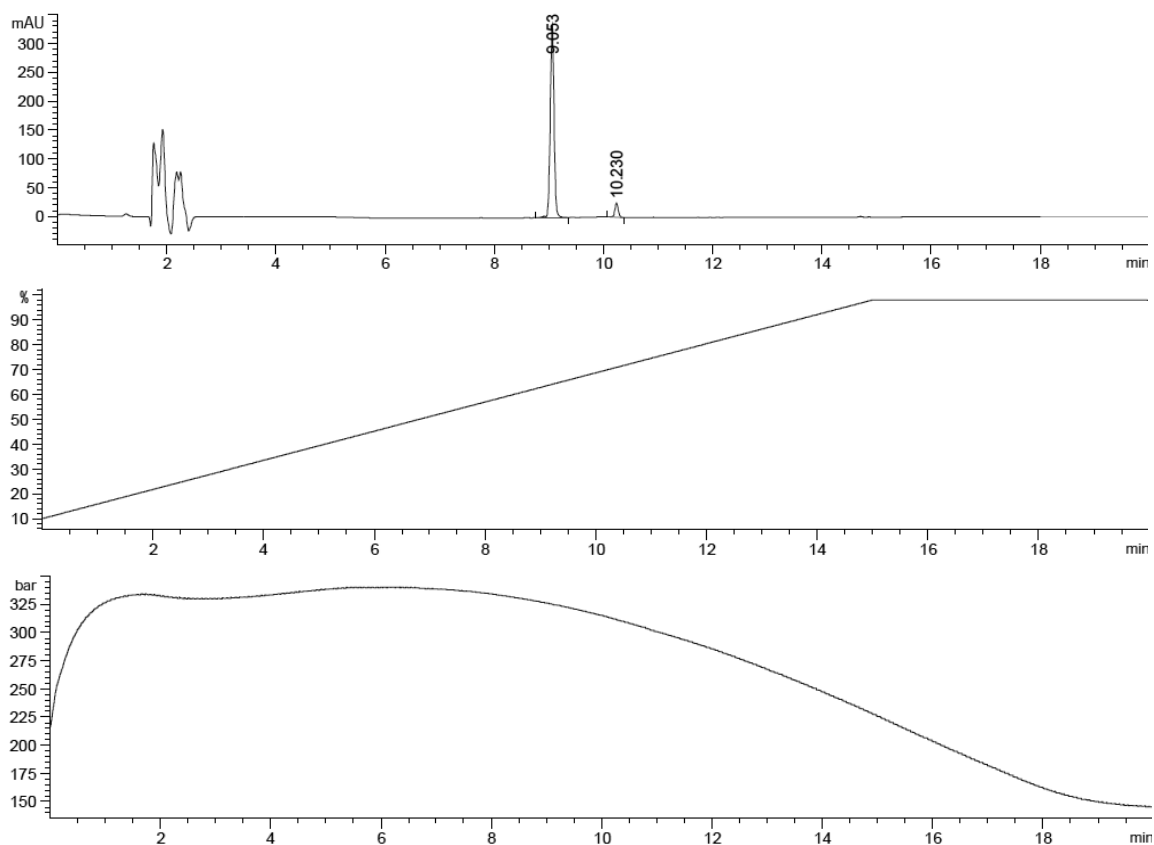
Peak #	RetTime [min]	Type	Width [min]	Area [mAU*s]	Height [mAU]	Area %
1	10.771	VB R	0.0743	118.93340	21.96607	5.6250
2	11.946	VV R	0.0754	1995.42334	403.11578	94.3750

Appendix

Irradiation with $\lambda = 365$ nm for conversion from *trans*-isomer to *cis*-isomer.

Detection at 297 nm: t_R *cis*-isomer = 9.053 min (94%), t_R *trans*-isomer = 10.230 min (6%).

Figures of analytical HPLC trace, solvent gradient (acetonitrile/H₂O + 0.01% TFA), pressure profile and data analysis:



Signal 1: DAD1 A, Sig=297,4 Ref=off

Peak #	RetTime [min]	Type	Width [min]	Area [mAU*s]	Height [mAU]	Area %
1	9.053	VB R	0.0747	1643.58459	335.45016	93.8331
2	10.230	BB	0.0666	108.01983	24.92130	6.1669

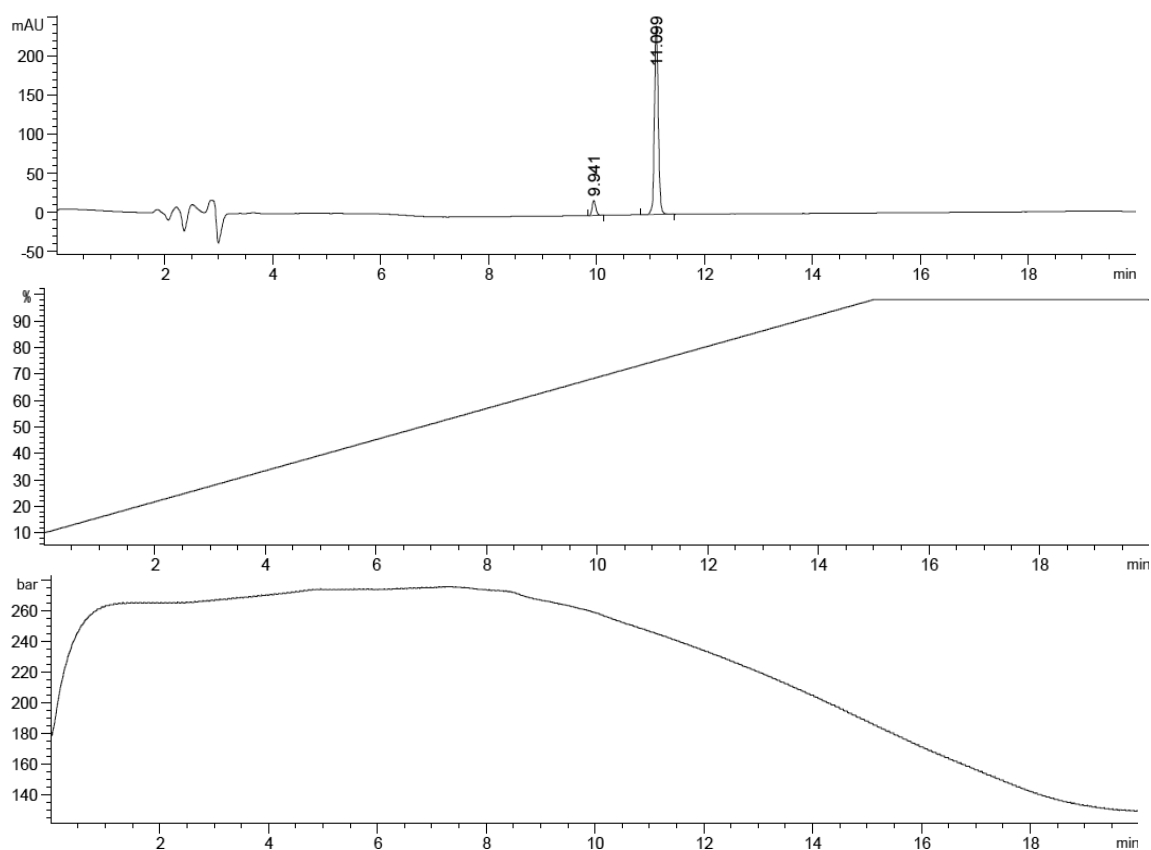
Appendix

Compound 3a (50 μ M solution in TrisHCl Buffer + 0.5% DMSO, pH 7.5, injection volume 10 μ L):

Irradiation with $\lambda = 528$ nm for conversion from *cis*-isomer to *trans*-isomer.

Detection at 290 nm: t_R *cis*-isomer = 9.941 min (7%), t_R *trans*-isomer = 11.099 min (93%).

Figures of analytical HPLC trace, solvent gradient (acetonitrile/H₂O + 0.01% TFA), pressure profile and data analysis:



Signal 3: DAD1 C, Sig=290,4 Ref=off

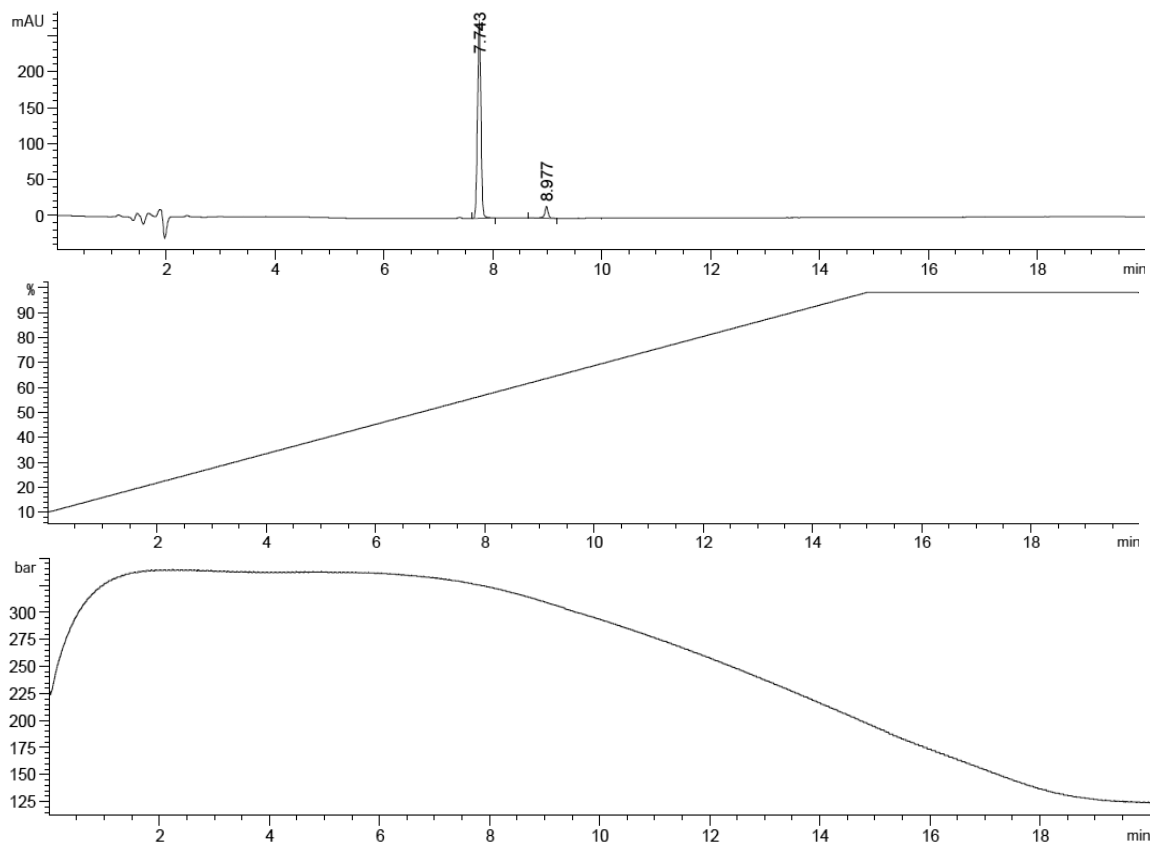
Peak #	RetTime [min]	Type	Width [min]	Area [mAU*s]	Height [mAU]	Area %
1	9.941	BB	0.0730	91.82278	19.46816	7.1141
2	11.099	BB	0.0780	1198.88672	240.98196	92.8859

Appendix

Irradiation with $\lambda = 365$ nm for conversion from *trans*-isomer to *cis*-isomer.

Detection at 290 nm: t_R *cis*-isomer = 7.743 min (94%), t_R *trans*-isomer = 8.977 min (6%).

Figures of analytical HPLC trace, solvent gradient (acetonitrile/H₂O + 0.01% TFA), pressure profile and data analysis:



Signal 3: DAD1 C, Sig=290,4 Ref=off

Peak #	RetTime [min]	Type	Width [min]	Area [mAU*s]	Height [mAU]	Area %
1	7.743	BB	0.0669	1186.94019	271.91513	94.2678
2	8.977	BB	0.0653	72.17484	16.41975	5.7322

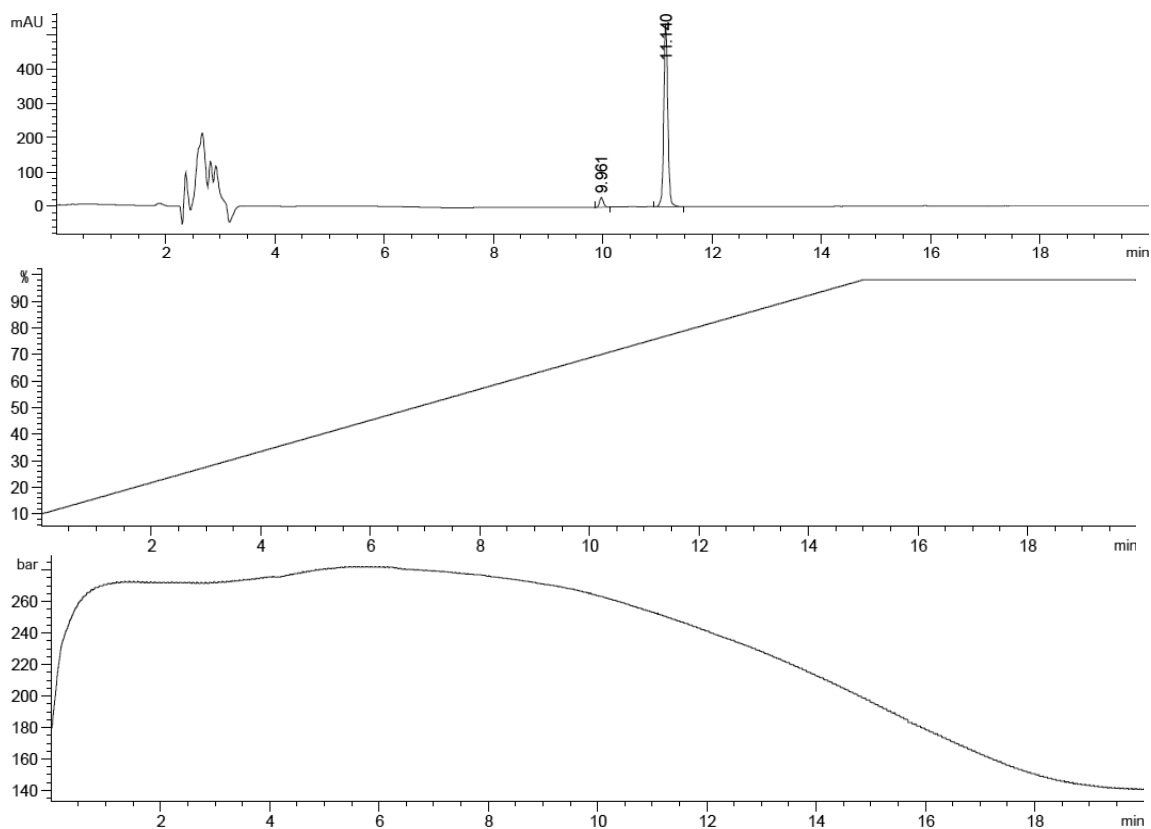
Appendix

Compound 3a (50 μ M solution in DMSO, injection volume 10 μ L):

Irradiation with $\lambda = 528$ nm for conversion from *cis*-isomer to *trans*-isomer.

Detection at 300 nm: t_R *cis*-isomer = 9.961 min (5%), t_R *trans*-isomer = 11.140 min (95%).

Figures of analytical HPLC trace, solvent gradient (acetonitrile/H₂O + 0.01% TFA), pressure profile and data analysis:



Signal 7: DAD1 G, Sig=300,4 Ref=off

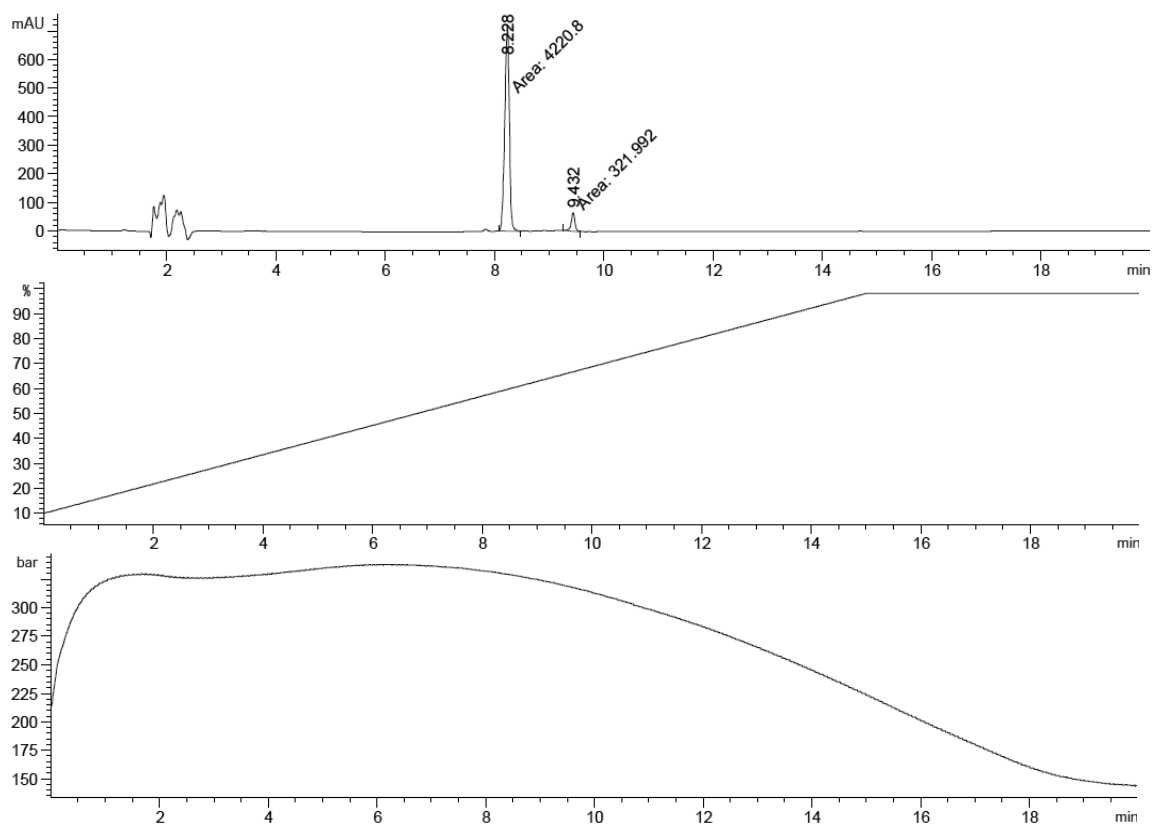
Peak #	RetTime [min]	Type	Width [min]	Area [mAU*s]	Height [mAU]	Area %
1	9.961	BB	0.0763	135.44861	28.06516	4.7216
2	11.140	BB	0.0797	2733.22607	534.48822	95.2784

Appendix

Irradiation with $\lambda = 365$ nm for conversion from *trans*-isomer to *cis*-isomer.

Detection at 300 nm: t_R *cis*-isomer = 8.228 min (93%), t_R *trans*-isomer = 9.432 min (7%).

Figures of analytical HPLC trace, solvent gradient (acetonitrile/H₂O + 0.01% TFA), pressure profile and data analysis:



Signal 7: DAD1 G, Sig=300,4 Ref=off

Peak #	RetTime [min]	Type	Width [min]	Area [mAU*s]	Height [mAU]	Area %
1	8.228	MM	0.0969	4220.80273	725.84991	92.9120
2	9.432	MM	0.0824	321.99194	65.15233	7.0880

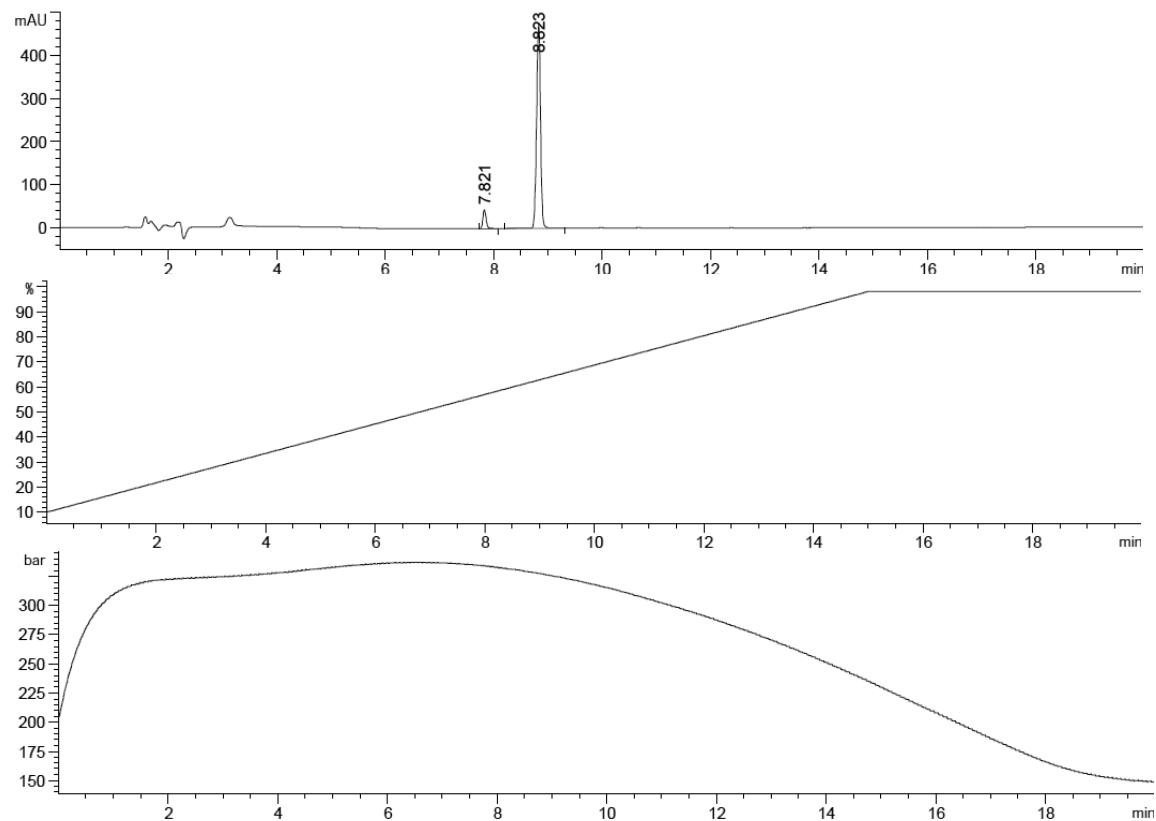
Appendix

Compound 3b (50 μ M solution in TrisHCl Buffer + 0.5% DMSO, pH 7.5, injection volume 10 μ L):

Irradiation with $\lambda = 528$ nm for conversion from *cis*-isomer to *trans*-isomer.

Detection at 297 nm: t_R *cis*-isomer = 7.821 min (7%), t_R *trans*-isomer = 8.823 min (93%).

Figures of analytical HPLC trace, solvent gradient (acetonitrile/H₂O + 0.01% TFA), pressure profile and data analysis:



Signal 3: DAD1 C, Sig=297,4 Ref=off

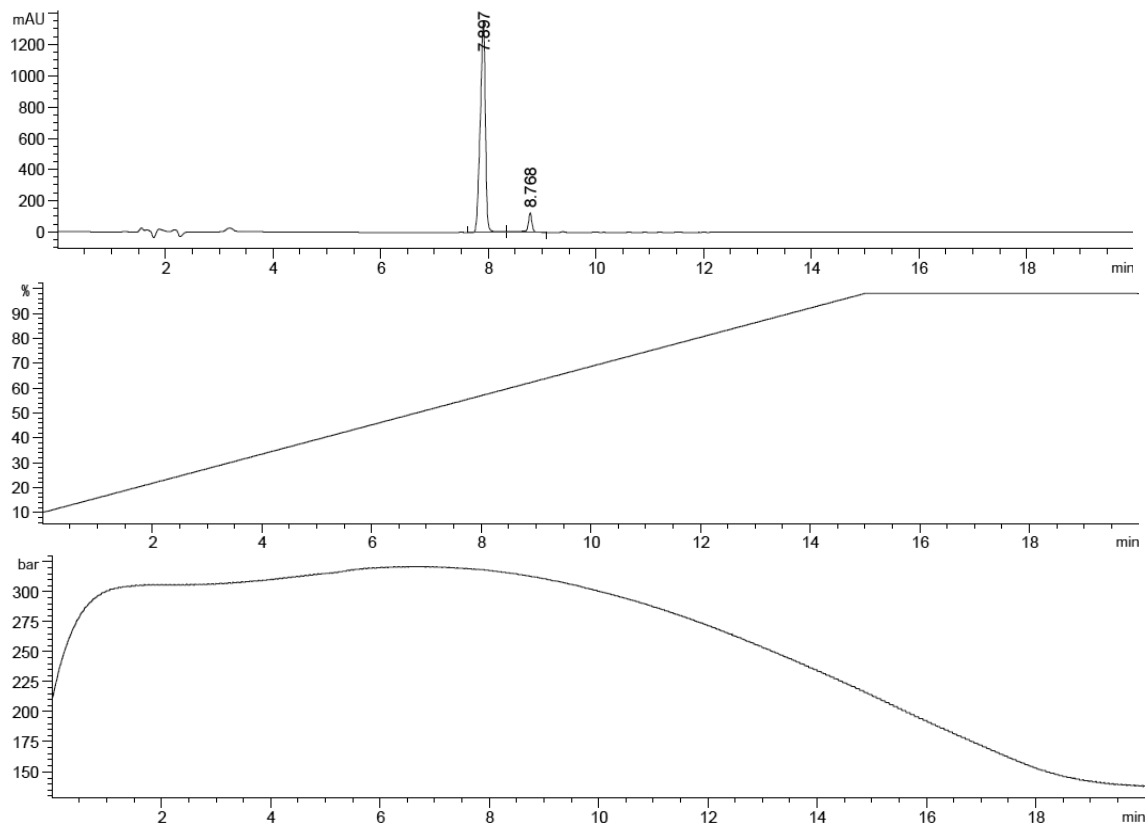
Peak #	RetTime [min]	Type	Width [min]	Area [mAU*s]	Height [mAU]	Area %
1	7.821	BB	0.0634	179.10533	44.08815	6.8857
2	8.823	VV R	0.0768	2422.00635	479.68219	93.1143

Appendix

Irradiation with $\lambda = 365$ nm for conversion from *trans*-isomer to *cis*-isomer.

Detection at 297 nm: t_R *cis*-isomer = 7.897 min (93%), t_R *trans*-isomer = 8.768 min (7%).

Figures of analytical HPLC trace, solvent gradient (acetonitrile/H₂O + 0.01% TFA), pressure profile and data analysis:



Signal 3: DAD1 C, Sig=297,4 Ref=off

Peak #	RetTime [min]	Type	Width [min]	Area [mAU*s]	Height [mAU]	Area %
1	7.897	BV R	0.0970	8982.23438	1351.64453	92.7435
2	8.768	VV R	0.0833	702.79816	124.06384	7.2565

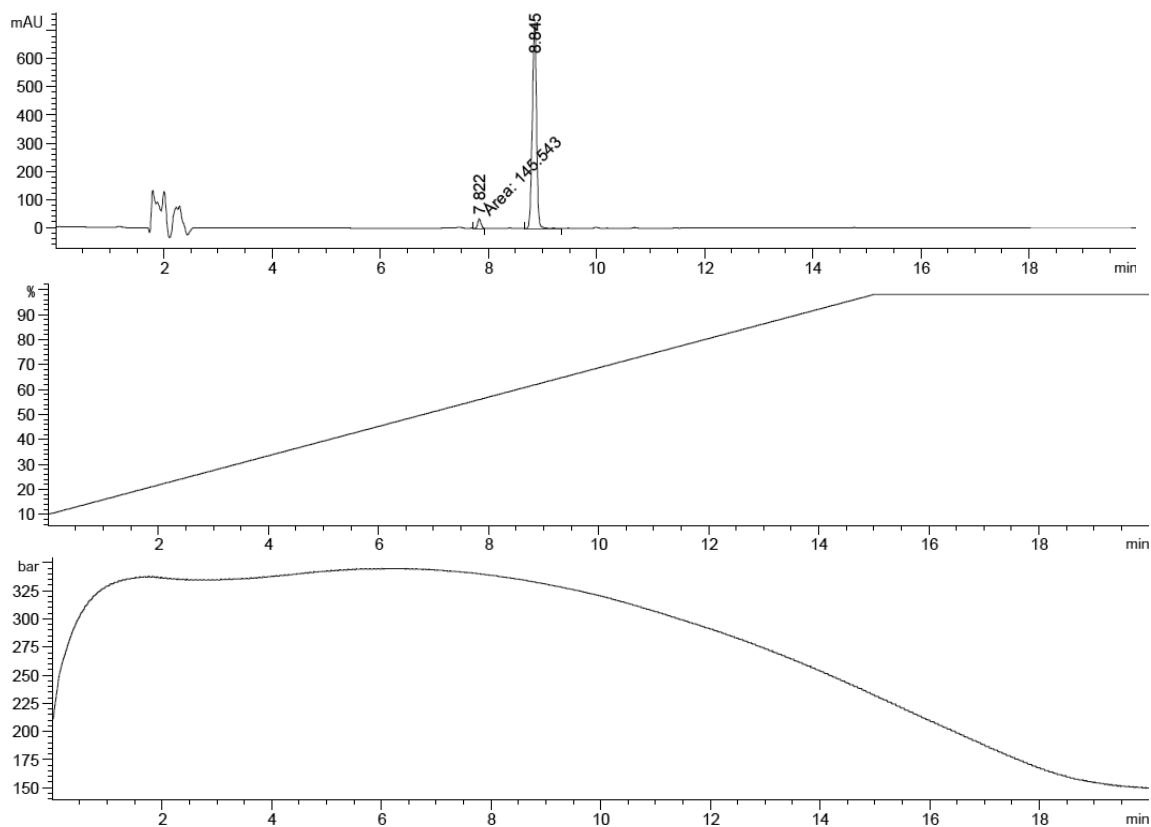
Appendix

Compound 3b (50 μ M solution in DMSO, injection volume 10 μ L):

Irradiation with $\lambda = 528$ nm for conversion from *cis*-isomer to *trans*-isomer.

Detection at 301 nm: t_R *cis*-isomer = 7.822 min (4%), t_R *trans*-isomer = 8.845 min (96%).

Figures of analytical HPLC trace, solvent gradient (acetonitrile/H₂O + 0.01% TFA), pressure profile and data analysis:



Signal 7: DAD1 G, Sig=301,4 Ref=off

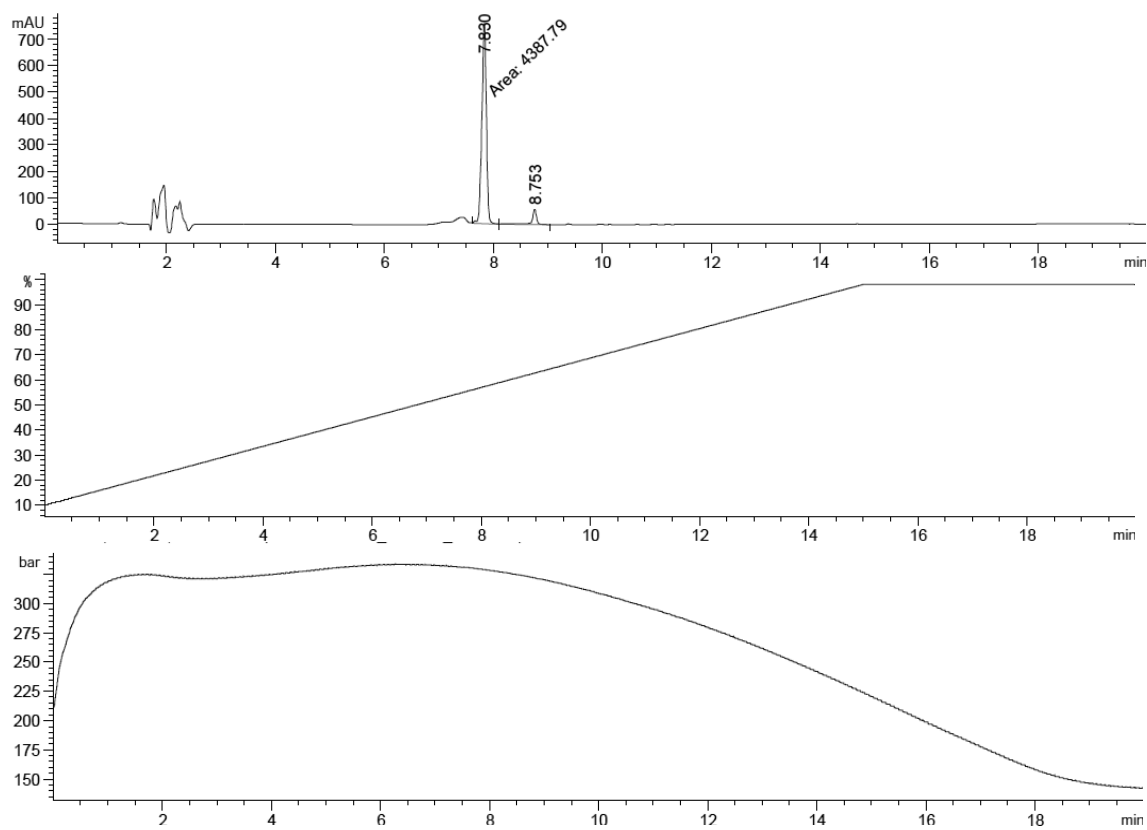
Peak #	RetTime [min]	Type	Width [min]	Area [mAU*s]	Height [mAU]	Area %
1	7.822	MM	0.0720	145.54337	33.69057	3.5492
2	8.845	BV R	0.0834	3955.23389	728.08710	96.4508

Appendix

Irradiation with $\lambda = 365$ nm for conversion from *trans*-isomer to *cis*-isomer.

Detection at 301 nm: t_R *cis*-isomer = 7.830 min (93%), t_R *trans*-isomer = 8.753 min (7%).

Figures of analytical HPLC trace, solvent gradient (acetonitrile/H₂O + 0.01% TFA), pressure profile and data analysis:



Signal 7: DAD1 G, Sig=301,4 Ref=off

Peak #	RetTime [min]	Type	Width [min]	Area [mAU*s]	Height [mAU]	Area %
1	7.830	MM	0.0964	4387.78564	758.81024	93.0113
2	8.753	VV R	0.0800	329.69113	57.61179	6.9887

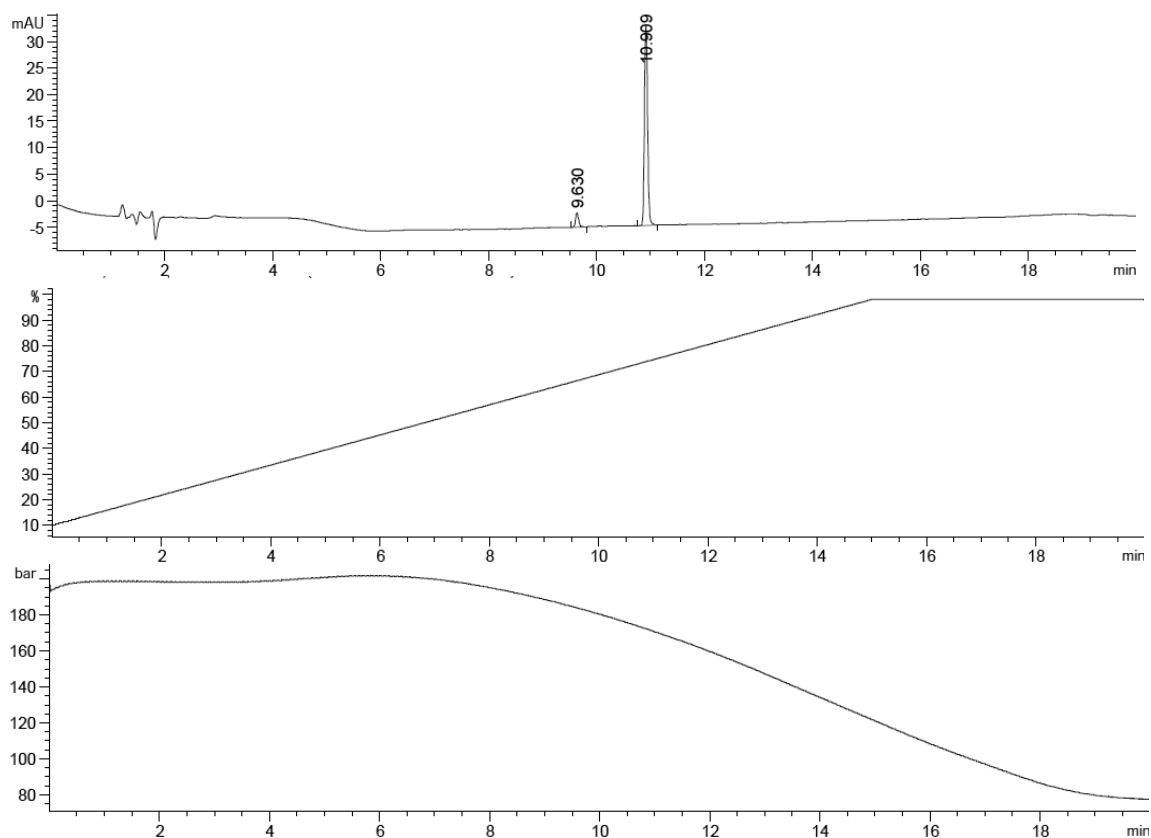
Appendix

Compound 3c (20 μ M solution in TrisHCl Buffer + 0.2% DMSO, pH 7.5, injection volume 10 μ L):

Irradiation with $\lambda = 528$ nm for conversion from *cis*-isomer to *trans*-isomer.

Detection at 291 nm: t_R *cis*-isomer = 9.630 min (7%), t_R *trans*-isomer = 10.909 min (93%).

Figures of analytical HPLC trace, solvent gradient (acetonitrile/H₂O + 0.01% TFA), pressure profile and data analysis:



Signal 3: DAD1 C, Sig=291,4 Ref=off

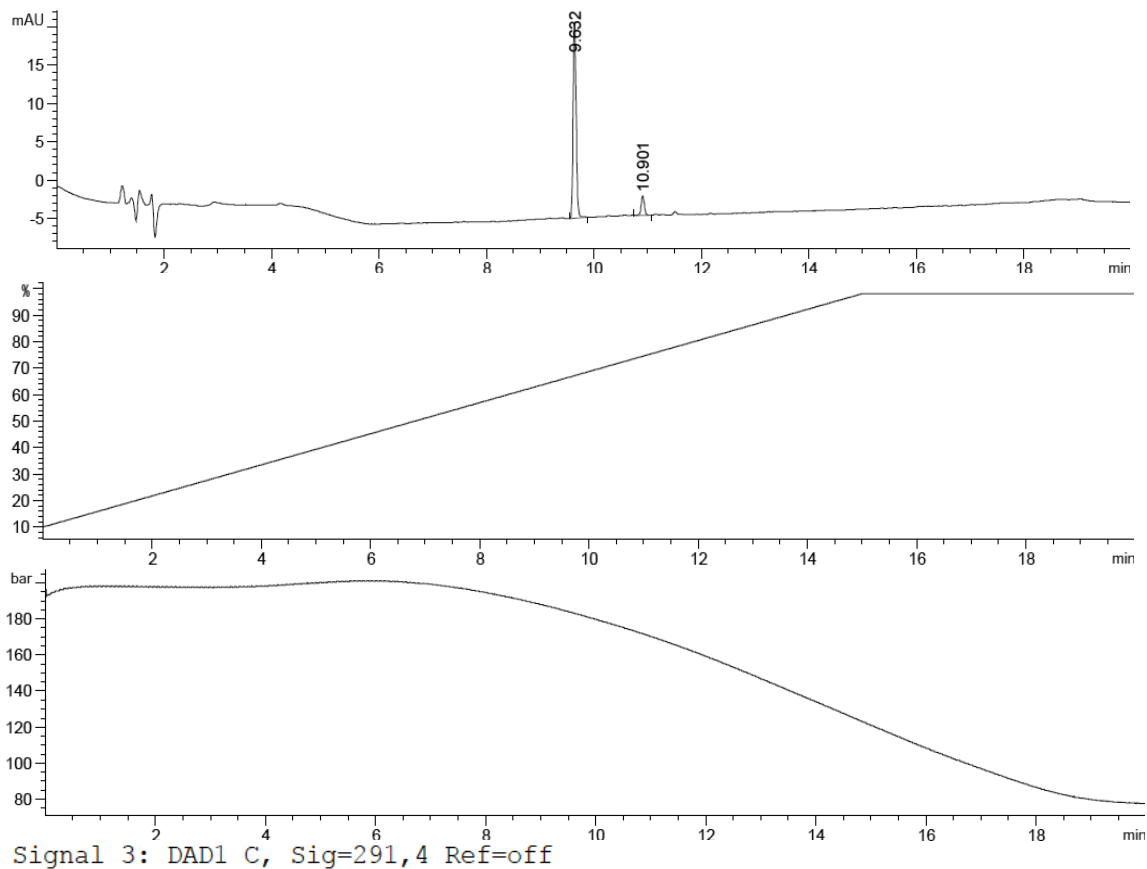
Peak #	RetTime [min]	Type	Width [min]	Area [mAU*s]	Height [mAU]	Area %
1	9.630	BB	0.0631	10.74787	2.66116	6.5235
2	10.909	BB	0.0633	154.00816	37.97816	93.4765

Appendix

Irradiation with $\lambda = 365$ nm for conversion from *trans*-isomer to *cis*-isomer.

Detection at 291 nm: t_R *cis*-isomer = 9.632 min (91%), t_R *trans*-isomer = 10.901 min (9%).

Figures of analytical HPLC trace, solvent gradient (acetonitrile/H₂O + 0.01% TFA), pressure profile and data analysis:



Signal 3: DAD1 C, Sig=291,4 Ref=off

Peak #	RetTime [min]	Type	Width [min]	Area [mAU*s]	Height [mAU]	Area %
1	9.632	BB	0.0623	101.88867	25.64798	90.6958
2	10.901	BB	0.0647	10.45243	2.50319	9.3042

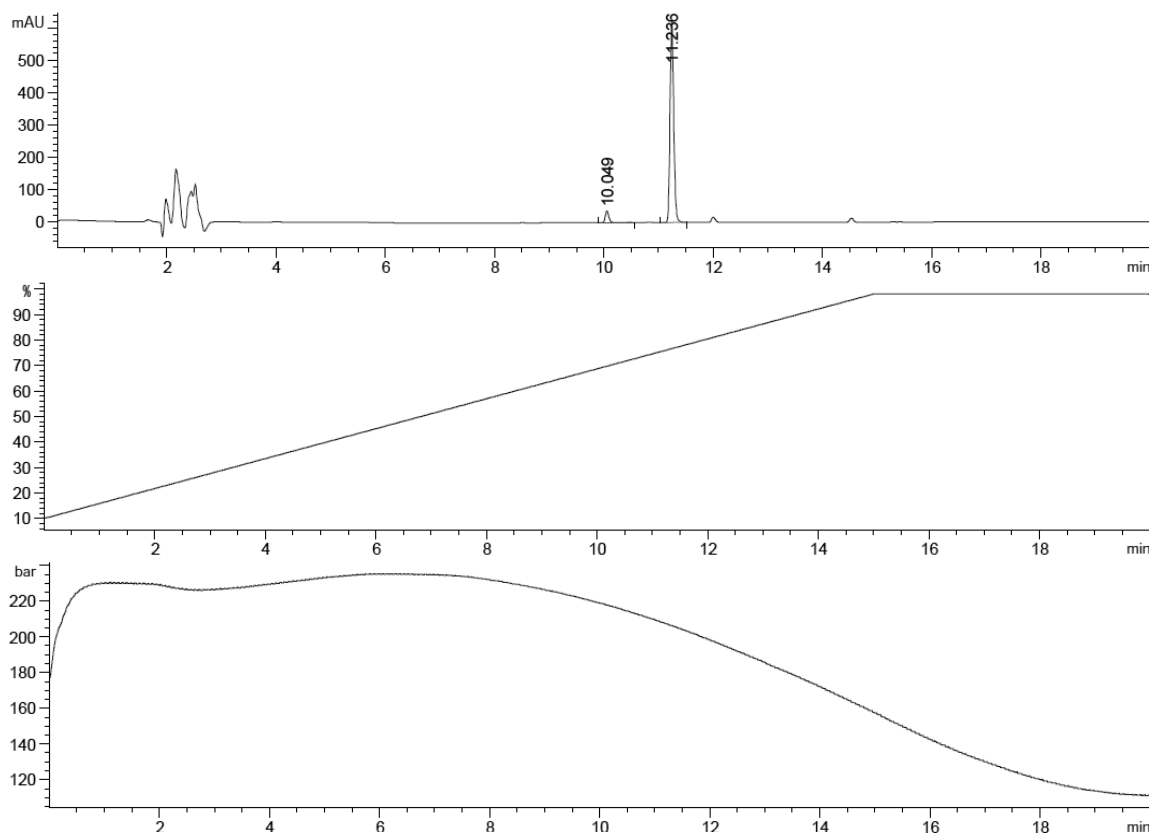
Appendix

Compound 3c (50 μ M solution in DMSO, injection volume 10 μ L):

Irradiation with $\lambda = 528$ nm for conversion from *cis*-isomer to *trans*-isomer.

Detection at 303 nm: t_R *cis*-isomer = 10.049 min (6%), t_R *trans*-isomer = 11.236 min (94%).

Figures of analytical HPLC trace, solvent gradient (acetonitrile/H₂O + 0.01% TFA), pressure profile and data analysis:



Signal 7: DAD1 G, Sig=303,4 Ref=off

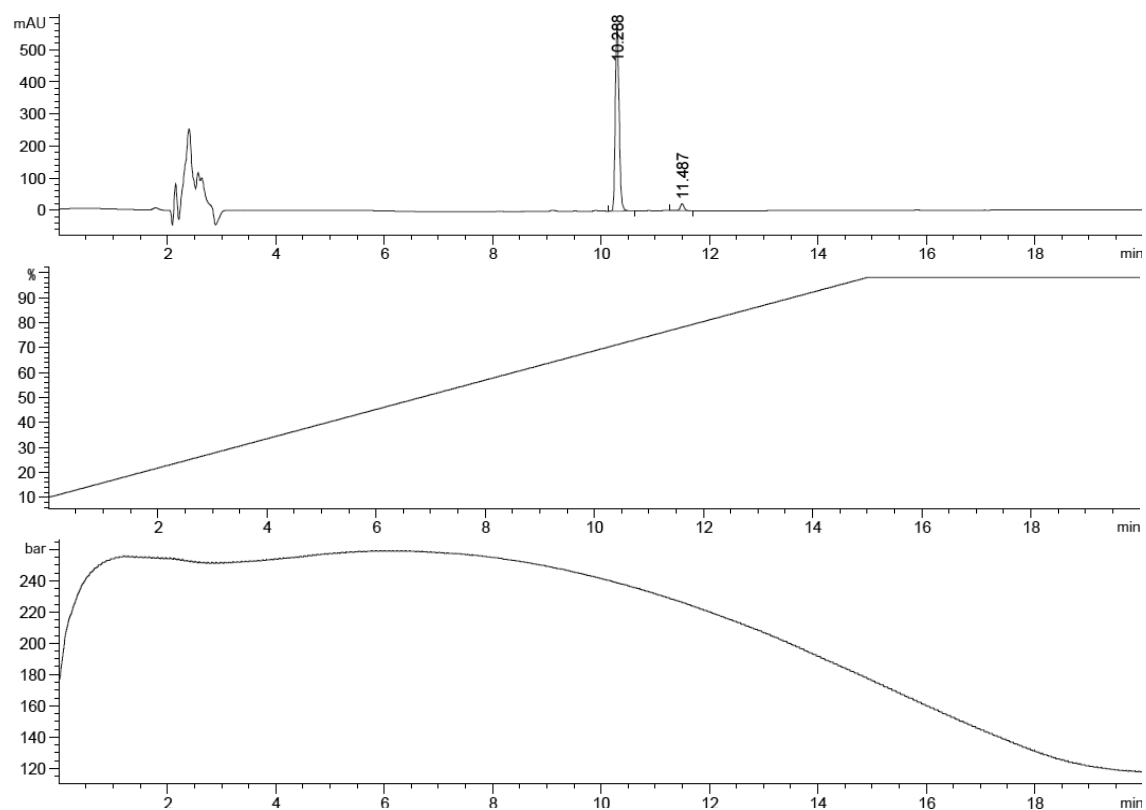
Peak #	RetTime [min]	Type	Width [min]	Area [mAU*s]	Height [mAU]	Area %
1	10.049	VV R	0.0719	172.46210	35.95505	5.5812
2	11.236	BB	0.0734	2917.61401	614.87427	94.4188

Appendix

Irradiation with $\lambda = 365$ nm for conversion from *trans*-isomer to *cis*-isomer.

Detection at 303 nm: t_R *cis*-isomer = 10.288 min (96%), t_R *trans*-isomer = 11.487 min (4%).

Figures of analytical HPLC trace, solvent gradient (acetonitrile/H₂O + 0.01% TFA), pressure profile and data analysis:

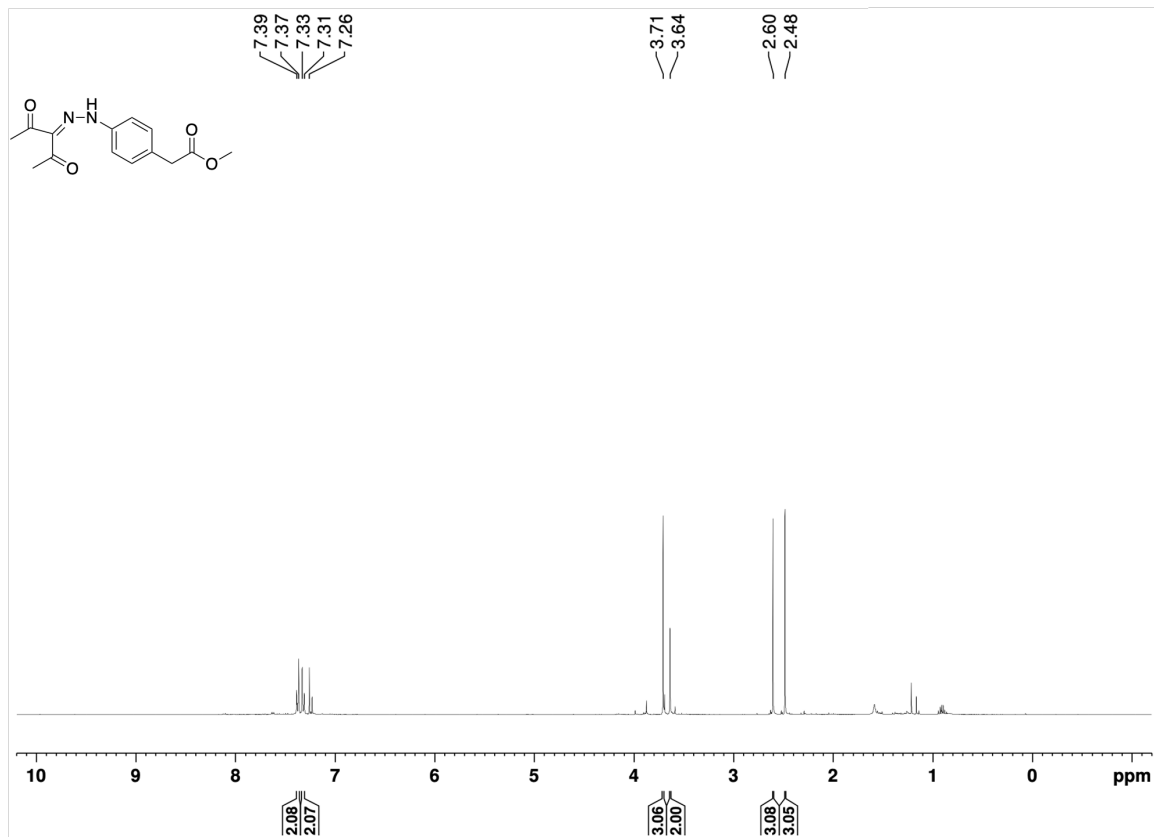


Signal 7: DAD1 G, Sig=303,4 Ref=off

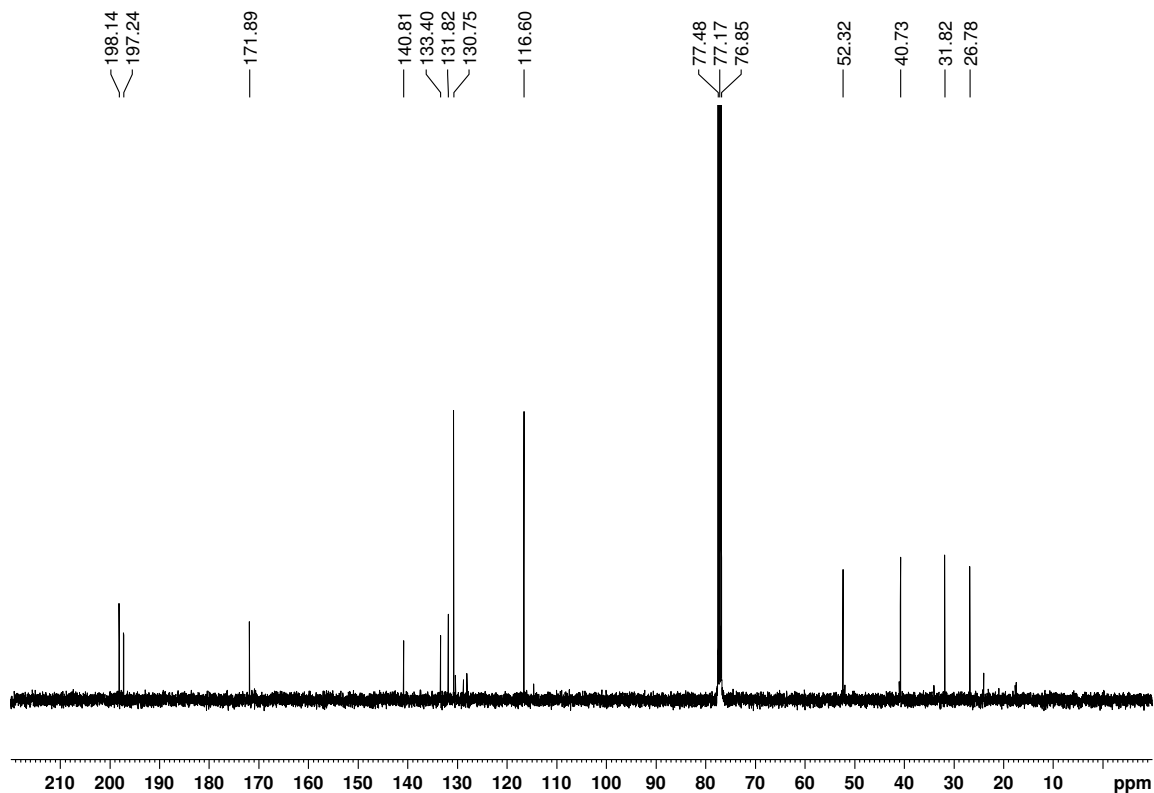
Peak #	RetTime [min]	Type	Width [min]	Area [mAU*s]	Height [mAU]	Area %
1	10.288	VB	0.0745	2821.02271	582.58197	96.3605
2	11.487	BB	0.0785	106.55003	21.23673	3.6395

7.2.3 NMR Spectra

^1H spectrum of **6** (400 MHz, CDCl_3):

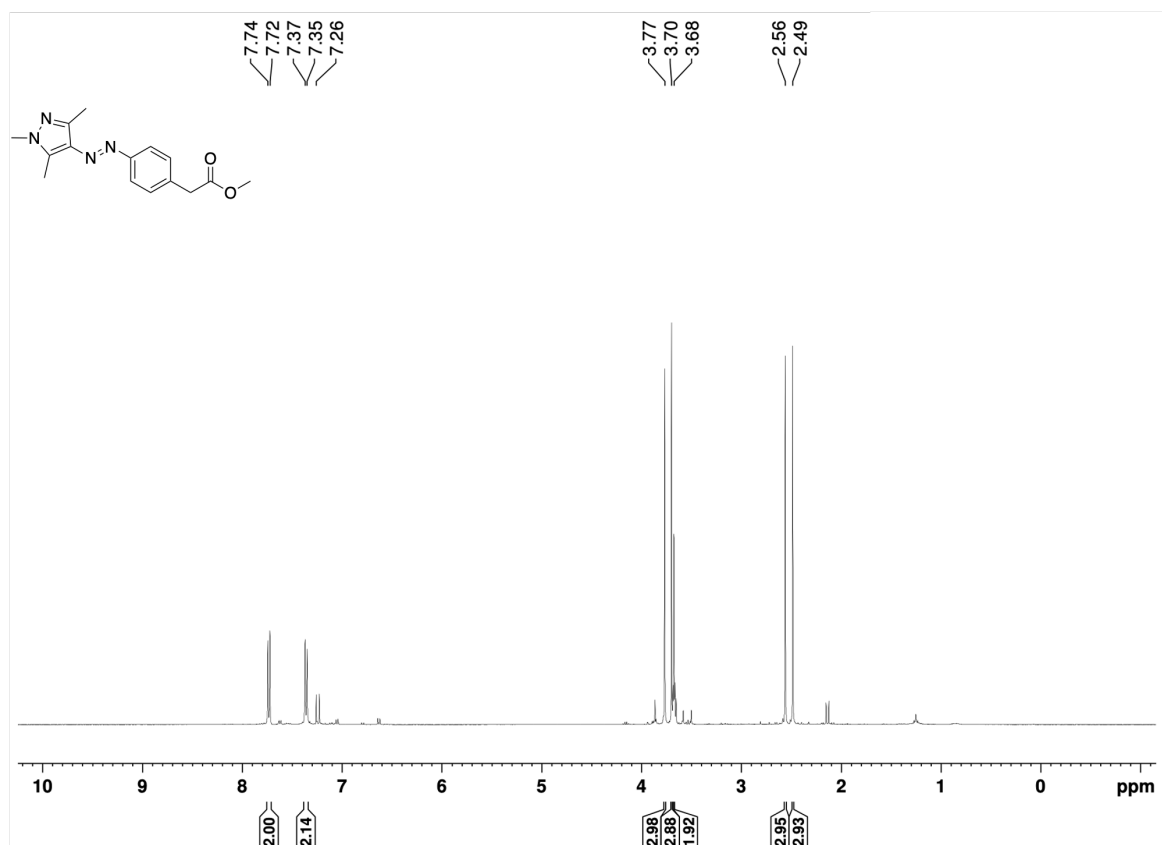


^{13}C spectrum of **6** (101 MHz, CDCl_3):

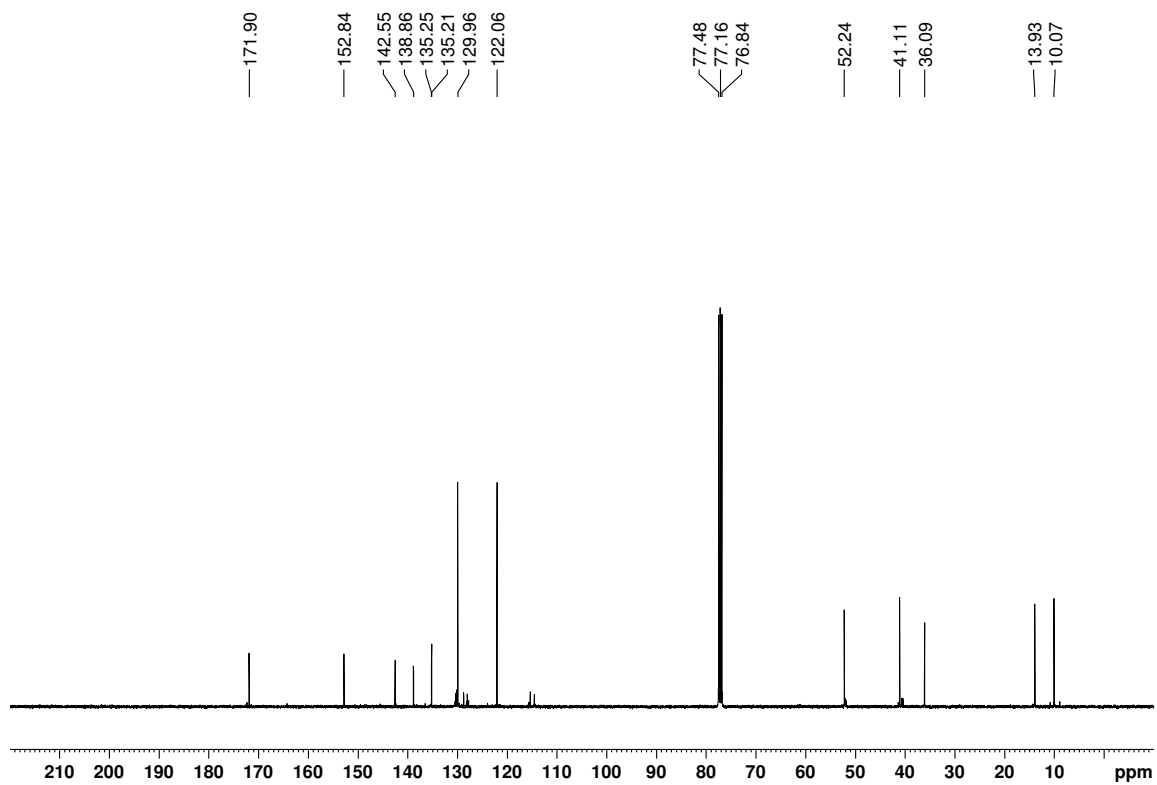


Appendix

^1H spectrum of **7** (400 MHz, CDCl_3):

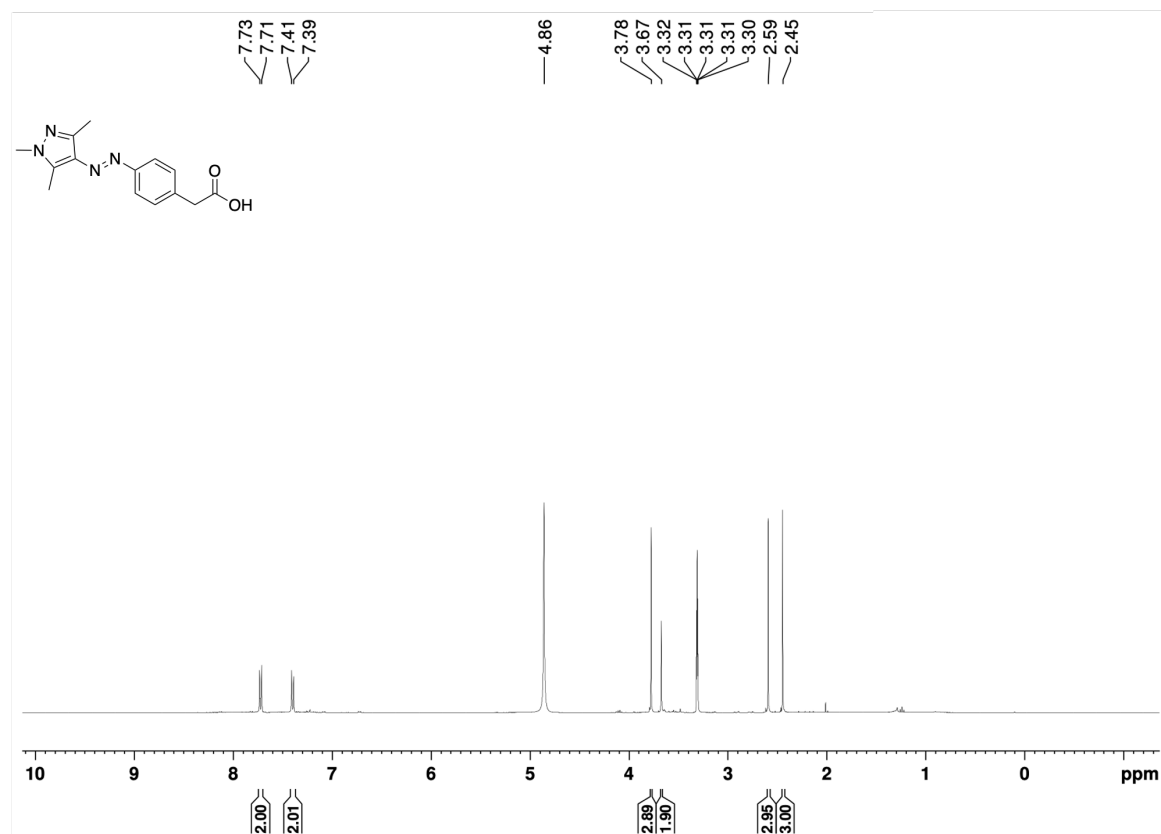


^{13}C spectrum of **7** (101 MHz, CDCl_3):

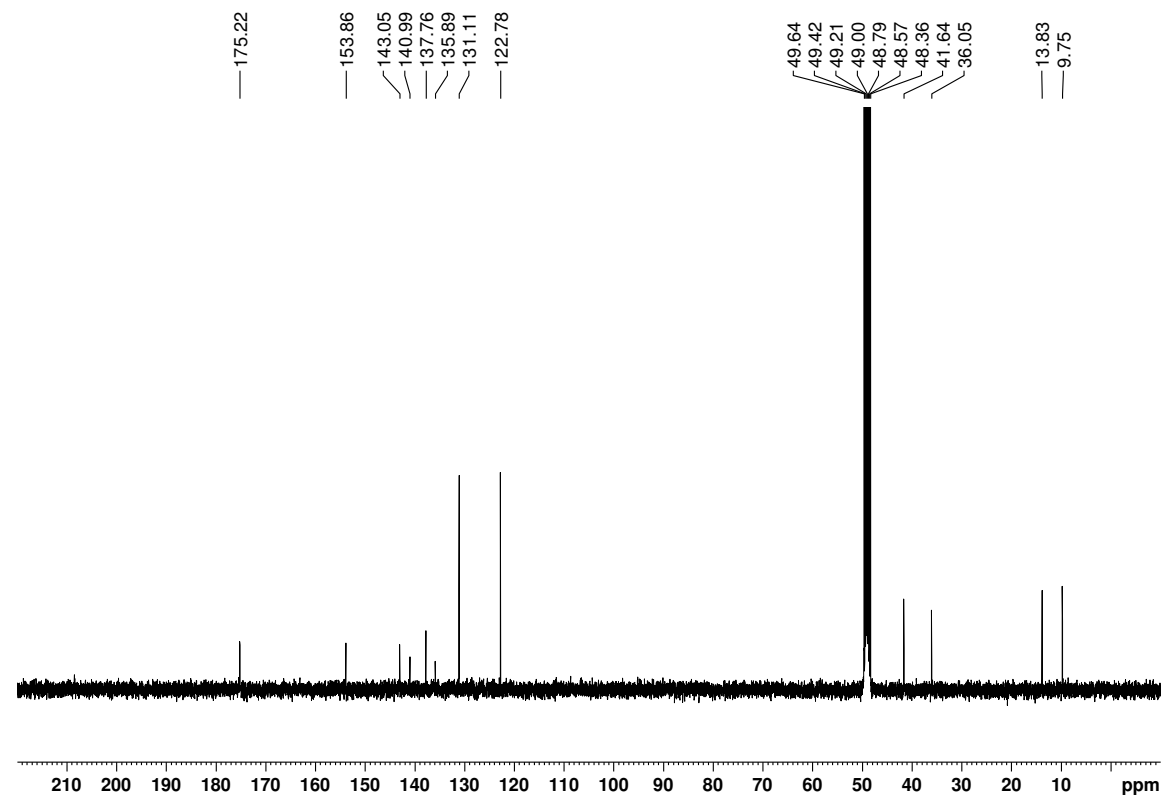


Appendix

^1H spectrum of **8** (400 MHz, MeOD):

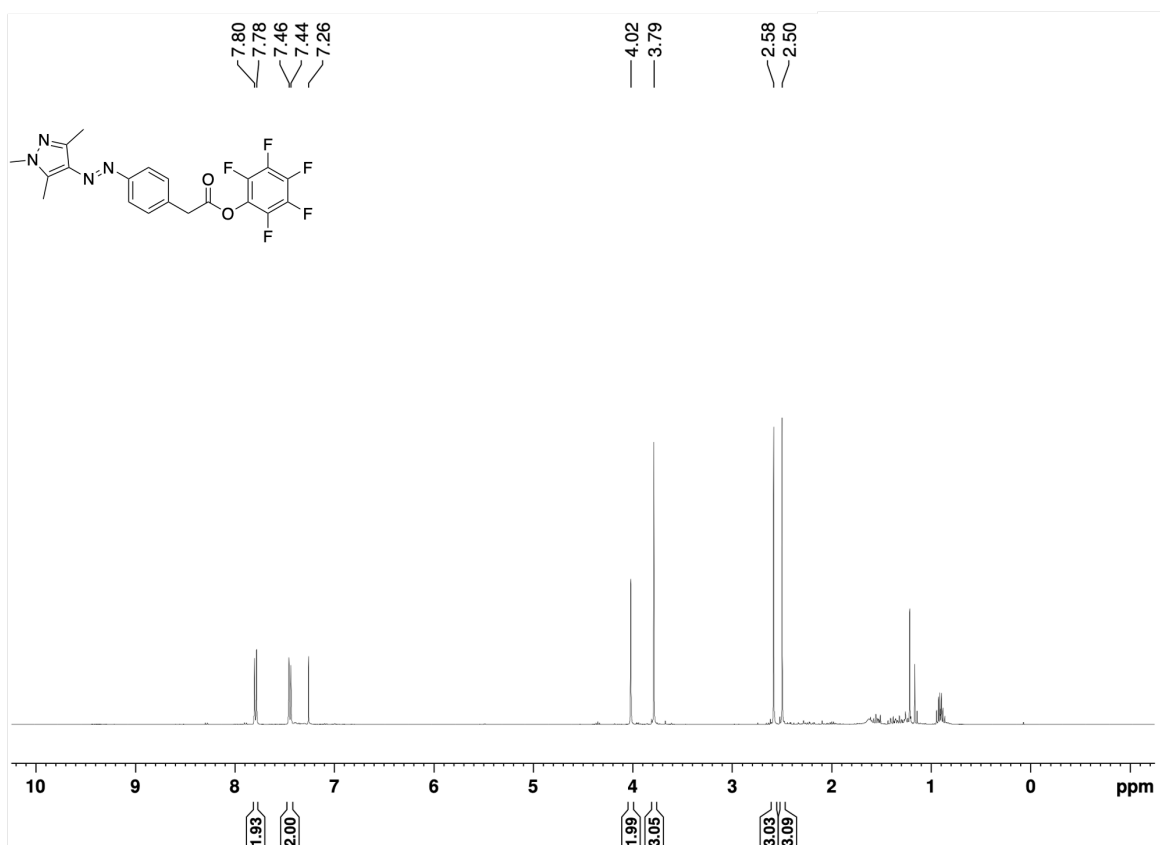


^{13}C spectrum of **8** (101 MHz, MeOD):



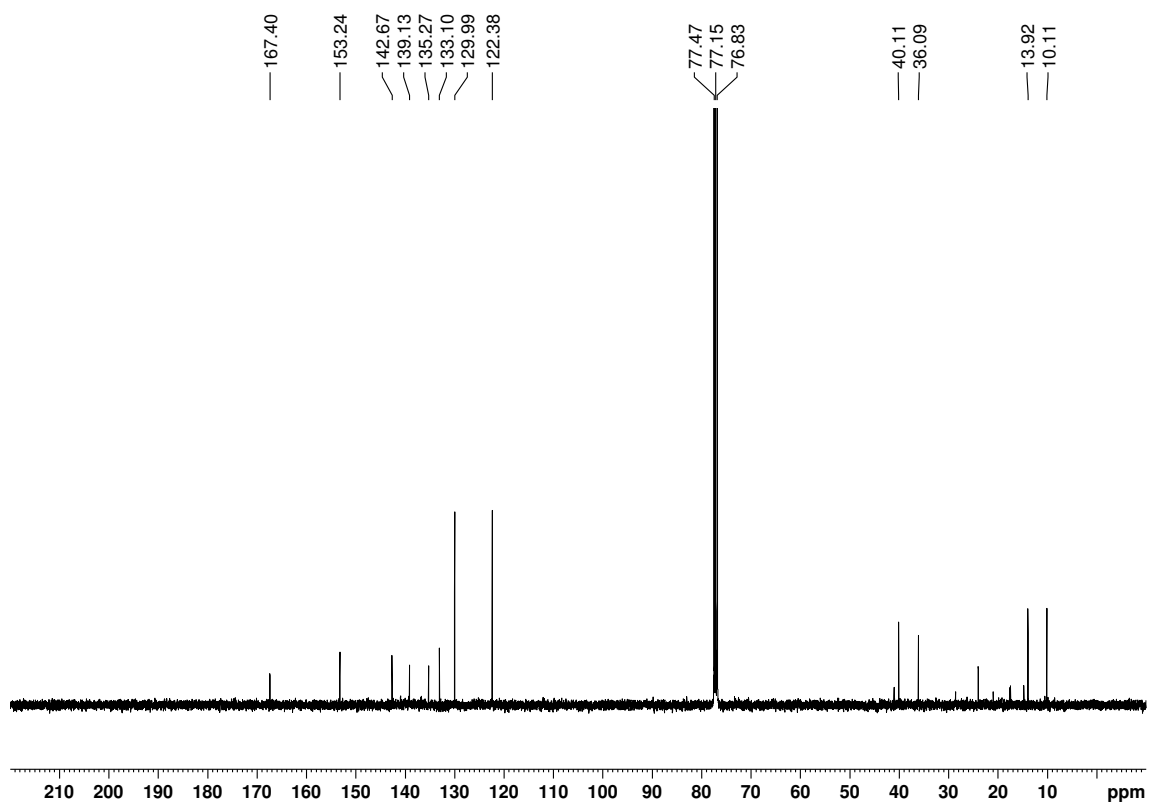
Appendix

^1H spectrum of **9** (400 MHz, CDCl_3):



*Contains grease.

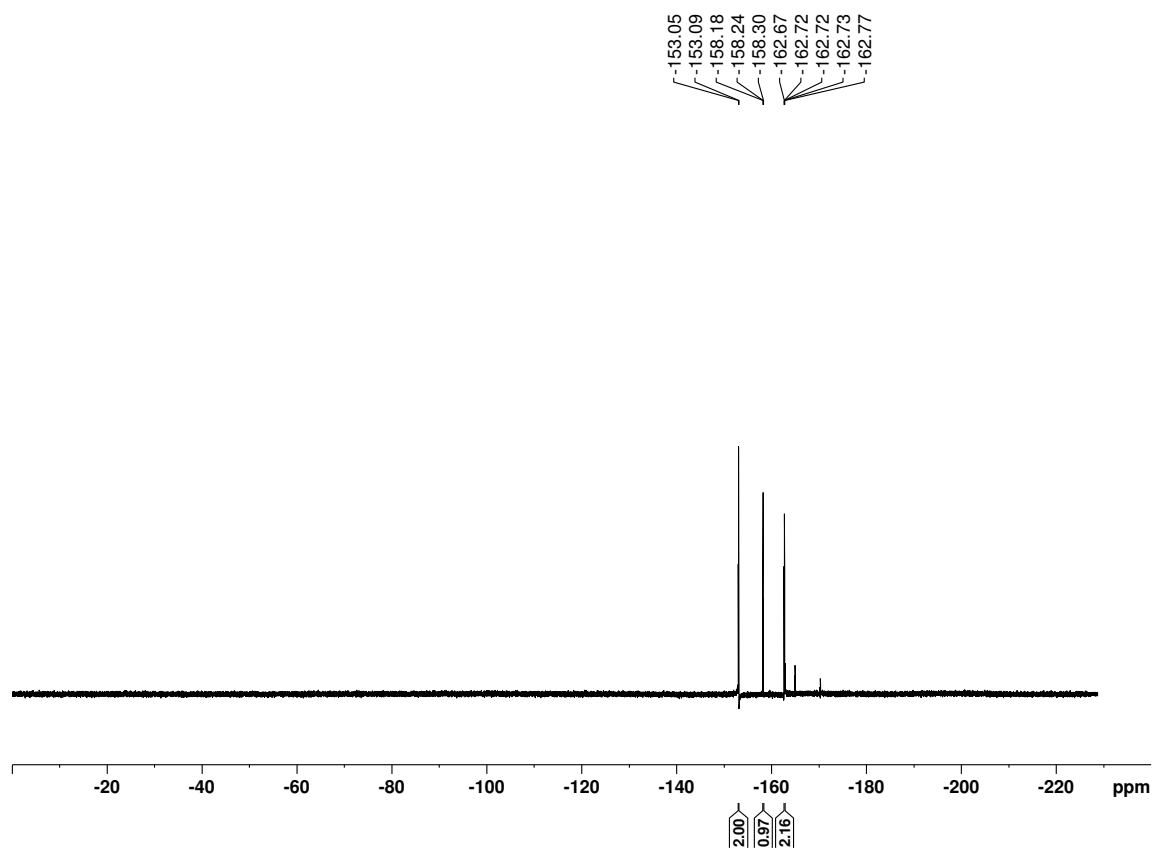
^{13}C spectrum of **9** (101 MHz, CDCl_3):



*Contains grease.

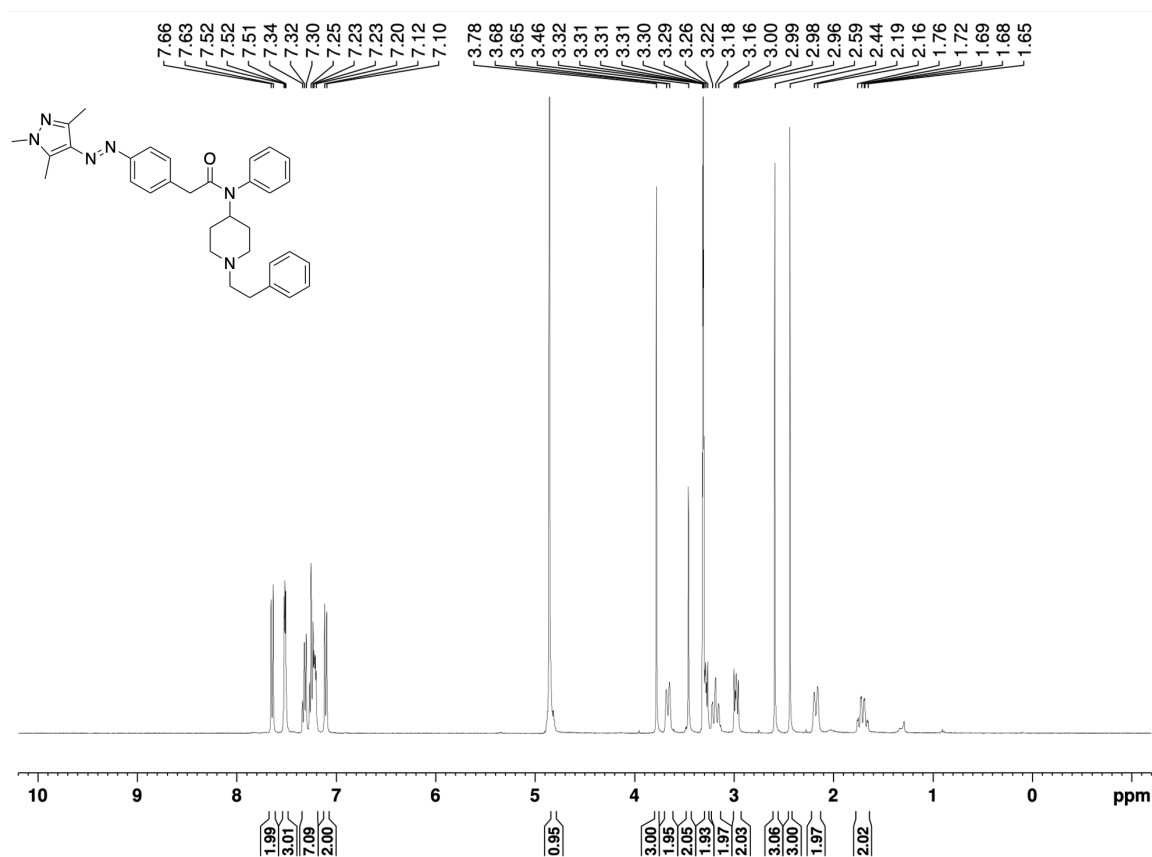
Appendix

^{19}F spectrum of **9** (377 MHz, CDCl_3):



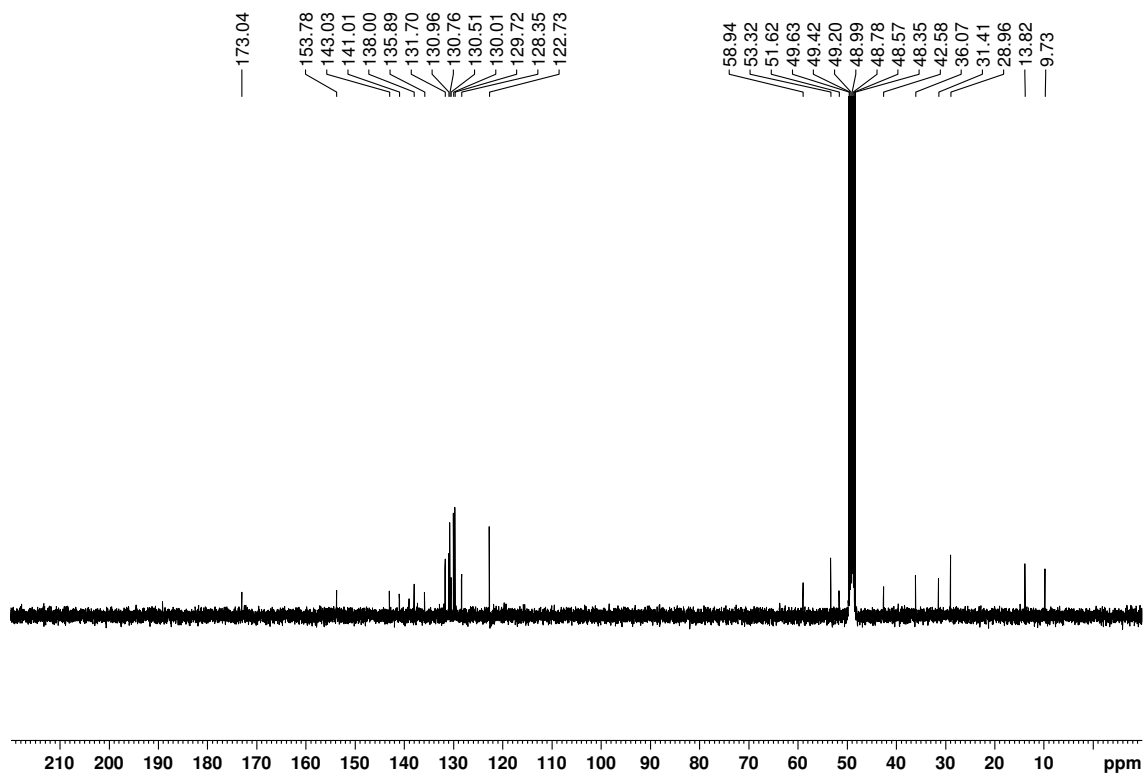
Appendix

^1H spectrum of **1** (400 MHz, MeOD):



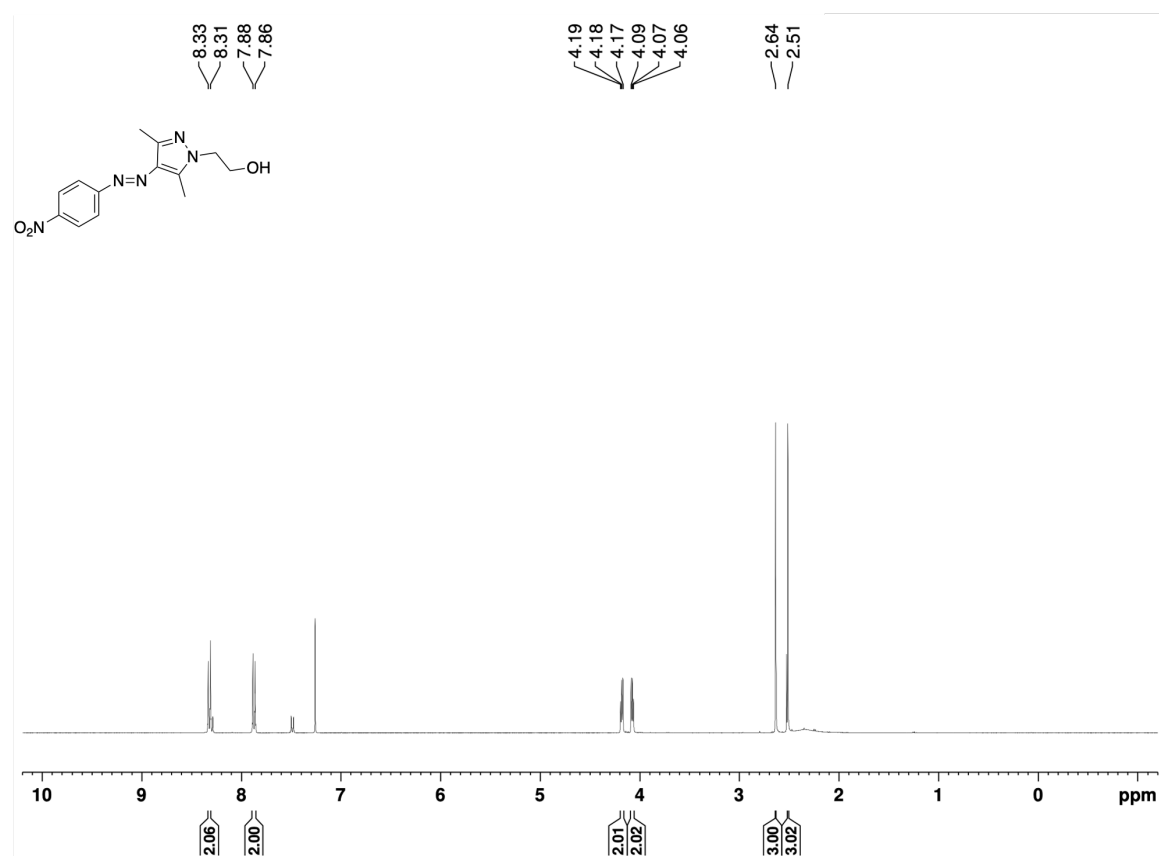
*Contains water present in MeOD.

^{13}C spectrum of **1** (101 MHz, MeOD):

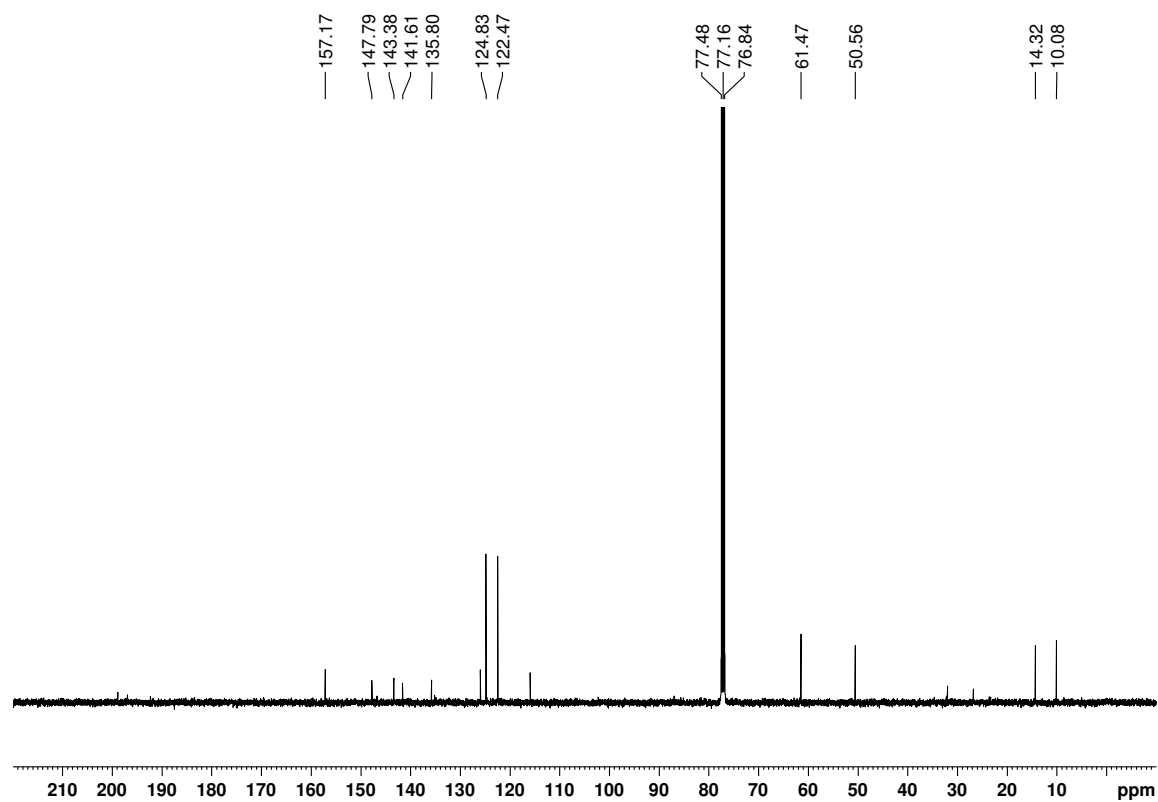


Appendix

^1H spectrum of **11** (400 MHz, CDCl_3):

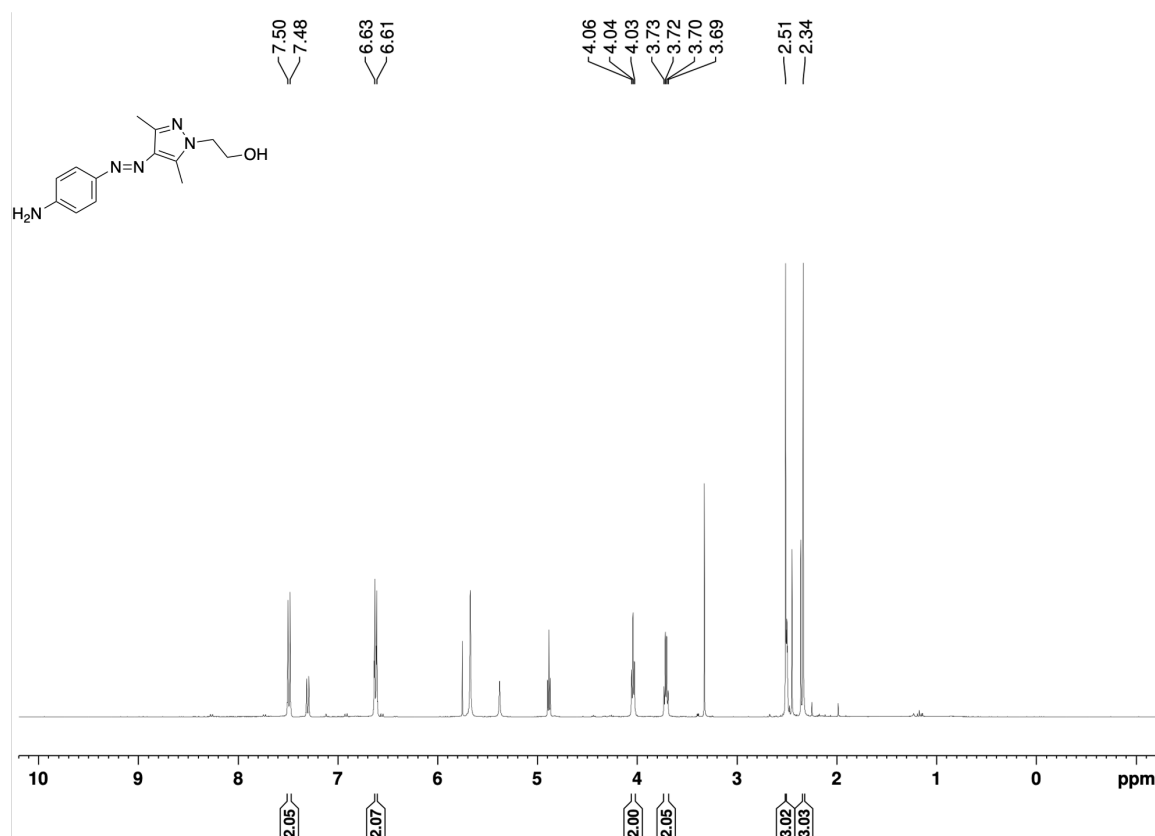


^{13}C spectrum of **11** (101 MHz, CDCl_3):

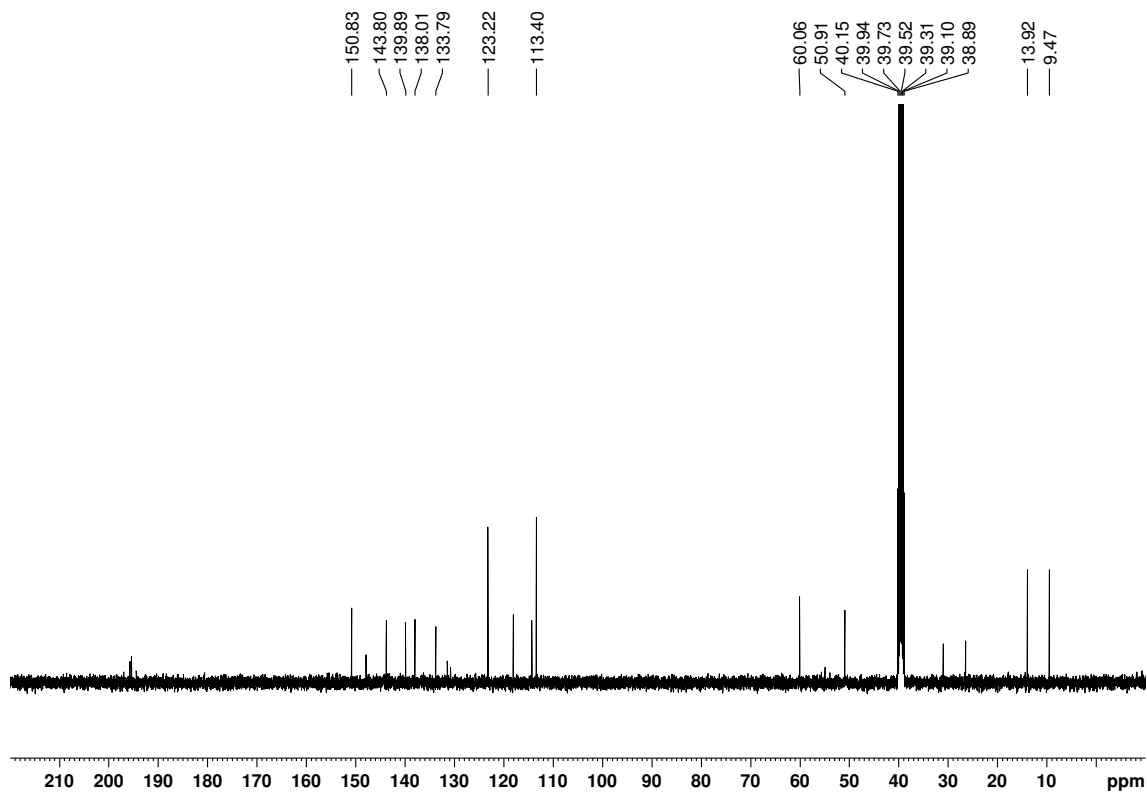


Appendix

^1H spectrum of **12** (400 MHz, $\text{DMSO-}D_6$):

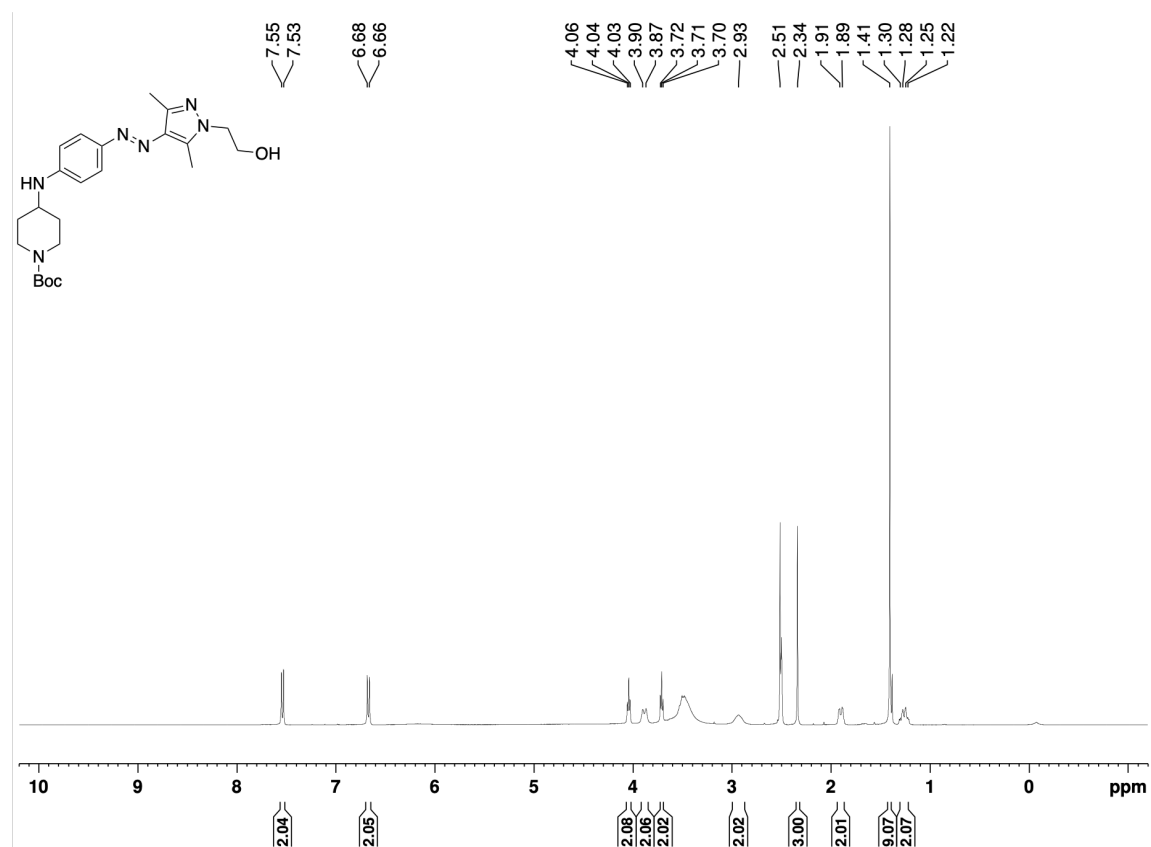


^{13}C spectrum of **12** (101 MHz, $\text{DMSO-}D_6$):

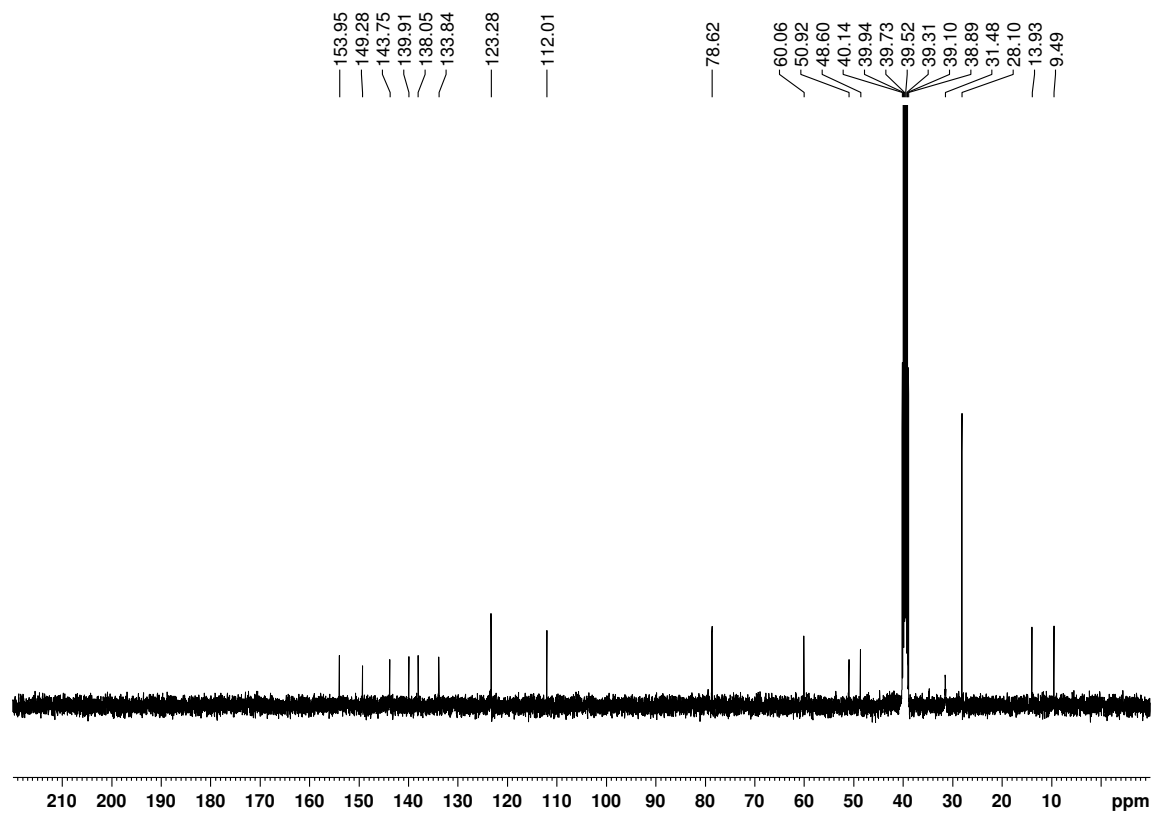


Appendix

^1H spectrum of **13** (400 MHz, DMSO-D_6):

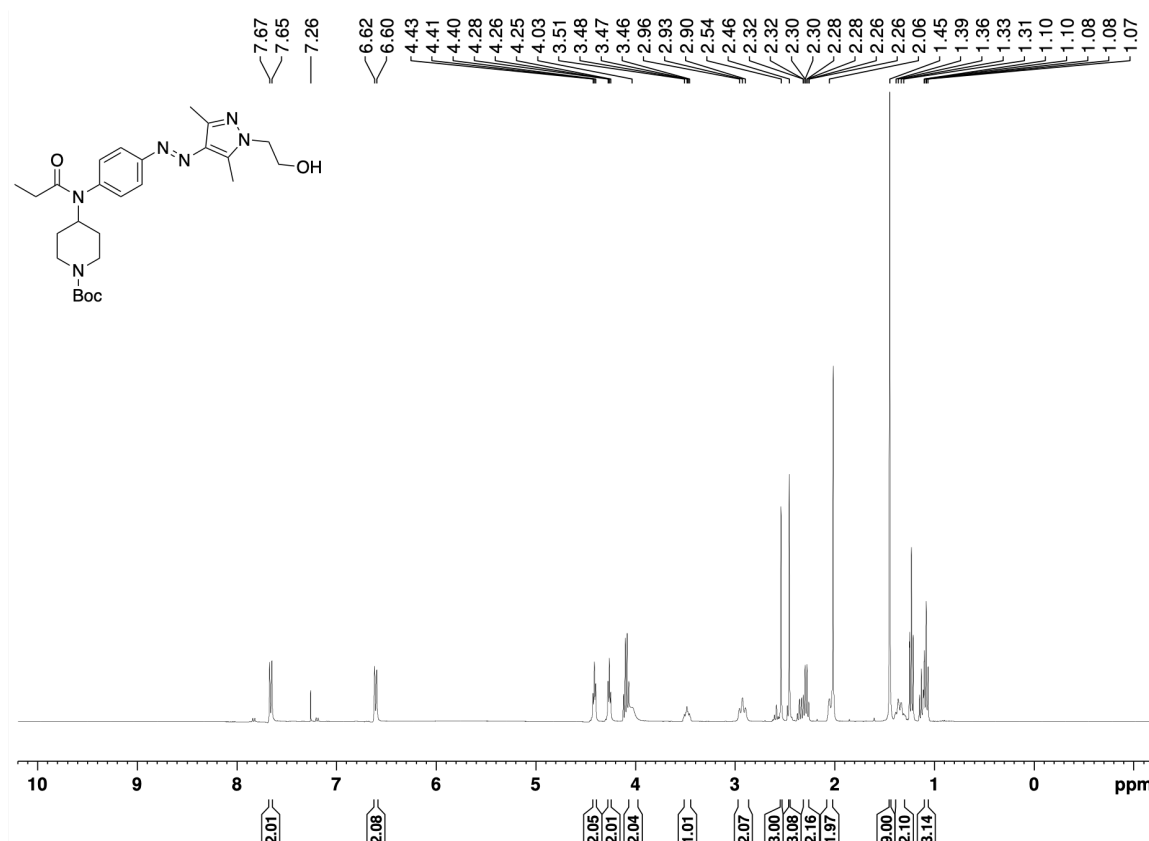


^{13}C spectrum of **13** (101 MHz, DMSO-D_6):



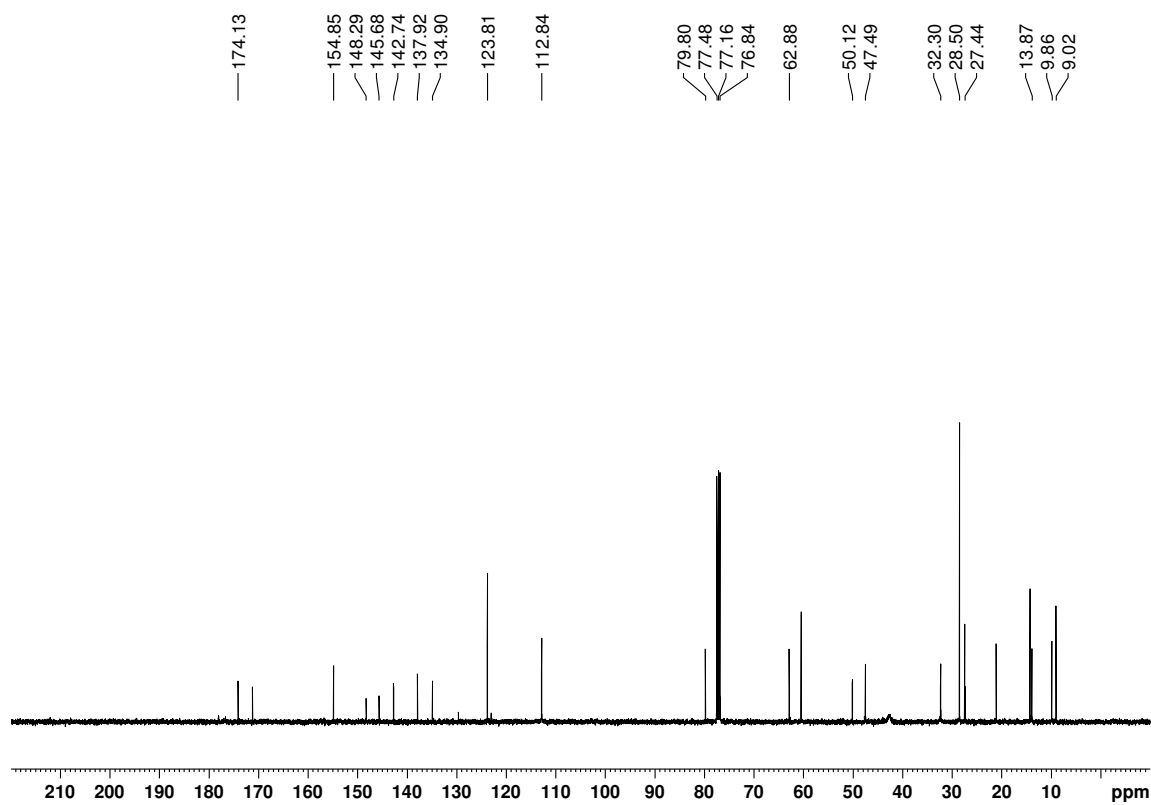
Appendix

^1H spectrum of **14** (400 MHz, CDCl_3):



*Contains ethyl acetate

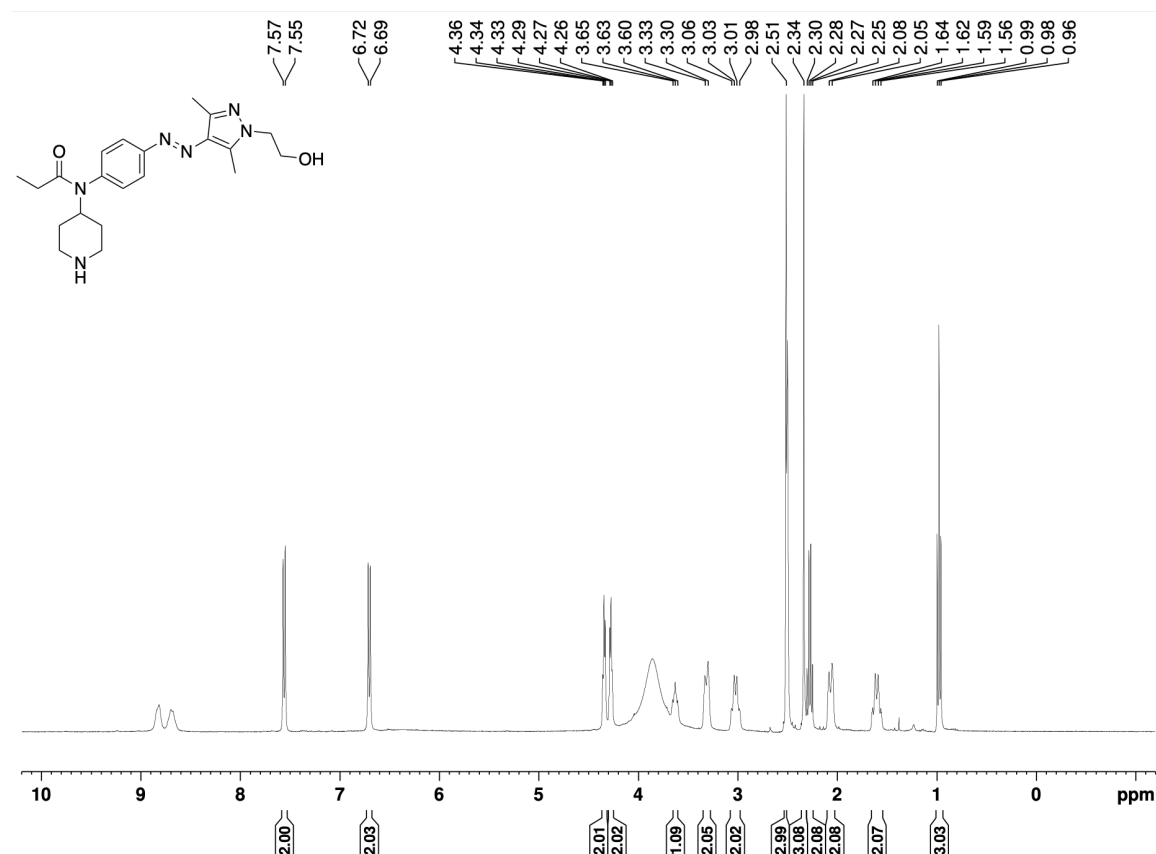
^{13}C spectrum of **14** (101 MHz, CDCl_3):



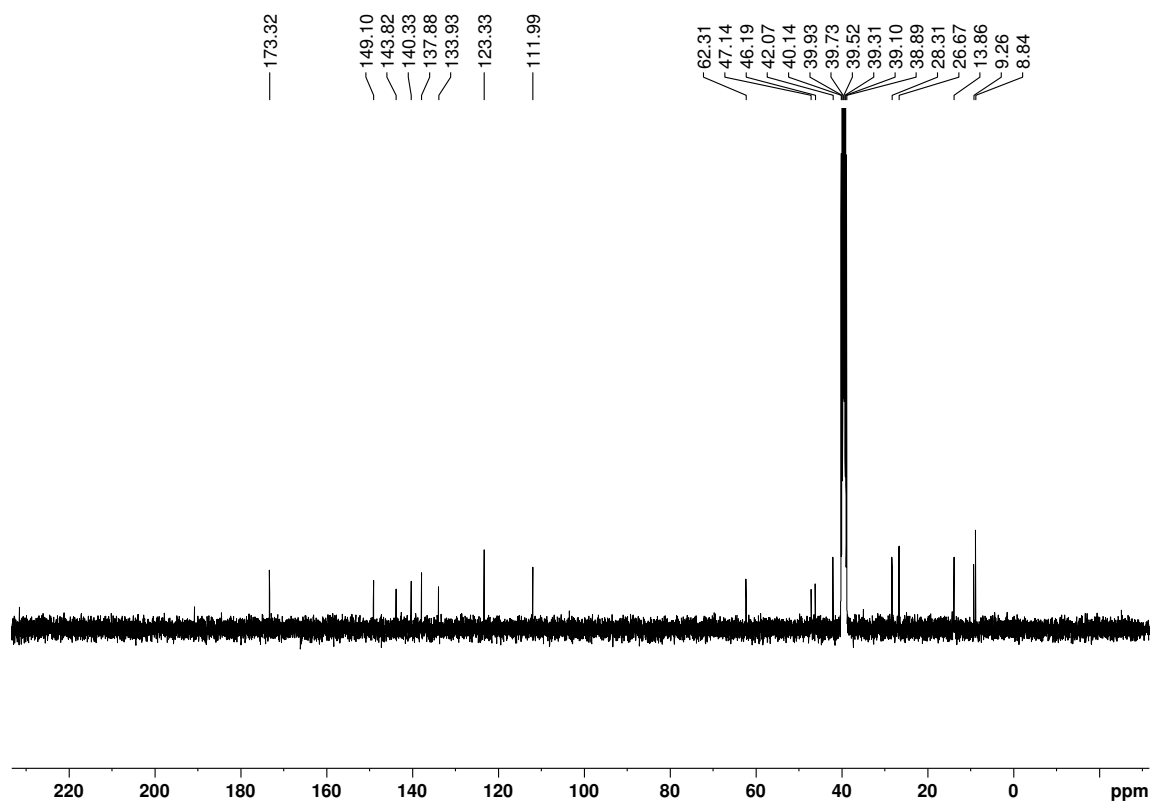
*Contains ethyl acetate

Appendix

^1H spectrum of **15** (400 MHz, DMSO-D_6):

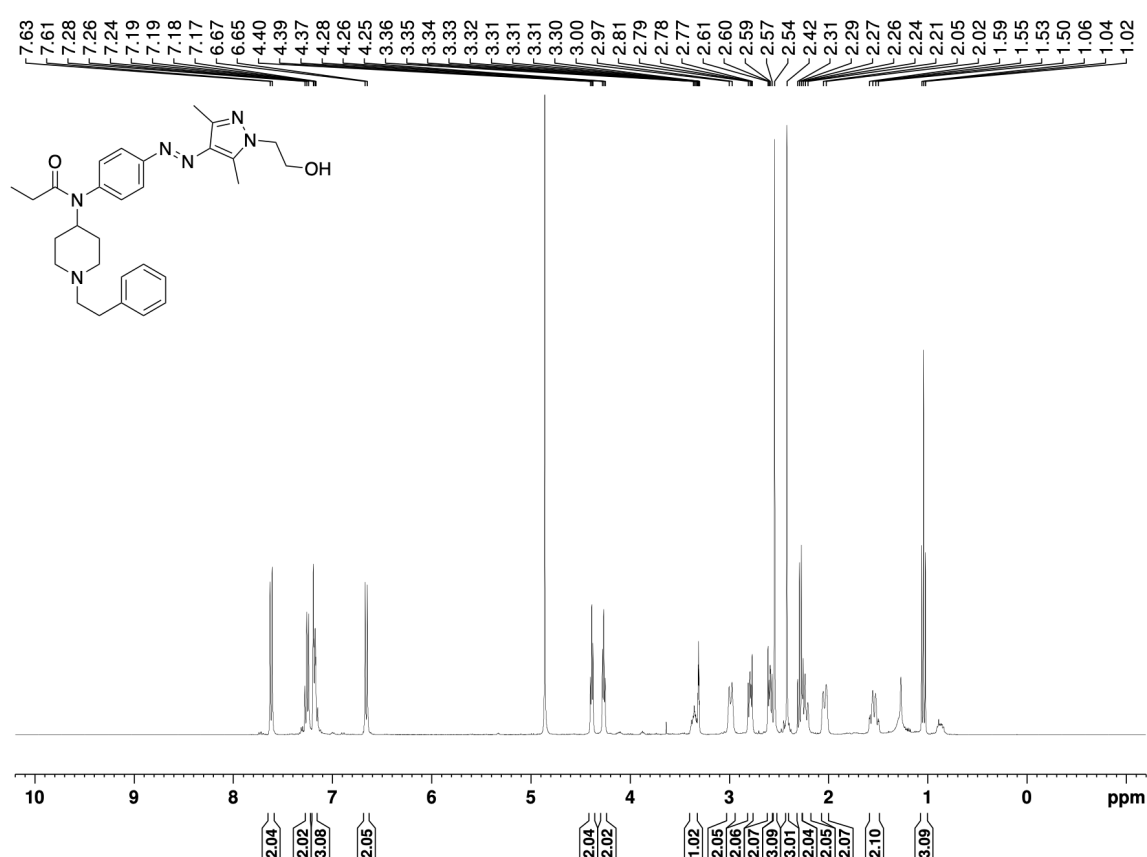


^{13}C spectrum of **15** (101 MHz, DMSO-D_6):



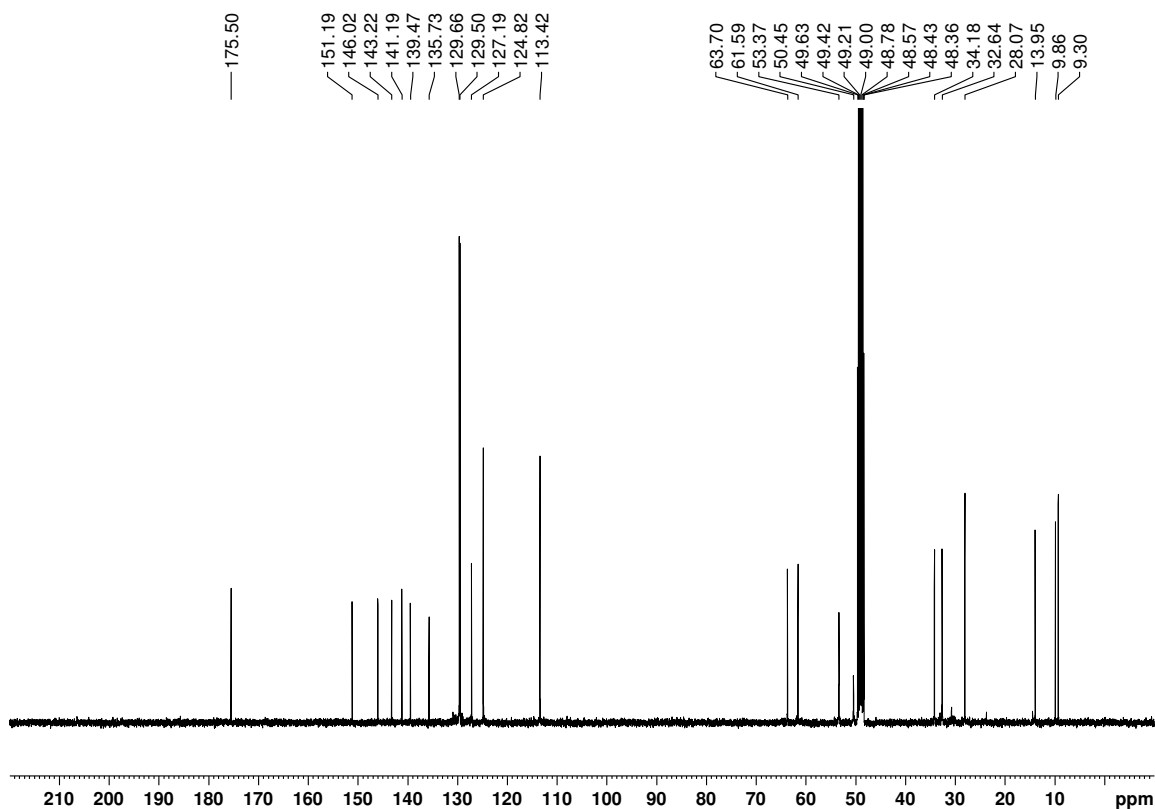
Appendix

^1H spectrum of **2** (400 MHz, MeOD):



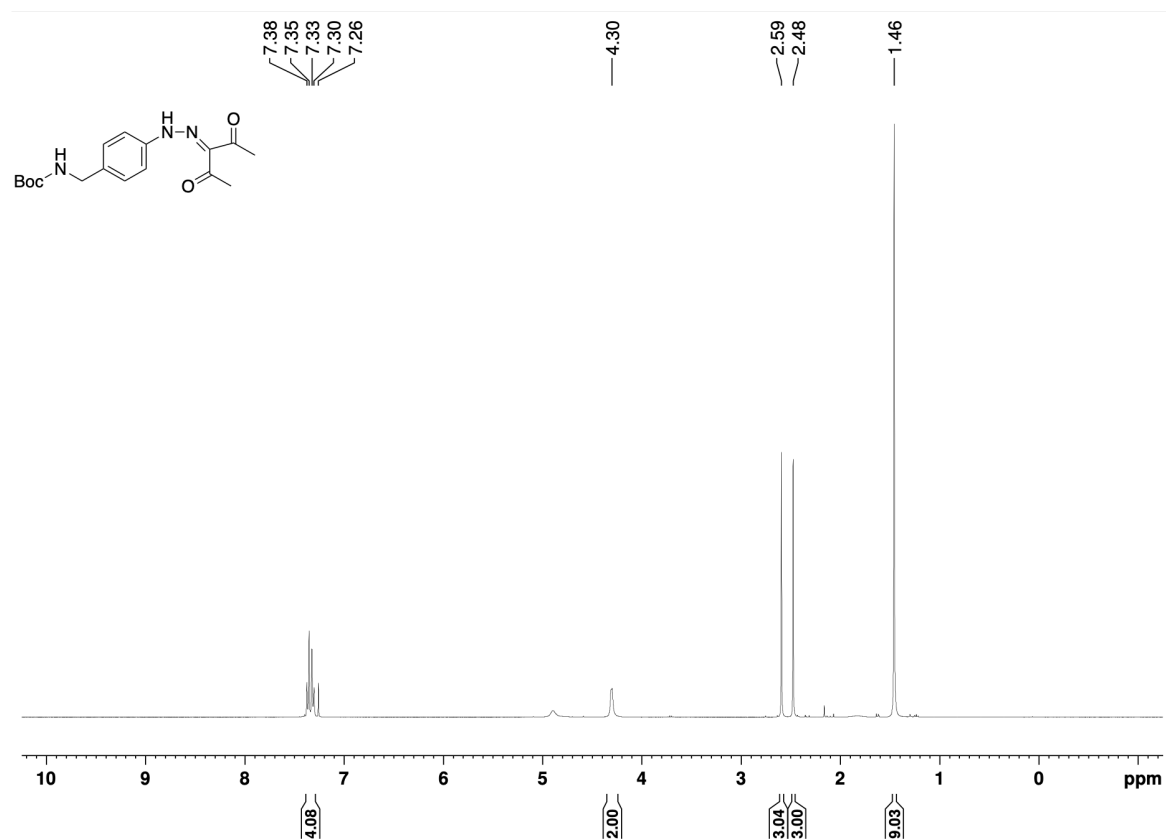
*Contains water that was present in MeOD and trace amounts of grease.

^{13}C spectrum of **2** (101 MHz, MeOD):

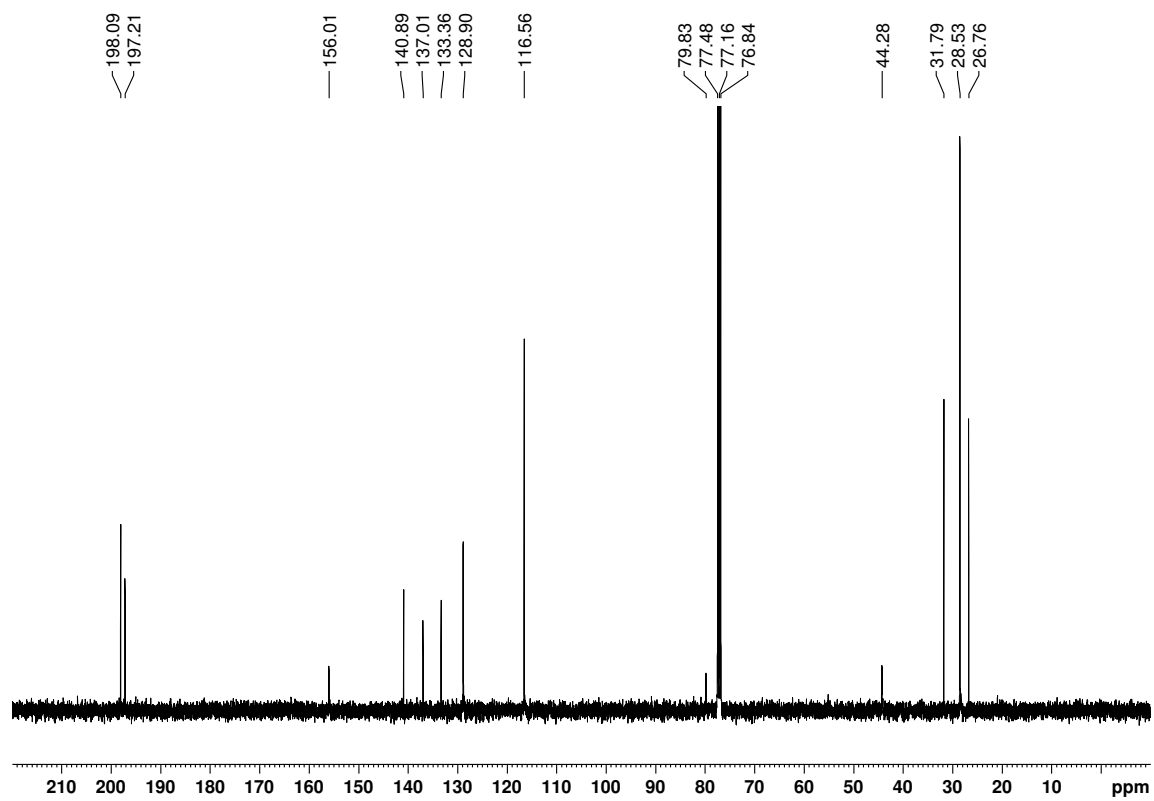


Appendix

^1H spectrum of **17** (400 MHz, CDCl_3):

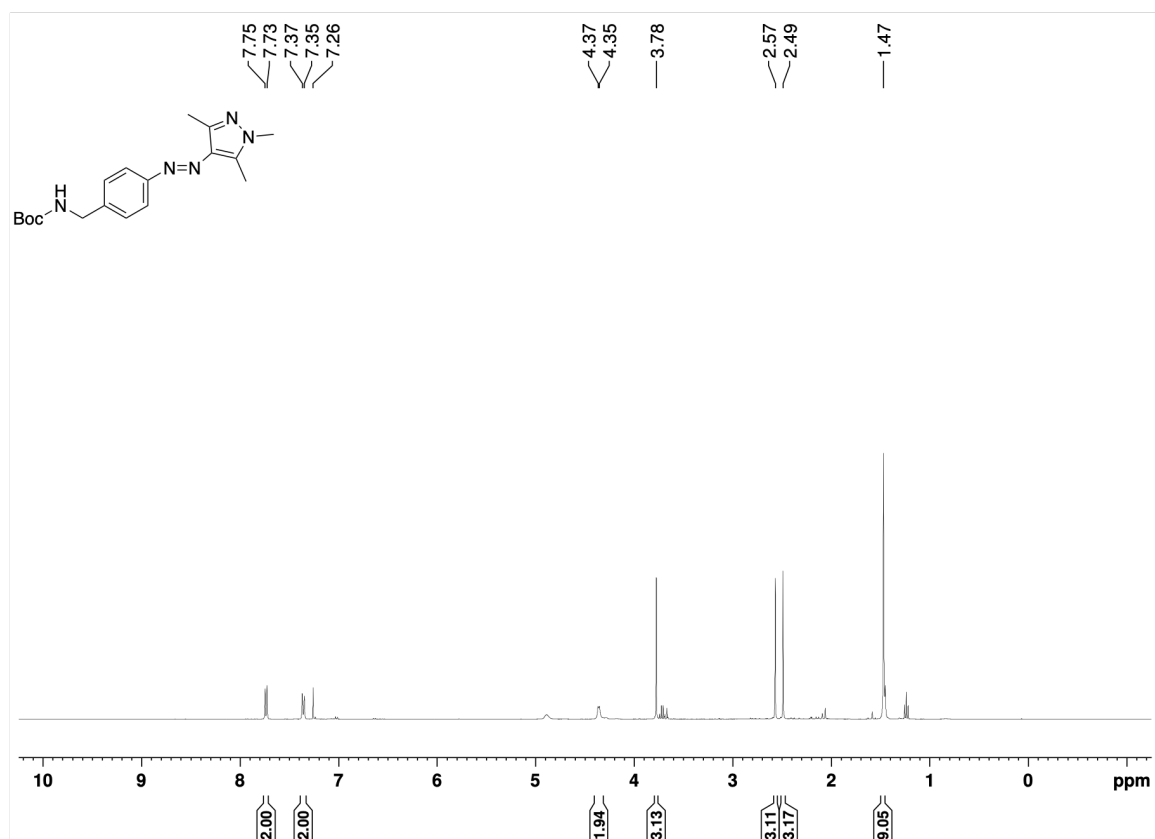


^{13}C spectrum of **17** (101 MHz, CDCl_3):



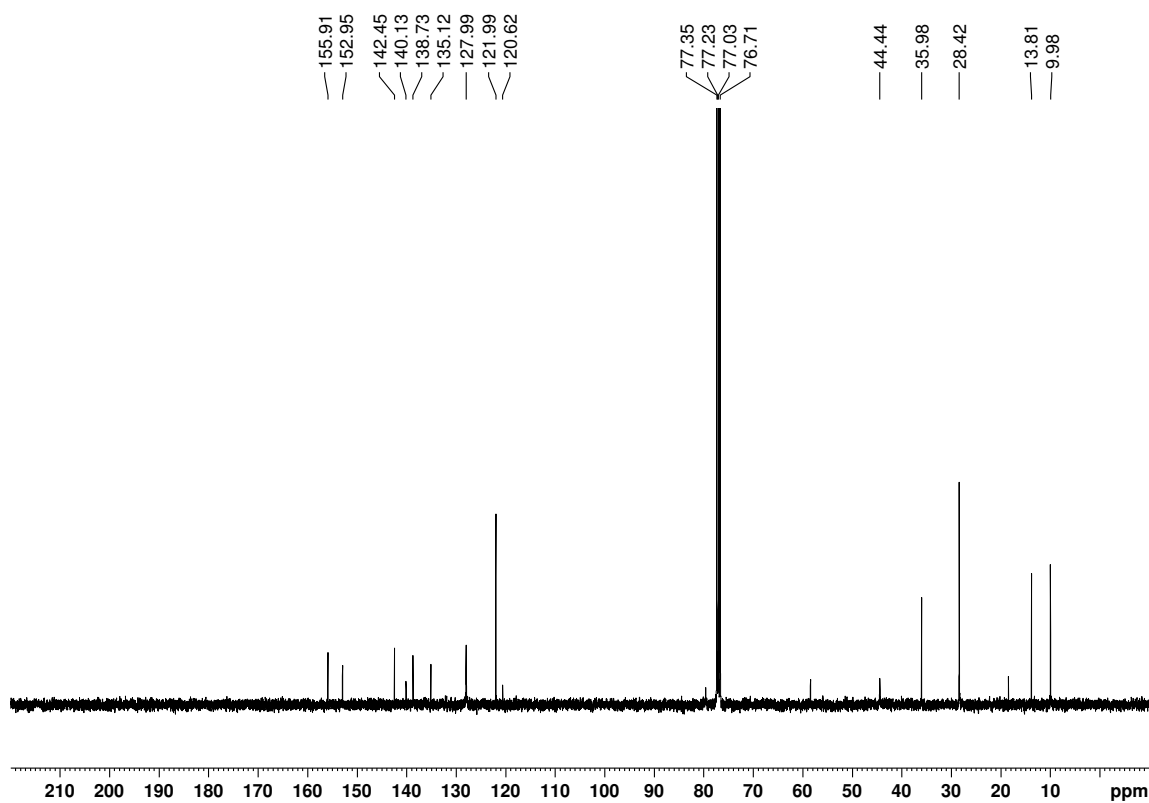
Appendix

^1H spectrum of **18** (400 MHz, CDCl_3):



*Contains ethanol. Yield was obtained after further drying.

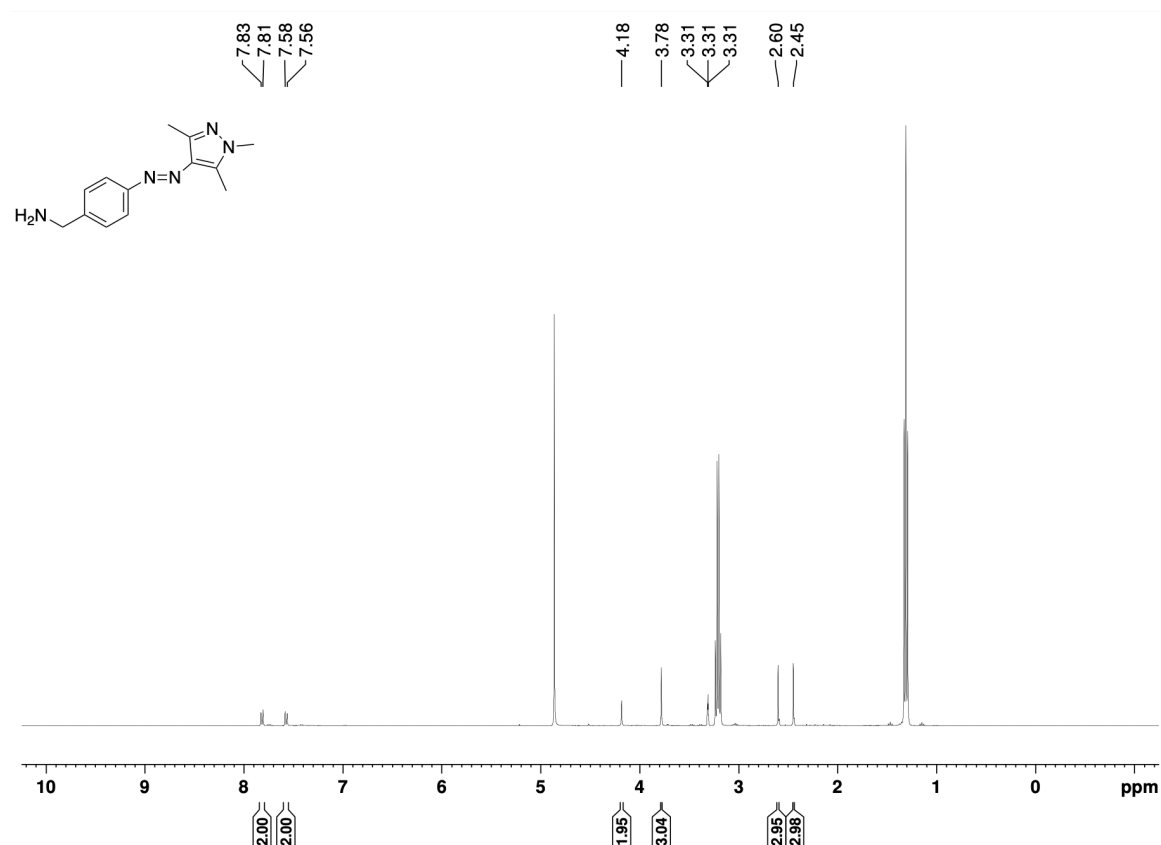
^{13}C spectrum of **18** (101 MHz, CDCl_3):



*Contains ethanol. Yield was obtained after further drying.

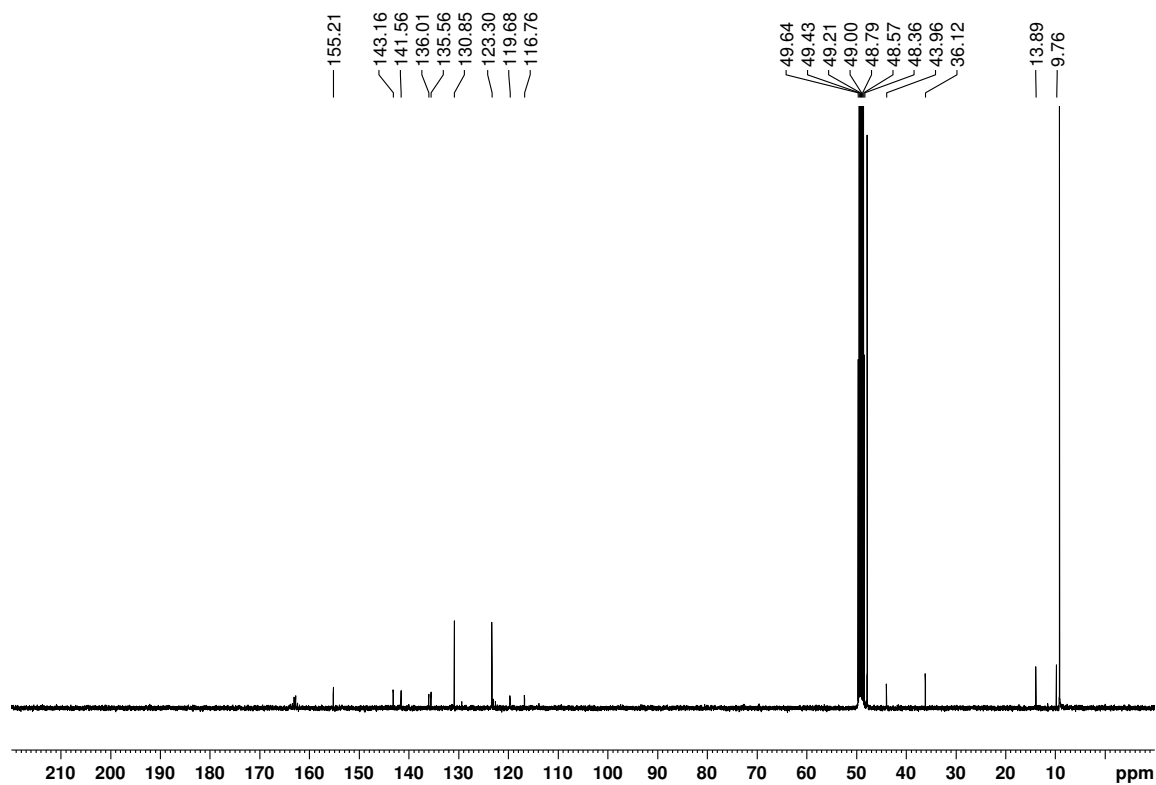
Appendix

^1H spectrum of **19** (400 MHz, MeOD):



*Contains water and diethyl ether. Yield was obtained after further drying.

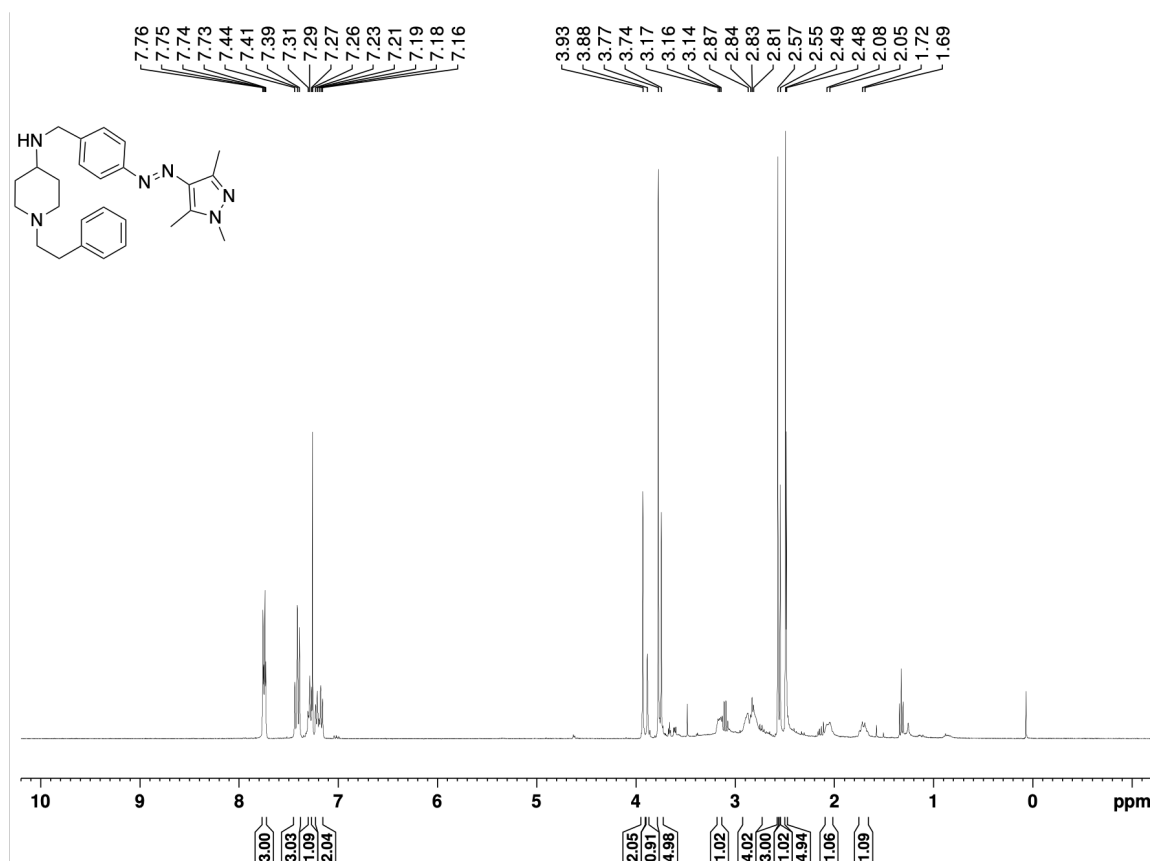
^{13}C spectrum of **19** (101 MHz, MeOD):



*Contains diethyl ether. Yield was obtained after further drying.

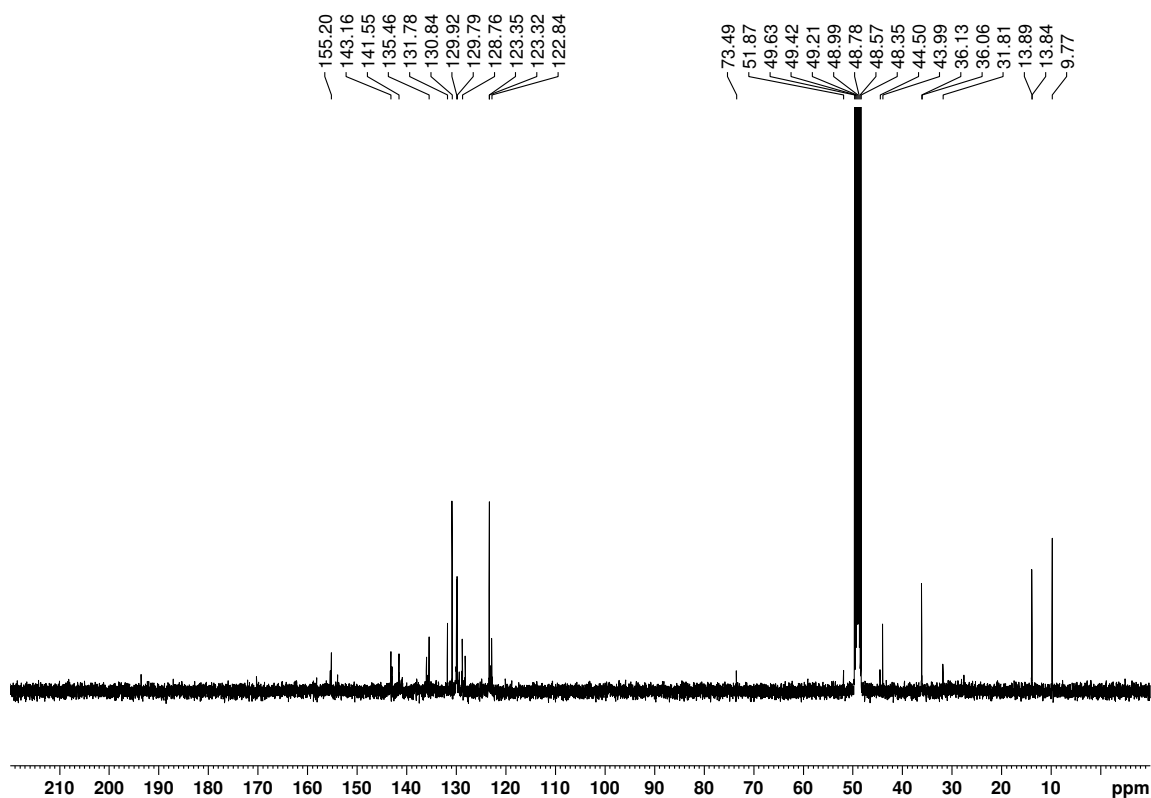
Appendix

^1H spectrum of **20** (400 MHz, CDCl_3):



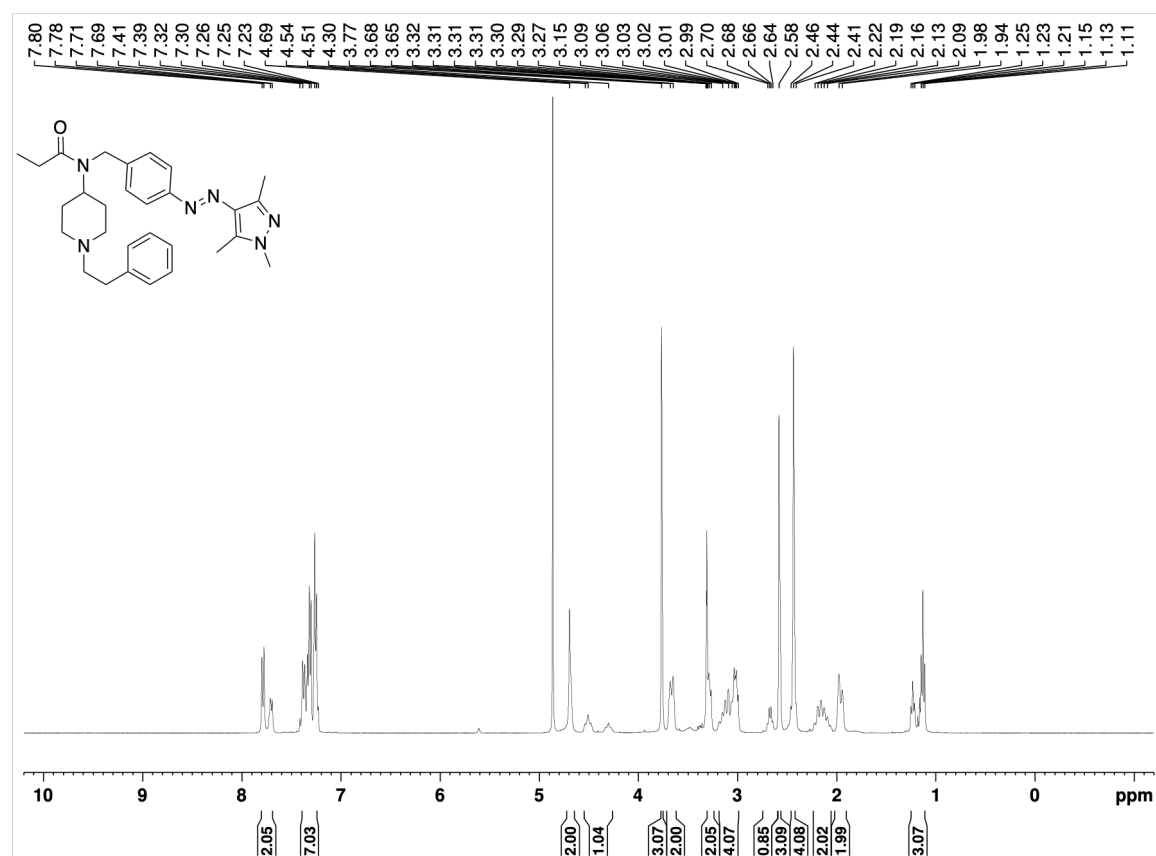
*Contains trace amount of grease and solvents that were used during synthesis.

^{13}C spectrum of **20** (101 MHz, MeOD):

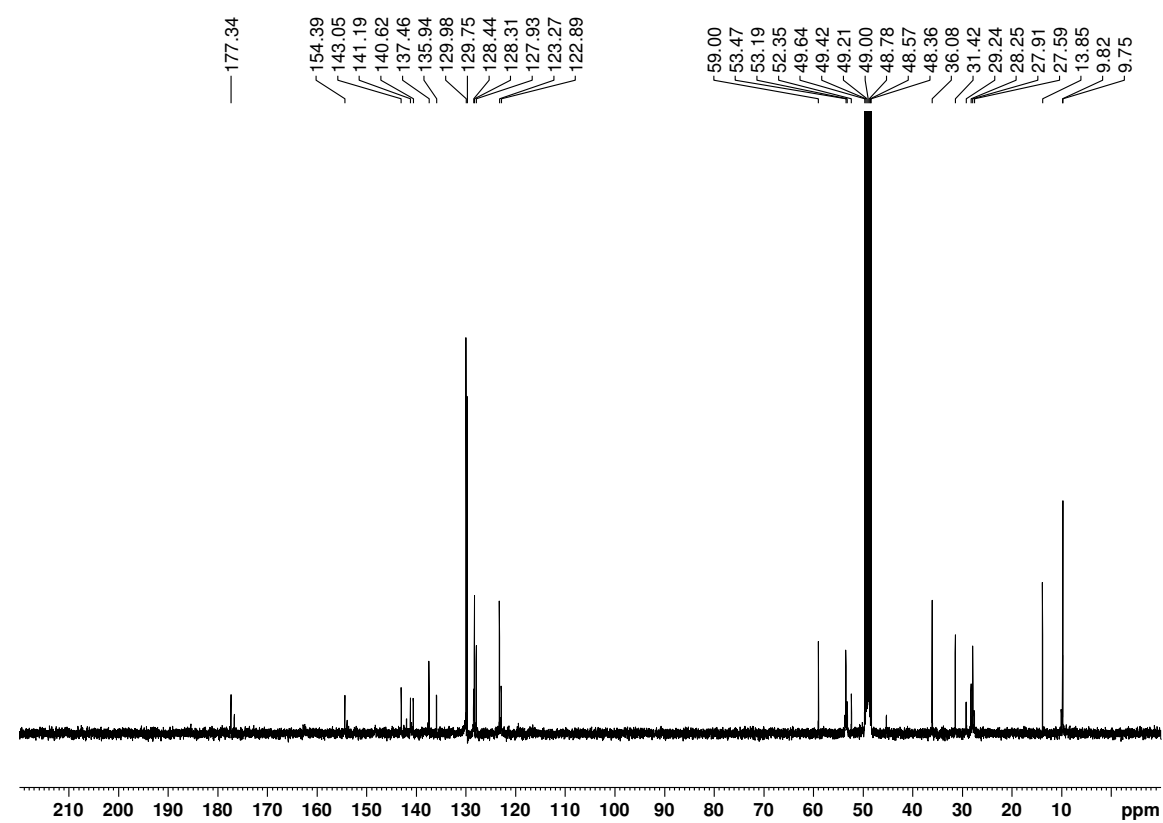


Appendix

^1H spectrum of **3a** (400 MHz, MeOD):

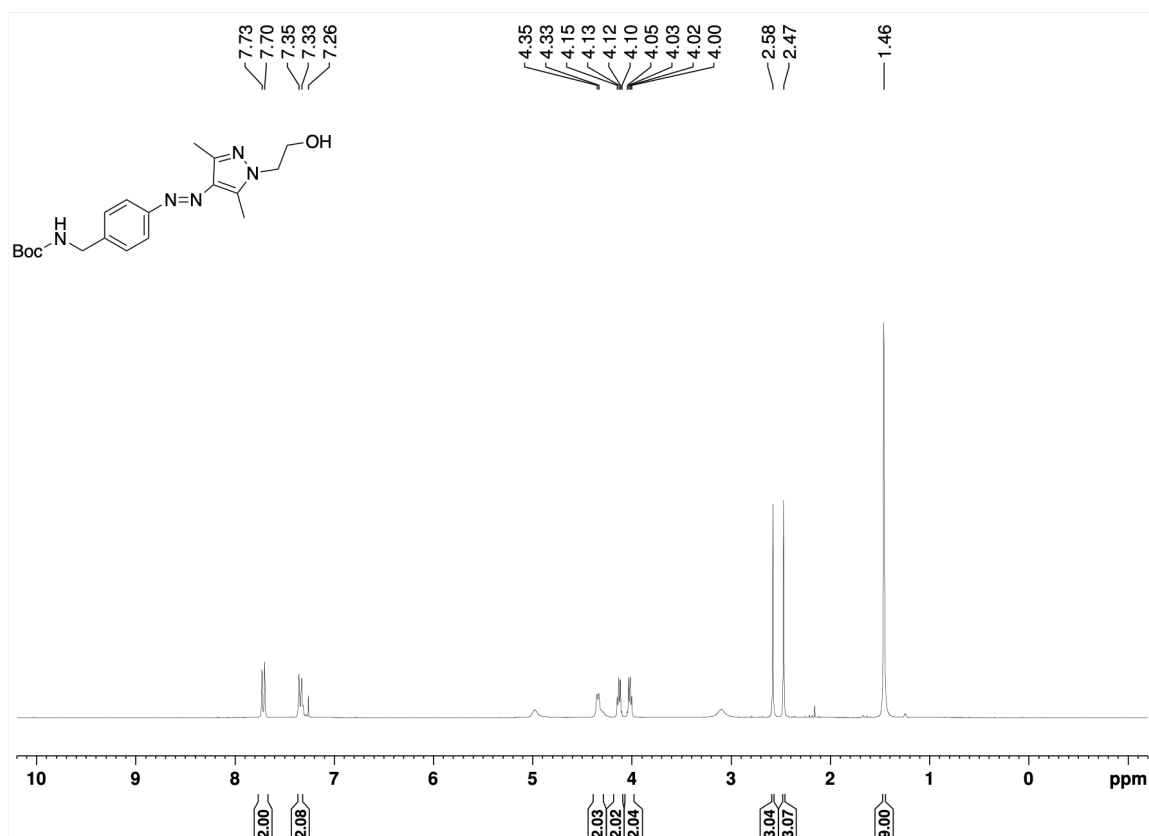


^{13}C spectrum of **3a** (101 MHz, MeOD):

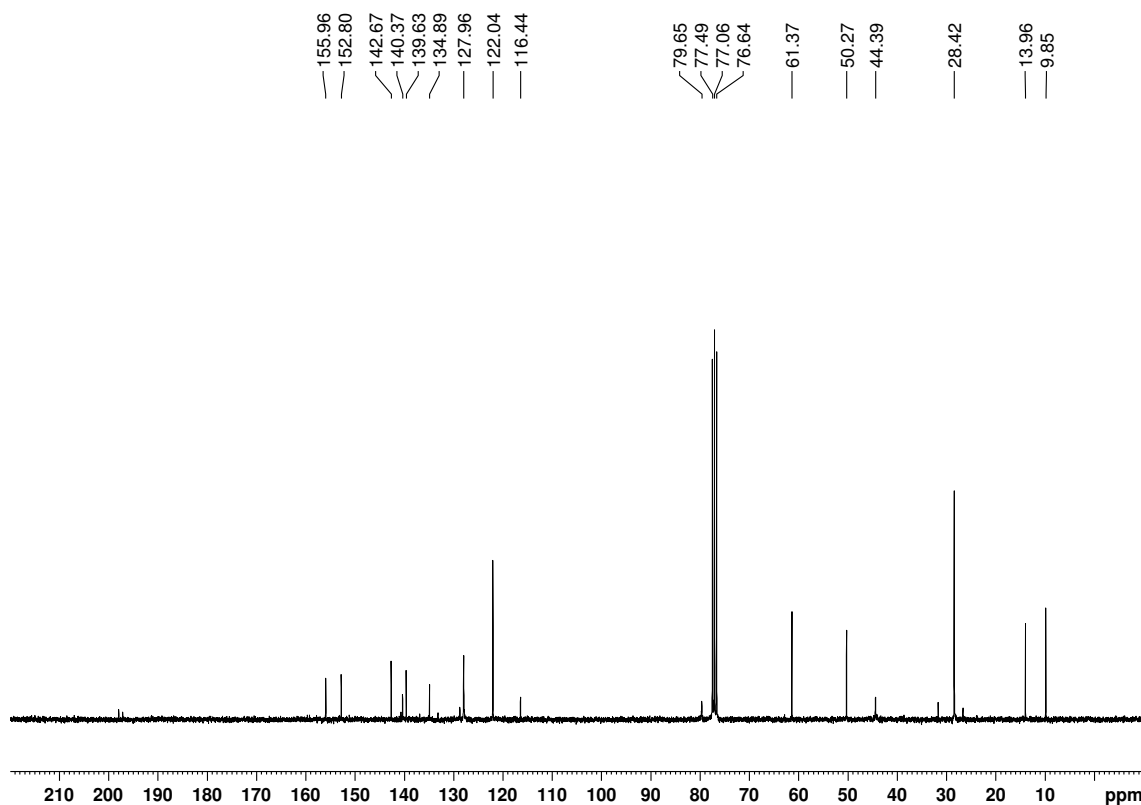


Appendix

^1H spectrum of **21** (400 MHz, CDCl_3):

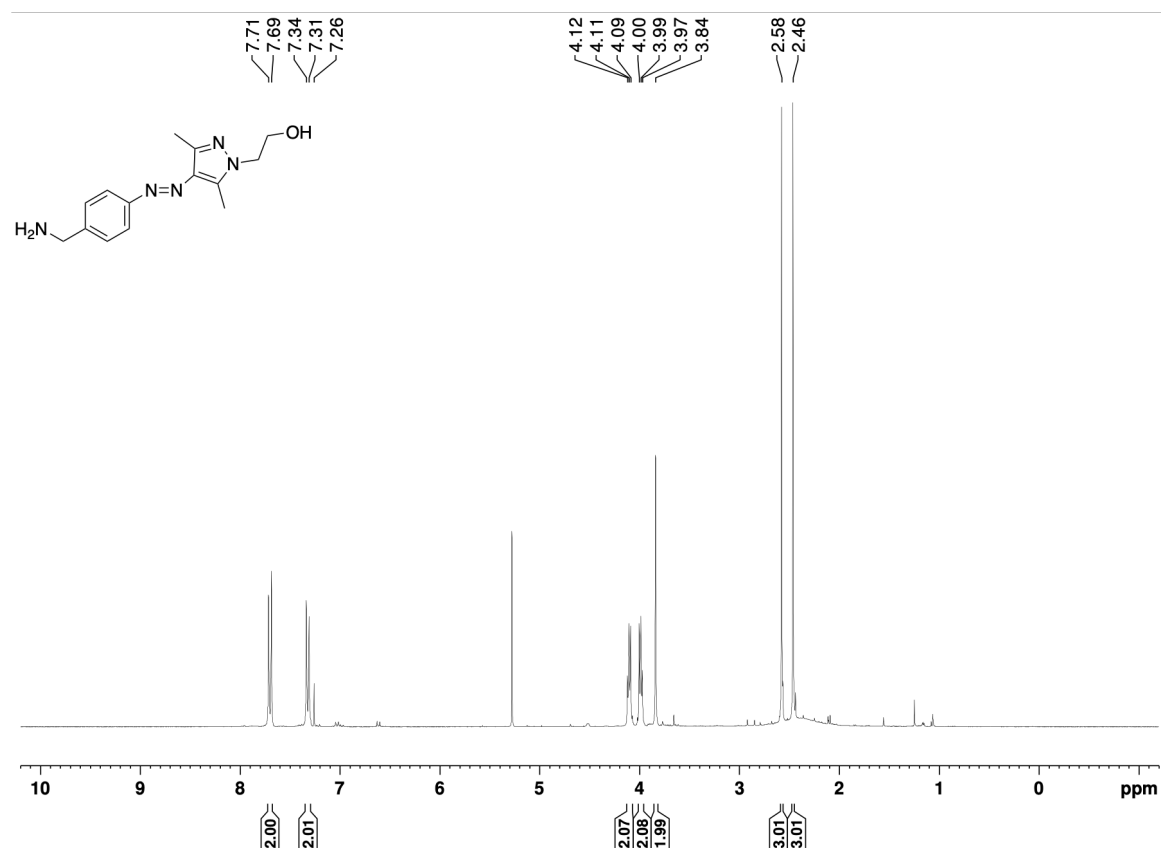


^{13}C spectrum of **21** (101 MHz, CDCl_3):



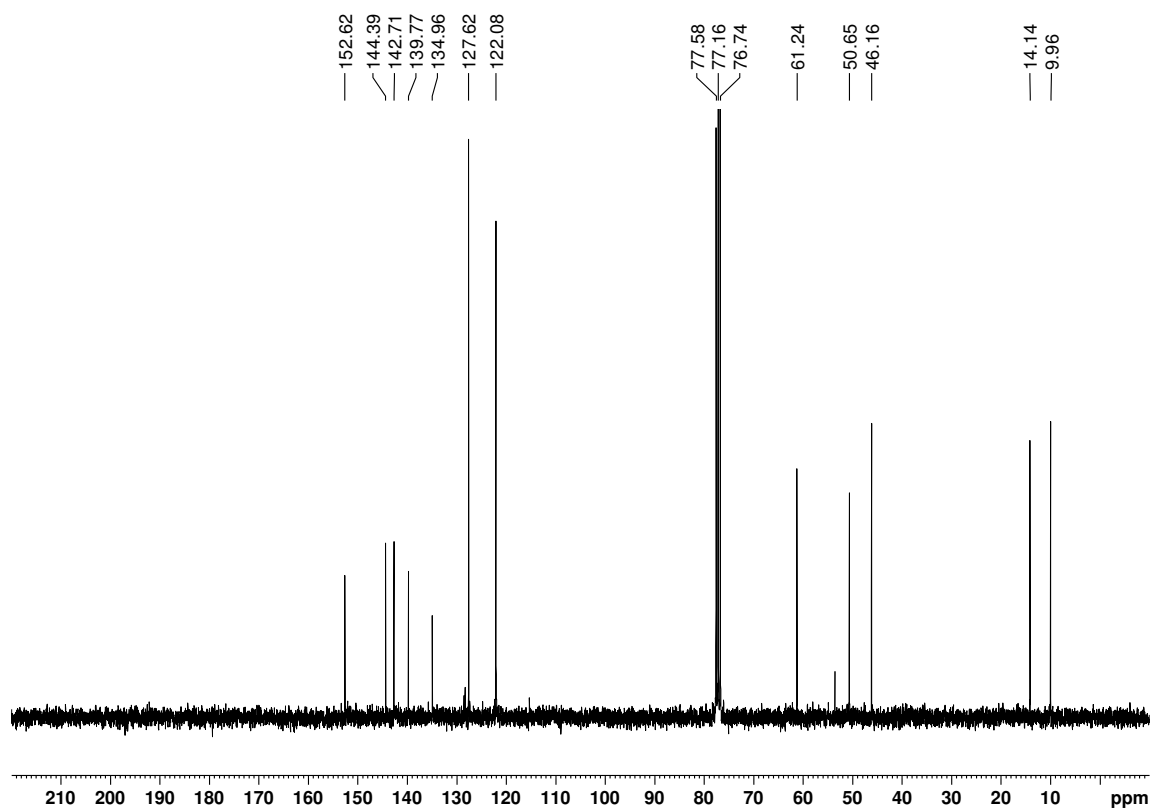
Appendix

^1H spectrum of **22** (400 MHz, CDCl_3):



*Contains traces of DCM

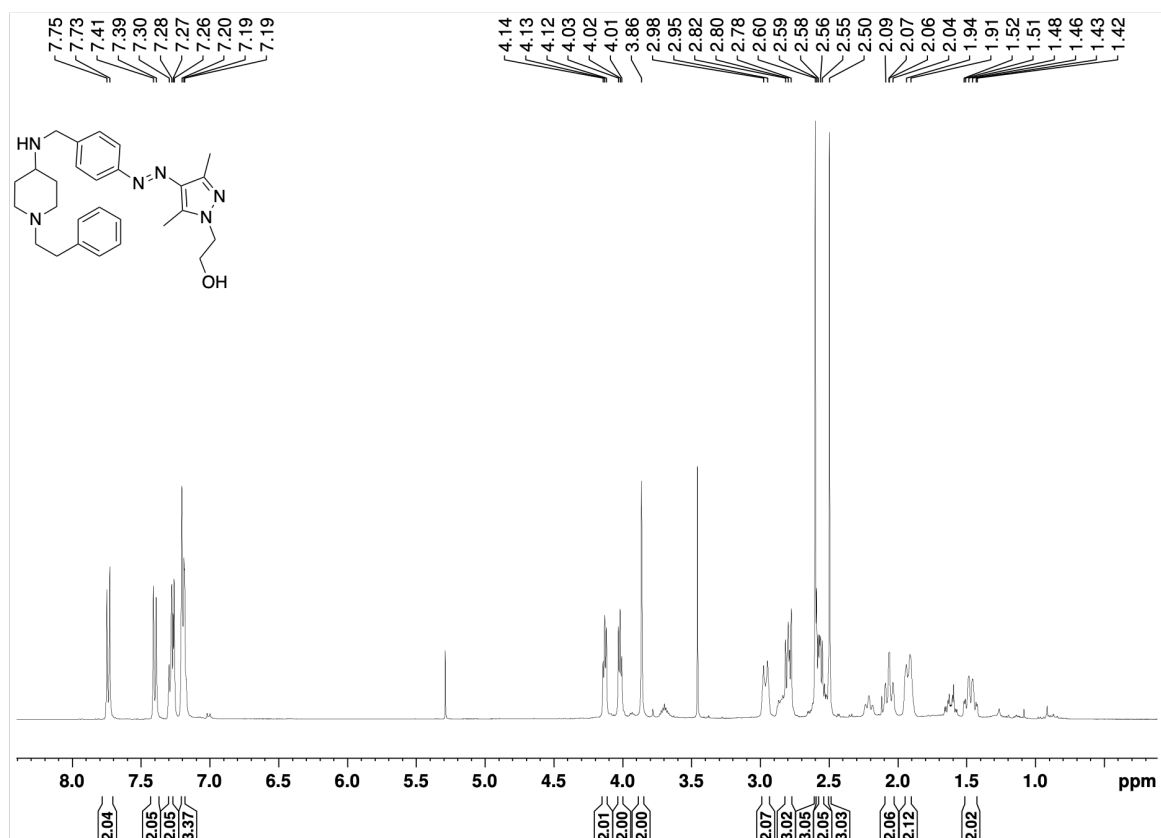
^{13}C spectrum of **22** (101 MHz, CDCl_3):



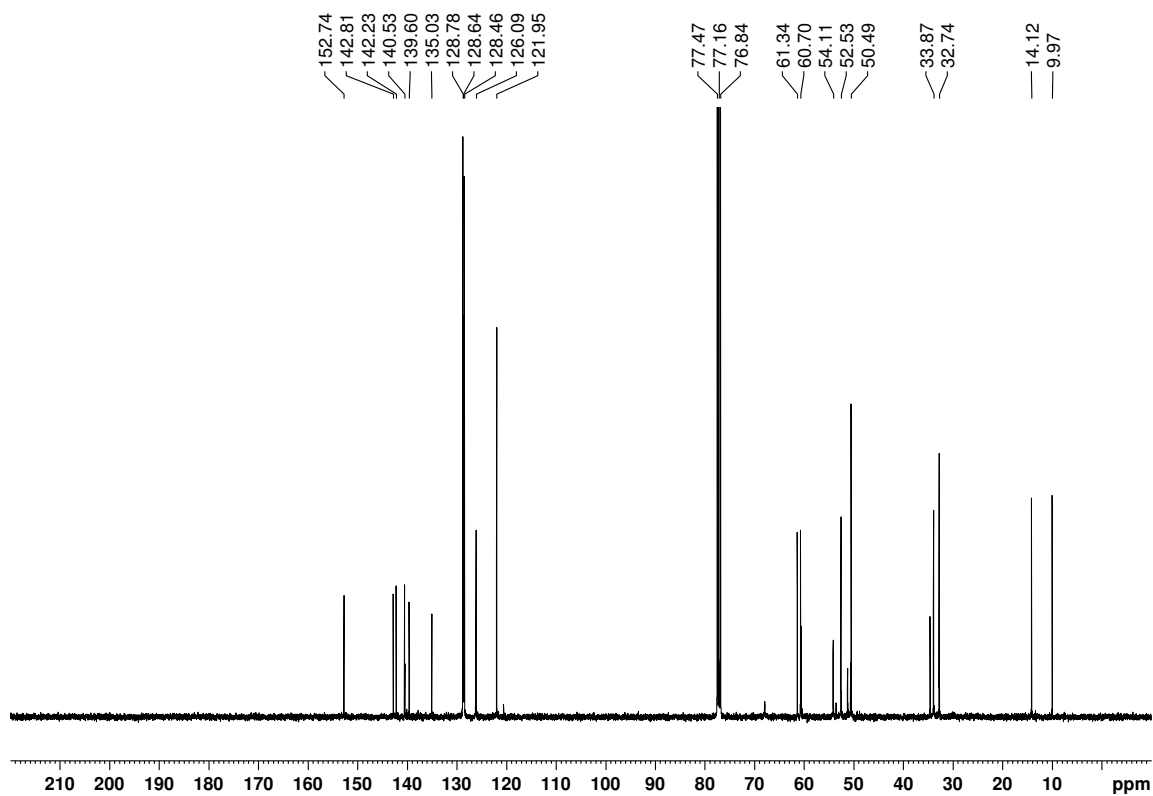
*Contains traces of DCM

Appendix

^1H spectrum of **23** (400 MHz, CDCl_3):

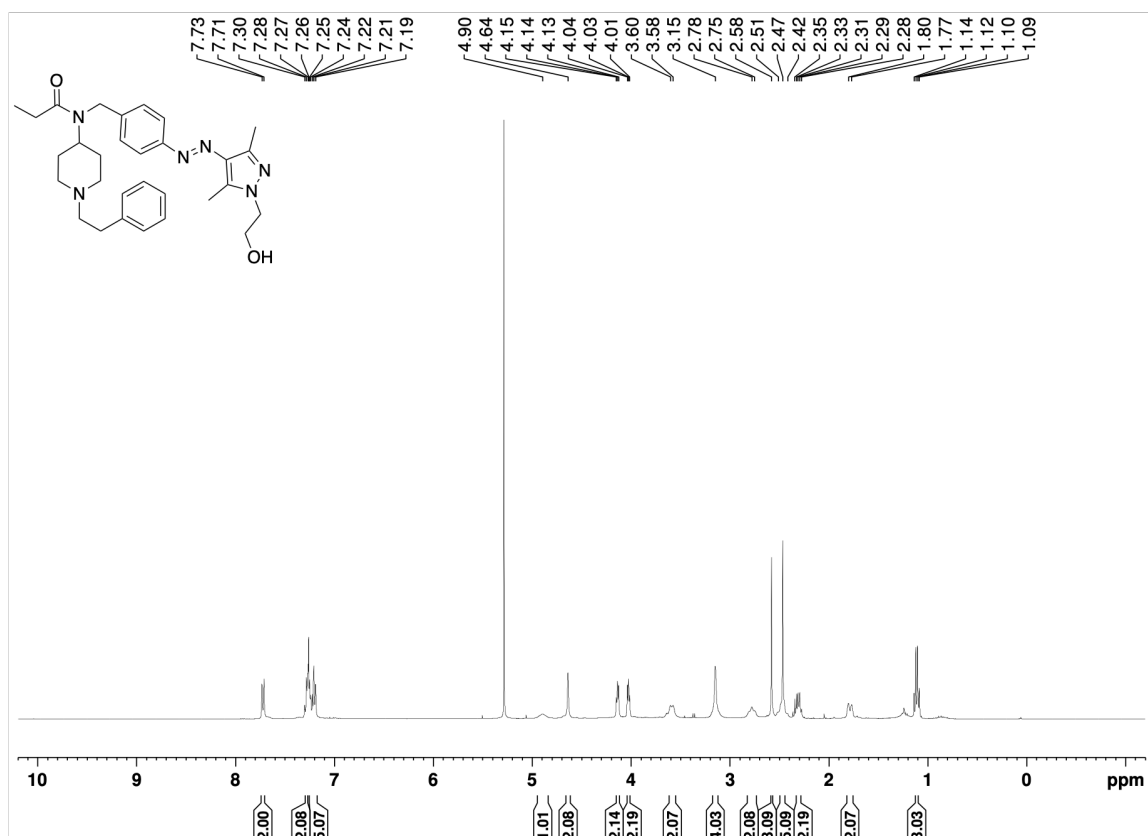


^{13}C spectrum of **23** (101 MHz, CDCl_3):



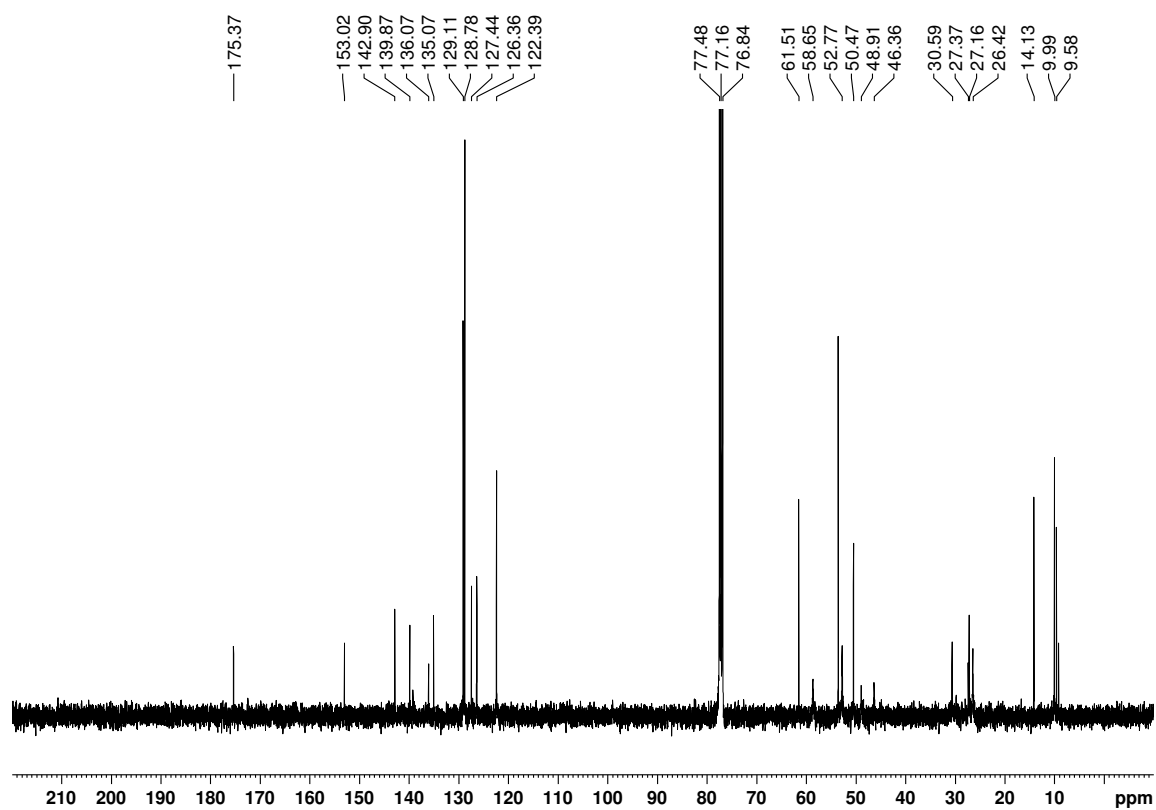
Appendix

^1H spectrum of **3b** (400 MHz, CDCl_3):



*Contains DCM.

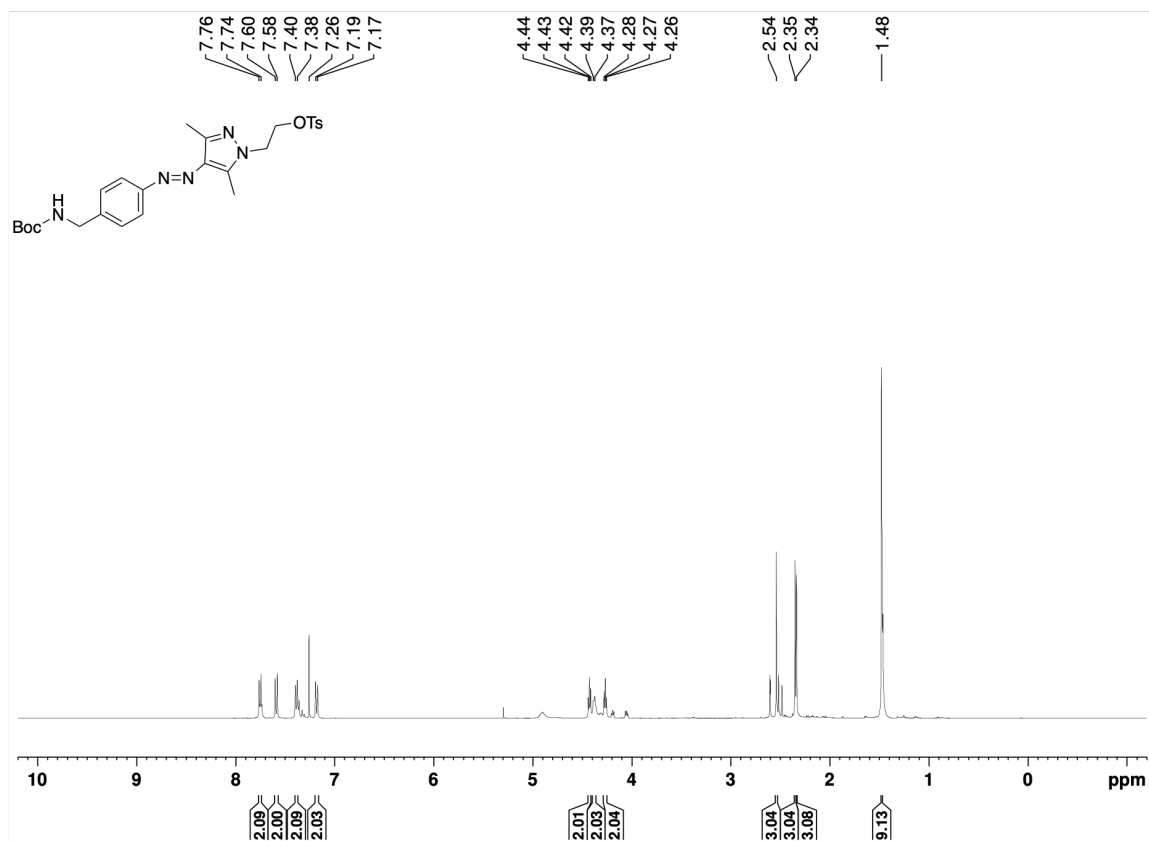
^{13}C spectrum of **3b** (101 MHz, CDCl_3):



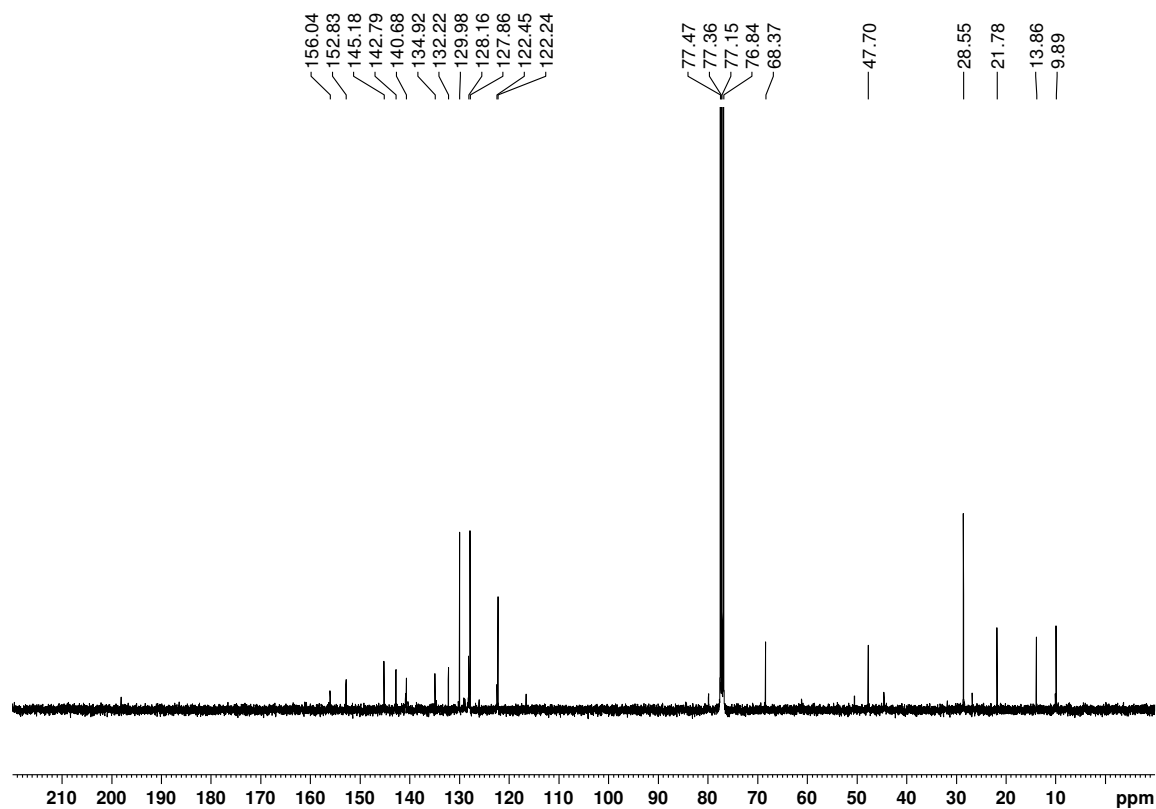
*Contains DCM

Appendix

^1H spectrum of **24** (400 MHz, CDCl_3):

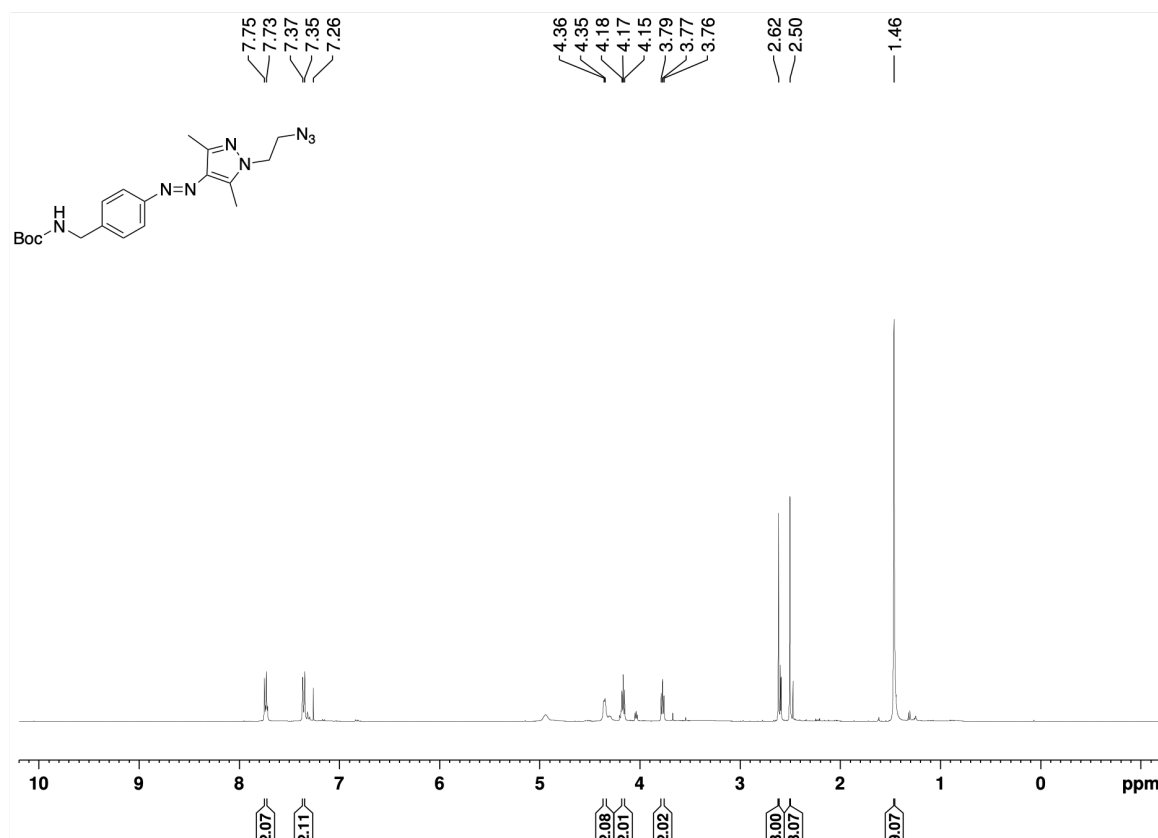


^{13}C spectrum of **24** (101 MHz, CDCl_3):

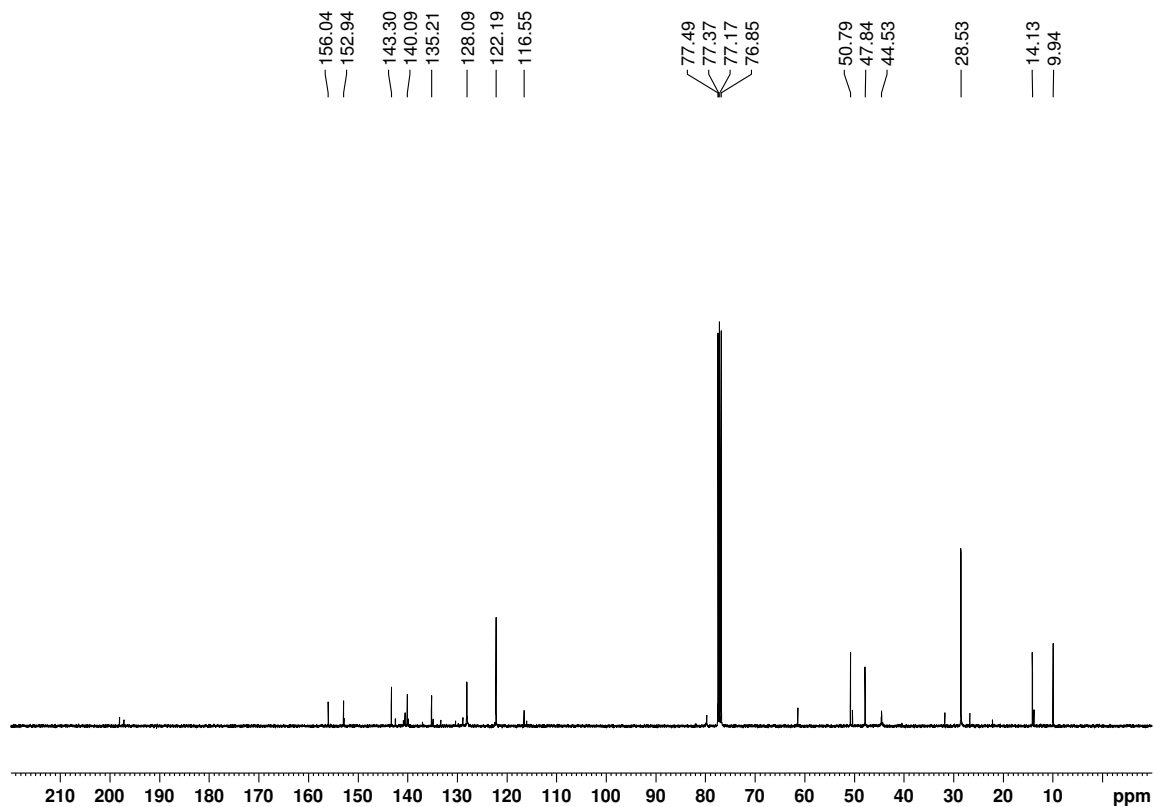


Appendix

^1H spectrum of **25** (400 MHz, CDCl_3):

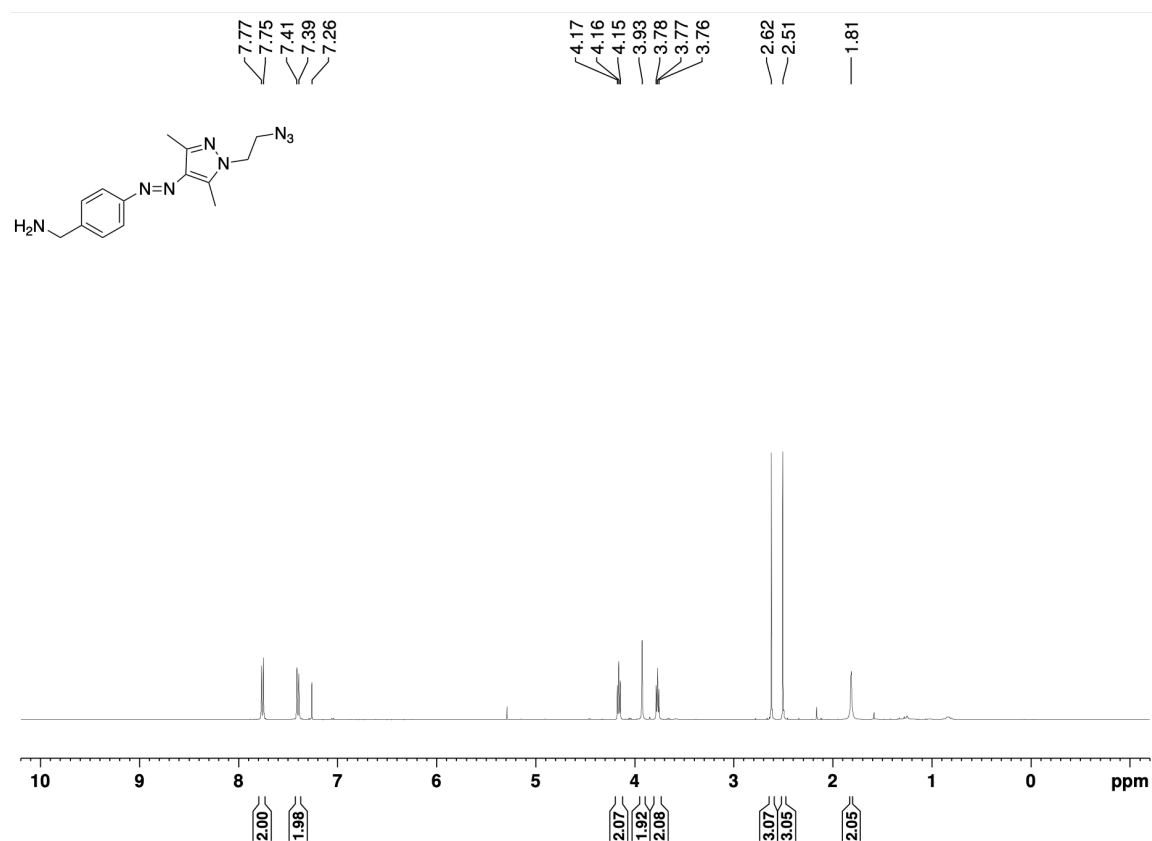


^{13}C spectrum of **25** (101 MHz, CDCl_3):

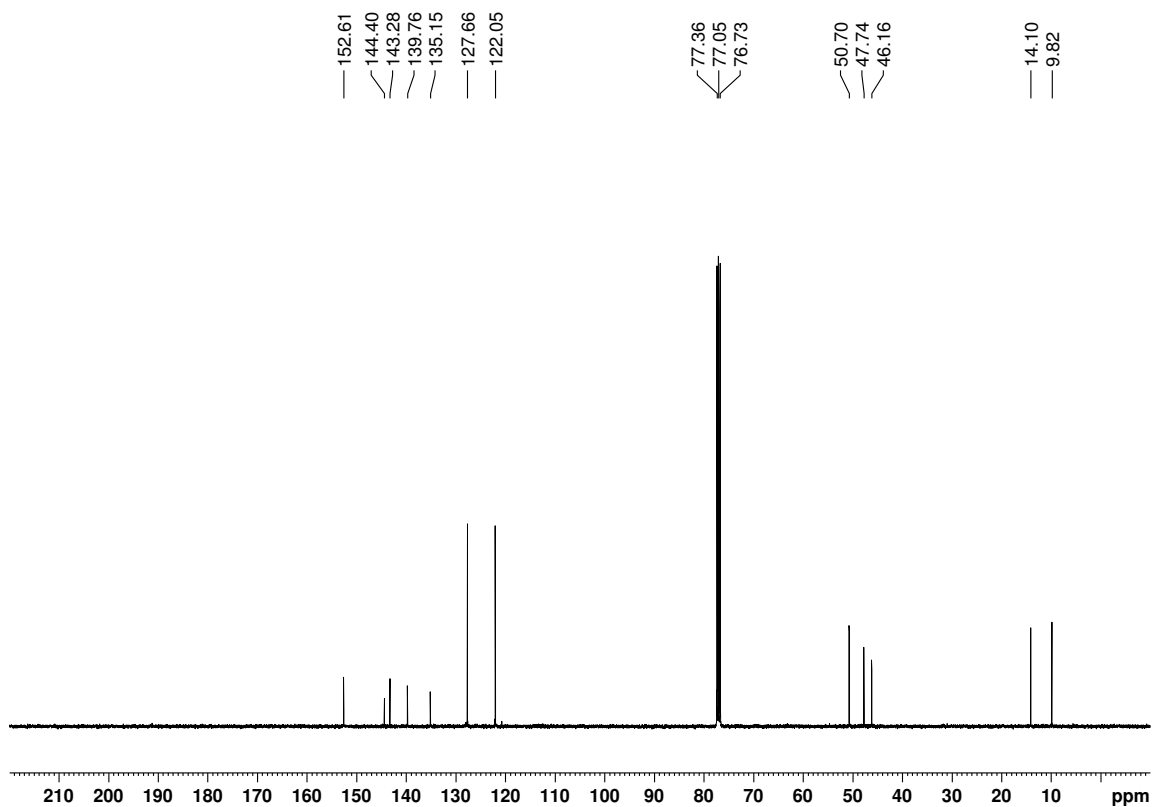


Appendix

^1H spectrum of **26** (400 MHz, CDCl_3):

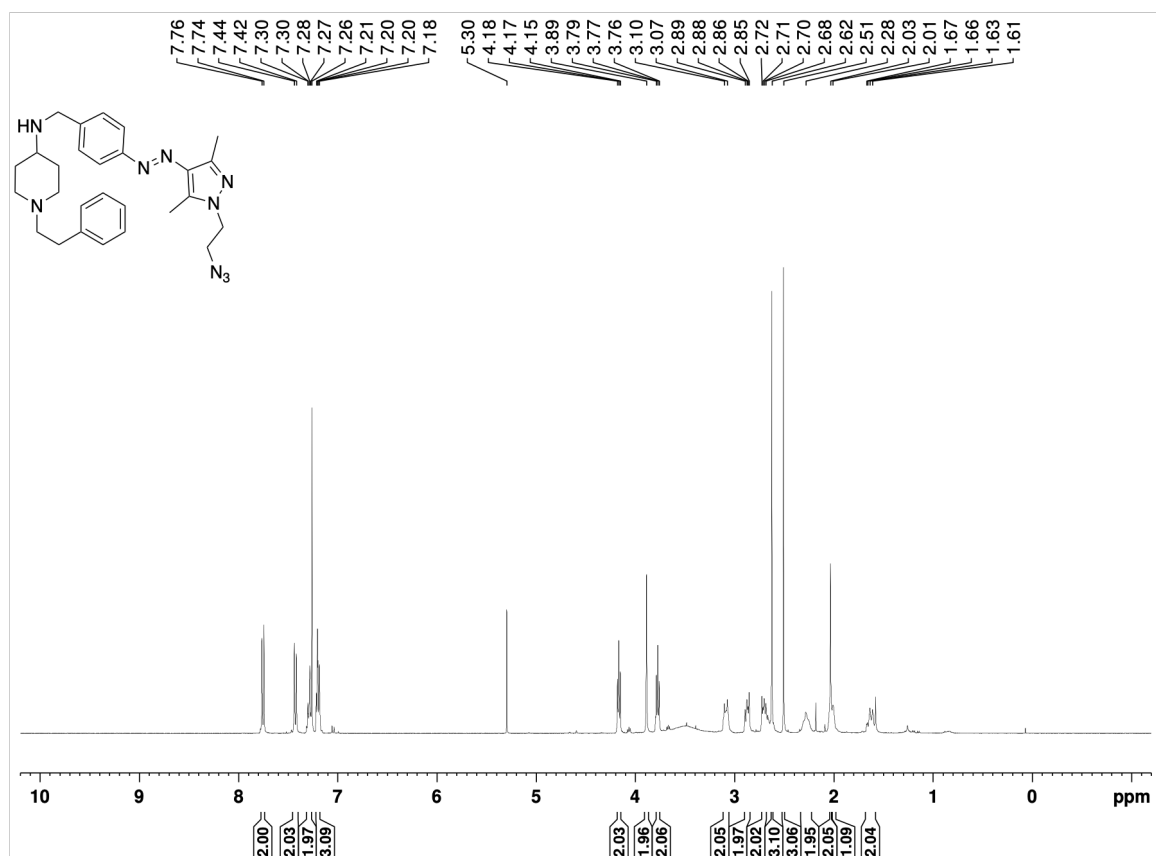


^{13}C spectrum of **26** (101 MHz, CDCl_3):



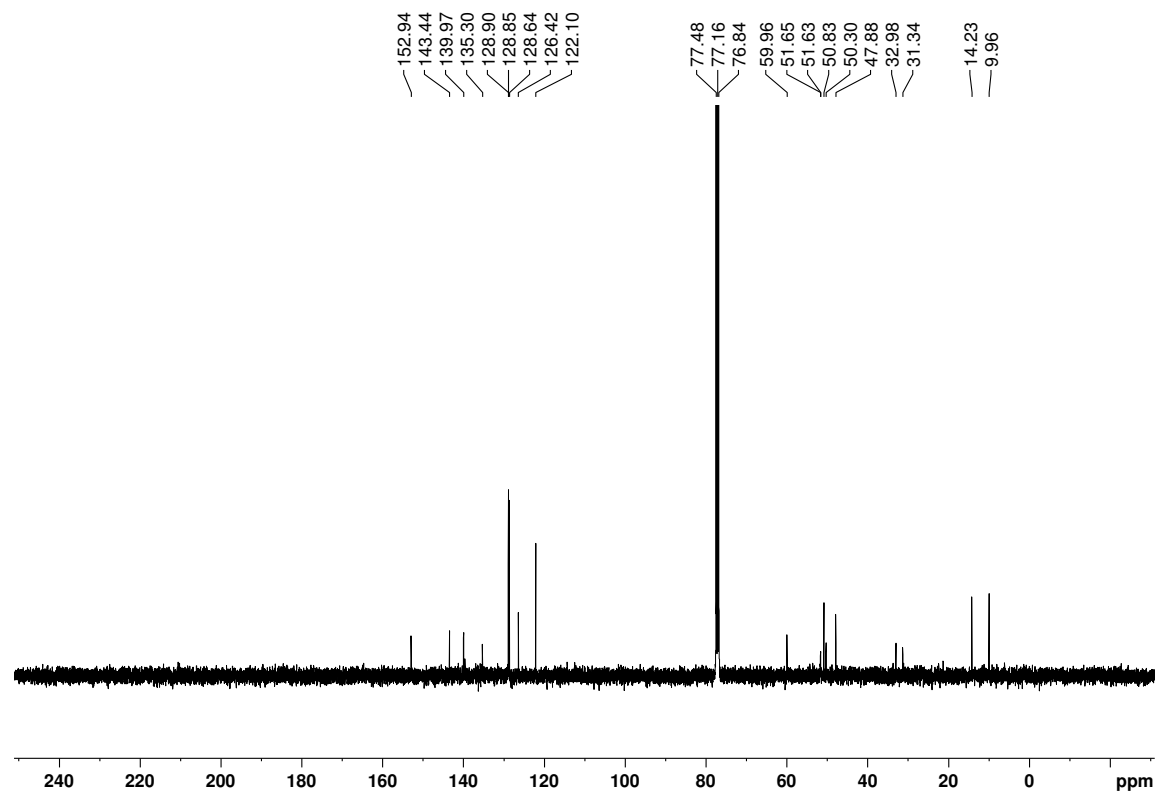
Appendix

^1H spectrum of **27** (400 MHz, CDCl_3):



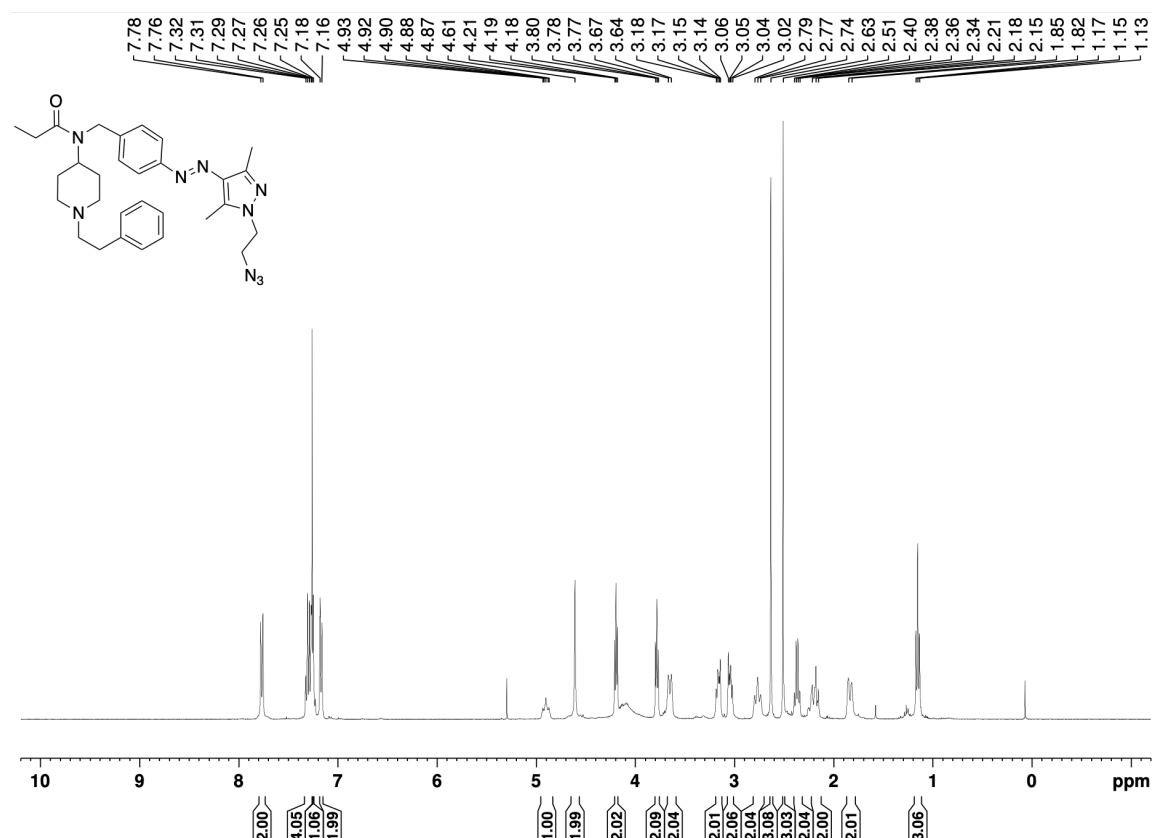
*Contains DCM.

^{13}C spectrum of **27** (101 MHz, CDCl_3):

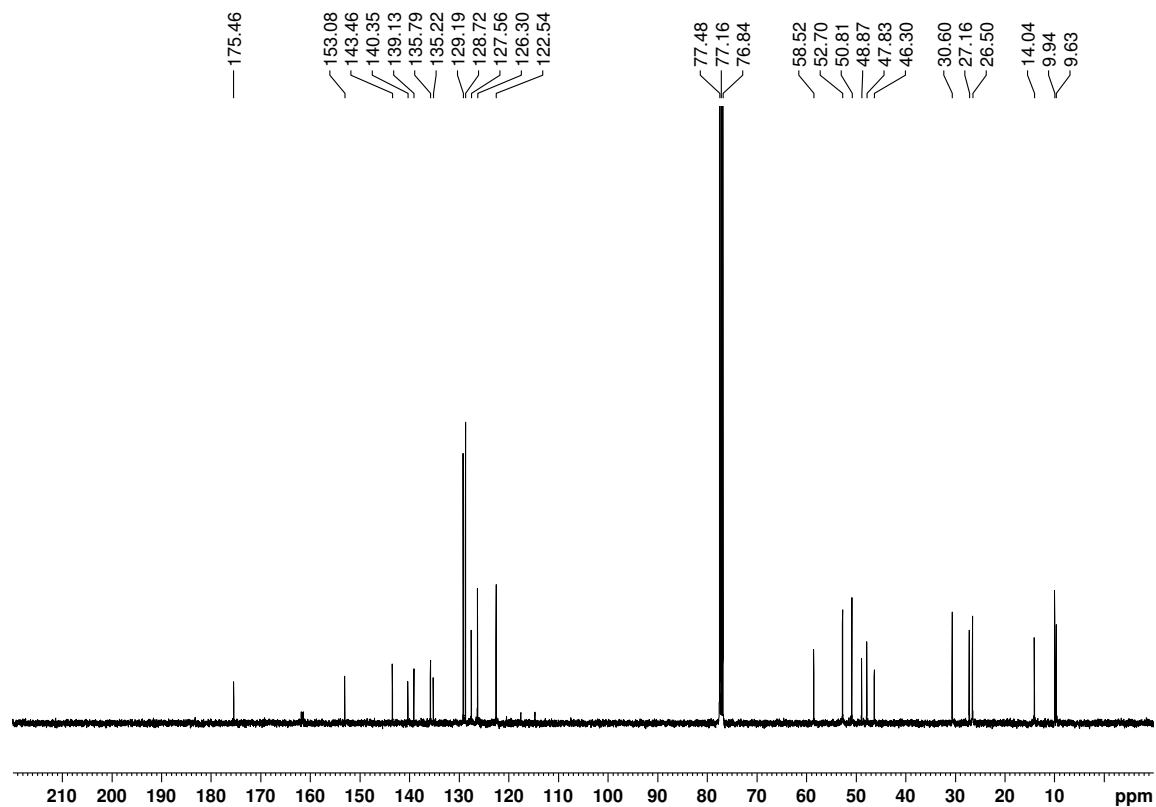


Appendix

^1H spectrum of **3c** (400 MHz, CDCl_3):

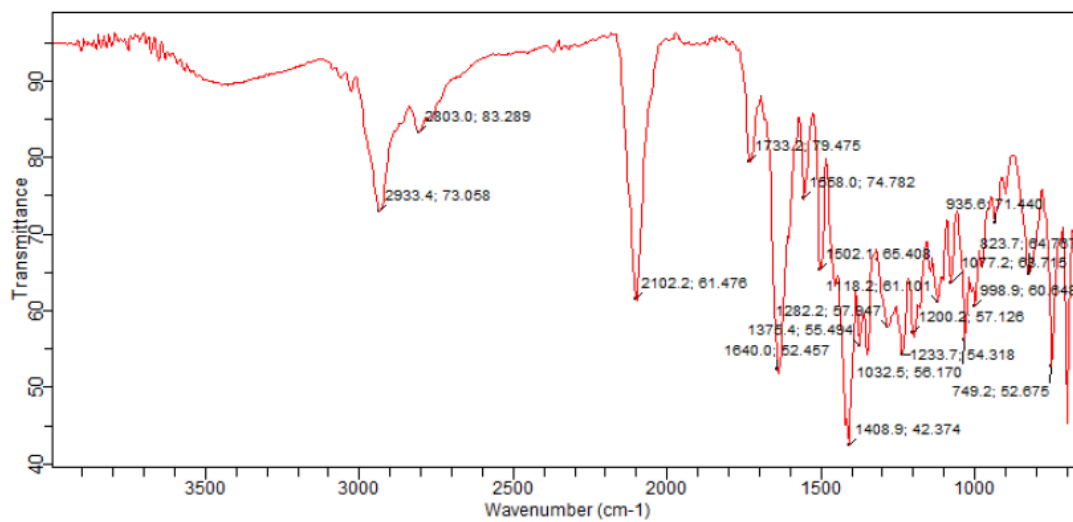


^{13}C spectrum of **3c** (101 MHz, CDCl_3):



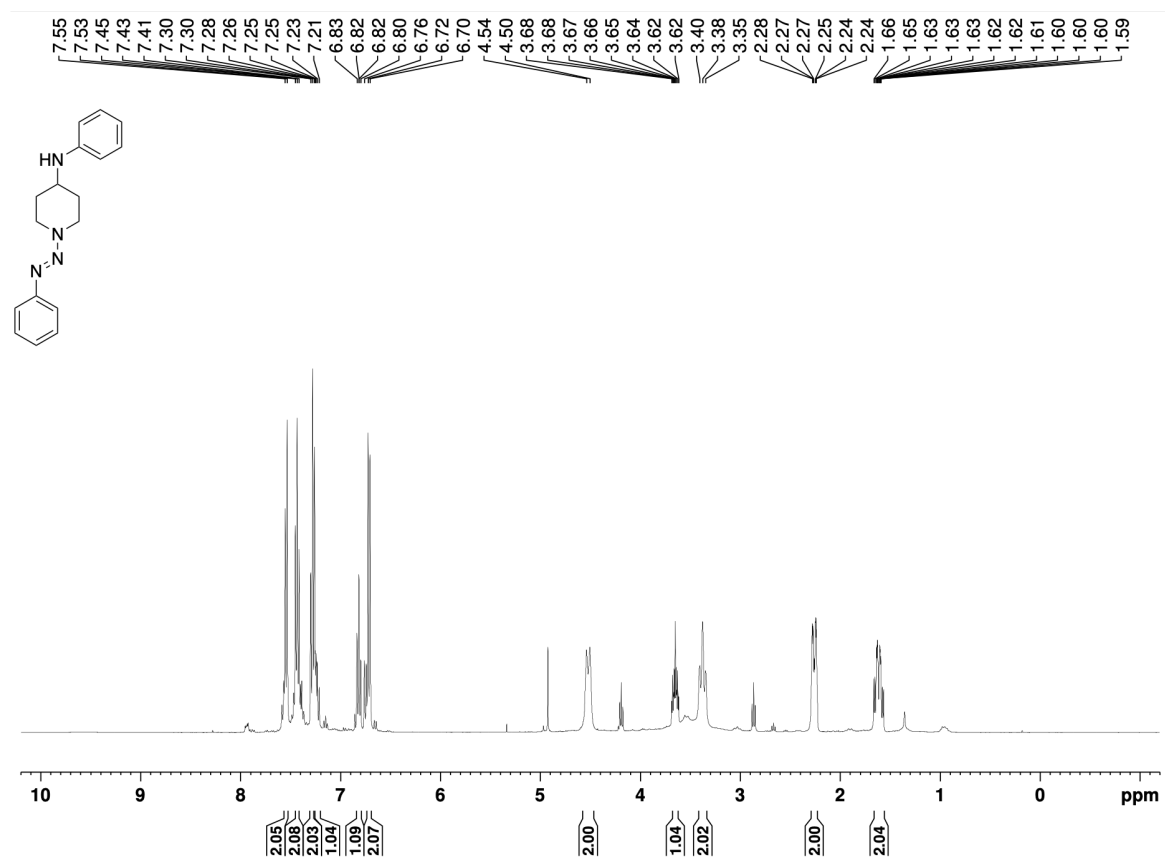
Appendix

Additional spectrum (IR):

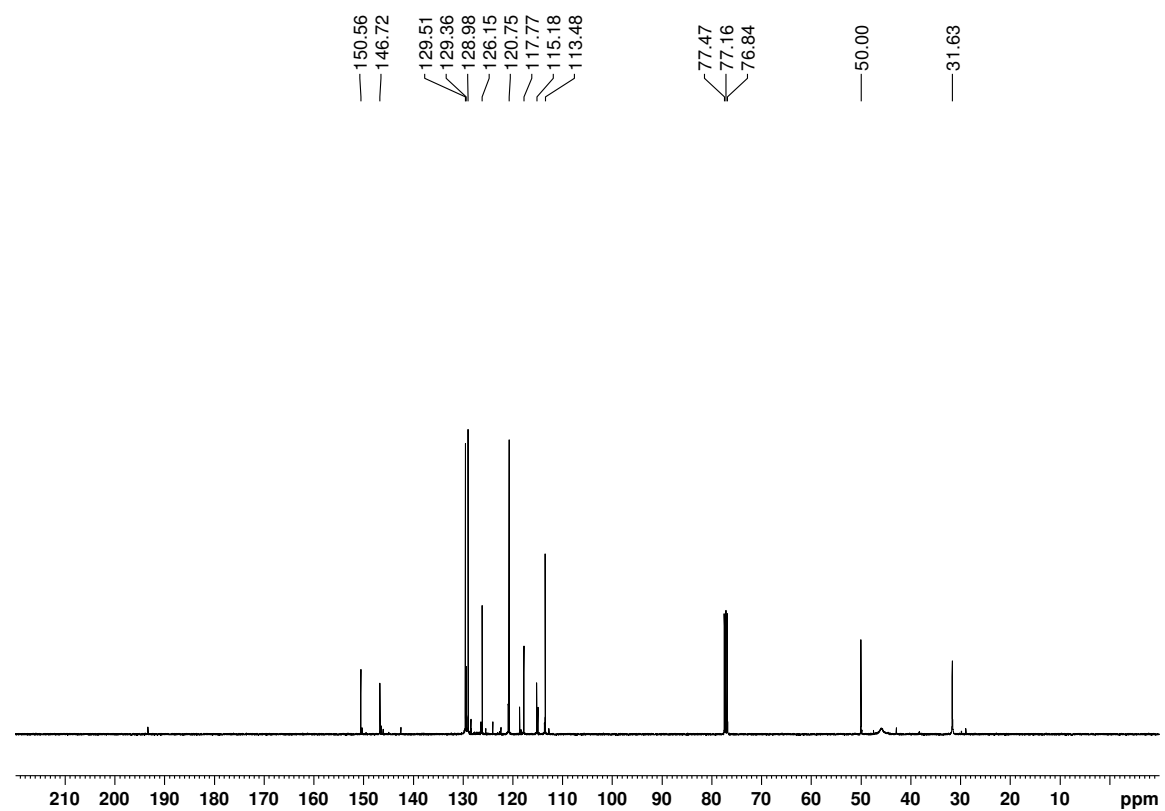


Appendix

^1H spectrum of **30** (400 MHz, CDCl_3):

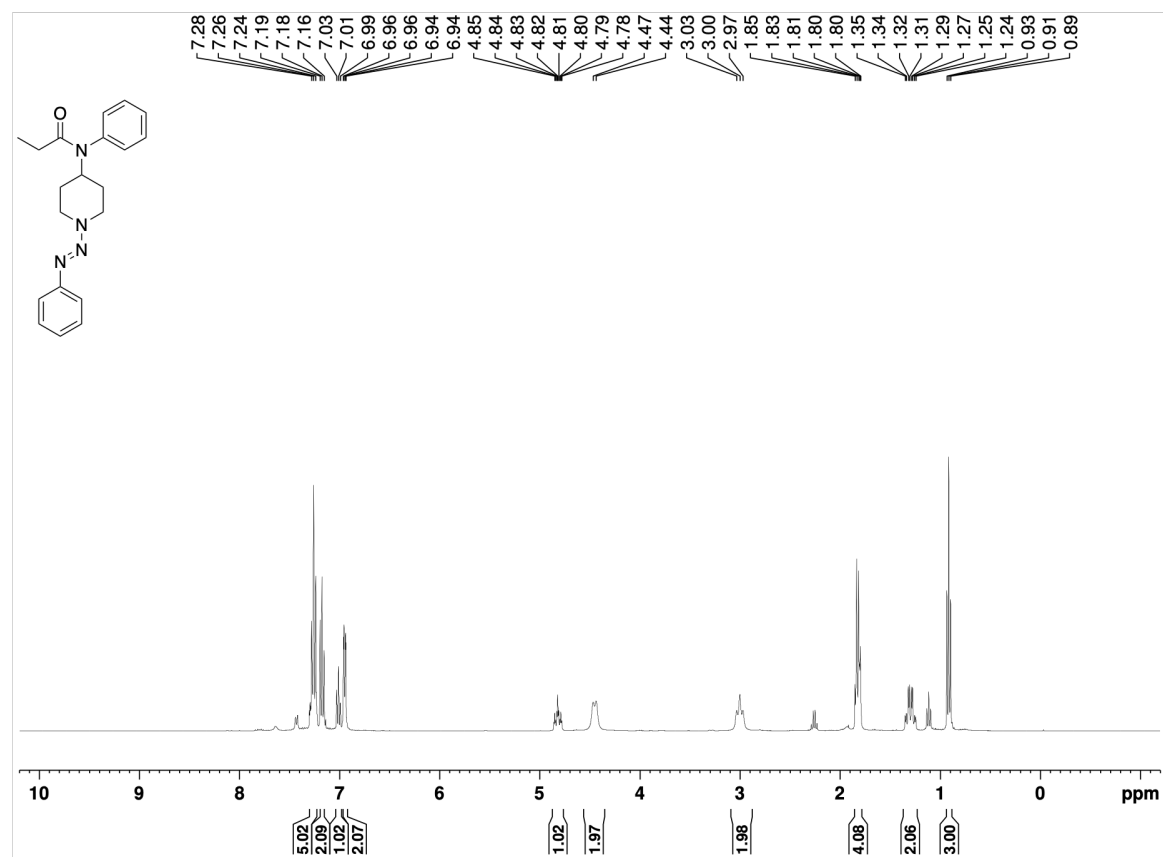


^{13}C spectrum of **30** (101 MHz, CDCl_3):

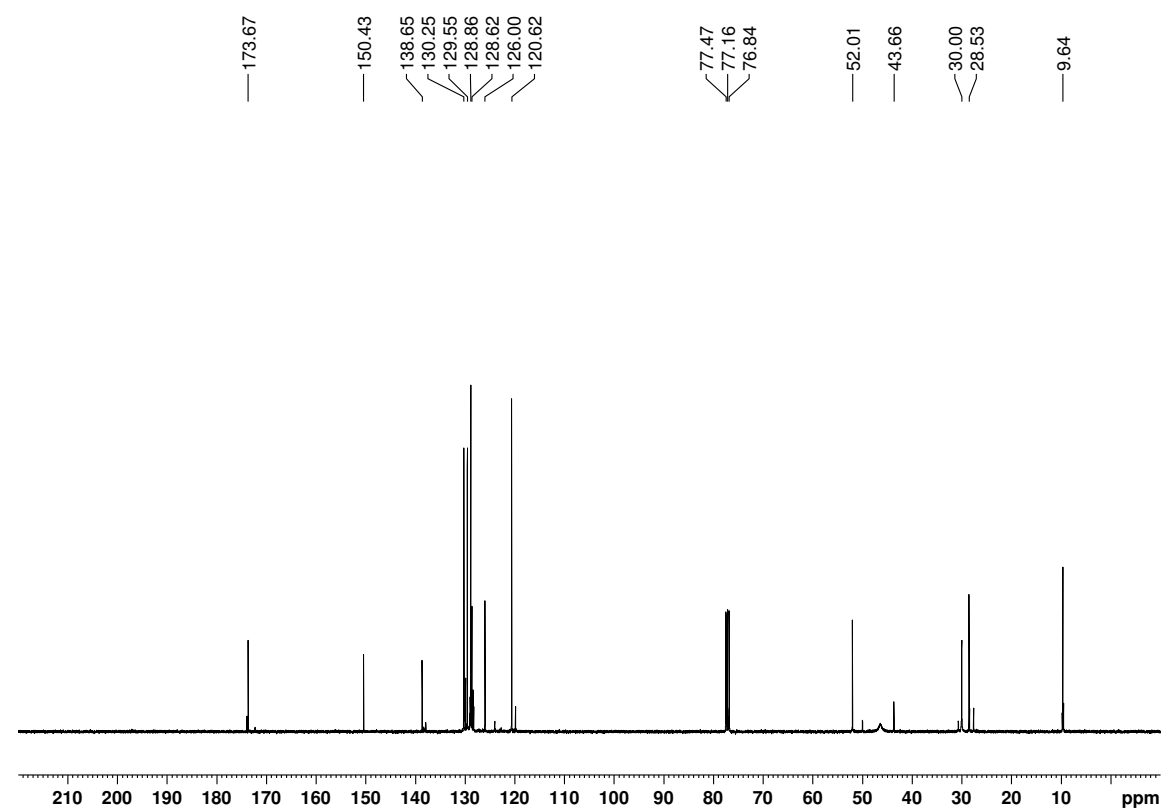


Appendix

^1H spectrum of **4** (400 MHz, CDCl_3):



^{13}C spectrum of **4** (101 MHz, CDCl_3):



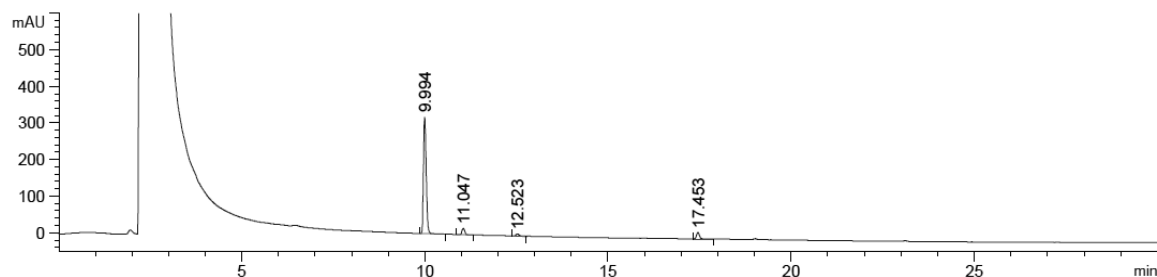
7.3 Appendix for Chapter 2

7.3.1 Analytical HPLC Chromatograms for Purity Determination

Experiments in this section were evaluated in DMSO.

Compound **tFAPz 1**:

Detection at 220 nm: 93% purity

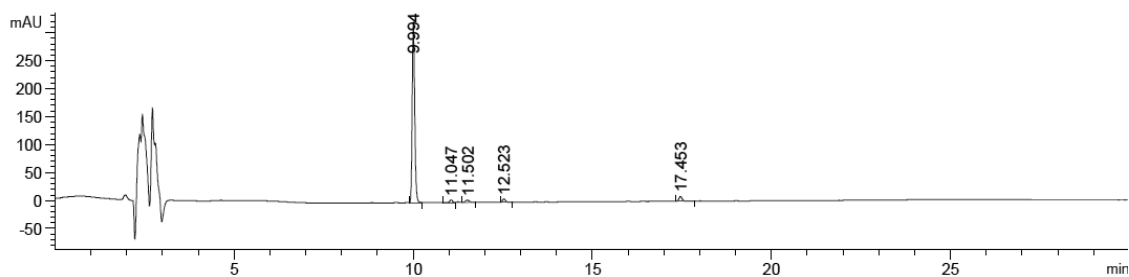


Signal 2: DAD1 B, Sig=220,4 Ref=off

Peak #	RetTime [min]	Type	Width [min]	Area [mAU*s]	Height [mAU]	Area %
1	9.994	BB	0.0828	1658.63428	318.44315	87.6508
2	11.047	BB	0.0855	92.54971	17.01028	4.8908
3	12.523	BB	0.0860	33.60691	6.12868	1.7760
4	17.453	BB	0.0936	107.52983	18.02739	5.6824

*Peak 1 and Peak 2 are *cis*- and *trans*-isomers of compound **1**, respectively.

Detection at 254 nm: 94% purity



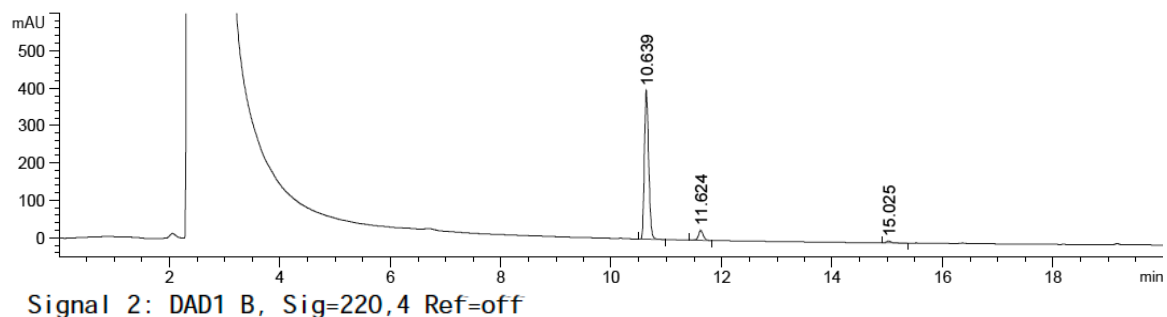
Signal 1: DAD1 A, Sig=254,4 Ref=off

Peak #	RetTime [min]	Type	Width [min]	Area [mAU*s]	Height [mAU]	Area %
1	9.994	BB	0.0803	1655.91150	320.23785	92.3736
2	11.047	BV	0.0845	23.91369	4.46610	1.3340
3	11.502	VB	0.1188	29.51271	3.87857	1.6463
4	12.523	BB	0.0845	31.68449	5.91059	1.7675
5	17.453	BV R	0.0925	51.60131	8.53963	2.8785

*Peak 1 and Peak 2 are *cis*- and *trans*-isomers of compound **1**, respectively.

Compound **tFAPz 2a**:

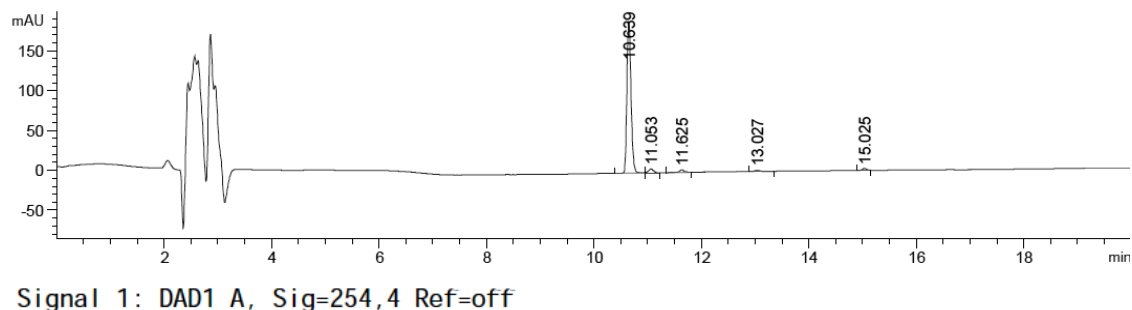
Detection at 220 nm: 99% purity



Peak #	RetTime [min]	Type	Width [min]	Area [mAU*s]	Height [mAU]	Area %
1	10.639	BB	0.0824	2135.17773	399.08350	92.0636
2	11.624	BB	0.0906	155.07411	26.35446	6.6864
3	15.025	BB	0.0884	28.99094	4.94135	1.2500

*Peak 1 and Peak 2 are *cis*- and *trans*-isomers of compound **2a**, respectively.

Detection at 254 nm: 95% purity



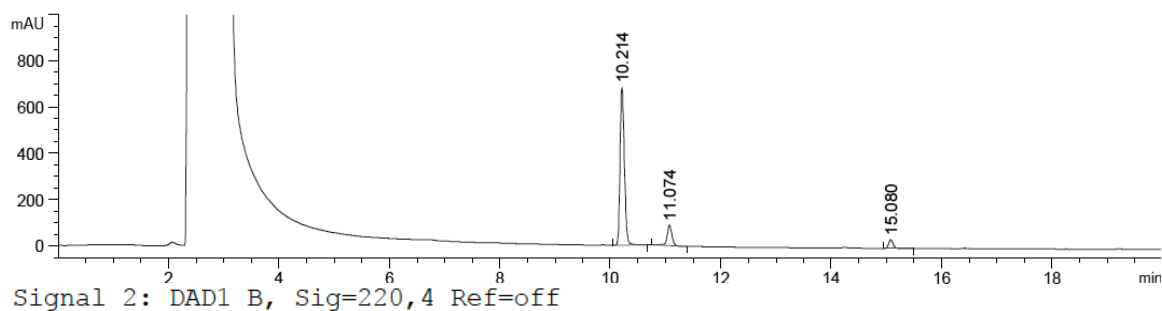
Peak #	RetTime [min]	Type	Width [min]	Area [mAU*s]	Height [mAU]	Area %
1	10.639	BV	0.0827	1023.22491	190.44737	93.3054
2	11.053	VB	0.0975	29.79934	4.73165	2.7173
3	11.625	BB	0.0964	19.92674	3.12388	1.8171
4	13.027	BB	0.1057	10.70113	1.49115	0.9758
5	15.025	BB	0.0867	12.98808	2.34076	1.1844

*Peak 1 and Peak 3 are *cis*- and *trans*-isomers of compound **2a**, respectively.

Appendix

Compound **tFAPz 2b**:

Detection at 220 nm: 95% purity

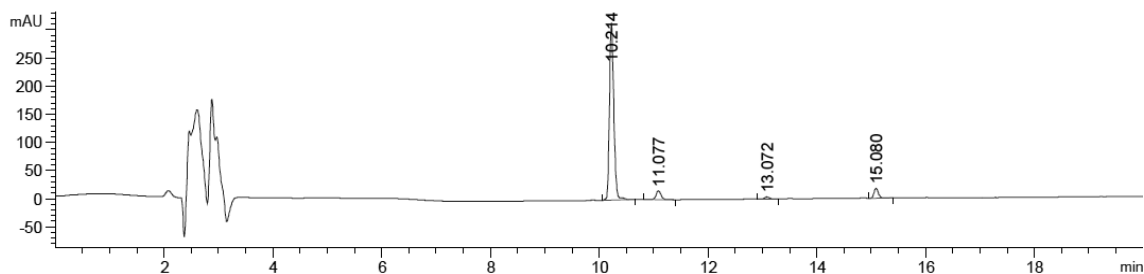


Signal 2: DAD1 B, Sig=220,4 Ref=off

Peak #	RetTime [min]	Type	Width [min]	Area [mAU*s]	Height [mAU]	Area %
1	10.214	BV R	0.0836	3706.82666	680.47638	82.9897
2	11.074	BB	0.0947	548.64825	88.08907	12.2833
3	15.080	BB	0.0884	211.13568	37.07842	4.7270

*Peak 1 and Peak 2 are *cis*- and *trans*-isomers of compound **2b**, respectively.

Detection at 254 nm: 94% purity



Signal 1: DAD1 A, Sig=254,4 Ref=off

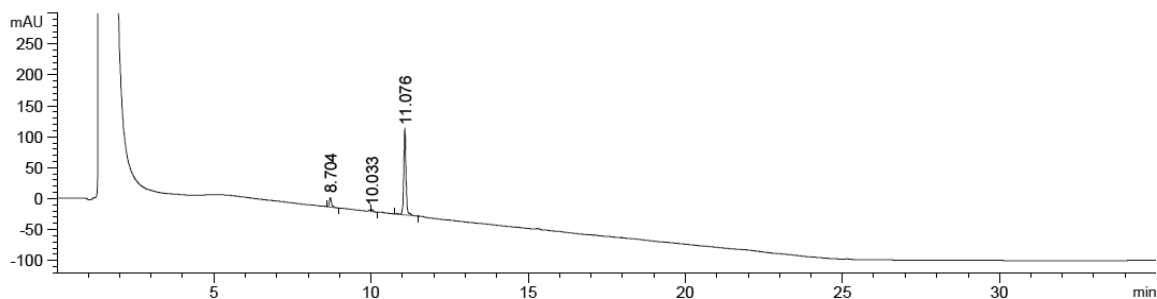
Peak #	RetTime [min]	Type	Width [min]	Area [mAU*s]	Height [mAU]	Area %
1	10.214	BV R	0.0836	1740.38220	315.49036	88.6088
2	11.077	BV R	0.1021	105.38597	15.73999	5.3656
3	13.072	BB	0.0910	19.80476	3.25597	1.0083
4	15.080	VB	0.0882	98.54634	17.36682	5.0173

*Peak 1 and Peak 2 are *cis*- and *trans*-isomers of compound **2b**, respectively.

Appendix

Compound **tFAPz 2c**:

Detection at 220 nm: >99% purity

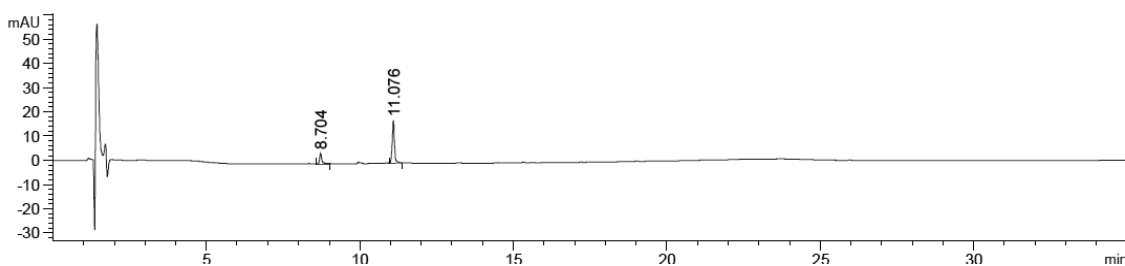


Signal 2: DAD1 B, Sig=220,4 Ref=off

Peak #	RetTime [min]	Type	Width [min]	Area [mAU*s]	Height [mAU]	Area %
1	8.704	BB	0.0689	75.14236	15.95775	9.5463
2	10.033	VB	0.0751	14.78739	3.02356	1.8786
3	11.076	VB R	0.0762	697.20984	138.36763	88.5751

*Peak 2 and Peak 3 are *cis*- and *trans*-isomers of compound **2c**, respectively, while Peak 1 is a solvent impurity.

Detection at 254 nm: >99% purity



Signal 1: DAD1 A, Sig=254,4 Ref=off

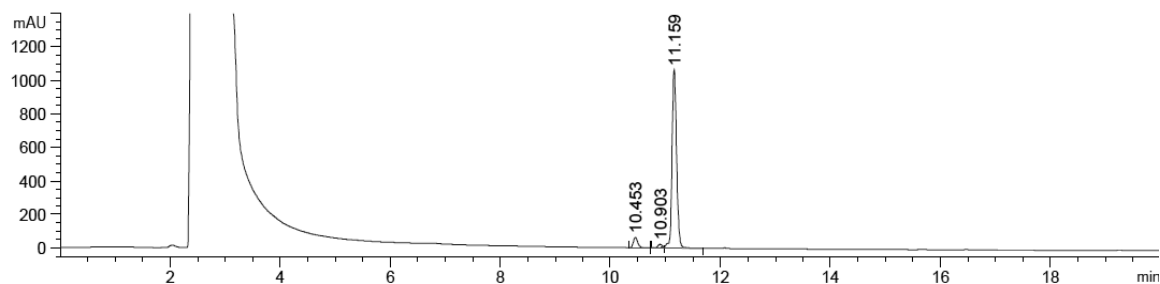
Peak #	RetTime [min]	Type	Width [min]	Area [mAU*s]	Height [mAU]	Area %
1	8.704	BB	0.0719	21.96865	4.42880	19.8383
2	11.076	BB	0.0776	88.77010	17.38212	80.1617

*Peak 2 is compound **2c**, while Peak 1 is a solvent impurity.

Appendix

Compound **tFAPz 2d**:

Detection at 220 nm: 98% purity

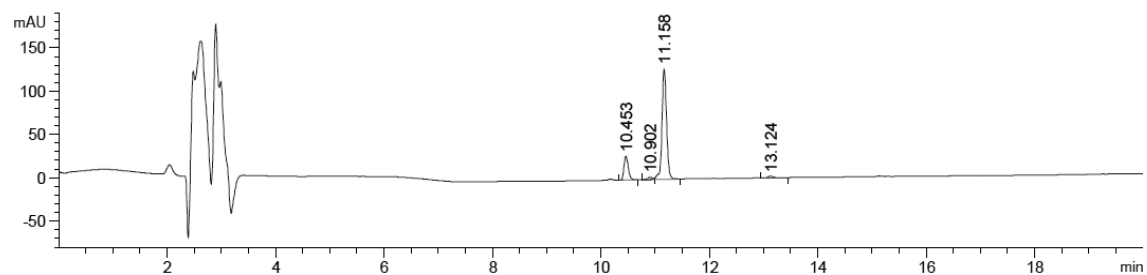


Signal 2: DAD1 B, Sig=220,4 Ref=off

Peak #	RetTime [min]	Type	Width [min]	Area [mAU*s]	Height [mAU]	Area %
1	10.453	BB	0.0856	334.06863	61.25165	5.1126
2	10.903	BV E	0.0820	101.85810	19.81578	1.5588
3	11.159	VB R	0.0889	6098.30371	1063.22681	93.3286

*Peak 1 and Peak 3 are *cis*- and *trans*-isomers of compound **2d**, respectively.

Detection at 254 nm: 97% purity



Signal 1: DAD1 A, Sig=254,4 Ref=off

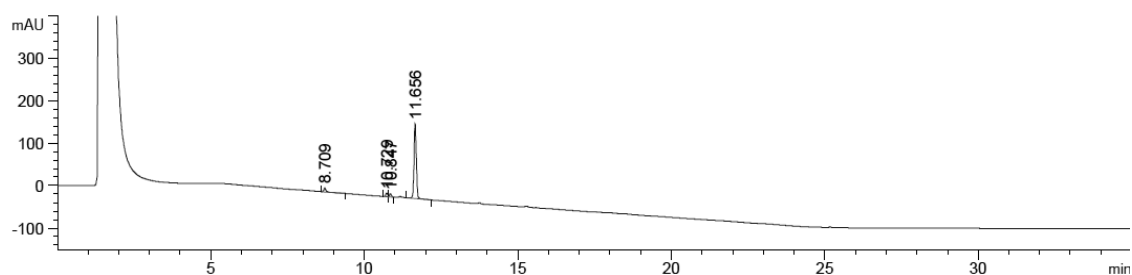
Peak #	RetTime [min]	Type	Width [min]	Area [mAU*s]	Height [mAU]	Area %
1	10.453	BB	0.0857	148.31471	27.17408	15.9015
2	10.902	BV E	0.0850	15.18391	2.72522	1.6279
3	11.158	VB R	0.0908	755.29016	128.07121	80.9781
4	13.124	BB	0.1016	13.92027	1.99098	1.4925

*Peak 1 and Peak 3 are *cis*- and *trans*-isomers of compound **2d**, respectively.

Appendix

Compound **tFAPz 2e**:

Detection at 220 nm: 96% purity

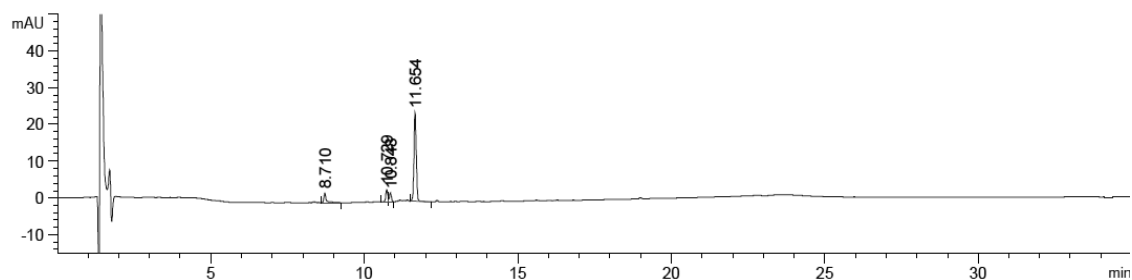


Signal 2: DAD1 B, Sig=220,4 Ref=off

Peak #	RetTime [min]	Type	Width [min]	Area [mAU*s]	Height [mAU]	Area %
1	8.709	BB	0.0773	49.76964	9.47899	4.8218
2	10.729	BV	0.0680	36.49594	8.18614	3.5358
3	10.847	VB	0.0671	30.32025	6.92202	2.9375
4	11.656	VB R	0.0805	915.59576	175.98161	88.7049

*Peak 3 and Peak 4 are *cis*- and *trans*-isomers of compound **2e**, respectively, while Peak 1 is a solvent impurity.

Detection at 254 nm: 90% purity



Signal 1: DAD1 A, Sig=254,4 Ref=off

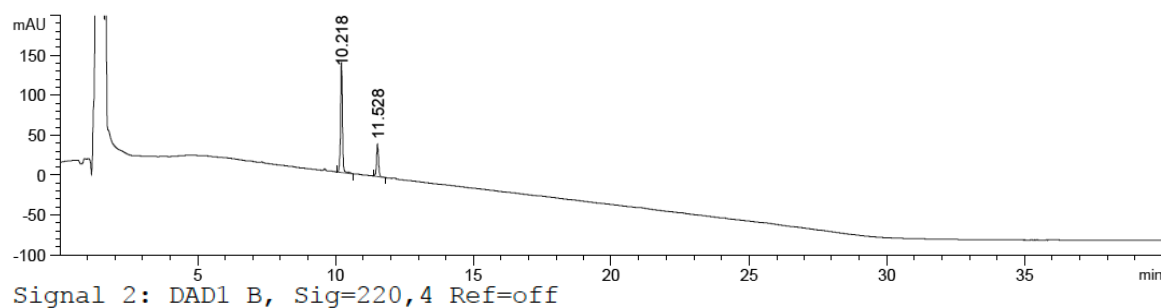
Peak #	RetTime [min]	Type	Width [min]	Area [mAU*s]	Height [mAU]	Area %
1	8.710	BB	0.0849	15.66210	2.65093	9.3402
2	10.729	BV	0.0689	15.56605	3.43198	9.2829
3	10.848	VB	0.0676	10.99482	2.48771	6.5569
4	11.654	BB	0.0809	125.46139	24.03287	74.8200

*Peak 3 and Peak 4 are *cis*- and *trans*-isomers of compound **2e**, respectively, while Peak 1 is a solvent impurity.

Appendix

Compound **tFAPz 2f**:

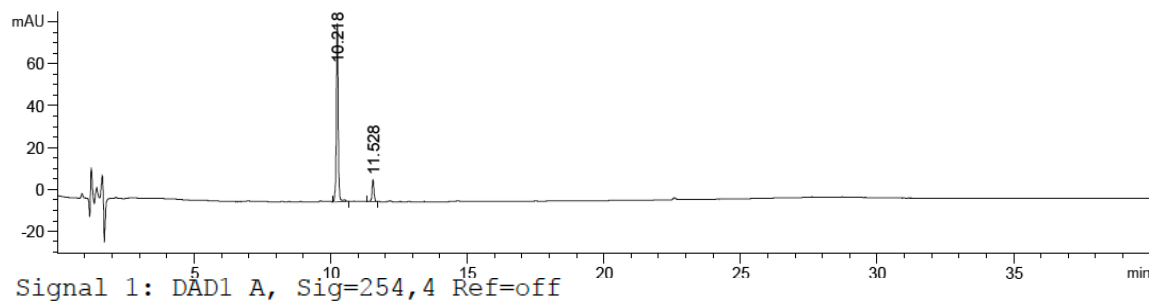
Detection at 220 nm: >99% purity



Peak #	RetTime [min]	Type	Width [min]	Area [mAU*s]	Height [mAU]	Area %
1	10.218	BV R	0.0743	684.29907	139.47960	77.2489
2	11.528	BB	0.0756	201.53714	40.82059	22.7511

*Peak 1 and Peak 2 are *cis*- and *trans*-isomers of compound **2f**, respectively.

Detection at 254 nm: >99% purity



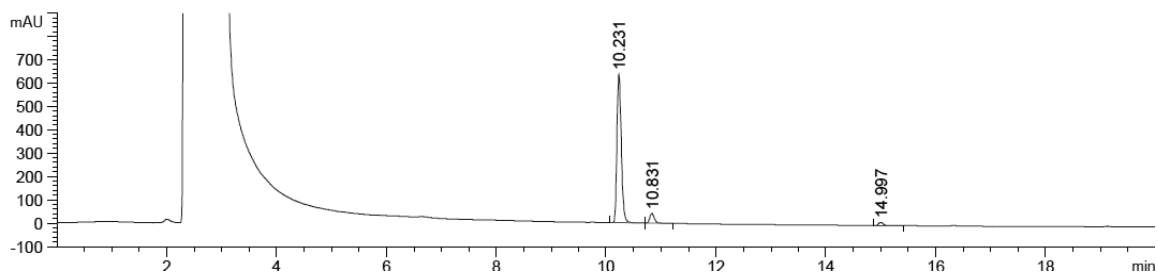
Peak #	RetTime [min]	Type	Width [min]	Area [mAU*s]	Height [mAU]	Area %
1	10.218	BV R	0.0731	420.10635	85.79062	89.2975
2	11.528	BB	0.0749	50.35044	10.32907	10.7025

*Peak 1 and Peak 2 are *cis*- and *trans*-isomers of compound **2f**, respectively.

Appendix

Compound **tFAPz 2g**:

Detection at 220 nm: 98% purity

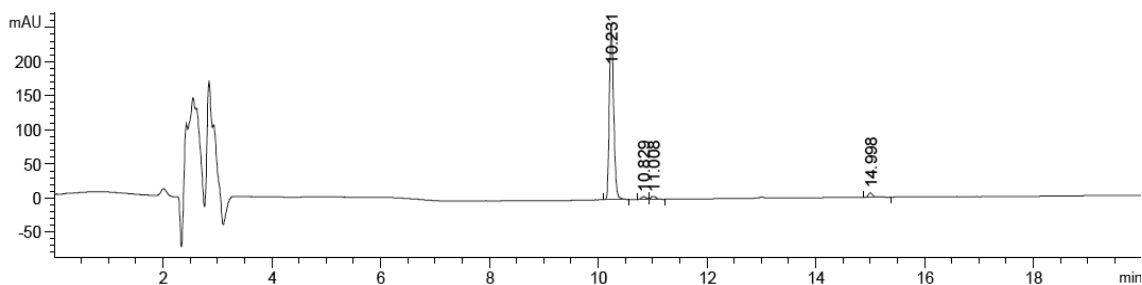


Signal 2: DAD1 B, Sig=220,4 Ref=off

Peak #	RetTime [min]	Type	Width [min]	Area [mAU*s]	Height [mAU]	Area %
1	10.231	BV	0.0862	3495.34033	634.78613	91.4535
2	10.831	VB	0.0905	246.91768	42.06487	6.4605
3	14.997	BB	0.0903	79.72755	13.61964	2.0860

*Peak 1 and Peak 2 are *cis*- and *trans*-isomers of compound **2g**, respectively.

Detection at 254 nm: 95% purity



Signal 1: DAD1 A, Sig=254,4 Ref=off

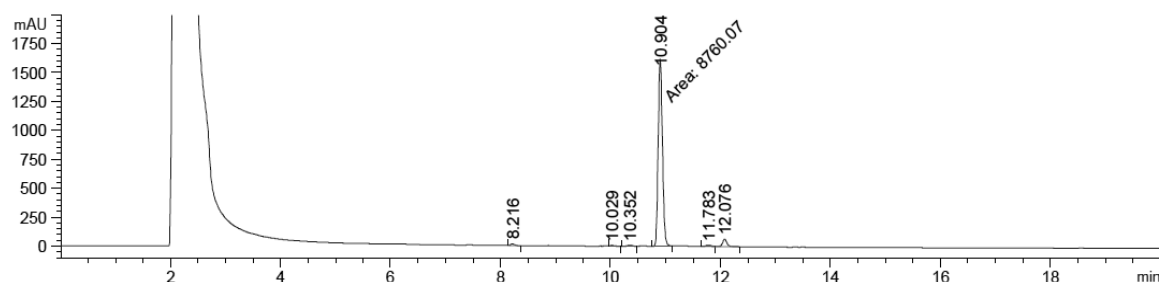
Peak #	RetTime [min]	Type	Width [min]	Area [mAU*s]	Height [mAU]	Area %
1	10.231	BB	0.0862	1421.64502	258.53427	93.9030
2	10.829	BV	0.0855	23.03539	4.10559	1.5215
3	11.008	VB	0.1009	30.08365	4.56190	1.9871
4	14.998	BB	0.0929	39.18709	6.44867	2.5884

*Peak 1 and Peak 2 are *cis*- and *trans*-isomers of compound **2g**, respectively.

Appendix

Compound **tFAPz 3**:

Detection at 220 nm: 98% purity

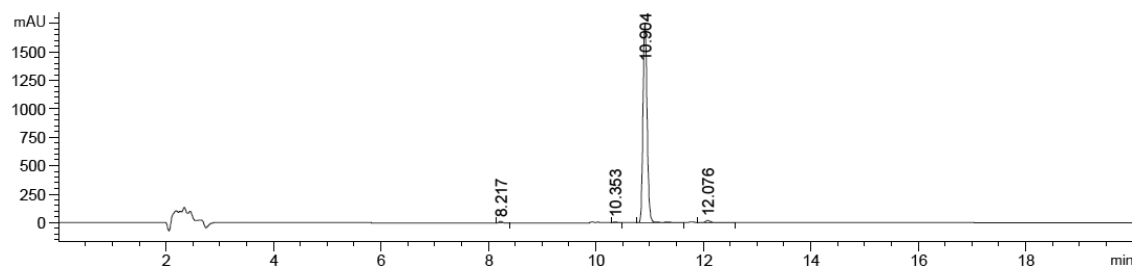


Signal 2: DAD1 B, Sig=220,4 Ref=off

Peak #	RetTime [min]	Type	Width [min]	Area [mAU*s]	Height [mAU]	Area %
1	8.216	BB	0.0718	70.83435	15.35261	0.7589
2	10.029	VB	0.0797	32.80803	6.20399	0.3515
3	10.352	BV	0.0854	53.05852	9.76781	0.5685
4	10.904	MM	0.0899	8760.07324	1624.20984	93.8531
5	11.783	BV E	0.0840	59.27827	10.81361	0.6351
6	12.076	VB R	0.0842	357.76056	65.03698	3.8330

*Peak 4 and Peak 6 are *cis*- and *trans*-isomers of compound **3**, respectively.

Detection at 254 nm: 99% purity



Signal 1: DAD1 A, Sig=254,4 Ref=off

Peak #	RetTime [min]	Type	Width [min]	Area [mAU*s]	Height [mAU]	Area %
1	8.217	BB	0.0723	73.87509	15.87974	0.7562
2	10.353	VB	0.0808	43.90155	8.42828	0.4494
3	10.904	BV R	0.0851	9516.02148	1751.78943	97.4068
4	12.076	VV R	0.1003	135.55783	18.70377	1.3876

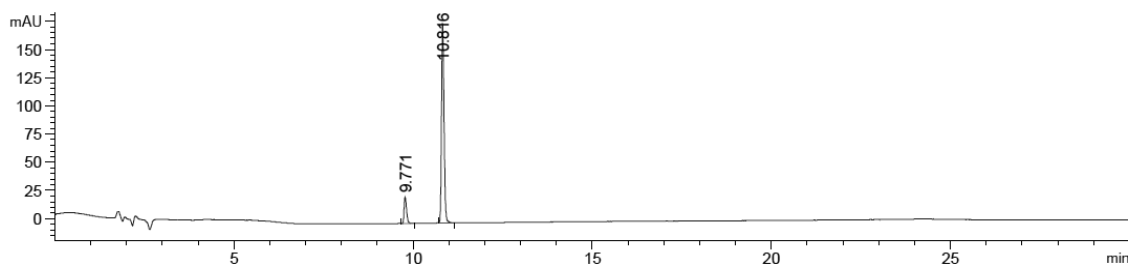
*Peak 3 and Peak 4 are *cis*- and *trans*-isomers of compound **3**, respectively.

7.3.2 Analytical HPLC Chromatogram for PSS Determination

Compound **tFAPz 1** (50 μ M solution in TrisHCl Buffer + 0.5% DMSO, pH 7.5, injection volume 5 μ L):

Irradiation with $\lambda = 528$ nm for conversion from *cis*-isomer to *trans*-isomer.

Detection at 298 nm: t_R *cis*-isomer = 9.771 min (11%), t_R *trans*-isomer = 10.816 min (89%).

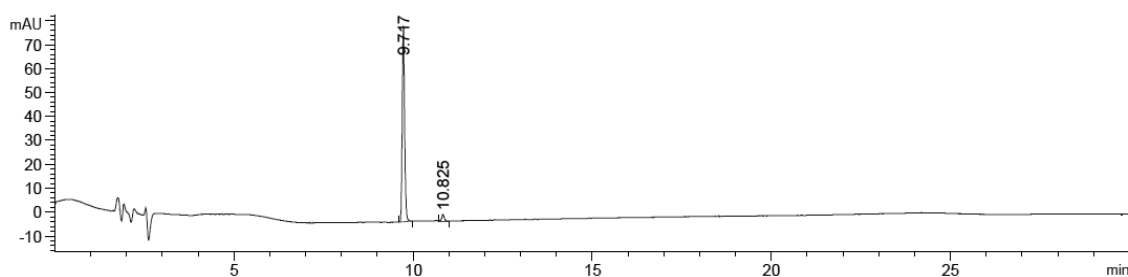


Signal 4: DAD1 D, Sig=298,4 Ref=off

Peak #	RetTime [min]	Type	Width [min]	Area [mAU*s]	Height [mAU]	Area %
1	9.771	BB	0.0745	112.47044	23.24260	11.2017
2	10.816	BB	0.0767	891.57690	177.14558	88.7983

Irradiation with $\lambda = 365$ nm for conversion from *trans*-isomer to *cis*-isomer.

Detection at 298 nm: t_R *cis*-isomer = 9.717 min (97%), t_R *trans*-isomer = 10.825 min (3%).



Signal 4: DAD1 D, Sig=298,4 Ref=off

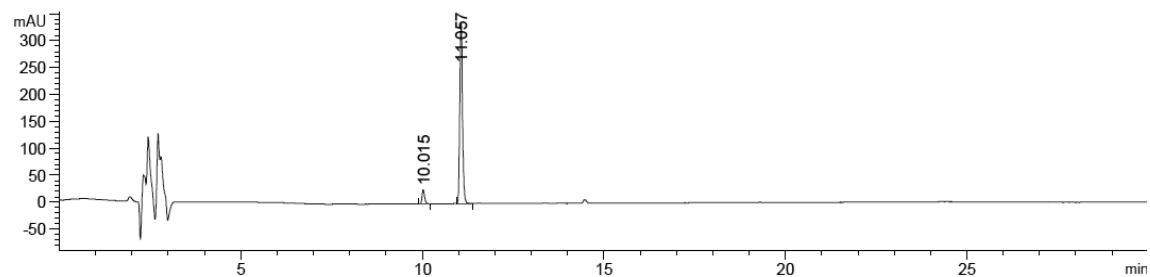
Peak #	RetTime [min]	Type	Width [min]	Area [mAU*s]	Height [mAU]	Area %
1	9.717	BB	0.0742	395.26639	82.05482	96.7450
2	10.825	BB	0.0772	13.29880	2.62116	3.2550

Appendix

Compound **tFAPz 1** (50 μ M solution in DMSO, injection volume 5 μ L):

Irradiation with $\lambda = 528$ nm for conversion from *cis*-isomer to *trans*-isomer.

Detection at 298 nm: t_R *cis*-isomer = 10.015 min (7%), t_R *trans*-isomer = 11.057 min (93%).

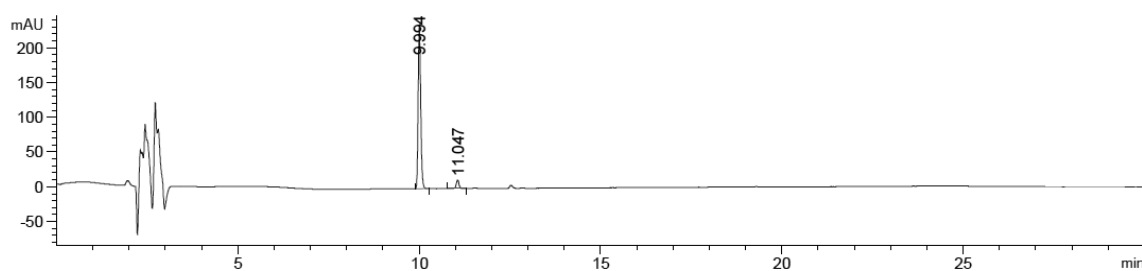


Signal 4: DAD1 D, Sig=298,4 Ref=off

Peak #	RetTime [min]	Type	Width [min]	Area [mAU*s]	Height [mAU]	Area %
1	10.015	BB	0.0794	134.98250	26.49073	6.9416
2	11.057	BB	0.0848	1809.57202	336.35025	93.0584

Irradiation with $\lambda = 365$ nm for conversion from *trans*-isomer to *cis*-isomer.

Detection at 298 nm: t_R *cis*-isomer = 9.994 min (95%), t_R *trans*-isomer = 11.047 min (5%).



Signal 4: DAD1 D, Sig=298,4 Ref=off

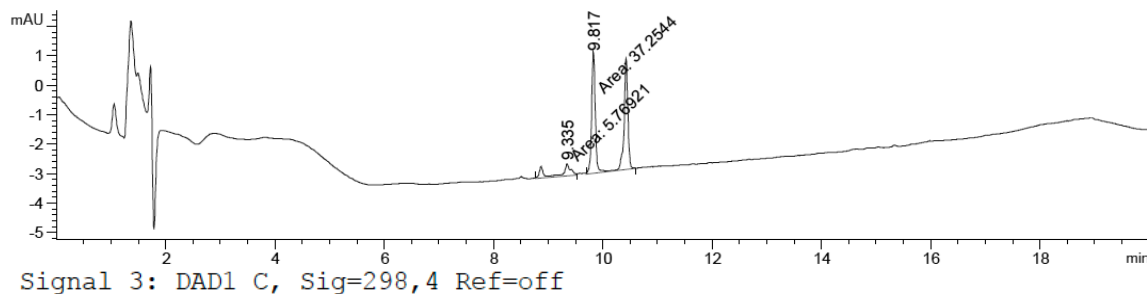
Peak #	RetTime [min]	Type	Width [min]	Area [mAU*s]	Height [mAU]	Area %
1	9.994	BB	0.0804	1217.11560	235.06967	94.7067
2	11.047	BB	0.0876	68.02588	12.09581	5.2933

Appendix

Compound **tFAPz 2a** (20 μ M solution in TrisHCl Buffer + 0.5% DMSO, pH 7.5, injection volume 5 μ L):

Irradiation with $\lambda = 528$ nm for conversion from *cis*-isomer to *trans*-isomer.

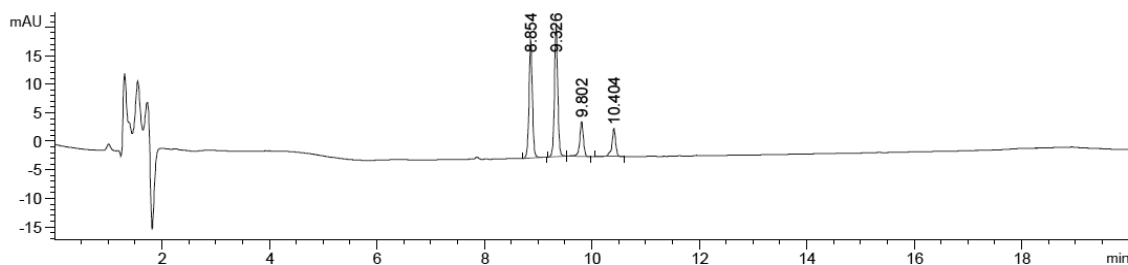
Detection at 298 nm: t_R *cis*-isomer = 9.335 min (13%), t_R *trans*-isomer = 9.817 min (87%).



Peak #	RetTime [min]	Type	Width [min]	Area [mAU*s]	Height [mAU]	Area %
1	9.335	MM	0.2332	5.76921	4.12265e-1	13.4094
2	9.817	MM	0.1498	37.25441	4.14439	86.5906

Irradiation with $\lambda = 365$ nm for conversion from *trans*-isomer to *cis*-isomer.

Detection at 298 nm: t_R *cis*-isomer = 8.854-9.326 min (78%), t_R *trans*-isomer = 9.802-10.404 min (22%).



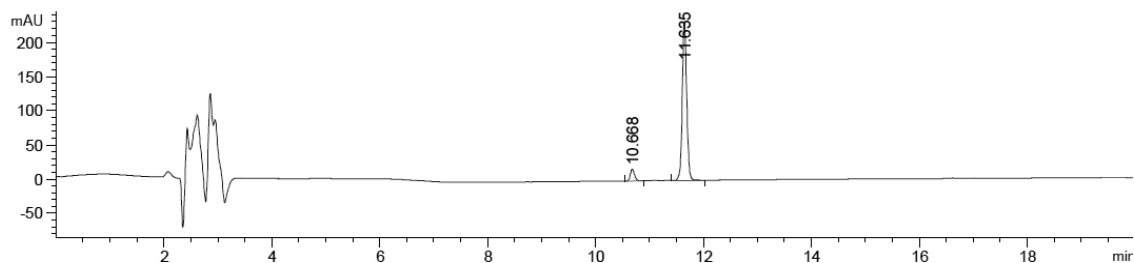
Peak #	RetTime [min]	Type	Width [min]	Area [mAU*s]	Height [mAU]	Area %
1	8.854	BB	0.0673	91.19453	20.75854	37.2684
2	9.326	BB	0.0656	99.64082	23.41810	40.7202
3	9.802	BB	0.0714	28.97844	6.10159	11.8426
4	10.404	BB	0.0747	24.88278	4.94866	10.1688

Appendix

Compound **tFAPz 2a** (20 μ M solution in DMSO, injection volume 5 μ L):

Irradiation with $\lambda = 528$ nm for conversion from *cis*-isomer to *trans*-isomer.

Detection at 299 nm: t_R *cis*-isomer = 10.668 min (7%), t_R *trans*-isomer = 11.635 min (93%).

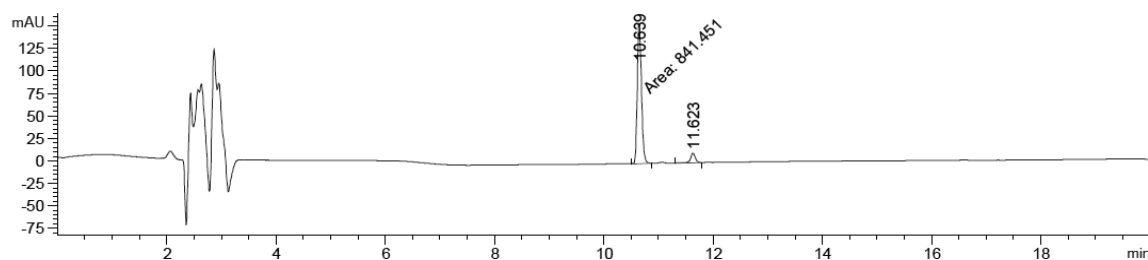


Signal 7: DAD1 G, Sig=299,4 Ref=off

Peak #	RetTime [min]	Type	Width [min]	Area [mAU*s]	Height [mAU]	Area %
1	10.668	BB	0.0830	94.37758	17.47907	6.6843
2	11.635	BB	0.0883	1317.55786	231.71507	93.3157

Irradiation with $\lambda = 365$ nm for conversion from *trans*-isomer to *cis*-isomer.

Detection at 299 nm: t_R *cis*-isomer = 10.639 min (93%), t_R *trans*-isomer = 11.623 min (7%).



Signal 7: DAD1 G, Sig=299,4 Ref=off

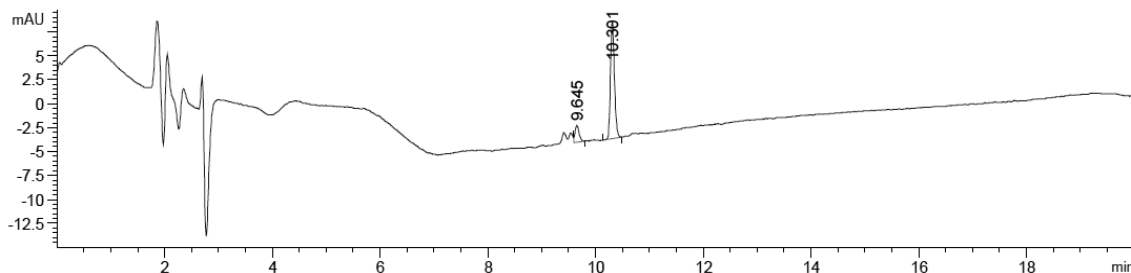
Peak #	RetTime [min]	Type	Width [min]	Area [mAU*s]	Height [mAU]	Area %
1	10.639	MM	0.0897	841.45099	156.29002	93.1209
2	11.623	BB	0.0911	62.16061	10.49891	6.8791

Appendix

Compound **tFAPz 2b** (20 μ M solution in TrisHCl Buffer + 0.2% DMSO, pH 7.5, injection volume 5 μ L):

Irradiation with $\lambda = 528$ nm for conversion from *cis*-isomer to *trans*-isomer.

Detection at 296 nm: t_R *cis*-isomer = 9.645 min (13%), t_R *trans*-isomer = 10.301 min (87%).

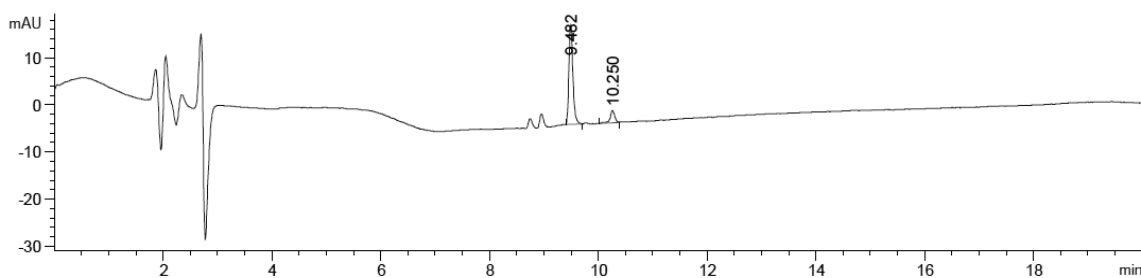


Signal 3: DAD1 C, Sig=296,4 Ref=off

Peak #	RetTime [min]	Type	Width [min]	Area [mAU*s]	Height [mAU]	Area %
1	9.645	VB	0.0803	9.18132	1.71801	12.7987
2	10.301	BB	0.0796	62.55503	12.23667	87.2013

Irradiation with $\lambda = 365$ nm for conversion from *trans*-isomer to *cis*-isomer.

Detection at 296 nm: t_R *cis*-isomer = 9.482 min (88%), t_R *trans*-isomer = 10.250 min (12%).



Signal 3: DAD1 C, Sig=296,4 Ref=off

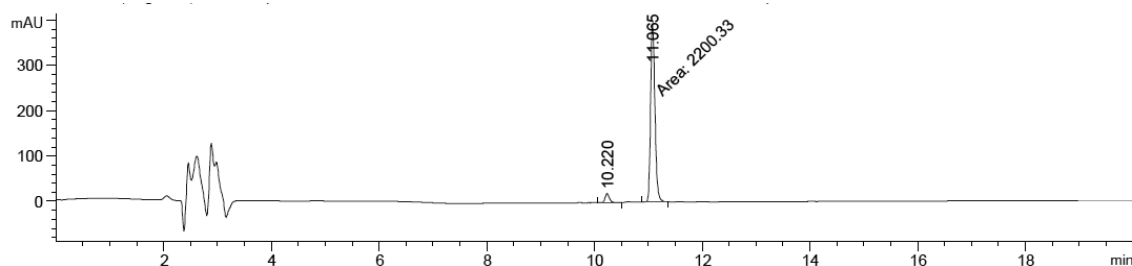
Peak #	RetTime [min]	Type	Width [min]	Area [mAU*s]	Height [mAU]	Area %
1	9.482	BB	0.0772	107.02318	21.07575	87.6282
2	10.250	BB	0.0885	15.11014	2.57241	12.3718

Appendix

Compound **tFAPz 2b** (50 μ M solution in DMSO, injection volume 5 μ L):

Irradiation with $\lambda = 528$ nm for conversion from *cis*-isomer to *trans*-isomer.

Detection at 303 nm: t_R *cis*-isomer = 10.220 min (5%), t_R *trans*-isomer = 11.065 min (95%).

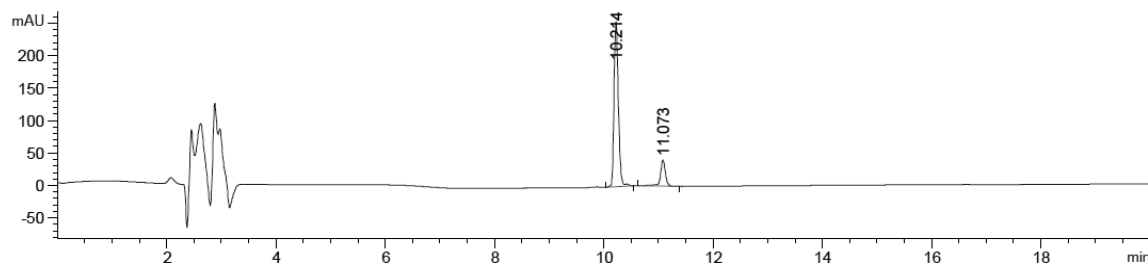


Signal 7: DAD1 G, Sig=303,4 Ref=off

Peak #	RetTime [min]	Type	Width [min]	Area [mAU*s]	Height [mAU]	Area %
1	10.220	BB	0.0858	109.35136	19.98429	4.7345
2	11.065	MM	0.0934	2200.32959	392.57013	95.2655

Irradiation with $\lambda = 365$ nm for conversion from *trans*-isomer to *cis*-isomer.

Detection at 303 nm: t_R *cis*-isomer = 10.214 min (85%), t_R *trans*-isomer = 11.073 min (15%).



Signal 7: DAD1 G, Sig=303,4 Ref=off

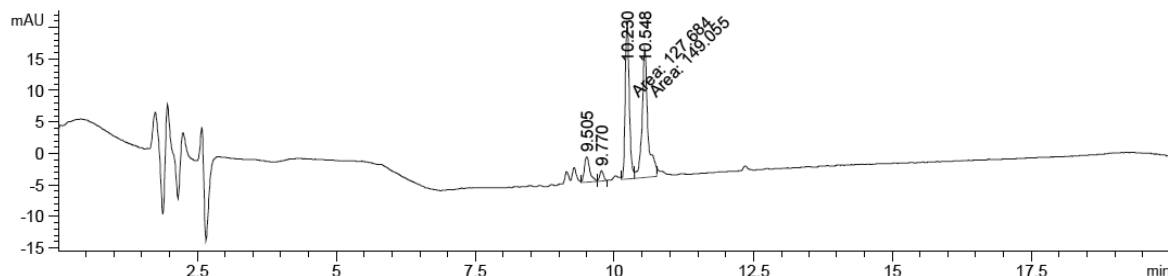
Peak #	RetTime [min]	Type	Width [min]	Area [mAU*s]	Height [mAU]	Area %
1	10.214	BV R	0.0834	1398.79175	254.29042	84.5831
2	11.073	BB	0.0958	254.95663	40.29276	15.4169

Appendix

Compound **tFAPz 2c** (20 μ M solution in TrisHCl Buffer + 0.2% DMSO, pH 7.5, injection volume 5 μ L):

Irradiation with $\lambda = 528$ nm for conversion from *cis*-isomer to *trans*-isomer.

Detection at 296 nm: t_R *cis*-isomer = 9.505-9.770 min (11%), t_R *trans*-isomer = 10.230-10.548 min (89%).

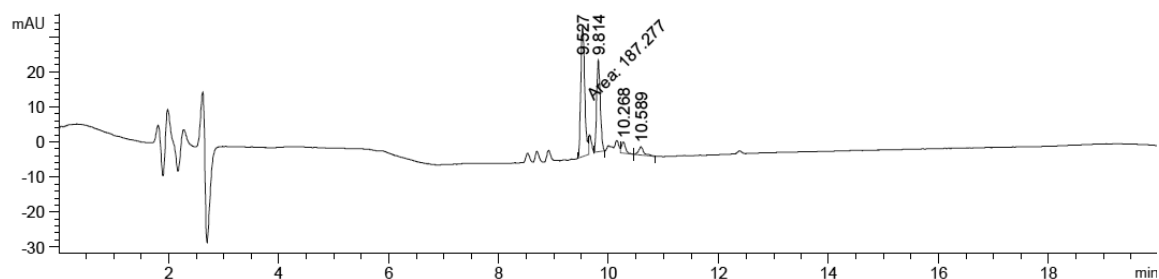


Signal 1: DAD1 C, Sig=296,4 Ref=off

Peak #	RetTime [min]	Type	Width [min]	Area [mAU*s]	Height [mAU]	Area %
1	9.505	VV	0.1021	27.07076	4.04305	8.6958
2	9.770	VB	0.0755	7.49859	1.57586	2.4087
3	10.230	FM	0.0849	127.68445	25.07917	41.0154
4	10.548	MF	0.1209	149.05498	20.54736	47.8801

Irradiation with $\lambda = 365$ nm for conversion from *trans*-isomer to *cis*-isomer.

Detection at 296 nm: t_R *cis*-isomer = 9.527 and 9.814 min (90%), t_R *trans*-isomer = 10.268-10.589 min (10%).



Signal 1: DAD1 C, Sig=296,4 Ref=off

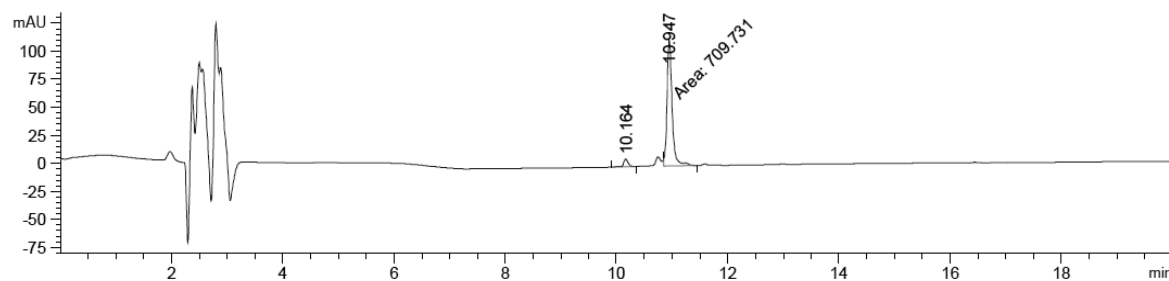
Peak #	RetTime [min]	Type	Width [min]	Area [mAU*s]	Height [mAU]	Area %
1	9.527	MF	0.0828	187.27718	37.68084	55.0929
2	9.814	BB	0.0715	120.29916	26.21181	35.3894
3	10.268	VB	0.0795	16.69783	3.16587	4.9121
4	10.589	BB	0.0985	15.65585	2.32536	4.6056

Appendix

Compound **tFAPz 2c** (20 μ M solution in DMSO, injection volume 5 μ L):

Irradiation with $\lambda = 528$ nm for conversion from *cis*-isomer to *trans*-isomer.

Detection at 300 nm: t_R *cis*-isomer = 10.164 min (5%), t_R *trans*-isomer = 10.947 min (95%).

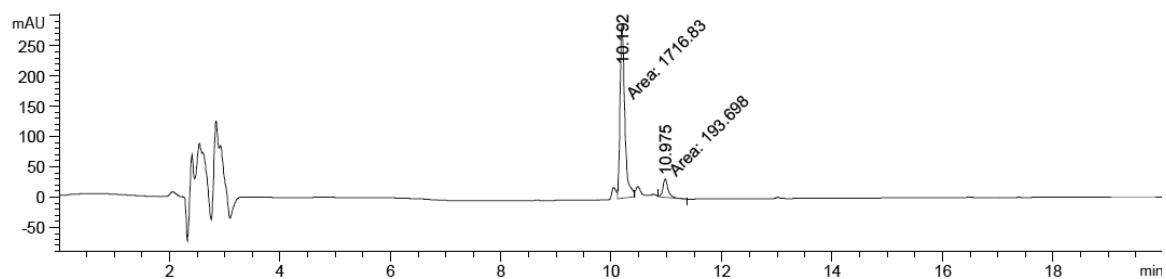


Signal 1: DAD1 G, Sig=300,4 Ref=off

Peak #	RetTime [min]	Type	Width [min]	Area [mAU*s]	Height [mAU]	Area %
1	10.164	VB R	0.0862	39.25893	6.91466	5.2416
2	10.947	FM	0.1050	709.73065	112.62199	94.7584

Irradiation with $\lambda = 365$ nm for conversion from *trans*-isomer to *cis*-isomer.

Detection at 300 nm: t_R *cis*-isomer = 10.192 min (90%), t_R *trans*-isomer = 10.975 min (10%).



Signal 1: DAD1 G, Sig=300,4 Ref=off

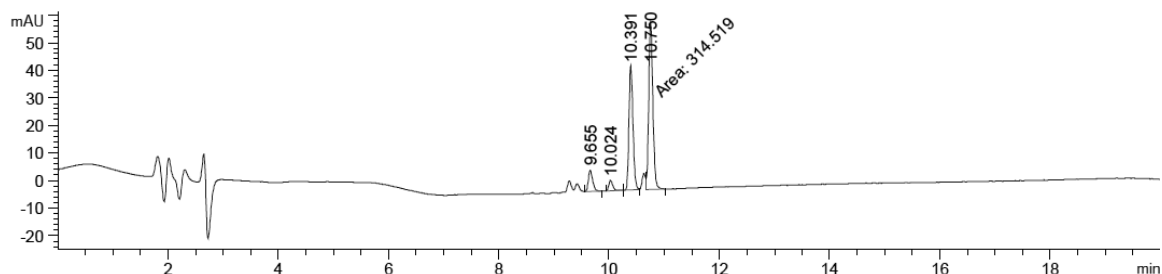
Peak #	RetTime [min]	Type	Width [min]	Area [mAU*s]	Height [mAU]	Area %
1	10.192	MF	0.0994	1716.83276	287.75098	89.8616
2	10.975	MM	0.1074	193.69769	30.05741	10.1384

Appendix

Compound **tFAPz 2d** (20 μ M solution in TrisHCl Buffer + 0.2% DMSO, pH 7.5, injection volume 5 μ L):

Irradiation with $\lambda = 528$ nm for conversion from *cis*-isomer to *trans*-isomer.

Detection at 298 nm: t_R *cis*-isomer = 9.655-10.024 min (10%), t_R *trans*-isomer = 10.391 and 10.750 min (90%).

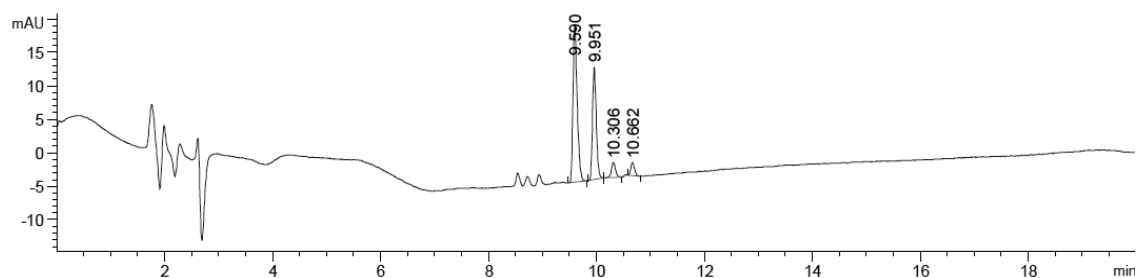


Signal 3: DAD1 C, Sig=298,4 Ref=off

Peak #	RetTime [min]	Type	Width [min]	Area [mAU*s]	Height [mAU]	Area %
1	9.655	VB	0.0836	42.35640	7.77229	6.9905
2	10.024	BB	0.0788	18.58157	3.68441	3.0667
3	10.391	BV	0.0795	230.45750	45.15563	38.0347
4	10.750	FM	0.0864	314.51907	60.65613	51.9082

Irradiation with $\lambda = 365$ nm for conversion from *trans*-isomer to *cis*-isomer.

Detection at 298 nm: t_R *cis*-isomer = 9.590-9.951 min (91%), t_R *trans*-isomer = 10.306-10.662 min (9%).



Signal 3: DAD1 C, Sig=298,4 Ref=off

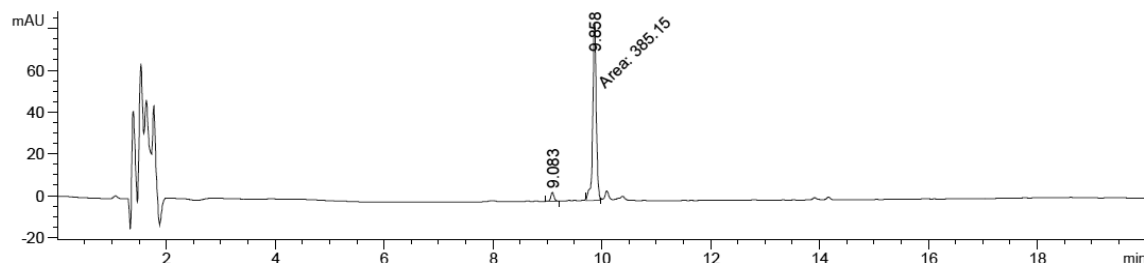
Peak #	RetTime [min]	Type	Width [min]	Area [mAU*s]	Height [mAU]	Area %
1	9.590	BB	0.0831	127.36843	23.54895	55.2091
2	9.951	BB	0.0772	82.41076	16.82096	35.7217
3	10.306	BB	0.0792	11.79682	2.24769	5.1134
4	10.662	BB	0.0733	9.12590	1.92439	3.9557

Appendix

Compound **tFAPz 2d** (20 μ M solution in DMSO, injection volume 5 μ L):

Irradiation with $\lambda = 528$ nm for conversion from *cis*-isomer to *trans*-isomer.

Detection at 298 nm: t_R *cis*-isomer = 9.083 min (4%), t_R *trans*-isomer = 9.858 min (96%).

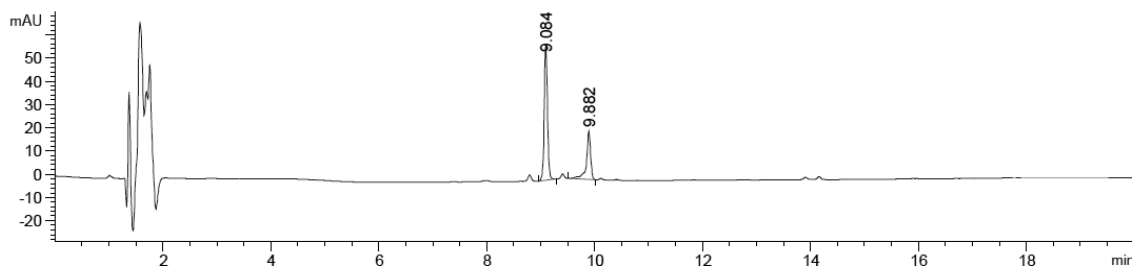


Signal 3: DAD1 C, Sig=298,4 Ref=off

Peak #	RetTime [min]	Type	Width [min]	Area [mAU*s]	Height [mAU]	Area %
1	9.083	BB	0.0647	17.21897	4.12223	4.2794
2	9.858	MM	0.0749	385.14972	85.64902	95.7206

Irradiation with $\lambda = 365$ nm for conversion from *trans*-isomer to *cis*-isomer.

Detection at 298 nm: t_R *cis*-isomer = 9.084 min (69%), t_R *trans*-isomer = 9.882 min (31%).



Signal 3: DAD1 C, Sig=298,4 Ref=off

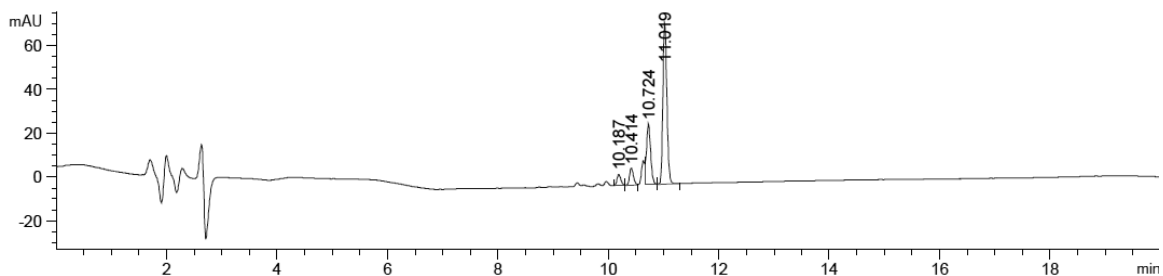
Peak #	RetTime [min]	Type	Width [min]	Area [mAU*s]	Height [mAU]	Area %
1	9.084	BB	0.0652	245.38435	58.17034	68.6012
2	9.882	BB	0.0787	112.31232	20.89488	31.3988

Appendix

Compound **tFAPz 2e** (20 μ M solution in TrisHCl Buffer + 0.2% DMSO, pH 7.5, injection volume 5 μ L):

Irradiation with $\lambda = 528$ nm for conversion from *cis*-isomer to *trans*-isomer.

Detection at 298 nm: t_R *cis*-isomer = 10.187-10.414 min (11%), t_R *trans*-isomer = 10.724-11.019 min (89%).

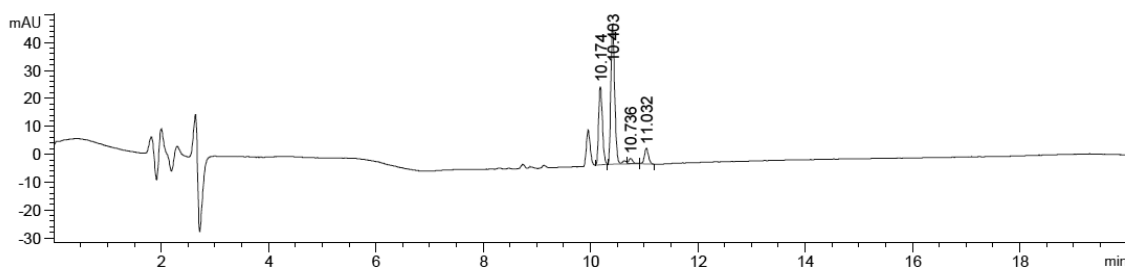


Signal 3: DAD1 C, Sig=298,4 Ref=off

Peak #	RetTime [min]	Type	Width [min]	Area [mAU*s]	Height [mAU]	Area %
1	10.187	BV	0.0770	24.57039	5.02689	4.2091
2	10.414	VV	0.0783	38.74809	7.75246	6.6378
3	10.724	VV	0.0801	147.53575	27.69523	25.2739
4	11.019	VB	0.0789	372.89377	73.86233	63.8792

Irradiation with $\lambda = 365$ nm for conversion from *trans*-isomer to *cis*-isomer.

Detection at 298 nm: t_R *cis*-isomer = 10.174-10.403 min (91%), t_R *trans*-isomer = 10.736-11.032 min (9%).



Signal 3: DAD1 C, Sig=298,4 Ref=off

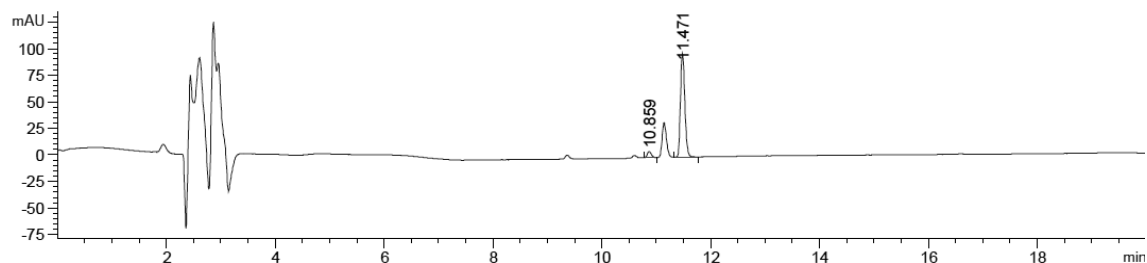
Peak #	RetTime [min]	Type	Width [min]	Area [mAU*s]	Height [mAU]	Area %
1	10.174	VB	0.0763	135.63310	28.09234	31.9714
2	10.403	BV R	0.0772	250.65239	50.12748	59.0837
3	10.736	VB E	0.0781	9.42633	1.83033	2.2220
4	11.032	BB	0.0793	28.52058	5.61447	6.7229

Appendix

Compound **tFAPz 2e** (20 μ M solution in DMSO, injection volume 5 μ L):

Irradiation with $\lambda = 528$ nm for conversion from *cis*-isomer to *trans*-isomer.

Detection at 302 nm: t_R *cis*-isomer = 10.859 min (5%), t_R *trans*-isomer = 11.471 min (95%).

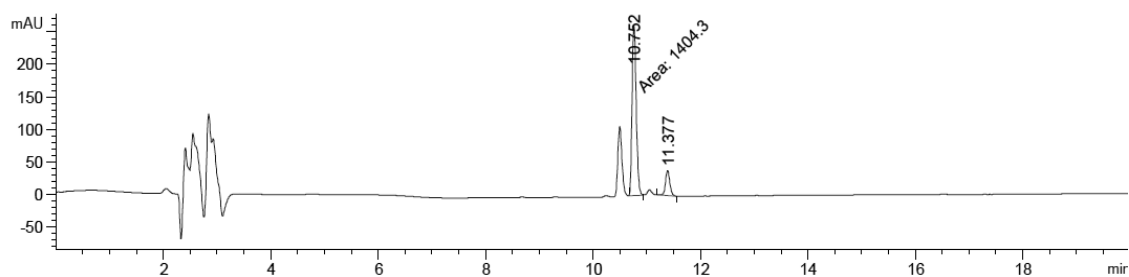


Signal 7: DAD1 G, Sig=302,4 Ref=off

Peak #	RetTime [min]	Type	Width [min]	Area [mAU*s]	Height [mAU]	Area %
1	10.859	BB	0.0813	30.50995	5.80463	5.3379
2	11.471	VB	0.0845	541.06525	97.93122	94.6621

Irradiation with $\lambda = 365$ nm for conversion from *trans*-isomer to *cis*-isomer.

Detection at 302 nm: t_R *cis*-isomer = 10.752 min (87%), t_R *trans*-isomer = 11.377 min (13%).



Signal 7: DAD1 G, Sig=302,4 Ref=off

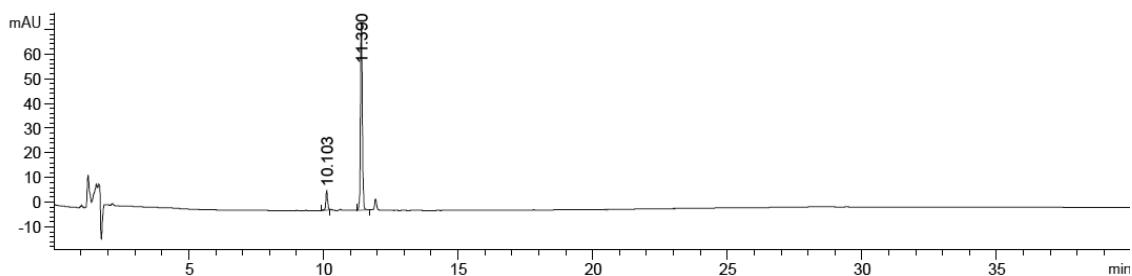
Peak #	RetTime [min]	Type	Width [min]	Area [mAU*s]	Height [mAU]	Area %
1	10.752	MM	0.0885	1404.29565	264.35718	86.7021
2	11.377	BB	0.0853	215.38411	38.46201	13.2979

Appendix

Compound **tFAPz 2f** (20 μ M solution in TrisHCl Buffer + 0.2% DMSO, pH 7.5, injection volume 5 μ L):

Irradiation with $\lambda = 528$ nm for conversion from *cis*-isomer to *trans*-isomer.

Detection at 292 nm: t_R *cis*-isomer = 10.103 min (9%), t_R *trans*-isomer = 11.390 min (91%).

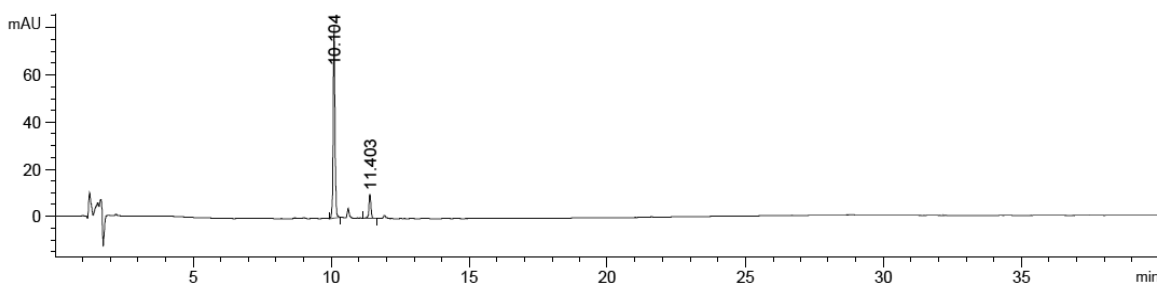


Signal 3: DAD1 C, Sig=292,4 Ref=off

Peak #	RetTime [min]	Type	Width [min]	Area [mAU*s]	Height [mAU]	Area %
1	10.103	BB	0.0708	35.83818	7.92365	8.9431
2	11.390	BB	0.0744	364.89911	75.53328	91.0569

Irradiation with $\lambda = 365$ nm for conversion from *trans*-isomer to *cis*-isomer.

Detection at 292 nm: t_R *cis*-isomer = 10.104 min (88%), t_R *trans*-isomer = 11.403 min (12%).



Signal 3: DAD1 C, Sig=292,4 Ref=off

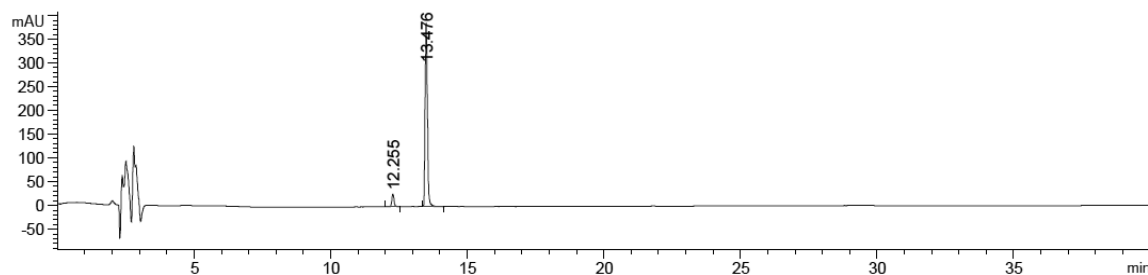
Peak #	RetTime [min]	Type	Width [min]	Area [mAU*s]	Height [mAU]	Area %
1	10.104	BB	0.0705	382.21686	81.89484	88.3790
2	11.403	BB	0.0738	50.25768	10.14672	11.6210

Appendix

Compound **tFAPz 2f** (50 μ M solution in DMSO, injection volume 5 μ L):

Irradiation with $\lambda = 528$ nm for conversion from *cis*-isomer to *trans*-isomer.

Detection at 300 nm: t_R *cis*-isomer = 12.255 min (6%), t_R *trans*-isomer = 13.476 min (94%).

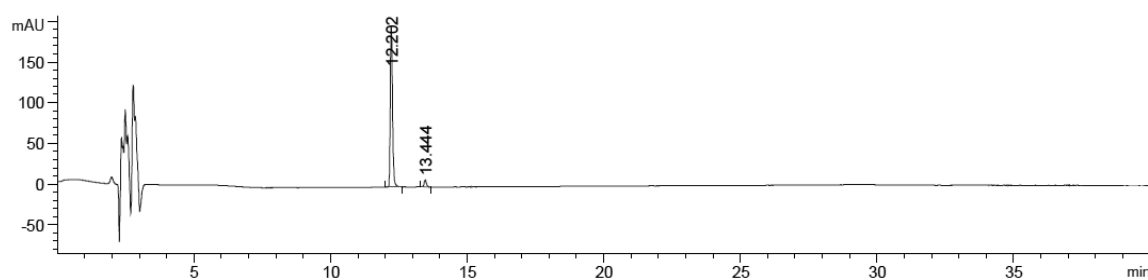


Signal 4: DAD1 D, Sig=300,4 Ref=off

Peak #	RetTime [min]	Type	Width [min]	Area [mAU*s]	Height [mAU]	Area %
1	12.255	BB	0.0891	156.33333	27.19328	6.4887
2	13.476	BV R	0.0900	2252.98145	386.68185	93.5113

Irradiation with $\lambda = 365$ nm for conversion from *trans*-isomer to *cis*-isomer.

Detection at 300 nm: t_R *cis*-isomer = 12.202 min (96%), t_R *trans*-isomer = 13.444 min (4%).



Signal 4: DAD1 D, Sig=300,4 Ref=off

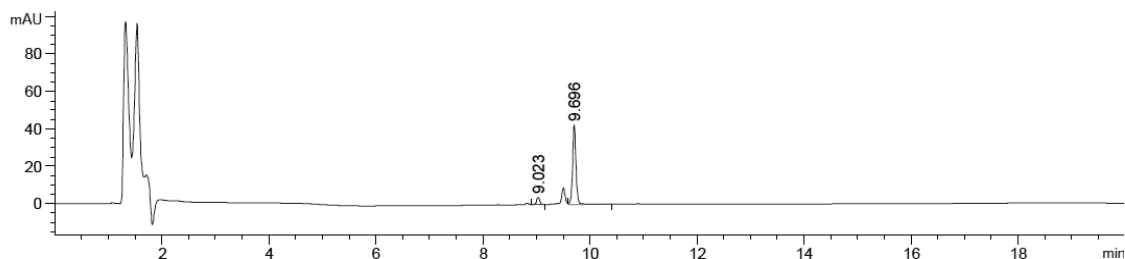
Peak #	RetTime [min]	Type	Width [min]	Area [mAU*s]	Height [mAU]	Area %
1	12.202	BB	0.0854	1105.94214	197.25192	95.8403
2	13.444	BB	0.0904	48.00014	8.18558	4.1597

Appendix

Compound **tFAPz 2g** (20 μ M solution in TrisHCl Buffer + 0.2% DMSO, pH 7.5, injection volume 5 μ L):

Irradiation with $\lambda = 528$ nm for conversion from *cis*-isomer to *trans*-isomer.

Detection at 296 nm: t_R *cis*-isomer = 9.023 min (8%), t_R *trans*-isomer = 9.696 min (92%).

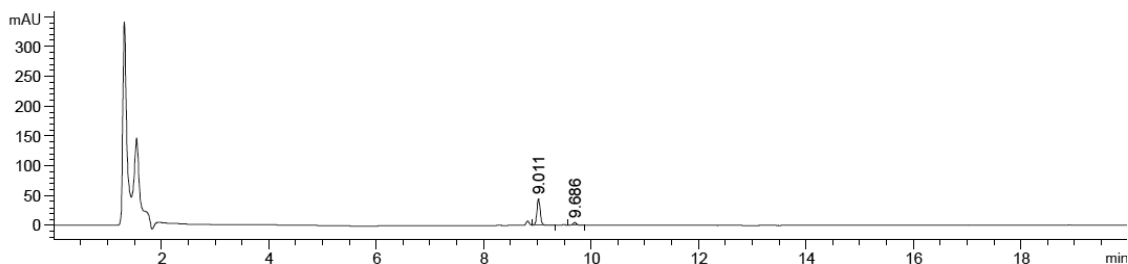


Signal 3: DAD1 C, Sig=296,4 Ref=off

Peak #	RetTime [min]	Type	Width [min]	Area [mAU*s]	Height [mAU]	Area %
1	9.023	BB	0.0652	16.45210	3.90064	8.0208
2	9.696	VB	0.0681	188.66501	42.24470	91.9792

Irradiation with $\lambda = 365$ nm for conversion from *trans*-isomer to *cis*-isomer.

Detection at 296 nm: t_R *cis*-isomer = 9.011 min (90%), t_R *trans*-isomer = 9.686 min (10%).



Signal 3: DAD1 C, Sig=296,4 Ref=off

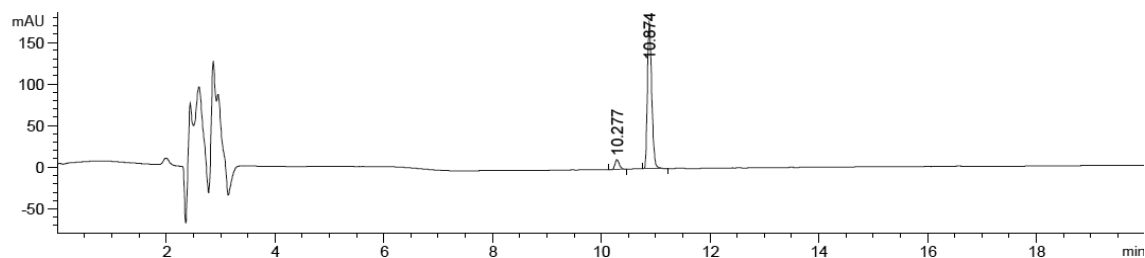
Peak #	RetTime [min]	Type	Width [min]	Area [mAU*s]	Height [mAU]	Area %
1	9.011	VV R	0.0658	188.76802	44.19389	89.9828
2	9.686	VB	0.0673	21.01425	4.77621	10.0172

Appendix

Compound **tFAPz 2g** (50 μ M solution in DMSO, injection volume 5 μ L):

Irradiation with $\lambda = 528$ nm for conversion from *cis*-isomer to *trans*-isomer.

Detection at 301 nm: t_R *cis*-isomer = 10.277 min (6%), t_R *trans*-isomer = 10.874 min (94%).

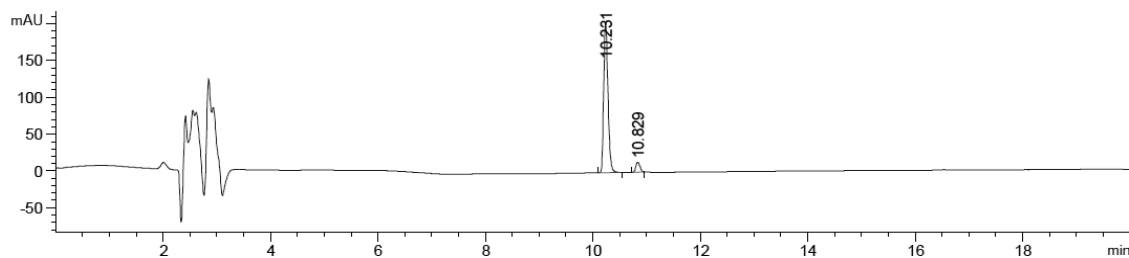


Signal 7: DAD1 G, Sig=301,4 Ref=off

Peak #	RetTime [min]	Type	Width [min]	Area [mAU*s]	Height [mAU]	Area %
1	10.277	BB	0.0836	64.21375	11.78767	6.1705
2	10.874	BB	0.0867	976.44653	176.06561	93.8295

Irradiation with $\lambda = 365$ nm for conversion from *trans*-isomer to *cis*-isomer.

Detection at 301 nm: t_R *cis*-isomer = 10.231 min (94%), t_R *trans*-isomer = 10.829 min (6%).



Signal 7: DAD1 G, Sig=301,4 Ref=off

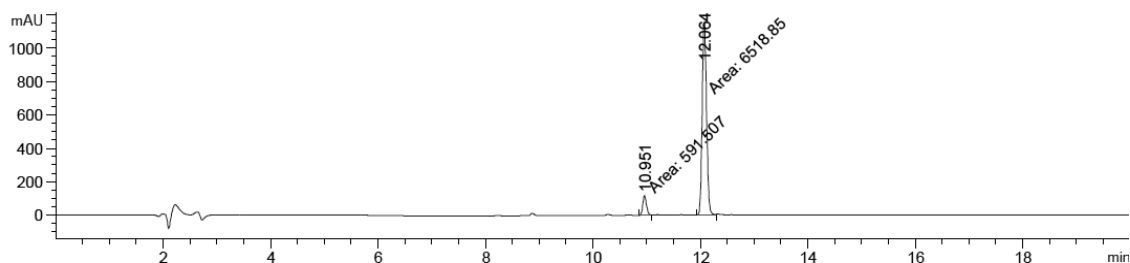
Peak #	RetTime [min]	Type	Width [min]	Area [mAU*s]	Height [mAU]	Area %
1	10.231	BB	0.0862	1130.77295	205.58601	94.0348
2	10.829	BB	0.0821	71.73136	13.47175	5.9652

Appendix

Compound **tFAPz 3** (50 μ M solution in TrisHCl Buffer + 0.5% DMSO, pH 7.5, injection volume 4 μ L):

Irradiation with $\lambda = 528$ nm for conversion from *cis*-isomer to *trans*-isomer.

Detection at 297 nm: t_R *cis*-isomer = 10.951 min (8%), t_R *trans*-isomer = 12.064 min (92%).

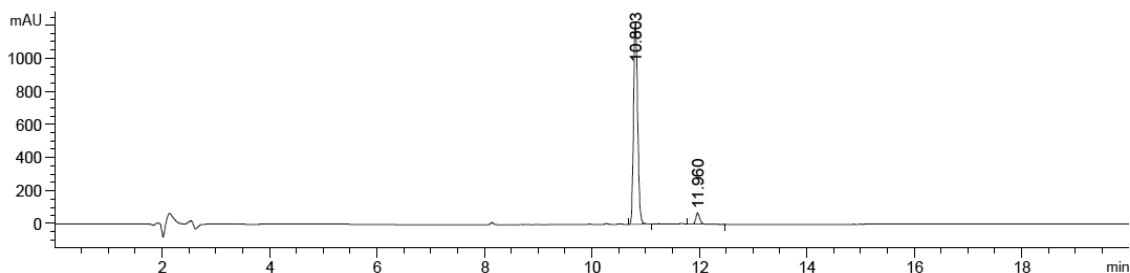


Signal 3: DAD1 C, Sig=297,4 Ref=off

Peak #	RetTime [min]	Type	Width [min]	Area [mAU*s]	Height [mAU]	Area %
1	10.951	MM	0.0830	591.50659	118.82800	8.3189
2	12.064	MM	0.0939	6518.85449	1156.71521	91.6811

Irradiation with $\lambda = 365$ nm for conversion from *trans*-isomer to *cis*-isomer.

Detection at 297 nm: t_R *cis*-isomer = 10.803 min (95%), t_R *trans*-isomer = 11.960 min (5%).



Signal 3: DAD1 C, Sig=297,4 Ref=off

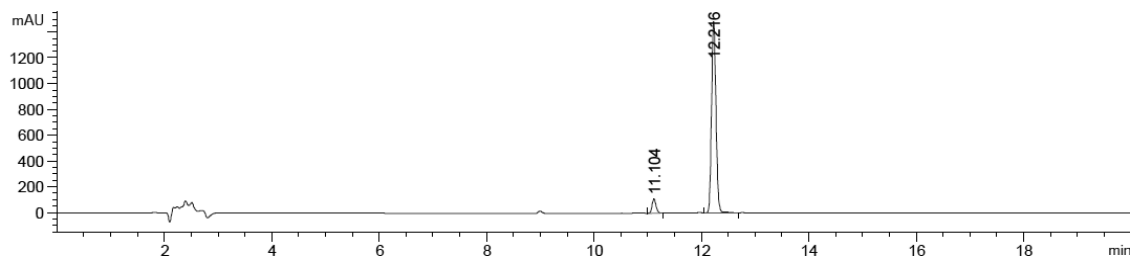
Peak #	RetTime [min]	Type	Width [min]	Area [mAU*s]	Height [mAU]	Area %
1	10.803	BB	0.0818	6491.63672	1225.00757	95.0036
2	11.960	VV R	0.0780	341.40857	66.34266	4.9964

Appendix

Compound **tFAPz 3** (50 μ M solution in DMSO, injection volume 4 μ L):

Irradiation with $\lambda = 528$ nm for conversion from *cis*-isomer to *trans*-isomer.

Detection at 300 nm: t_R *cis*-isomer = 11.104 min (6%), t_R *trans*-isomer = 12.216 min (94%).

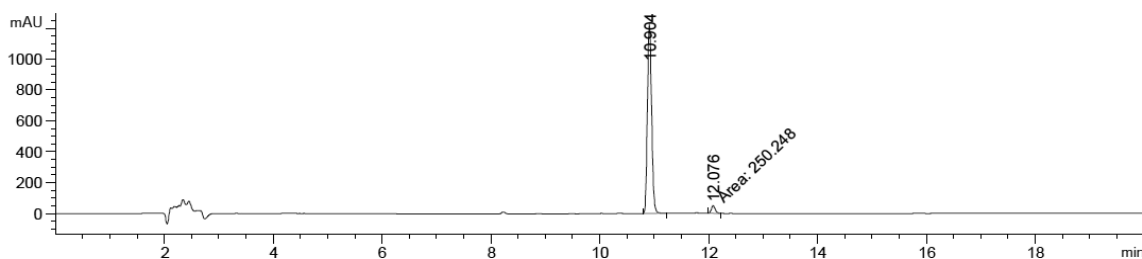


Signal 7: DAD1 G, Sig=300,4 Ref=off

Peak #	RetTime [min]	Type	Width [min]	Area [mAU*s]	Height [mAU]	Area %
1	11.104	BB	0.0784	559.88293	111.78555	6.1565
2	12.216	BV R	0.0906	8534.29688	1489.73401	93.8435

Irradiation with $\lambda = 365$ nm for conversion from *trans*-isomer to *cis*-isomer.

Detection at 300 nm: t_R *cis*-isomer = 10.904 min (96%), t_R *trans*-isomer = 12.076 min (4%).

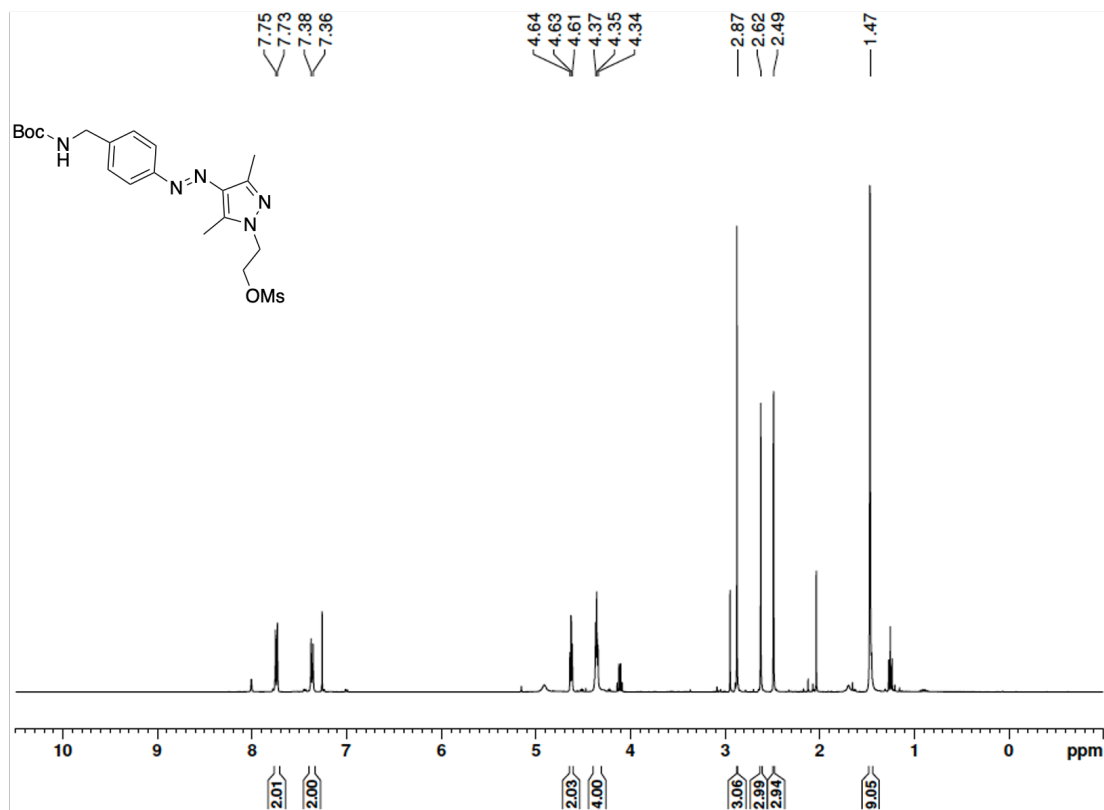


Signal 7: DAD1 G, Sig=300,4 Ref=off

Peak #	RetTime [min]	Type	Width [min]	Area [mAU*s]	Height [mAU]	Area %
1	10.904	BB	0.0847	6622.77881	1232.27710	96.3590
2	12.076	MM	0.0856	250.24759	48.73035	3.6410

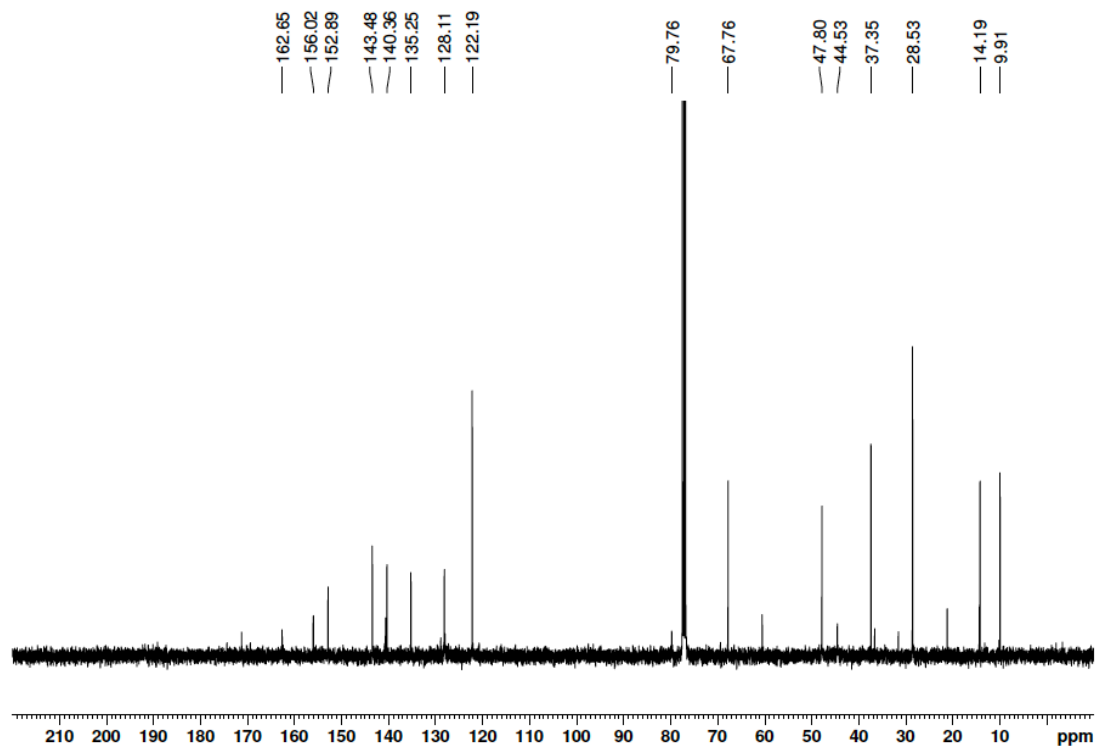
7.3.3 NMR Spectra

^1H spectrum of **5** (400 MHz, CDCl_3):



*Contains ethyl acetate. Yield was obtained after further drying.

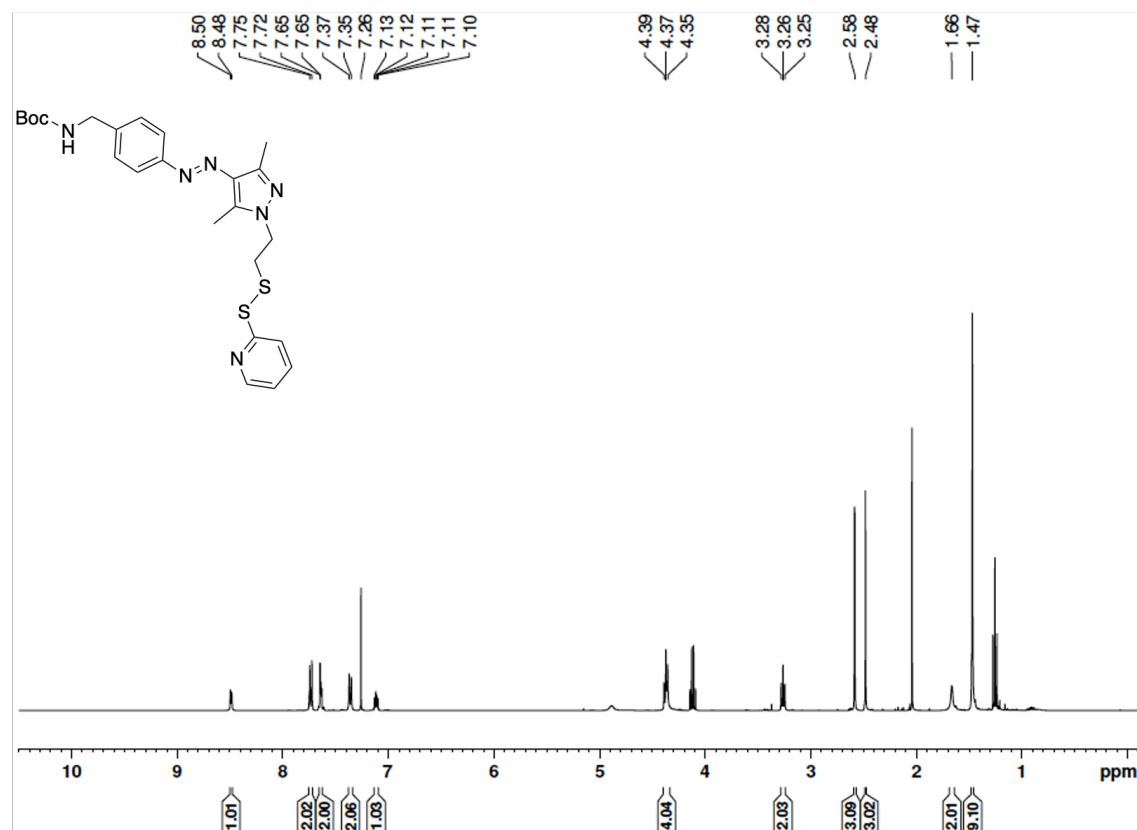
^{13}C spectrum of **5** (101 MHz, CDCl_3):



*Contains ethyl acetate. Yield was obtained after further drying.

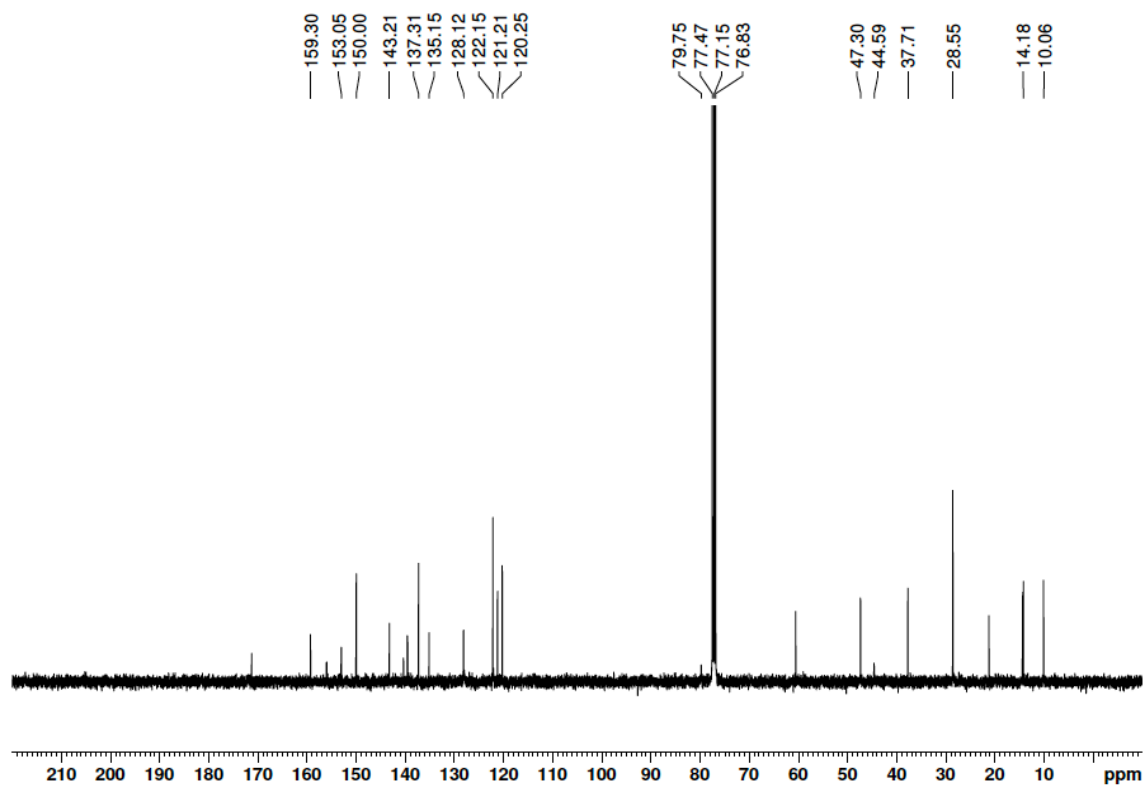
Appendix

^1H spectrum of **6** (400 MHz, CDCl_3):



*Contains ethyl acetate. Yield was obtained after further drying.

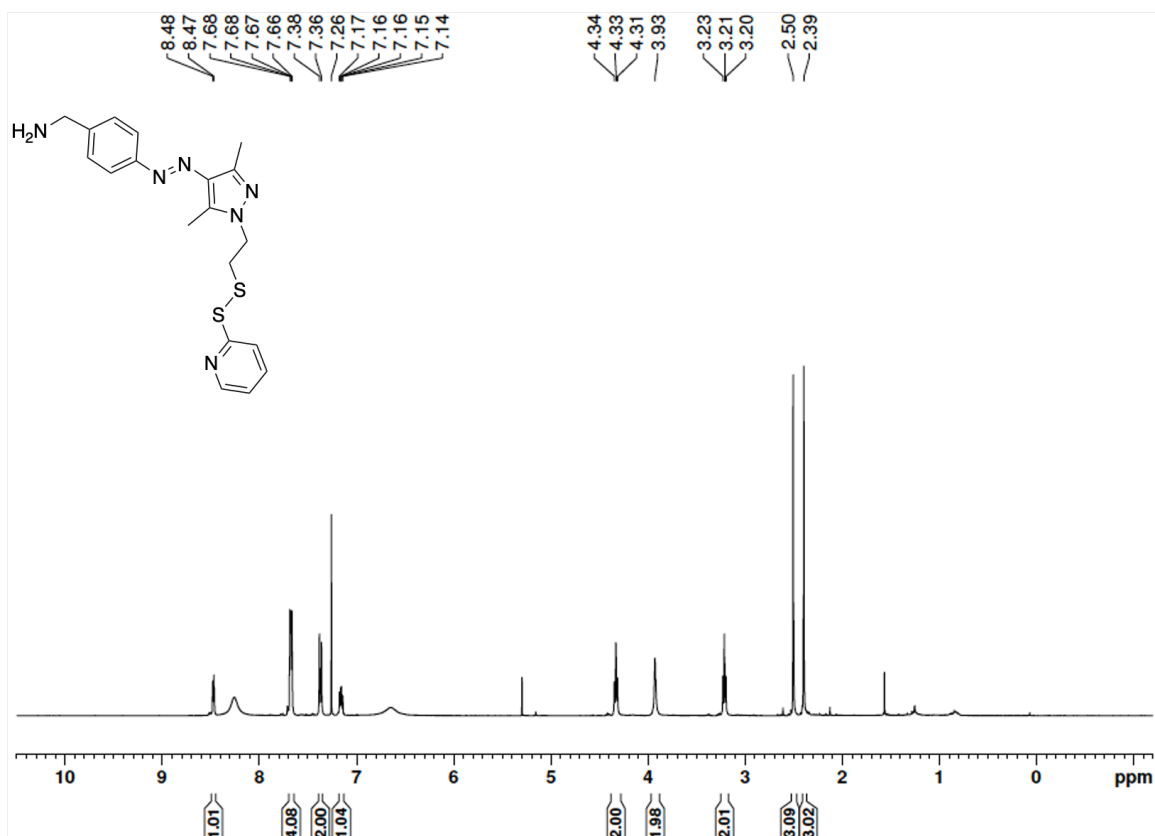
^{13}C spectrum of **6** (101 MHz, CDCl_3):



*Contains ethyl acetate. Yield was obtained after further drying.

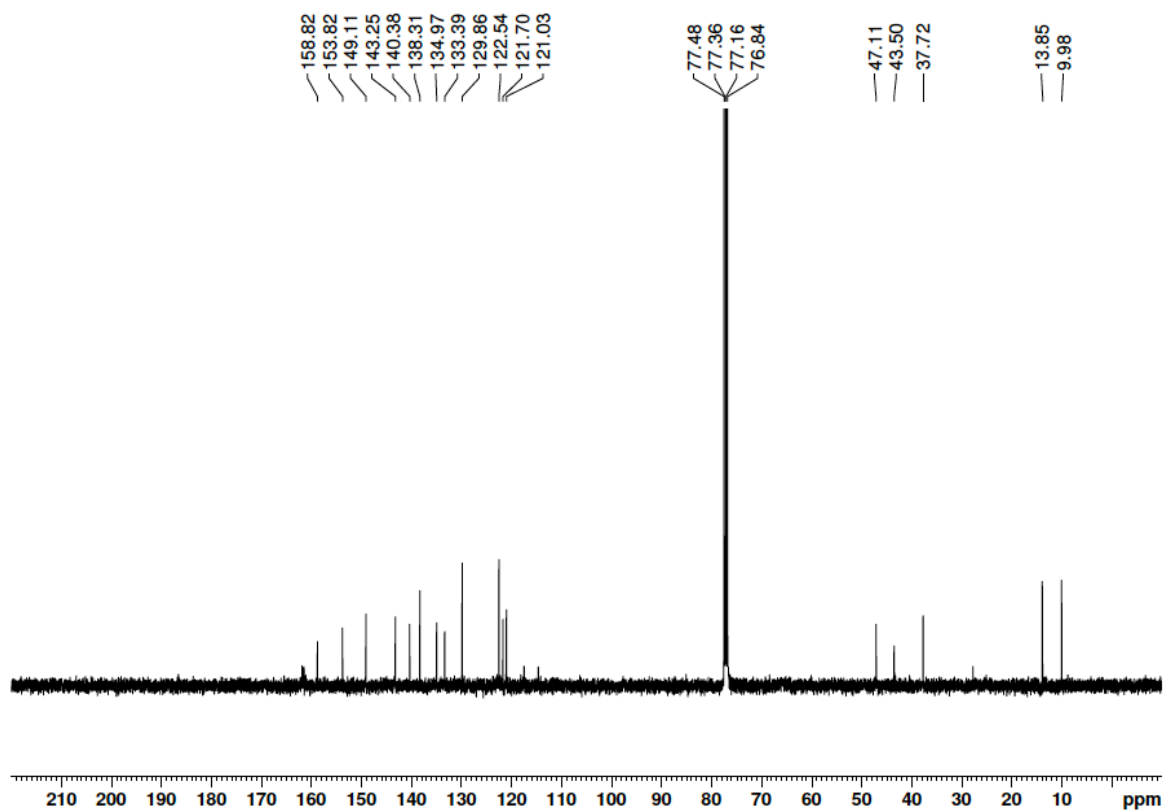
Appendix

^1H spectrum of **7** (400 MHz, CDCl_3):



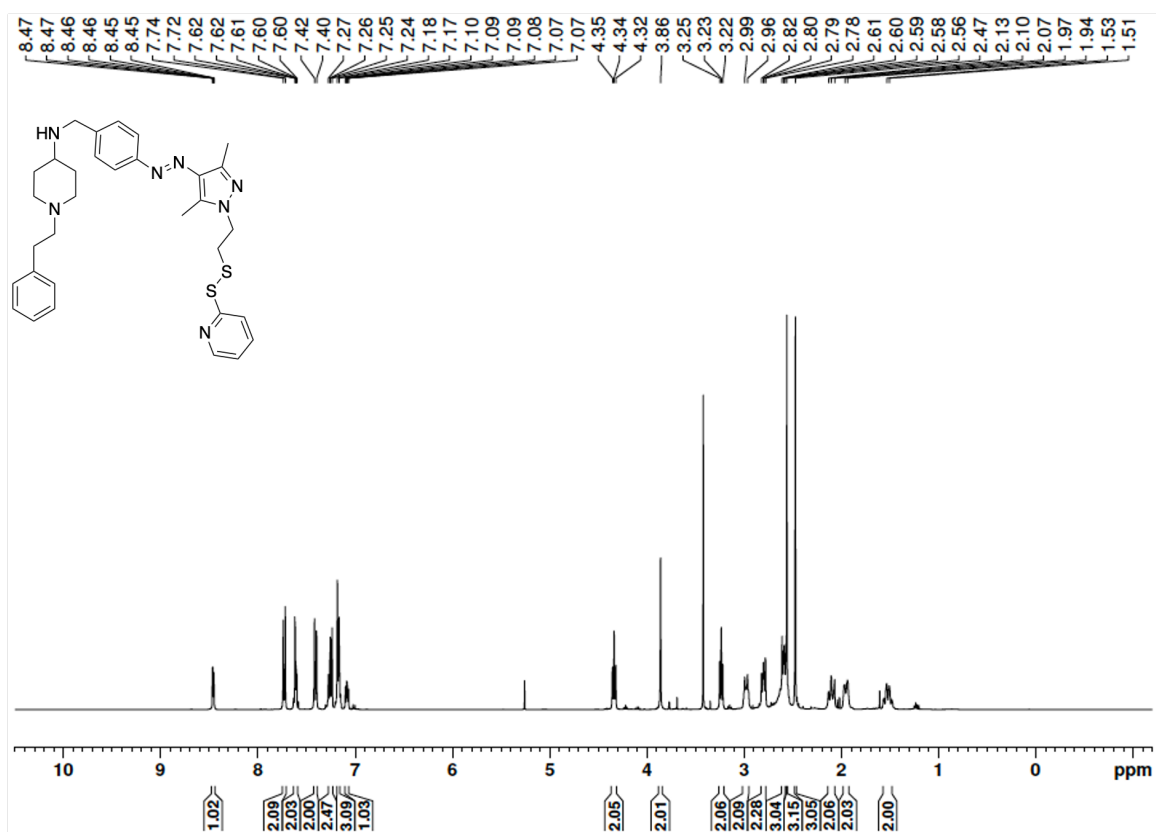
*Contains trace amounts of DCM. Yield was obtained after further drying.

^{13}C spectrum of **7** (101 MHz, CDCl_3):

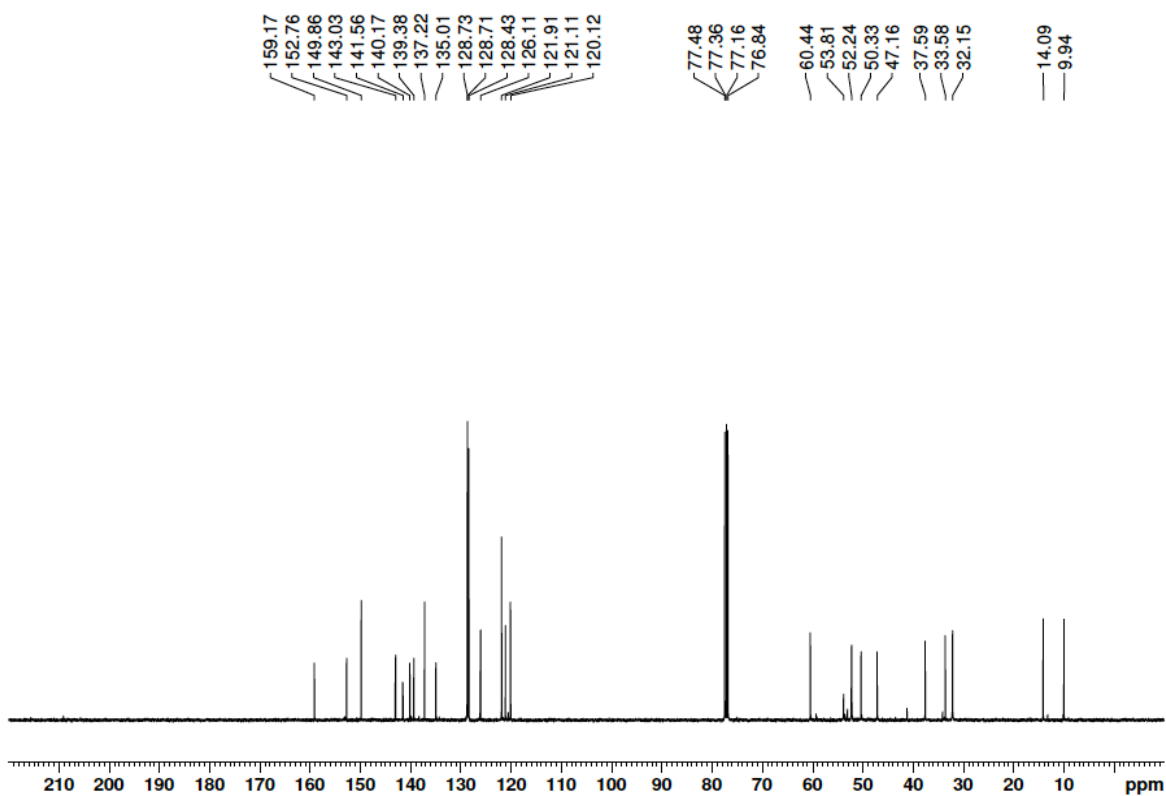


Appendix

^1H spectrum of **8** (400 MHz, CDCl_3):

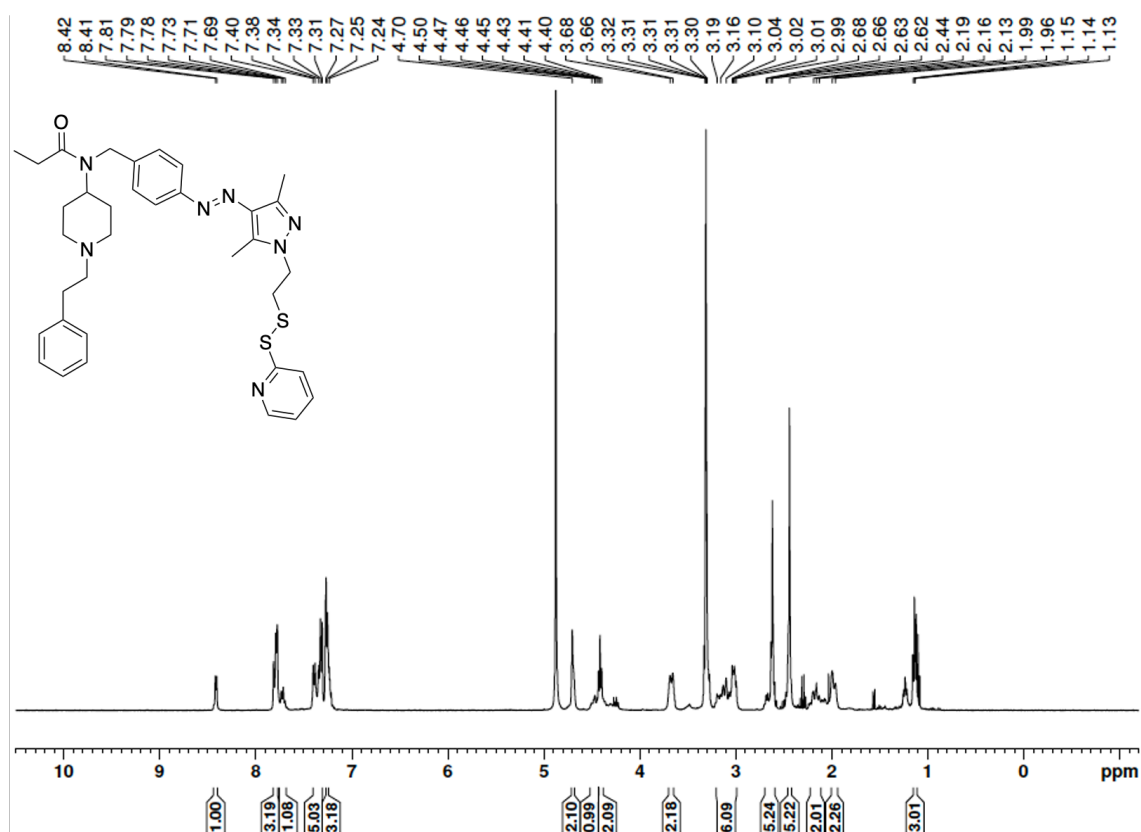


^{13}C spectrum of **8** (101 MHz, CDCl_3):



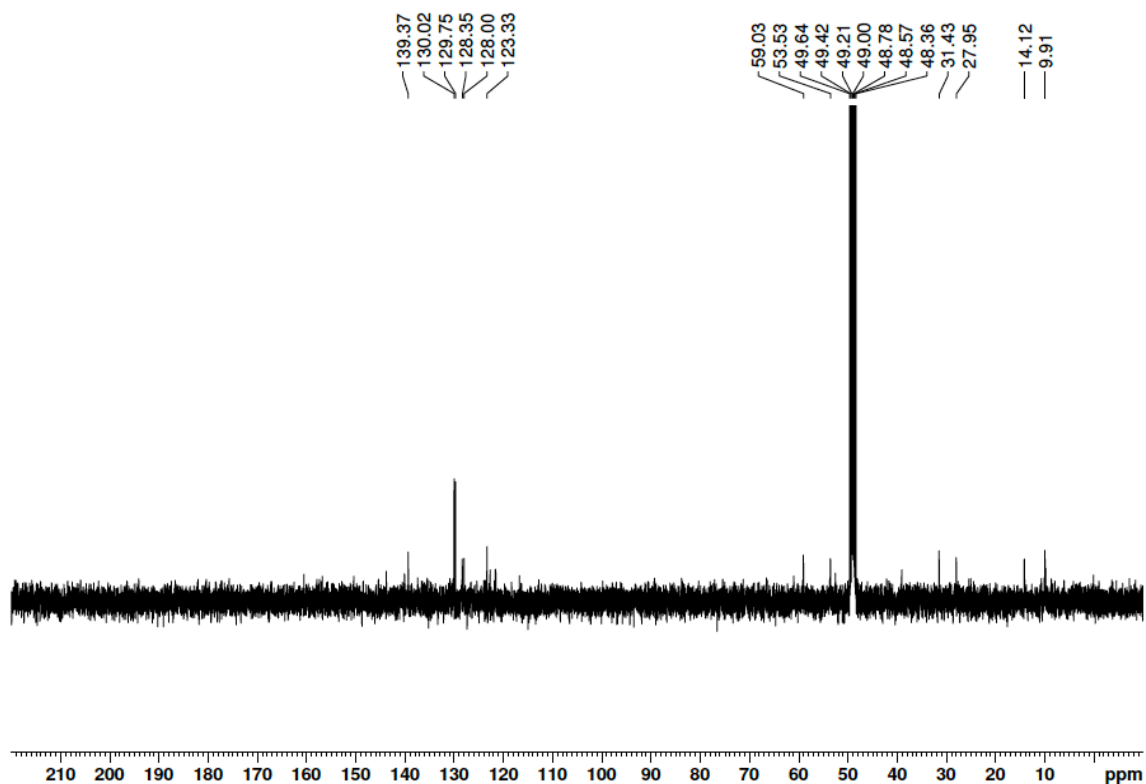
Appendix

^1H spectrum of **9** (400 MHz, MeOD):



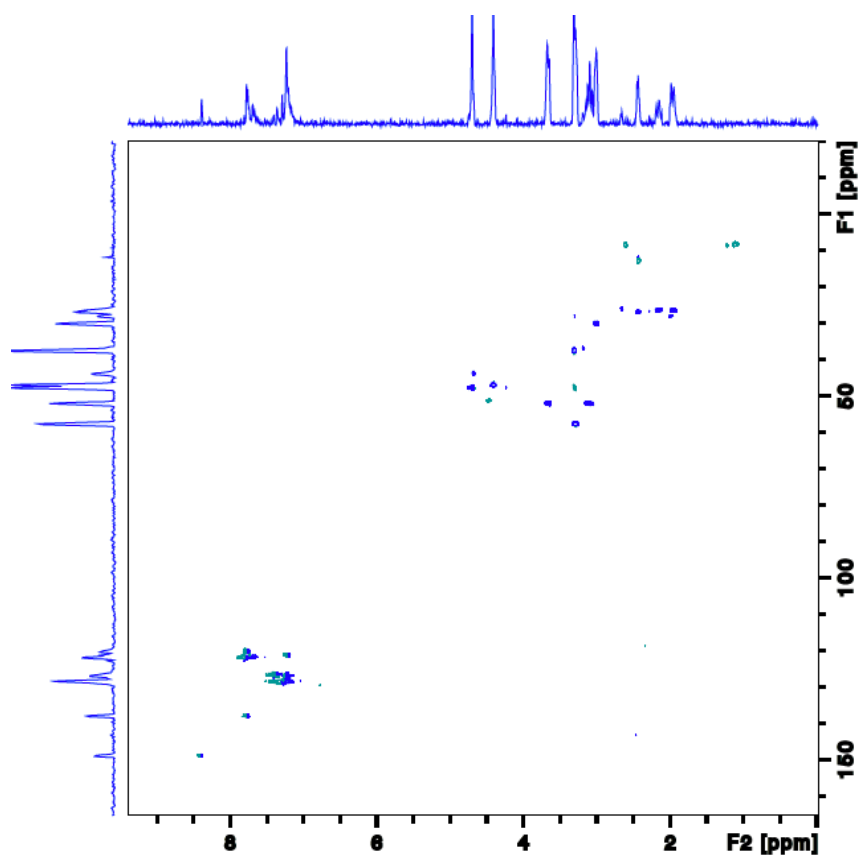
*Contains water that was present in MeOD, as well as traces of acetonitrile.

^{13}C spectrum of **9** (101 MHz, MeOD):



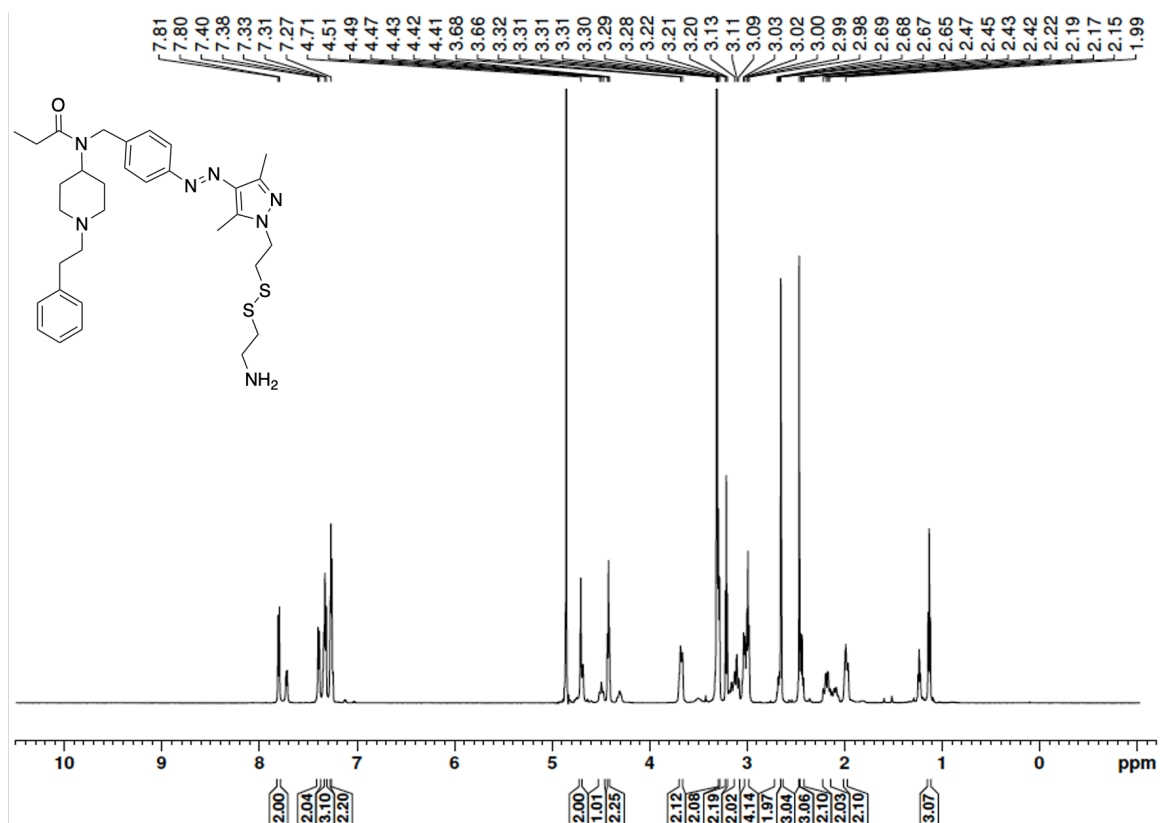
Appendix

HSQC(DET) spectrum of **9** (F1:101 MHz; F2: 400 MHz, MeOD):



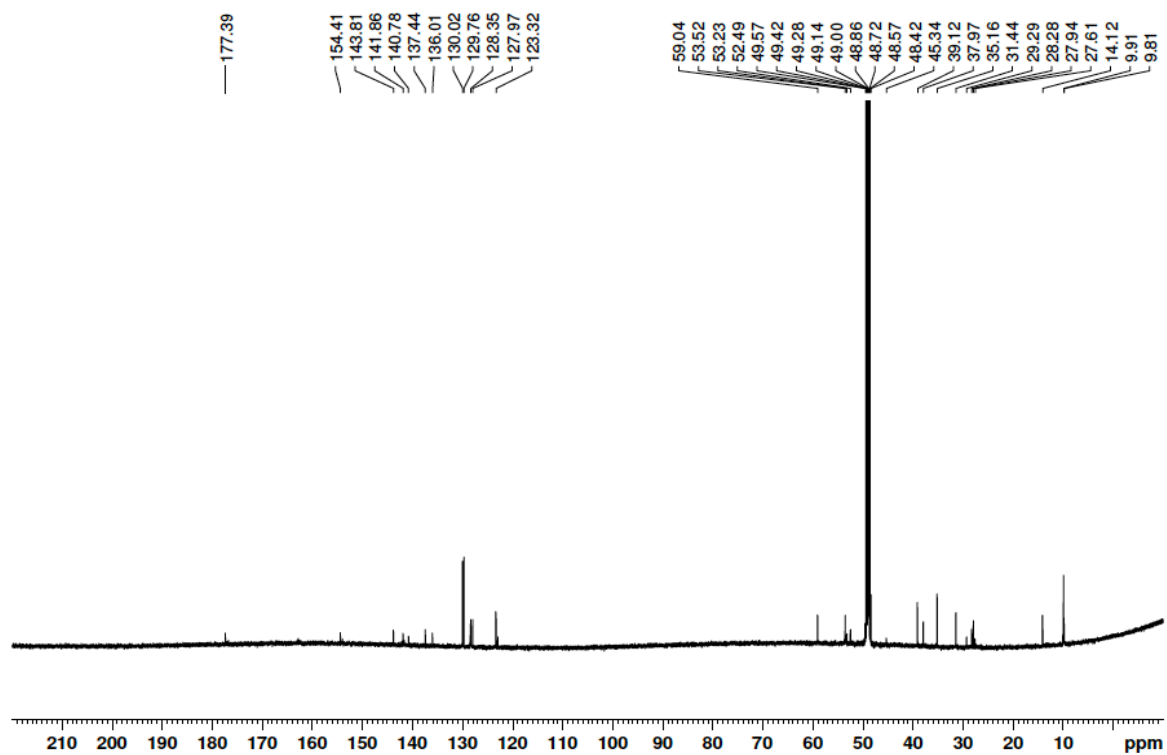
Appendix

^1H spectrum of **tFAPz 1** (400 MHz, MeOD):



*Contains water that was present in MeOD. Contains traces of *cis*-isomer.

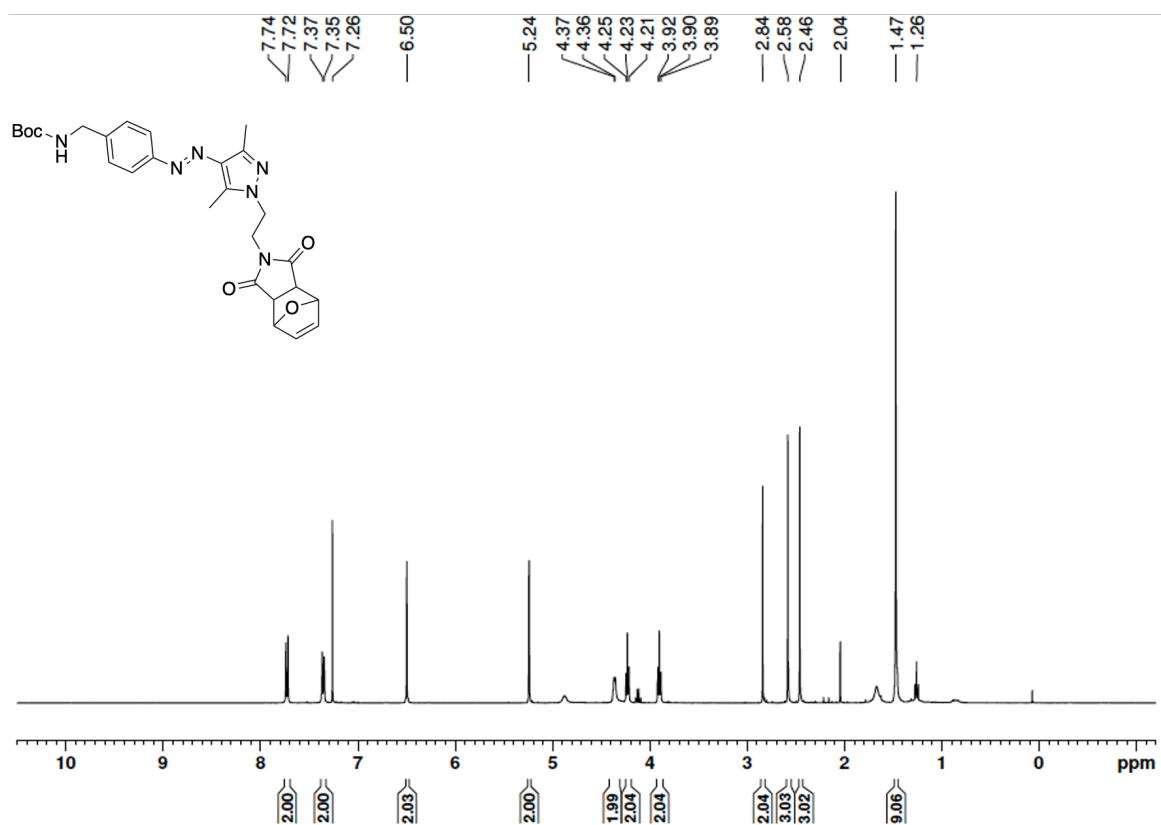
^{13}C spectrum of **tFAPz 1** (101 MHz, MeOD):



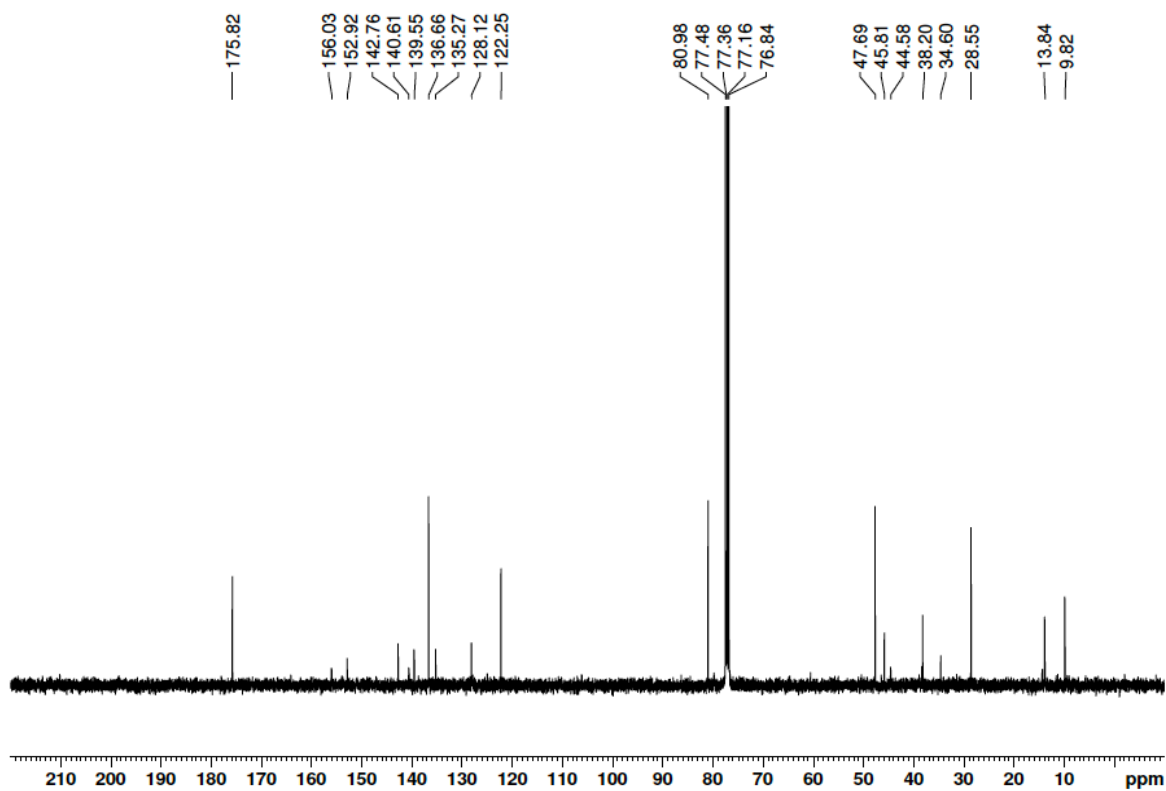
*Contains water that was present in MeOD. Contains traces of *cis*-isomer.

Appendix

^1H spectrum of **12** (400 MHz, CDCl_3):

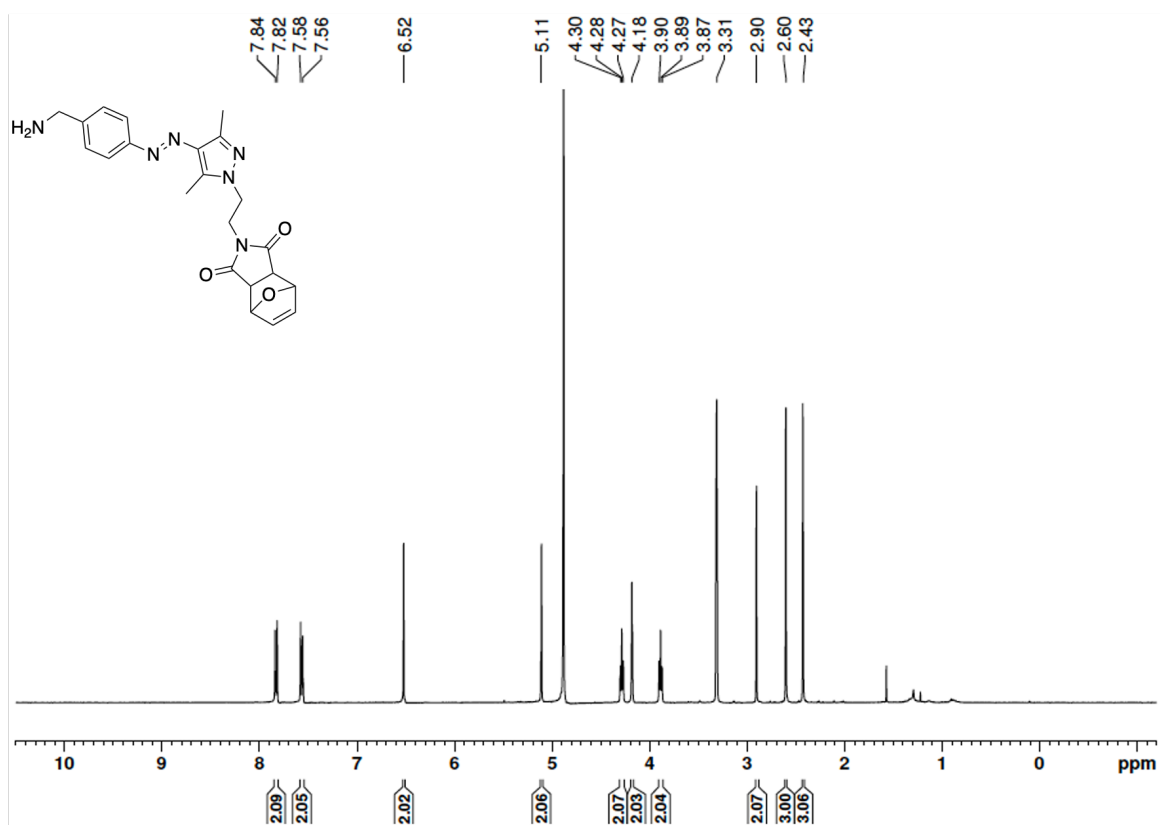


^{13}C spectrum of **12** (101 MHz, CDCl_3):



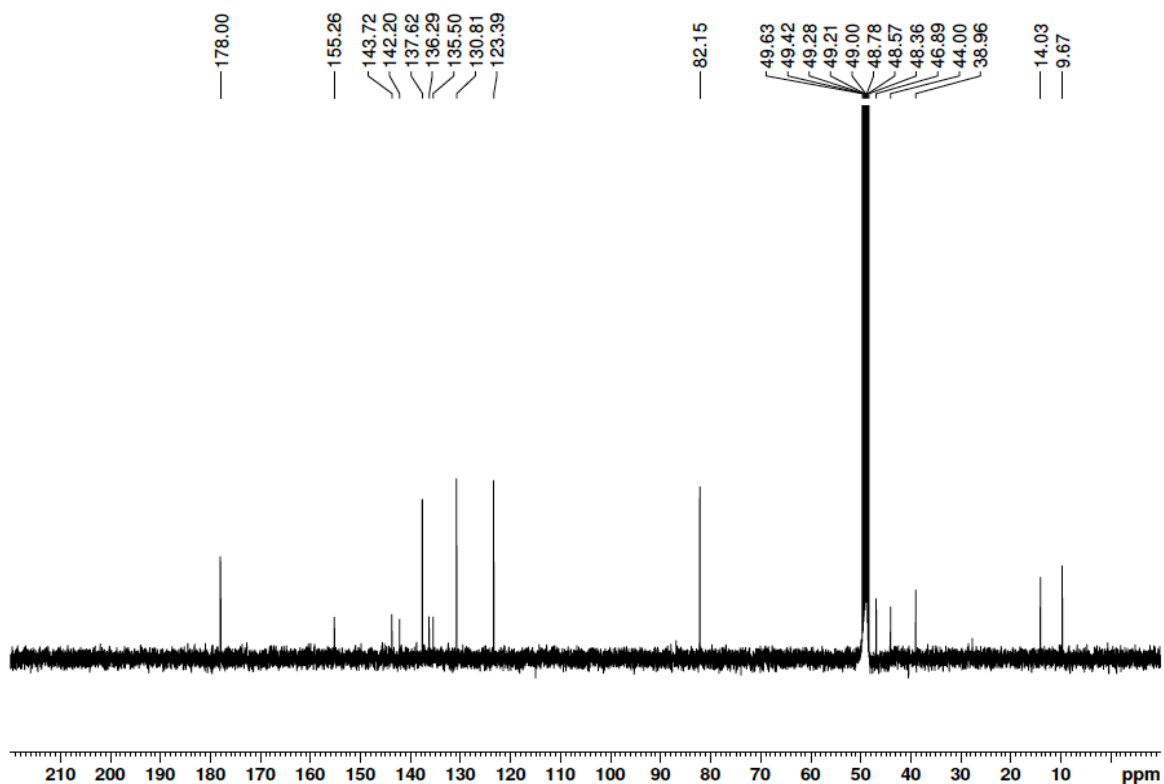
Appendix

^1H spectrum of **13** (400 MHz, MeOD):



*Contains water that was present in MeOD.

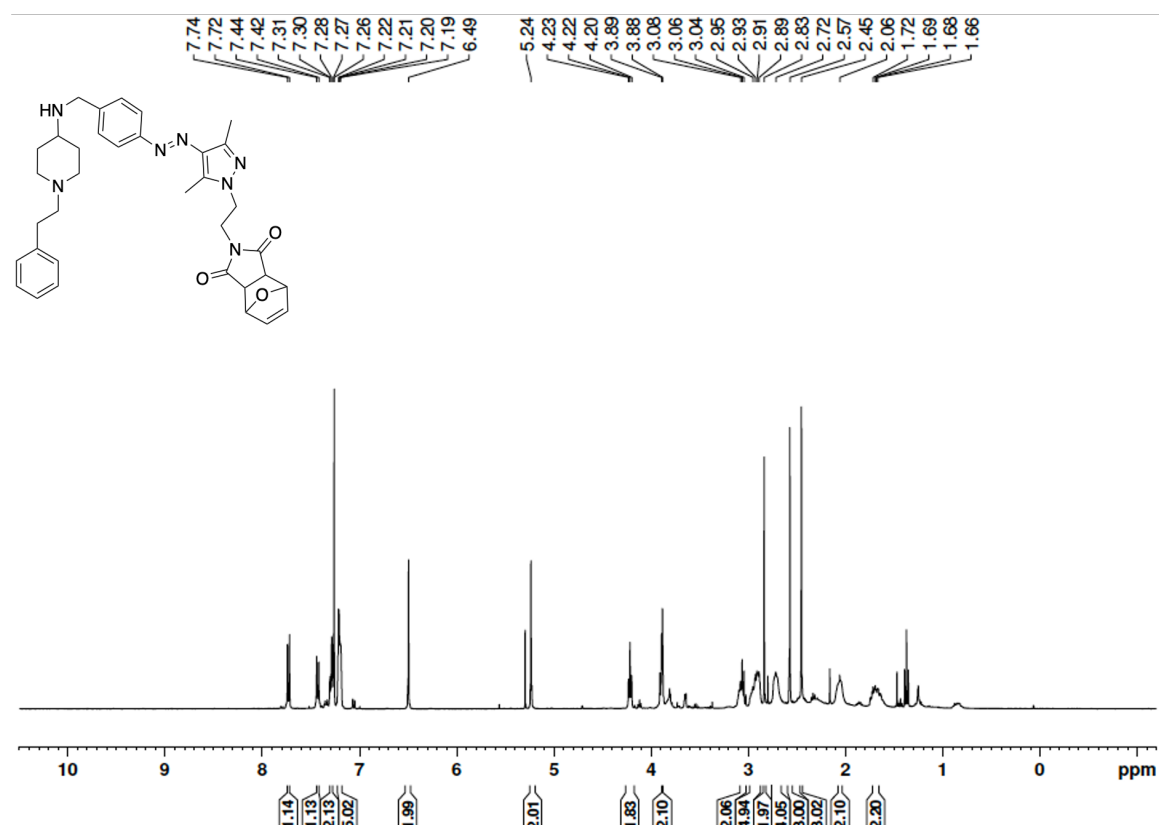
^{13}C spectrum of **13** (101 MHz, MeOD):



*Contains water that was present in MeOD.

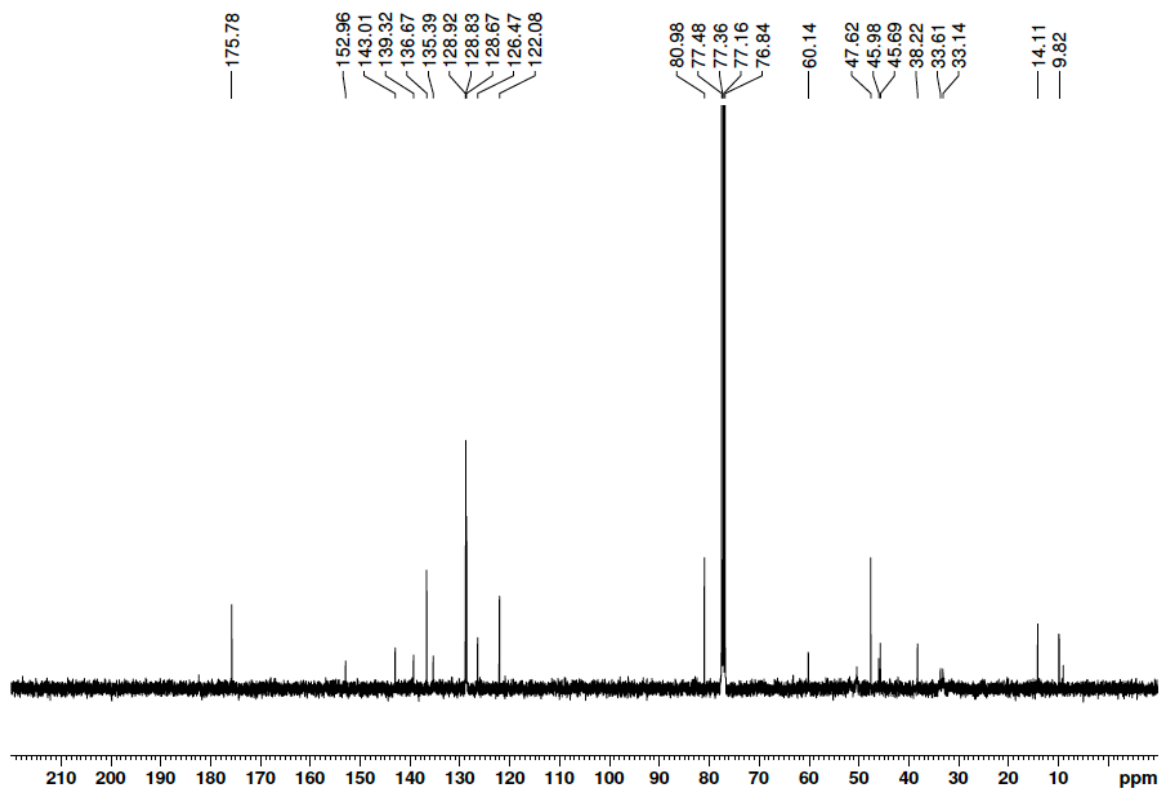
Appendix

^1H spectrum of **14** (400 MHz, CDCl_3):



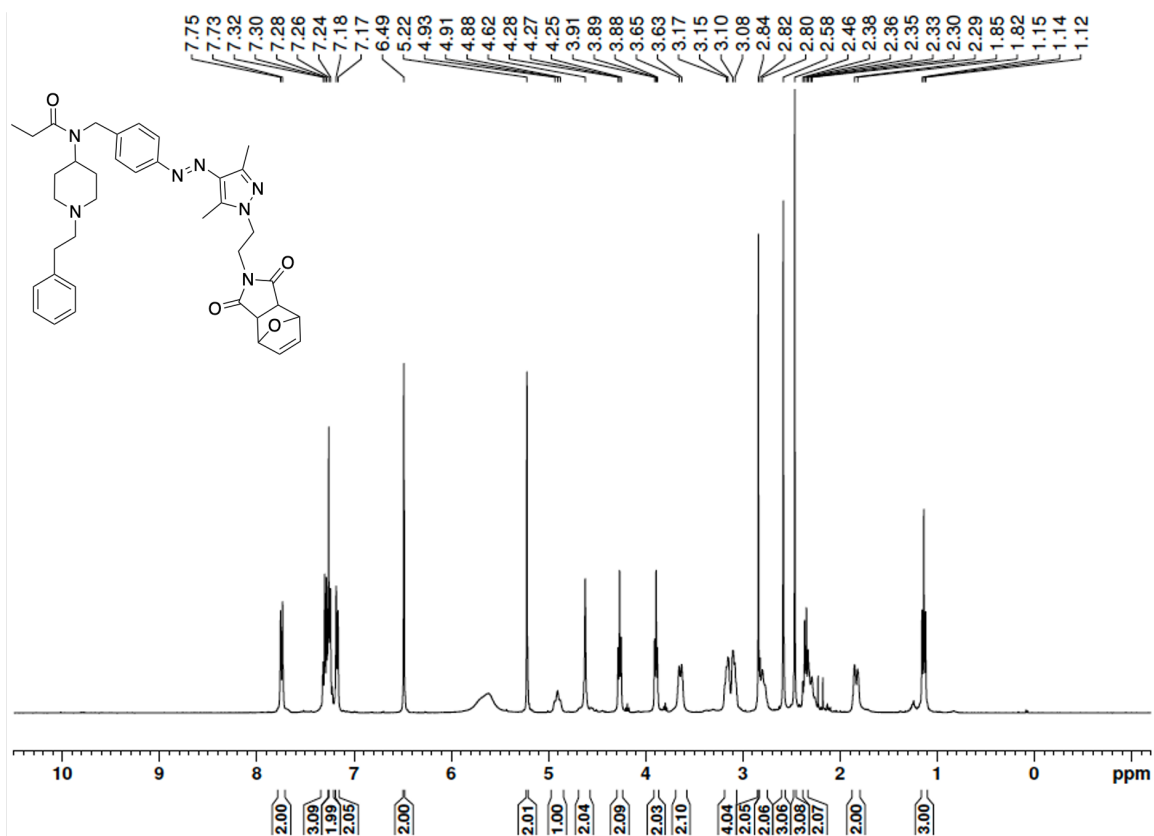
*Contains ethyl acetate and DCM. Yield was obtained after further drying.

^{13}C spectrum of **14** (101 MHz, CDCl_3):

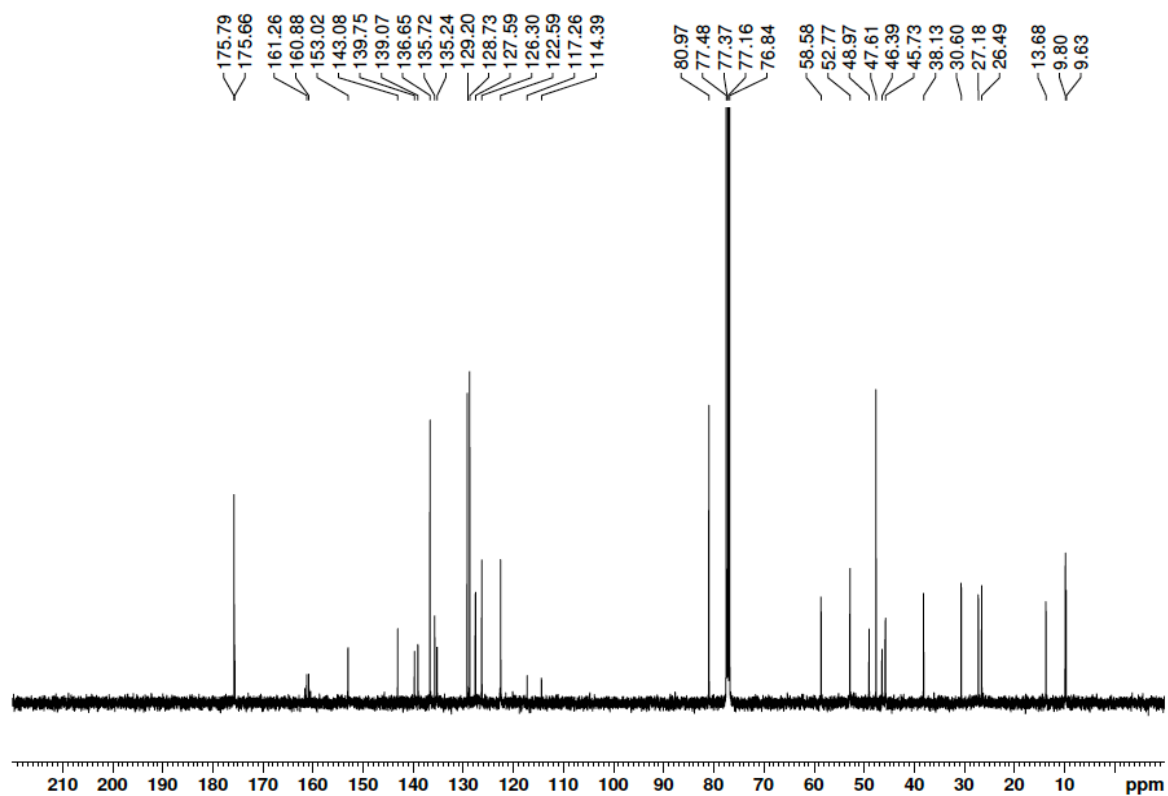


Appendix

^1H spectrum of **15** (400 MHz, CDCl_3):

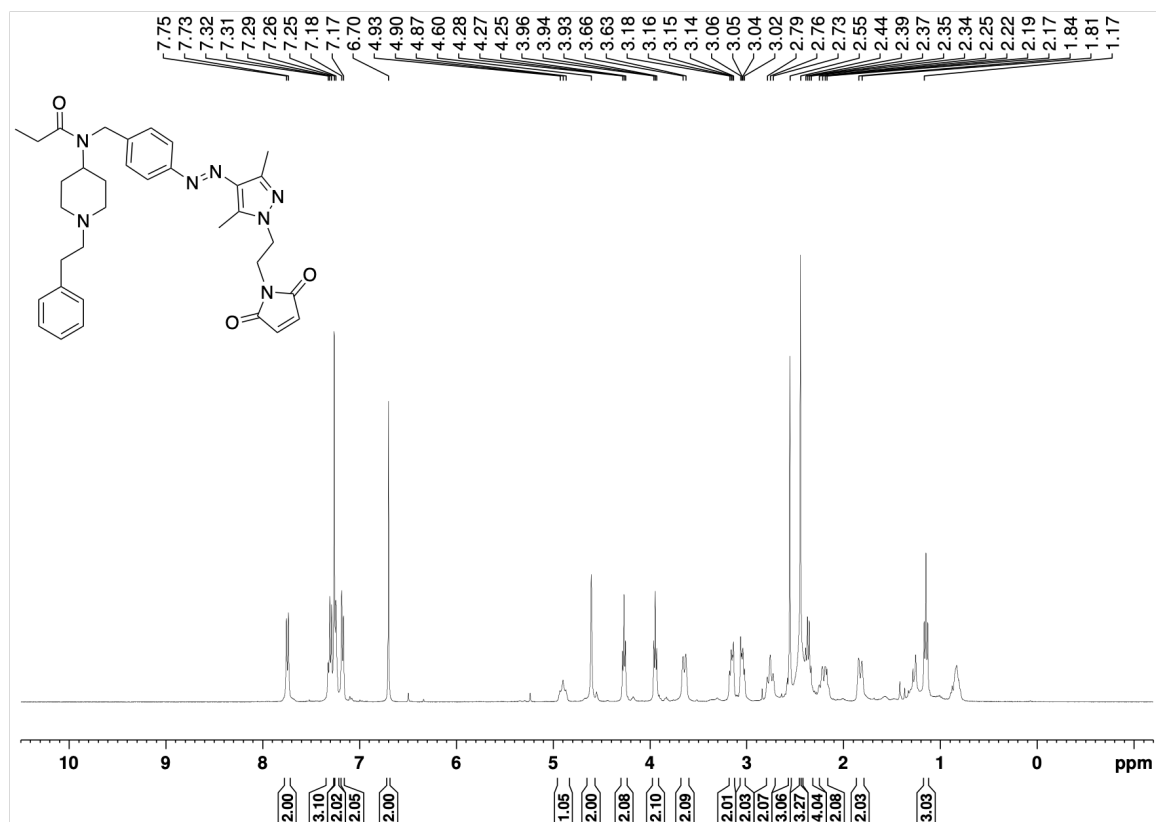


^{13}C spectrum of **15** (101 MHz, CDCl_3):



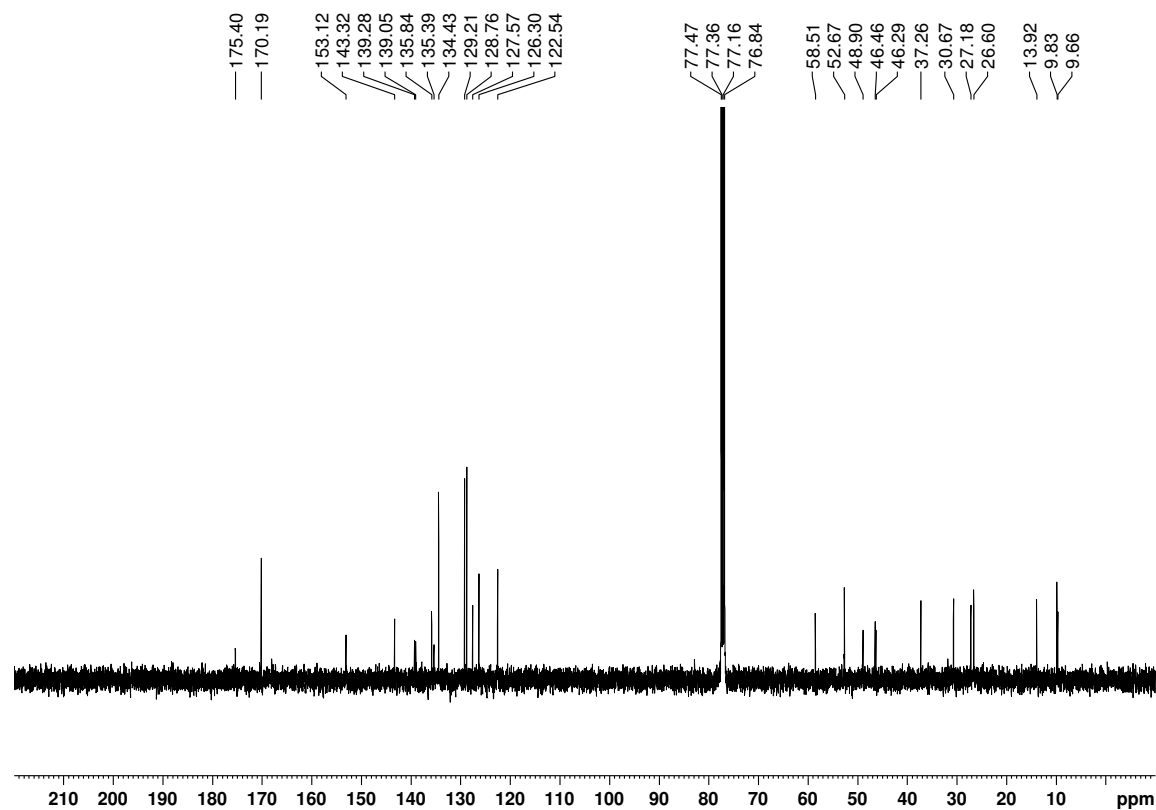
Appendix

^1H spectrum of **tFAPz 2a** (400 MHz, CDCl_3):



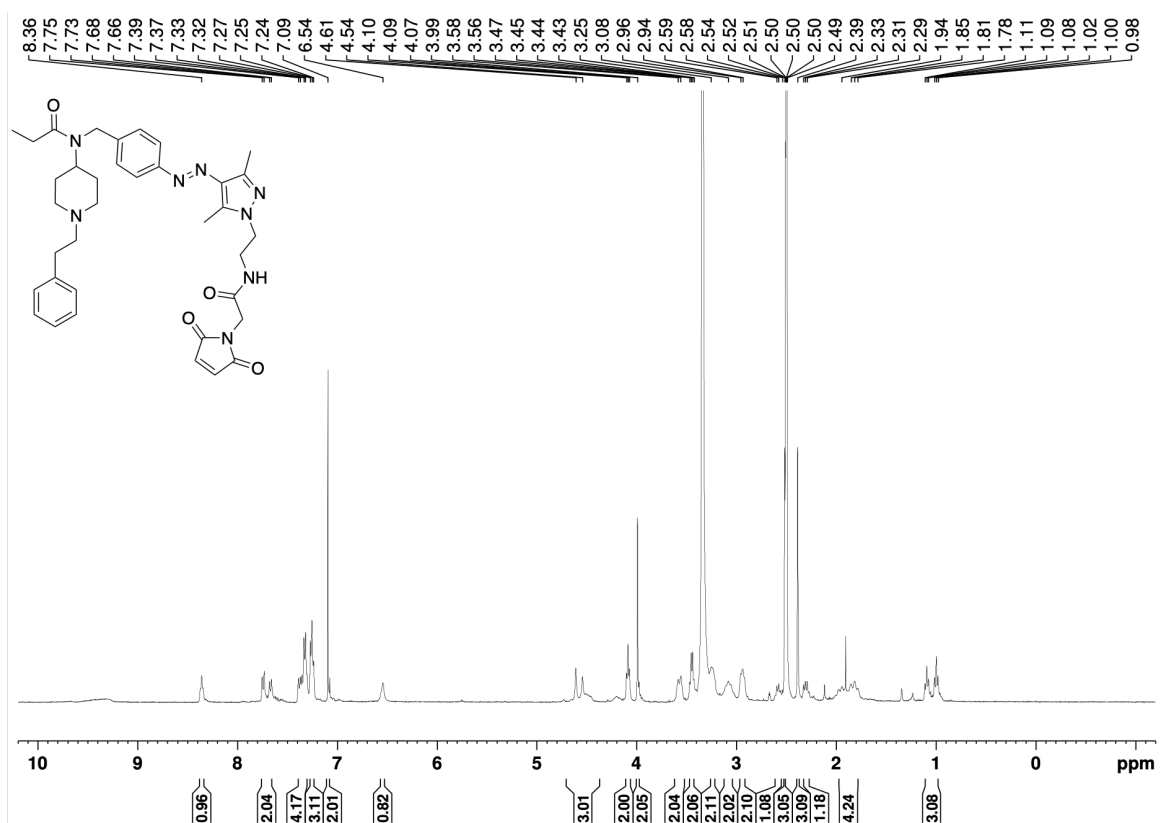
*Contains traces of grease.

^{13}C spectrum of **tFAPz 2a** (101 MHz, CDCl_3):



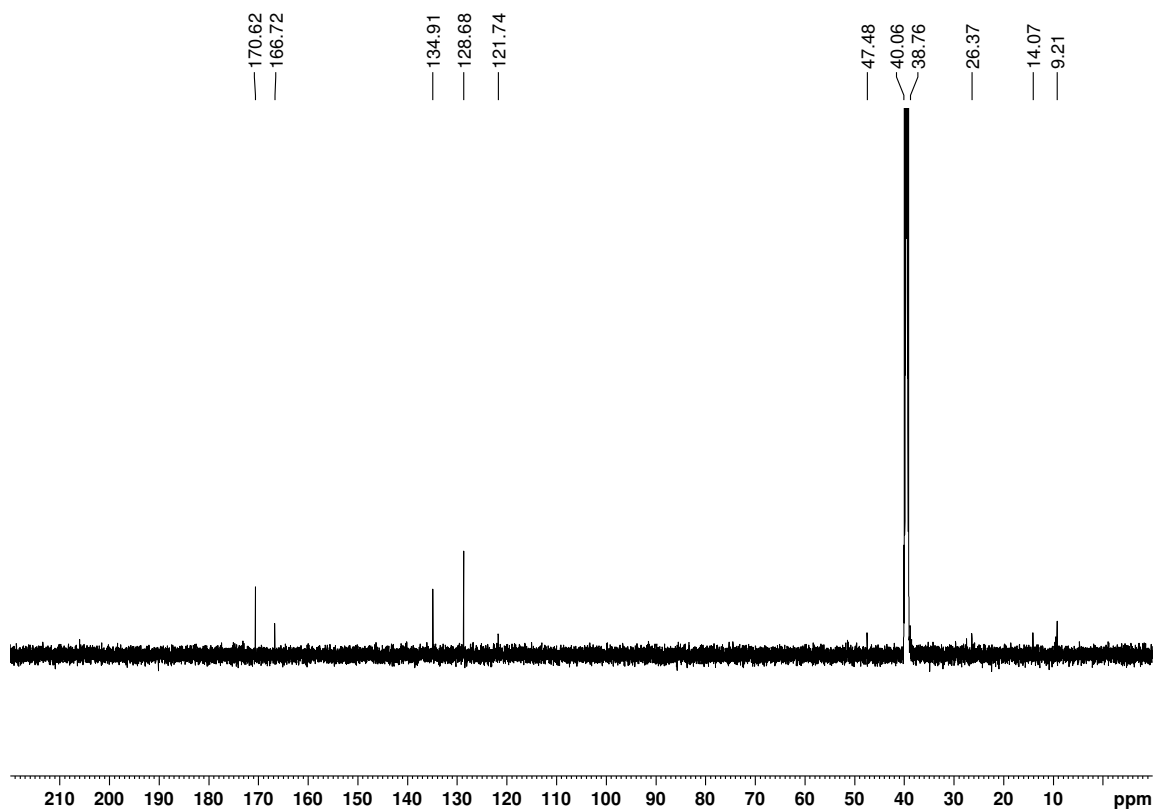
Appendix

¹H spectrum of **tFAPz 2b** (400 MHz, DMSO-D₆):



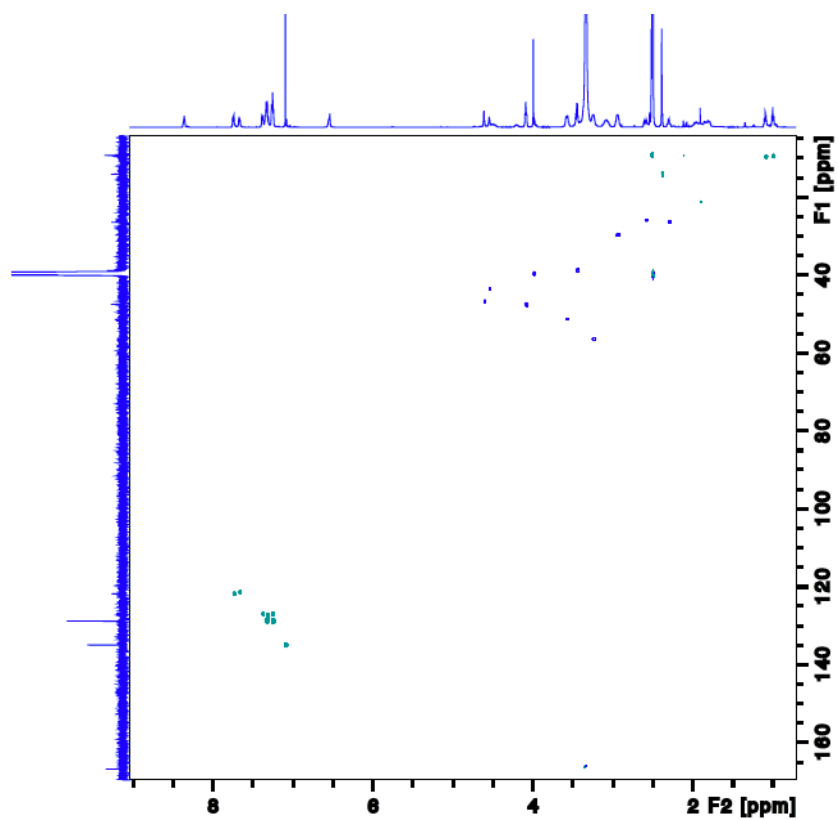
*Contains water that was present in DMSO-D₆.

¹³C spectrum of **tFAPz 2b** (151 MHz, DMSO-D₆):



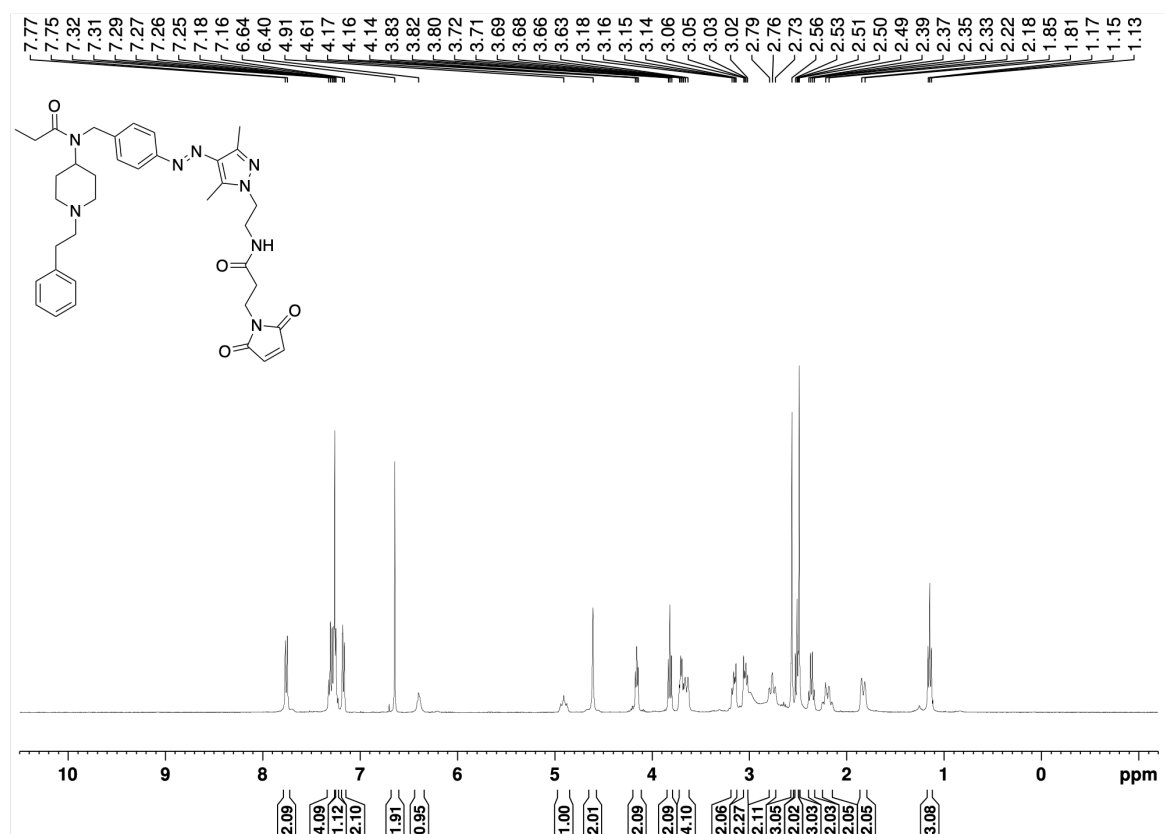
Appendix

HSQC(DET) spectrum of **tFAPz 2b** (F1:151 MHz; F2: 600 MHz, DMSO-D₆):

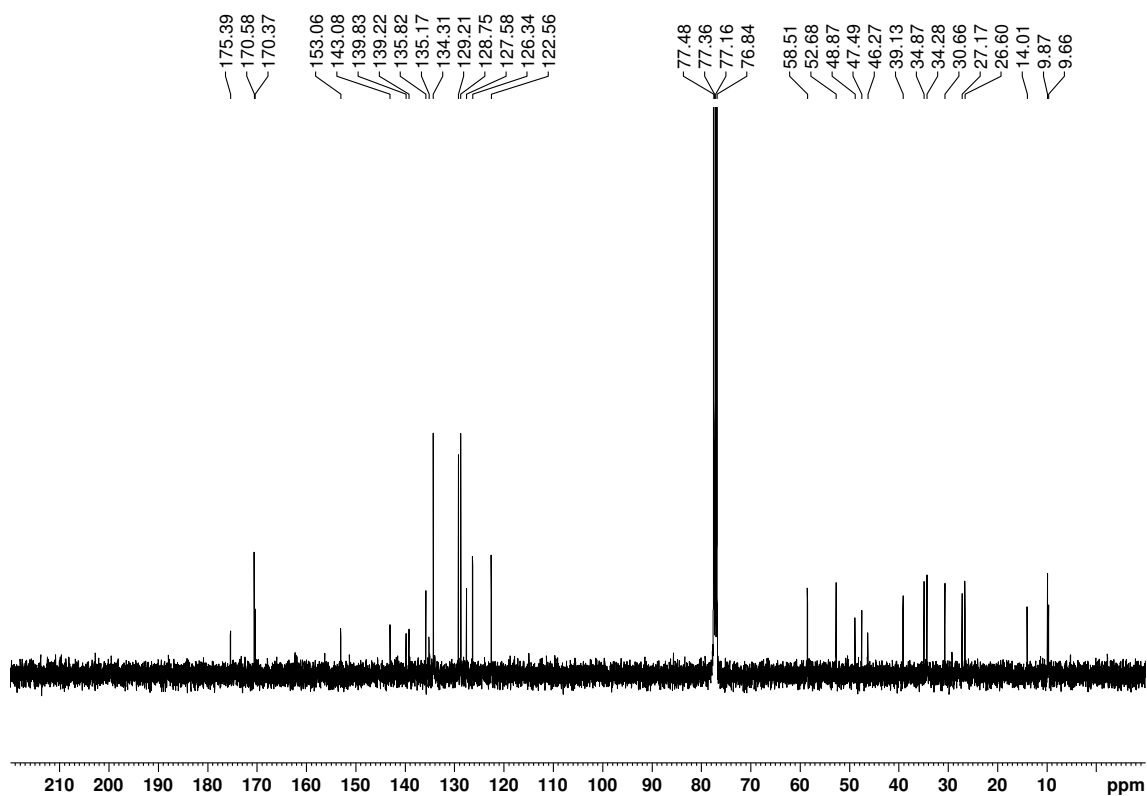


Appendix

^1H spectrum of **tFAPz 2c** (400 MHz, CDCl_3):

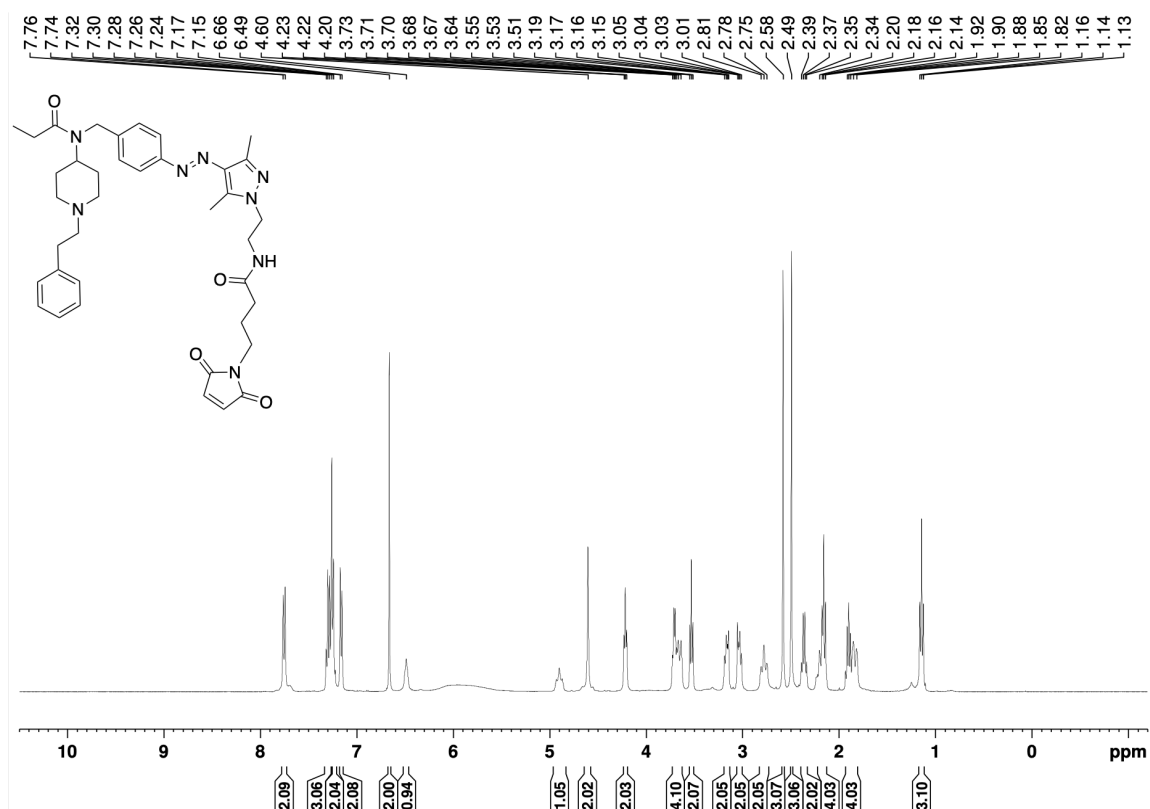


^{13}C spectrum of **2c** (101 MHz, CDCl_3):

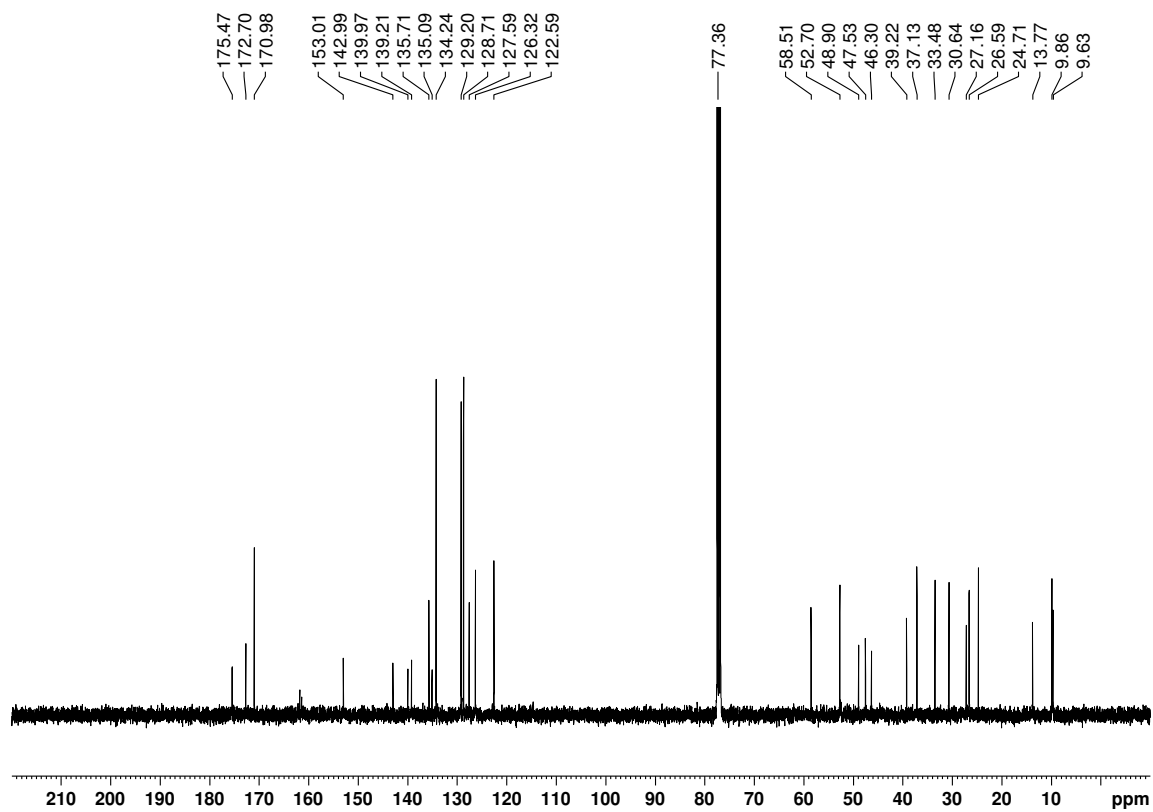


Appendix

^1H spectrum of **tFAPz 2d** (400 MHz, CDCl_3):

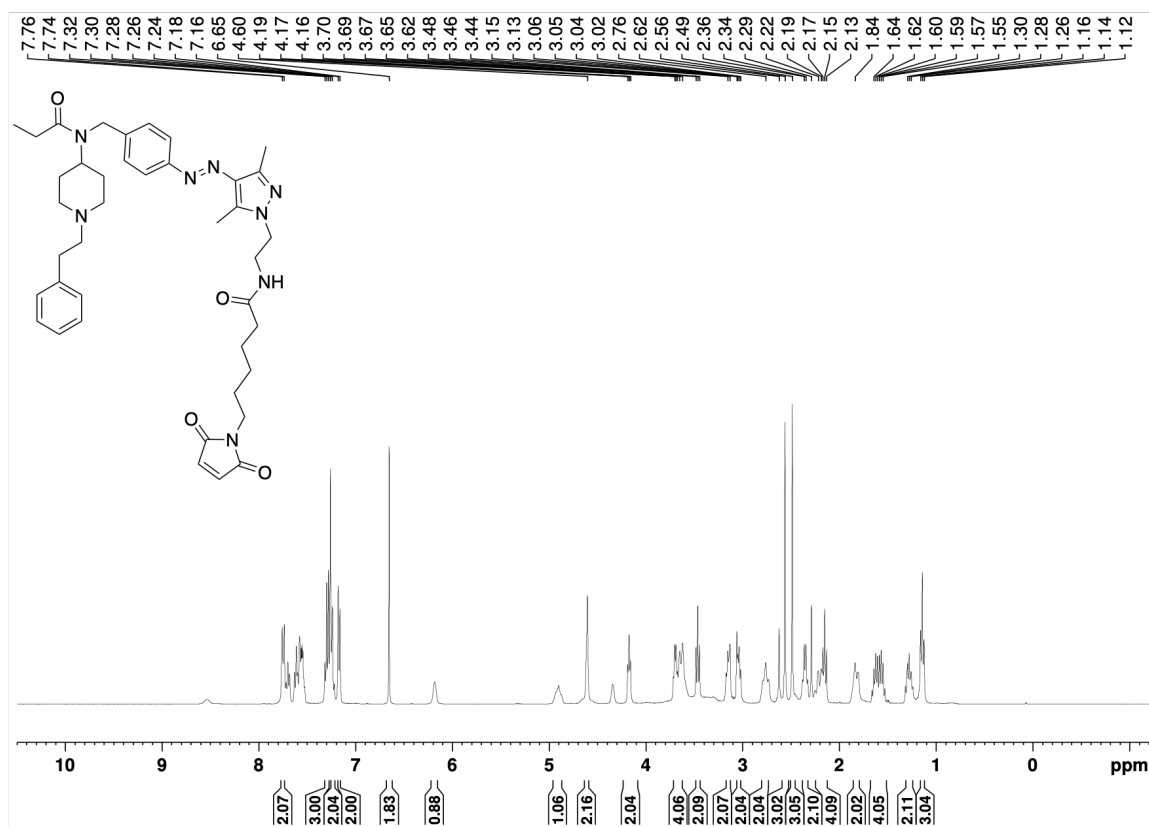


^{13}C spectrum of **tFAPz 2d** (101 MHz, CDCl_3):



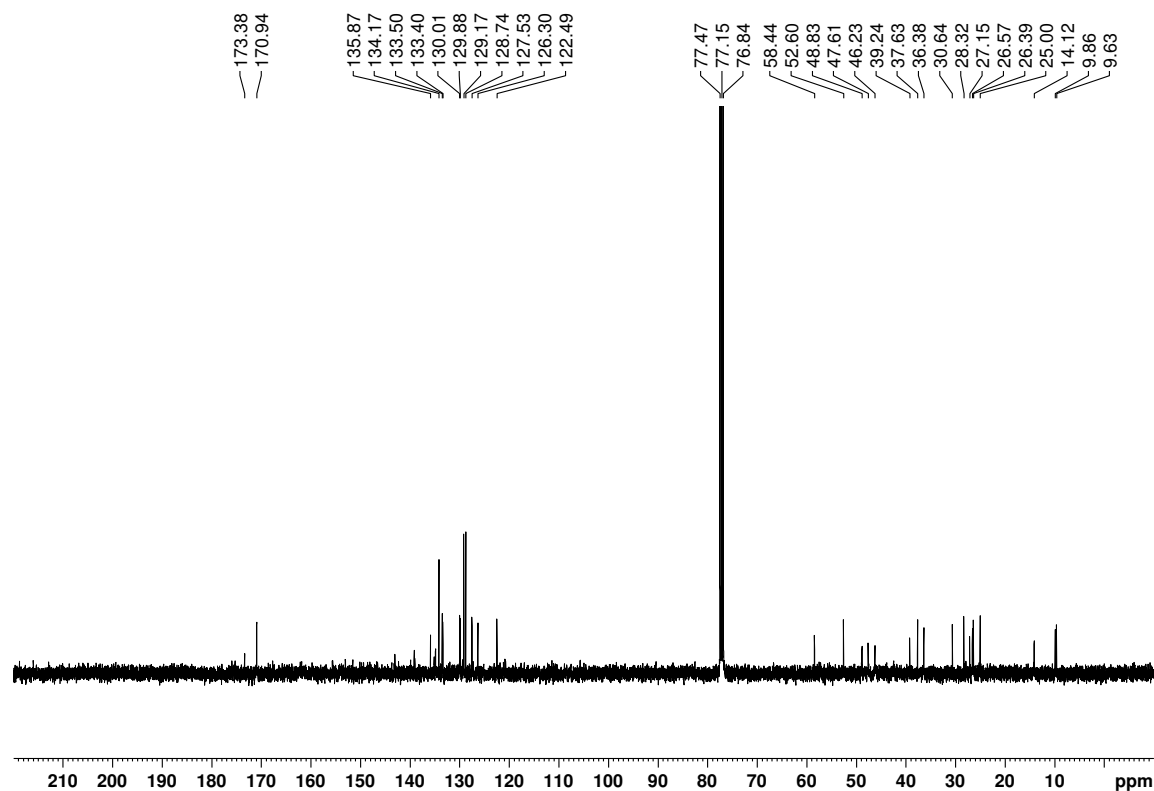
Appendix

^1H spectrum of **tFAPz 2e** (400 MHz, CDCl_3):



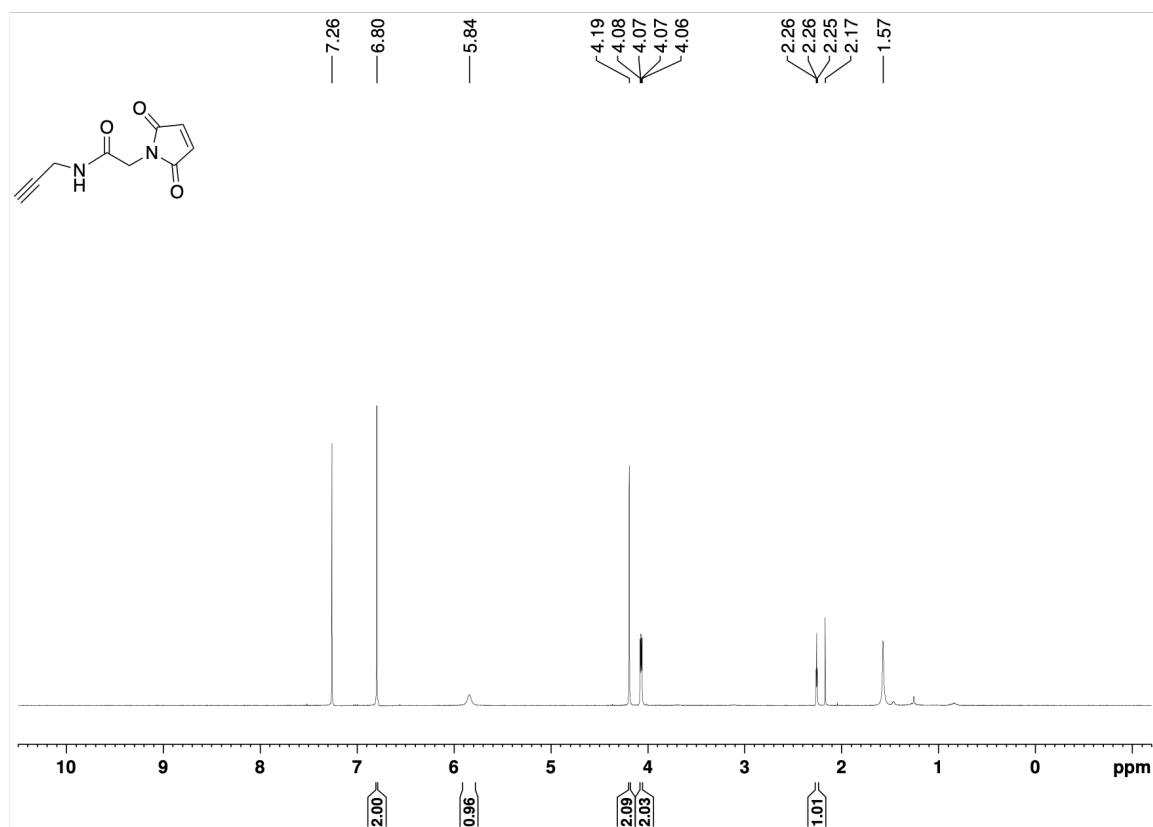
*Contains pyridine. Yield was obtained after further drying.

^{13}C spectrum of **tFAPz 2e** (101 MHz, CDCl_3):



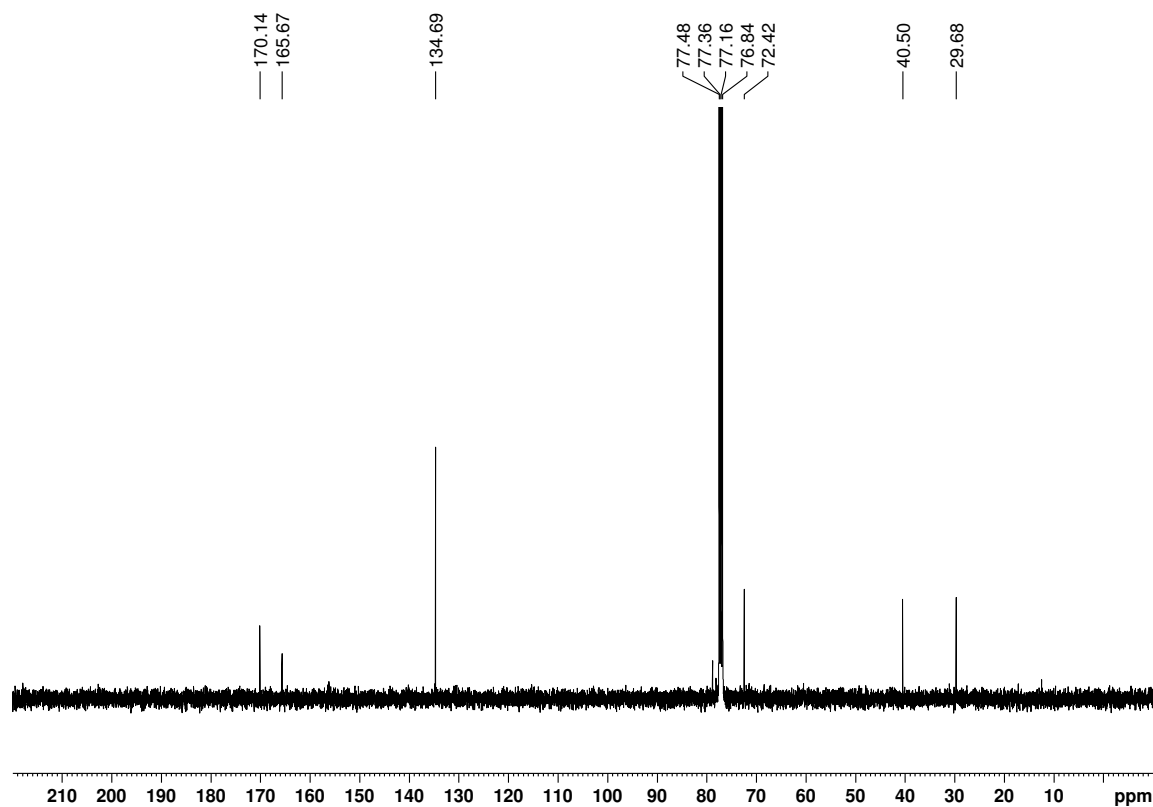
Appendix

^1H spectrum of **16** (400 MHz, CDCl_3):



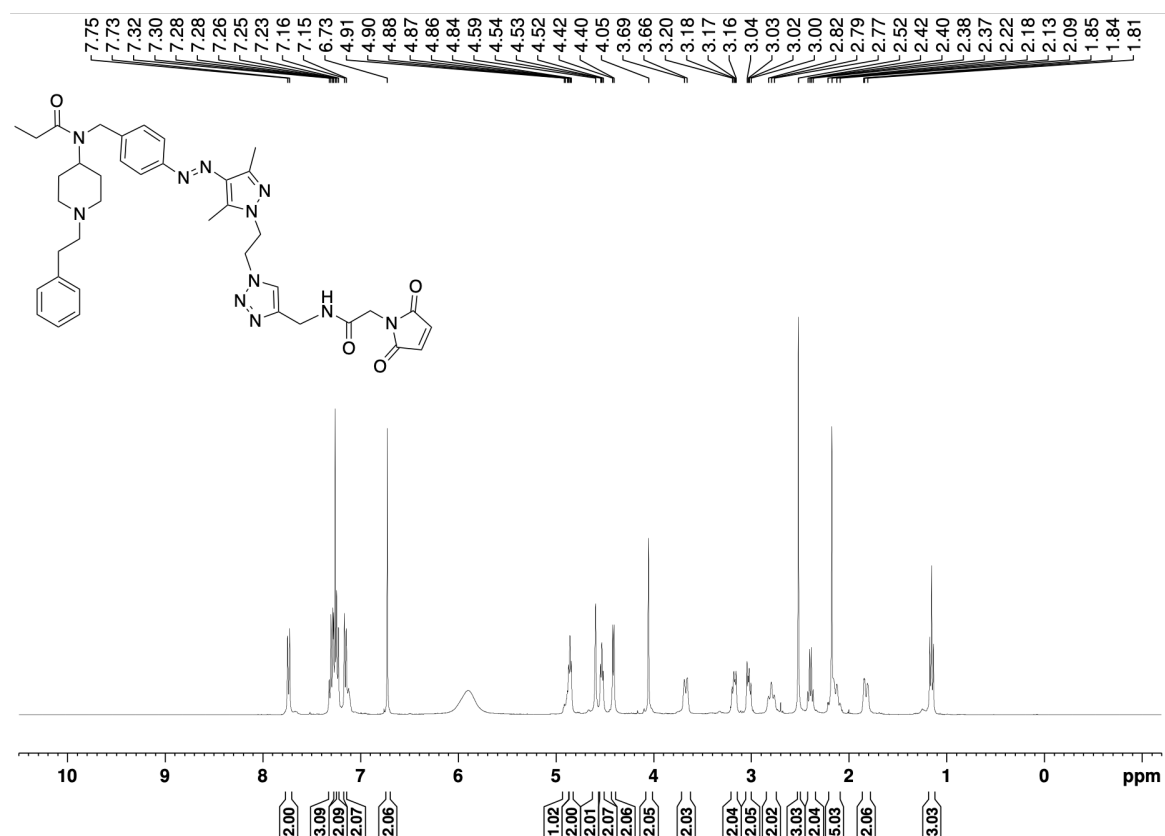
*Contains traces of acetone and H_2O . Yield was obtained after further drying.

^{13}C spectrum of **16** (101 MHz, CDCl_3):

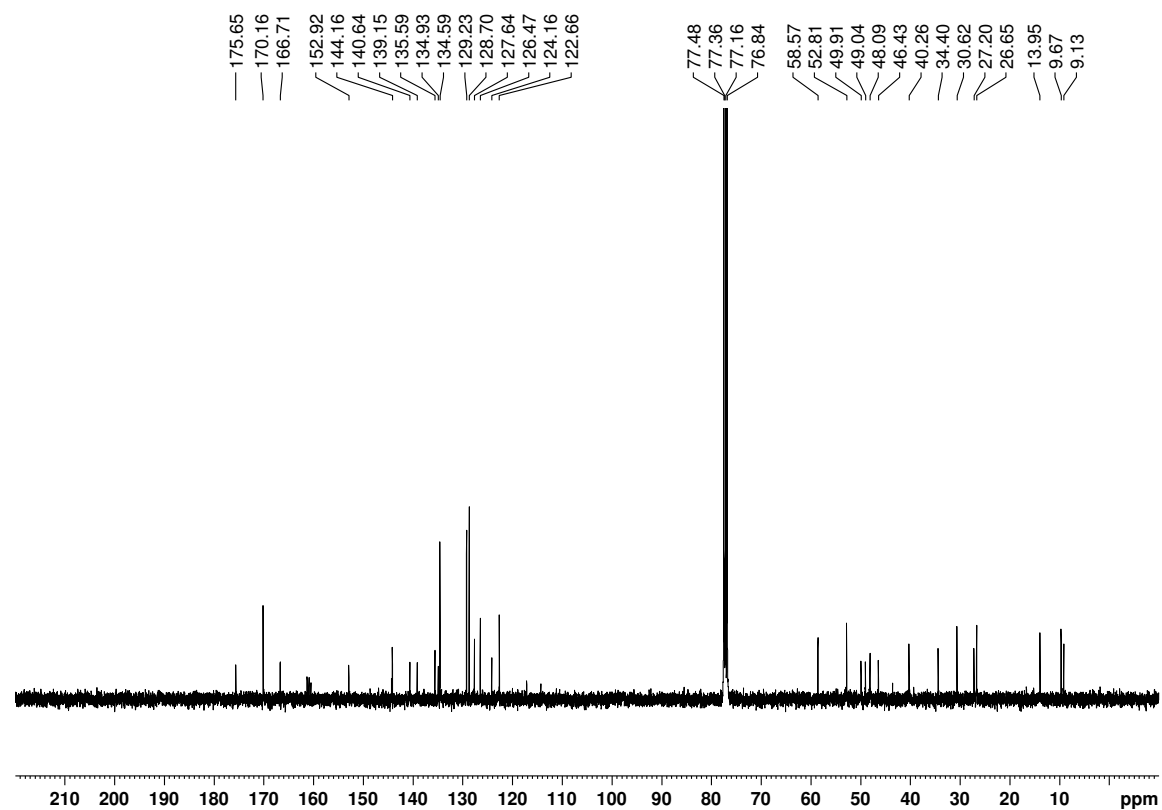


Appendix

^1H spectrum of **tFAPz 2f** (400 MHz, CDCl_3):

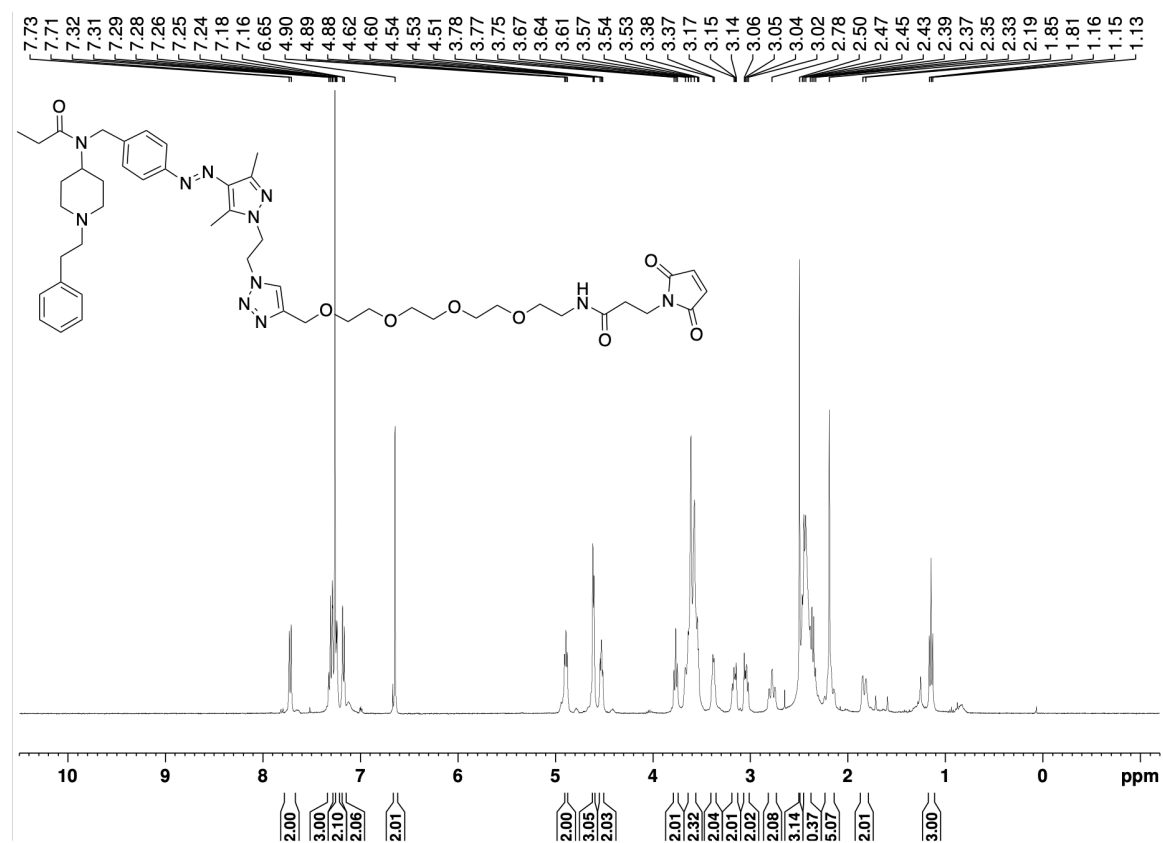


^{13}C spectrum of **tFAPz 2f** (101 MHz, CDCl_3):

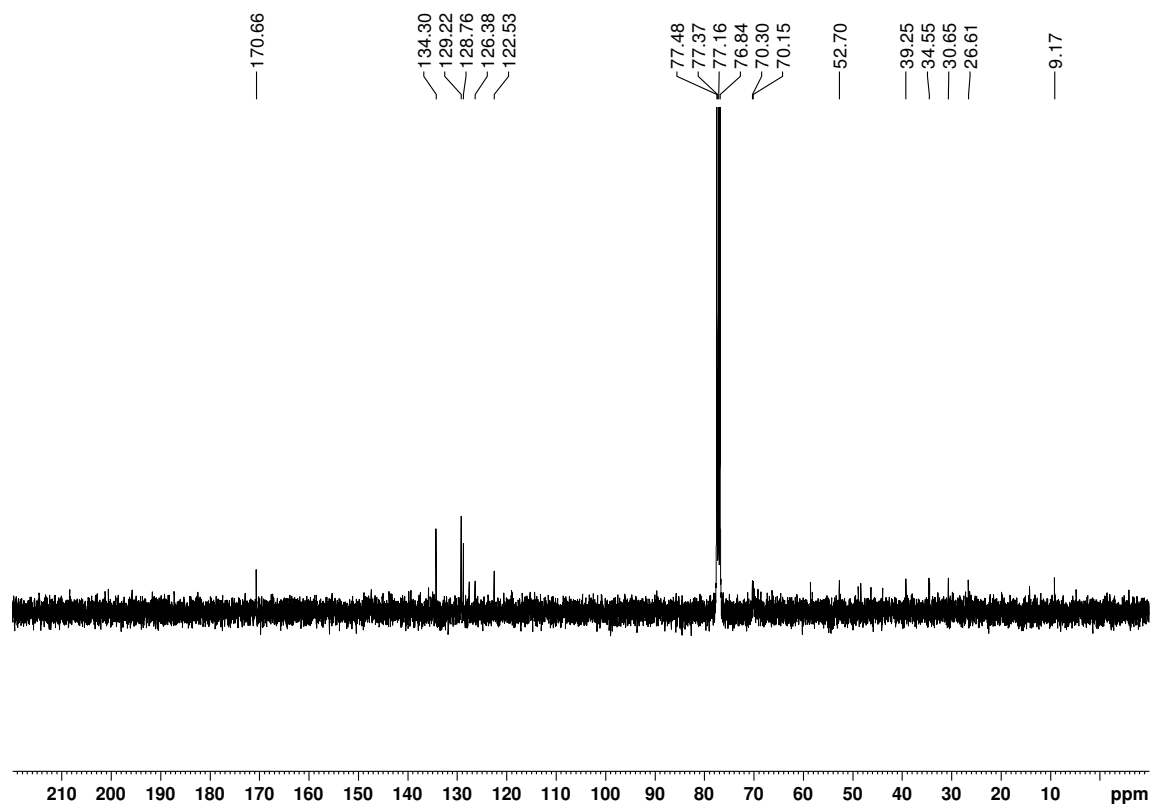


Appendix

^1H spectrum of **tFAPz 2g** (400 MHz, CDCl_3):

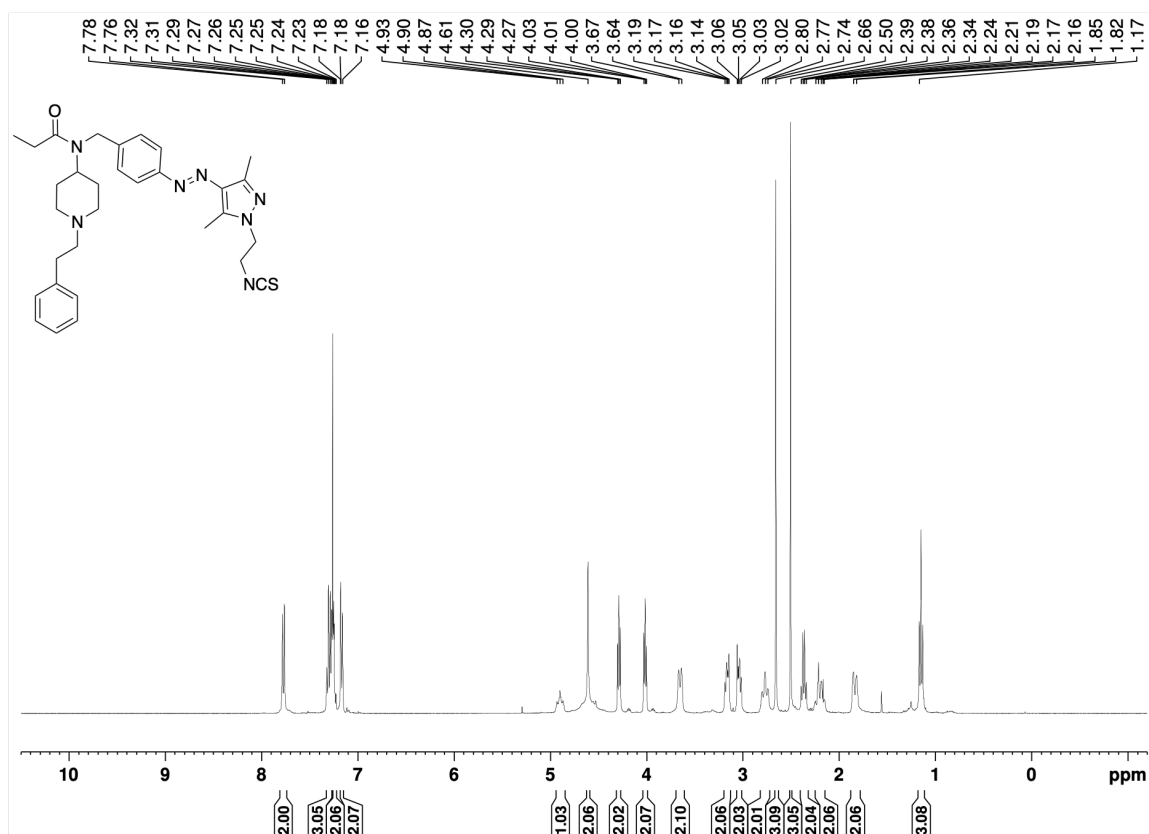


^{13}C spectrum of **tFAPz 2g** (101 MHz, CDCl_3):

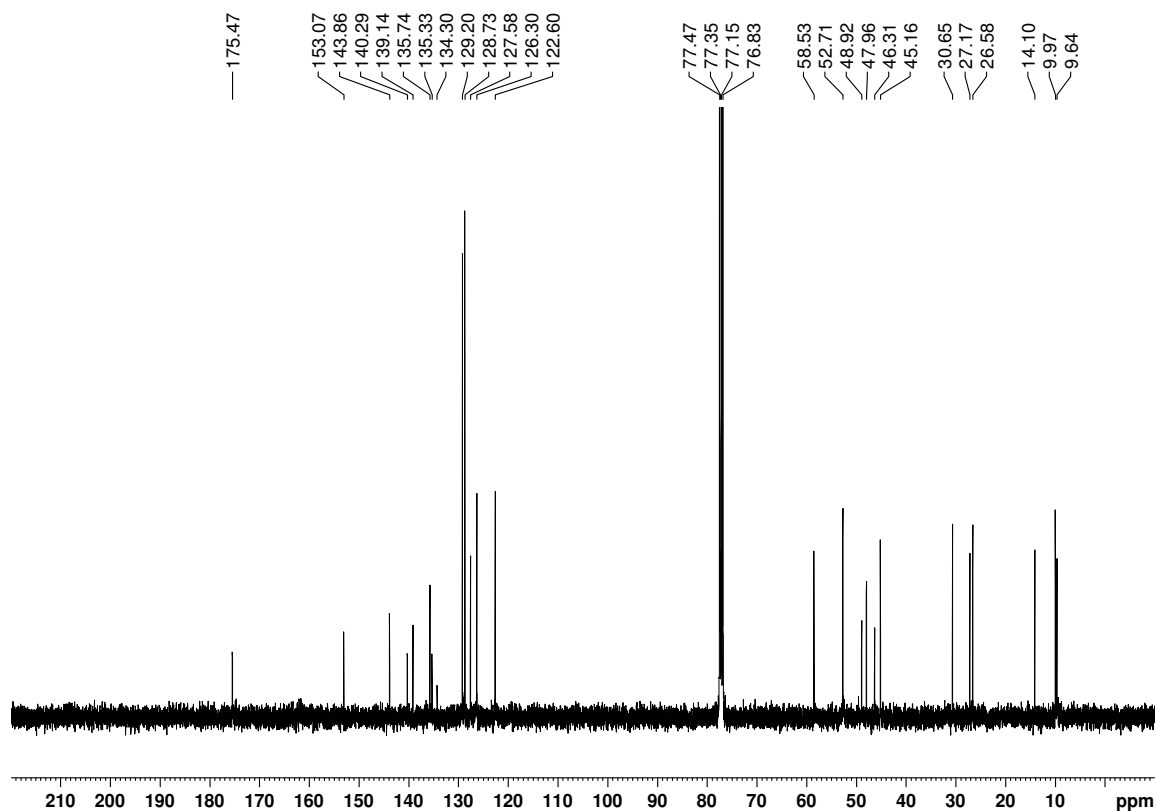


Appendix

^1H spectrum of **tFAPz 3** (400 MHz, CDCl_3):



^{13}C spectrum of **tFAPz 3** (101 MHz, CDCl_3):



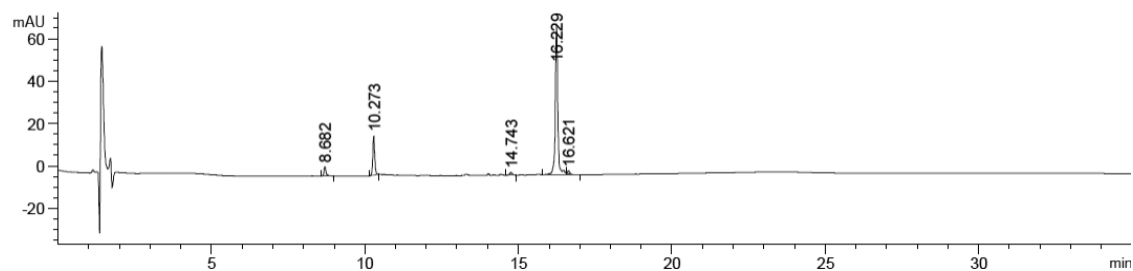
7.4 Appendix for Chapter 3

7.4.1 Analytical HPLC Chromatograms for Purity Determination

Experiments in this section were evaluated in DMSO.

Compound **2a**:

Detection at 254 nm: 92% purity



Signal 1: DAD1 A, Sig=254,4 Ref=off

Peak #	RetTime [min]	Type	Width [min]	Area [mAU*s]	Height [mAU]	Area %
1	8.682	BB	0.0740	22.55994	4.54125	4.2630
2	10.273	BB	0.0676	81.28781	18.37691	15.3604
3	14.743	BB	0.0844	7.65057	1.34372	1.4457
4	16.229	BV R	0.0835	407.58231	71.41820	77.0182
5	16.621	VB E	0.0886	10.12162	1.67230	1.9126

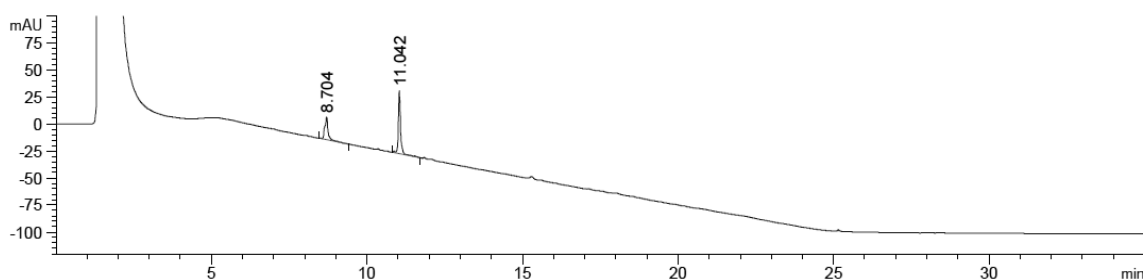
*Peak 2 and Peak 4 are *cis*- and *trans*-isomers of compound **2a**, respectively.

Compound **2a** did not substantially absorb at 220 nm in comparison to 254 nm, therefore, data for 254 nm was analyzed for compound purity.

Appendix

Compound 2b:

Detection at 220 nm: >99% purity

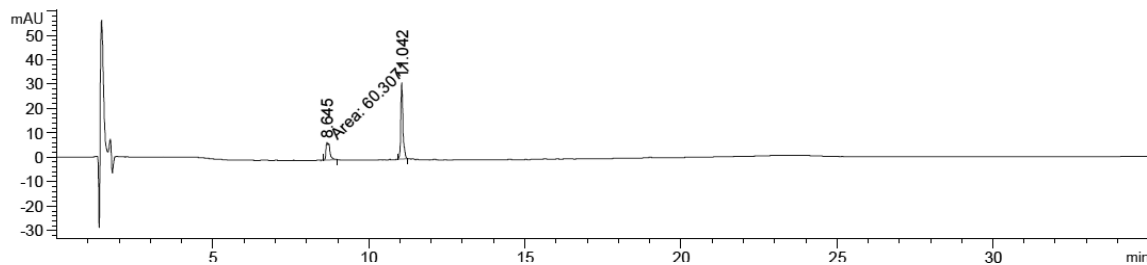


Signal 2: DAD1 B, Sig=220,4 Ref=off

Peak #	RetTime [min]	Type	Width [min]	Area [mAU*s]	Height [mAU]	Area %
1	8.704	VB R	0.1029	160.38322	21.04614	34.8308
2	11.042	VV R	0.0759	300.08087	58.40069	65.1692

*Peak 1 and Peak 2 are *cis*- and *trans*-isomers of compound 2b, respectively.

Detection at 254 nm: >99% purity



Signal 1: DAD1 A, Sig=254,4 Ref=off

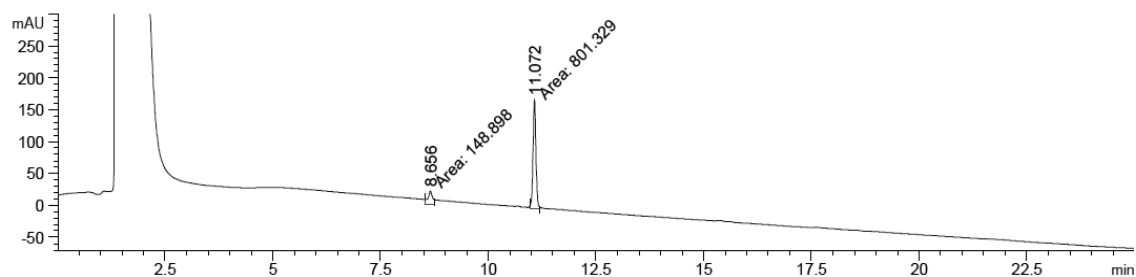
Peak #	RetTime [min]	Type	Width [min]	Area [mAU*s]	Height [mAU]	Area %
1	8.645	MM	0.1398	60.30715	7.18843	28.0809
2	11.042	BB	0.0731	154.45531	31.58138	71.9191

*Peak 1 and Peak 2 are *cis*- and *trans*-isomers of compound 2b, respectively.

Appendix

Compound **2c**:

Detection at 220 nm: >99% purity

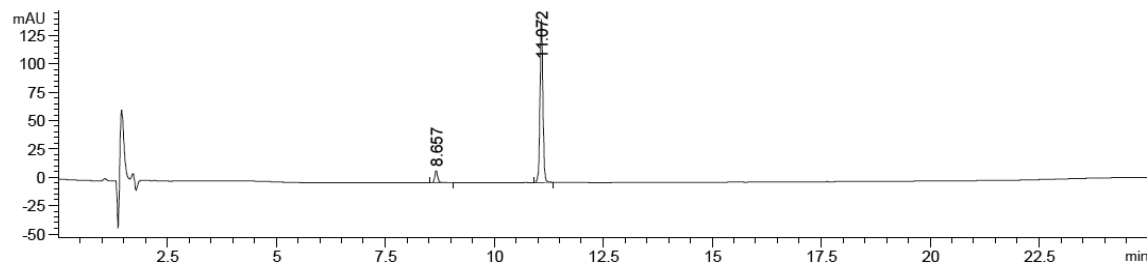


Signal 2: DAD1 B, Sig=220,4 Ref=off

Peak #	RetTime [min]	Type	Width [min]	Area [mAU*s]	Height [mAU]	Area %
1	8.656	MM	0.1226	148.89751	20.24962	15.6697
2	11.072	MM	0.0785	801.32935	170.19341	84.3303

*Peak 1 and Peak 2 are *cis*- and *trans*-isomers of compound **2c**, respectively.

Detection at 254 nm: >99% purity



Signal 1: DAD1 A, Sig=254,4 Ref=off

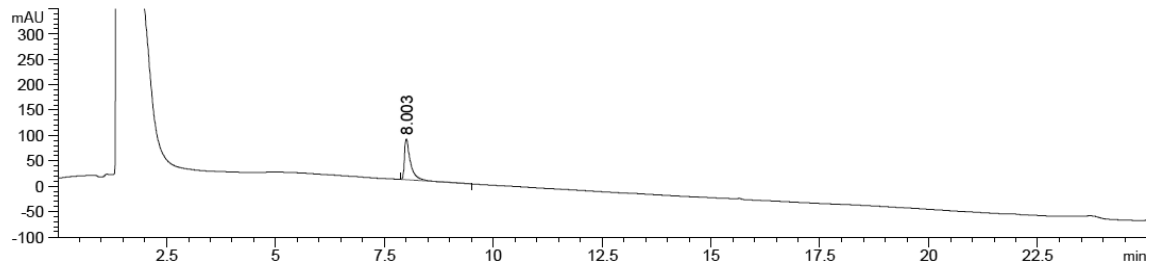
Peak #	RetTime [min]	Type	Width [min]	Area [mAU*s]	Height [mAU]	Area %
1	8.657	BB	0.0767	56.20324	10.80707	7.6833
2	11.072	BB	0.0731	675.29492	142.96805	92.3167

*Peak 1 and Peak 2 are *cis*- and *trans*-isomers of compound **2c**, respectively.

Appendix

Compound **2d**:

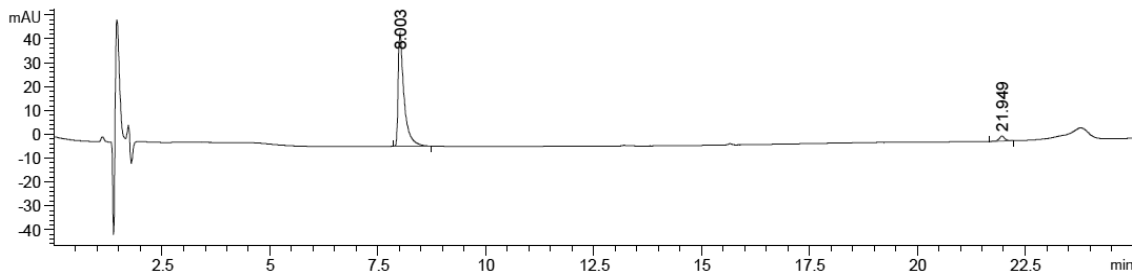
Detection at 220 nm: >99% purity



Signal 2: DAD1 B, Sig=220,4 Ref=off

Peak #	RetTime [min]	Type	Width [min]	Area [mAU*s]	Height [mAU]	Area %
1	8.003	BB	0.1398	786.65485	80.66946	100.0000

Detection at 254 nm: 96% purity



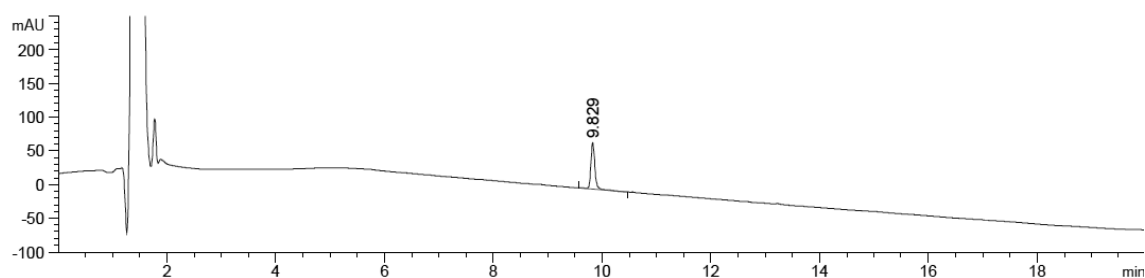
Signal 1: DAD1 A, Sig=254,4 Ref=off

Peak #	RetTime [min]	Type	Width [min]	Area [mAU*s]	Height [mAU]	Area %
1	8.003	BB	0.1379	454.01617	47.34629	96.1046
2	21.949	BB	0.1309	18.40272	2.12772	3.8954

Appendix

Compound **2e**:

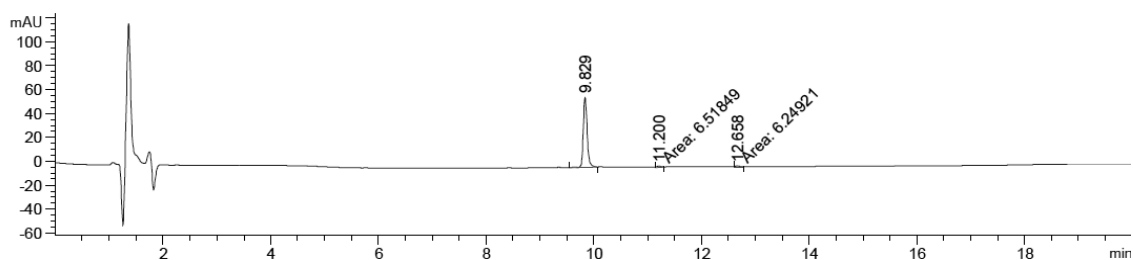
Detection at 220 nm: >99% purity



Signal 2: DAD1 B, Sig=220,4 Ref=off

Peak #	RetTime [min]	Type	Width [min]	Area [mAU*s]	Height [mAU]	Area %
1	9.829	VV R	0.0780	355.32703	69.05930	100.0000

Detection at 254 nm: 96% purity



Signal 1: DAD1 A, Sig=254,4 Ref=off

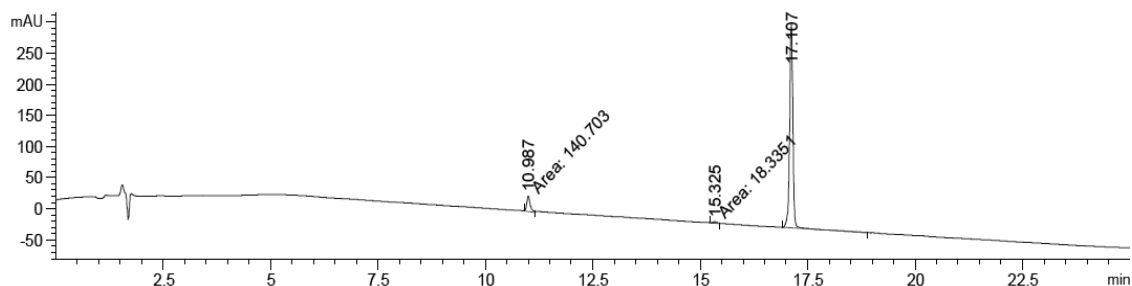
Peak #	RetTime [min]	Type	Width [min]	Area [mAU*s]	Height [mAU]	Area %
1	9.829	VB R	0.0758	289.81271	58.45004	95.7804
2	11.200	MM	0.0951	6.51849	1.14216	2.1543
3	12.658	MM	0.1005	6.24921	1.03646	2.0653

*Peak 1 is compound **2e**.

Appendix

Compound 3a:

Detection at 220 nm: 99% purity

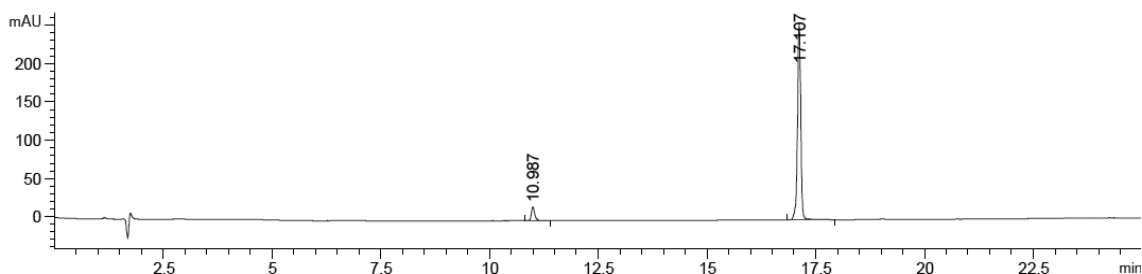


Signal 2: DAD1 B, Sig=220,4 Ref=off

Peak #	RetTime [min]	Type	Width [min]	Area [mAU*s]	Height [mAU]	Area %
1	10.987	MM	0.0950	140.70300	24.67721	7.5132
2	15.325	MM	0.1170	18.33514	2.61243	0.9791
3	17.107	BB	0.0787	1713.70752	329.15683	91.5078

*Peak 1 and Peak 3 are *cis*- and *trans*-isomers of compound 3a, respectively.

Detection at 254 nm: >99% purity



Signal 1: DAD1 A, Sig=254,4 Ref=off

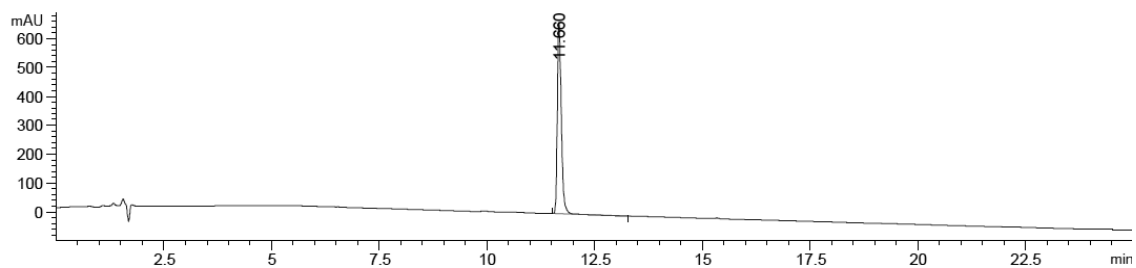
Peak #	RetTime [min]	Type	Width [min]	Area [mAU*s]	Height [mAU]	Area %
1	10.987	BB	0.0809	97.46942	18.09208	6.8212
2	17.107	BB	0.0785	1331.45911	256.60541	93.1788

*Peak 1 and Peak 2 are *cis*- and *trans*-isomers of compound 3a, respectively.

Appendix

Compound **3b**:

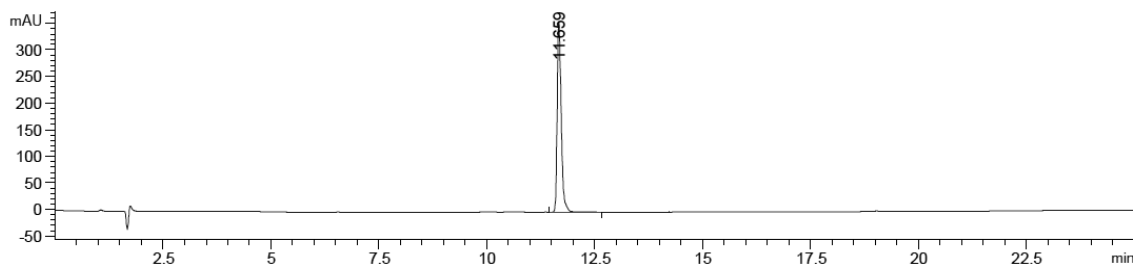
Detection at 220 nm: >99% purity



Signal 2: DAD1 B, Sig=220,4 Ref=off

Peak #	RetTime [min]	Type	Width [min]	Area [mAU*s]	Height [mAU]	Area %
1	11.660	BB	0.0998	4303.63818	662.59735	100.0000

Detection at 254 nm: >99% purity



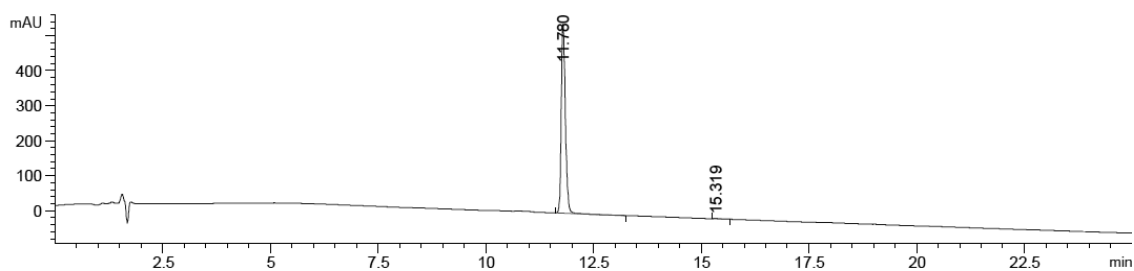
Signal 1: DAD1 A, Sig=254,4 Ref=off

Peak #	RetTime [min]	Type	Width [min]	Area [mAU*s]	Height [mAU]	Area %
1	11.659	BB	0.1001	2335.53735	358.12900	100.0000

Appendix

Compound 3c:

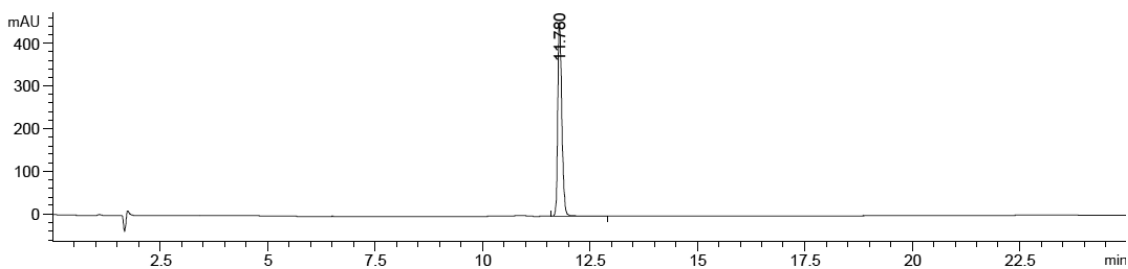
Detection at 220 nm: >99% purity



Signal 2: DAD1 B, Sig=220,4 Ref=off

Peak #	RetTime [min]	Type	Width [min]	Area [mAU*s]	Height [mAU]	Area %
1	11.780	BB	0.1013	3576.99707	539.67877	99.6279
2	15.319	BB	0.0918	13.35999	2.17008	0.3721

Detection at 254 nm: >99% purity



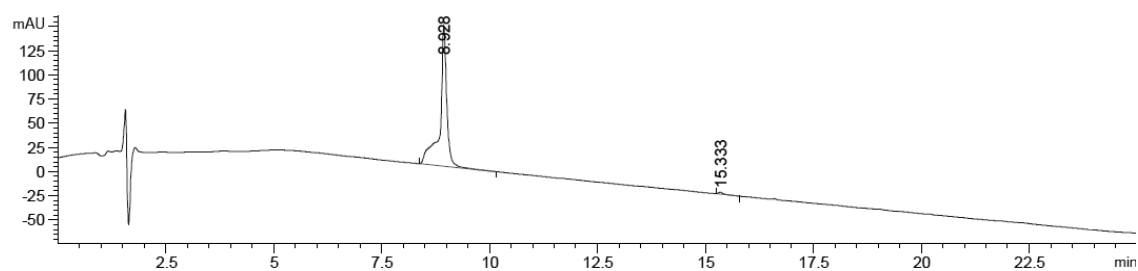
Signal 1: DAD1 A, Sig=254,4 Ref=off

Peak #	RetTime [min]	Type	Width [min]	Area [mAU*s]	Height [mAU]	Area %
1	11.780	BB	0.1010	2993.83301	453.61435	100.0000

Appendix

Compound **3b-NH₂**:

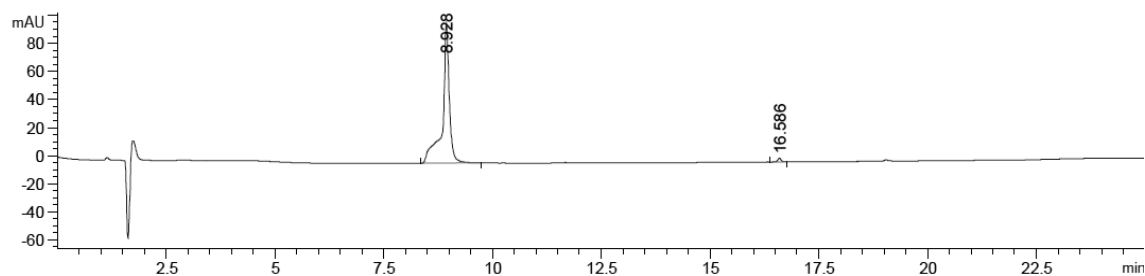
Detection at 220 nm: 99% purity



Signal 2: DAD1 B, Sig=220,4 Ref=off

Peak #	RetTime [min]	Type	Width [min]	Area [mAU*s]	Height [mAU]	Area %
1	8.928	BB	0.1520	1625.66235	145.84552	99.1665
2	15.333	BB	0.0953	13.66377	2.11821	0.8335

Detection at 254 nm: 99% purity



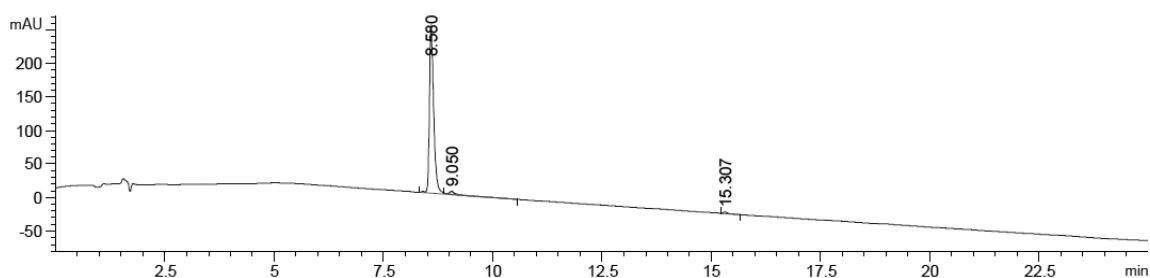
Signal 1: DAD1 A, Sig=254,4 Ref=off

Peak #	RetTime [min]	Type	Width [min]	Area [mAU*s]	Height [mAU]	Area %
1	8.928	BB	0.1511	1102.16919	99.62576	98.7085
2	16.586	BB	0.0830	14.42022	2.66910	1.2915

Appendix

Compound **3d**:

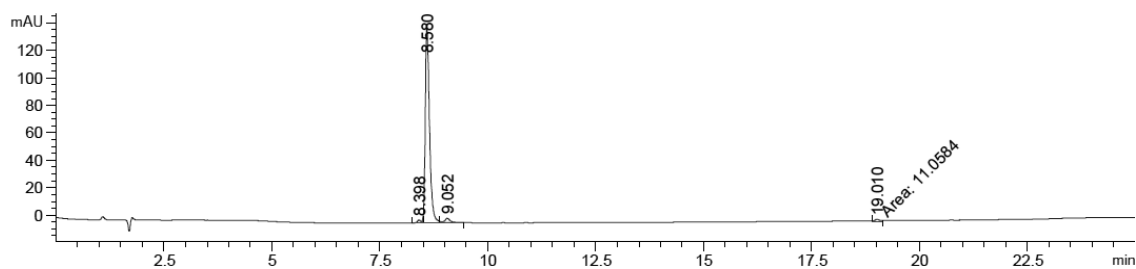
Detection at 220 nm: 96% purity



Signal 2: DAD1 B, Sig=220,4 Ref=off

Peak #	RetTime [min]	Type	Width [min]	Area [mAU*s]	Height [mAU]	Area %
1	8.580	VV R	0.1013	1704.31018	249.28183	96.2516
2	9.050	VB E	0.1519	53.15728	4.77326	3.0021
3	15.307	BB	0.0920	13.21583	2.20284	0.7464

Detection at 254 nm: 95% purity



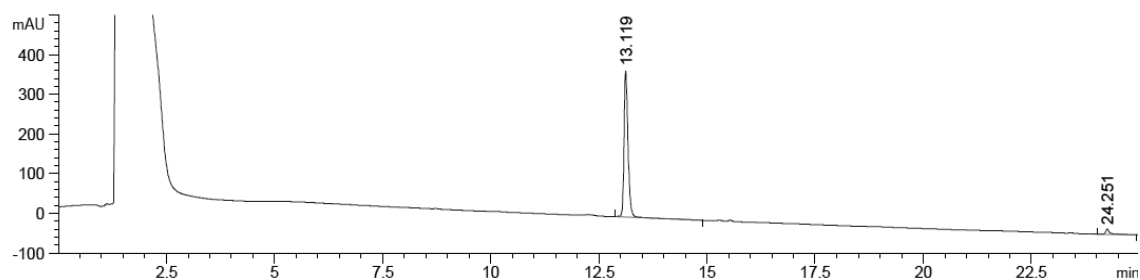
Signal 1: DAD1 A, Sig=254,4 Ref=off

Peak #	RetTime [min]	Type	Width [min]	Area [mAU*s]	Height [mAU]	Area %
1	8.398	BV E	0.0766	9.91450	1.97380	0.9595
2	8.580	VV R	0.1013	985.64587	144.98233	95.3888
3	9.052	VB E	0.1204	26.67387	3.16301	2.5814
4	19.010	MM	0.1365	11.05842	1.35036	1.0702

Appendix

Compound **3e**:

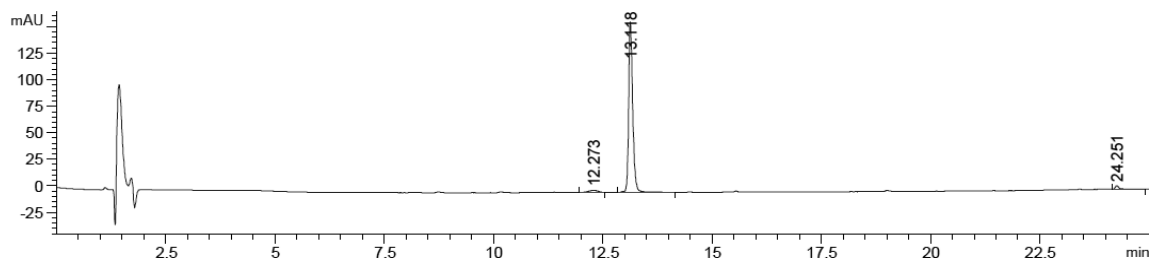
Detection at 220 nm: 96% purity



Signal 2: DAD1 B, Sig=220,4 Ref=off

Peak #	RetTime [min]	Type	Width [min]	Area [mAU*s]	Height [mAU]	Area %
1	13.119	VB R	0.0973	2389.11963	370.13995	96.0276
2	24.251	VBAR	0.1037	98.83099	13.45837	3.9724

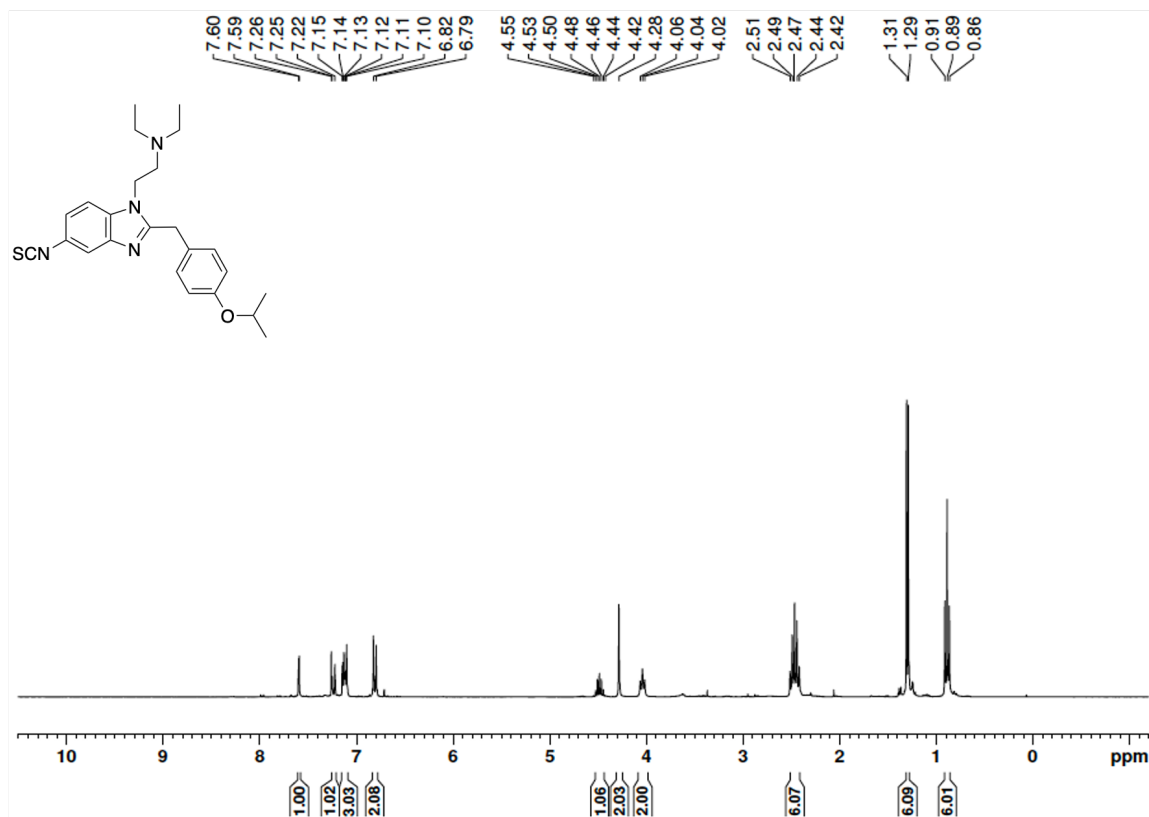
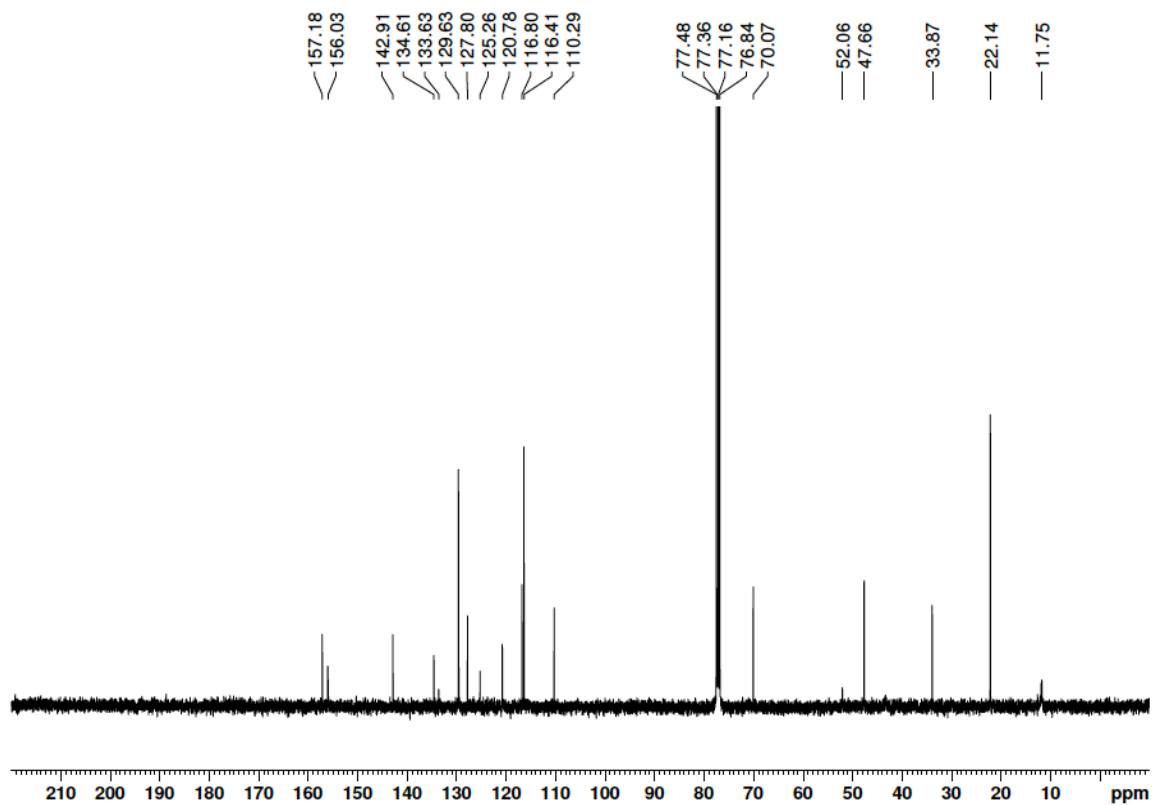
Detection at 254 nm: 96% purity



Signal 1: DAD1 A, Sig=254,4 Ref=off

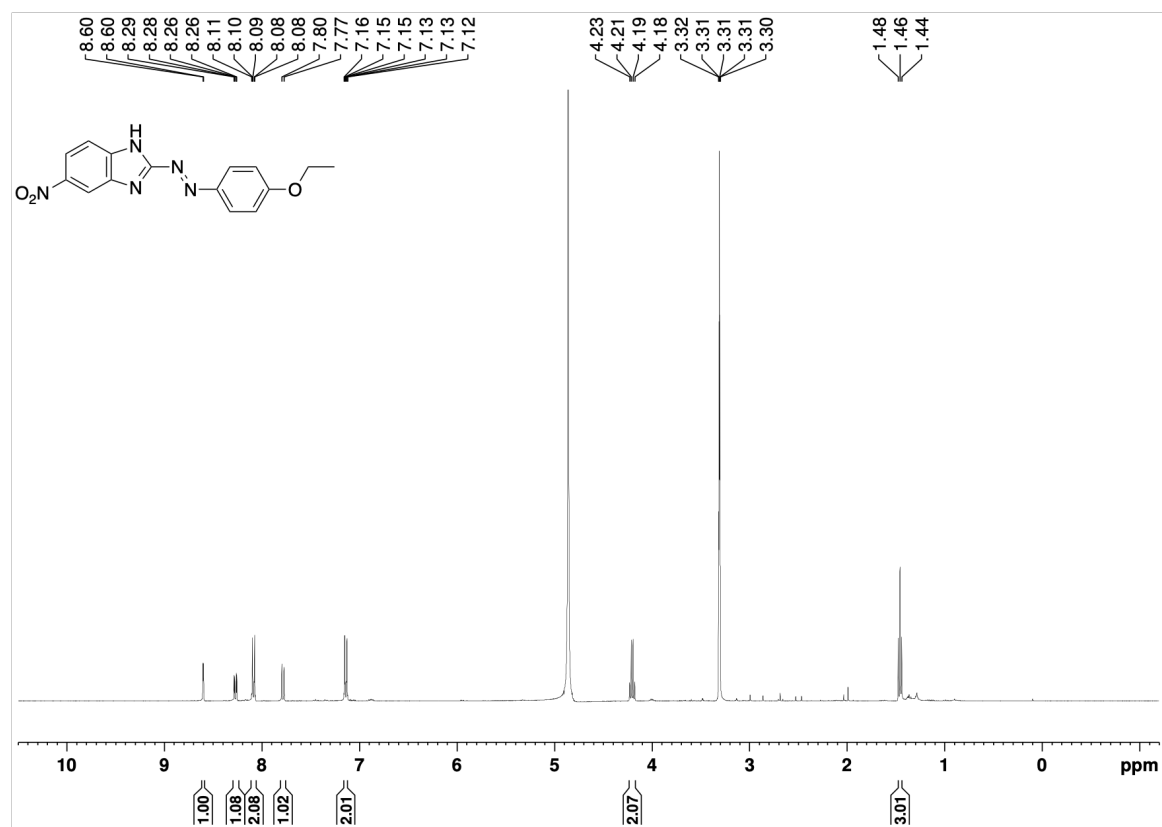
Peak #	RetTime [min]	Type	Width [min]	Area [mAU*s]	Height [mAU]	Area %
1	12.273	BB	0.2348	29.41046	1.87658	2.7044
2	13.118	BB	0.0992	1039.89966	161.25882	95.6242
3	24.251	BBA	0.0831	18.17627	3.25509	1.6714

7.4.2 NMR Spectra

 ^1H spectrum of **1** (400 MHz, CDCl_3): ^{13}C spectrum of **1** (101 MHz, CDCl_3):

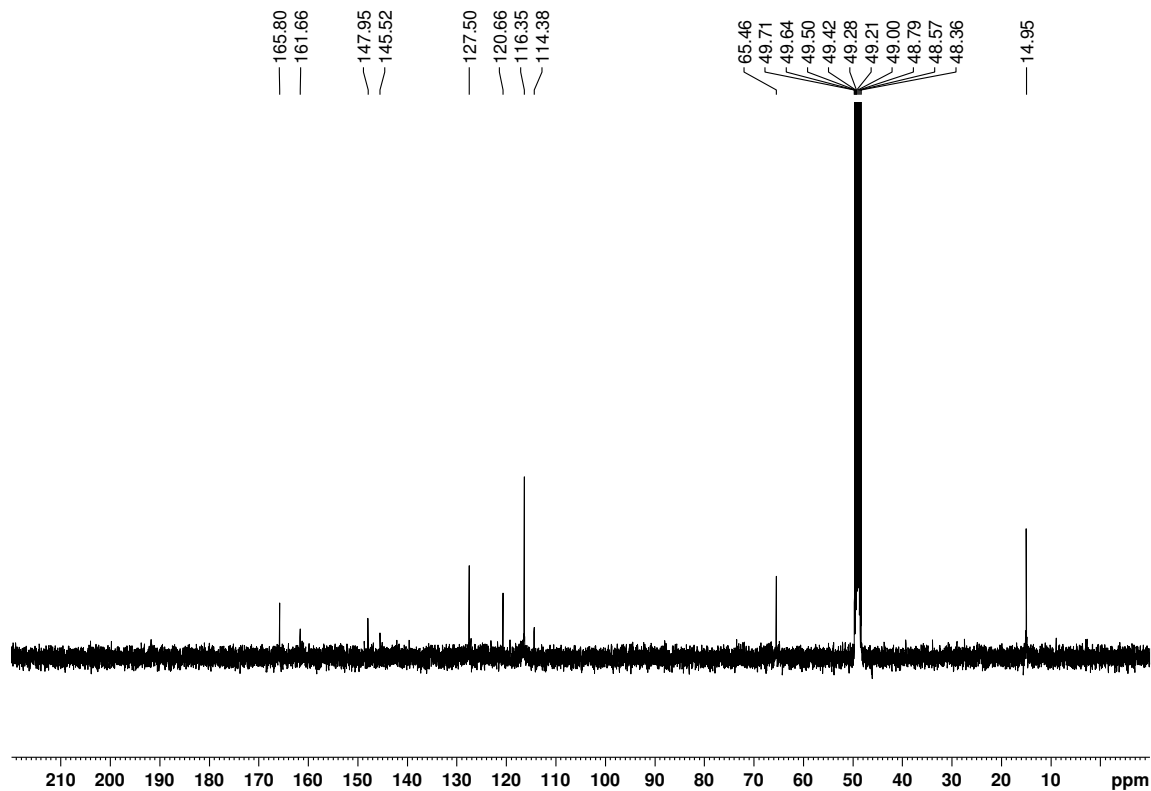
Appendix

^1H spectrum of **2a** (400 MHz, MeOD):



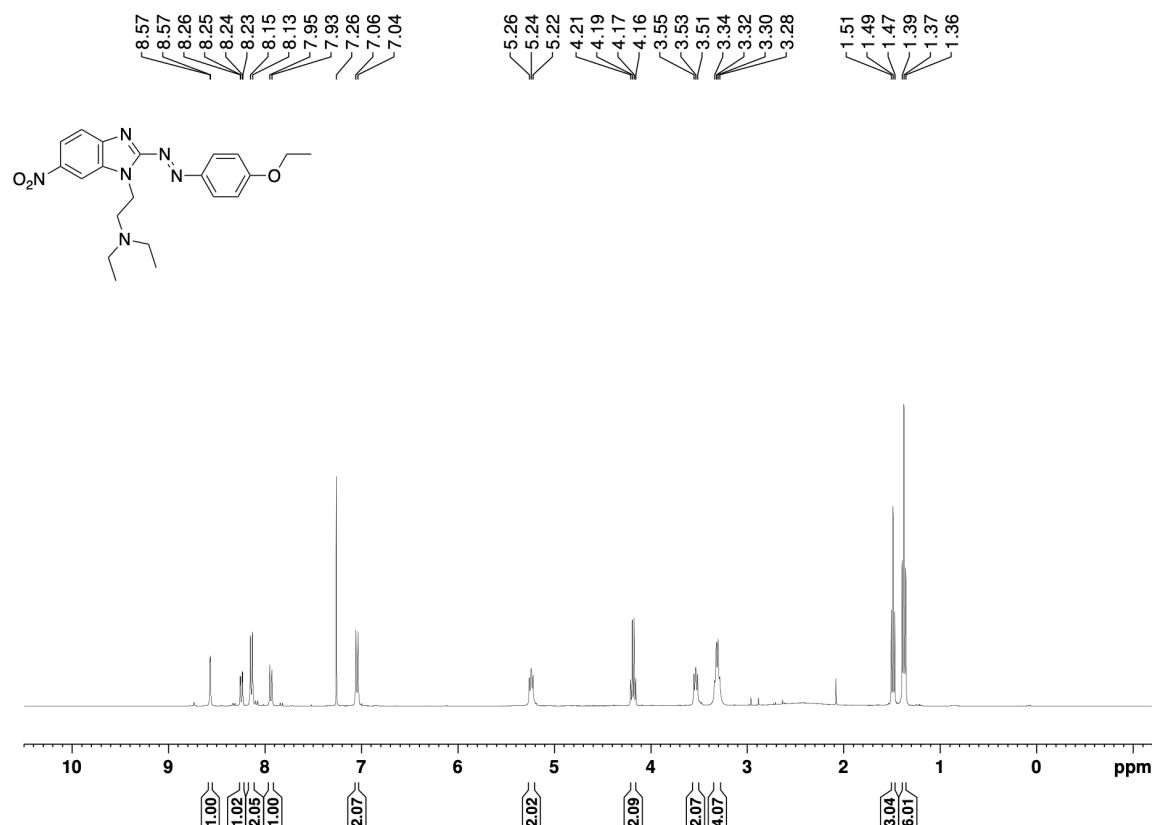
*Contains H_2O present in MeOD.

^{13}C spectrum of **2a** (101 MHz, MeOD):

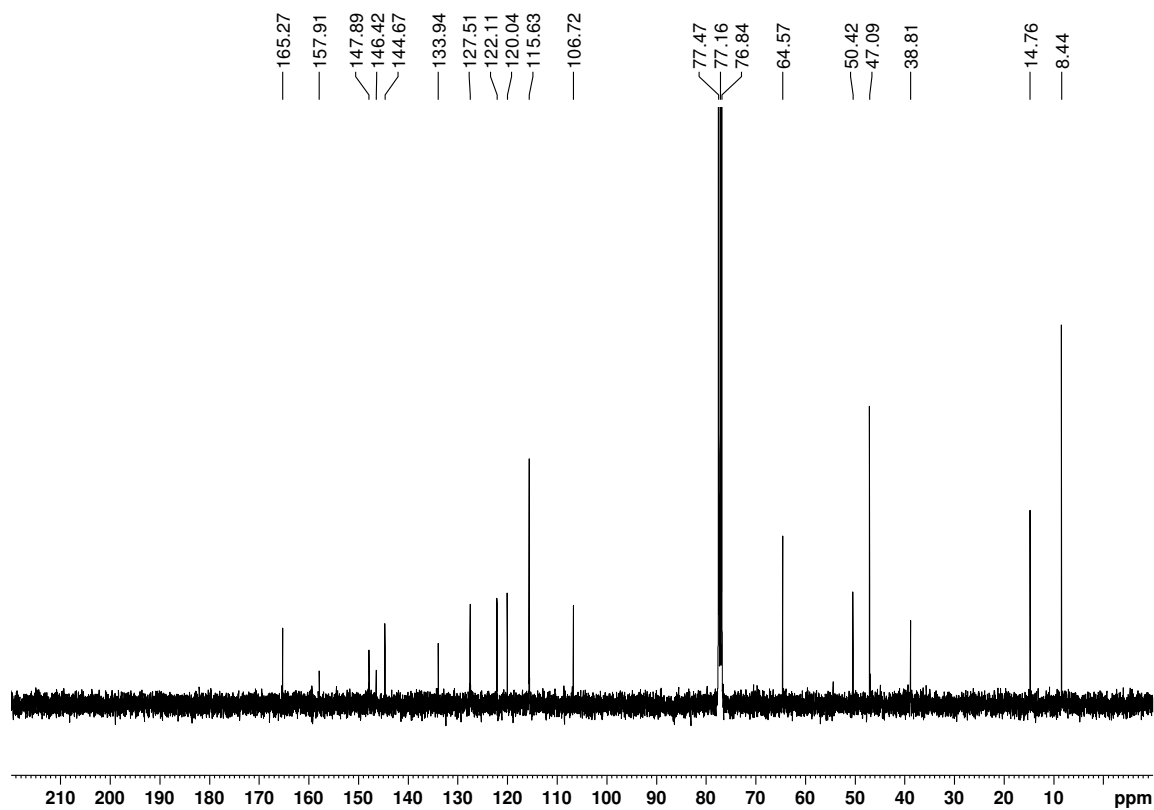


Appendix

^1H spectrum of **2b** (400 MHz, CDCl_3):

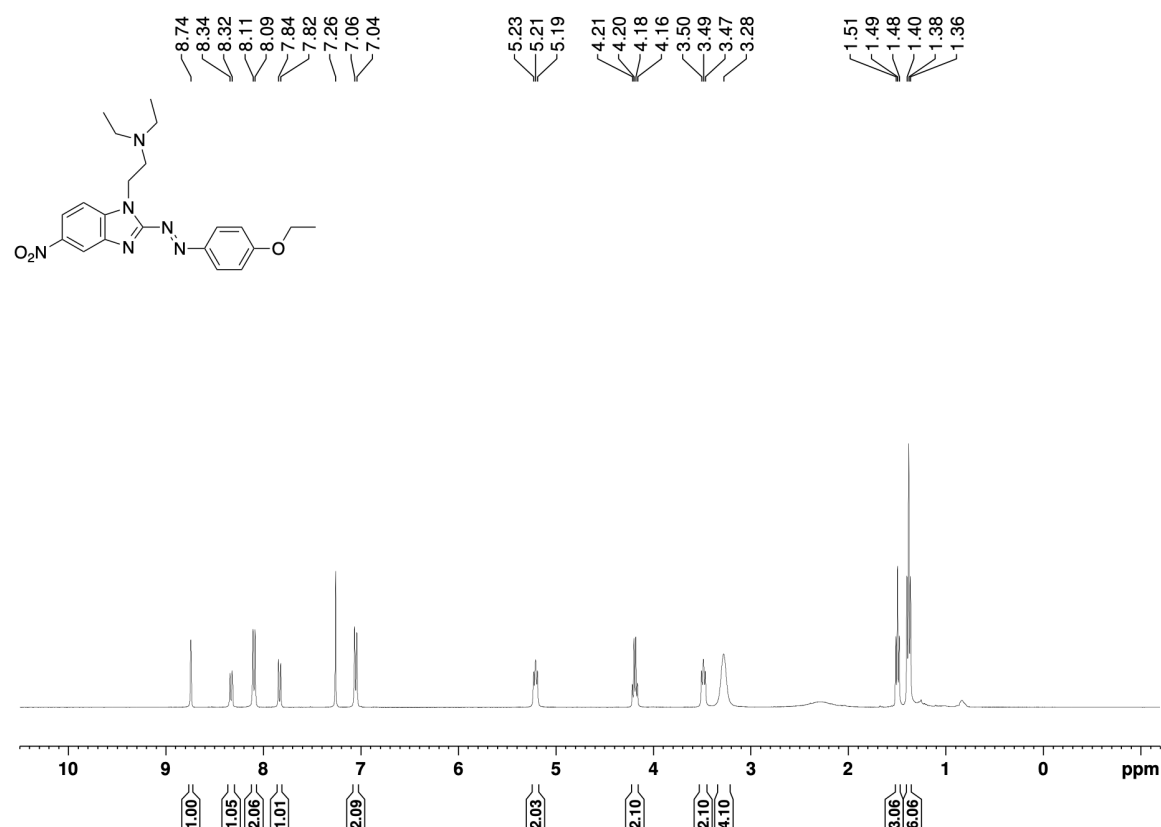


^{13}C spectrum of **2b** (101 MHz, CDCl_3):

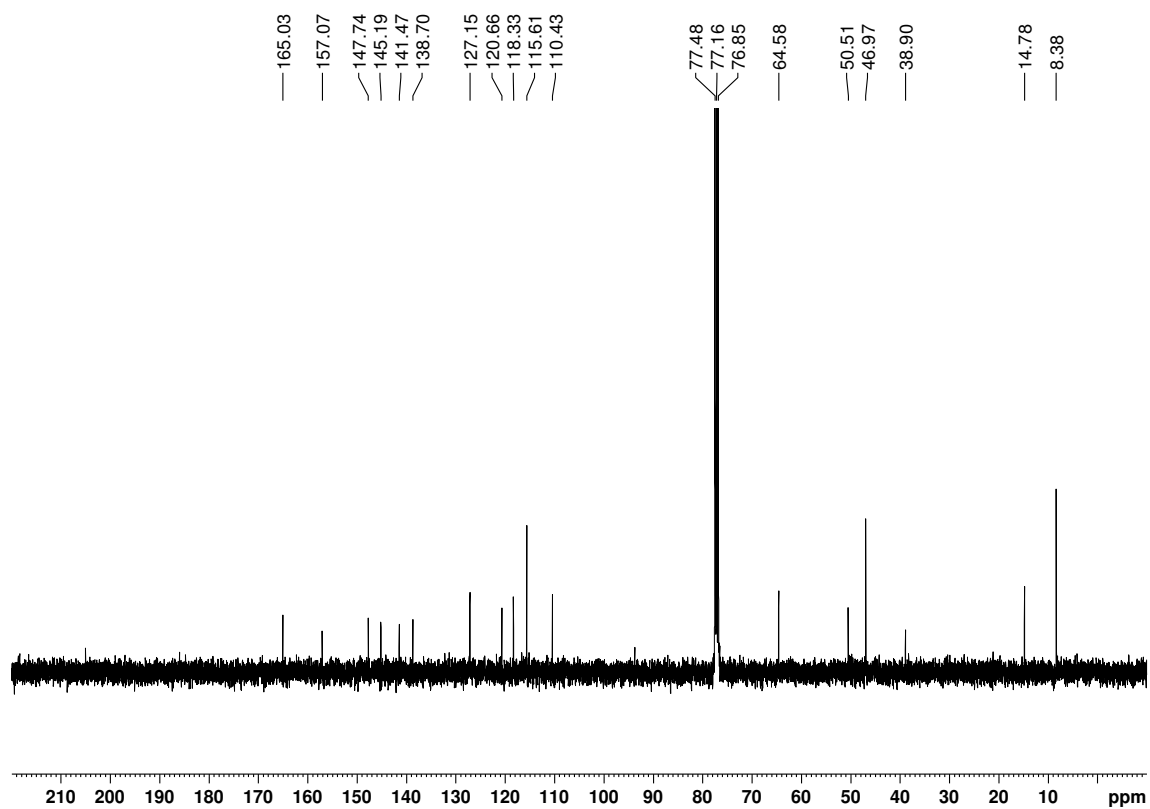


Appendix

^1H spectrum of **2c** (400 MHz, CDCl_3):

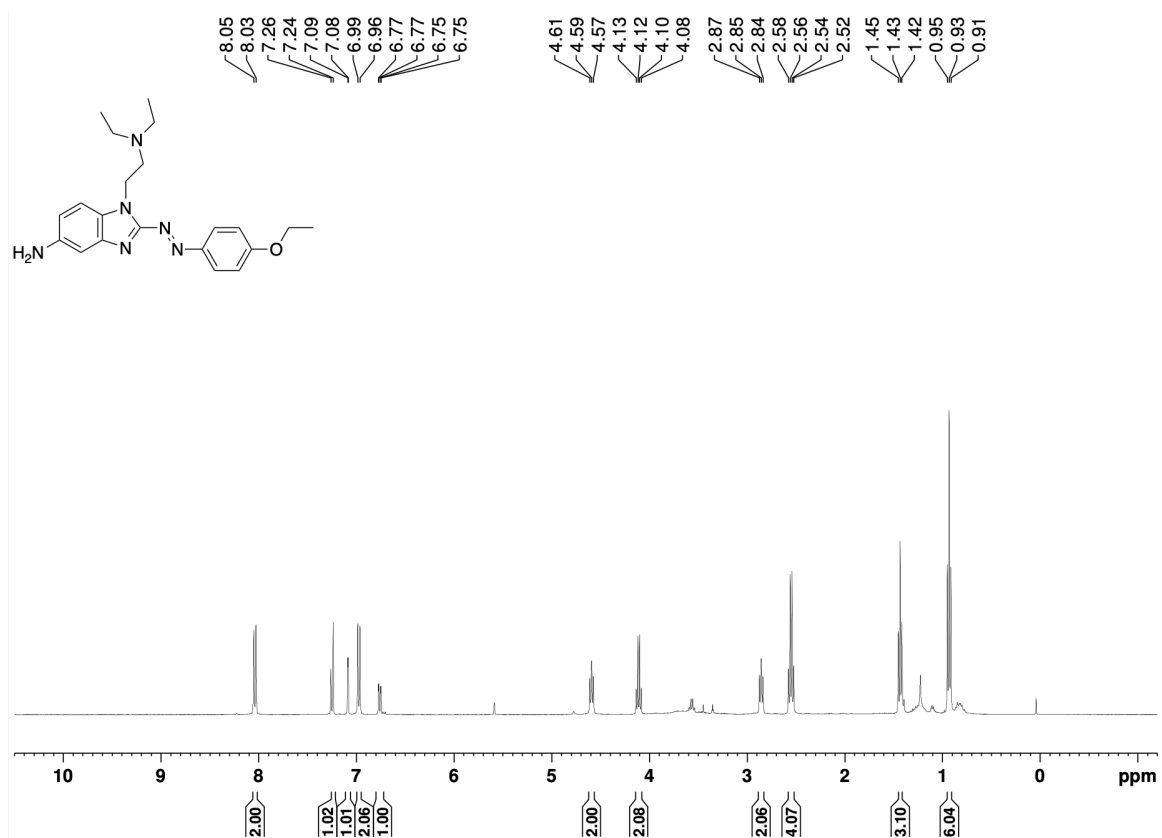


^{13}C spectrum of **2c** (101 MHz, CDCl_3):

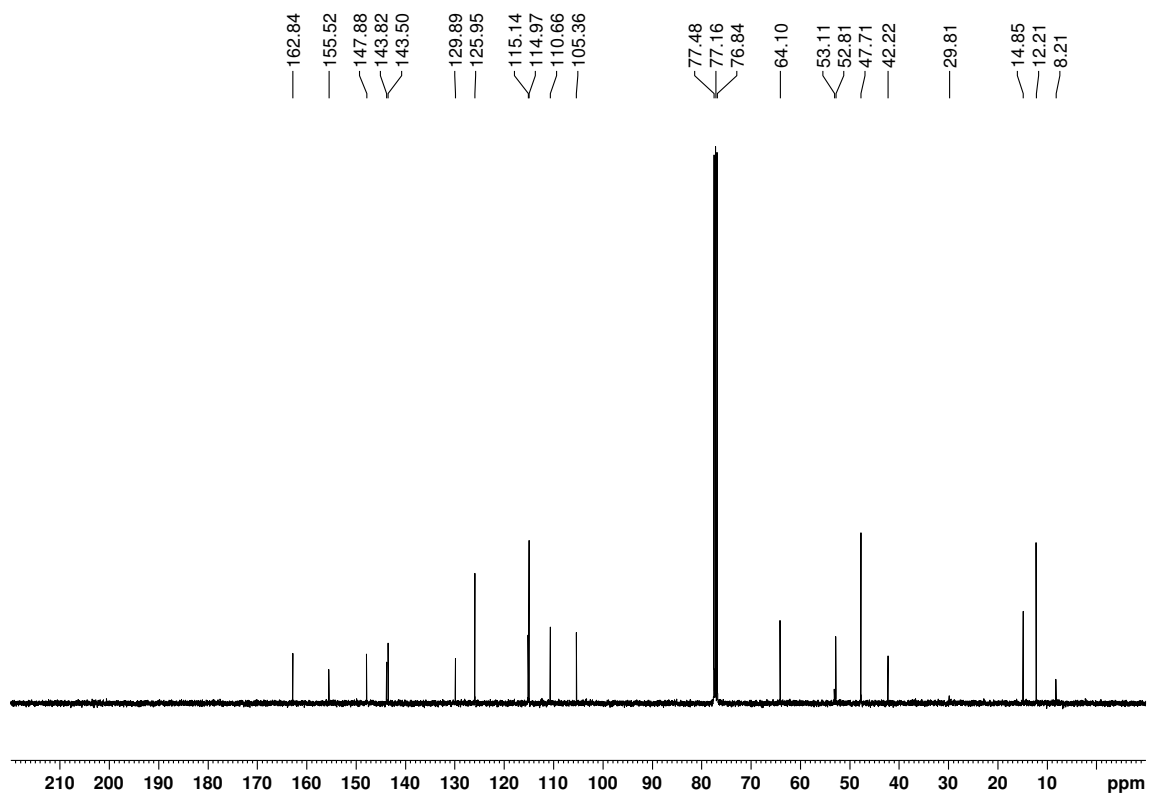


Appendix

^1H spectrum of **2d** (400 MHz, CDCl_3):

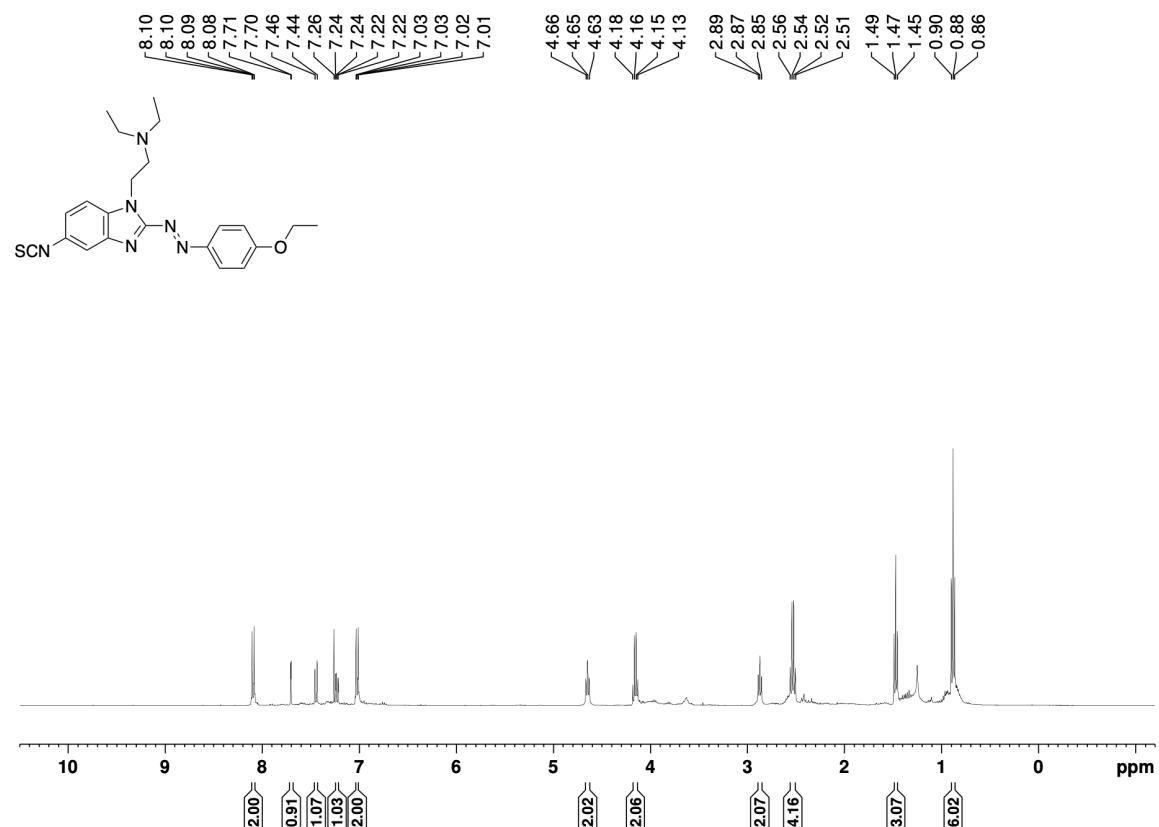


^{13}C spectrum of **2d** (101 MHz, CDCl_3):

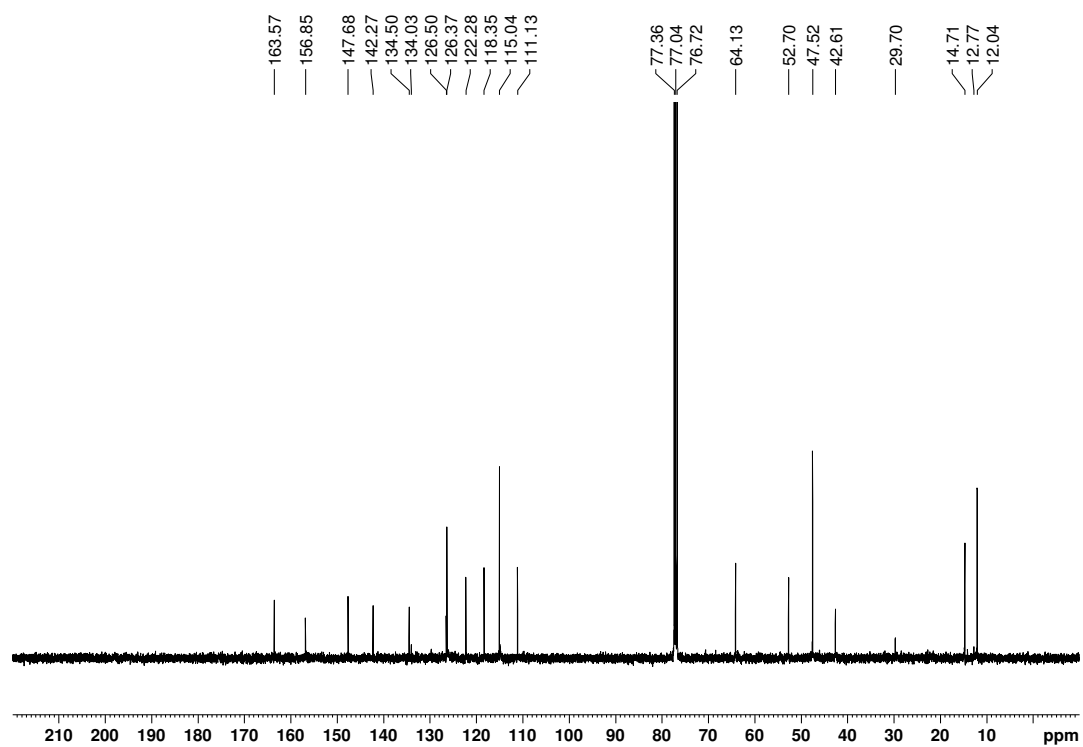


Appendix

^1H spectrum of **2e** (400 MHz, CDCl_3):

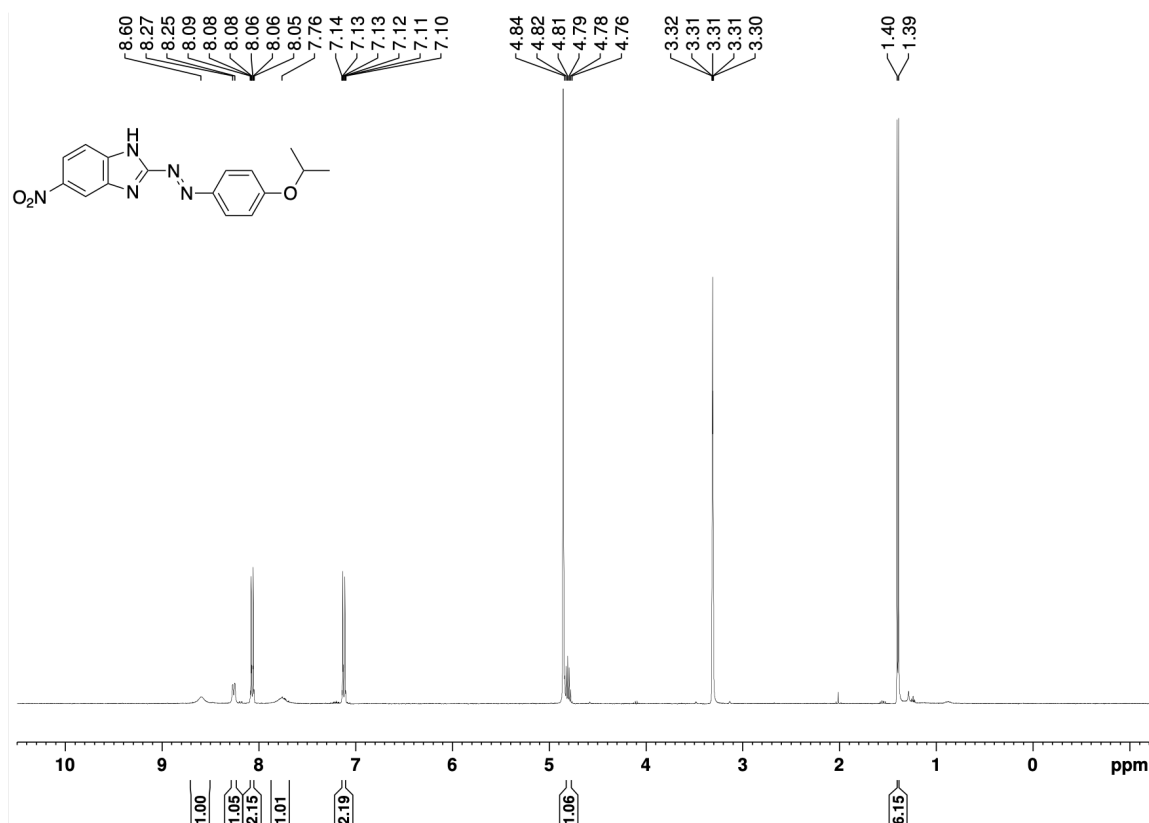


^{13}C spectrum of **2e** (101 MHz, CDCl_3):



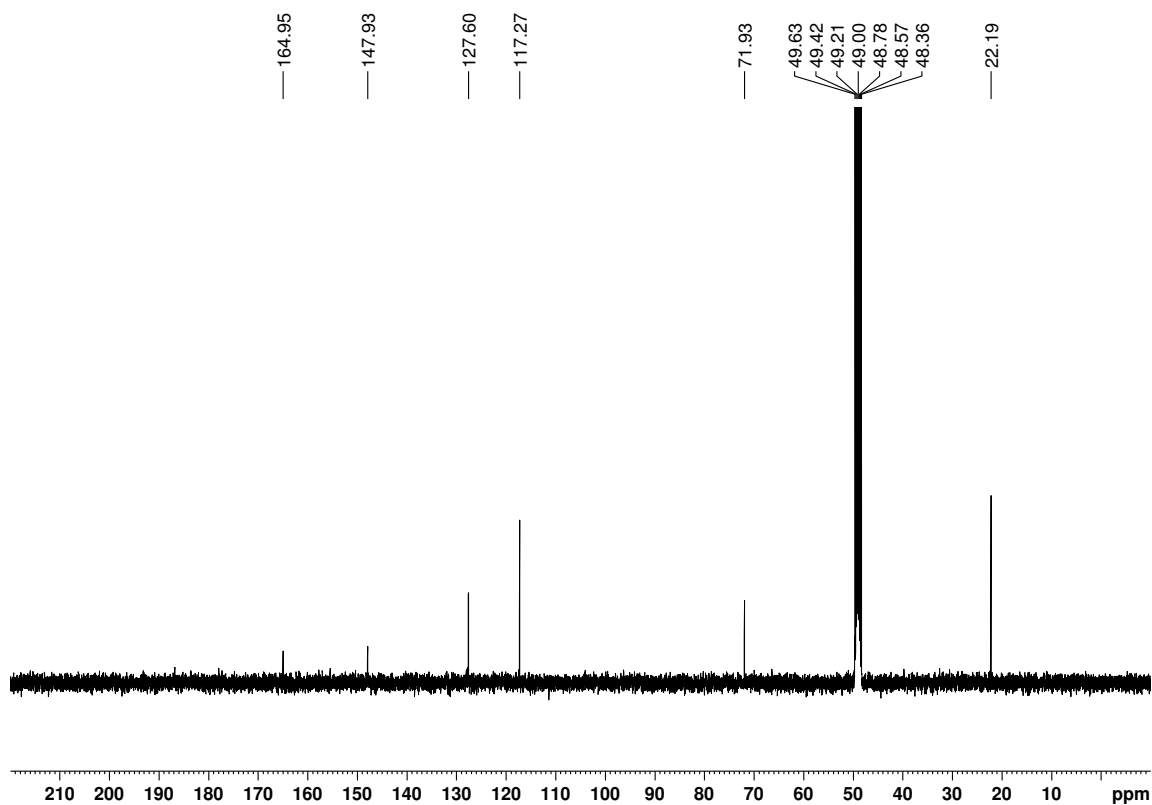
Appendix

^1H spectrum of **3a** (400 MHz, MeOD):



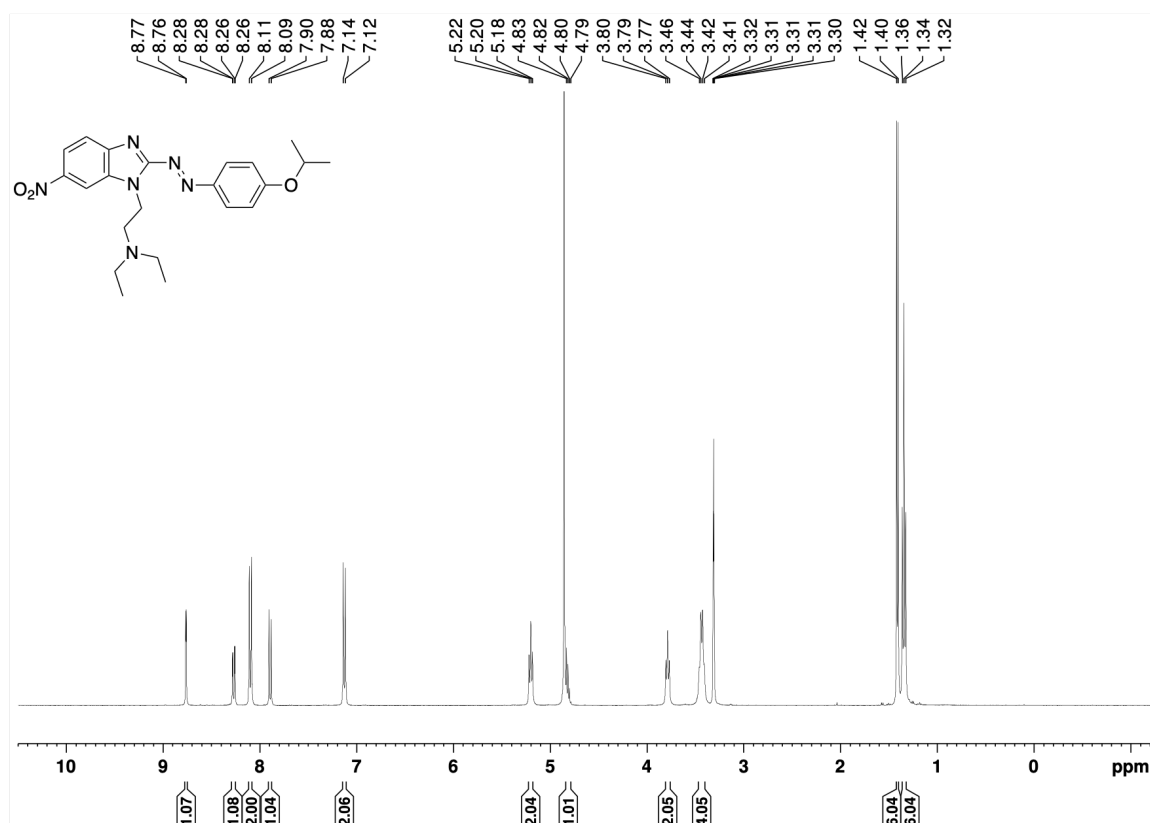
*Contains H_2O present in MeOD.

^{13}C spectrum of **3a** (101 MHz, MeOD):



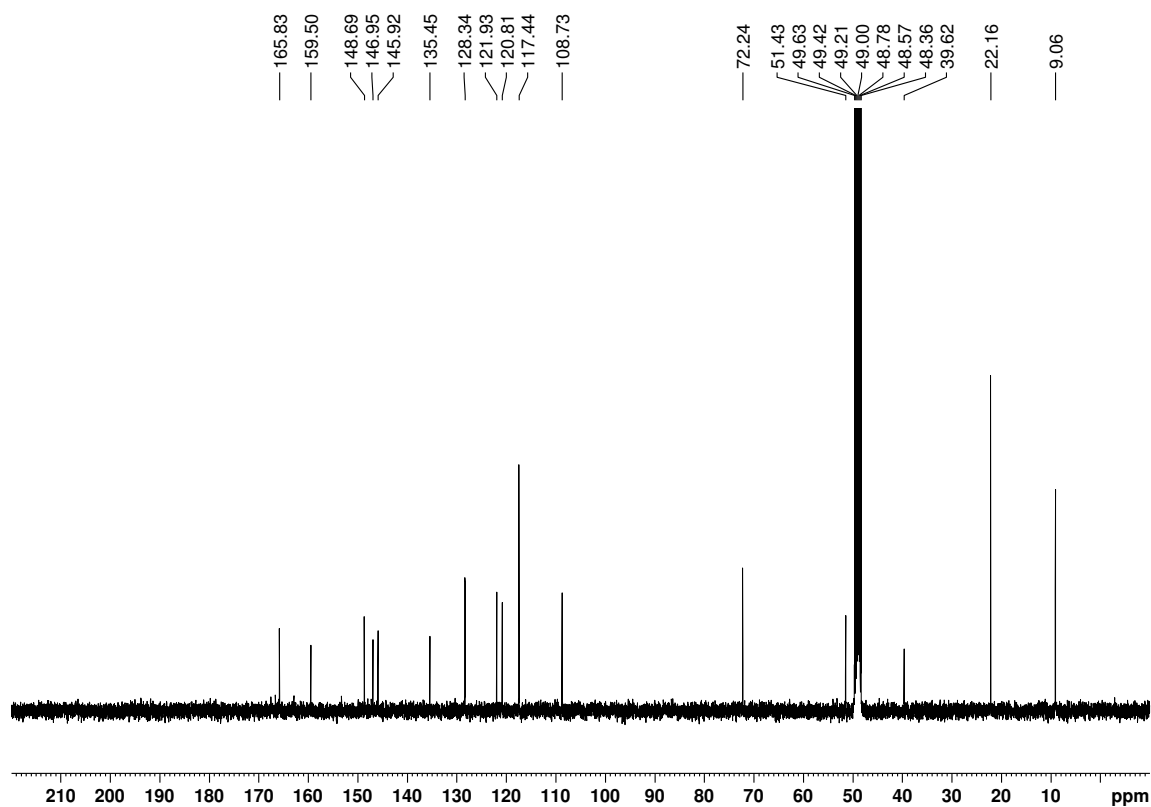
Appendix

^1H spectrum of **3b** (400 MHz, MeOD):



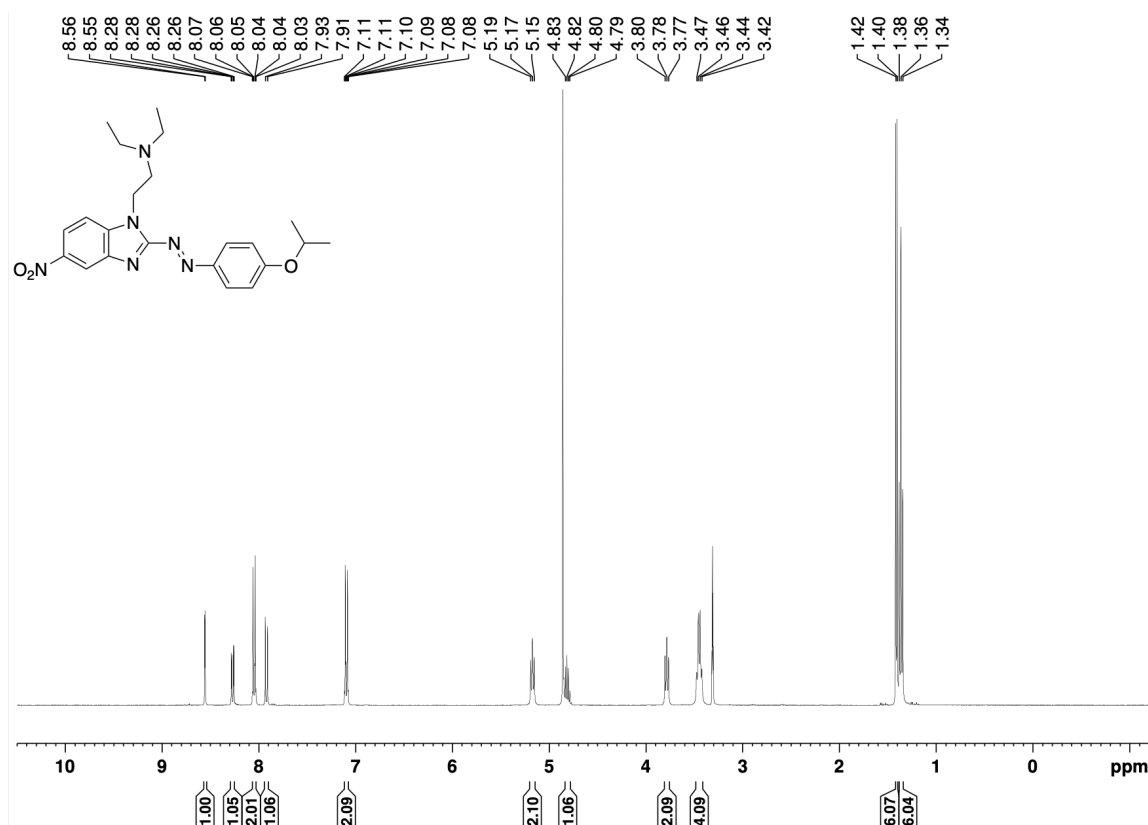
*Contains H₂O present in MeOD.

^{13}C spectrum of **3b** (101 MHz, MeOD):



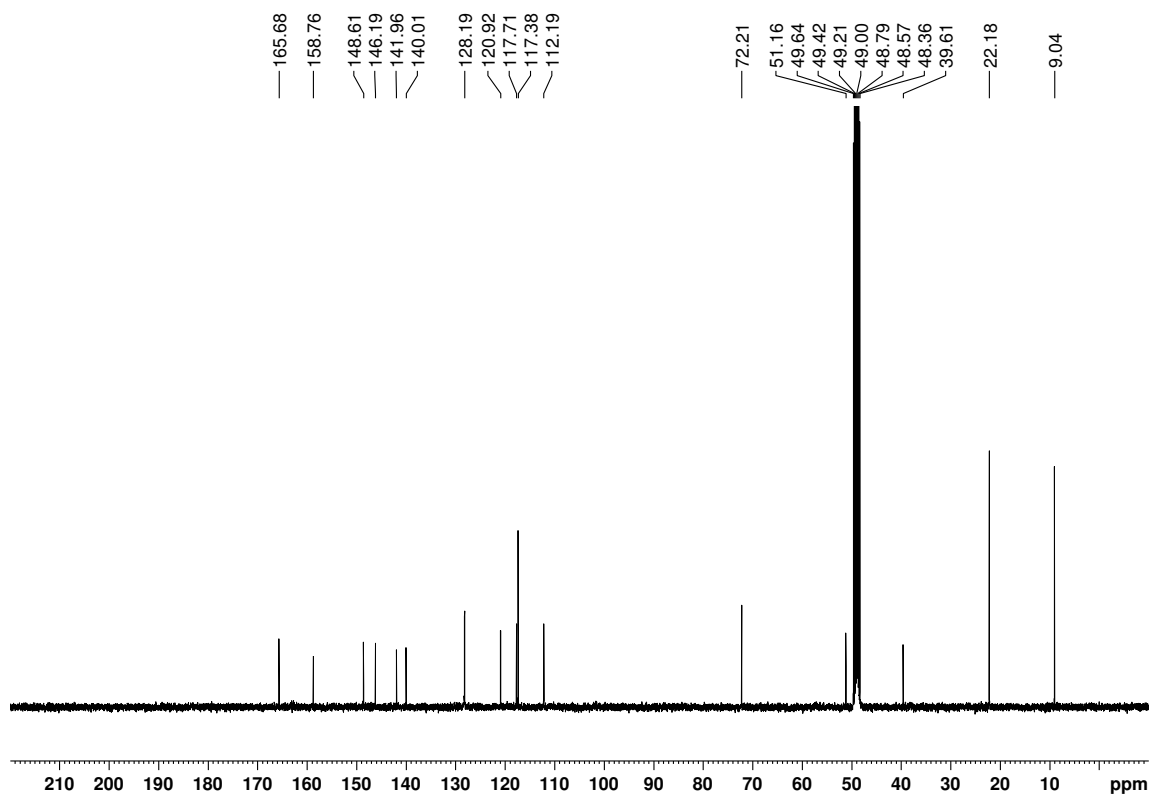
Appendix

^1H spectrum of **3c** (400 MHz, MeOD):



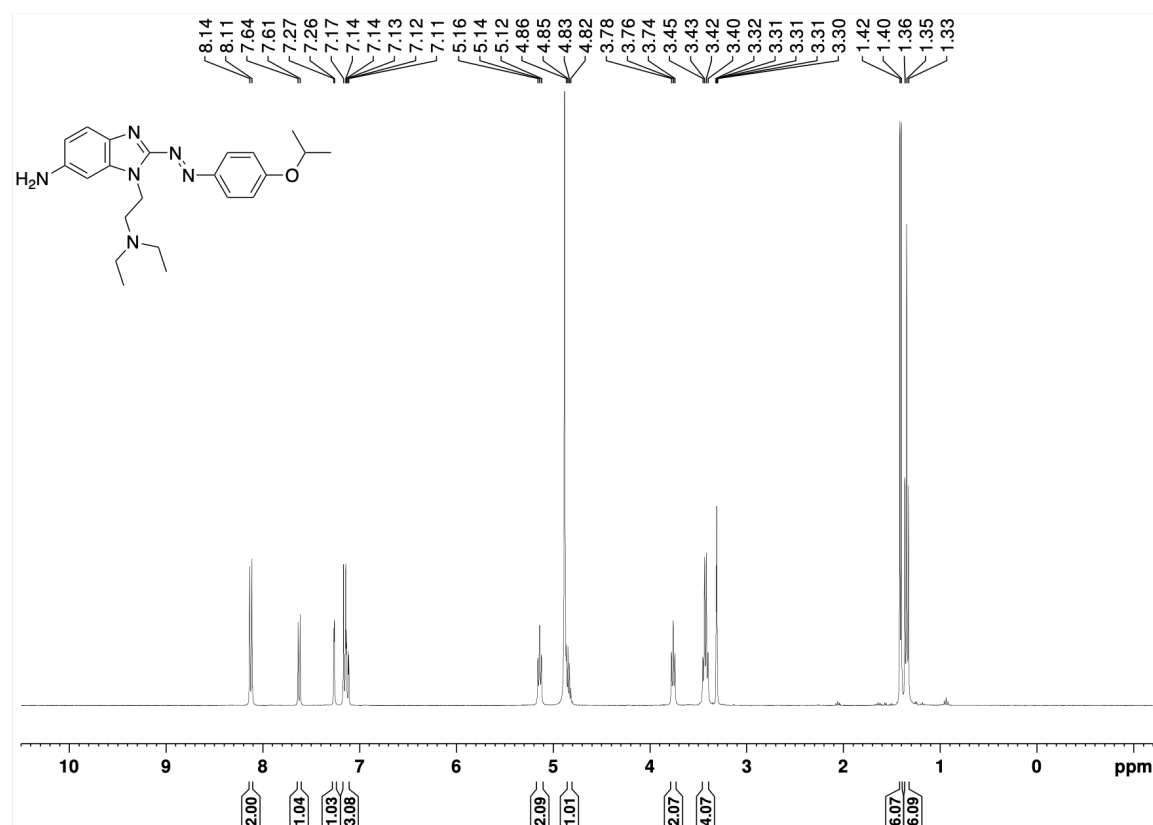
*Contains H_2O present in MeOD.

^{13}C spectrum of **3c** (101 MHz, MeOD):



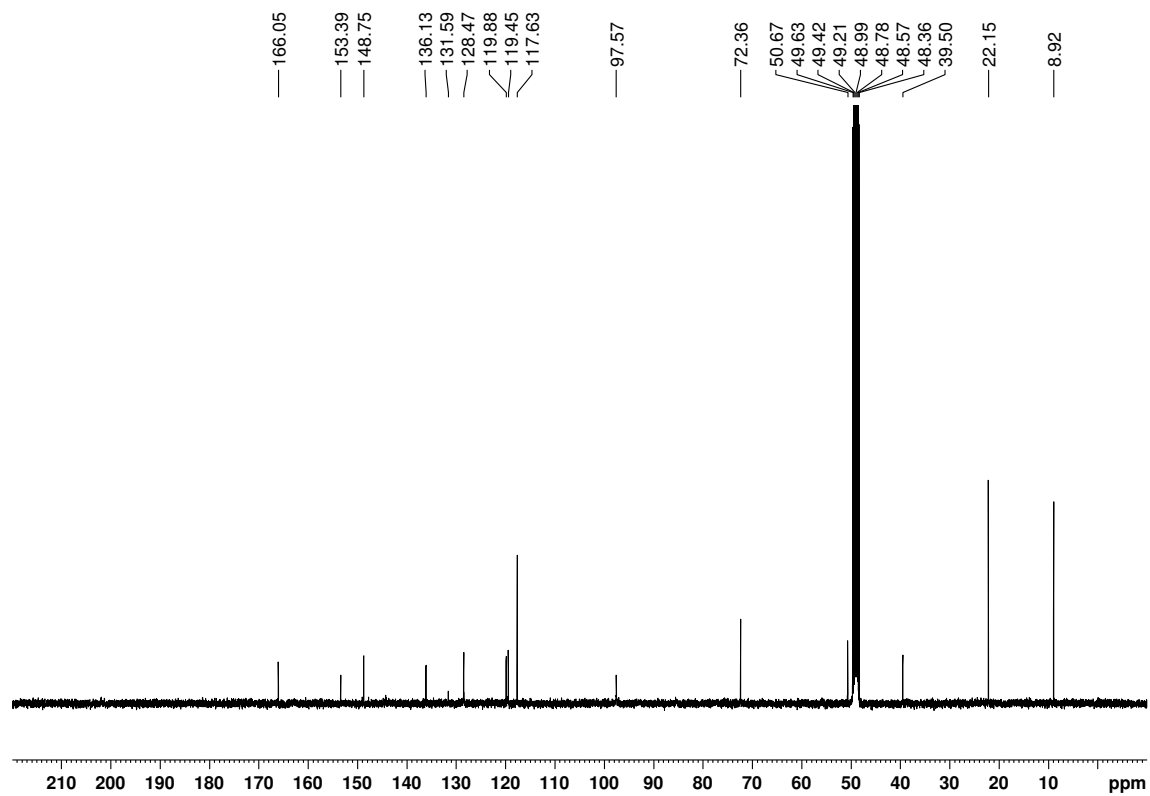
Appendix

^1H spectrum of **3b-NH₂** (400 MHz, MeOD):



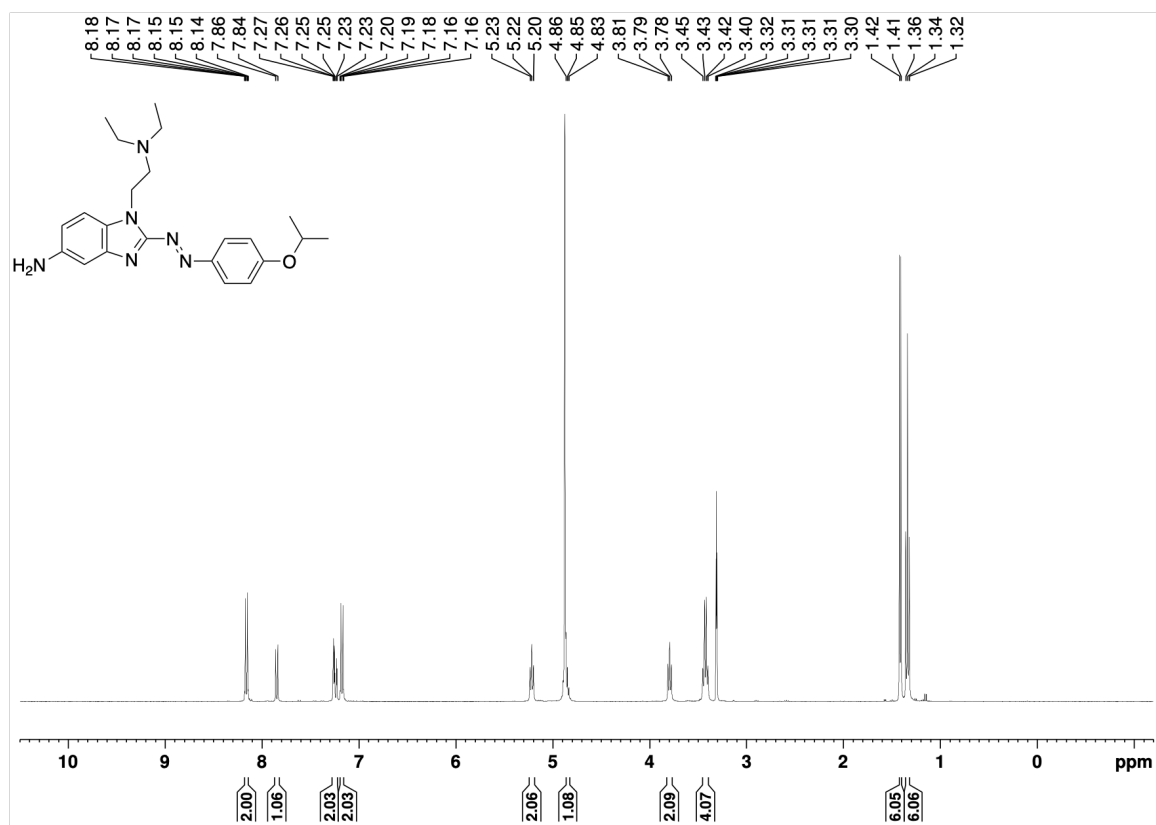
*Contains H₂O present in MeOD.

^{13}C spectrum of **3b-NH₂** (101 MHz, MeOD):



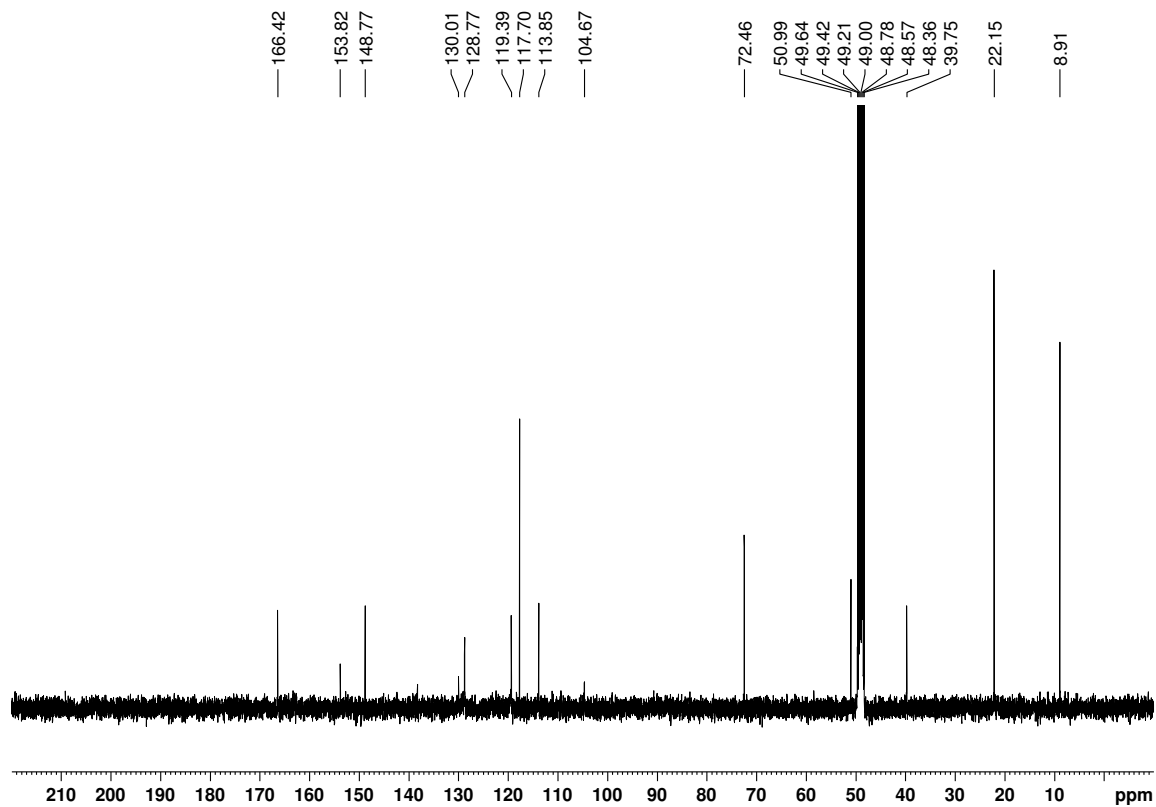
Appendix

^1H spectrum of **3d** (400 MHz, MeOD):



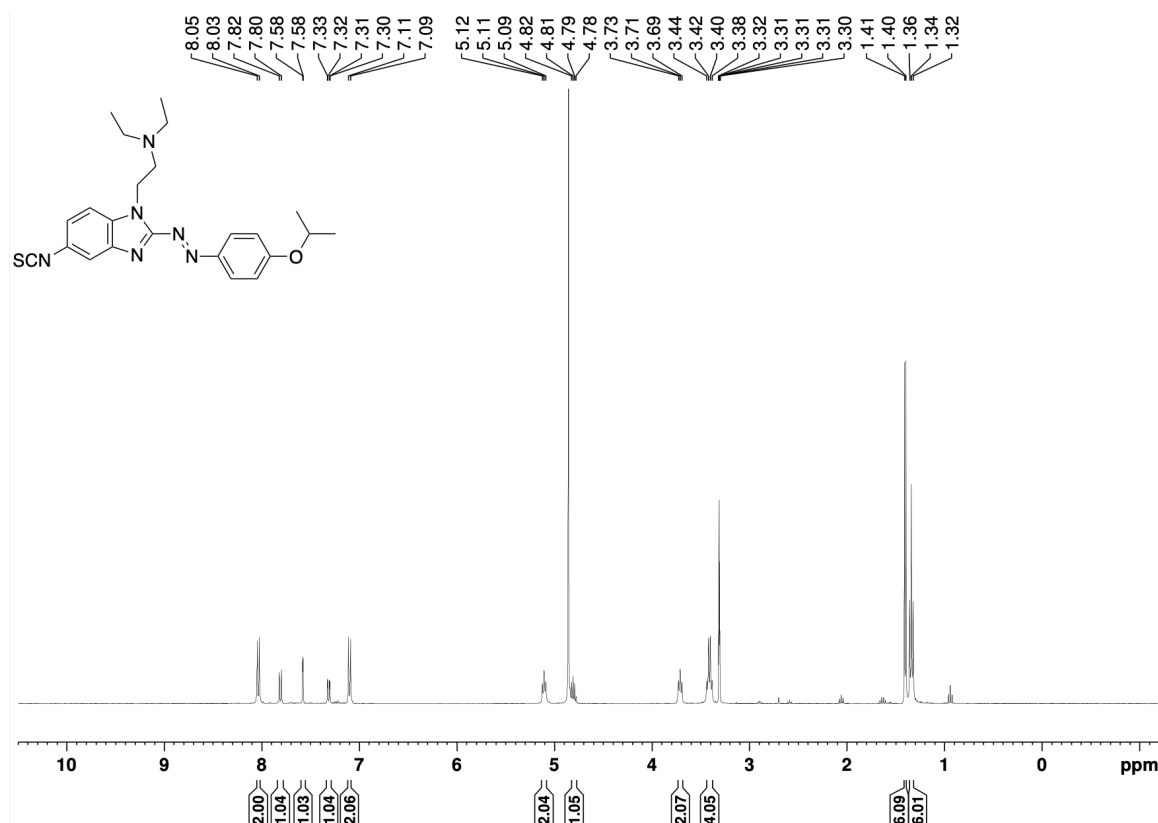
*Contains H_2O present in MeOD.

^{13}C spectrum of **3d** (101 MHz, MeOD):



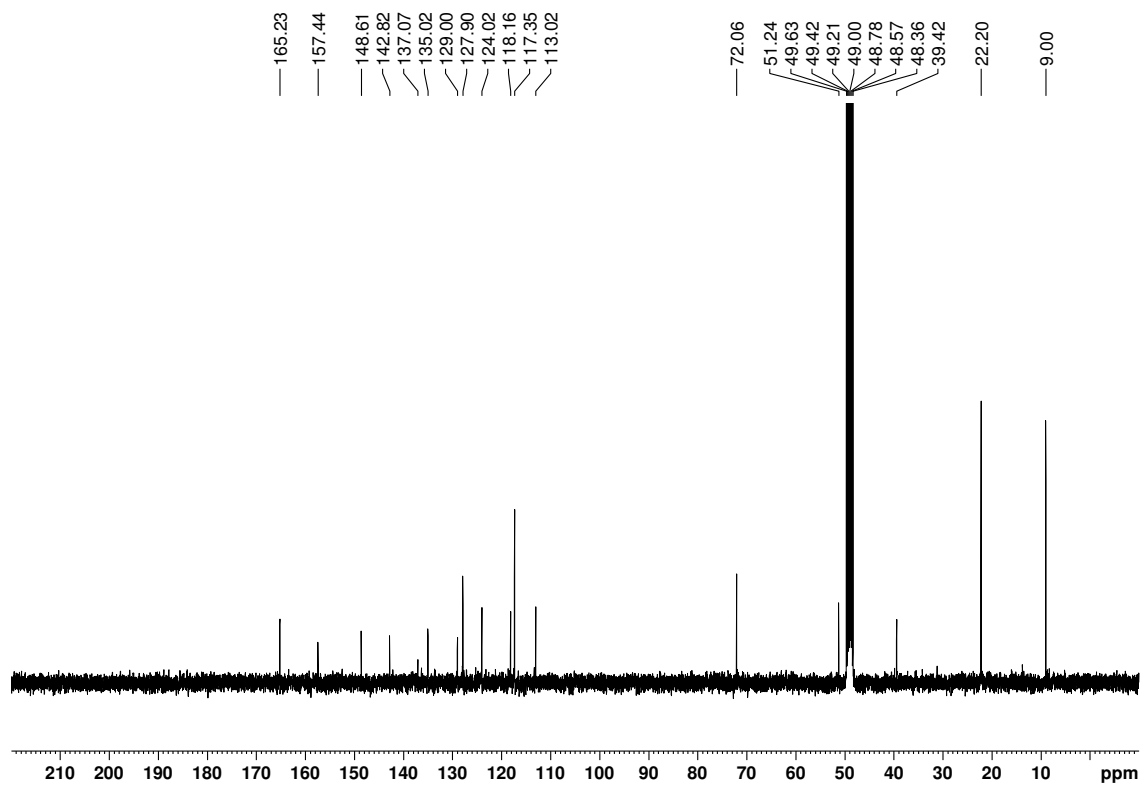
Appendix

^1H spectrum of **3e** (400 MHz, MeOD):



*Contains H_2O present in MeOD.

^{13}C spectrum of **3e** (101 MHz, MeOD):



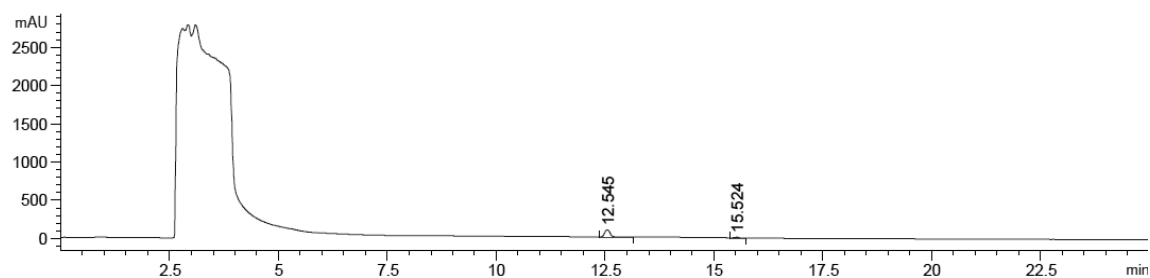
7.5 Appendix for Chapter 5

7.5.1 Analytical HPLC Chromatograms for Purity Determination

Experiments in this section were evaluated in DMSO.

Compound **AapF1**:

Detection at 220 nm: >99% purity

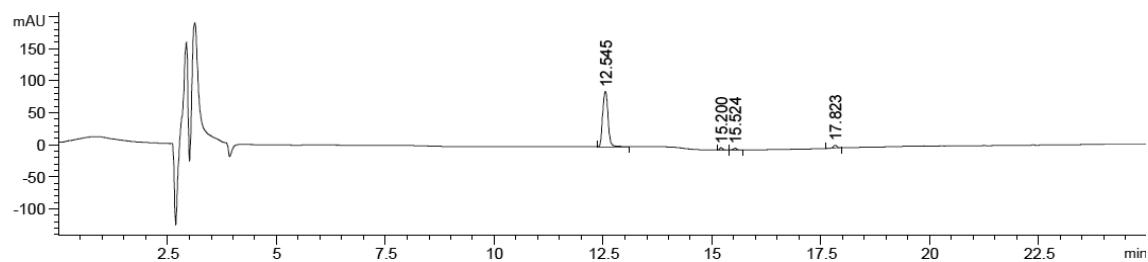


Signal 2: DAD1 B, Sig=220,4 Ref=off

Peak #	RetTime [min]	Type	Width [min]	Area [mAU*s]	Height [mAU]	Area %
1	12.545	BB	0.1400	812.61566	94.78011	93.7906
2	15.524	VB	0.0889	53.79906	8.85210	6.2094

*Peak 1 and Peak 2 are *cis*- and *trans*-isomers of compound **AapF1**, respectively.

Detection at 254 nm: 95% purity



Signal 3: DAD1 C, Sig=254,4 Ref=off

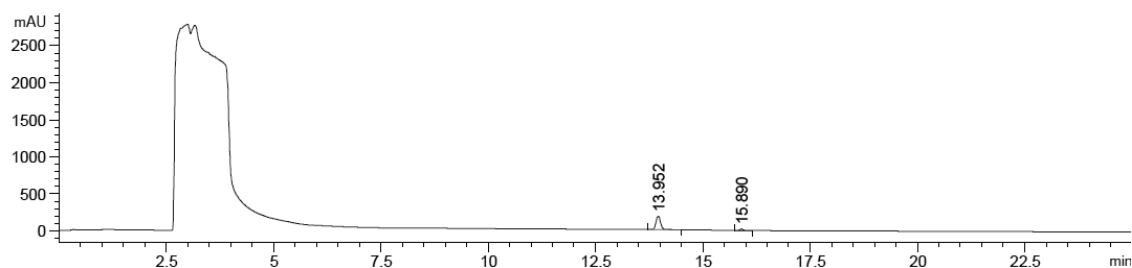
Peak #	RetTime [min]	Type	Width [min]	Area [mAU*s]	Height [mAU]	Area %
1	12.545	BB	0.1400	737.66748	86.08880	92.3711
2	15.200	BV	0.0756	18.31343	3.71112	2.2932
3	15.524	VB	0.0883	17.21208	2.94155	2.1553
4	17.823	BB	0.0899	25.39849	4.36699	3.1804

*Peak 1 and Peak 3 are *cis*- and *trans*-isomers of compound **AapF1**, respectively.

Appendix

Compound **AapF2**:

Detection at 220 nm: >99% purity

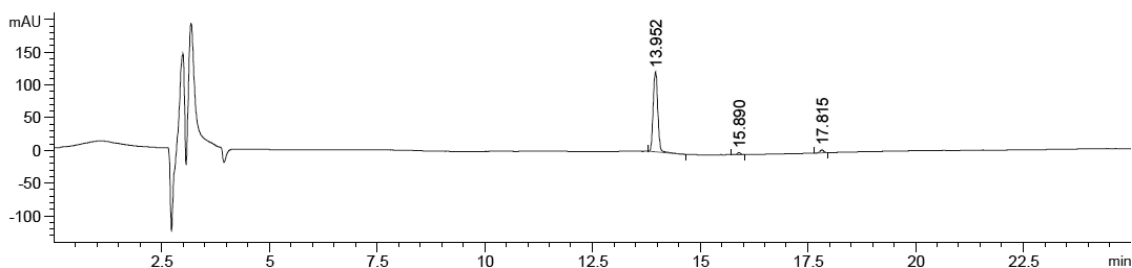


Signal 2: DAD1 B, Sig=220,4 Ref=off

Peak #	RetTime [min]	Type	Width [min]	Area [mAU*s]	Height [mAU]	Area %
1	13.952	BB	0.1192	1363.40710	182.31255	93.8208
2	15.890	BV R	0.0790	89.79578	17.18268	6.1792

*Peak 1 and Peak 2 are *cis*- and *trans*-isomers of compound **AapF2**, respectively.

Detection at 254 nm: 97% purity



Signal 3: DAD1 C, Sig=254,4 Ref=off

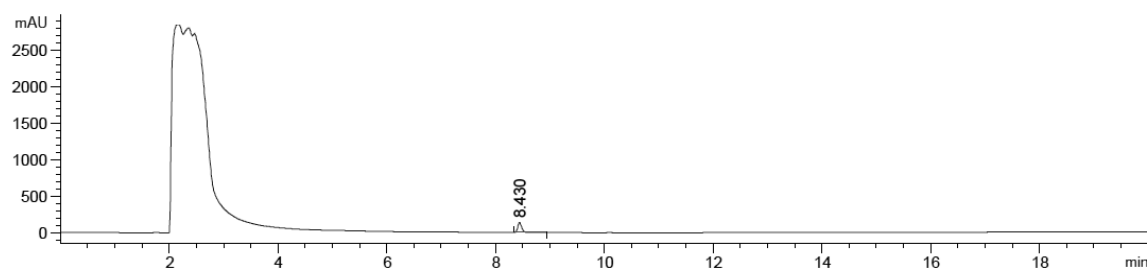
Peak #	RetTime [min]	Type	Width [min]	Area [mAU*s]	Height [mAU]	Area %
1	13.952	BB	0.1198	920.41302	122.24872	95.6745
2	15.890	BB	0.0779	17.20122	3.35076	1.7880
3	17.815	BB	0.0880	24.41133	4.31412	2.5375

*Peak 1 and Peak 2 are *cis*- and *trans*-isomers of compound **AapF2**, respectively.

Appendix

Compound **AapF3**:

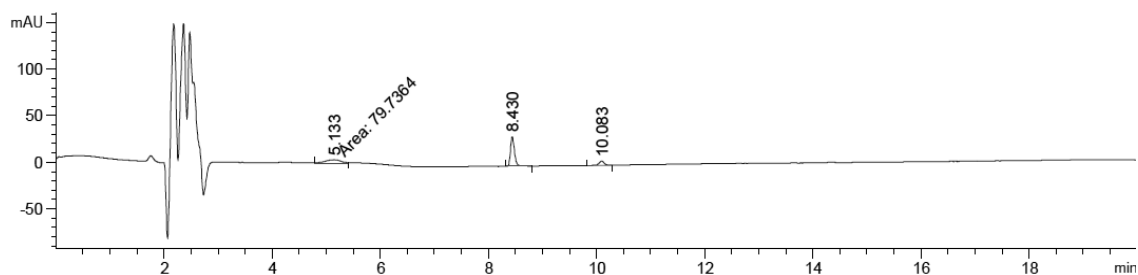
Detection at 220 nm: 99% purity



Signal 2: DAD1 B, Sig=220,4 Ref=off

Peak #	RetTime [min]	Type	Width [min]	Area [mAU*s]	Height [mAU]	Area %
1	8.430	BB	0.0791	692.04163	136.56175	100.0000

Detection at 254 nm: 90% purity



Signal 1: DAD1 A, Sig=254,4 Ref=off

Peak #	RetTime [min]	Type	Width [min]	Area [mAU*s]	Height [mAU]	Area %
1	5.133	MM	0.3588	79.73637	3.70372	29.4834
2	8.430	BB	0.0799	162.58618	31.68982	60.1181
3	10.083	BB	0.0979	28.12228	4.44107	10.3985

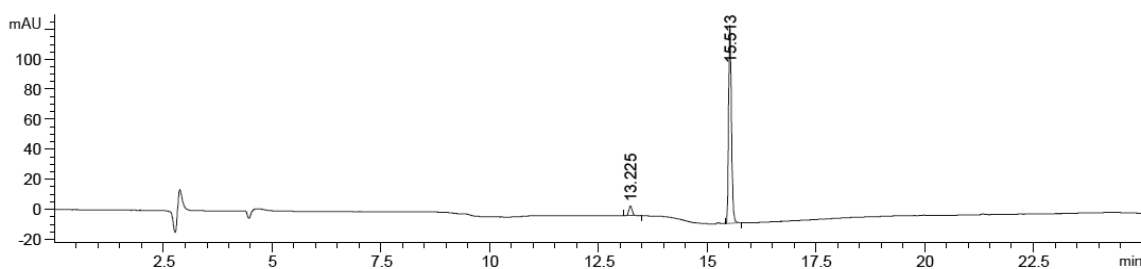
*Peak 1 and Peak 2 are *cis*- and *trans*-isomers of compound **AapF3**, respectively.

7.5.2 Analytical HPLC Chromatogram for PSS Determination

Compound **AapF1** (50 μ M in 50 mM TrisHCl Buffer + 0.5% DMSO, pH 7.5, injection volume 5 μ L):

Thermal equilibrium:

Detection at 285 nm: t_R *cis*-isomer = 13.225 min (6%), t_R *trans*-isomer = 15.513 min (94%).

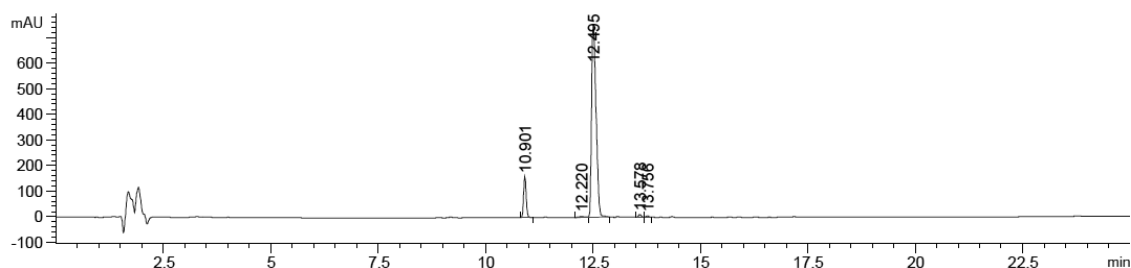


Signal 1: DAD1 A, Sig=285,4 Ref=off

Peak #	RetTime [min]	Type	Width [min]	Area [mAU*s]	Height [mAU]	Area %
1	13.225	BB	0.0859	37.22353	6.59052	5.7525
2	15.513	BB	0.0695	609.86530	133.03673	94.2475

Irradiation with $\lambda = 420$ nm for conversion from *cis*-isomer to *trans*-isomer:

Detection at 285 nm: t_R *cis*-isomer = 12.355 min (34%), t_R *trans*-isomer = 15.361 min (66%).



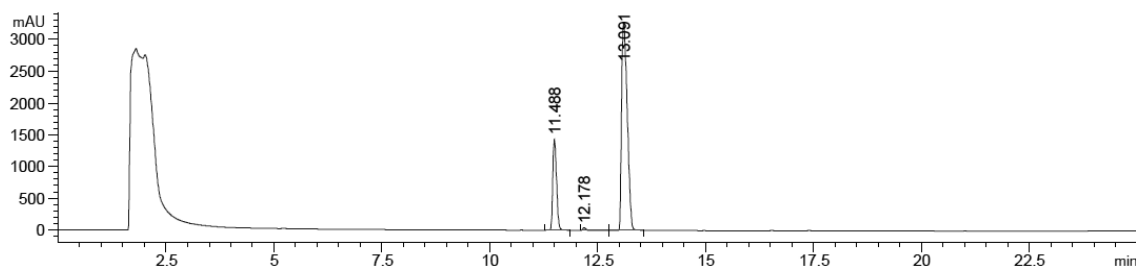
Signal 1: DAD1 A, Sig=285,4 Ref=off

Peak #	RetTime [min]	Type	Width [min]	Area [mAU*s]	Height [mAU]	Area %
1	12.355	BB	0.0903	168.05438	28.72329	33.8159
2	15.361	BB	0.0723	328.91464	70.69030	66.1841

Appendix

Irradiation with $\lambda = 340$ nm for conversion from *trans*-isomer to *cis*-isomer:

Detection at 285 nm: t_R *cis*-isomer = 12.362 min (94%), t_R *trans*-isomer = 15.333 min (6%).



Signal 1: DAD1 A, Sig=285,4 Ref=off

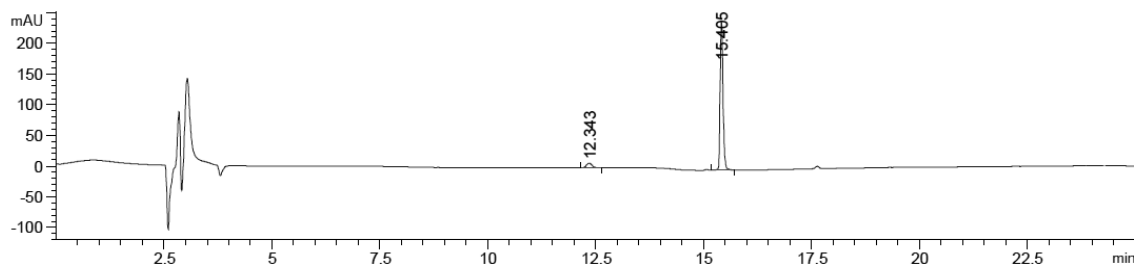
Peak #	RetTime [min]	Type	Width [min]	Area [mAU*s]	Height [mAU]	Area %
1	12.362	BB	0.0906	656.69287	111.68710	93.8153
2	15.333	BB	0.0823	43.29214	7.85349	6.1847

Appendix

Compound **AapF1** (50 μ M in DMSO, pH 7.5, injection volume 5 μ L):

Thermal equilibrium:

Detection at 285 nm: t_R *cis*-isomer = 12.343 min (5%), t_R *trans*-isomer = 15.405 min (95%).

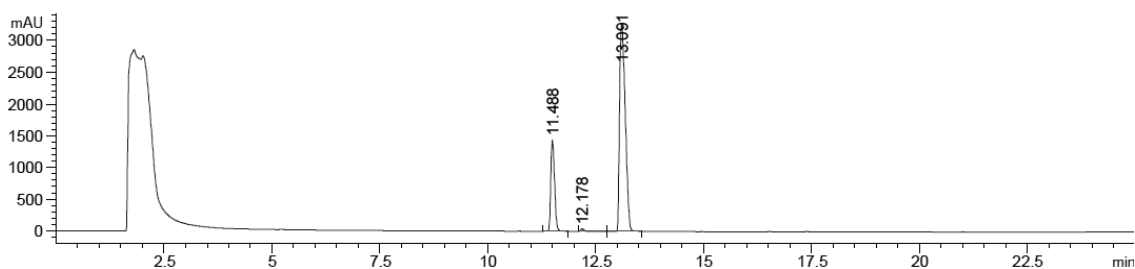


Signal 1: DAD1 A, Sig=285,4 Ref=off

Peak #	RetTime [min]	Type	Width [min]	Area [mAU*s]	Height [mAU]	Area %
1	12.343	BB	0.1387	58.74947	6.94258	4.9159
2	15.405	BB	0.0727	1136.34766	242.29875	95.0841

Irradiation with $\lambda = 420$ nm for conversion from *cis*-isomer to *trans*-isomer:

Detection at 285 nm: t_R *cis*-isomer = 12.559 min (31%), t_R *trans*-isomer = 15.561 min (69%).



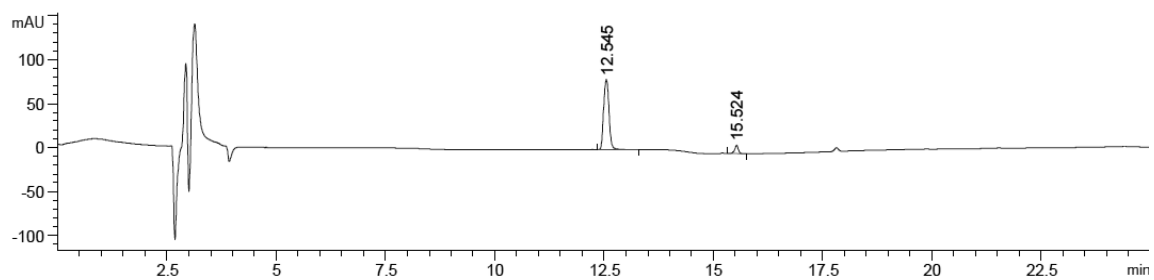
Signal 1: DAD1 A, Sig=285,4 Ref=off

Peak #	RetTime [min]	Type	Width [min]	Area [mAU*s]	Height [mAU]	Area %
1	12.559	BB	0.1380	312.54120	36.47517	31.4622
2	15.561	BB	0.0762	680.84454	141.31747	68.5378

Appendix

Irradiation with $\lambda = 340$ nm for conversion from *trans*-isomer to *cis*-isomer:

Detection at 285 nm: t_R *cis*-isomer = 12.545 min (92%), t_R *trans*-isomer = 15.524 min (8%).



Signal 1: DAD1 A, Sig=285,4 Ref=off

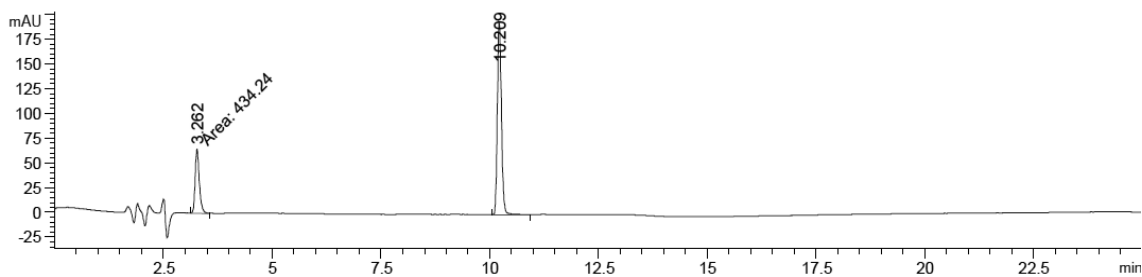
Peak #	RetTime [min]	Type	Width [min]	Area [mAU*s]	Height [mAU]	Area %
1	12.545	BB	0.1403	684.48907	79.62872	92.4134
2	15.524	BB	0.0882	56.19221	9.61071	7.5866

Appendix

Compound **AapF2** (50 μ M in 50 mM TrisHCl Buffer + 0.5% DMSO, pH 7.5, injection volume 5 μ L):

Thermal equilibrium:

Detection at 291 nm: t_R *cis*-isomer = 3.262 min (25%), t_R *trans*-isomer = 10.209 min (75%).

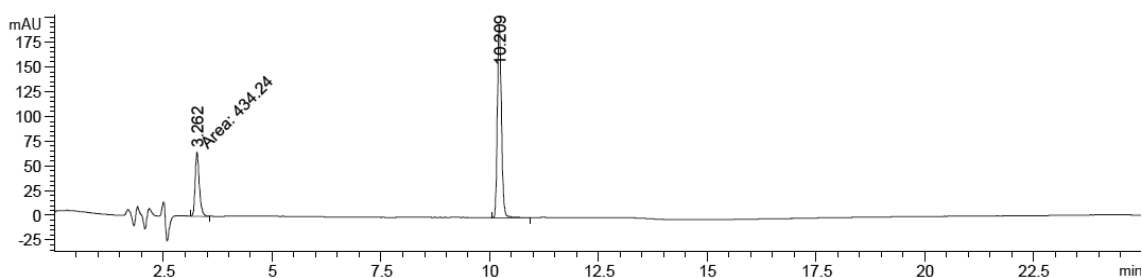


Signal 1: DAD1 A, Sig=291,4 Ref=off

Peak #	RetTime [min]	Type	Width [min]	Area [mAU*s]	Height [mAU]	Area %
1	3.262	MM	0.1110	434.23972	65.18752	25.4913
2	10.209	BB	0.1023	1269.24084	194.00095	74.5087

Irradiation with $\lambda = 420$ nm for conversion from *cis*-isomer to *trans*-isomer:

Detection at 291 nm: t_R *cis*-isomer = 3.260 min (39%), t_R *trans*-isomer = 10.226 min (61%).



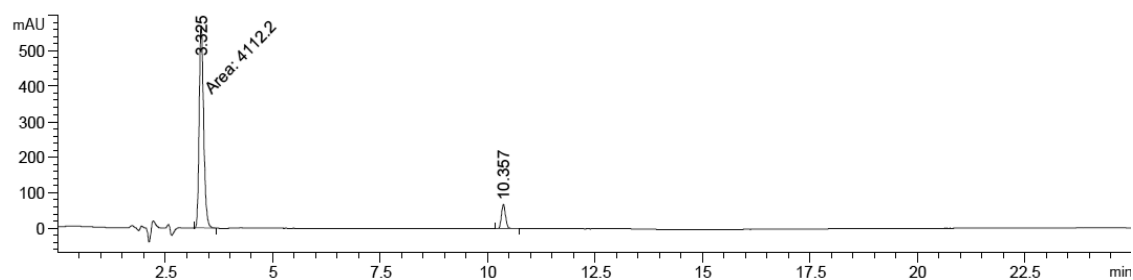
Signal 1: DAD1 A, Sig=291,4 Ref=off

Peak #	RetTime [min]	Type	Width [min]	Area [mAU*s]	Height [mAU]	Area %
1	3.260	MM	0.1103	482.52933	72.91040	38.6972
2	10.226	BB	0.1026	764.40546	116.44802	61.3028

Appendix

Irradiation with $\lambda = 365$ nm for conversion from *trans*-isomer to *cis*-isomer:

Detection at 291 nm: t_R *cis*-isomer = 3.325 min (90%), t_R *trans*-isomer = 10.357 min (10%).



Signal 1: DAD1 A, Sig=291,4 Ref=off

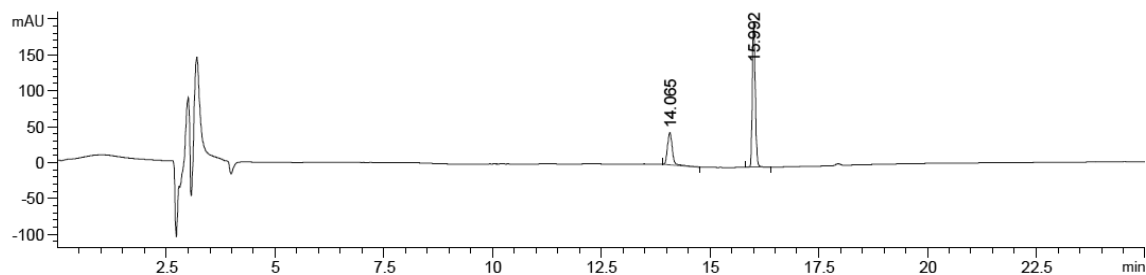
Peak #	RetTime [min]	Type	Width [min]	Area [mAU*s]	Height [mAU]	Area %
1	3.325	MM	0.1200	4112.20459	571.19824	90.0405
2	10.357	BB	0.1030	454.85400	68.92821	9.9595

Appendix

Compound **AapF2** (50 μ M in DMSO, pH 7.5, injection volume 5 μ L):

Thermal equilibrium:

Detection at 291 nm: t_R *cis*-isomer = 14.065 min (26%), t_R *trans*-isomer = 15.992 min (74%).

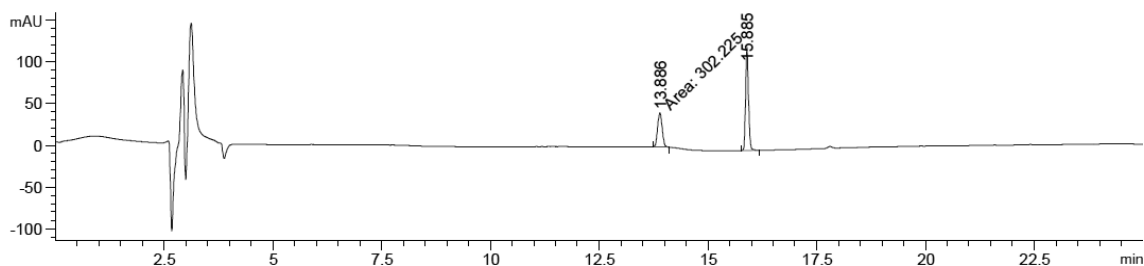


Signal 1: DAD1 A, Sig=291,4 Ref=off

Peak #	RetTime [min]	Type	Width [min]	Area [mAU*s]	Height [mAU]	Area %
1	14.065	BB	0.1223	343.31113	44.35573	26.2544
2	15.992	BB	0.0739	964.32141	201.37875	73.7456

Irradiation with $\lambda = 420$ nm for conversion from *cis*-isomer to *trans*-isomer:

Detection at 291 nm: t_R *cis*-isomer = 13.886 min (35%), t_R *trans*-isomer = 15.885 min (65%).



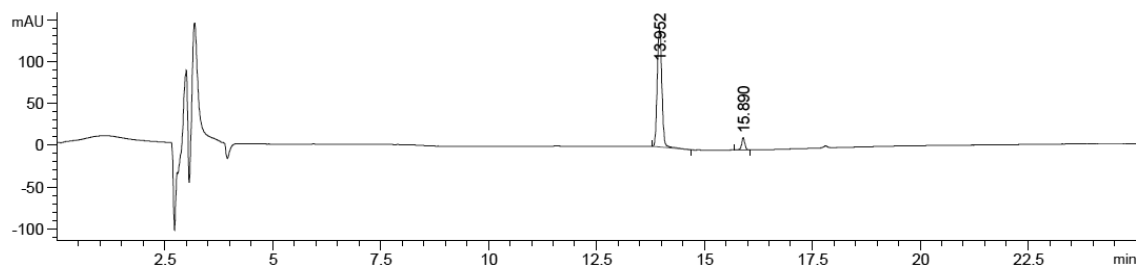
Signal 1: DAD1 A, Sig=291,4 Ref=off

Peak #	RetTime [min]	Type	Width [min]	Area [mAU*s]	Height [mAU]	Area %
1	13.886	MM	0.1230	302.22507	40.94640	34.6336
2	15.885	BB	0.0733	570.41144	120.43083	65.3664

Appendix

Irradiation with $\lambda = 365$ nm for conversion from *trans*-isomer to *cis*-isomer:

Detection at 291 nm: t_R *cis*-isomer = 13.952min (93%), t_R *trans*-isomer = 15.890 min (7%).



Signal 1: DAD1 A, Sig=291,4 Ref=off

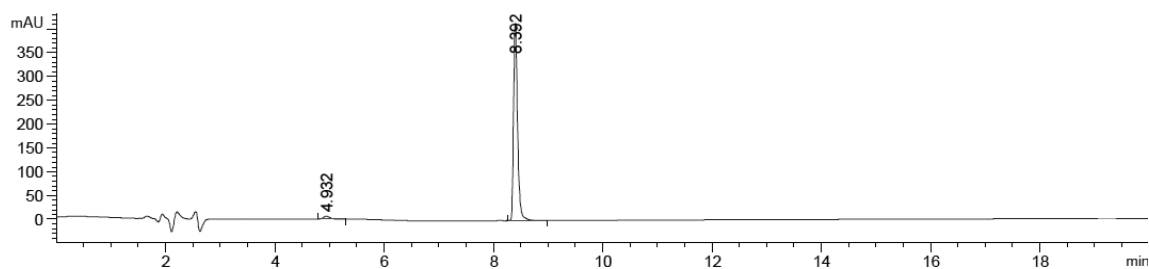
Peak #	RetTime [min]	Type	Width [min]	Area [mAU*s]	Height [mAU]	Area %
1	13.952	BB	0.1194	1051.34814	140.26959	93.3428
2	15.890	BB	0.0773	74.98245	14.76414	6.6572

Appendix

Compound **AapF3** (50 μ M in 50 mM TrisHCl Buffer + 0.5% DMSO, pH 7.5, injection volume 5 μ L):

Thermal equilibrium:

Detection at 296 nm: t_R *cis*-isomer = 4.932 min (2%), t_R *trans*-isomer = 8.392 min (98%).

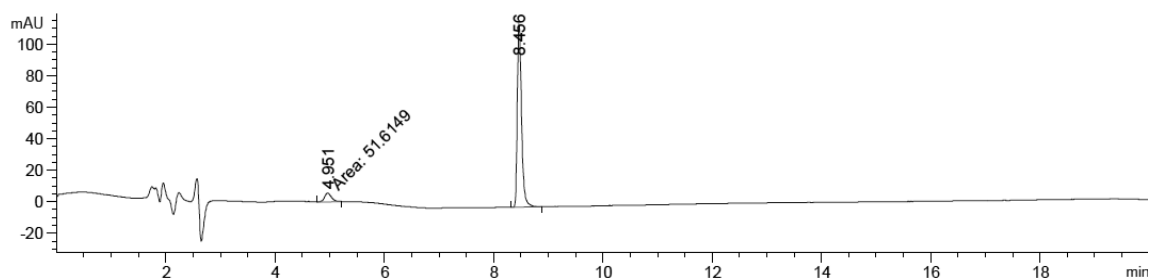


Signal 3: DAD1 C, Sig=296,4 Ref=off

Peak #	RetTime [min]	Type	Width [min]	Area [mAU*s]	Height [mAU]	Area %
1	4.932	BB	0.1260	51.27573	6.23096	2.3582
2	8.392	BB	0.0779	2123.07593	413.48053	97.6418

Irradiation with $\lambda = 528$ nm for conversion from *cis*-isomer to *trans*-isomer:

Detection at 296 nm: t_R *cis*-isomer = 4.951 min (8%), t_R *trans*-isomer = 8.456 min (92%).



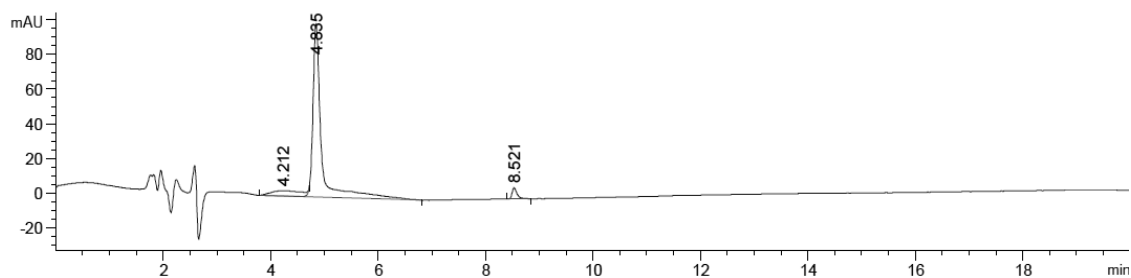
Signal 3: DAD1 C, Sig=296,4 Ref=off

Peak #	RetTime [min]	Type	Width [min]	Area [mAU*s]	Height [mAU]	Area %
1	4.951	MM	0.1522	51.61485	5.65268	7.5786
2	8.456	BB	0.0833	629.44934	116.08516	92.4214

Appendix

Irradiation with $\lambda = 365$ nm for conversion from *trans*-isomer to *cis*-isomer:

Detection at 296 nm: t_R *cis*-isomer = 4.835 min (97%), t_R *trans*-isomer = 8.521 min (3%).



Signal 3: DAD1 C, Sig=296,4 Ref=off

Peak #	RetTime [min]	Type	Width [min]	Area [mAU*s]	Height [mAU]	Area %
1	4.212	BV E	0.4682	118.53583	2.99194	9.3389
2	4.835	VB R	0.1600	1109.85620	99.60580	87.4403
3	8.521	BB	0.0971	40.88054	6.35290	3.2208

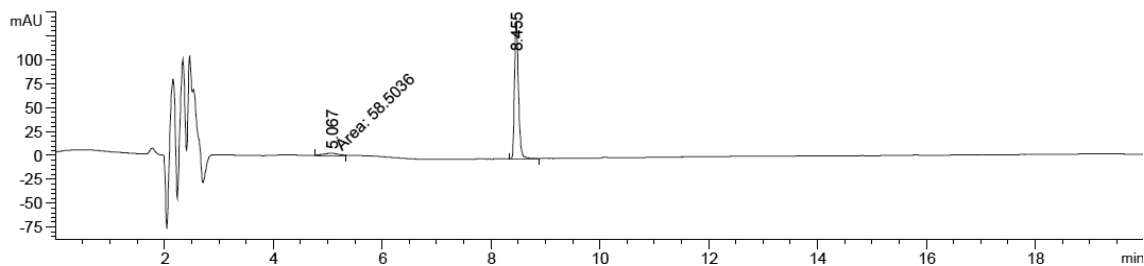
*Peak 1 and Peak 2 are considered to be the *cis*-isomer, while Peak 3 is the *trans*-isomer.

Appendix

Compound **AapF3** (50 μ M in DMSO, pH 7.5, injection volume 5 μ L):

Thermal equilibrium:

Detection at 301 nm: t_R *cis*-isomer = 5.067 min (7%), t_R *trans*-isomer = 8.455 min (93%).

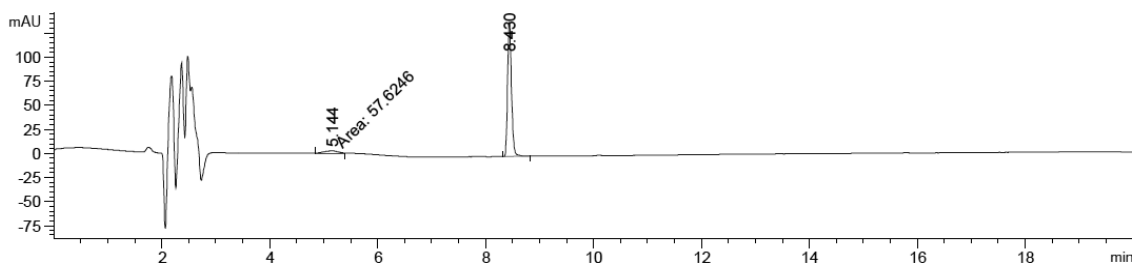


Signal 7: DAD1 G, Sig=301,4 Ref=off

Peak #	RetTime [min]	Type	Width [min]	Area [mAU*s]	Height [mAU]	Area %
1	5.067	MM	0.3721	58.50362	2.62046	7.4389
2	8.455	BB	0.0773	727.95471	143.25841	92.5611

Irradiation with $\lambda = 528$ nm for conversion from *cis*-isomer to *trans*-isomer:

Detection at 301 nm: t_R *cis*-isomer = 5.144 min (8%), t_R *trans*-isomer = 8.430 min (92%).



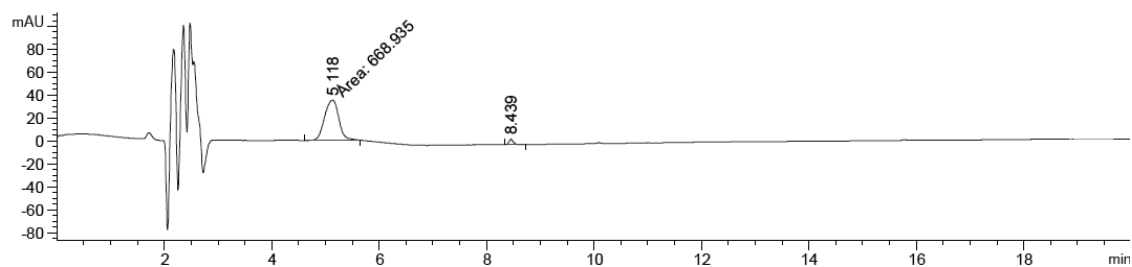
Signal 7: DAD1 G, Sig=301,4 Ref=off

Peak #	RetTime [min]	Type	Width [min]	Area [mAU*s]	Height [mAU]	Area %
1	5.144	MM	0.3257	57.62464	2.94907	7.5955
2	8.430	BB	0.0767	701.04749	139.24420	92.4045

Appendix

Irradiation with $\lambda = 365$ nm for conversion from *trans*-isomer to *cis*-isomer:

Detection at 301 nm: t_R *cis*-isomer = 5.118 min (96%), t_R *trans*-isomer = 8.439 min (4%).

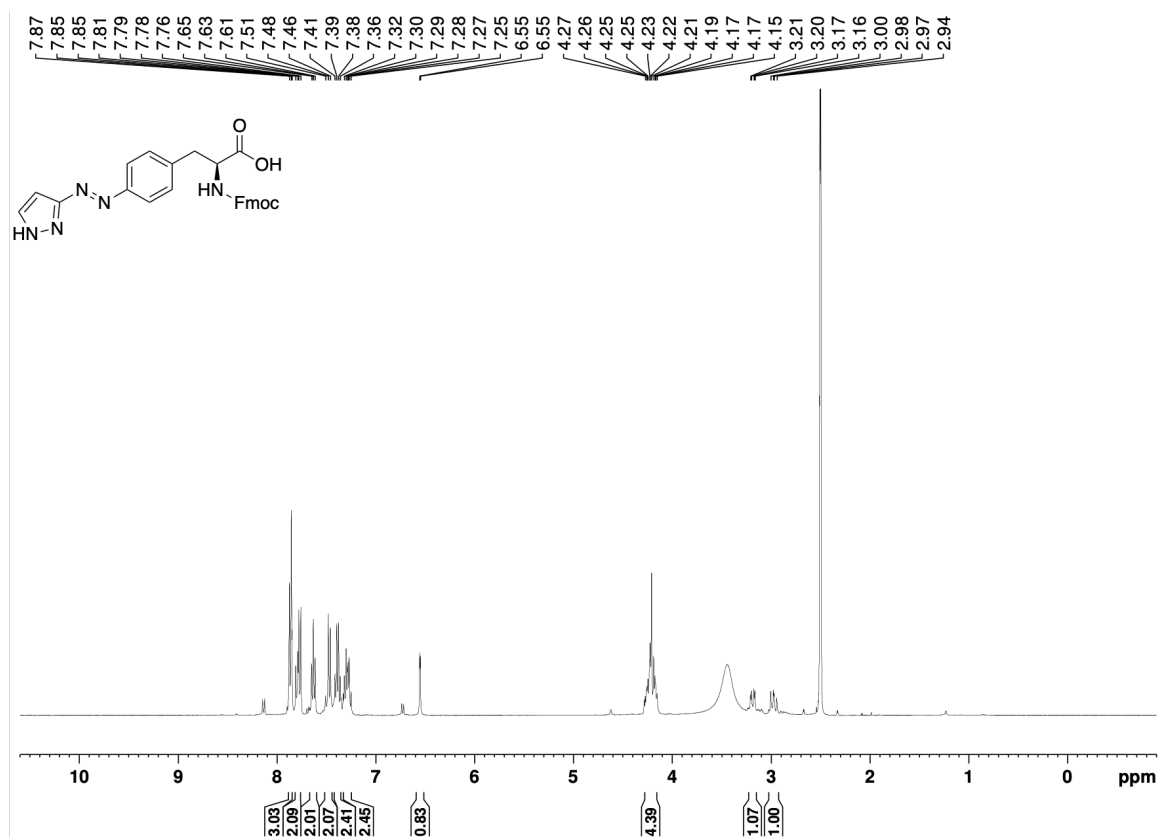


Signal 7: DAD1 G, Sig=301,4 Ref=off

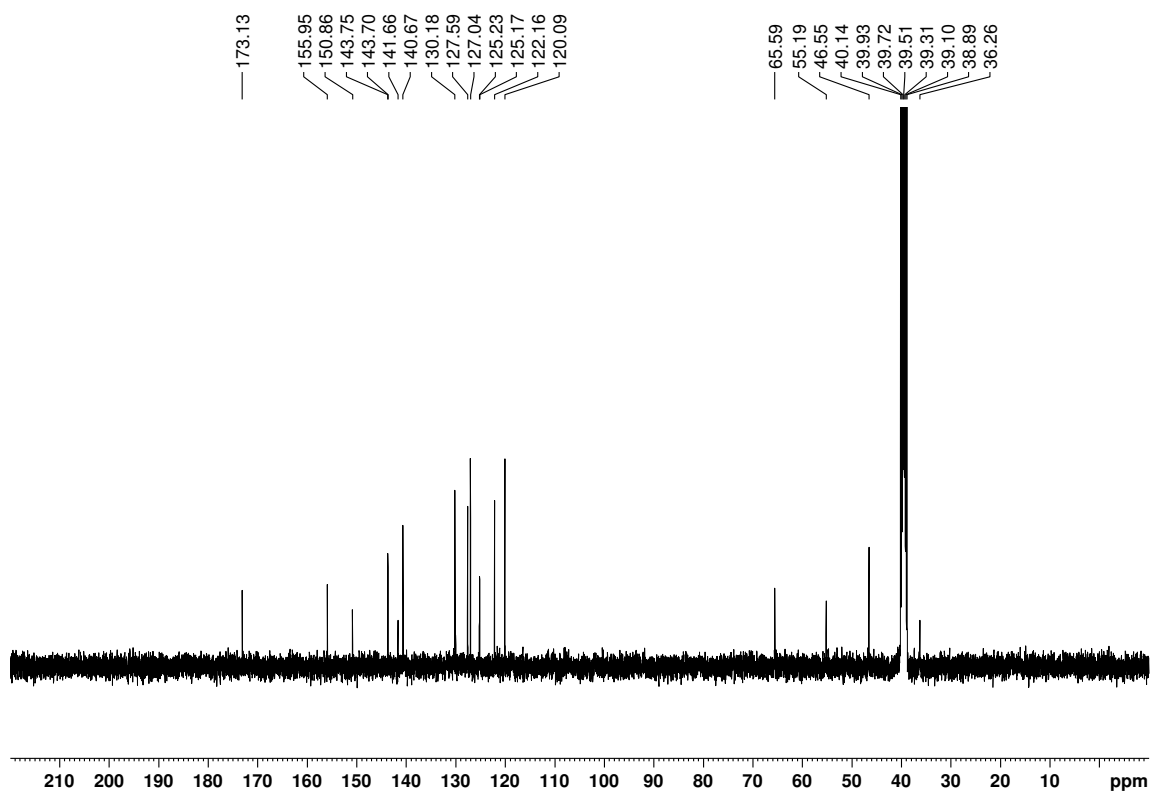
Peak #	RetTime [min]	Type	Width [min]	Area [mAU*s]	Height [mAU]	Area %
1	5.118	MM	0.3134	668.93469	35.57063	96.3372
2	8.439	BB	0.0870	25.43335	4.56446	3.6628

7.5.3 NMR Spectra

^1H spectrum of **3** (400 MHz, $\text{DMSO-}d_6$):

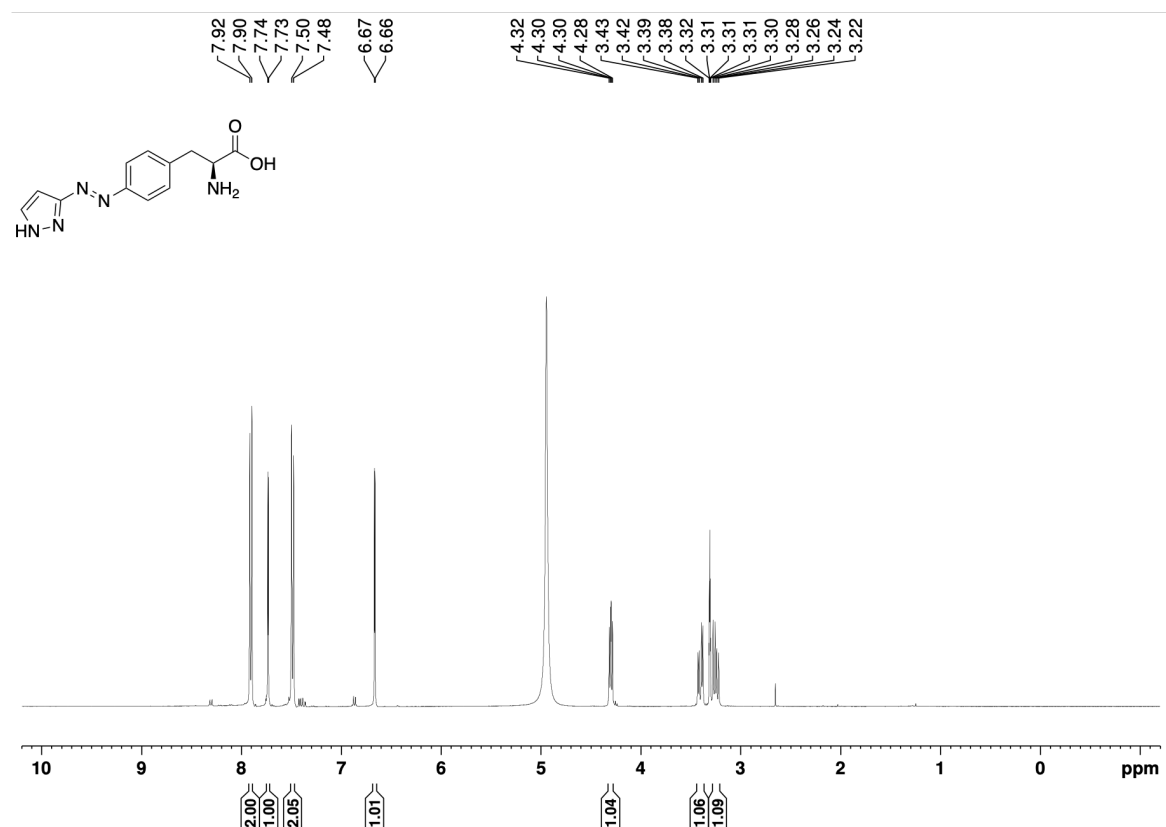


^{13}C spectrum of **3** (101 MHz, $\text{DMSO-}d_6$):

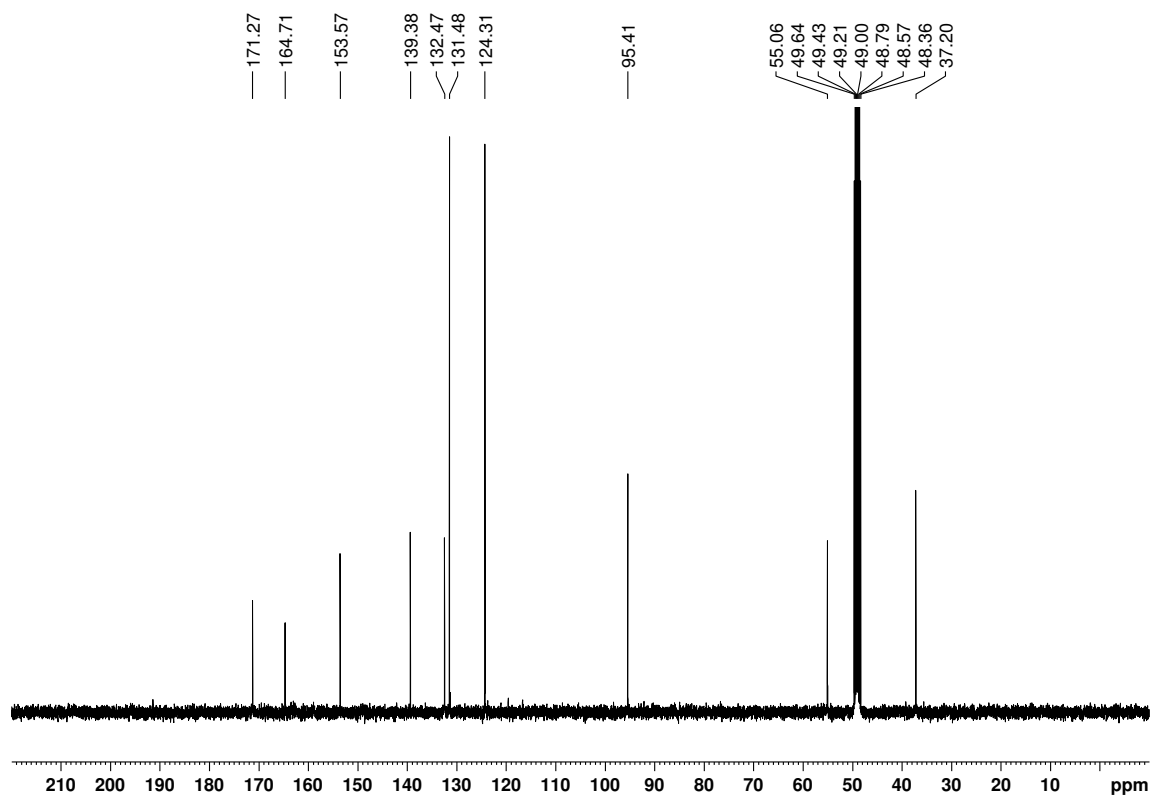


Appendix

^1H spectrum of **AapF1** (400 MHz, MeOD):

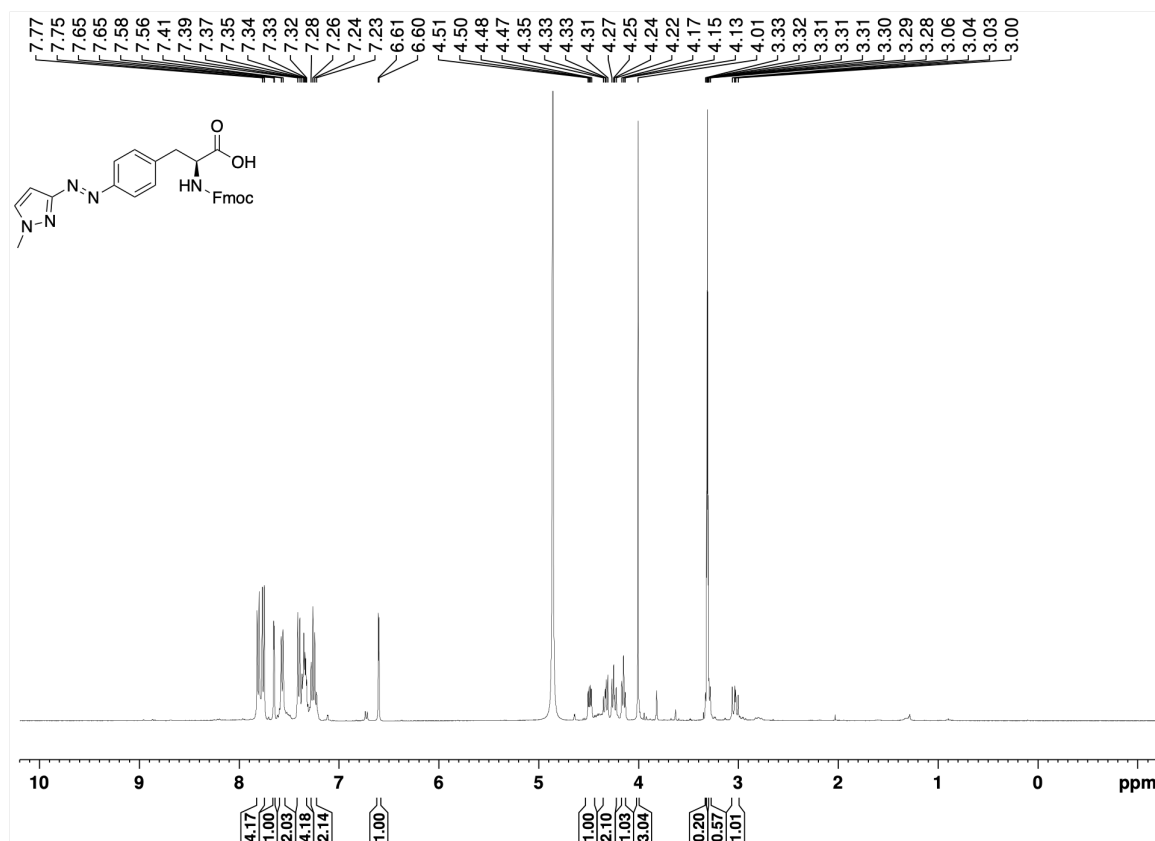


^{13}C spectrum of **AapF1** (101 MHz, MeOD):

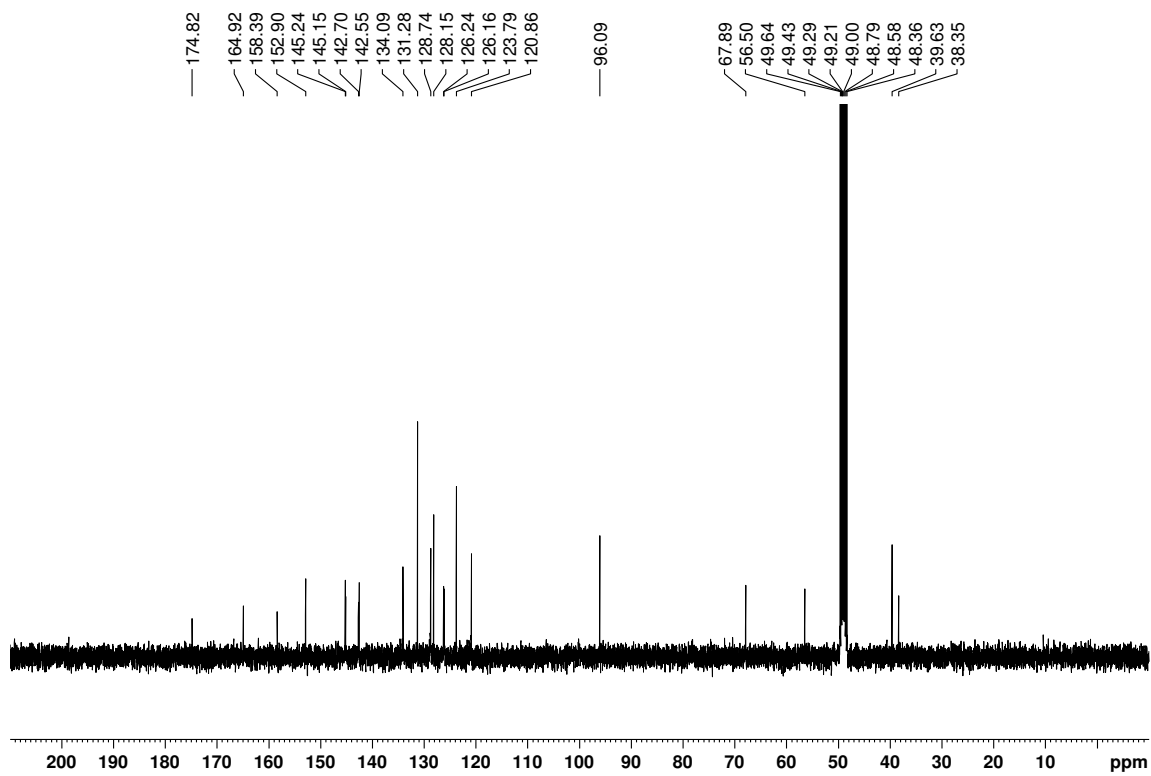


Appendix

^1H spectrum of **4** (400 MHz, MeOD):

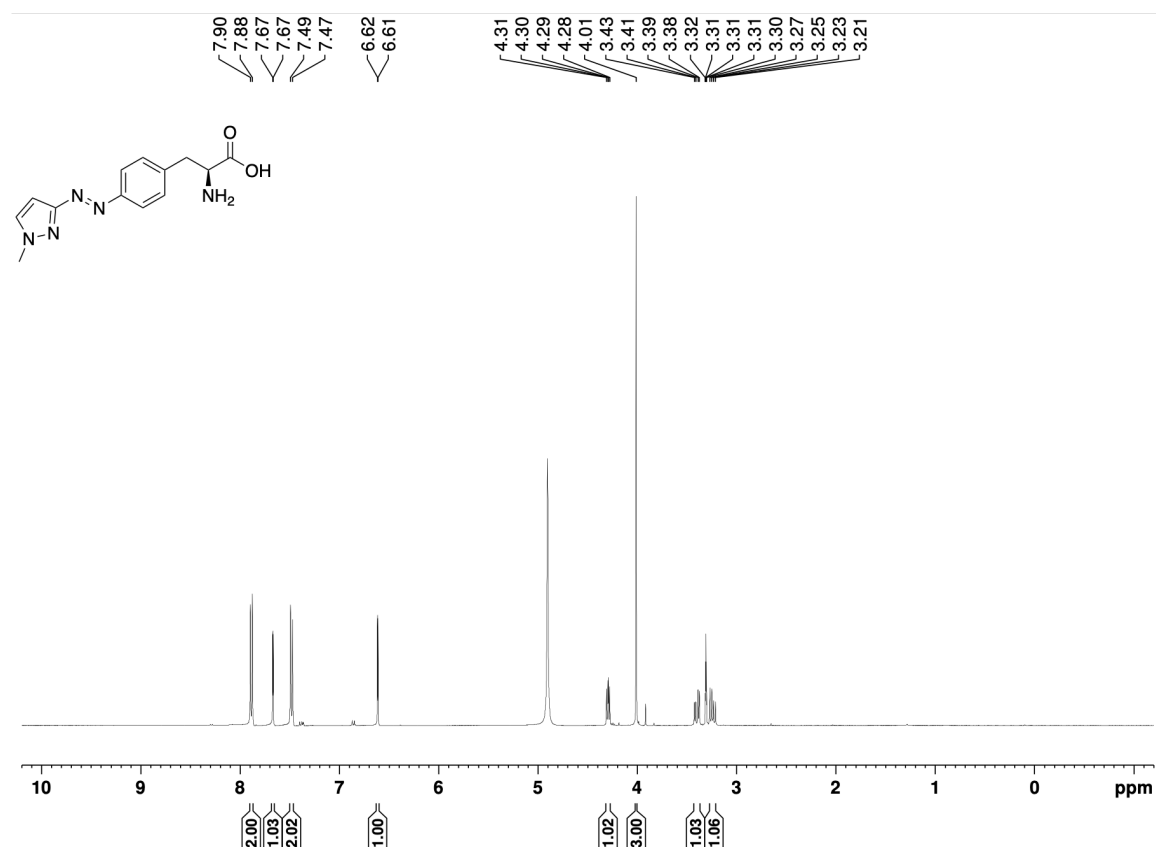


^{13}C spectrum of **4** (101 MHz, MeOD):

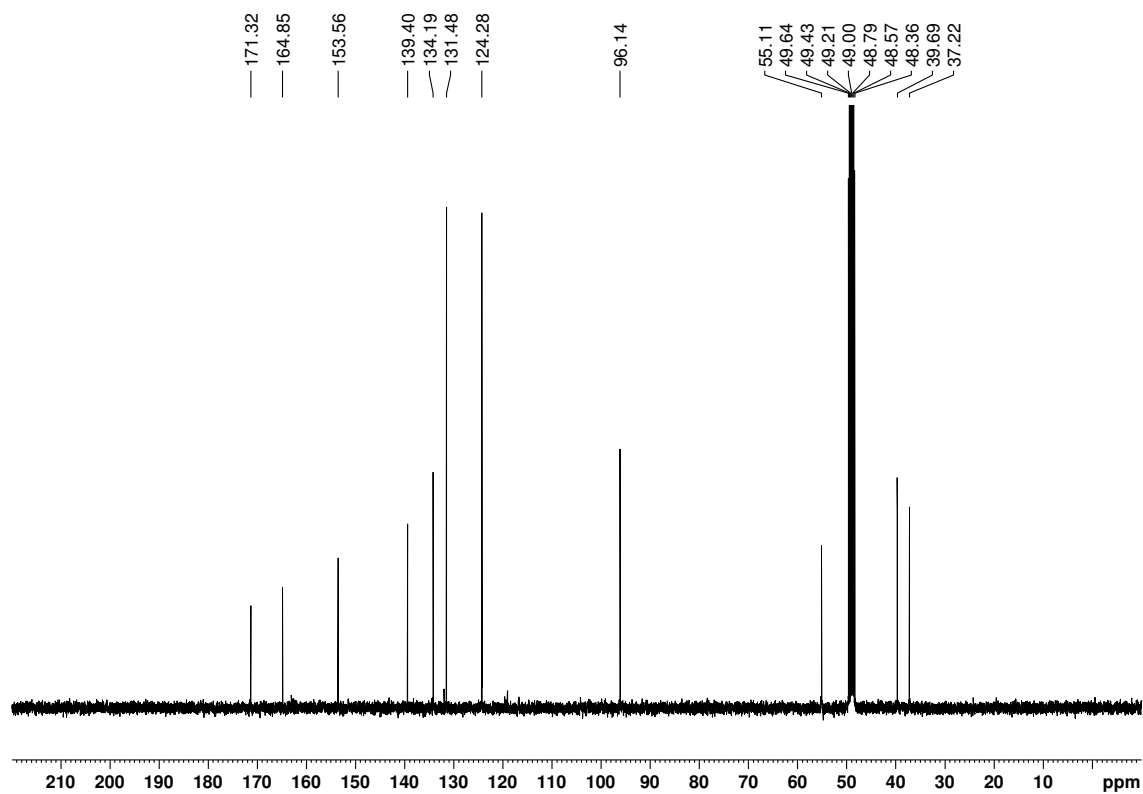


Appendix

^1H spectrum of **AapF2** (400 MHz, MeOD):

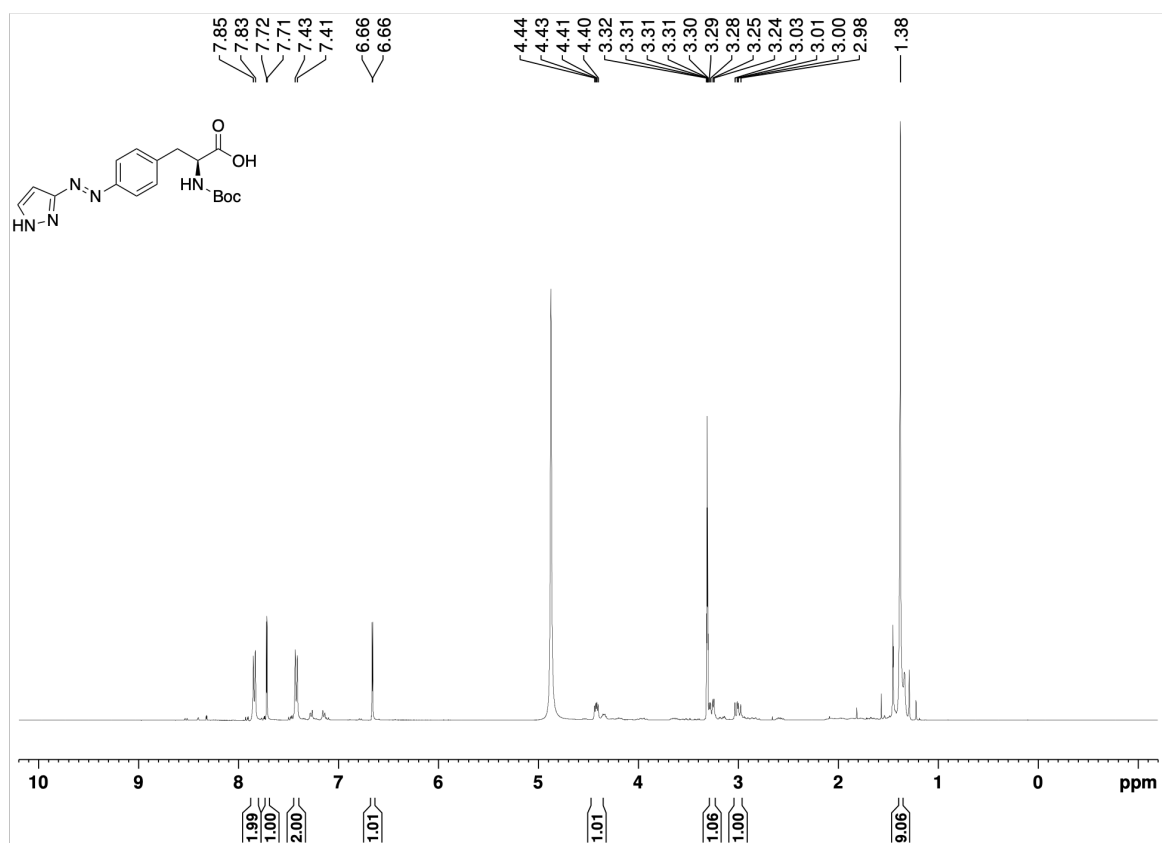


^{13}C spectrum of **AapF2** (101 MHz, MeOD):

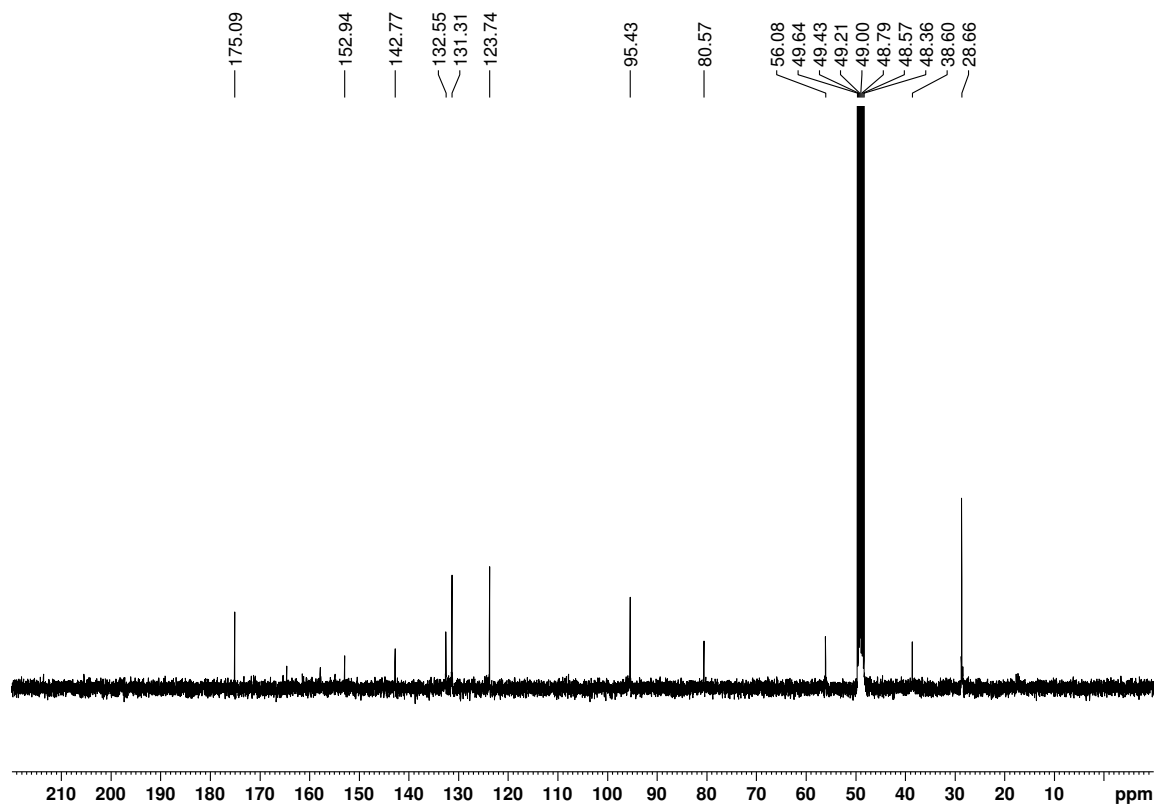


Appendix

^1H spectrum of **7** (400 MHz, MeOD):

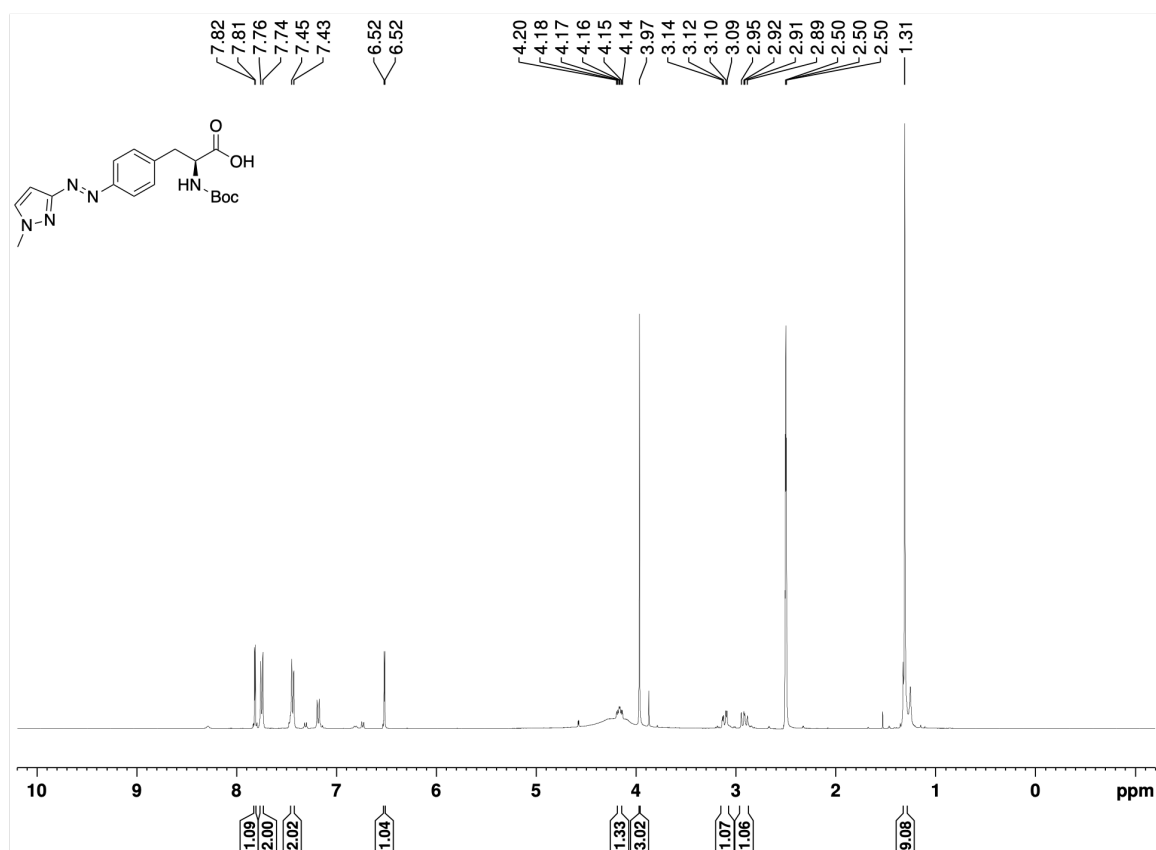


^{13}C spectrum of **7** (101 MHz, MeOD):

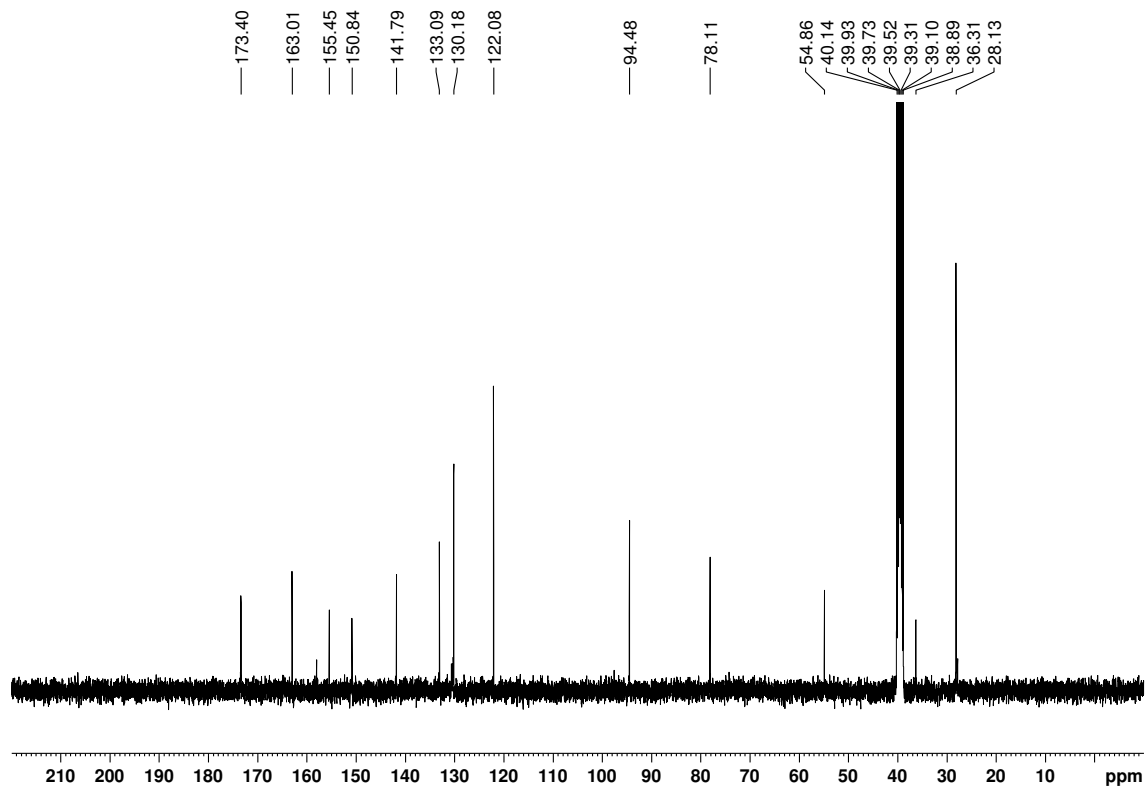


Appendix

^1H spectrum of **8** (400 MHz, $\text{DMSO-}d_6$):

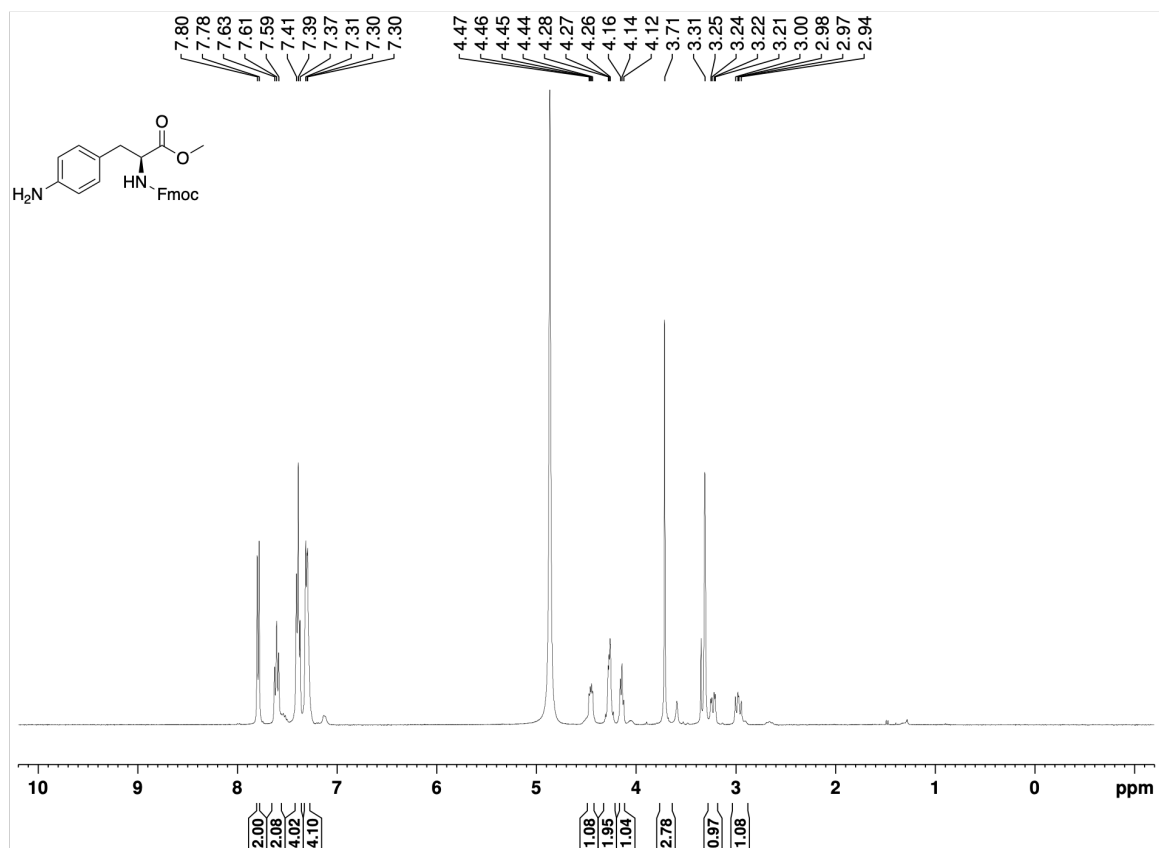


^{13}C spectrum of **8** (101 MHz, $\text{DMSO-}d_6$):

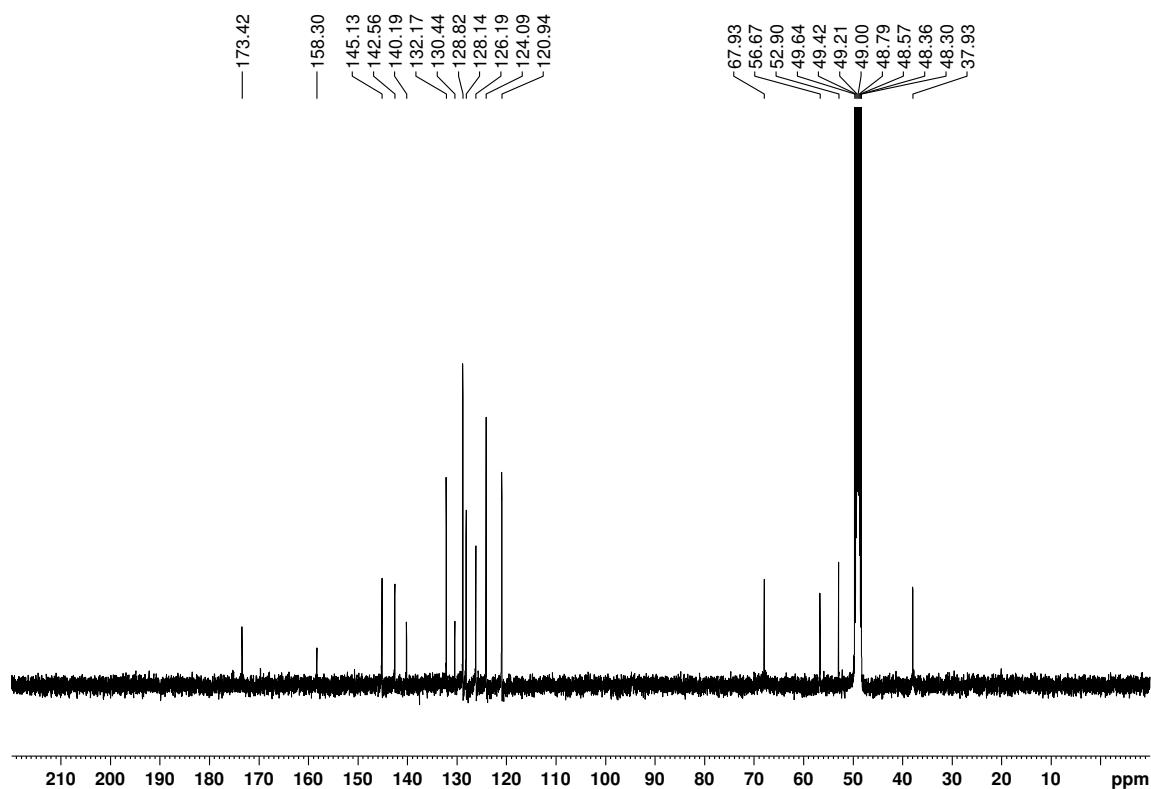


Appendix

^1H spectrum of **9** (400 MHz, MeOD):

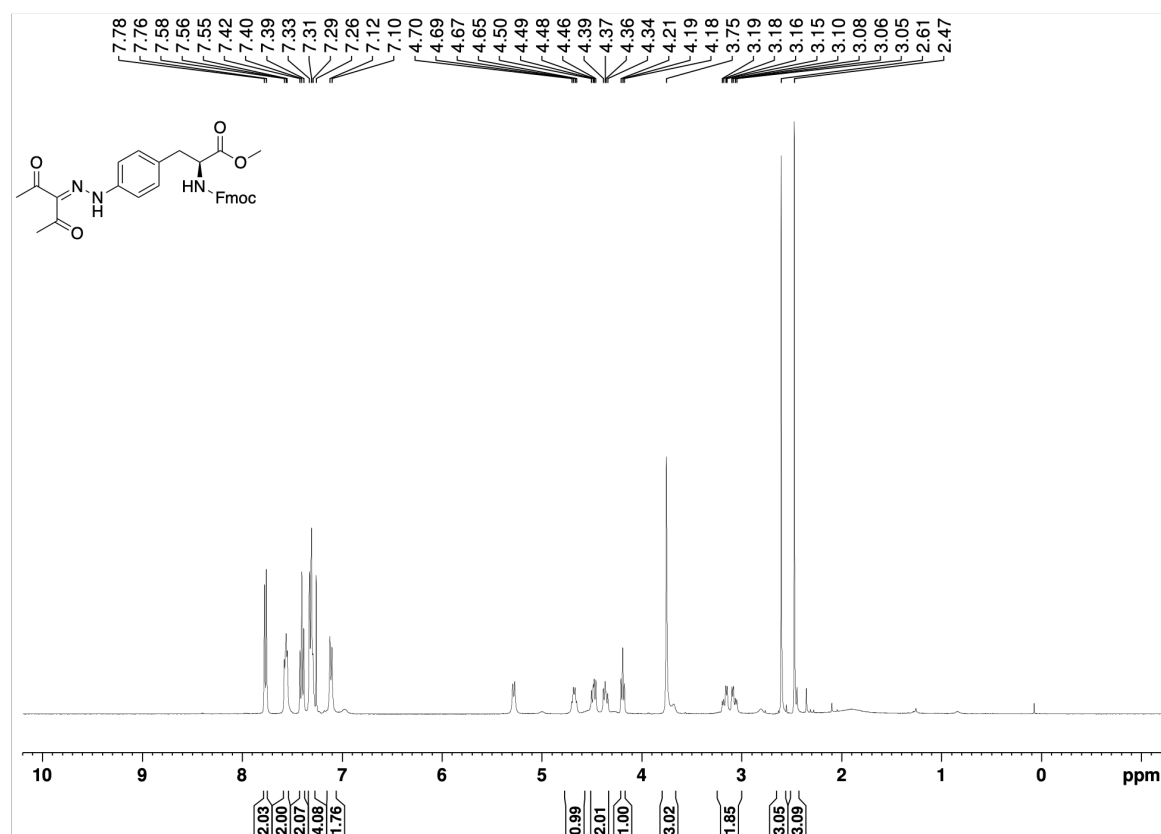


^{13}C spectrum of **9** (101 MHz, MeOD):

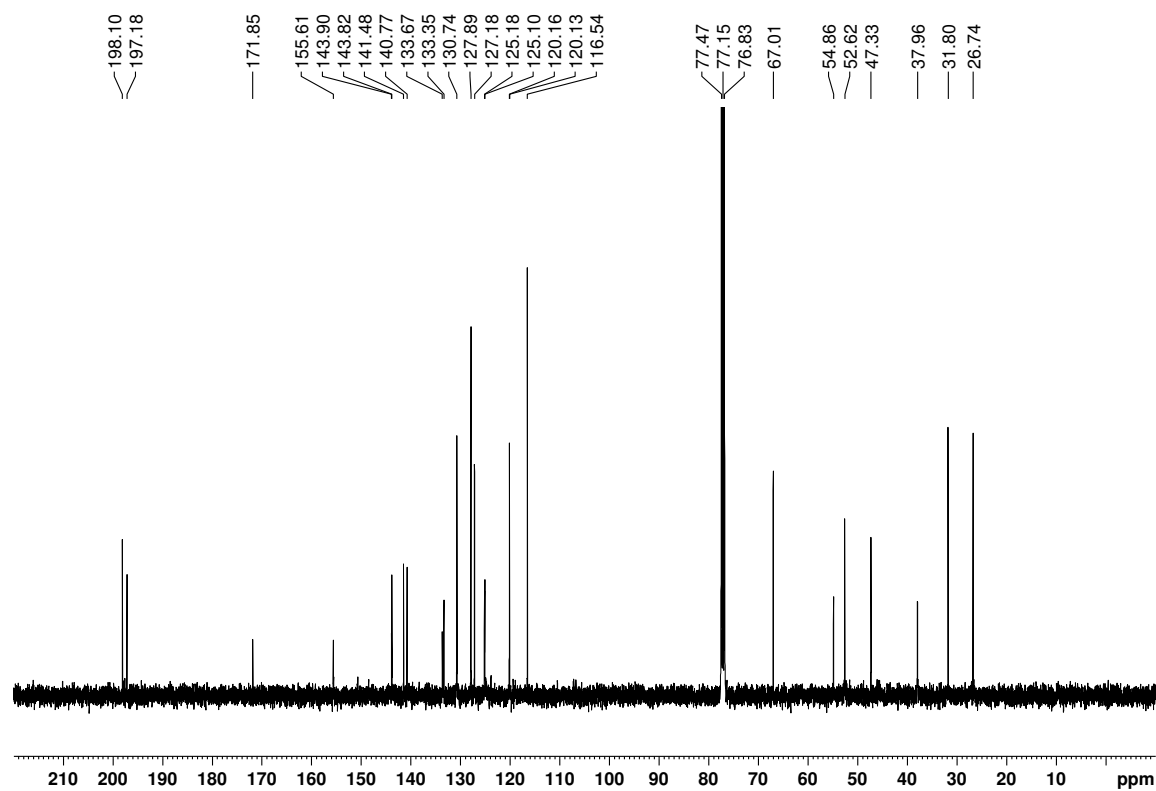


Appendix

^1H spectrum of **10** (400 MHz, CDCl_3):

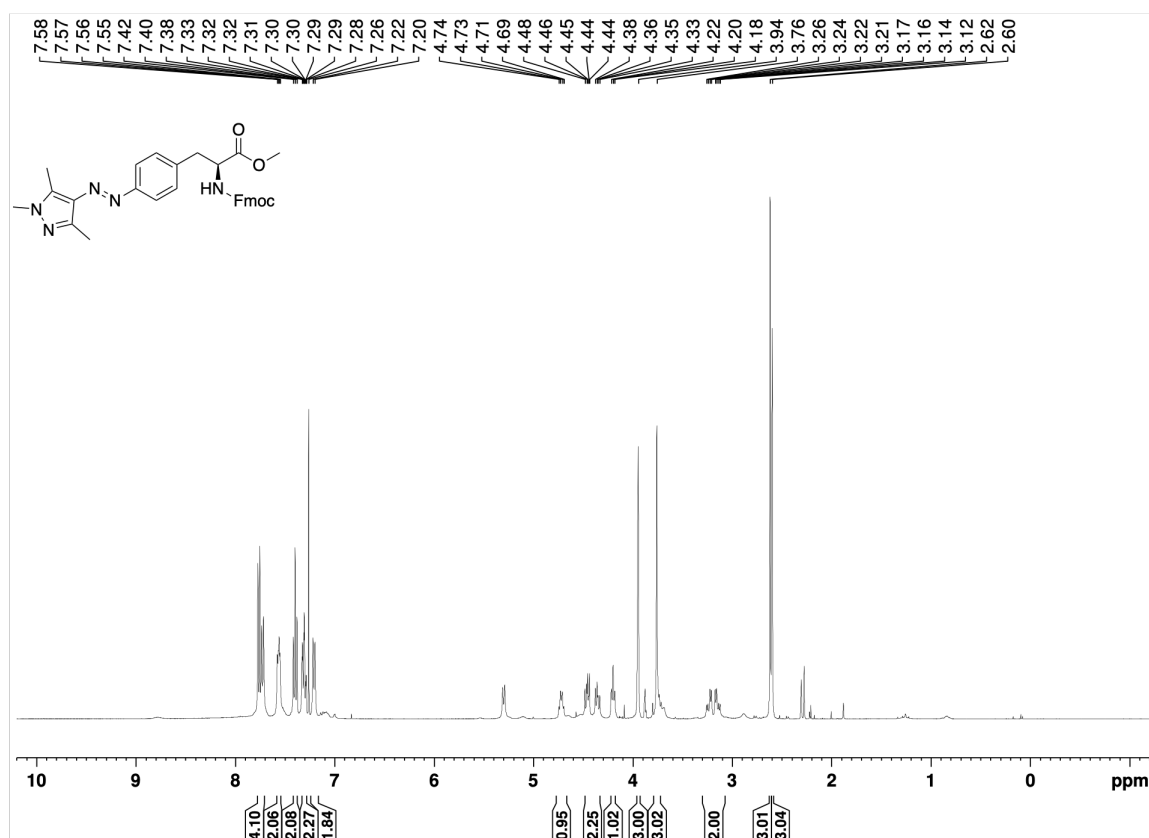


^{13}C spectrum of **10** (101 MHz, CDCl_3):

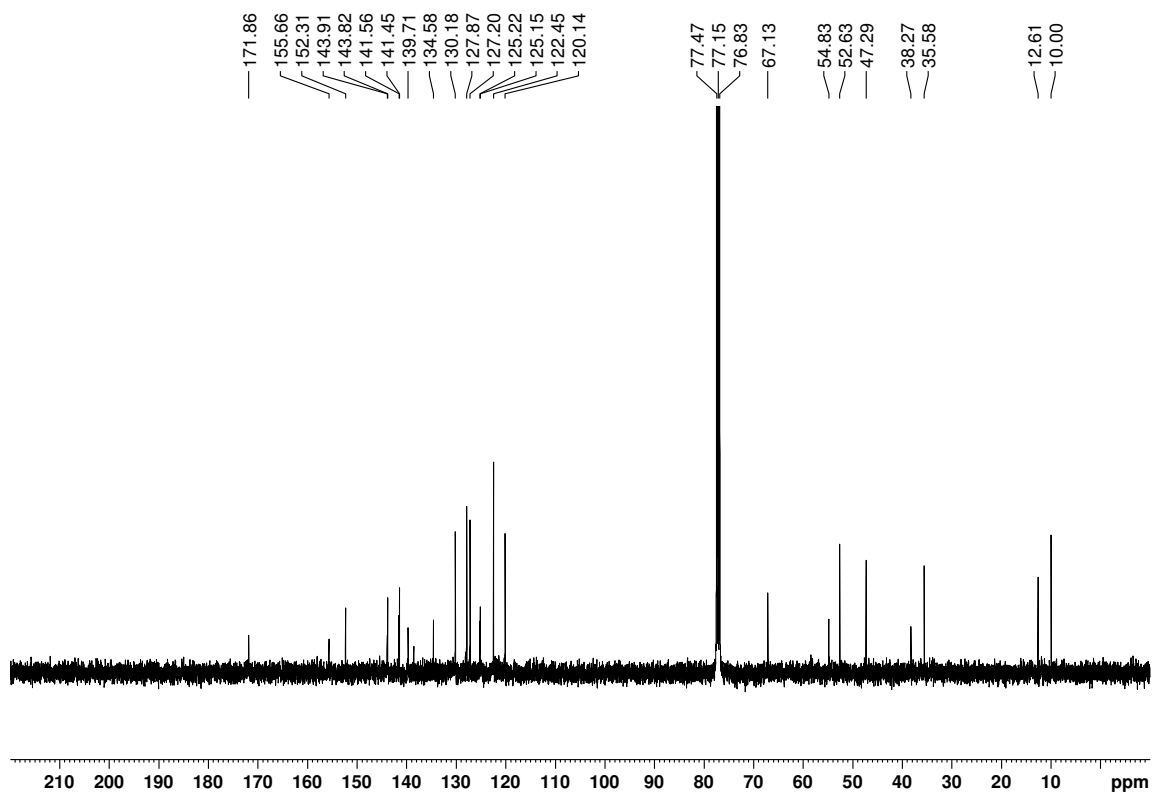


Appendix

^1H spectrum of **11** (400 MHz, CDCl_3):

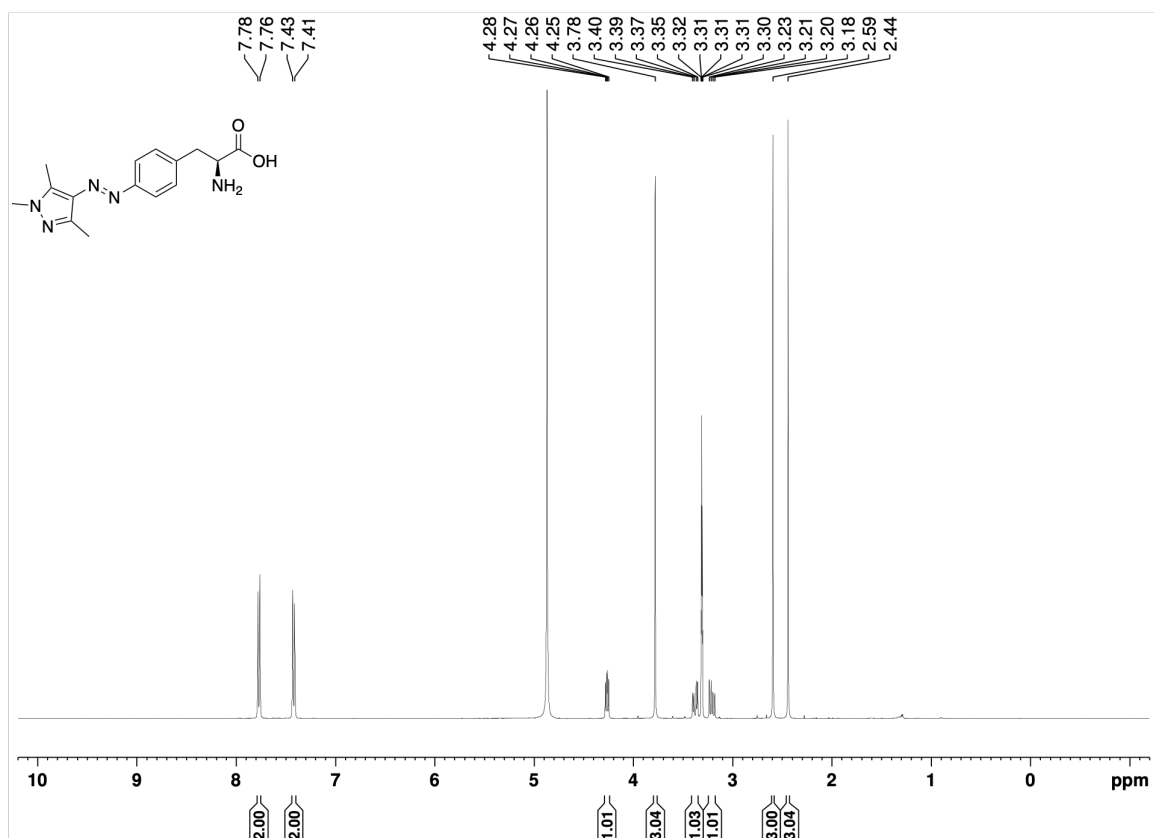


^{13}C spectrum of **11** (101 MHz, CDCl_3):

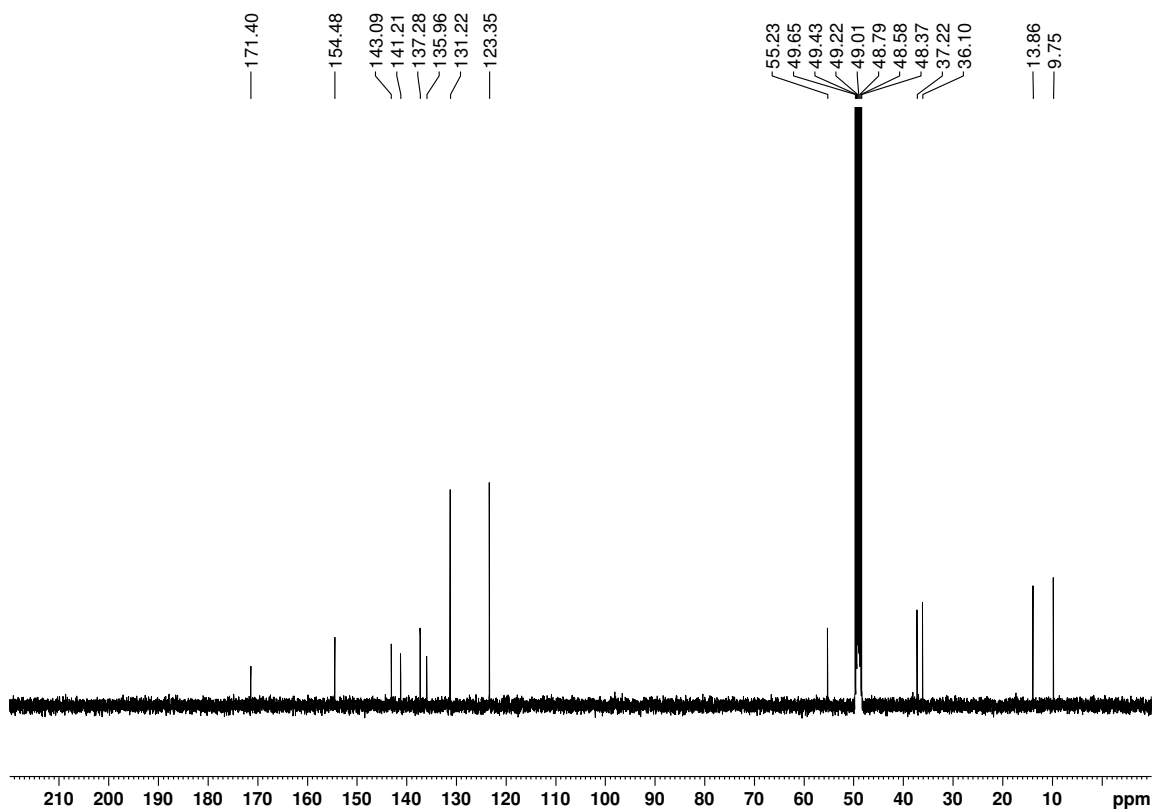


Appendix

^1H spectrum of **AapF3** (400 MHz, MeOD):



^{13}C spectrum of **AapF3** (101 MHz, MeOD):



Scientific Publications

'Development of Photoswitchable Tethered Ligands that Target the μ -Opioid Receptor' 10/2023

R. Lahmy, H. Hübner, D. Lachmann, P. Gmeiner, B. König,
ChemMedChem. **2023**, e202300228.

'Photochromic Fentanyl Derivatives for Controlled μ -Opioid Receptor Activation' 07/2022

R. Lahmy, H. Hübner, M. F. Schmidt, D. Lachmann, P. Gmeiner, B. König, *Chem. Eur. J.* **2022**, 28, e202201515.

'Fulgimides as Light-Activated Tools in Biological Investigations' 03/2019

D. Lachmann, R. Lahmy, B. König, *Eur. J. Org. Chem.* **2019**, 2019, 5018-5024.

Scientific Contributions and Committees

Associate Member of GRK1910 Research Training Group 03/2018 – 06/2022
Oral Presentations (Germany): 07/2018, 07/2019 and 08/2020

Emil Fischer Graduate Programme Research Day (via Zoom) 07/2020
Oral Presentation

9th International Symposium on Photochromism (France) 09/2019
Oral Presentation

6th Prague-Weizmann Summer School 2019 (Czech Republic) 09/2019
Poster Presentation

IUPAC Paris 2019 (France) 07/2019
Poster Presentation

II International Symposium on Photopharmacology 2018 (Spain) 11/2018
Poster Presentation

Member of iGEM University of Melbourne Team (Australia) 04/2013 – 11/2014

Further Awards and Achievements

Among Top 10% Most Downloaded Papers of 2018/2019 <i>Publication recognized in European Journal of Organic Chemistry</i>	04/2020
Minerva Stiftung Fellowship <i>For PhD research at the University of Regensburg</i>	03/2019
Australian Postgraduate Award Scholarship <i>University of Melbourne/Australian Government (declined for PhD in Germany)</i>	02/2016
Alan W Harris Scholarship – Honours Research Scholarship <i>Walter and Eliza Hall Institute of Medical Research</i>	02/2015
Co-Author of a Children's Science Book Makogon, B.; Lahmy, R., <i>The Adventures of E. coli</i> , <i>MoshPit Publishing</i> , 2014 , 1925219208.	10/ 2014
Outstanding Result Achievement Letter <i>University of Melbourne – Bachelor Degree Subject 'Pharmacology – How Drugs Work'</i>	08/2013

9. Acknowledgements

I am sincerely grateful to numerous individuals and associations who have contributed to the completion of this doctoral thesis. Your support, guidance, inspiration and encouragement have been invaluable throughout my academic journey.

First and foremost, I extend my gratitude to Prof. Burkhard König for providing me with the opportunity to pursue my PhD under his supervision. Coming from Australia, your generosity, support and guidance has not only instilled in me a great passion for chemistry but has significantly and positively shaped the past few years of my life. I am honored to have had the opportunity to learn from you and be part of your research group – thank you. I wish to express my sincere appreciation to the members of my examination board, Prof. Oliver Reiser as second examiner, Prof. Joachim Wegener as third examiner and Apl. Prof. Rainer Müller as chair of my doctoral colloquium. I would like to additionally thank Prof. Oliver Reiser for further support in securing my PhD position at the University of Regensburg.

This thesis would not have been possible without fruitful and impactful collaborations. I am grateful to Prof. Peter Gmeiner, Dr. Harald Hübner, Dr. Maximilian Schmidt and Dr. Jonas Kaindl from the Friedrich-Alexander-Universität for the successful collaboration across several projects. I would like to further thank Dr. Harald Hübner for countless scientific discussions – I am grateful to have worked with you and to have learned from you. I would like to extend my sincere gratitude to Prof. Reinhard Sterner, Dr. Andrea Kneuttinger and Caroline Hiefinger from the University of Regensburg for the strong and valuable collaboration across our respective projects. In addition, I would like to thank Prof. Remco Sprangers, Prof. Ruth Gschwind, Prof. Ralph Witzgall, Prof. Reinhard Rachel, Anita Zügner and Willibald Stockerl from the University of Regensburg, as well as Prof. Rafal Klajn from the Weizmann Institute of Science, for insightful collaborations in further projects that were outside the scope of this thesis. I would like to thank the GRK1910 for further collaboration opportunities, helpful discussions and scientific workshops.

I extend my thanks to Julia Zach, Barbara Bauer, Regina Hoheisel, Ernst Lautenschlager, Britta Badziura, Dr. Rudolf Vasold, Simone Strauß and Katharina Nickl for their help in all technical and organizational matters. I would like to additionally thank Julia Zach for her valuable help in developing LED-related equipment and further support. My gratitude also goes out to personnel of the mass spectroscopy department, in particular Josef Kiermaier,

Acknowledgements

the NMR department, the electronics workshop, the mechanics workshop and the chemical store at the University of Regensburg.

In addition, I would like to thank all current and former members of the König research group for the enjoyable working environment and valuable support. I would especially like to thank the following people for welcoming me upon my arrival to Germany: Dr. Alexander Wimmer, Dr. Andreas Graml, Dr. Ulrike Wirth, Dr. Daniel Lachmann, Dr. Daniel Petzold, Dr. Indrajit Ghosh, Dr. Nadja Simeth, Dr. Antonín Králík, Dr. Tobias Karl, Dr. Karsten Donabauer, Dr. Karin Rustler, Dr. Anna Berger, Dr. Simon Düsel, Dr. Shun Wang and Dr. Stefano Crespi. I thank you all for helpful scientific discussions and for the incredible and unforgettable memories made both inside and outside the laboratory environment. I would like to especially thank Dr. Daniel Lachmann for his invaluable scientific mentorship during the earlier stages of my PhD. I would like to extend a further thanks to my interns Fjoralba Zeqiri, Ritu Singh and Magdalena Koch.

In addition to Prof. Burkhard König, my gratitude also goes out to the Minerva Stiftung, which provided me with a scholarship to carry out this research. I would additionally like to thank Prof. Chiara Cabrele (University of Salzburg) for support in obtaining this scholarship. Furthermore, I would like to deeply thank Prof. Uta Wille (University of Melbourne/Bio21 Institute) for directing me to and connecting me with Prof. Burkhard König in the first place, as well as Dr. Brad Sleebs (WEHI) and A. Prof. Chris Burns (WEHI) for support in my pursuit of a PhD abroad.

Lastly, I would like to thank my friends and family for their encouragement during this academic journey. A special thanks to my parents Coco and Anna, as well as my brother Doron, who have taught me the importance of perseverance, resilience and a passion for life that proved valuable throughout this academic endeavour. I would also like to thank my fiancé Dr. Alexander Wimmer, whom I met in this research group, for the unwavering support.

This thesis reflects a collective effort and support of many individuals and associations. Each one of you has played an essential role in shaping my academic and personal growth, and for that, I am truly grateful.

Thank you,


Ranit Lahmy

DECLARATION

Eidesstattliche Erklärung

Ich erkläre hiermit an Eides statt, dass ich die vorliegende Arbeit ohne unzulässige Hilfe Dritter und ohne Benutzung anderer als der angegebenen Hilfsmittel angefertigt habe; die aus anderen Quellen direkt oder indirekt übernommenen Daten und Konzepte sind unter Angabe des Literaturzitats gekennzeichnet.

Die Arbeit wurde bisher weder im In- noch im Ausland in gleicher oder ähnlicher Form einer anderen Prüfungsbehörde vorgelegt.

Unterschrift: 

Ort, Datum: Regensburg, 28.11.2023

Ranit Lahmy